IV
FUSION
ROME
1970

IV EUROPEAN CONFERENCE ON CONTROLLED FUSION AND PLASMA PHYSICS

C. N. E. N.

Contributions to the

"FOURTH EUROPEAN CONFERENCE ON CONTROLLED FUSION AND PLASMA PHYSICS"

ROME, *Italy*, August 31 - September 4, 1970

This book will be made available free of charge to all participants of the Conference. Further copies can be ordered at a price of Lit. 2,500.=

C.N.E.N.

Divisione Affari Internazionali e
Studi Economici
Ufficio Edizioni Scientifiche
V.le Regina Margherita, 125
I-00198 ROMA

CONTENTS

PREFACE

These proceedings contain the papers to be presented at the *"IV European Conference on Controlled Fusion and Plasma Physics"*, which will take place in Rome, Italy, from 31 August to 4 September 1970. The Conference is the fourth in a series of which the previous three took place in Munich (1965), in Stockholm (1967), and in Utrecht (1969), and the first to be organized by the European Physical Society (EPS) through its Plasma Physics Division.

The papers have been selected for presentation by the Paper Selection and Programme Committee. The responsibility for the contents of the contributions (received on 1 June 1970) is exclusively that of the authors. In the proceedings, the papers have been arranged in groups of related subjects, reflecting the order of their presentation.

Sincere thanks are due to the authors for their co-operation.

The Organizing Committee,

Frascati, 18 June, 1970

COMMITTEES AND SUPPORTING ORGANIZATIONS

Organizing Committee

B. Brunelli *chairman*

F. Engelmann

Mrs. M. Fiorini

M. Iannuzzi

B. Rumi

R. Verbeek

Paper Selection and Programme Committee

B. Lehnert, *Stockholm, Sweden*

R.S. Pease, *Culham, United Kingdom*
(during the Committee meeting replaced by D.E.T.F. Ashby)

D. Pfirsch, *Garching, Federal Republic of Germany*

M. Trocheris, *Fontenay-aux-Roses, France*

Financial Support

The organizations mentioned below have contributed financially to the Conference. Their support is gratefully acknowledged:

Comitato Nazionale per l'Energia Nucleare, Rome

Commission of the European Communities, Brussels

International Atomic Energy Agency, Vienna.

Invited Lecture

CONCLUSIONS OF THE TRIESTE "WORKSHOP" ON THEORETICAL PLASMA PHYSICS

B. B. Kadomtsev*

International Centre for Theoretical Physics, Trieste, Italy.

ABSTRACT. A short review of the main results of the plasma physics group at ICTP is given. Both papers and results of discussions are included.

The main topics of the work and seminars of the plasma physics group during April-August 1970, were toroidal plasma confinement and non-linear phenomena in plasmas.

Concerning toroidal plasma confinement, many related problems were considered, namely equilibrium and diffusion, instabilities and cooperative phenomena. In addition to the usual diffusion in rare plasma, the effect of plasma compression by longitudinal electric fields in toroidal discharges was investigated. It was shown that in the case of very low collision frequencies, so-called banana and plateau regimes, the plasma compression is very effective so that it dominates the diffusion at $\beta_p = 8\pi p/B_\theta^2 < 1$.**) This result is in qualitative agreement with the experimental data on Tokamak-3 concerning the very long time of particle confinement. Probably better understood is the ion heating process on Tokamak-3 which can be explained on the basis of the usual electron-ion energy exchange and neoclassical ion thermoconductivity. The mechanism of drift temperature instability may also be involved. But the problem of electron thermoconduction is not solved uniquely. It follows both from the analysis of energy balance and from the overheating instability that electron thermoconductivity is considerably higher than classical thermoconductivity. One possible way to explain this effect is given by trapped electron instability; there may be another possibility which would be coupled with the anomalous resistivity cooperative phenomena.

---

*) On leave from Kurchatov Institute of Atomic Energy, Moscow, USSR.

**) This effect was considered independently by Galeev and Sagdeev at Novosibirsk.

Different types of toroidal plasma instabilities were considered. In particular, a more refined theory of instability of trapped particles was developed. It was very nice to learn that, predicted purely theoretically, trapped particle instability has recently been discovered experimentally on the spherator device. More detailed theory of flute type instability on tokamaks, both with circular and elliptical cross-sections, was developed. Some specific problems of anisotropic and rotating plasma diffusion were also considered.

The detailed theory of the cone and drift-cone plasma instabilities which takes into account the longitudinal inhomogeneity of a magnetic field was given. It shows that the restriction on longitudinal dimensions of adiabatic magnetic traps are more severe than was given previously. But, at the same time it shows that restrictions on the radius of the adiabatic trap is not so severe as was previously believed so that some discrepancy between the theory of the drift-cone instability and the experimental data was overcome.

Much of the effort of the plasma group concerned investigations of different types of cooperative non-linear plasma phenomena. A new approach to the problems of plasma turbulence was suggested. It takes into account the two-particle correlation in its motion which corresponds to some sort of coherent motion appearing as macro-particles or "clumps." These clumps behave like new particles with great charge; they can generate waves and interact with each other. At a strongly turbulent situation they can explain the anomalous resistivity; at beam-plasma interaction they make a qualitative explanation possible of two-exponential type electron distribution at the final state. The different types of anomalous resistivity and some approaches to strong turbulence treatment were discussed.

The participants of the plasma group also investigated and discussed many problems such as wave propagation, interaction of waves with plasma, and non-linear wave interaction.

All participants of the plasma group are grateful to Professor Abdus Salam and the International Atomic Energy Agency and UNESCO for hospitality at the International Centre for Theoretical Physics, Trieste.

TOROIDAL CONFINEMENT (THEORY)

EFFECT OF LONGITUDINAL ELECTRIC FIELD ON TOROIDAL DIFFUSION

by
P. Rutherford, L. Kovrizhnikh and M. Rosenbluth
International Centre for Theoretical Physics, Trieste, Italy.

ABSTRACT: The driving toroidal electric field in tokamaks is shown to lead to a significant pinching effect. For $\beta_\theta < 1$ this pinching is more rapid than outward diffusion in the banana and plateau regimes.

It was pointed out by Ware [1] that the driving toroidal electric field in tokamaks produces a much larger drift than the usual $ExB/B^2 \approx EB_\theta/B^2$. We employ the usual toroidal co-ordinates with concentric circular flux surfaces of radius r, θ measuring the azimuthal angle round the magnetic axis and ϕ the azimuthal angle round the major axis. The major radius is $R = R_0 + r\cos\theta$, and $\partial/\partial\phi = 0$. Ware reasoned that if one looked at trapped particles and used the conservation of angular momentum

$$\frac{d}{dt}\left(Rmv_{\parallel} + ReA_\phi\right) = 0 \qquad (1)$$

then, since $v_{\parallel}$ vanishes at a particle reflection point, it follows that over many bounce periods

$$\frac{d}{dt}RA_\phi = \dot{r}\frac{\partial}{\partial r}RA_\phi + R\frac{\partial A_\phi}{\partial t} = -\dot{r}RB_\theta - E_\phi R = 0$$

so that

$$\dot{r} = -\frac{E_\phi}{B_\theta} \gg \frac{E_\phi B_\theta}{B^2} \qquad (2)$$

This somewhat surprising result may also be understood by noting that the azimuthal electric field acts like a θ-varying static potential for the trapped particles. Hence the "bananas" are displaced and now have an up-down asymmetry. Due to this asymmetry the usual magnetic radial drifts no longer cancel and a simple calculation of the effect yields eq.(2). However, this simple picture is not adequate since the effect of the electric field on untrapped particles is rather complex. More important, the collisional friction between particles perturbs the orbits in a similar way to the electric field. Since the equilibrium field necessary to drive the current must be of the order of the frictional forces, a self-consistent solution of the problem must be sought.

We start from the Vlasov equation in the guiding centre limit:

$$v_{dr}\frac{\partial f_0}{\partial r} + \frac{e}{m}E_\phi\frac{\partial f_0}{\partial v_{\parallel}} + v_{\parallel}\,n\cdot\nabla f_1 = C(f_1) \qquad (3)$$

Here v_{dr} is the usual magnetic drift, $v_{\parallel} = \sqrt{2(\mathcal{E}-\mu B)}$ is the velocity parallel to the magnetic field, f_0 is the Maxwellian distribution and $f_1(\theta,\mu,\mathcal{E})$ the perturbed distribution induced by the electric field and collisional effects; $C(f_1)$ represents the collision operator; $n\cdot\nabla$ indicates a derivative along the magnetic field taken at constant energy $\mathcal{E}$, and magnetic moment μ. From eq.(1) we may write

$$v_{dr} = \frac{m}{eRB_\theta}v_{\parallel}\,n\cdot\nabla(v_{\parallel}R) \qquad (4)$$

The surface averaged radial flux is now given by

$$\Gamma_r = \frac{1}{R_0}\left\langle R\int v_{dr}f_1\,d^3v\right\rangle \qquad (5)$$

where $\langle\ \rangle$ denotes an average over θ. Using eq.(4), integrating by parts on θ, and substituting for $n\cdot\nabla f$ from eq.(3) (with $\partial f_0/\partial r = 0$) we obtain for the flux due to the electric field

$$\Gamma_r = \frac{m}{eRB_\theta}\frac{1}{R_0}\left\langle R^2\int v_{\parallel}\left[\frac{e}{m}E_\phi\frac{\partial f_0}{\partial v_{\parallel}} - C(f_1)\right]d^3v\right\rangle \qquad (6)$$

This expression immediately shows the flux to be ambipolar. It will then suffice to calculate the electron diffusion and to use only electron-ion collision terms in eq.(6). We must now solve eq.(3) for f_1. We use a Lorentz collision operator

$$C(f_1) = \frac{\nu(v)\,v_{\parallel}}{B}\frac{\partial}{\partial\mu}\mu v_{\parallel}\frac{\partial f_1}{\partial\mu} \qquad (7)$$

The calculation now proceeds in the usual way. Thus in the low collision frequency (banana) limit the dominant term in the equation is $v_{\parallel}\,n\cdot\nabla f_1$. This yields to lowest order $\partial f_1/\partial\theta = 0$ and to next order by averaging over θ we obtain an equation for determining $f_1(\mathcal{E},\mu)$. The solution is

$$f_1 = \frac{eE_\phi f_0}{\nu T}\int_{\mu}^{\mathcal{E}/B_{max}}\frac{B_\theta\,d\mu}{\langle v_{\parallel}\rangle} \qquad \text{(untrapped particles)}$$

$$f_1 = 0 \qquad \text{(trapped particles)} \qquad (8)$$

The averages of $v_{\parallel}$ are expressible in terms of elliptic integrals for the tokamak geometry, and substituting into eq.(6) we find for the flux, after numerically evaluating the μ integrals

$$\Gamma_r = -1.6\,\frac{nE_\phi}{B_\theta}\left(\frac{r}{R}\right)^{1/2} \qquad (9)$$

The minus sign indicates an inward flux. Note that the result is roughly equal to that which would be obtained by multiplying Ware's drift by the fraction of trapped particles. However, if we examine the flux in detail we find that it does not come from trapped particles but mostly from the boundary layer between trapped and untrapped particles. Evidently in this region of velocity space a large unbalanced collisional friction exists leading to a large modification of the orbits and particle diffusion. It should also be noted that the displacement of orbits leads to a large charge separation and hence a self-consistent potential. However, it is easily shown that introduction of this potential and the drifts resulting from it into eq.(3) does not modify the flux.

Finally, we note that if we had kept the first term in eq.(3) rather than the second as the driving term, we would have recovered the usual banana-diffusion result. Hence it is simple to compare the flux due to electric field with the usual diffusion flux. Neglecting electron-electron collisions (and the possible role of anomalous resistivity) we obtain

$$\Gamma_{electric}/\Gamma_{diffusion} \approx -2/\beta_\theta \qquad (10)$$

where $\beta_\theta = 8\pi p_{centre}/B^2_{\theta\,surface}$. Under the usual conditions of tokamak experiments $\beta_\theta \lesssim 1$ and we might expect an inward flow of plasma. However, it must be pointed out that both the experimental time scale and the time scale for thermal diffusion are shorter by an order of magnitude than the time scale for particle diffusion discussed here.

Finally, the above-described calculations may be performed for other collisional regimes. In the "plateau" regime eq.(10) remains approximately valid, while in the hydrodynamic regime the effect of the electric field becomes small although the details of the transition are not yet clear.

It has been pointed out to us by L. Artsimovich that similar results have recently been obtained by Galeev and Sagdeev.

REFERENCE

1) A. Ware, Sherwood Theoretical Meeting (Princeton, April 1970).

TOROIDAL CONFINEMENT (THEORY)

Classical Diffusion in Tokomak

W. Feneberg, Institut für Plasmaphysik GmbH, 8046 Garching near Munich, Federal Repuolic of Germany

Abstract: The mass flow perpendicular to the magnetic surfaces is calculated for rotational symmetric systems .The influence of an induced electric field on the classical diffusion is included. The formula will be simplified for a special self-consistent Tokomak case with magnetic surfaces of nearly circular cross section. It will be shown that a stationary equilibrium with vanishing mass flow has no physical meaning for realistic Tokomak conditions.

The influence of an induced electric field produced by ohmic heating in a toroidal discharge has not been taken into account in the work of Pfirsch-Schlüter on classical diffusion [1]. The effect of this electric field consists in an additional $\vec{E} \times \vec{B}$ drift which decreases the classical diffusion. If we want to calculate this effect we must start with the magnetohydrodynamic equation

$$\vec{i} = -\frac{c}{B^2}[\nabla p \times \vec{B}] + \lambda \vec{B} \qquad (1)$$

From the condition $\nabla \vec{i} = 0$ there results the differential equation for λ,

$$\frac{\partial \lambda}{\partial \varrho}\frac{\partial F}{\partial z} - \frac{\partial \lambda}{\partial z}\frac{\partial F}{\partial \varrho} = -\frac{2c\varrho}{B_0 R}\frac{dp}{dF}\frac{\partial F}{\partial z} \qquad (2)$$

which is to be solved by the general solution:

$$\lambda = -\frac{dp}{dF}\frac{c\varrho^2}{B_0 R} + \lambda_0(F) \qquad (3)$$

Here we have used cylindrical coordinates (ϱ, θ, z), with ϱ - the distance from the torus axis, θ - the direction of the main magnetic field $B_\theta = B_0 \frac{R}{\varrho}$, R - the distance of the center of the discharge vessel from the torus axis, z - the distance from the torus plane. We shall also introduce a system of polar coordinates:

$$z = r \sin\vartheta$$
$$\varrho - R = -r\cos\vartheta \qquad (4)$$

It is known that the magnetic field can be generated by a scalar function F [2],

$$B_r = -\frac{1}{\varrho r}\frac{\partial F}{\partial \vartheta}, \quad B_\vartheta = \frac{1}{\varrho}\frac{\partial F}{\partial r} \qquad (5)$$

where the lines F = const coincide with the lines p = const. The contribution of the magnetic field of the diamagnetic currents to the main magnetic field B_θ is neglected.

$$\beta_\theta = \frac{8\pi p}{B_0^2} \ll 1, \text{ p - the plasma pressure} \qquad (6)$$

In equation (2) the assumption was made $|B| = |B_\theta|\left(1+\frac{B_M^2}{B_\theta^2}\right)^{1/2} \cong |B_\theta|$, where $B_M^2 = \frac{1}{\varrho^2}\left(\left(\frac{\partial F}{\partial r}\right)^2 + \frac{1}{r^2}\left(\frac{\partial F}{\partial \vartheta}\right)^2\right)$. This assumption is not used in the following equations.

The free function $\lambda_0(F)$ is determined by Ohm's law:

$$\vec{E} + \frac{1}{c}[\vec{v} \times \vec{B}] = \frac{m}{ne^2\tau}\left(-\frac{c}{B^2}[\nabla p \times \vec{B}] + \frac{1}{2}\lambda\vec{B}\right) + \frac{1}{2ne}\nabla p \qquad (7)$$

Ohm's law in this form can be received only for constant temperature.

(That means: $\vec{v}$ - Mass velocity, n - particle density, e -electron charge, m - electron mass, τ - electron-ion collision time.)The difference between the conductivity parallel and perpendicular to the magnetic field is taken into account by a factor 2.The electric field

$$\vec{E} = -\nabla\phi + \frac{1}{c}\frac{\partial \vec{A}}{\partial t} \qquad (8)$$

consists of a scalar field in the meridional (ϱ, z) plane and the induced field in direction $-\theta$.

$$\left(\frac{1}{c}\frac{\partial \vec{A}}{\partial t}\right)_\theta = E_\theta, \quad E_\theta = E_0\frac{R}{\varrho} \qquad (9)$$

If we multiply equation (7) scalar with $\vec{B}$ and integrate over a magnetic surface F = const, we obtain:

$$\lambda_0(F) = \frac{c}{B_0 R}\frac{dp}{dF}\frac{\int_0^{2\pi} \varrho\left(\frac{\partial F}{\partial r}\right)^{-1} d\vartheta}{\int_0^{2\pi} \varrho^{-1}\left(\frac{\partial F}{\partial r}\right)^{-1} d\vartheta} + \frac{2ne^2\tau E_0}{m B_0}\left\{1 - \frac{\int_0^{2\pi} \varrho^{-1}\frac{B_M^2}{B_\theta^2}\left(\frac{\partial F}{\partial r}\right)^{-1} d\vartheta}{\int_0^{2\pi}\left(\frac{\partial F}{\partial r}\right)^{-1}\varrho^{-1} d\vartheta}\right. \qquad (10)$$

The formula for the mass flow M is obtained using the vector product of equation (7) with $\vec{B}$:

$$M = \int_0^{2\pi}\left(nv, \frac{\nabla F}{|\nabla F|}\right) 2\pi\varrho \frac{|\nabla F|}{\left|\frac{\partial F}{\partial r}\right|} d\vartheta =$$

$$-\frac{2\pi mc^2}{e^2\tau B_0^2}\frac{dp}{dF}A(F) - \frac{\pi mc^2}{e^2\tau}\frac{dp}{dF}B(F) - \frac{2\pi nc E_0}{B_0^2 R}C(F) \qquad (11)$$

with

$$A(F) = \int_0^{2\pi}\varrho\frac{(\nabla F)^2}{\left|\frac{\partial F}{\partial r}\right|} d\vartheta, \quad B(F) = \int_0^{2\pi}\varrho^3\left|\frac{\partial F}{\partial r}\right| d\vartheta - \frac{\left(\int_0^{2\pi}\varrho\left(\frac{\partial F}{\partial r}\right)^{-1} d\vartheta\right)\left(\int_0^{2\pi}\varrho\left|\frac{\partial F}{\partial r}\right|^{-1} d\vartheta\right)}{\int_0^{2\pi}\varrho^{-1}\left(\frac{\partial F}{\partial r}\right)^{-1} d\vartheta}$$

$$C(F) = \frac{\left(\int_0^{2\pi}\left(\frac{\partial F}{\partial r}\right)^{-1}\varrho^{-1}(\nabla F)^2 d\vartheta\right)\left(\int_0^{2\pi}\varrho\left|\frac{\partial F}{\partial r}\right|^{-1} d\vartheta\right)}{\int_0^{2\pi}\varrho^{-1}\left(\frac{\partial F}{\partial r}\right)^{-1} d\vartheta} \qquad (12)$$

The first term A(F) accounts for the classical diffusion in a straight cylinder, the second term B(F) contains the Pfirsch-Schlüter diffusion and the third term C(F) gives the contribution of the electric field.

In the following now we shall look for a special simple Tokomak case. The Maxwell equation for the meridional magnetic field is:

$$rot\,\vec{B}_M = \frac{4\pi}{c} i_\theta \qquad (13)$$

This equation will be solved in the approximation of a high discharge current.

$$i_\theta \approx \frac{2ne^2\tau}{m} E_\theta = \frac{2ne^2\tau E_0}{m}\frac{R}{\varrho} \qquad (14)$$

We apply a homogeneous vertical magnetic field

$$B_z = \frac{Ja^2}{RC\,b^2} \qquad (15)$$

(J - total current, a-plasma radius) and obtain the solution for the magnetic surfaces:

$$F = \frac{\alpha}{4}\left(x^2 - \frac{\varepsilon}{4}x^3\cos\vartheta\right), \quad x = \frac{r}{b}, \quad \alpha = \frac{8\pi ne^2\tau E_0 R b^2}{mc} \qquad (16)$$

In this configuration with nearly circularly shaped surfaces we can use a simplified expression for the mass flow:

$$M = -\frac{4\pi^2 R\tau mc^2}{e^2\tau B_0^2}\left(1+\frac{4\pi^2}{\iota^2}\right)\frac{dp}{dt} - 4\pi^2\tau^2\frac{E_0 cn}{B_0}\left(\frac{\iota}{2\pi}\right), \quad \frac{\iota}{2\pi} = \frac{\alpha}{2b^2 B_0} \qquad (17)$$

For M = 0 it follows for the density profile:

$$n = n_0\left(1 - \frac{\gamma r^2}{2n_0}\right), \quad \gamma = \frac{\iota^3 eE_0 ne^2\tau B_0}{16\pi^3 Rmc\,kT} \qquad (18)$$

For the conditions realized in T-3 we have $\frac{\gamma}{n_0} \approx 10^3$, that means that the electric field in realistic cases is too small to prevent the plasma diffusion. An interesting stationary stage with M = 0 can be achieved only when a temperature gradient is considered [3, 4].

References

1 Pfirsch, D., Schlüter, A.: MPI/PA 7/62
2 Lüst, R., A. Schlüter: Zeitschr.f.Naturforschg.12a,850(1957)
3 Shafranov,V.D., Reviews of Plasma Physics, Vol. 2,p.145
4 Feneberg, W., IPP 3/84

This work was performed as part of the agreement between the Institut für Plasmaphysik GmbH, Munich-Garching, and Euratom to conduct joint research in the field of plasma physics.

TOROIDAL CONFINEMENT (THEORY)

Plasma Equilibria of Tokamak Type

H.P. Zehrfeld, B.J. Green, Institut für Plasmaphysik GmbH, Garching near Munich, Federal Republic of Germany

We present a general formalism for the description of an axisymmetric plasma equilibrium. This is a model for the steady operation of a Tokamak device. We use the hydromagnetic equations taking into account effects such as tensorial resistivity and finite thermal conductivity. The reformulation of this set leads to an equivalent set, including the generalisation to toroidal geometry of the Bennett-Pinch relation, and an expression for the resistive plasma loss which shows explicitly the effect of the discharge current. This mathematically concise presentation of the full resistive equilibrium problem is appropriate to practical calculations. As an example we consider a steady state on the resistive time scale and for the case of small inverse aspect-ratio calculate the plasma displacement, and the radial distributions of all equilibrium quantities.

To describe the stationary state of a Tokamak plasma, we use the following MHD equations in M.K.S. units and standard notation

$$\mathrm{rot}\,\underline{B} \times \underline{B} = \mu_0 \nabla p \tag{1}$$

$$\mathrm{div}\,\underline{B} = 0 \tag{2}$$

$$\underline{E} + \underline{v} \times \underline{B} = \eta \underline{j} \quad ; \quad \underline{E} = -\nabla\varphi - \frac{U}{2\pi}\nabla\zeta \tag{3}$$

$$\mathrm{div}\,\rho\underline{v} = Q \tag{4}$$

$$\mathrm{div}\,e\rho\underline{v} = \eta \underline{j}\underline{j} - p\,\mathrm{div}\,\underline{v} + \mathrm{div}(\kappa\nabla T) + Q_E \tag{5}$$

$$\eta = \eta_\perp \mathbf{1} - (\eta_\perp - \eta_\parallel)\underline{B}\underline{B}/B^2 \tag{6}$$

The expression for $\underline{E}$ follows from the assumption that there is no time variation of $\underline{B}$ in the plasma region. U is the ring voltage, ζ the angle about the axis of symmetry and e the specific internal energy. To complete the system we add the ideal gas equation of state. We assume that the temperature T is constant along field lines. We imagine that the plasma is enclosed in an ideally conducting container.

The following observations should be made:

(1) We consider a stationary state, by which is meant that the time variation is slow enough to neglect all partial derivatives with respect to time.

(2) The plasma losses due to ion-electron collisions, as described by the resistivity η are balanced by a plasma source Q.

(3) In the stationary state under investigation, plasma flows are retained but are such that inertia effects are negligible.

The usual description of an axisymmetric situation is carried out with the use of cylindrical coordinates. The introduction of flux functions leads to a more elegant and convenient description [1]. We employ for $\underline{B}$ and $\underline{j}$ the fluxes the "long" and "short" way, where each flux is evaluated in the appropriate direction between the magnetic axis and a magnetic surface. We call the magnetic fluxes the long and the short way F and G respectively. The corresponding fluxes of $\underline{j}$, the currents, we call I and J. By their definition, the equations used and the assumption on T, F,G,I,J,T, p and ρ are surface quantities. The labeling of magnetic surfaces can be done in terms of any one of these, we usually emplpy the poloidal magnetic flux G and denote derivatives with respect to this variable by a dot.

A straightforward analysis reveals that the basic equations can be rewritten in the following form

$$\mathrm{div}\,\frac{\nabla G}{R^2} + \frac{\Lambda\dot{\Lambda}}{R^2} + 4\pi^2\mu_0\dot{p} = 0 \tag{7}$$

$$\Lambda I - \Lambda\dot{I} = \frac{U}{\eta_\parallel \iota} \tag{8}$$

$$\dot{I} + \frac{1}{\mu_0 \iota}\dot{\Lambda} + \dot{p}\dot{V} = 0 \tag{9}$$

$$\int_{F(x)=F} Q\,d^3\tau = M = \left\{\eta_\perp \int_{F(x)=F} \frac{|\nabla p|}{B^2}\,dS - \eta_\parallel \frac{p'\Lambda^2}{\iota^2}\left(\int_{F(x)=F}\frac{1}{B^2}\frac{dS}{|\nabla F|} - \frac{V'^2}{\Lambda+\mu_0\iota I}\right) + \frac{\mu_0 I U V'}{\Lambda+\mu_0\iota I}\right\}\zeta \tag{10}$$

$$p = \rho k T/m \tag{11}$$

$$\frac{k\gamma}{m(\gamma-1)}(TM)^{\cdot} + U\dot{I} = \frac{d}{dG}\left\{\tilde{T}\frac{d}{dG}\left(\int \kappa |\nabla G|^2 d^3\tau\right) + \int Q_E\, d^3\tau\right\} \tag{12}$$

(7) is the fundamental equilibrium equation. (8) is Ohm's law in the flux formulation and (9) is the differential form of the Bennett-Pinch relation in the toroidal case. The last two equations express mass and energy balance. The quantities needed to explain this system we list in the following lines

$$\underline{B} = \frac{1}{2\pi}(\nabla\zeta \times \nabla G + \Lambda\nabla\zeta) \quad , \quad \Lambda = \mu_0(J_\Lambda - J) \tag{13}$$

$$\frac{1}{\iota} \equiv \dot{F} = \Lambda \frac{d}{dG}\int \frac{d^3\tau}{(2\pi R)^2} \quad , \quad V \equiv \int d^3\tau \tag{14}$$

$$M \equiv \int_{F(x)=F} \rho \underline{v}\cdot d\underline{S} \quad , \quad ' = \frac{d}{dF} \tag{15}$$

R is the distance from the axis of symmetry. We note that the determination of the six quantities G, Λ, I, p, T and ρ from (7) to (12) determines the flows, so that the velocity $\underline{v}$ consists of two parts

$$\underline{v} = \hat{\underline{v}} + (\psi_s - \frac{\Lambda}{B^2}\dot{\varphi}_s)\underline{B} + \frac{\varphi_s}{B^2}\underline{B}\times\nabla G \tag{16}$$

(1) $\hat{\underline{v}}$, which is calculable from G, Λ and ρ, and (2) the remaining part, which is divergencefree and everywhere tangent to the magnetic surfaces. This part depends on arbitrary surface quantities ψ_s and φ_s, which come from the integration of two magnetic differential equations.

(10) is the expression for the resistive plasma loss and is made up of three different terms:

(1) the so called "Classical Diffusion" term involving $\underline{j}_\perp$,

(2) the correction due to toroidicity, first derived by Pfirsch and Schlüter [2]. By Schwarz's inequality this term can quite generally be shown to be always positive,

(3) a new term, involving the ring voltage and always negative.

The structure of the derived set of equations suggests the following procedure for an approximate determination of all equilibrium quantities. Leaving for a moment the equilibrium equation (7) out of discussion, closer investigation of the remaining relations shows that the prescription of any family of nested toroidal surfaces G=const. allows the calculation of the surface quantities I, J, p, ρ and T by ordinary differential equations. However the question now is do the solutions so found, satisfy the equilibrium condition? Certainly they do not on average violate the equilibrium condition, because (9) is (7) averaged over a magnetic surface. But this does not avoid local violation of equation (7).

What is possible and what we propose, is to choose a family of surfaces, in other words a coordinate system, which anticipates the expected geometry of the magnetic surfaces and which is provided with largely arbitrary built-in functions. After solving for the surface quantities we can use the built-in functions to modify shape and position of the magnetic surfaces in such a manner that the approximation with respect to the equilibrium equation is as good as possible.

As an example we have done this for a large aspect-ratio torus and for the special case of no mass and energy sources. The results will be presented.

This work is part of the joint programme between IPP and Euratom.

[1] M.D. Kruskal, R.M. Kulsrud, Phys.Fluids 1, 265 (1958)
[2] D. Pfirsch, A. Schlüter, MPI/PA/7/62 (1962).

PLASMA DIFFUSION IN TOROIDAL SYSTEMS WITH ANISOTROPIC PRESSURE

M. Dobrowolny(+) and O. Pogutse(*)

International Centre for Theoretical Physics, Trieste, Italy.

Abstract: The problem of resistive diffusion of a plasma with anisotropic pressure in a toroidal system is considered. The diffusion decreases, with respect to the isotropic pressure case, when $P_{\parallel} > P_{\perp}$ and increases in the opposite case.

It is well known that collisional diffusion of a plasma in toroidal systems exceeds that in a similar straight device. The enhancement factor is due to the combined effect of the toroidal particle drifts and finite resistivity along magnetic field lines and was first calculated by Pfirsch and Schlüter / 1 /.

We investigate here how this toroidal effect is modified in a plasma with anisotropic pressure. Such anisotropy is actually present both in toroidal machines with Joule heating (Tokamak's for example) where $P_{\parallel} > P_{\perp}$ / 2 / and when electron cyclotron resonance is used to heat the plasma (then $P_{\perp} > P_{\parallel}$).

The basic equations of our calculation are

$$\nabla \cdot \vec{P} = [\underline{J} \times \underline{B}] \tag{1}$$

$$\underline{E} + [\underline{v} \times \underline{B}] = \frac{\underline{J}_{\parallel}}{\sigma_{\parallel}} + \frac{\underline{J}_{\perp}}{\sigma_{\perp}} \tag{2}$$

$$\nabla \cdot \underline{J} = 0 \tag{3}$$

where the pressure tensor $\vec{P}$ is assumed to be given by

$$(\vec{P})_{\perp} = P_{\perp} (\delta_{\perp} - \frac{B_{\perp} B_{\perp}}{B^2}) + P_{\parallel} \frac{B_{\perp} B_{\perp}}{B^2} \tag{4}$$

(+) - On leave of absence from Laboratori Gas Ionizzati (Ass. EURATOM-CNEN) - Frascati, Italy.

(*) - On leave of absence from Kurchatov Institute of Atomic Energy, Moscow, USSR.

and the other symbols do not need explanation. Several authors have examined more complete fluid equations, in the isotropic pressure case, including ion inertia and viscosity in Eq. (1), electron pressure gradient in (2) and allowing also for a plasma rotation due to a radially directed electric field / 3, 4 /. As it has been finally concluded / 5, 6 / that when all dissipative terms are correctly taken into account, only small corrections to the Pfirsch and Schlüter result are obtained in the cases which are more interesting experimentally, we restrict our attention here to the simpler equations (1) - (3).

These equations are applied to an axisymmetric toroidal system with large aspect ratio ($\epsilon = \frac{r}{R} \ll 1$ where r and R are the minor and major radius of the torus, respectively). In the usual toroidal co-ordinate system, with the element of length given by $ds^2 = dr^2 + r^2 d\theta^2 + (1 + \epsilon \cos\theta)^2 dz^2$, the magnetic field can be taken as

$$\underline{B} \simeq (0, B_{\theta}(r), B_0(1 - \epsilon \cos\theta)) \tag{5}$$

with B_0 = const and $\frac{B_{\theta}}{B_0} \ll 1$. All quantities can be expanded in the toroidicity parameter ϵ so that $n = n_0(r) + \epsilon \tilde{n}(r,\theta), \phi = \epsilon \tilde{\phi}(r,\theta)$, etc. The final quantity to be calculated is the toroidal contribution to the diffusion flux across a magnetic surface which can be simply obtained from

$$q_r^t = \langle (n_0 + \epsilon \tilde{n}) \frac{\epsilon}{|B|} \frac{1}{r} \frac{\partial \tilde{\phi}}{\partial \theta} (1 + \epsilon \cos\theta) \rangle \tag{6}$$

where $\langle \rangle \equiv \frac{1}{2\pi} \int_0^{2\pi} d\theta$ and the factor $1 + \epsilon \cos\theta$ is the element of area per unit length in toroidal co-ordinates. The total diffusion will be given by

$$q = q_r^t + q_{class} \tag{7}$$

where q_{class} is the radial average flux in a plane cylinder. Multiplying scalarly Eq. (1) by $\underline{B}$ we obtain for the toroidal correction to parallel plasma pressure

$$\frac{\partial \tilde{P}_{\parallel}}{\partial \theta} - (P_{\perp 0} - P_{\parallel 0}) \frac{B_z}{B^2} \frac{\partial B_z}{\partial \theta} + \frac{\iota}{|B|} (P_{\perp 0} - P_{\parallel 0}) \frac{\partial |B|}{\partial \theta} = 0 \tag{8}$$

where, using (5) and supposing an adiabatic law $\frac{P_{\parallel}}{n^{\gamma}} = \text{const}$ ($\gamma = 1$ for the isothermal case), we obtain for the density correction

$$\tilde{n} = n_0 \frac{P_{\perp 0} - P_{\parallel 0}}{\gamma P_{\parallel 0}} \cos\theta . \tag{9}$$

The parallel component of Ohm's law (2) together with (3) gives, after some algebra

$$\frac{1}{|B|} \frac{1}{r} \frac{\partial \Phi}{\partial \theta} = \frac{1}{B_{\theta}^2} \frac{1}{\sigma_{\parallel}} \frac{\partial}{\partial r} (P_{\perp 0} + P_{\parallel 0}) \cos\theta . \tag{10}$$

Using (3) and (10) in (6) and (7) we finally get

$$q = D \frac{\partial}{\partial r} (P_{\perp 0} + P_{\parallel 0}) \tag{11}$$

where

$$D = D_{ps} \left[1 + \frac{P_{\perp 0} - P_{\parallel 0}}{\gamma P_{\parallel 0}} \right], \quad D_{ps} = \frac{\epsilon^2 n_0}{2 B_{\theta}^2 \sigma_{\perp}} \left(1 + \frac{2\sigma_{\perp}}{\sigma_{\parallel}} \frac{\delta \pi^2}{\iota^2} \right). \tag{12}$$

D_{ps} is the Pfirsch-Schlüter diffusion coefficient, ι being the rotational transform. The quantity, $1 + \frac{P_{\perp 0} - P_{\parallel 0}}{\gamma P_{\parallel 0}}$ now represents the additional correction factor to the Pfirsch-Schlüter result, related to pressure anisotropy. Since all plasma quantities have been expanded to first order in ϵ, it is clearly valid only for $\frac{\gamma P_{\parallel 0}}{P_{\perp 0}} \gtrsim \epsilon$. The derivation of the result itself shows the physical reason for it. The additional contribution to diffusion related to pressure anisotropy arises because, for $P_{\perp} \neq P_{\parallel}$, contrary to the case of isotopic pressure, surfaces of constant density are displaced with respect to magnetic surfaces. When $P_{\perp} > P_{\parallel}$, the plasma is displaced towards regions of stronger magnetic field, so that particle flux outwards dominates over inward flux. In the opposite case $P_{\parallel} > P_{\perp}$ the inverse situation occurs. These tendencies clearly appear in our result. On the other hand, it is seen that, for small pressure anisotropy, the Pfirsch and Schlüter diffusion is not appreciably changed(*).

(*) This differs from a result found by Wimmel / 7 / in the low density collisionless regime.

We have thus pointed out a new physical effect associated with pressure anisotropy, contributing to radial resistive diffusion in toroidal plasmas.

Acknowledgements: The authors are grateful to Prof. B.B. Kadomtsev for useful discussions. They wish to thank Prof. Abdus Salam, the International Atomic Energy Agency and UNESCO for hospitality at the International Centre for Theoretical Physics, Trieste.

References

/ 1 / D. Pfirsch and A. Schlüter, Max-Plank-Inst. Report No. MPI/PA/7/62 (1962) (unpublished).

/ 2 / A. Bobrovskii, N.D. Vinogradov, E.N. Kuznetsov and K.A. Razumova, Zh. Eksperim. i Teor. Fiz. (Pisma) 9, 261 (1969).

/ 3 / T.E. Stringer, Phys. Rev. Letts. 22, 770 (1969).

/ 4 / M.N. Rosenbluth and J.B. Taylor, Phys. Rev. Letts. 23, 367 (1969).

/ 5 / A.A. Galeev, JETP Letts. 10, 225 (1969).

/ 6 / O.P. Pogutse, to be published in Nucl. Fusion 1970.

/ 7 / H.K. Wimmel, Inst. for Plasma Physik, Garching, IPP 6/78 August 1969.

Invited Lecture

NUCLEAR FUSION REACTOR DESIGN-A REVIEW

by

M. Kristiansen and M. O. Hagler

Plasma Laboratory, Department of Electrical Engineering

Texas Tech University, Lubbock, Texas, 79409, USA

Abstract: Reasons for recent interest in fusion reactor design are discussed. The various efforts and studies underway, particularly in the USA, are described. The most significant results to date and the most apparent needs for further research are summarized. An appraisal is made of the current state of fusion reactor development and possible development time schedules are discussed.

Motivation: Since the last IAEA Conference on Plasma Physics and Controlled Nuclear Fusion Research at Novosibirsk, USSR, in August 1968 there has been a considerable resurgence of optimism for the future of thermonuclear fusion reactors. This optimism is based on experimental evidence, presented in part at Novosibirsk, that plasmas do not necessarily diffuse across the confining magnetic fields at the relatively fast Bohm rate ($\sim 1/B$). Such evidence, consisting of significant improvement in confinement times in several countries rather than a single major break-through, indicates that under certain conditions, the diffusion rate across the confining magnetic field may approach the relatively slow classical rate ($\sim 1/B^2$). Additional interest has been stimulated by the advantages fusion reactors offer over fast breeder reactors in terms of environmental and safety factors. These advantages include potentially high thermal efficiency, non-proliferation of weapons grade materials, inherent safety from nuclear explosions, negligible after heat, and relatively low inventory of radioactive material.

Summary of Activities: Early fusion reactor studies in the USA were conducted by Professor D. J. Rose at MIT, Dr. R. G. Mills at Princeton University Plasma Physics Laboratory, and Dr. F. L. Ribe at Los Alamos Scientific Laboratory. The first international conference on Nuclear Fusion Reactors was held at Culham Laboratory in September, 1969, and was followed by a very successful Working Study Week. Approximately 50% of the papers at this conference were from the USA, 45% from the U.K., and the rest from the Federal Republic of Germany, France, and the USSR. These percentages give a fairly correct picture of the relative interest in the various countries at that time. The European interest has apparently increased since that time and several countries seem to be planning larger study efforts. The USAEC has also conducted several informal fusion technology meetings over the past 1 1/2 - 2 years. In June, 1970, a Symposium on Fusion Reactor Design, designed to stimulate interest in fusion reactor design problems, was co-sponsored by the USAEC and Texas Tech University with participation from several national laboratories, industry, foreign countries and different U.S. universities [1].

The four USAEC supported national laboratory plasma research groups at Los Alamos, New Mexico; Livermore, California; Oak Ridge, Tennessee, and Princeton, New Jersey are all now carrying out limited design studies. Several U.S. universities are also engaged in fusion reactor studies, including MIT, University of Wisconsin, Texas Tech University, and others. The USAF, NASA, and several universities are giving consideration to the use of fusion reactors in space [1]. The U.K. apparently is continuing its efforts indicated by the Culham Conference and the Federal Republic of Germany is at least considering an increased effort in this area.

Studies and Problem Areas: The various design studies conducted to date have made a bold assumption, namely that the plasma stability problem has been solved. Very little consideration has been given to specific problems in how to stabilize the plasma, except in some cases to allow for power consumption to provide feedback or dynamic stabilization.

In spite of ignoring the stability problem and in spite of the various assumptions of continuous versus pulsed and toroidal versus mirror reactors, certain basic features and troublesome problem areas are becoming apparent. It appears that fusion reactors will necessarily be quite large. A commonly quoted figure is 5000 MW(t). A D-T reactor will be an efficient tritium breeder. Experimental data on wall damage, both due to neutrons and charged particles, are insufficient. No satisfactory solution has been suggested to simulate the intense 14 Mev neutron flux from a D-T reactor. Unless turbulent heating or shock and compressional heating is successful the heating problem appears to be extremely severe. There are no apparent easy ways of incorporating auxiliary heating structures, such as RF coils, into the reactor design. Injection of fuel into an operating reactor is another major problem. Theoretical calculations indicate that the only feasible scheme may be pellet injection. Even assuming that neutral particle or ion injection will succeed in penetrating into the interior of the reactor one is faced with truly impressive requirements on beam flux and energy. Many researchers are actually more worried about heating and injection problems than stability problems.

Several very clever ideas and concepts that have caused much discussion and interest include, among others, the direct energy conversion scheme proposed by R. F. Post, the "Fusion Torch" proposed by B. J. Eastlund and W. C. Gough, Urban Complex Design proposed by A. P. Fraas, Vacuum Wall Free Blankets Using Heat Pipes proposed by R. W. Werner, and Cryogenic Energy Storage proposed by F. L. Ribe. In the space allotted, proper credit cannot be given to all the interesting and clever ideas that already have resulted from a very limited study effort.

Recommendations and Conclusions: Whether or not fusion reactors can successfully compete with fast breeder reactors depends on the final analysis on the economics of the two systems. It is very clear, however, that any meaningful economic analysis must include future cost factors due to environmental and societal considerations. The economic analyses conducted so far have largely been carried out by engineers and scientists and not by professional economists. Environmental and societal factors have usually been ignored. This omission gives reason for considerable concern and it appears that any truly meaningful economic evaluation must be performed by a team of engineers, scientists, economists, ecologists, sociologists, lawyers, and others. Some of the most critical technology research areas are: plasma heating, fuel injection, wall damage, direct energy conversion, cryogenic energy storage, blanket design, and heat transfer.

If fusion research is continued at the present world wide effort, a successful, on-line, fusion reactor will not be built in this century. If environmental, political, or societal considerations make the development of fusion reactors a national or international priority then planned, accellerated funding can speed the development up so as to provide such a reactor in less than 20 years. A "scientific feasibility" experiment will probably be reported within 5 years even at the present level of effort.

REFERENCE

1. Proceedings of the Symposium on Fusion Reactor Design, M. Kristiansen and M. O. Hagler, Eds., Special Report No. 1 on AEC Contract AT-(40-1)-3778, Department of Electrical Engineering, Texas Tech University, Lubbock, Texas, 79409, June 15, 1970.

This work was supported in part by the USAEC and NSF.

ON CLASSICAL DIFFUSION OF PLASMA IN TOROIDAL SYSTEMS

by

O. Fogutse *

International Centre for Theoretical Physics, Trieste, Italy.

Abstract: The problems of resistive diffusion and thermal conductivity of a rotating toroidal plasma are considered. It is shown that the coefficient of thermal conductivity is strongly decreased in the case of sufficiently large collision frequency. A large transverse electric field is presented in the plasma and its direction depends on the collision frequency.

We consider the problem of classical diffusion of hydrodynamical plasma in toroidal systems taking into account its azimuthal rotation (Stringer's effect [1]). In contrast with works of Rosenbluth and Taylor [2] and Galeev [3] we use the complete system of hydrodynamical equations, including the heat-balance equations:

$$\frac{\partial n}{\partial t} = -\operatorname{div} n\vec{v}_i = -\operatorname{div} n\vec{v}_e, \tag{1}$$

$$m_i n \frac{d_i \vec{v}_i}{dt} + \nabla p_i = en\left(\vec{E} + \frac{1}{c}[\vec{v}_i \vec{B}]\right) - en\frac{\vec{j}}{\sigma} - \operatorname{Div}\hat{\pi}_i - \vec{R}_T, \tag{2}$$

$$\nabla p_e = -en\left(\vec{E} + \frac{1}{c}[\vec{v}_e \vec{B}]\right) + en\frac{\vec{j}}{\sigma} + \vec{R}_T, \tag{3}$$

$$\frac{3}{2} n \frac{d_i T_i}{dt} + p_i \operatorname{div}\vec{v}_i = -\operatorname{div}\vec{q}_i, \tag{4}$$

$$\frac{3}{2} n \frac{d_e T_e}{dt} + p_e \operatorname{div}\vec{v}_e = -\operatorname{div}\vec{q}_e. \tag{5}$$

In the continuity Eqs.(1), the ion and electron densities are assumed to be equal; Eq.(2) represents the equation of ion motion; $\hat{\pi}_i$ is the viscosity tensor; Eq.(3) is the equation of electron motion, where we neglected electron inertia and viscosity; Eqs.(4) and (5) represent the heat-balance equations; $d_j/dt \equiv \partial/\partial t + v_j \nabla'$; $\sigma = e^2 n \tau_e / m_e$ is the plasma conductivity, R_T is the thermal force, q_j is the thermal flux. In the viscosity tensor we take into account only the magnetic viscosity and the longitudinal ion viscosity $\eta_H \nabla_H^2 \vec{V}_i$. The thermal fluxes include drift heat fluxes $q_{dj} = \frac{5}{2}\frac{cnT_j}{e_j B^2}\left[B \nabla T_j\right]$ and longitudinal heat fluxes $q_{Hj} = -\kappa_{Hj} \nabla_H T_j$.

The system (1)-(5) gives the possibility of taking into account some effects not considered in the previous papers [2),3)] and very important in this problem. For example, in contrast with Ref.2, we take into account the effect of parallel viscosity, which is much larger than that of transverse viscosity considered in Ref.2; longitudinal ion and electron thermal conductivity and displacement of the surfaces T_j = const from magnetic surfaces. In contrast with Ref.3 we take into account ion viscosity and thermal conductivity and displacement of T_i = const surfaces from magnetic surfaces.

The system of equations is solved by a perturbation technique in which all quantities are expanded with respect to the inverse aspect ratio $\varepsilon = r/R$ (where r is the radius of a given magnetic surface, R the major radius of the torus). To simplify the calculation we introduce three assumptions: 1) no zeroth order current $j_{\theta 0} = 0$; 2) the longitudinal thermal conductivity $\chi_{\parallel e}$ is very large so that we can expand all quantities in $1/\chi_{\parallel e}$. This assumption is valid only in the weakly collisional case $qR/\lambda < (m_i/m_e)^{\frac{1}{2}}$ (where $q = RB_z/RB_\theta$, B_z is the toroidal component of the magnetic field; B_θ is the azimuthal magnetic field; λ is the particle mean free path; 3) the larmor radius of ions is small: $\rho_i/r \ll B_\theta/B_z$.

With these assumptions the fluxes of particles and heat due to toroidicity can easily be calculated. These fluxes are functions of the rotational velocity $v_0 = (E \times B)/B^2$. In order to determine this velocity we derive an additional equation (analogous to that used in Ref.2).

The results of the calculation are best shown in the following diagram (Fig.1):

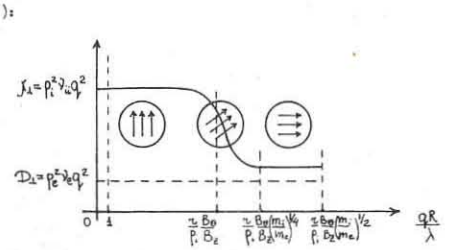

For all the region of validity of our treatment $1 < \frac{qR}{\lambda} < \frac{r}{\rho_0}\frac{B_\theta}{B_z}\left(\frac{m_i}{m_e}\right)^{\frac{1}{2}}$, there is a stable rotating state with velocity of the order of the drift velocity. When $1 < \frac{qR}{\lambda} < \frac{r}{\rho_i}\frac{B_\theta}{B_z}\left(\frac{m_0}{m_e}\right)^{\frac{1}{4}}$, this rotation is determined by ion longitudinal viscosity and thermal conductivity; in the case $\frac{B_\theta}{B_z}\frac{r}{\rho_0} < \frac{qR}{\lambda} < \frac{r}{\rho_0}\frac{B_\theta}{B_z}\left(\frac{m_i}{m_e}\right)^{\frac{1}{2}}$, stable rotation is determined by the electron parallel thermal conductivity. The toroidal correction to the coefficient of ion thermal conductivity is strongly decreased, where $\frac{qR}{\lambda} > \frac{r}{\rho_i}\frac{B_\theta}{B_z}$. In this case we have the ordinary expression for a cylindrical plasma. The coefficient of diffusion within a factor ~2 is constant in the entire region considered. In the case where the temperature gradient is of the order of the density gradient, a large transverse electric field exists. This field in the region $1 < \frac{qR}{\lambda} < \frac{r}{\rho_i}\frac{B_\theta}{B_z}$ is $\left(\frac{m_i}{m_e}\right)^{\frac{1}{2}}$ times larger than the Pfirsch Schluter field. The direction of this field depends on the collision frequency as is shown graphically in Fig.1.

ACKNOWLEDGMENTS

The author is grateful to Dr. M. Dobrowolny for useful discussions. He wishes to thank Professor Abdus Salam, the International Atomic Energy Agency and UNESCO for hospitality at the International Centre for Theoretical Physics, Trieste.

REFERENCES

1) T.E. Stringer, Phys. Rev. Letters 22, 770 (1969).
2) M.N. Rosenbluth and J.B. Taylor, Phys. Rev. Letters 23, 367 (1969).
3) A.A. Galeev, JETP Letters 10, 225 (1969).

* On leave from Kurchatov Institute of Atomic Energy, Moscow, USSR.

TOROIDAL CONFINEMENT (THEORY)

CLASSICAL DIFFUSION IN AN AXISYMMETRIC TOROIDAL PLASMA FOR ARBITRARY COLLISION FREQUENCIES

by

J.W. CONNOR and T.E. STRINGER

United Kingdom Atomic Energy Authority,
Research Group, Culham Laboratory, Abingdon, Berkshire, England

Abstract: Expressions are obtained for classical diffusion in an axisymmetric torus, valid over a wide range of conditions which includes the intermediate and highly collisional regimes. Various limiting cases are considered and the ambipolar condition discussed.

Introduction: Classical diffusion in large aspect ratio, ε^{-1}, axisymmetric torii has previously been discussed in certain limiting cases characterised by the value of the ratio $\frac{2\pi\lambda}{L_c}$ where λ is the collisional mean free path and L_c the connection length. These are: $\frac{2\pi\lambda}{L_c} \ll 1$ where resistivity, viscosity and thermal conductivity are the main dissipative processes associated with the diffusion[1,2,3]; (ii) $1 \ll \frac{2\pi\lambda}{L_c} \ll \varepsilon^{-\frac{3}{2}}$ where dissipation is provided by Landau damping[4], and (iii) $\varepsilon^{-\frac{3}{2}} \ll \frac{2\pi\lambda}{L_c}$ where trapped particle effects are important[4]. In many experiments the variation of L_c with radius carries $\frac{2\pi\lambda}{L_c}$ from region (i) to region (ii)[2]. Thus a theory is required which is valid across the transition between these regimes. In addition the theory should cover a wide range of another relevant parameter $\frac{a_i}{r_n\Theta}$ where a_i is the ion Larmor radius in the main toroidal field B_o, Θ is the ratio of poloidal and toroidal fields and r_n is the density scale length.

The General Diffusion Expression: The variation in the equilibrium parameters over magnetic surfaces is obtained from the guiding-centre kinetic equation[5] with a Bhatnagar-Gross-Krook collision term[6]. For simplicity the isothermal BGK term is used, which does not properly describe thermal conductivity effects. The equation is solved by expanding in ε with the assumption that the zero-order distribution is Maxwellian. This excludes case (iii) since the distribution function for trapped particles cannot be expanded in ε. Integrating the radial drift over velocity and then over a magnetic surface gives a net outward flux of order ε^2. The velocity integration introduces the plasma dispersion function[5] $I(z_j)$ where $z_j = x_j + iy_j$, $x_j = -\frac{V_o}{c_j\Theta}$ and $y_j = \frac{L_c}{2\pi\lambda_j}$, c_j is the thermal speed of the j^{th} species, and $V_o = -E_r/B_o$ is the azimuthal drift due to a zero-order radial electric field. The diffusion velocity for the j^{th} species can be written:

$$V_{dj} = V_{dj}^{(A)} + V_{dj}^{(B)} + V_{dj}^{(C)} - \frac{m_j}{e_j B_o}\frac{\partial V_o}{\partial t}.$$

The slow variation in the azimuthal drift, of order ε^2, is determined by the ambipolarity condition, $V_{di} = V_{de}$. In the above:

$$V_{dj}^{(A)} = \frac{\varepsilon^2 T_j}{2rB_o e_j}\left(1 + \frac{U_{jn}}{V_o}\right)\left\{\mathcal{I}m\left[\frac{x_j}{z_j}(I_j - 1)\right] + \frac{\Lambda_j^I}{F^2+L^2}\left(\left[\alpha\left(1 + \frac{U_{kn}}{V_o}\right)\Lambda_k^R + \beta_j\frac{U_{in}}{V_o}(1+\tau)\right]^2 + \left[\alpha\left(1 + \frac{U_{kn}}{V_o}\right)\Lambda_k^I\right]^2\right)\right\}$$

$$V_{dj}^{(B)} = -\frac{\varepsilon^2 T_j \eta e \beta_j p'}{B^2\Theta^2 T_e e_j (F^2+L^2)}\left\{\left(1 - \beta_j\frac{U_{in}}{V_o}\right)\alpha\left[\Lambda_i^R\Lambda_e^R\left(1 + \frac{U_{en}}{V_e}\right) + \tau\Lambda_e^R\Lambda_i^R\left(1 + \frac{U_{in}}{V_o}\right)\right] - \left(\frac{U_{jn} - U_{kn}}{V_o}\right)\left[\left(1 + \frac{U_{jn}}{V_o}\right)\left(\beta_j^2\Lambda_j^2 + 2\tau\Lambda_e^I\Lambda_i^I\right) + \tau\left(1 + \beta_j\frac{U_{in}}{V_o}\right)\left(\Lambda_i^R\Lambda_e^R - \Lambda_i^I\Lambda_e^I\right)\right] + F^2 + L^2\right\}$$

$$V_{dj}^{(C)} = \frac{2\varepsilon^2 T_j \tau\beta_j e^2 rp'^2\eta^2}{B^2\Theta^4 T_e^2 e_j}\quad\frac{(\Lambda_i^I\Lambda_e^2 + \tau\Lambda_e^I\Lambda_i^2)}{F^2+L^2}$$

where p' is the gradient of the plasma pressure, η is the resistivity and U_{jn} the diamagnetic velocity of species j. k denotes the species complementary to j. We have defined

$$\mathcal{I}_e = -1\ ,\quad \beta_i = \tau = \frac{T_e}{T_i}\ ,\quad \alpha = 1 + \tau + 2x_i^2 + 2\tau x_e^2\ ,$$

and

$$F + iL = \tau\left(1 + \frac{U_{in}}{V_o}\right)\Lambda_i + \left(1 + \frac{U_{en}}{V_o}\right)\Lambda_e$$

where:

$$\Lambda_j = \Lambda_j^R + i\Lambda_j^I = \frac{I_j}{I_j\left(1 + 2ix_jy_j - \frac{x_j}{z_j}\right) + \frac{x_j}{z_j}}$$

$F + iL$ is proportional to the dielectric constant and near its zeros there is an enhancement of V_{dj}. The dissipative process responsible for $V_{dj}^{(A)}$ changes from Landau damping to viscosity as $\frac{2\pi\lambda}{L_c}$ decreases, $V_{dj}^{(B)}$ is a generalisation of resistive diffusion and $V_{dj}^{(C)}$ is a small term proportional to η^2 and common to both species.

Special Cases: When $|z_j| < 1$ or $|z_j| \gg 1$, approximate forms may be used for $I(z_j)$ and the diffusion expression simplifies. This allows the following limiting cases to be treated analytically:

(a) $x_i \ll y_i$, $x_e \ll y_e$, $y_e, y_i \gg 1$. Here both ions and electrons behave as highly collisional fluids. We find considerable modifications to the expressions given in reference 2 because of a more exact treatment of viscosity, but the actual ambipolar diffusion is hardly changed. Over part of this range electron thermal conductivity, which is not correctly described by the equations, is important[5].

(b) $x_i \gg y_i$, $x_e \ll y_e$, $y_e, y_i \gg 1$. In this case both species are described by fluid-like equations but only the electrons are collision dominated. The region is important experimentally but has not previously been investigated theoretically. We find the ambipolar results:

$V_o \sim -U_{in}$, $V_d \sim V_{ps}$ when $1 < \frac{a_i}{r_n\Theta} < \left(\frac{m_i}{m_e}\right)^{\frac{1}{4}}$

$V_o \sim -U_{en}$, $V_d \sim V_{ps}\left(\frac{m_e}{m_i}\right)^{\frac{1}{2}}\left(\frac{a_i}{r_n\Theta}\right)^6$ when $\frac{a_i}{r_n\Theta} > \left(\frac{m_i}{m_e}\right)^{\frac{1}{4}}$

The latter case can show considerable enhancement over the Pfirsch-Schlüter velocity V_{ps}.

(c) $x_i, x_e \ll 1$, $y_i, y_e \ll 1$. This case corresponds to ions and electrons undergoing Landau damping. We reproduce the results of reference 5, but find they are restricted to $\frac{a_i}{r_n\Theta} \lesssim 1$. When $\frac{a_i}{r_n\Theta} \gg 1$ we must use the results of (d).

(d) $x_i \gg 1$, $x_e \ll 1$, $y_i, y_e \ll 1$. This implies that the electrons are Landau damped, while the ions behave as a weakly collisional fluid. We find the ambipolar state $V_o \sim -U_{en}$, $V_d \sim V_{ps}$, valid for $\frac{a_i}{r_n\Theta} > 5$.

Conclusions: General equations are derived for the diffusion valid over most of parameter space of experimental interest. In the case (c) these expressions agree with earlier analyses, while in case (a) they lead to a modification of earlier results. The limiting cases (b) and (d) have not previously been treated. The general result could be evaluated numerically to find the diffusion rate when the parameters fall within the transition regions.

References

1. PFIRSCH, D. and SCHLÜTER, A. Max-Plank Institute Report No. MPI/PA/7/62, (1962) unpublished.
2. STRINGER, T.E. Phys. Fluids, (to be published)
3. GALEEV, A.A. ZhETF Letters, 10, 353, (1969)
4. GALEEV, A.A. and SAGDEEV, R.Z., Sov. Phys. J.E.T.P., 26, 233, (1968)
5. STRINGER, T.E. Phys. Fluids, 13, 810, (1970)
6. MIKHAILOVSKII, A.B. and POGUTSE, O.P. Sov. Phys. Tech. Phys. 11, 153, (1966).

BULK VISCOSITY, MAGNETIC-FIELD CORRUGATIONS, AND CONTAINMENT IN TOROIDAL CONFIGURATIONS*

by

J. M. Dawson, N. K. Winsor, E. C. Bowers, and J. L. Johnson†

Princeton University Plasma Physics Laboratory, Princeton, N. J., USA

Abstract: The dissipation associated with hydrodynamic flow through magnetic field corrugations reduces the ability of a plasma to compensate for $\underline{E}\times\underline{B}$, gradient B, and other drifts by flow parallel to $\underline{B}$. This effect is investigated for toroidal confinement.

Magnetic field corrugations or field strength variations are common in toroidal devices, being produced by the finite spacings of the coils, by helical windings, and even by the toroidal nature of the field itself. Dissipation due to flow through these field irregularities restricts the flow along the field and leads to more rapid plasma loss then would otherwise be predicted. Further, calculations[1] show that resistivity causes a toroidal plasma to rotate, but indicate no preferred direction. The viscosity associated with electron flow removes this degeneracy; the plasma rotates in such a way as to make the magnetic axis positive.

We modify a previously described numerical model[2] by introducing a viscous drag represented by phenomenological terms $\mu_i V_i$ and $\mu_e V_e$ in the respective ion and electron momentum equations. The magnitude of these coefficients can be estimated by noting that plasma behavior in moving through the magnetic field corrugations is similar to that of a static plasma in a time-varying magnetic field. In the analogous magnetic pumping model,[3] collisions increase the temperature of the plasma through the dissipation associated with the finite relaxation time between the parallel and perpendicular degrees of freedom. For the flowing plasma this energy is obtained at the expense of translational kinetic energy.

Berger et al.[3] studied magnetic pumping associated with collisions. From their equation for energy dissipation we obtain the coefficient for viscous drag

$$\mu = \frac{\epsilon^2\omega^2\nu}{3(4\omega^2+9\nu^2)}\,\frac{V_{th}^2}{V^2} \approx \frac{(2\pi\epsilon V_{th}/\lambda)^2}{27\nu}\ ,$$

$\omega \ll \nu$; ϵ, ω and λ measure the field variations seen by the fluid, $B = B_o(1+\epsilon\cos\omega t)$, and ν is classical 90° collision time. The frequency ν_e for the electrons is larger than that for the ions by the square root of the mass ratio $(m_i/m_e)^{1/2}$ provided the temperatures are equal. For the stellarator model the pumping frequency $\omega/2\pi$ is roughly the mean velocity along the field lines divided by the field period λ. The electron velocity is larger than the ion velocity, and ω_e is about $(m_i/m_e)^{1/2}$ larger than ω_i. Therefore we find that μ_e is larger than μ_i by approximately this ratio. In order to include these viscous stresses we introduce the terms $\mu_i\rho\underline{V}$ and $\mu_e m_e \underline{J}/e$ into the parallel component of the momentum equation and modify the value of $\eta_{\|}$ in Ohm's law. This last modification is normally numerically small (though not necessarily fundamentally so) compared to classical resistivity. Thus the equations we adopt are

$$\rho\frac{d\underline{V}}{dt} = \frac{1}{c}\underline{J}\times\underline{B} - V_{th}^2\,\underline{\nabla}\rho - \underline{e}_B\underline{e}_B : [\mu_i\rho\underline{V} - \mu_e m_e \underline{J}/e]\ ,$$

$$-\underline{\nabla}\phi + \frac{1}{c}\underline{V}\times\underline{B} = [\eta\underline{I} + (4\pi\mu_e/\omega_{pe}^2)\underline{e}_B\underline{e}_B]\cdot\underline{J}\ ,$$

$$\underline{\nabla}\cdot\underline{J} = 0\ , \qquad \partial\rho/\partial t + \underline{\nabla}\cdot\rho\underline{V} = 0\ .$$

These provide momentum balance for an isothermal plasma, an Ohm's law with resistivity, charge neutrality, and mass continuity.

For our numerical calculations we choose typical laboratory values for the density, temperature, B, and rotational transform, take μ_e and μ_i constant in space and time with $\mu_e = (m_i/m_e)^{1/2}\mu_i$, and follow the time evolution of the fluid until its flow becomes steady.

Fig. 1

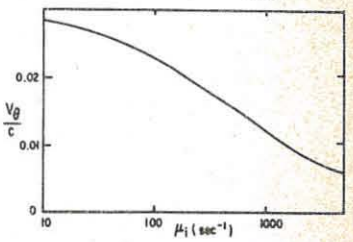

The magnitude of the rotation velocity is plotted as a function of μ_i in the first figure. To the left it approaches its free rotation velocity, while to the right it approaches zero. Over this range $1/\mu_i$ is short compared to resistive diffusion times, but long compared to acoustic times.

Fig. 2

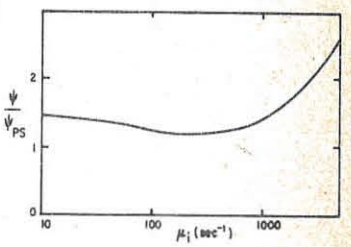

The second figure shows the material flux through a magnetic surface vs μ_i. For small μ, the rotation velocity reaches its maximum value and there is a pronounced outward shift of the pressure surface relative to the magnetic surfaces. For large μ, parallel flow is greatly restricted and the plasma drifts out of the system. In the intermediate range there is a slight decrease in the flux, but in all cases it is greater than the Pfirsch-Schlüter value.

The change in the flux caused by viscosity results from modifying the density variations on magnetic surfaces by restricting flow along the field. The calculations confirm qualitative expectations regarding the influence of viscosity in enhancing loss, and agree with other calculations in limiting cases. The dependence of flux on parameters such as temperature and magnetic field is determined by the scaling of μ.

Rotation (poloidal flows) leads to similar behavior, and the short periodicity length λ makes this dissipation a very effective mechanism for reducing the radial electric field. In a more realistic model, Hall terms in Ohm's law would lead to larger flow velocities and make viscous effects more important. Other dissipative processes (heat conduction, Landau damping, etc.) would also contribute to the damping.

* Supported by the U. S. Atomic Energy Commission, Contract AT(30-1)-1238, using facilities sponsored by National Science Foundation Grant NSF-GP 579.

† On loan from Westinghouse Research Laboratory; visiting Culham.

(1) T. E. Stringer, Phys. Rev. Letters 22, 770 (1969).

(2) N. K. Winsor, J. L. Johnson, and J. M. Dawson, J. Comp. Phys. (in press).

(3) J. M. Berger, W. A. Newcomb, J. M. Dawson, E. A. Frieman, R. M. Kulsrud and A. Lenard, Phys. Fluids 1, 301 (1958).

TOROIDAL CONFINEMENT (THEORY)

ROTATION AND DIFFUSION IN A SELF-CONSISTENT TOROIDAL PLASMA

by

M.G. Haines

Physics Department, Imperial College,

London, S.W.7, England

Abstract: An axisymmetric resistive toroidal plasma is considered in the Tokamak configuration in which plasma currents produce the rotational transform necessary for containment. The self consistent magnetic field resulting from all plasma currents is included in this fluid model, and the rotations and diffusion are found as functions of time. Several effects, additional to the Pfirsch-Schluter correction, and comparable in magnitude contribute to the diffusion, in particular one term depending on the shear and another on the outward displacement of the plasma relative to the magnetic axis.

The additional diffusion arising from resistive effects on the parallel neutralising currents has been calculated by Pfirsch and Schluter[1]. Stringer[2,3] and Rosenbluth and Taylor[4] included rotation about the minor axis, and predicted a resonant enhancement which is modified by viscosity. All these papers employ an inconsistent model in which the magnetic fields produced by plasma currents are ignored and yet their vacuum field is not curl-free. Here we consider a self consistent fluid model including also the correct time dependence of all quantities associated with the rotation. We expand in the inverse aspect ratio $\varepsilon = r/R_o$ and use the (r, θ, ϕ) coordinate system, and solve the time-dependent rotational problem with a computer.

The fluid equations used include parallel viscosity and finite Larmor radius effects, but, in this treatment, assume uniform temperature for each species. For convenience in the later applications of boundary conditions on the magnetic field we choose the geometric axis defined by the circular minor cross-section of the conducting walls, and expand about this. The magnetic field is

$$\frac{B_o}{1+\varepsilon\cos\theta}\left[\beta_{r2}(r,\theta),\beta_{\theta 1}(r)+\beta_{\theta 2}(r,\theta),1+\beta_{\phi 2}(r)\right]$$

to second order in ε, and the lowest order pressure balance is given by

$$j_{\theta o}(r) = \frac{(T_e + T_i)}{B_o}\frac{dn_o(r)}{dr} + j_{\phi-1}(r)\beta_{\theta 1}(r)$$

The component of Ampere's Law that relates the ordering of currents and fields is

$$\mu j_{\phi-1}(r) = \frac{B_o}{r}\frac{\partial}{\partial r}(r\beta_{\theta 1}(r))$$

In the expansion we find that the lowest order θ-dependent parameters have simple $\sin\theta$ and $\cos\theta$ dependence, and accordingly we write, for example,

$$\beta_{r2}(r,\theta) = \beta_{rs}(r)\sin\theta + \beta_{rc}(r)\cos\theta .$$

The ordering of $\frac{\partial}{\partial t}$ is essentially $\varepsilon^2\Omega_i$ where Ω_i is the ion-gyro frequency, whilst all centre-of-mass and diamagnetic velocity components are to lowest order ε times the ion thermal speed, except the electron velocity in $j_{\theta-1}$ which is of the order of the ion thermal speed. The resistivity is effectively ordered by the Hall parameter which is $\sim\varepsilon^{-2}$.

We find that the averaged second order radial flux of plasma $(\overline{nu_r})_2$ is given by

$$(\overline{nu_r})_2 = -\eta_\perp\frac{n_o j_{\theta o}}{B_o} + \eta_{11}\frac{2\varepsilon}{\beta_{\theta 1}}\left(\frac{\varepsilon}{\beta_{\theta 1}} + \frac{x_c(t)}{2}\right)\left[\frac{-n_o(T_e+T_i)}{B_o^2}\frac{dn_o}{dr} + \frac{n_o r\beta_{rs}}{2\varepsilon B_o}\frac{dj_{\phi-1}}{dr}\right] - \frac{r}{2}\frac{\beta_{rs}}{\beta_{\theta 1}}\frac{\partial n_c}{\partial t}$$

where $-\beta_{rs}(r)$ is a measure of the outward displacement of the magnetic surfaces from the geometric axis, and is determined by the solution of the inhomogeneous differential equation

$$\frac{d^2\beta_{rs}}{dr^2} + \frac{3}{r}\frac{d\beta_{rs}}{dr} - \frac{\mu_o}{B_o\beta_{\theta 1}}\frac{dj_{\phi-1}}{dr}\beta_{rs} = -\frac{2\mu_o(T_e+T_i)}{R_o\beta_{\theta 1}B_o^2}\frac{dn_o}{dr} + \frac{\varepsilon\beta_{\theta 1}}{r^2} .$$

β_{rc}, which determines the displacement of the magnetic surfaces parallel to the major axis, is essentially zero since it satisfies a homogeneous differential equation with an identical operator as above and must also obey the boundary conditions of zero at the metal wall. It is therefore omitted in the diffusion formula.

The quantity x_c measures the outward displacement of the plasma density relative to the magnetic surfaces and is defined by

$$x_c(t) = \frac{n_c(t)}{\beta_{\theta 1}n_o} - \frac{r}{n_o}\frac{dn_o}{dr}\frac{\beta_{rs}}{\beta_{\theta 1}^2}$$

where $n_1(r,\theta) = n_s(r)\sin\theta + n_c(r)\cos\theta$.

Writing $x_s = \frac{n_s}{\beta_{\theta 1}n_o}$ (with $\beta_{rc} = 0$), $c_s^2 = \frac{(T_e+T_e)n_o}{\rho_o}$, $V_\theta^{i,e} = \frac{T_{i,e}}{n_o eB_o}\frac{dn_o}{dr}$,

$$c_\eta = -\eta_{11}\frac{r}{n_o^2}\frac{dn_o}{dr}\frac{2\varepsilon}{\beta_{\theta 1}^3}\left[-\frac{n_o(T_e+T_i)}{B_o^2} + \frac{n_o r\beta_{rs}}{2\varepsilon B_o}\frac{dj_{\theta-1}}{dr}\right] \text{ and } c_\nu = \frac{4}{3}\frac{\nu}{r}$$

where ν is the kinematic viscosity, we find the time dependence of x_c, x_s and the velocities $u_{\theta o}$, $u_{\phi c}$ and $u_{\phi s}$ from

$$\frac{r\partial x_c}{\partial t} = (V_\theta^i + V_\theta^e - u_{\theta o})x_s - u_{\phi s} + c_\eta$$

$$\frac{r\partial x_s}{\partial t} = -(V_\theta^i + V_\theta^e - u_{\theta o})x_c + u_{\phi c} + \frac{2\varepsilon}{\beta_{\theta 1}}u_{\theta o}$$

$$\frac{r\partial u_{\theta o}}{\partial t} = -\frac{\varepsilon}{\beta_{\theta 1}}c_s^2\beta_{\theta 1}^2 x_s$$

$$\frac{r\partial u_{\phi c}}{\partial t} = -c_s^2\beta_{\theta 1}^2 x_s - c_\nu\beta_{\theta 1}^2(u_{\phi c} + \frac{\varepsilon}{\beta_{\theta 1}}u_{\theta o}) + (V_\theta^i - u_{\theta o})u_{\phi s}$$

$$\frac{r\partial u_{\phi s}}{\partial t} = c_s^2\beta_{\theta 1}^2 x_c - c_\nu\beta_{\theta 1}^2 u_{\phi s} - (V_\theta^i - u_{\theta o})u_{\phi c}$$

where $u_{\phi o}(r,\theta) = u_{\phi s}(r)\sin\theta + u_{\phi c}(r)\cos\theta$. The time behaviour has been found over a wide range of parameters and initial conditions. A typical result for $V_\theta^i = V_\theta^e = -1$, $c_s^2\beta_{\theta 1}^2 = 0.5$, $c_\eta = 0.1$, $\varepsilon/\beta_{\theta 1} = 2$, and $c_\nu\beta_{\theta 1}^2 = 0.2$ is illustrated below. In all cases a stable steady state was achieved.

In conclusion we have found the transient acceleration of the plasma leading to rotation about the major and minor axes. The diffusion of the plasma is enhanced by a term in $dj_{\phi-1}/dr$ which measures the shear of the magnetic field and also by x_c; the outward shift of the plasma relative to the magnetic surfaces. An initial transient term in $\partial x_c/\partial t$ is also present.

References

1. D. Pfirsch and A. Schluter, Max-Planck Institut, Report MPI/PA/1,62 .
2. T.E. Stringer, Phys. Rev. Letters 22, 110 (1969).
3. T.E. Stringer, Culham Laboratory Report, CLM-P215 (1969).
4. M.N. Rosenbluth and J.B. Taylor, Phys. Rev. Letters 23, 367 (1969).

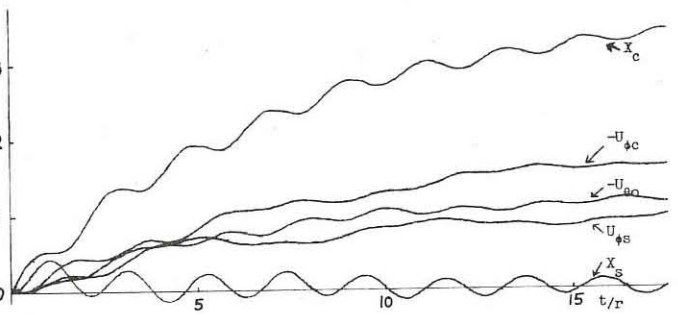

Effect of Inertia on Losses from a Plasma in Toroidal Equilibrium

B.J. Green, H.P. Zehrfeld, Institut für Plasmaphysik GmbH, Garching near Munich, Federal Republic of Germany

We investigate the magnetohydrodynamic equilibrium of a resistive, low-density plasma in a model stellarator field. The effect of inertia on plasma motion is treated exactly, and its influence on plasma loss determined. It is shown that the losses due to inertia are limited by the conditions for the existence of an equilibrium.

One of the basic theoretical problems in the fusion programme is the calculation of plasma loss from particular containment devices. However, because of the complexity of the problem, brought about by the choice of plasma model and the complicated geometry of realistic devices, to say nothing of boundary conditions, it has not been possible to carry through a completely satisfactory calculation. As an example we can consider the Pfirsch-Schlüter calculation [1] for plasma loss from a model stellarator or Levitron device. In this calculation the plasma flow velocity parallel to the magnetic field can become very large, and this casts strong doubts on the assumption that the plasma inertia is negligible.

In the present calculation we have included the effect of plasma inertia and investigated the modified losses from a model configuration. We describe the plasma by means of the one-fluid equations (see below, where "standard" notation is used), and treat the flows and geometry exactly, but consider resistive effects as a perturbation to the perfectly conducting plasma motion.

$$\rho \underline{v}\cdot\nabla\underline{v} = \underline{j}\times\underline{B} - c^2\nabla\rho$$

$$-\nabla\phi + \underline{v}\times\underline{B} = \eta\underline{j}$$

$$\nabla.\rho\underline{v} = Q$$

$$\nabla.\underline{j} = 0$$

The model magnetic field used, is the axisymmetric Pfirsch - Schlüter field where we used the cylindrical co-ordinate system R, Z, ζ and in a meridional cross-section, the polar co-ordinates r, θ.

Two assumptions deserve explicit mention a) isothermal plasma (i.e.c the sound speed is constant), and b) Q the mass source term that is necessary to replace losses, as we are considering stationary solutions. Closer investigation of the equations reveals that the differential part of them can be brought into a form $\frac{\partial G}{\partial\theta} = \eta R(G, \theta)$, where G indicates a column of four known algebraic functionals of quantities to be determined. Expansion in resistive effects leads to easily solvable differential equations $\frac{\partial G^{(n)}}{\partial\theta} = \eta R(G^{(n-1)}, \theta)$, so that the nth order solution is given by quantities in the order n-1, together with surface functions $S^{(n)}$ i.e. $G^{(n)} = \eta\int_0^\theta d\theta' R(G^{(n-1)}, \theta') + S^{(n)}(r)$. These surface functions in nth order are determined by the condition that the (n+1)th order solution is periodic in θ i.e. $\int_0^{2\pi} d\theta R(G^{(n)}, \theta) = 0$. Hence, once we have the zeroth order we have a systematic procedure to obtain all higher orders. What we have done is to solve the zeroth order, which corresponds to non-linear ideal MHD flows, and to derive the plasma loss expression in the resistive first order.

It is interesting to note that we are led to restrictions on the ideal plasma flow. In terms of the mass fluxes the long and the short way, these are shown in the figure. One can see (for definite values of aspect ratio and rotational transform), the possible departures from the quasistatic case, which corresponds to the neighbourhood of the origin. The quantities plotted are related to the mass fluxes Γ the short and Ψ the long way. The two regions where stationary solutions are possible, can be shown to correspond to super and subsonic meridional flow, where the appropriate sound speed is not c, but fc.

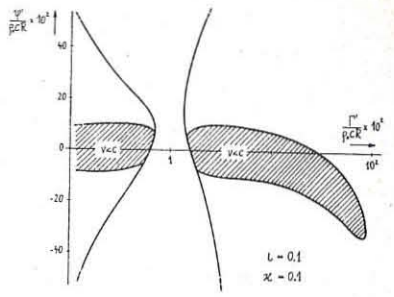

In first order the mass loss rate through a surface (where Q is located at r = 0) is

$$W^{(1)} = \int_{r(\zeta)=r} \rho \underline{v}^{(1)}\cdot d\underline{S}$$

$$= -\frac{4\pi^2\eta r R\bar{\zeta}}{B_0^2 f^2}\left\{\left\langle\rho\frac{\partial\rho}{\partial r}N^2\right\rangle - \frac{(1-\kappa^2)^{1/2}}{1+f^2}\langle\rho N\rangle\left\langle N\frac{\partial\rho}{\partial r}\right\rangle\right.$$

$$-\frac{1}{r}\left[\left\langle\rho^2N^2\left(\frac{v_r^2}{c^2} + K\frac{\cos\theta}{N}\frac{v_\theta^2}{c^2}\right)\right\rangle - \frac{(1-\kappa^2)^{1/2}}{1+f^2}\langle\rho N\rangle\left\langle\rho N\left(\frac{v_\theta^2}{c^2} + K\frac{\cos\theta}{N}\frac{v_r^2}{c^2}\right)\right\rangle\right] + \left\langle\rho N\frac{\partial}{\partial r}\left(\frac{1}{f}\rho N^2\frac{v_\theta}{c}\frac{v_r}{c}\right)\right\rangle - (1-\kappa^2)^{1/2}\langle\rho N\rangle\left\langle\frac{1}{N}\frac{\partial}{\partial r}\left(\frac{1}{f}\rho N^2\frac{v_\theta}{c}\frac{v_r}{c}\right)\right\rangle\Bigg\}$$

where each line can be identified with a particular force. Note that this expression is given in terms of zeroth order quantities, which can in principle be calculated from conditions on the first order solution, as we have pointed out earlier. These conditions are differential equations and their solution is a boundary value problem. We can, however, estimate losses without a full solution of these equations. Different estimates will be presented which indicate that in representative situations the "extra" losses caused by plasma flow are of the same order as the classical (quasi-static) resistive losses.

[1] D.Pfirsch, A.Schlüter: MPI/PA/7/62 (unpublished).

This work is part of the joint programme between IPP and Euratom.

ENHANCED DIFFUSION IN A NON-UNIFORM MAGNETIC FIELD

S. Puri

Institut für Plasmaphysik, Garching bei München, Germany

Abstract: A uniform electric field transverse to a spatially non-uniform magnetic field produces particle diffusion even when the electric field spectrum contains no dc component. This diffusion is additional to the usual $\underline{E} \times \underline{B}$ diffusion and occurs isotropically in the plane perpendicular to the magnetic field direction.

Analytical Solution: From Eq.(51) of Ref.1, the equation of transverse motion of a particle in a magnetic mirror and subject to a x-directed, spatially uniform electric field E(t) is given by

$$v_r(t) = -j\Omega(t)v_r(t) + j\Omega_r(t)v_z(t) + \eta E(t), \qquad (1)$$

where $v_r = v_x + jv_y$, $r = x + jy$, $\Omega(t) = \eta B_z(t)$, $\Omega_r(t) = \eta\left[B_x(t) + jB_y(t)\right]$ and B(t) implies $B\left[x(t), y(t), z(t)\right]$ at the instantaneous position of the particle. For paraxial particles $r \to 0$, $\Omega_r \to 0$, and Eq.(1) gives

$$v_r(t) = \exp\left[-j\omega_c t\right] G^*(t) \left\{ \iint_{-\infty}^{\infty} \eta\, \tilde{E}(\omega)\tilde{G}(g)\, d\omega\, dg\, \frac{\exp\left[j(\omega+\omega_c+g)t\right] - 1}{j(\omega+\omega_c+g)} + v_r(0) \right\} \qquad (2)$$

where $\Omega(t) = \omega_c + \omega_c(t)$, $G(t) = \exp \int_0^t j\omega_c(t)\, dt$, and tilde denotes Fourier-transformation. Integrating Eq.(2) we obtain

$$r(t) = -\eta \iiint_{-\infty}^{\infty} \tilde{E}(\omega)\tilde{G}(g-s)\tilde{G}^*(g)\, \frac{d\omega\, ds\, dg}{\omega_c + g} \left\{ \frac{\exp\left[j(\omega-s)t\right] - 1}{\omega - s} + \exp\left[-j(\omega_c + g)t\right] \cdot \frac{\exp\left[j(\omega + \omega_c + g - s)t\right] - 1}{\omega + \omega_c + g - s} \right\} + jv_r(0) \int_{-\infty}^{\infty} \tilde{G}^*(g)\, dg\, \frac{\exp\left[-j(\omega_c+g)t\right] - 1}{\omega_c + g} + r(0) \qquad (3)$$

By applying l'Hôpital rule to Eq.(3) it is readily verified that the first branch of poles at $\omega = s$ represents guiding center drift. The second branch at $\omega = s - \omega_c - g$ represents the effect of expanding particle orbits due to particle acceleration from the corresponding poles in the velocity equation. This spiraling motion does not contribute to guiding center motion. Unlike the above poles, the pole at $\omega_c = -g$ produces a drift with a quadratic dependence on time; however, its contribution is negligibly small in practical confinement systems.

In order to simplify further analysis, we consider an ideal parabolic mirror in which $\omega_c(t) = \omega_c A \cos(pt + \theta)$, where $p/2$ is the longitudinal frequency of the particle along the mirror axis, θ its initial position, and $A = (R-1)/(R+1)$, R being the ratio of the maximum to the minimum magnetic field seen by the particle. We further assume that E(t) is vanishingly small so as to leave $\omega_c(t)$ unaffected; this being tantamount to assuming that E(t) and G(t) are independent. Then $\tilde{G}(g) = 2\pi \exp\left[-j\beta \sin\theta\right] \sum_n J_n(\beta) \exp(jn\theta) \cdot \delta(g - np)$ and Eqs.(2) and (3) become ($\beta = A\omega_c/p$)

$$v_r(t) = \exp\left[-j\omega_c t - j\beta \sin(pt+\theta)\right] \left[\sum_n \eta \int_{-\infty}^{\infty} \tilde{E}(\omega)\, d\omega \exp(jn\theta) \cdot \frac{\exp\left[j(\omega + \omega_c + np)t\right] - 1}{j(\omega + \omega_c + np)} + v_r(0) \exp(j\beta \sin\theta) \right] \qquad (4)$$

and,

$$r(t) = \eta \sum_s \sum_m J_m(\beta) J_{m-s}(\beta)\, \frac{\exp(-js\theta)}{\omega_c + mp} \int_{-\infty}^{\infty} \tilde{E}(\omega)\, d\omega \qquad (5)$$

$$\cdot \left[- \frac{\exp\left\{j(\omega - sp)t\right\} - 1}{\omega - sp} + \exp\left\{-j(\omega_c + mp)t\right\} \frac{\exp\left\{j(\omega + \omega_c + mp - sp)t\right\} - 1}{\omega + \omega_c + mp - sp} \right]$$

$$+ jv_r(0) \exp(j\beta \sin\theta) \sum_m J_m(\beta) \exp(-jm\theta)\, \frac{\exp\left[-j(\omega_c + mp)t\right] - 1}{\omega_c + mp} + r(0)$$

where all summations extend from $-\infty$ to $+\infty$. In this paper we shall circumvent the singularity at $\omega_c + mp = 0$ (which gives rise to the quadratic drift term) by requiring ω_c/p to be a non-integer. For a stationary random electric field E(t) we obtain from Eq.(5),

$$\frac{dr_g^2(t)}{dt} = 2\pi\eta^2 \sum_s \left[\sum_m \frac{J_m(\beta) J_{m-s}(\beta)}{\omega_c + mp} \right]^2 \phi(sp), \quad t \to \infty, \qquad (6)$$

where $\phi(\omega)$ is the power spectrum of E(t) and the subscript "g" denotes guiding center diffusion. Note that in general (including the case of spatially varying, correlated dc electric and magnetic fields) the calculations leading to Eq.(6) are not so easy to perform, since E(t) and G(t) may not be independent. It is to be remembered that the diffusion is isotropic for $s \neq 0$ and in the $\underline{E} \times \underline{B}$ direction for $s = 0$.

Using the identity $\sum_m J_m(\beta) J_{m-s}(\beta) = J_s(0)$, it is seen from Eq.(6) that for $\omega = sp \neq 0$, the magnitude of the diffusion term is small compared to the case $\omega = 0$, for comparable values of the electric field. However, the contribution to diffusion parallel to the electric field may still be important due to the presence of rather large ambipolar fields in the radial direction.

Physical Mechanism: Consider the case $\omega = p$ with the electric field "in phase" with the magnetic field as shown in Fig.1. The particle sees a stronger magnetic field during the positive half-cycle and a weaker magnetic field during the negative half-cycle of the electric field. Owing to different $\underline{E} \times \underline{B}$ rates in the two regions of the magnetic field, there is a net displacement of the guiding center in the y-direction.

Although such a simple explanation is not available for the x-direction drift, some insight may be gained by considering the velocity Eq.(4). For a dc electric field the particle velocity oscillates at the frequency $\omega = sp$, in addition to the frequency ω_c. During the positive half-cycle of the electric field of frequency $\omega = p$, the order of change in the particle velocity is E/ω_c and implies an x-displacement $\Delta x \sim E/\omega_c B$. Due to the absence of a pole at $\omega = p$ in Eq.(4), the particle is obliged to return this reactive energy during the subsequent negative half-cycle of the electric field, necessitating a further displacement Δx in the same direction.

The above drifts are first-order compared to the $\underline{E} \times \underline{B}$ drift at $\omega = 0$. There is yet a second-order drift due to the non-exact-adiabatic motion of the particle as evidenced by the pole at $\omega_c + g = 0$ in the term containing $v_r(0)$ in Eq.(3) and is shown in an exaggerated manner in Fig.(2). Since the particle velocity increases linearly in time, this drift component has a quadratic dependence on time. The maximum drift produced in a single transit across the mirror is $O(r_{max} - r_{min})$; therefore the magnitude of this drift is negligibly small for $\omega_c \gg p$.

Discussion: Both the first and the second order drifts would be somewhat reduced by the inclusion of the term containing ω_{cr} in Eq.(1). Thus the longitudinal velocity v_z decreases and the duration of the particle's stay increases in the strong magnetic field region (and vice-versa), thereby partially compensating for the difference in the oppositely directed drifts. Similarly, the difference between the radii in Fig.(2) would be reduced, resulting in a still smaller second order drift.

For comparable electric field fluctuations, the drifts and the associated diffusion would be most marked in magnetic mirrors, bumpi-tori, and multipoles decreasing in relative importance for stellerators and tokomaks.

Acknowledgement: This work has been performed as part of the joint research program of the Institut für Plasmaphysik and Euratom.

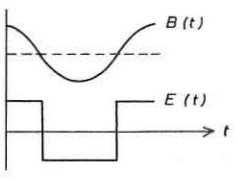

Fig. 1

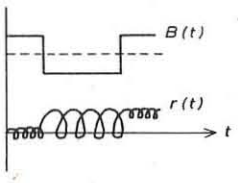

Fig. 2

References: 1. S. Puri, Phys. Fluids 8, 1743 (1968).

TOROIDAL CONFINEMENT (THEORY)

Stable Magnetohydrostatic Equilibria without Rotational Transform

by

Dietrich Lortz

Institut für Plasmaphysik, 8046 Garching

bei München, W. Germany

Abstract: The general class of vacuum fields $\underline{B} = \nabla\phi$ with closed lines of force in the neighborhood of a given closed curve C was investigated, where $\underline{B}$ is tangential on C and $q = \oint |\underline{B}|^{-1} d\ell$ has a maximum on C.

The condition that a toroidal MHD equilibrium have closed lines of force and vanishing longitudinal current can be met by the following symmetry:

(A) The current density $\underline{j}$ has reflexional symmetry to a plane and $\underline{B}$ the respective antisymmetry such that $\underline{j}$ is tangential and $\underline{B}$ is normal on the symmetry plane.

Such equilibria with symmetry (A) have three major advantages:

a) The existence of a toroidal finite β equilibrium can be proved [1] (in contrast to a stellarator configuration)

b) No interior conductors are necessary (in contrast to multipoles)

c) Sufficient stability criteria can be satisfied (in contrast to axisymmetric configurations without interior conductors).

It is well known [2], [3] that for the stability of closed line configurations without a longitudinal current it is sufficient to construct a vacuum field

(1) $\underline{B} = \nabla\phi = \nabla\Psi \times \nabla\chi$

such that the function

$$q(\Psi(\underline{x}), \chi(\underline{x})) = \oint |\underline{B}|^{-1} d\ell$$

posseses a local maximum. Several special configurations of this kind have already been discussed [4], [5], [6], [7].

In this paper the general conditions are derived that in the neighborhood of a given closed curve C there exists a vacuum field with symmetry (A) which is tangential on C and such that q has a maximum on C. If the independent variables $\underline{x}$ are interchanged with the dependent variables ϕ, Ψ, χ then eq. (1) is equivalent to

(2) $$\frac{\partial \underline{x}}{\partial \phi} = \frac{\partial \underline{x}}{\partial \Psi} \times \frac{\partial \underline{x}}{\partial \chi}$$

A solution of eq. (2) has the advantage that the field lines are explicitly known. If the curve C is described by $\underline{x}(\phi, 0, 0)$ one can find a systematic expansion of $\underline{x}(\phi, \Psi, \chi)$ with respect to Ψ and χ. The n-th order derivative of eq. (2) represents a system of 3 (n+1) inhomogeneous linear algebraic equations for the 3 (n+2) (n+1)-order derivatives

$$\frac{\partial^{n+1}\underline{x}}{\partial\Psi^{n-\tau+1}\partial\chi^{\tau}} \quad , \quad (\tau = 0, 1, 2, \dots, n+1)$$

on C, the inhomogeneities depending on the lower order derivatives. It is found that the rank of the system is 2 n+3 if $|\underline{B}|$ is everywhere finite on C. So there are n solubility conditions for the right-hand sides. If the field has the symmetry (A), then these conditions can always be satisfied and in each order two functions of ϕ can be arbitrarily prescribed.

If the curve C with curvature $\varkappa$ lies in the plane $\Psi = 0$ and $\underline{B}$ has reflexional symmetry to this plane, then the condition that q have a maximum on C veduces to

$$\partial q/\partial\chi = -2\int_0^{2\pi} f^{-1} h' d\ell = 0 \qquad h' = \varkappa f$$

$$\partial^2 q/\partial\Psi^2 = 2\int_0^{2\pi} f^{-5}(f'^2 f - f h g' - 2 f' h' h)\, d\ell < 0$$

$$\partial^2 q/\partial\chi^2 = 2\int_0^{2\pi} (f'^2 + 2h'^2 + h g')\, d\ell < 0$$

where $|\underline{B}| = 1$ has been chosen on C. $f, g, \varkappa$ are symmetric periodic functions of the arc length ℓ with period 2π and $f > 0$. If $\underline{t}$ is the tangential unit vector, $\underline{n}$ the unit normal on C, and $\underline{b} = \underline{t} \times \underline{n}$, then

$$\partial\underline{x}/\partial\chi = f\underline{n}, \quad \partial\underline{x}/\partial\Psi = -f^{-1}\underline{b}, \quad \partial^2\underline{x}/\partial\Psi^2 = v\underline{t} + V\underline{n},$$

$$\partial^2\underline{x}/\partial\chi^2 = u\underline{t} + v\underline{n}, \quad \partial^2\underline{x}/\partial\Psi\partial\chi = f^{-1} g\underline{b}, \quad V = f^{-3} f', \quad u = -f'/f,$$

$$v = g f - \varkappa f^2, \quad f^4 (f^{-1} V)' + g' + 2\varkappa f' = 0.$$

A configuration of this kind has been plotted in the figure: a) half of the curve C $(0 \le \ell \le 8\pi)$, b) - g) cross sections of the surfaces q = const perpendicular to C for the values $\ell = k\pi/5$ $(k = 0, 1, \dots, 5)$. The figures b) – g) are magnified by a factor of 100 relative to figure a). Ψ, χ has been restricted in such a way that the neglected terms cubic in Ψ, χ are absolutely less than 5 % of the linear terms. This results in $\delta q/q \sim 1.5\ \%$.

[1] Lortz, D., ZAMP, 21, 196 (1970)

[2] Kadomtsev, B.B., Plasma Physics and the Problem of Controlled Thermonuclear Reactions, Vol. IV, Pergamon Press London 1960

[3] Solov'ev, L.S., Soviet Phys. JETP, 26, 1167 (1968)

[4] Johnson, J. and Mosher, D., Plasma Phys. 8, 489 (1966)

[5] Shafranov, V.D., Soviet Atomic Energy 22, 449 (1968)

[6] McNamara, B., Plasma Phys. 10, 309 (1968)

[7] Glagolev, V.M., Plasma Phys. 11, 621 (1969)

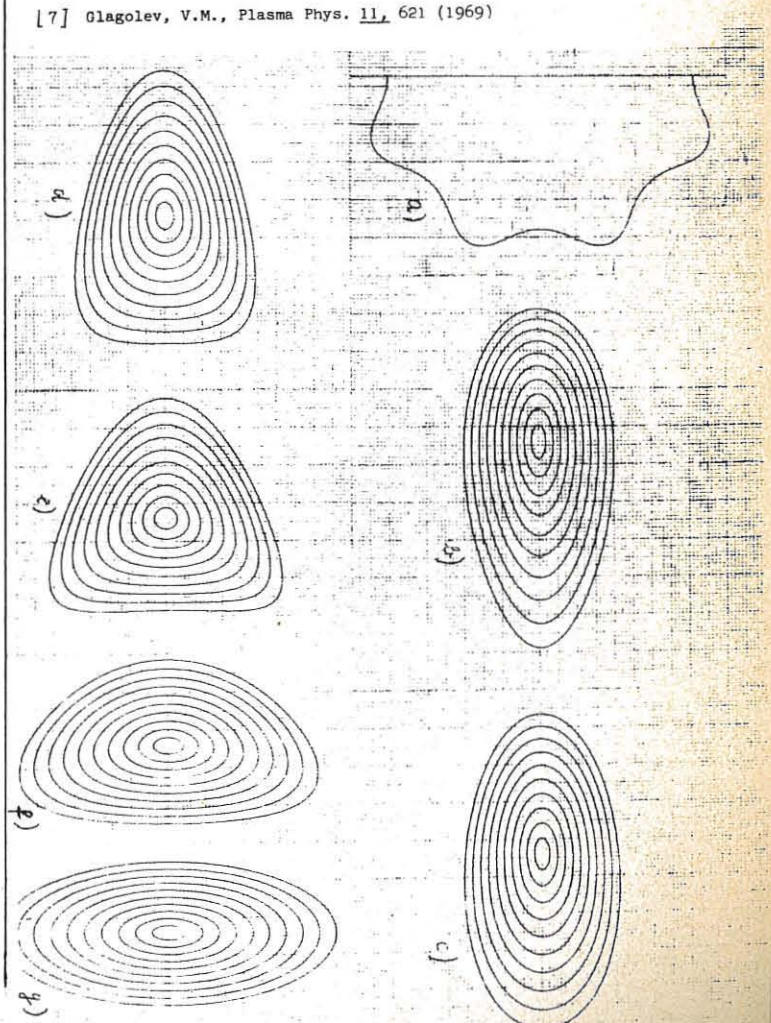

STABILITY OF AXISYMMETRIC MULTIPOLE CONFIGURATIONS WITH CLOSED MERIDIONAL FIELD LINES

by

Eckhard Rebhan

INSTITUT FÜR PLASMAPHYSIK

D-8046 Garching bei München, Germany

Abstract: The stability of axisymmetric equilibria having meridional field lines only is investigated. In order to obtain stability, a hard core must be placed inside the plasma. The pressure distribution can be chosen such that absolute stability is obtained. However, a low pressure layer extends up to the wall.

We consider axisymmetric equilibria with closed meridional magnetic field lines produced by toroidal currents. By using a stream function $\psi(r,z)$ the magnetic field $\underline{B}$ can be written

$$\underline{B} = -\underline{e}_\Theta \times \nabla\psi/r \qquad (1)$$

in cylindrical coordinates r,Θ,z. ($\underline{e}_\Theta$ is the unit vector in the Θ direction). The toroidal current $\underline{j} = j\underline{e}_\Theta$ is related to the pressure distribution $p(\psi)$ by the relation

$$p'(\psi) = j/r . \qquad (2)$$

For equilibria of this type the following form of the energy principle has been given in ref.[1]

$$\delta W = \frac{1}{2\pi}\left(L' + \frac{V'}{\gamma p}\right) f^2 + \int d\chi \left[\frac{1}{r^2 B^2 J}\left(\frac{\partial X}{\partial \chi}\right)^2 + p' J D X^2\right] \geq 0 \qquad (3)$$

with

$$L' = 2\pi \int d\chi\, J/B^2 \;, \quad V' = 2\pi \int d\chi\, J \;, \quad J = 1/B\,|\nabla\chi|$$

$$D = -\frac{2}{rB}(\underline{e}\cdot\underline{\kappa}) \;, \quad f = (2\pi \int d\chi\, J D X)/(L' + V'/\gamma p)$$

Thereby χ =const. are trajectories orthogonal to the flux surfaces ψ = const., $\underline{\kappa}$ is the vector of curvature of the $\underline{B}$-lines, and $\underline{e}_\psi = \nabla\psi/|\nabla\psi|$. From (3), Bernstein et al. have derived a necessary stability criterion and in two limiting cases (low ß and almost circular field lines) necessary and sufficient criteria.

It is possible to derive further stability criteria in the general finite ß case and to show that stable equilibria exist. Expanding δW around the center line of the flux surfaces one can show that the plasma is always unstable unless a current carrying hard dore is placed inside the plasma. Since the plasma should be separated from the hardcore we assume that the plasma starts with p = o on a $\underline{B}$-line at some distance from the hardcore. From (3) it is obvious that we have stability in the region immediately behind since p>o. Towards the wall the pressure must decrease and therefore ∇p must reverse direction on some flux surface. According to $\nabla p = \underline{j} \times \underline{B}$, ∇p reverses if $\underline{j}$ or $\underline{B}$ reverses. However, it can be shown that the second case would be unstable, and therefore j and $p(\psi) = j/r$ must change sign.

Except for very singular situations one can further show that the average curvature of the field lines must be positive:

$$\frac{1}{2}\int JD\,d\chi = \int \kappa \frac{J}{rB}\, d\chi \geq 0 \;. \qquad (4)$$

If X is decomposed into $X_I + X_{II}$ with $\int X_I X_{II}\, d\chi = 0$ and $\frac{\partial X_{II}}{\partial \chi} = 0$ then (3) splits into the two independent criteria

$$\delta W_I = \int d\chi \left[\frac{1}{r^2 B^2 J}\left(\frac{\partial X_I}{\partial \chi}\right)^2 + p' J D X_I^2\right] \geq 0 \qquad (5)$$

and

$$\delta W_{II} = X_{II}^2 \left[\frac{2\pi\gamma p \left(\int d\chi\, JD\right)^2}{V' + \gamma p L'} + p' \int JD\, d\chi\right] \geq 0 \qquad (6)$$

Inequality (5) can be fulfilled by making $|p'|$ smaller than a certain upper limit. If $D \geq 0$ in the whole region of ascending pressure, then this limitation applies only to the region with $p' \leq 0$. From (6), which is the criterion given in ref.[1], no restriction follows for the region with $p' \geq 0$ because of (4). On the other hand, the pressure in the region with $p' \leq 0$ may not drop to zero again within a finite distance from the outer wall. It may however decay rather fast towards the wall (in a straight cylinder $p \sim 1/r^{4\beta}$). Since finite restivity and other diffusion effects will enforce a low pressure layer extending to the wall even in cases where an ideal MHD equilibrium would be separated from this by a vacuum region, the low pressure layer obtained here will be no serious disadvantage.

---

[1] I.B. Bernstein, E.A. Frieman, M.B. Kruskal and R.M. Kulsrud; Proc. Roy. Soc. (London) A 244, 17 (1958)

TOKAMAK EQUILIBRIUM*

by

J. L. Johnson,† J. M. Greene, and K. E. Weimer

Princeton University Plasma Physics Laboratory

Princeton, New Jersey, U. S. A.

Abstract: Axisymmetric hydromagnetic equilibria are obtained to determine how externally applied magnetic fields, that support the configuration, must be altered to compress the plasma to a smaller major radius and thus obtain additional heating.

A promising technique for heating a tokamak plasma, above that obtained with anomalous resistivity, is to increase the strength of an externally applied vertical field to adiabatically compress the plasma by pushing it inward into a region of higher toroidal field.(1) The purpose of this work is to determine how this field must be shaped to maintain an equilibrium and adjusted to achieve the desired heating.

To solve the equilibrium we make the standard tokamak ordering in an aspect ratio expansion

$$\frac{a}{R} \sim \frac{B_p}{B_t} \sim \left(\frac{8\pi p}{B_t^2}\right)^{1/2} \ll 1, \qquad \iota \sim \left(\frac{8\pi p}{B_p^2}\right) \sim 1 .$$

Here R and a are the major and minor radii of the plasma, B_p and B_t are the poloidal and toroidal components of the field, and ι is the rotational transform. We obtain expressions for the stream function for the poloidal field in the region near the plasma where the aspect ratio expansion is applicable and in the external region where r/R is finite and then asymptotically match.

In the inner region we generalize Shafranov's formalism,(2) introducing an r, θ, ϕ coordinate system with r constant on the magnetic surfaces, $p = p(r)$. Thus

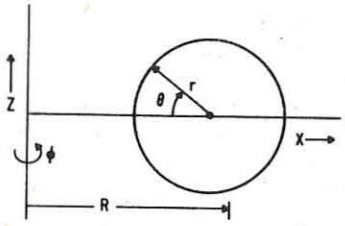

$$X = R - r\cos\theta - \Delta(r) + [E(r) + P(r)]\cos\theta + \ldots$$

$$Z = r\sin\theta + [E(r) - P(r)]\sin\theta + \ldots .$$

Here $\Delta(r)$ denotes the shift of the center of a surface of radius r from the magnetic axis, $E(r)$ is the ellipticity of the surface, and $P(r)$ modifies its label. The magnetic field is

$$\underline{B} = R\bar{B}\left[f(r)\underline{\nabla}\phi \times \underline{\nabla} r + g(r)\underline{\nabla}\phi\right]$$

with $\bar{B}$ a constant. We prescribe the pressure $p(r)$ and rotational transform $\iota(r)$, and solve the equilibrium equation $\underline{J} \times \underline{B} = \underline{\nabla} p$ order by order.

In the outside region we separate the field into two parts, $\underline{B} = \underline{B}_{out} + \underline{B}_{ext}$, with $\underline{B}_{out}$ associated with current in the plasma and $\underline{B}_{ext}$ due to currents in external conductors. Adopting a set of toroidal coordinates, we write an exact expression for $\underline{B}_{out}$ that satisfies the boundary conditions that $\underline{B}_{out}$ vanish on the toroidal axis and far from the plasma. We write an expression for $\underline{B}_{ext}$ in terms of its vertical component $B_\perp$ and its curvature κ at the plasma.

Asymptotically matching these expressions, $\underline{B}_{in} = \underline{B}_{out} + \underline{B}_{ext}$ in the vicinity of the plasma, completes the equilibrium calculation;

$$\frac{B_\perp}{\bar{B}} = -\frac{a f_a}{2R}\left[\ln\frac{8R}{a} + \frac{R\Delta_a'}{a} - \frac{3}{2}\right]$$

$$\kappa R = -\frac{3}{4} + \frac{\left[\frac{1}{16} + \frac{R\Delta_a'}{2a} + \frac{R^2\Delta_a'^2}{2a^2} + \frac{R^2}{a^3}(rE)_a'\right]}{\left[\ln\frac{8R}{a} + \frac{R\Delta_a'}{a} - \frac{3}{2}\right]} .$$

Primes represent derivatives with respect to r; the subscript a denotes evaluation on the plasma surface $r = a$. Note that this equation relates the eccentricity of the plasma surface to the curvature of the external field.

If the rotational transform is constant and the pressure distribution is parabolic inside this surface,

$$R\Delta_a'/a = (1 + 2\beta/f_a^2)/4 ,$$

$$R^2(rE)_a'/a^3 = 2R^2E_a/a^3 - (3 + 4\beta^2/f_a^4)/32 .$$

To see how the equilibrium scales, we assume that the current responsible for the toroidal field is changed so that $R\bar{B} = R_o\bar{B}_o\tau^2$ and $\underline{B}_{ext}$ is adjusted so that $R = R_o/\sigma^2$. Then conservation of toroidal flux, poloidal flux, and mass determines the scaling of r, f, p (assuming an adiabatic equation of state), etc.:

$$p = p_o\sigma^{20/3}\tau^{10/3} + \ldots ,$$

$$\frac{B_{ext}}{\bar{B}} = -\underline{e}_z\frac{\iota a_o^2\sigma^4}{4\pi R_o^2}\left(\ln\frac{8R_o\tau}{a_o\sigma} - \frac{5}{4} + \frac{2\pi^2\beta_o R_o^2\sigma^{2/3}\tau^{4/3}}{\iota^2 a_o^2}\right)$$

$$+ (\underline{e}_x\sin\theta - \underline{e}_z\cos\theta)\frac{3\iota a_o^3\sigma^5}{16\pi R_o^3}\left(\ln\frac{8R_o\tau}{a_o\sigma} - \frac{17}{12}\right) + \ldots .$$

For the parameters of a device proposed at Princeton – $R_o = 90$ cm, $\iota/2\pi = 1/3$, $\beta_{\theta o} = 0.56$, R/a varying from 5.3 to 3.3 with $R\bar{B}$ maintained constant – the ion temperature should increase from 0.3 kV to 1.0 kV with the configuration changing as shown.

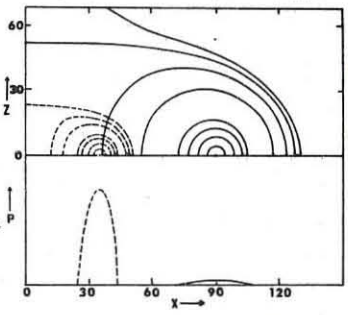

* Supported by the U. S. Atomic Energy Commission, Contract AT(30-1)-1238.

† On loan from Westinghouse Research Laboratory; visiting U. K. A. E. K. Culham Laboratory, England.

(1) H. P. Furth and S. Yoshikawa, Bull. Am. Phys. Soc. II, 15, 534 (1970).

(2) V. D. Shafranov, Reviews of Plasma Physics, M. A. Leontovich, Ed., Consultants Bureau, New York, 1966, Vol. 2, p. 103.

SPACE-TIME EVOLUTION OF A TOKOMAK TYPE PLASMA.

by

C. Mercier and Soubbaramayer

ASSOCIATION EURATOM-CEA
Département de la Physique du Plasma et de la Fusion Contrôlée
Centre d'Etudes Nucléaires
Boîte Postale n° 6 - **92 Fontenay-aux-Roses** (France)

Abstract : A mathematical model is set up to compute the space-time evolution of a TOKOMAK type plasma. Two examples of applications show that the model can be used to do extrapolation calculations of TOKOMAK machines or to carry out numerical experiments to test possible interpretations of measurements.

EQUATIONS.

The behaviour of a plasma stabilized by a strong longitudinal magnetic field and submitted to a discharge current can be described macroscopically [1] with a one or two fluid magnetohydrodynamic model. In one fluid, the system includes MAXWELL equations, OHM's law, mass continuity, momentum equation, energy balance and a state equation.

$$\vec{\nabla}\times\vec{E}=-\frac{\partial\vec{B}}{\partial t} \qquad \vec{\nabla}\times\vec{B}=\mu_0\vec{J} \qquad \vec{\nabla}\cdot\vec{B}=0$$

$$\vec{J}=\sigma(\vec{E}+\vec{V}\times\vec{B}) \qquad \frac{\partial n}{\partial t}+\vec{\nabla}\cdot(n\vec{V})=s \qquad \vec{\nabla}p=\vec{J}\times\vec{B} \qquad (1)$$

$$\sigma^{-1}\vec{J}^2=\frac{3}{2}kn\frac{dT}{dt}+p\,\vec{\nabla}\cdot\vec{V}+\vec{\nabla}\cdot(-\kappa\vec{\nabla}T)+P_c+P_r$$

$$p=knT$$

The system (1) is written with usual notations and in electromagnetic C.G.S units. s is a local source of mass, P_c charge exchange loss and P_r radiation loss (Bremsstrahlung and cyclotron radiation). We assume that a flux $\mathcal{N}_0$ of cold neutral atoms enters the plasma from the wall. This flux may be emitted directly from the wall or constituted by the fraction of the diffused flux from the plasma which is not pumped and which is absorbed and reemitted by the wall . One part of the flux $\mathcal{N}_0$ gets ionized by collisions with electrons (source of mass) and another part collides with hot ions exchanging its charge (charge exchange loss). The system (1) is much simplified in the case of cylindrical symetry. But in that approximation, the derivation of the average diffusion velocity shows that one cannot give account of the toric effect nor the trapped particles effects. We have replaced the diffusion term in the average velocity by an effective diffusion taking into account the toric effect or more generally any instability effect. The system (1) in cylindrical symetry and this assumption are our basic model. The computations are carried out with a IBM-91 computer. The values of the longitudinal magnetic field, the radius of the plasma, the major radius of the torus , the shape of the discharge current function of time, the initial mass , the coefficient of reemission of neutrals by the wall, cross sections of ionization and charge exchange are introduced as data. The model can work with any given function of the electrical resistivity , diffusion and thermal conductivity.

EXAMPLES OF APPLICATIONS OF THE MODEL.

Two examples of applications of the model will be given here.

1) - Quasi-stationary solution. Such a solution may be considered as valid at the end of a sufficiently long rectangular current discharge. We do $\frac{\partial}{\partial t}=0$ in all equations except the mass continuity where we replace $\frac{\partial n}{\partial t}$ by $(-\omega n)\omega$, being an eigen value. Physically the solution means that all quantities are stationary except the density which is slowly decreasing. This model has been tested in the case of ROBINSON's [2] experiments and there is an excellent agreement between measurements and computations. We can use this model to do extrapolation calculations of TOKOMAK machines.

2) - Possible interpretation of MIRNOV's measurements.

MIRNOV observed a strong cooling and deterioration of plasma containment during a second rise of the discharge current. One of the possible explanations of this phenomena may be due to the influence of the shear. The second current rise decreases the shear over the boundary region of the plasma and excites some instability previously stabilized by the shear. This instability increases the dissipation coefficients and causes the cooling observed. We use our model to do numerical experiments to test this possible explanation. As in these experiments , thermal losses are predominant, we have considered only one dissipative coefficient (thermal conductivity K). To fix the ideas we assume that instabilities are excited when the absolute value of the shear θ , at the point of radial coordinate 9/10 of the plasma radius , decreasesbelow a critical value θ_c and we assume the following rough law :

$$|\theta(0.9)|\geq\theta_c \qquad k=K_{Galeev} \; ; \quad |\theta(0.9|<\theta_c \qquad K=\lambda K_{Bohm}$$

λ being a factor. The FIGURE shows the energy evolution computed for one

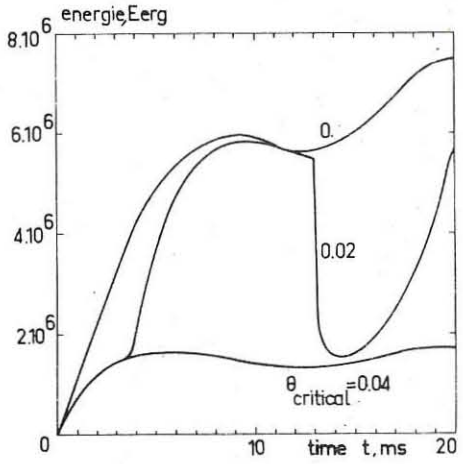

value of λ and three values of θ_c. We see that during the second increase of the current, this explanation may lead to an energy decrease of the same order as it was observed. A stematic computation shows the existence of a very narrow region (λ, θ_c) leading to a similar result .

Moreover MIRNOV observed the appearance of instabilities in the oscillogram of the current derivative at a time Δt after the beginning of the second current rise. This interval Δt corresponds to a current increase ΔI. MIRNOV observed that this current increase ΔI does not depend on the initial level I_0 from which the second current rise occurs but exhibits a dependence on the steepness of this current rise (an increase in the steepness of the rise causes a decrease in ΔI). These two phenomena are tested also in our model and the computations are in qualitative agreement with experimental results. The explanation of MIRNOV'S results by the influence of the shear is therefore plausible. Other explanations, like the influence of the tearing mode may be tested in the same way.

References :

[1] H.LUC , C.MERCIER, SOUBBARAMAYER
International Symposium on closed confinement systems, DUBNA 1969.

[2] D.C.ROBINSON and al, NATURE, Vol.224, Nov.1, 1969.

[3] S.V. MIRNOV, Nuclear Fusion, Vol.9 , n°1, 1969.

Current Diffusion and Energy Balance in Tokamak Systems.

Y.N. Dnestrovskii, D.P.Kostomarov, N.L.Pavlova,

Moscow State University, Moscow USSR.

Abstract. The transport processes in Tokamak systems with the anomalous resistance and electron thermoconductivity of plasma are considered. The computational results are in good agreement with the experiments on two Tokamak devices.

1. In our report /1/ the energy balance in Tokamak systems with classical trasport coefficients /2-4/ was researched. The results of calculations for the ion and electron temperatures were in good correspondence with the experimental data. At the same time the measurements of the plasma resistance have shown that its value exceeds the classical resistance in several times /5-6/. Furthermore the calculations of the current diffusion lead to the large skin-effect for current and electron temperature if the classical transport coefficients are used. In this report we study the current diffusion with some phenomenological picture of anomal resistance and electron thermoconductivity.

2. We have used the following system of equations on ion and electron temperatures ($T_i(x,t)$ and $T_e(x,t)$ in ev) and current magnetic field He:

$$\frac{\partial T_i}{\partial t} = \frac{1}{nx}\frac{\partial}{\partial x}\left(xn\chi_i\frac{\partial T_i}{\partial x}\right) - \frac{Cn}{T_e^{3/2}}(T_i - T_e)$$

$$\frac{\partial T_e}{\partial t} = \frac{1}{nx}\frac{\partial}{\partial x}\left(xn\chi_e\gamma_1\frac{\partial T_e}{\partial x}\right) + \frac{Cn}{T_e^{3/2}}(T_i - T_e) + \frac{B\gamma}{nT_e^{3/2}}\left[\frac{1}{x}\frac{\partial}{\partial x}(x^2 j_n)\right]^2 \qquad (1)$$

$$\frac{\partial j_n}{\partial t} = \frac{A}{x}\frac{\partial}{\partial x}\left[\frac{\gamma}{T_e^{3/2}}\frac{1}{x}\frac{\partial}{\partial x}(x^2 j_n)\right]$$

Here t is time in msec, $j_n = \frac{1}{q} = \frac{R H_e}{2 H}$, H is the longitudinal magnetic field in koe, $n(x) = N(1 - \frac{1}{2}x^2)$ is the plasma density in 10^{13} cm^{-3}, $x = \frac{r}{a}$, R and a are the large and little radii of plasma torus (in cm). $A = 6100/\lambda^2$, $B = 2\cdot10^7 H^2/R^2$, $C = 470/\rho$, ρ is the relative ion mass. The classical thermoconductivity coefficients χ_j ($j = i, e$) are given by the equations /2-4/:

$$\chi_j = 300\frac{F_j n \lambda^2}{a^2 H^2 \sqrt{T_j}}\begin{cases}\left(\frac{R}{2}\right)^{3/2} J(\alpha_j) & (\alpha_j \le \alpha_0)\\ 1.6 & (\alpha_j \ge \alpha_0)\end{cases} \qquad (2)$$

Here $\alpha_j = 420\frac{R^5 n^2 q^2}{T_j^4 f_j}$, $\alpha_0 = 1.25\left(\frac{R}{2}\right)^{3/2}$, $J(\alpha) = 2.3\int_0^\infty \frac{e^{-z}z^3 dz}{\sqrt{2+\alpha}}$; $J(0) = 1$,

$F_j = \sqrt{\rho}$ ($j = i$) or $\frac{5}{43}$ ($j = e$), $f_j = 1$ ($j = i$) or 4 ($j = e$)

In the system(1) there are functions $\gamma(x,t)$ and $\gamma_1(x,t)$ allowing us to describe the anomalous resistance and electron thermoconductivity. In the simplest case $\gamma(x,t)$ equals constant, which determinds from the mean experimental value of the plasma resistance ("middle" model). Nevertheless this model leads usually to too slowly current diffusion. Therefore we have used also the "local" model connected with an idea on ion-sound instability causing the anomality in trasnport coefficients/7/. On this model γ is the function of the local relation of the current electron velocity u to the velocity of ion-sound c_s: $\gamma = \gamma(\theta)$, $\theta = \frac{u}{c_s}$. If $\theta < 1$ then $\gamma = 1$ and plasma is classical. If $\theta > 1$ then γ is fastly increasing. Usually we set that $\gamma(\theta) = 1 + \frac{1}{2}(\gamma_{max} - 1)\left(1 - \cos\sqrt{\pi}\frac{(\theta - 1)}{\Delta\theta}\right)$ if $1 < \theta \le 1 + \Delta\theta$ and $\gamma(\theta) = \gamma_{max}$ if $\theta > 1 + \Delta\theta$.

In computations we set $\Delta\theta \sim 2$ and γ_{max} was chosen so as to correspond to the experimental values of the plasma resistance. For T-3 device $\theta \sim 1 \div 3$. For TM-3 $\theta > 5$ and $\gamma(\theta) = \gamma_{max} = \text{const}$ (in this case the local model coincides with the middle model).

3. The system (1) was solved by computer with the following boundary and initial conditions: $T_j(1,t) = T_{j0}$, $j_n(1,t) = 0.2\frac{RJ(t)}{a^2 H} \equiv j_{n0}(t)$, $T_j(x,0) = T_{j0}$, $j_n(x,0) = j_{n0}$, $J(t) = \left[J_1 + (J_2 - J_1)t/t_1\right]$ if $0 < t < t_1$, $J(t) = J_2$ if $t > t_1$, $J(t)$ is the total current in ka. On fig.1-5 the results of calculations are plotted for T-3 device /5/ ($R = 100$, $a = 12$, $H = 30$, $J_1 = 5$, $J_2 = 110$, $t_1 = 7$, $N = 4$, $T_{i0} = 10$) for mixture plasma with 30% hydrogen and 70% deiterium. For the comparison of the various anomality models on fig.1-2 the current distributions in space are drown for the different moments of time.

On fig.1 the dotted lines correspond to classical plasma ($\gamma = \gamma_1 = 1$),

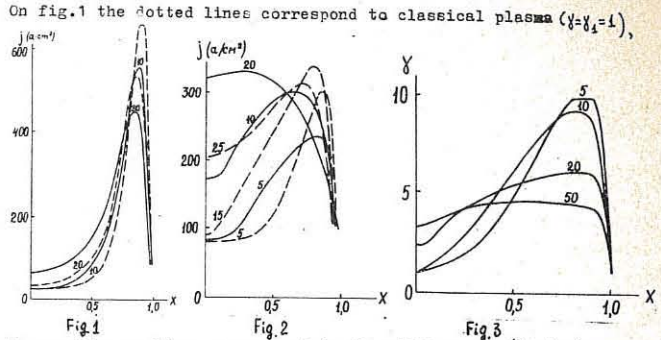

Fig.1 Fig.2 Fig.3

the continuous lines correspond to the middle model ($\gamma = 4, \gamma_1 = 1$). On fig.2 for dotted lines $\gamma = \gamma(\theta)$, $\gamma_1 = 1$, for continuous lines $\gamma = \gamma_1 = \gamma(\theta)$ ($\Delta\theta = 2$, $\gamma_{max} = 10$). It is easily seen that only the last model leads to the sufficiently fast current diffusion. On fig.3 for this model the distributions of $\gamma(x,t)$ are plotted. The curves show very high anomality near the plasma boundary at the initial moments of time. After this the current distributions are smoothing approximating the value $\gamma \sim 4$ which fits to the experimental data. On fig.4 the electron temperature distributions $T_e(x,t)$

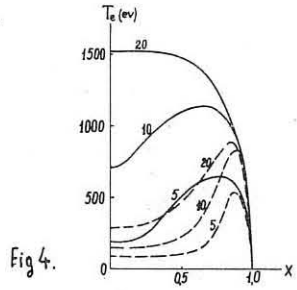

Fig 4.

are traced for two models: $\gamma = \gamma_1 = 1$ (dotted lines) and $\gamma = \gamma_1 = \gamma(\theta)$ (continuous lines). The fast smoothing of the continuous lines is in good coincidence with experiment /8/. On fig.5 for these two models also the dependence max Te, max Ti and energetical time τ_E on time are plotted.

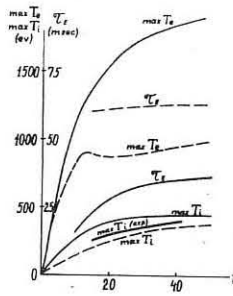

Fig.5

The fat curve corresponds to the experiment. On the last fig.6 the analogous dependences for TM-3 device are traced (R=40, a=8, H=27, J_1=1, J_2=27, t_1=2, N=2, γ_{max} =6). The good conformity between the theoretical and experimental results indicates the resonableness of the used model of plasma anomality.

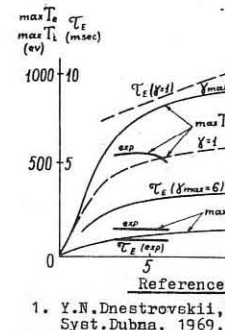

Fig.6

The authors thank acad. L.A.Arzimovich for stating the problem and very useful discussions.

References.

1. Y.N.Dnestrovskii, D.P.Kostomarov, Int.Conf.on Closed Syst.Dubna, 1969.
2. V.D.Shafranov, Atomnaya Energia, 19, 120 (1965)
3. A.A.Galeev, R.Z.Sagdeev, JETP, 53, 348 (1967)
4. L.M.Kovrijnych, JETP, 56, 877 (1969)
5. L.A.Arzimovich et all. Int.Conf.on Closed Syst.Dubna 1969
6. G.A.Bobrovskii, E.I.Kuznetzov, K.A.Rasumova, Int.Conf.on Closed Syst., Dubna, 1969.
7. H.A.B.Bodin, J.McCartan, Int. Conf.on Closed Syst., Dubna 1969.
8. H.J.Peacock, D.C.Robinson, V.V.Sannikov, P.D.Wilcock, Int.Conf. on Closed Syst., Dubna, 1969.

THE ENERGY BALANCE AND THE LIFETIME OF IONS IN PLASMA OF TOKAMAK T-3

L.A.Artsimovich, A.V.Glukhov, E.P.Gorbunov, M.P.Petrov.
I.V.Kurchatov Institute of Atomic Energy, Moscow, USSR
A.F.Ioffe Physico-Technical Institute, Leningrad, USSR

Abstract: The energy balance of ions in the tokamak device T-3 was examined using ion temperature, obtained from the analysis of energy spectrum of charge-exchange atoms. The values of ion energy lifetimes are given. It is shown that the ion energy losses are mainly caused by the classical heat conductivity with trapped particles taken into account.

In closed toroidal devices of tokamak type, where the plasma coil is heated by the current, flowing throught it, and is stabilized by the strong magnetic field, the energy life-time of ions is quite important characteristics of the plasma thermoinsulation. Introducing this characteristics one can write the equation of ion energy balance in the following form:

$$0{,}4\cdot10^{-17}\frac{n^2}{A\,T_i^{1/2}}=\frac{3}{2}nk\frac{dT_i}{dt}+\frac{3}{2}nk\frac{T_i}{\tau_E} \qquad (1)$$

where A is the atomic weight of the matter (hydrogen or deuterium), T_i is the ion temperature, n is the plasma density. The left-hand term of the equation is the energy passed from electrons to ions by the Coulomb collisions per sec in I cm^3. The electron temperature T_e is not included in this term, because the flux of energy from electrons to ions quite weakly depends on T_e in the range of T_e/T_i from I.6 to IO. The experimental value of the ratio T_e/T_i is always in this range. The equation (I) assumes that the ions are mainly heated by the Coulomb collisions with electrons. Several experimental facts confirm this assumption, when the density of the plasma is not very low /see for instance [I]/.

Fig.I presents the dependences of T_i, n and τ_E on the discharge time in the center region of plasma column in T-3.

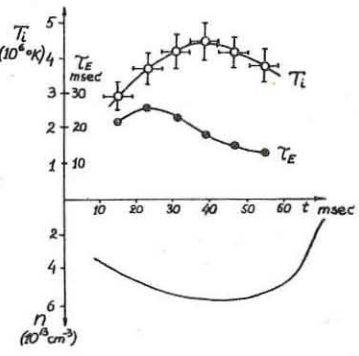

FIG.I

τ_E values presented have been calculated from equation (I), using T_i and n shown in fig.I. The vaiues of T_i have been recieved from the analysis of charge-exchange atomic spectra and the values of n - from radiointerferometry.

The energy losses from ion component of the plasma are caused by:
I) heatconductivity,
2) diffusion, 3) charge-exchange of ions on the residual gas. Hence:

$$\frac{1}{\tau_E}=\frac{1}{\tau_H}+\frac{1}{\tau_d}+\frac{1}{\tau_c} \qquad (2)$$

, where τ_H is the energy lifetime due to heat conductivity, τ_d is diffusion lifetime (or lifetime of charged particles), τ_c is charge-exchange lifetime of ions. The comparison of time values including in eq. (2) characterises the contribution of these three processes into the ion energy losses. The values τ_c and τ_d are determined by the following equations: $\tau_c=\frac{1}{n_a\langle\sigma v\rangle_c}$ (3) and in the stationary case for pure hydrogen plasma: $\tau_d=\frac{1}{n_a\langle\sigma v\rangle_i}$ (4), where n_a is the density of atomic hydrogen or deuterium in the central region of the plasma column, (we are considering here the energy losses just for this region), $\langle\sigma v\rangle_c$ and $\langle\sigma v\rangle_i$ are averaged by the Maxwellian velocity distribution products of resonance charge-exchange and electron ionisation cross sections by ion and electron velocities respectively.

The value n_a included in (3) and (4) has been measured in tokamak TM-3 by the registration of absolute intensities of Balmer hydrogen spectral lines [2]. There were no such measurements in T-3 device. However, here it is possible to evaluate the density n_a, using the absolute atomic charge-exchange flux emitted by the central region of the plasma column. The values n_a thus obtained for typical regimes of T-3 during the stationary period of the discharge are within the limits of $(1.5 \div 3.0)\cdot10^8$ at/cm^3. By the way, such evaluation for TM-3 gives the values of n_a close to 10^9 at/cm^3, which are in satisfactory agreement with the spectroscopic data. The values of τ_c and τ_d calculated by eq.(3) and (4), applying the above values of n_a, essensially prevail O.I sec. The comparison of such values with τ_E, equal to I5 ÷ 20 msec during the stationary period (see fig.I), shows that the main part of the ion energy losses in the central region of the plasma is caused by the heat conductivity.

The theoretical consideration of the classical ion heat conductivity in toroidal systems with regard to trapped particles is carried out in [3]. The theory developed gives the necessary formula for calculation of heat conductivity coefficients for various experimental conditions. Using these formula as well as energy balance equation (I), it can be shown, that the ion temperature in tokamaks should be proportional to $\sqrt[3]{IH_z^2R^2\bar{n}}\cdot A^{-1/2}$, where I is the discharge current, R is the main radius of the toroidal system, H_z is the strength of the longitudinal magnetic field, $\bar{n}$ is the average density of the plasma. The proportionality coefficient can be found by solving the heat conductivity equation at the given current and density distributions by the plasma column cross-section. Fig.2 shows the experimental data of maximum ion temperature in T-3. The ion temperature in the central region of the plasma column during the stationary period is plotted on the ordinate-axis. The values of $\sqrt[3]{IH_z^2R^2\bar{n}}\cdot A^{-1/2}$ are plotted on the abscissa-axis. Experimental values of T_i have been measured at $\bar{n}$ being from 1.5×10^{13} cm^{-3} to 3.8×10^{13} cm^{-3}, I - from 60 kA to II0 kA, H_z - from 25 kOe to 38 kOe. R in T-3 is equal to I00 cm. Black spots are the experimental data corresponding to hydrogen, the white spots - to deuterium. It is clear that the experimental results are in good agreement with the function $\sqrt[3]{IH_z^2R^2\bar{n}}\cdot A^{-1/2}$. Straight lines I and II shown in fig.2 present the function of T_i calculated on the base of classical theory of ion heat conductivity [3] with two different assumptions on current and density distributions in the plasma. Line I corresponds to the uniform current and density distributions by the cross-section of the plasma column. Line II is calculated for the case when current and density have square-parabolic radial distributions. The straight line, which approximates the experimental data, lies between I and II (it is shown by dashed line). So it is follows from the experimental data given in fig.2, that in the range of $\sqrt[3]{IH_z^2R^2\bar{n}}\cdot A^{-1/2}$ from 4×10^8 to 9.2×10^8 (where I - in A, H_z - in Oe, R - in cm, $\bar{n}$ - in cm^{-3}) the following formula takes place:

$$T_i=(5{,}9\pm0{,}5)\cdot10^{-7}\sqrt[3]{IH_z^2R^2\bar{n}}\cdot A^{-1/2} \qquad (5)$$

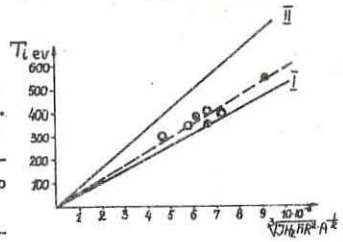

Fig. 2.

This result confirm the assumption that the ion energy losses in T-3 plasma in the considered range of physical parameters are caused mainly by the classical heat conductivity.

REFERENCES

I. L.A.Artsimovich et all. Plasma Physics and Controlled Nuclear Fusion Research, IAEA, Vienna I969, vol.I,page I57.

2. E.I.Kuznetsov, N.D.Vinogradova J.E.T.P. Letters 8, 59 (I968)

3. A.A.Galeev, R.Z.Sagdeev J.E.T.P. 53, 348 (I967)

THE PLASMA ENERGY IN TOKAMAK T3 FROM ELECTRICAL AND THOMSON SCATTERING MEASUREMENTS

by

E.P. Gorbunov+, D.P. Ivanov+, N.J. Peacock*, D.C. Robinson*, V. . Strelkov+

* U.K.A.E.A., Culham Laboratory, Abingdon, Berks. England
+ I.V. Kurchatov Institute of Atomic Energy, Moscow, USSR.

Abstract: The radial distributions of the electron density and temperature have been measured as functions of time from photon scattering together with μ-wave interferometer measurements, and have been compared with the total energy derived from the diamagnetic signal and the electrical waveforms. There is agreement between the two methods of estimating the plasma energy throughout the range of ohmic heating currents 40-150 kA and densities in the range 1-4·5 x 10^{13} cm^{-3}. The transverse electron energy scales as the square of the current. Beta with respect to the field of the current is about 0.5 but increases with time to greater than 2 towards the end of the current pulse. Anomalous resistivity is observed under most plasma conditions.

Introduction: Preliminary measurements[1] of the transverse temperature using the technique of laser light scattering on Tokamak T3 have shown that local temperatures can be higher than 1 keV and that essentially all the electrons, at least on the magnetic axis, have a Maxwellian distribution of velocities. The photon scattering results confirm[2] in order of magnitude the previous diamagnetic temperatures reported for T3 with a short (15 msec) current pulse.

The total electron plasma energy deduced from the values of T_e and n_e obtained by Thomson scattering has been compared with the total plasma energy evaluated from the electrical measurements throughout the same discharge and over a wide range of discharge parameters. The toroidal field, B_o has in general been chosen so that $q = \frac{B_o r}{B_\theta R} \gtrsim 2.5$, although mildly unstable conditions, $q < 2.5$, have also been studied.

The Radial Distribution of Electron Pressure: In order to evaluate the total electron energy in the plasma column, $2\pi \int_0^a r\, n_e(r)\, T_e(r)\, dr$, it is convenient to calculate the mean radius of the plasma pressure distribution from the radial density and temperature profiles. The profiles found from the Thomson scattering were symmetric about the magnetic axis (taking into account any small displacements of the plasma column). The temperature distribution during the middle of the current pulse is shown in Fig.1, each point being the mean from up to 10 discharges. The profile is described by $T_e = T_{eo}(1-(r/a)^4)^2$, where T_{eo} is the value on the magnetic axis and a = 17.5 cms is the limiter radius. A similar radial dependence is found for the density from microwave and scattering measurements. The electron energy per cm in the plasma column in these conditions is given by $\pi r_p^2 n_{eo} T_{eo}$; where r_p = 11.7 cms. The temperature distribution early in the discharge was somewhat different, e.g. for times ≲ 4 msec from the initial current rise, a temperature increase on the outside of the plasma (of up to 1.5 times the central value) was observed due to skin currents.

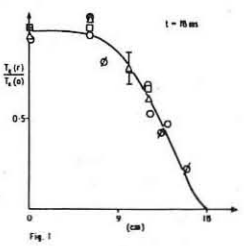

Fig. 1

Comparison of $2\pi \int_0^a r\, n_e(r) T_e(r)\, dr$ and the Diamagnetic Energy: The total transverse energy was calculated from the magnetic flux in the plasma column by a method described by Mirnov[3] and improved by Anashin. The result is compared with the scattering measurements throughout a typical discharge in Fig.2. Taking into account the mean ion energies[4] (about 150 eV in Fig.2), and the respective errors, there is agreement between the two values. Over the whole range of parameters studied the agreement is less good (up to 50% difference). The diamagnetic temperature depends critically on the mean current radius calculated from the electrical circuit equations[5]. This

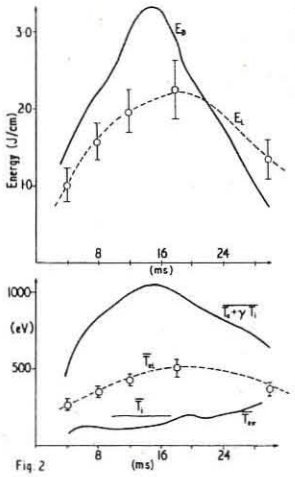

Fig. 2

radius is in general somewhat less than the mean plasma radius, r_p, and this results in a diamagnetic plasma temperature equal to or higher than the scattering temperature measurements. The examples where there is poorest agreement are correlated with the largest differences between the calculated current distribution and the electron pressure distribution. A comparison between the mean transverse diamagnetic temperature, $T_e + \gamma T_i$, the mean transverse ion temperature, T_i, the mean electron temperature T_e from the laser measurements and finally T_{eo}, the conductivity temperature throughout the same discharge, is shown in Fig.3. The electron temperature and density obtained by the laser technique on the magnetic axis remains practically constant after the first 10 millisec. (Fig.4); on the other hand, the diagmagnetic temperature is more sensitive to irregularities in the current waveform due to plasma drift and peripheral instabilities. Even when the plasma becomes weakly unstable during the current pulse the decrease in the temperature on the magnetic axis is not more than 10 to 20%.

The Value of Beta: The temporal variation of T_e and n_e on the axis is shown in Fig.4. The value of β_θ i.e. $I^2\beta_\theta = 2\,NkT$, is about 0.45 near the middle of the current pulse when the transverse energy is a maximum. β_θ can however exceed 2 late in the discharge as the current decreases.

Scaling Relations: For the whole range of discharge conditions studied T_e and the transverse energy are practically independent of the toroidal field

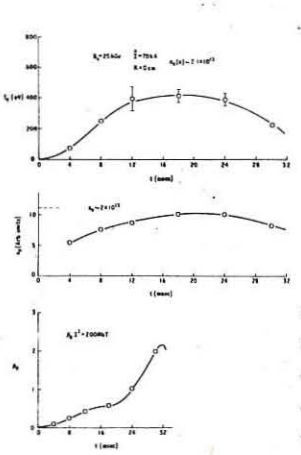
Fig. 3

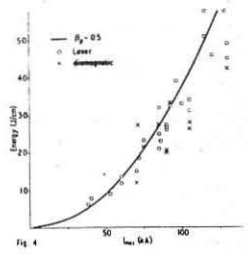

Fig. 4

B_o. The dependence of the temperature on n_e and I is marked however and characterised by β_θ = 0.5 for the time of maximum energy content in the plasma column. The maximum total energy from the laser and diamagnetic measurements is shown plotted against the heating current over the range of discharge conditions studied in Fig.4.

Conclusion: The total energy determined from diamagnetic signals is in agreement with the sum of electron energy obtained from Thomson scattering, and the ion energy. The total energy increases as the square of the current and the value of β_θ at current maximum is always about 0.45.

References

(1) Peacock, N.J. et al. Nature 224,488(1969)

(2) Gorbunov, E.P. et al. Nuc. Fus. 10, 43 (1970)

(3) Mirnov, S.V. Atomnaya Energiya 26, 458 (1969)

(4) Afrosimov,V.V. Zh. Tech. Fiz. 37, 1195 (1967)

(5) Artsimovich, L.A. et al. Proc. 4th. Int. Conf. Controlled Fusion Novosibirsk, I.A.E.A., Vol. 1, 157

DESIGN OF ALCATOR-THE MIT HIGH FIELD TORUS*

by
ALCATOR DESIGN GROUP**
(Paper presented by L. M. Lidsky)
RESEARCH LABORATORY OF ELECTRONICS
and
FRANCIS BITTER NATIONAL MAGNET LABORATORY
MASSACHUSETTS INSTITUTE OF TECHNOLOGY
CAMBRIDGE, MASSACHUSETTS U.S.A.

Abstract: ALCATOR is a new plasma containment experiment characterized by high magnetic field, good control of symmetry, and copious diagnostic access. It will be operated first in the Tokamak mode with major radius R = 54cm, minor radius a = 12cm, and centerline field of 120kg. The initial operation will exploit the high allowable plasma current density to explore the limits of ohmic heating, and to study the questions of enhanced resistivity and thermal transfer. Major aspects of the experimental design are described.

ALCATOR is an acronym for the high field toroidal plasma experiment under construction by MIT and the Bitter National Laboratory. It will be operated first as an ohmically heated Tokamak but other configurations are easily achieved within the basic design--noncircular minor cross sections, high shear stellarators, etc.

Initial Goals The advanced technology developed at the Francis Bitter National Magnet Laboratory makes possible the use of magnetic fields in the range 100-200kg in devices of moderate size. This field can be exploited in Tokamak devices to yield high current densities [recall that $j \propto (B_T/qR)$] which results in very high energy input rates and the possibility of maintaining enhanced resistivity (i.e. $\eta > \eta_{spitzer}$) even for quite large values of density and temperature. ALCATOR should be able to maintain enhanced resistivity within the Kruskal-Schafranov limit even for densities of $10^{14}/cm^3$ at electron temperatures of several keV. Our initial experimental object will be to explore the limits of ohmic heating in Tokamak-like devices with particular attention given to measurements of electrical resistivity and possible enhanced thermal transfer to the ions. The aspect ratio of ALCATOR was decided on by simultaneous consideration of the achievable current density, energy confinement time and available pulsed power(32MW). The final dimensions represent a compromise of achievable current density in order to allow significant ion heating.

Experimental Design ALCATOR is a pulsed toroidal device using LN_2 cooled composite copper-steel Bitter plates to produce 120kg on the toroidal center line--the peak toroidal field in the plasma region is 158kg. The 2.5mm thickness of steel in each plate supports the majority of the stress, approaching 65% of yield at the point of peak stress. The plasma current is induced by an air core transformer capable of supplying 1.2volt-seconds of excitation. The 300 turn primary has a 20kv voltage limit and can supply a maximum of 65 volts to the plasma. Peak calculated fringe vertical fields at the plasma edge are ± 5gauss. The copper stabilizing shell, also LN_2 cooled, is outside the vacuum chamber. The time constant for transverse field generated by this shell is in excess of 250msec. The limiter will be inserted through a full width 2cm transverse slot in such a fashion that its size, shape and position can be changed easily and quickly. Full power repetition rate will be one pulse every ten minutes with reduced power pulses proportionally more often. The major specifications are detailed in table 1.

TABLE I: DESIGN SPECIFICATIONS

Major Radius	54cm	Minor Radius (liner)	13cm
Toroidal Field	120kg	Pulse Duration	200msec
B_T Coil Power	21MW	Transformer Prod.	1.2v-sec
" " Current	130kA	" energy	5.6MJ
" " I.D.	32.5cm	" field	144kg
Cu Shell Radius	15.5cm	Prog. vert field	600g
" " Thickness	1.25cm	B_v Field(8cm) Uniformity	±15g

Diagnostics The major diagnostic access ports are illustrated in figure 1. There are four 2cm wide "T" sections, two pairs of oblique access tubes, and two axial tubes. These penetrations can be made with very small perturbations of the toroidal magnetic field. The oblique holes inherently cause little perturbation because the current redistribution in the Bitter plates reduces first order field perturbation. The transverse "T" sections are compensated by reducing the thickness of the Bitter plates near the slots to increase the local density. The maximum field perturbation caused by diagnostic access is 2% at the 12cm limiter radius. One of the diagnostic ports will be completely devoted to a 7 spatial channel Thomson scattering experiment to measure the velocity spectrum of the electrons. One of the oblique pair will be used for the simultaneous measurement of T_i and T_e for the electrons. Other experimental techniques that will be used, in addition to the important magnetic field sensing schemes so well-developed in the Soviet Tokamak experiments, will include a 337μ laser interferometer, bremsstrahlung monitors and several methods of measuring ion distributions--charge exchange neutral spectra, doppler shifted L_α radiation, and analysis of fusion reaction products.

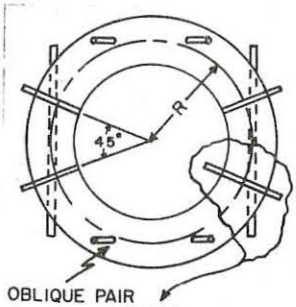

1- DIAGNOSTIC ACCESS

Operating Regimes The experimental design was, of course, based on the expected behavior of the plasma in ALCATOR. The accuracy of these predictions is limited by lack of prior plasma experiments in the particular regimes to be explored, but reasonable extrapolations can be based on existing theoretical considerations and experimental results. The transient heating and confinement of plasmas in Tokamaks is a complex nonlinear problem involving questions of varying particle and energy confinement times, widely changing resistivity, rapidly changing and possibly anomalous thermal transfer, current redistribution and many other such features. We have carried out extensive numerical analyses taking these factors into account. Typical transient and steady state plasma conditions are plotted in figures 2 and 3. The results are based on an accurate model of ALCATOR geometry, classical transfer of energy from electrons to ions, energy containment time as given by Gorbunov[1] and enhanced resistivity according to the model developed by Coppi[2] where the scaling parameters have been chosen to fit the existing data. In the operating regimes near the maximum ion temperature, β_p is of order 0.2. Similar calculations allowing for the possibility of enhanced transfer of energy from electrons to ions shows great sensitivity to small changes in this rate.

Ref: (1) E. P. Gorbunov et al. IAE-1681 (1968)
(2) B. Coppi and E. Mazzucato MATT-720 (1969)

* Supported by the United States Atomic Energy Commission

** The ALCATOR Design Group is comprised of B. Coppi, D. B. Montgomery, G. Bekefi, A. Bers, R. Blanken, R. Briggs, H. Kolm, L. M. Lidsky, R. Parker, P. Politzer and K. Thomassen, and has been augmented at times by other members of RLE and the Bitter Laboratory.

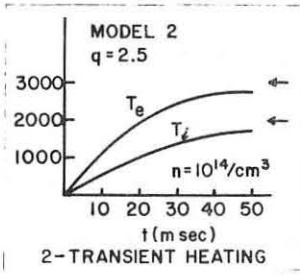

2-TRANSIENT HEATING

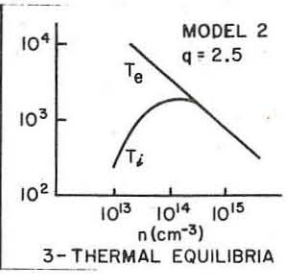

3-THERMAL EQUILIBRIA

LONGITUDINAL HEAT CONDUCTIVITY INVESTIGATION ON "TUMAN" DEVICE

M.G.Kaganski, S.G.Kalmikov, K.G.Shahovetz

A.F.Ioffe Physico-Technical Institute, Leningrad
USSR

Abstract: Measurements of a temperature gradient along the magnetic field are made in "Tuman" device. Measured plasma longitudinal heat conductivity coefficient is in agreement with a theory at plasma densities 10^{14}-10^{15} cm^{-3} and electron temperatures 10-20ev.

At ohmic heating in Tuman mashine the energy input is mainly in narrow toroidal parts while a main plasma bulk is in straight parts (figI). It is pointed out in the work [1] that a finite plasma heat conductivity along a magnetic field lines can lead to a temperature difference between the toroidal and the straight parts.

In this work experimental data on electron temperature are obtained for ohmic heating period. In the toroidal parts electron temperature is determined from plasma conductivity measurments. At the centre of the straight part electron temperature is determined from plasma diamagnetism and density measurments. The electron temperature is assumed much higher than the ion one in accordance with the work [1]. Experimental conditions and diagnostics are discribed in the work [1].

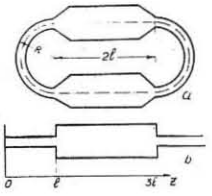

Fig.I. a. The real plasma configuration in "Tuman" device. b. The model used for calculation. $\pi R = 2\ell$

Results obtained from oscillograms for a typical regime are shown in fig.2. The changes in plasma density and conductivity temperature are small after 100 μsec. However in the straight part electron temperature rapidly falls with a decrease of energy input rate in the end of the discharge. A comparison of the curves (b) and (c) in fig.2 shows an existence of a temperature gradient in Tuman mashine. Measurments carried out over range of hydrogen pressures show a strong dependence of the temperature gradient on plasma density. Experimental data are presented in fig.3.

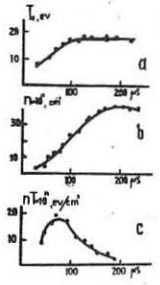

Fig.2.
a. Electron temperature obtained from conductivity measurments.
b. Plasma density.
c. Plasma diamagnetism. The discharge conditions p = 5mtorr, U = 750v, B_t = I8kG, B_s = 0,9 kG.

The balance equation for electron component energy is

$$\frac{\partial}{\partial t}\left(\frac{3}{2} n \kappa T_e\right) = q_h - q_{//} - q_{ei} - q_e - q_o - q_L \quad (I)$$

Here q_h is the energy input rate per Icm^{-3}; $q_{//}$ is the energy loss rate caused by heat flow along the magnetic field; q_{ei} - the energy loss rate due to electron-ion collisions; the energy losses q_e, q_o, q_L are due to light emission, diffusion and heat conductivity across the magnetic field.

Plasma column configuration in "Tuman" device is shown in fig.I (a). A correlation between plasma cross-sections in the toroidal and the straight parts is determined by a longitudinal magnetic field strength. In a typical regime B_t = I8 kG, B_s = = 0,9 kG. For the case of equal plasma conductivity the energy input rate $q_h = \frac{I^2}{\sigma}$ in the toroidal parts is 400 times higher then the energy input rate in the straight parts. Therefore we can neglect the direct energy input in the straight parts. An estimation shows that the basic role in the energy balance for the toroidal parts plays the heat stream along the magnetic field stimulated by longitudinal conductivity. The heat stream can be written in the form $q_{//} = -\varkappa \frac{\partial T_e}{\partial z}$. The heat conductivity coefficient $\varkappa$ can be taken [2] as $\varkappa = \alpha T_e^{5/2}$. For the toroidal parts equation (I) can be reduced to

$$\frac{\partial}{\partial t}\left(\frac{3}{2} n \kappa T_e\right) = q_h + \frac{\partial}{\partial z}\left(\varkappa \frac{\partial T_e}{\partial z}\right) \quad (2)$$

If the energy loss occurs along the magnetic field only our tusk is close to the problem of plasma energy loss in theta pinch [3].

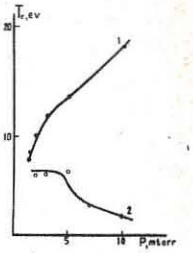

Fig.3. Variation of conductivity (I) and diamagnetic temperature (2) with pressure.

For the second half of a discharge plasma density and conductivity changes are small. Suppose $\frac{\partial}{\partial t}(n T_e) \approx 0$ we have

$$q_h + \frac{\partial}{\partial z}\left(\varkappa \frac{\partial T_e}{\partial z}\right) = 0 \quad (3)$$

In real conditions $q_h = q(z,t)$ but an essential change of the energy input takes place only near $z = \ell$. Therefore we assume for simplicity $q_h = q(t)$.

The equation (3) is solved at boundary conditions $\frac{\partial T_e}{\partial z} = 0$ at z = 0 (the condition of simmetry) and T_e = 0 at $z = \ell$. The condition $T_e = 0$ is a limiting case of a very strong plasma cooling in the straight part.

The solution of the eguation (3) has the form

$$T_e^{7/2} = \frac{7 q(t) \ell^2}{4\alpha}\left[1 - \frac{z^2}{\ell^2}\right] \quad (4)$$

This solution gives a correct description of some experimental results. The weak dependence of electron temperature from the energy input rate is in agreement with experimental data. The solution (4) also shows the plasma temperature doesn't depend on plasma density. In experiments some temperature raise was observed with an increase of density.

For plasma energy balance kanalisis in the straight parts the electron cooling caused by energy transfer to ions must be taken into account. The energy loss rate $q_{ei} = \frac{3 n k (T_e - T_i)}{2 \tau_{ei}}$ rapidly increases with a density raise. This effect can explain the experimental data shown in fig.3.

The equation (4) permits to determine the longitudinal heat conductivity coefficient. Temperature calculated from conductivity measurments is taken as T_e at z = 0; the ohmic heating energy input is calculated from plasma current and voltage oscillograms; ℓ = 30cm. The values of α obtained from the equation (4) are given by points in fig.4. The theoretical values of α obtained by Spitzer [2] are given in the same fig.4. (solid line). The plasma longitudinal conductivity over the range of experimental conditions is in agreement with the theory.

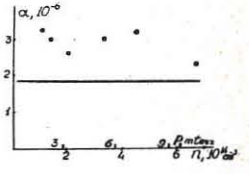

Fig.4.

REFERENCES

I. V.E.Golant and others. Plasma Phys., v.I, 277 (1969).
2. L.Spitzer, R.Harm. Phys.Rev., 82, 422, (1951).
3. T.S.Green and others. Phys.Fluids, 10, I663, (1967).

MAGNETIC SURFACES IN A QUADRUPOLE

by

J. H. Williamson, UKAEA Culham Laboratory, Abingdon, England.

ABSTRACT: Local imperfections in the magnetic field can alter the topology of the magnetic surfaces, thereby allowing plasma to escape. A modest longitudinal magnetic field will maintain the nested surfaces near the plasma boundary, so that the residual topological charges near the separatrix become unimportant.

The stability of plasma in a toroidal multipole is not much affected by the presence of an axisymmetric toroidal field B_ϕ as this merely opens out the closed lines of force to produce nested magnetic surfaces[1]. However, in any real device local imperfections will destroy the perfect symmetry and so cause the magnetic surfaces to break up and possibly reach the walls. On the whole, the toroidal curvature does not play an important role, so the results which follow were computed for a straight unshielded quadrupole. The closed lines of force in the unperturbed system were labelled by the coordinate z and the z-component of vector potential $A_z \equiv \Psi$. The origin of Ψ was chosen to be the separatrix, and ideally, plasma can be contained between the critical surface $\Psi = 1$ and $\Psi = -3.5$ which represents the surface of the conductors in CLIMAX[2].

One important class of local imperfections arises from defective joints in the conductors within the plasma. Measurements on CLIMAX showed that the peak perturbation field B_1 was greatest close to the conductor surface and at a distance of ±2 cm from the joint. Before the joints were properly tightened, B_1 was as large as 30% of B_0, but it has now been reduced to less than 3% at all joints.

If the perturbation B_1 is small enough, then the adiabatic approximation (the method of averaging) can be used. This assumes that lines of force follow their original closed orbits except for a slow drift in Ψ and z. As no lines of force may cross a magnetic surface, the flux threading any cross-section intersecting the surface is invariant. By Stokes' theorem this can be written as $\oint \underline{A}.d\underline{\ell}$ taken around the line of intersection which for convenience is chosen to be the unperturbed orbit. This integral is

$$\alpha(\Psi,z) = \oint \frac{\underline{A}_1 . \underline{B}_0 d\chi}{B_0^2}$$

because the zero-th order term $A_0.B_0$ vanishes everywhere. Fig. 1 shows the trajectories in Ψ, z space of the magnetic surfaces when B_1 is the field of a magnetic dipole centred on one conductor at z = 0 with its polar axis in the x direction. The trajectories do not depend on the magnitude of B_1: all that happens as B_1 is increased is that the surfaces are traced out more quickly. The full lines represent the surfaces which encircle only the defective conductor or both, while the broken lines represent those which encircle only the other conductor.

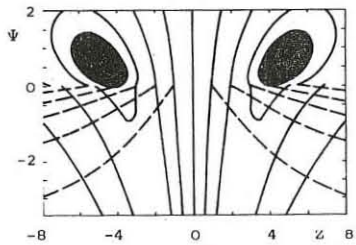

Fig.1 Projection of the surfaces

Because the separatrix $\Psi = 0$ has a field zero, the adiabatic approximation must break down in its vicinity. However, the magnetic surfaces are well defined for both positive and negative Ψ, and the region of invalidity shrinks as B_1 is reduced. We may therefore join up the surfaces across the separatrix.

In the stippled regions in Fig. 1, the magnetic surfaces are nested tori surrounding the two magnetic axes. The rest of the Ψ, z plane is occupied by a single surface with a rather complicated configuration. It can be thought of as being made up of a series of gloves having a thumb and only one finger, Fig. 2, one inside the other. The digits of each glove are pulled inside out and the finger sticks out through its own wrist, and ends by merging onto the wrist of a larger sized surrounding glove. The thumb ends while still inside the hand, so it merges onto the wrist of a glove which is smaller than its own. Lines of force move from one glove to another and, unless they chance upon the right mixture of thumbs and fingers, quickly reach a wall or conductor. Thus, no matter how small B_1 is, only the volume represented by the stippled regions can be used to confine plasma for an indefinite period.

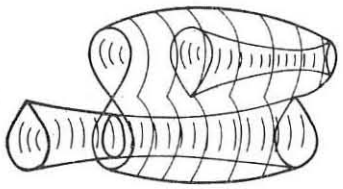

Fig. 2 Topology

The time scale for the drift motion depends on the size of the perturbation. When B_1 is 3% B_0, 5 eV electrons on the critical surface at z = 0 can reach the conductor in only 4 μs, compared with the observed plasma lifetime of 2 ms.

One way of trying to suppress the effects of local imperfections is to apply a uniform longitudinal field B_z of the same order as B_1. The vector potential can be taken to be $A_x = -yB_z$ and hence the invariant (which is the flux the long way round) is

$$\phi = \oint \underline{A}_1 . \underline{B}_0 \, d\chi / B_0^2 - B_z \oint y dx = \alpha(\Psi,z) - B_z v(\Psi)$$

where v is volume enclosed per unit length within the orbit Ψ.

When $B_z = 6.5\% \times B_1$ is applied (Fig. 3), closed magnetic surfaces exist both inside and outside the separatrix so that the topology of the surfaces in between becomes irrelevant and plasma can be contained along the whole length of the machine. It is of course preferable for B_z/B_1 to be greater than this minimal value as the break-down of nesting near $\Psi = 0$ will allow anomalously fast transport of plasma there. Combined with the ordinary diffusion mechanism in the outer regions, this will lead to an enhanced plasma loss rate.

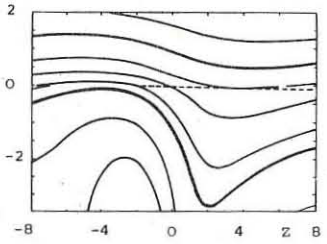

Fig.3 Effect of B_z

Further calculations have shown that if the perturbations remain within the scope of the adiabatic approximation ($B_1 \leq 10\% B_0$), the necessary B_z is minimised. For the worst perturbation now present in CLIMAX, B_1 = 3% B_0, B_z should be at least 0.17% B_0, typically 15G.

I am grateful to Dr. R. J. Bickerton for his critical appraisal of this work and to Dr. A. N. Dellis and his group who measured the perturbed field in CLIMAX.

References

1. FURTH, H.P., Advances in Plasma Phys. 1, 67, 1968. (Interscience, N.Y.)
2. ALLEN, T. K., et al, IIIrd European Conf. on Controlled Fusion and Plasma Physics, Utrecht, 8, 1969.

CONVECTIVE MOTION IN THE CLIMAX QUADRUPOLE PLASMA

J. H. P. C. Megaw, A. N. Dellis, R. Prentice and C. D. King
UKAEA Culham Laboratory, Abingdon, Berkshire, England

ABSTRACT: Measurements of plasma density and floating potential in CLIMAX indicate large scale convective flow, transporting plasma across the flux surfaces. A mechanism is proposed by which this flow can be set up due to localised regions of cold gas.

The Langmuir probe measurements of plasma ion saturation current, i_s, and floating potential, V_f, in the CLIMAX toroidal quadrupole [1], have been extended by simultaneously using six probes positioned around the major toroidal azimuth at angles θ = 27, 85, 155, 207, 295 and 333 degrees from the conical theta pinch gun (at θ = 0) used for plasma injection. Great care was taken to correct for slight differences in probe area by interchanging the probe positions.

Figure 1 is a plot of contours of equal i_s (representing plasma density n, in arbitrary units) in the Ψ,θ plane perpendicular to the magnetic lines of force, at time 600 μs after injection. The flux function Ψ measures the total magnetic flux between a given surface and the separatrix, Ψ = 0, where $\oint \frac{dl}{B} = \infty$. The minimum $\oint \frac{dl}{B}$ critical surface is labelled Ψ = +3 and the private flux surfaces inside the separatrix are given negative Ψ values. Figure 1 shows n to be strongly peaked near Ψ = 0, but with almost 2:1 variations in the θ direction. A plot 1 ms later shows this θ variation to be maintained as the overall density decays, in contradiction to what one would expect for plasma inside the critical surface, where $\underline{E} \times \underline{B}$ flow should be generated to equalise n along θ.

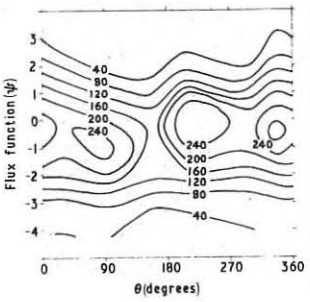

Fig.1

Figure 2 shows equipotential contours of V_f (in volts relative to the wall) in the same Ψ-θ plane. The arrows indicate the direction of $\underline{E} \times \underline{B}$. This plasma flow is essentially perpendicular to the expected equalising flow near Ψ = 0. Note the large disparity in linear scales between θ where 360° corresponds to ~500 cm and Ψ where Ψ = 0 and +3 average ~2 cm separation.

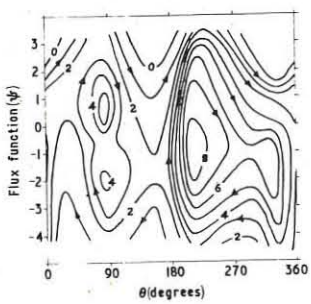

Fig. 2

One possible reason for the maintenance of the gradient $\partial n/\partial\theta$ is that the charge separation field produced by the ∇B particle flow is short-circuited because magnetic imperfections open out the lines of force to form magnetic surfaces, which connect regions of opposite space charge. These surfaces would correspond locally with the equipotentials. To test this, a 100 volt electron beam was injected along the field lines at θ = 90° on Ψ = -2 and intercepted, after undergoing ∇B toroidal drift, still on Ψ = -2 at θ = 27°. The observed equipotentials do not therefore coincide with the magnetic surfaces in this region. Further measurements will show whether there are field imperfections elsewhere.

The contour plots of n and V_f obtained on reversing the quadrupole ring current are shown in Figures 3 and 4 respectively. The regions of high density are still strongly correlated with those of most positive V_f so that the $\underline{E} \times \underline{B}$ flow is approximately reversed.

Although the base pressure in CLIMAX is ~10^{-8} torr, the

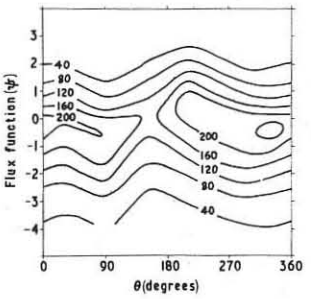

Fig. 3

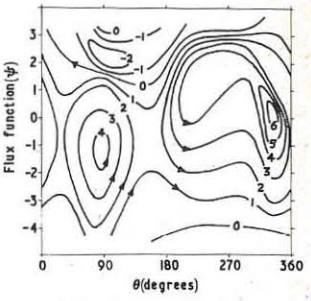

Fig. 4

0.06 cm^3 charge of hydrogen gas in the plasma gun will produce a diffusing cloud of neutral gas of pressure ~10^{-3} torr localised near the gun at about 1 ms after its release. This could be a major factor producing the convective flow observed. The initial ion energy ($T_i \approx$ 50 eV) will be removed in a few microseconds from ions ∇B drifting into this neutral gas. The direction of the ion ∇B drift velocity v_B reverses across Ψ = 0 and with the reversal of ring current, and is along +θ for negative Ψ in Figures 1 and 2. Since $v_B \propto T_i$, positive space charge will accumulate as the ions enter the neutral gas and are cooled. The negative space charge produced by the electron flow will be much less, since their rate of energy loss is less by a factor ~$(M/m)^{\frac{1}{2}}$.

This model is consistent with the observed sheared $\underline{E} \times \underline{B}$ flow at $\theta \sim 0$, and with the shift of the positive space charge centres across Ψ = 0 when the ring current direction is reversed. The θ components of $\underline{E} \times \underline{B}$ velocity are in the opposite direction to v_B and so a mechanism for limiting E to the order of T_i divided by the magnetic field scale length is produced. Larger E fields would prevent hot ions from reaching the neutral gas to produce the positive space charge.

The sheared $\underline{E} \times \underline{B}$ flow also observed near θ = 180° may be due to cold gas evolved from the wall during the initial injection phase.

Considerably help with the measurements by A. Marshall is gratefully acknowledged.

Reference

1. Allen, T. K., Dellis, A. N., Megaw, J.H.P.C., Prentice, R., Reynolds, D. A. and Ward, B. A; Proceedings of the 3rd European Conference on Plasma Physics and Controlled Fusion, Utrecht, 1969.

PLASMA MEASUREMENTS IN A LEVITATED PULSED OCTUPOLE

by

H. K. Forsen, D. W. Kerst, R. A. Breun, A. J. Cavallo
J. R. Drake and J. C. Sprott

PHYSICAL SCIENCES LABORATORY
THE UNIVERSITY OF WISCONSIN
Madison, Wisconsin U.S.A.

Abstract: Studies with levitated hoops in a pulsed toroidal octupole were undertaken with gun injected and microwave produced plasmas. Density decay rates were less than Bohm and were less with levitated hoops than with supported hoops.

A levitated toroidal octupole has been constructed to study plasmas in highly axisymmetric minimum B geometries in the absence of hoop supports. Major dimensions are shown in Fig. 1 and the magnetic field is supplied by a 5 kV, 0.6 MJ capacitor bank which provides 1.3 MA peak current with a half sine duration of 43 msec. Peak field is 14 kG and this gives a minimum of 22 gyroradii for 100 eV protons.

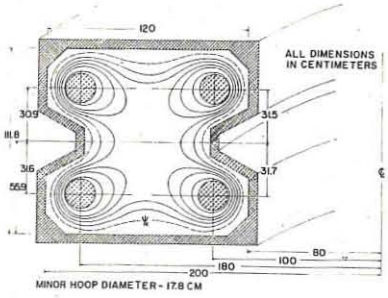

FIGURE 1

Magnetic field errors were minimized by distributing the primary and image current continuity windings to match the wall current density. The excitation gap edge was resistively trimmed to give an effective width proportional to the major radius. Tapered port plugs insure a thick skin contact when wedged in. Field errors at the surface of the hoops due to resistivity differences in the welds were measured and are less than 1%.

Sixteen pneumatically driven, bellows-sealed levators are used to support the four aluminum hoops whose total mass is 2300 kg. These supports are subsequently reinserted to catch the hoops.

Gun injection and vacuum pumping are all accomplished through a single 10 cm diameter opening. The aluminum vacuum tank of $8.6 \cdot 10^6$ cm^3 reaches a base pressure of $2 \cdot 10^{-6}$ torr with a turbo-molecular pump in parallel with a 25 cm diameter titanium orbitron pump. Pressures $2 \cdot 10^{-7}$ are reached using a single filament Mo-Ti wire located in the center of the lid but outside of $\Psi_{critical}$ and heated with 40 amperes to evaporate approximately 5 mg/hr.

Hot ion hydrogen plasmas with densities of $\approx 10^9$ cm^{-3} and $kT_e \approx 3$-5 eV are produced by a coaxial gun. Cold ion plasmas are produced in the field by electron cyclotron resonance heating using either high power (100 kW), pulsed (144 μsec), microwave heating at high pressure ($\approx 10^{-4}$ torr) to produce a plasma with $n \approx 10^8$ cm^{-3}, or by low power (100 W), CW heating at lower pressure ($\geq 3 \cdot 10^{-7}$ torr) to produce a plasma with $n \approx 10^9$-10^{10} cm^{-3} and $kT_e \approx 3$-5 eV. The CW source can be turned off abruptly to study the plasma decay in the afterglow. Hot electron plasmas in the kilovolt range are produced by gun injection or by CW microwave pre-ionization with subsequent high power pulsed microwave heating at low background pressure.

The decay of plasma density has been measured using Langmuir probes, 9 and 24 GHz microwave perturbation techniques and by integration of the ion flux to the wall, hoops, and supports. Electron temperatures have been measured using an admittance probe and a swept Langmuir probe.

For the hot ion, gun injected plasma and for the cold ion, microwave plasma, the density decay rate at peak magnetic field is somewhat slower than the rate calculated for Bohm diffusion and decreases slightly when the hoops are levitated, but further adjustments to attempt to decrease the decay rate have not yet been made. Figure 2 summarizes the results for gun injection.

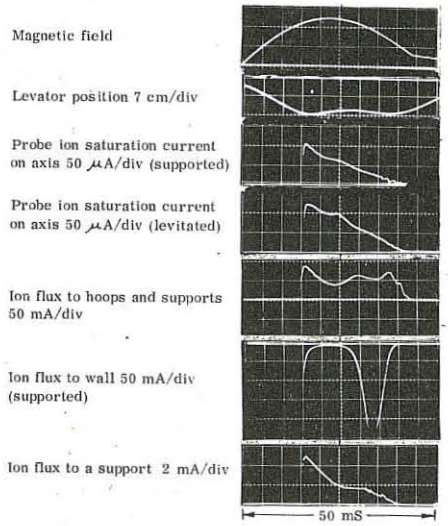

FIGURE 2

The lifetime of energetic electrons in the tail of the nonmaxwellian distribution, produced by pulsed microwave heating of gun injected plasma and measured with a scintillator probe near the edge of the plasma, shows a pronounced increase when the hoops are levitated, indicating that these electrons are lost primarily to the supports as suspected from measurements on the small octupole. The intensity and decay rate of the signal from the scintillator probe depends strongly on pressure even at the lowest pressure attained indicating that ionization losses are an important cooling mechanism for these electrons.

The density profile as measured by probes is peaked near the separatrix at early times with the peak moving out to the wall as the magnetic flux leaves the machine. The plasma is generally quiescent in the $\int dl/B$ stable region, but large ($\approx 100\%$) fluctuations in ion saturation current are observed in the flute unstable region near the wall. To get a measure of losses in the machine, and thus of plasma lifetime, the four hoops with their sixteen supports were used as ion collectors. Ion current to the hoops and supports was measured with all four hoops and their supports biased to -45 V relative to the tank wall. Ion current to the wall was measured by biasing the hoops and supports to +45 V. These measurements give a lifetime of $\approx$ 10-20 msec in agreement with measurements using Langmuir probes and microwave diagnostics.

Ion current to a single support was measured by withdrawing a support a short distance from the hoop and biasing it to -45 V. Ion flux to individual hoops and to hoops with and without supports are being measured to establish the validity of these loss measurements.

Acknowledgment: This work was supported by the U.S. Atomic Energy Commission. Fabrication was done by the staff of the Physical Sciences Laboratory, The University of Wisconsin.

CONTAINMENT TIME SCALING LAWS FOR PLASMA INJECTED INTO THE PROTO-CLEO STELLARATOR

D.J. Lees, R.A.E. Bolton, C.R.J. Hoffmann*, S.S. Medley* and P. Reynolds

U.K.A.E.A., Culham Laboratory, Abingdon, Berks., England.

(i) Introduction

It is important to establish the scaling properties of containment experiments in fusion since these can give useful guidance for the design of future experiments and illustrate the feasibility of a particular configuration as a possible reactor. This paper describes measurements made on the scaling of containment time with magnetic field and rotational transform using the PROTO-CLEO stellarator. The apparatus has already been described in its original form[1,2], but a 13 field period helical winding has now been fitted which gives almost twice the rotational transform and shear of the previous 7 field period windings. The parameters of the experiment in its later configuration are shown in Table 1.

Table 1
Parameters of PROTO-CLEO ℓ=3 stellarator experiment

Trap	
Major radius R	40 cm
Helical winding radius s	10 cm
Separatrix radius (to apex of trefoil) r_m	5 cm
Number of field periods on torus	13
Current at B_o = 5 kGauss. Helical winding I_ℓ	67 kA
Toroidal winding I_o	33 kA
Computed rotational transform at separatrix ι	1.08
Mean shear length $L_s = R/\iota$	37 cm
Mean shear parameter $\theta = r_m/L_s$	0.135
Useful time duration of magnetic fields	~ 10 msec
Plasma	
Injected from hydrogen occluded Titanium injector	
Initial density	3×10^{10} cm^{-3}
Electron temperature) measured 1 msec	4 eV
Ion temperature at 3 kGauss) after injection	20 eV

*National Research Council of Canada, Post-Doctorate Fellow CR70-92

(ii) Diagnostics

The average density across a diameter of the plasma is measured with a 16 mm microwave interferometer. In the absence of recycling the particle containment time is taken as equal to the density decay time. Electron and ion temperatures are measured with a swept double probe and a multigridded analyser respectively.

(iii) Scaling of containment time with magnetic field

The dependence of particle containment time on magnetic field is shown in Figs 1 & 2 for the 7 and 13 field period helical windings respectively. These measurements are made with the electron temperature, as far as possible, kept constant and with a constant ι, that is to say a constant ratio of B_o/I_ℓ. The ion temperature is however varying with field: it has been established that T_i is a linear function of B_o. This is possibly due to the method of injection in which the force driving plasma across field lines to within the separatrix depends on the value of the magnetic field.

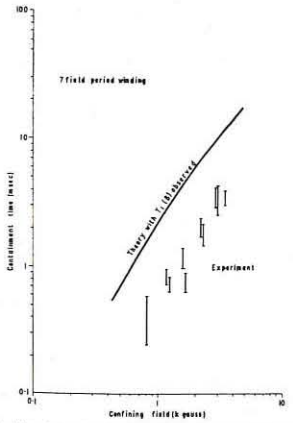

Fig.1 Containment time as a function of confining magnetic field for 7 field period helical winding.

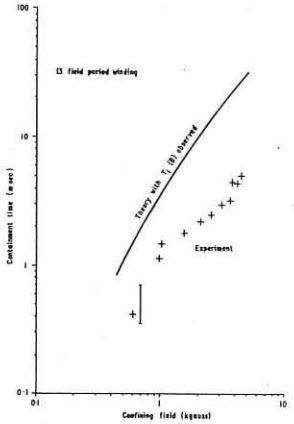

Fig.2 Containment time as a function of confining magnetic field for 13 field period winding.

(iv) Scaling of containment time with rotational transform

In this case the containment time is measured as a function of the current in the helical winding with the confining magnetic field, electron temperature and ion temperature constant. As I_ℓ is increased from zero the separatrix radius remains constant at ~ 0.8 s and ι increases until at a critical value of I_ℓ, ι has reached its maximum value of 30° per field period. As I_ℓ is increased beyond this ι remains constant but the separatrix radius decreases. The results of Fig.3 therefore show τ plotted against the computed value of $\iota_{max}\, r_m^2$, rather than as a function of I_ℓ for both 7 and 13 field period windings. It is seen that the results for both windings lie on a smooth curve.

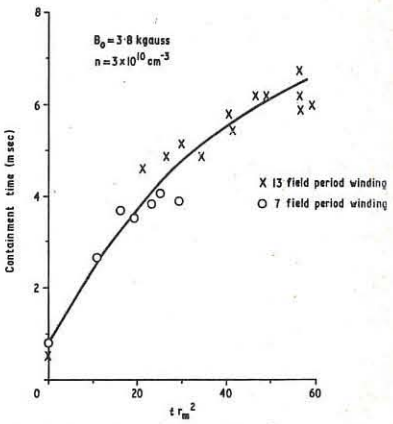

Fig.3 Containment time as a function of the maximum rotational transform × (separatrix radius)² for 7 and 13 field period helical windings.

(v) Discussion

The significance of Fig.3 lies in the fact that at the same value of ι the shear parameter at the separatrix for the 13 field period helical winding is about twice that of the 7 field period winding, but that nevertheless the results lie on the same curve for both windings. Thus the indications are that the containment time appears to scale with ιr_m^2 and not θ, at any rate in our case in which $\theta > 0.06$. Since the containment time is given, for a Bessel function distribution of density, in terms of the diffusion coefficient as $\tau = r_m^2/5.7\, D_\perp^{-1}$ thus we conclude that $D_\perp$ scales as ι^{-1}. This scaling appears to be true except at large values of ιr_m^2. It is possible here that the computed value of ι may be larger than the actual value due to non-closure of magnetic surfaces. This scaling is in agreement with the predictions of the theory of equilibrium in toroidal traps. Since for the case of PROTO-CLEO with the parameters given $R/\iota < \lambda_{ei} < R/\iota\ (R/r_m)^{3/2}$ where λ_{ei} is the electron-ion mean free path, the appropriate diffusion coefficient is that given by Galeev and Sagdeev[3,4] modified by Stringer[5], viz:- $D_\perp = \sqrt{\pi}/2\ r_{ce}/R_\iota\ k(T_e + T_i)/eB$. This predicts a containment time which should scale as B^2. If, however, we take the observed variation of T_i with B into account we find that the predicted containment time is given by the full curves of Fig.1 and 2. This scales with field approximately as the experimental points although the absolute value is greater than the observed value by a factor of ~ 5. It should be noted that the above formula applies only to the axisymmetric toroid. However in this density range localized particle diffusion is not expected to be important and thus we may expect the axisymmetric formula to be applicable to our results.

(vi) Conclusions

We have shown that if we fold in the observed variation of T_i with field the agreement between measured containment time and theory is correct in scaling and differs by only a factor 5 in magnitude for the intermediate collisional region, except for high values of rotational transform.

(vii) Acknowledgements

The authors gratefully acknowledge the experimental help given by Messrs P.A. Shatford and D.R.A. Webb: we are also grateful to Mr T.E. Stringer for helpful discussions. Finally we thank Dr R.J. Bickerton for his advice and encouragement throughout.

References

1. Adlam, J.H., et al., Plasma Physics and Controlled Nuclear Fusion Research, Novosibirsk Conf.Proc.1968, Vol.I.p.573.
2. Lees, D.J., et al., 3rd European Conference on Controlled Fusion and Plasma Physics, Utrecht Conference Proceedings 1969, p.4.
3. Galeev, A.A., and Sagdeev, R.Z., Sov.Phys.J.E.T.P. 26 (1968) 233.
4. Sagdeev, R.Z., and Galeev, A.A., Doklady Akademii Nauk, 189, (1969) 1204.
5. Stringer, T.E., Physics of Fluids 13 (1970) 810.

PLASMA LOSS RATE IN THE CLASP STELLARATOR
COMPARISON WITH CLASSICAL DIFFUSION

J. Hugill, G. W. Reid, K. B. Axon, W. G. F. Core
UKAEA Culham Laboratory, Abingdon, Berkshire, England

Abstract: Experiments on a small stellarator with $\ell = 3$ helical windings at field strengths up to 2000 Gauss show nearly classical confinement of an argon plasma with $n_e \sim 10^{10}cm^{-3}$, $T_e \sim 1$ eV. Experimental results are compared with the theory of Galeev and Sagdeev in the intermediate collisional regime.

Introduction

The Clasp stellarator has $\ell = 3$ helical windings with 8 field periods on the torus. The major radius is 300 mm and the helical winding mean radius 116 mm. The vacuum vessel is inside the helical windings and has a limiter with a radius of 58 mm. Field strengths up to 2000 Gauss are used.

We have studied the confinement of an argon plasma with $n_e \sim 10^{10}cm^{-3}$ and $T_e \sim 1$ eV as a function of field strength and rotational transform, with a view to establishing whether this is classical or Bohm-like[1].

Plasma production and diagnostics

The plasma is produced by the ionisation of neutral gas filling the vacuum vessel, by fast electrons from a hot tungsten filament stretched across the minor diameter. The emission current is 3 mA, and the bias -200 volts with respect to the conducting walls.

Plasma confinement is studied after switching off the filament and isolating it electrically.

The frequency shift of a cavity resonance near 20GHz is used as a measure of the total number of electrons in the vacuum vessel. Together with probe measurements of the plasma profile, this gives electron density, decay time and plasma radius.

The electron temperature is measured from the current - voltage characteristic of a probe obtained by applying a ramp waveform at intervals of 1 ms.

Results

Two scaling experiments were done:

1. The magnetic field strength, B, was varied from 500 to 1500 Gauss keeping the rotational transform, ι, constant. The plasma density decay time, τ, increased more slowly than B^2 because n_e and T_e increased with B. However, the magnitude of the decay time is within a factor 3 of the theoretical value, in the Galeev-Sagdeev intermediate collisional regime, and is 13 x the Bohm time.

2. ι was varied, keeping B constant, first at 1620 Gauss. For $\iota < 0.1$ radians, the plasma appeared to be in contact with the limiter. Under these conditions the equilibrium is influenced by currents which flow through the limiter or conducting vessel, and the diffusion time is approximately equal to the Bohm time[2]. As ι is increased the decay time increases while the Bohm time falls, because T_e increases slightly, and the plasma radius decreases. τ is within a factor of 2 of the theoretical value, for ι up to 0.8 radians.

At 810 Gauss ι can be increased up to 3.5 radians. Again τ is approximately equal to the theoretical value for $\iota < 1.4$ radians. At higher values of ι a larger discrepancy appears. The theoretical decay time continues to increase while τ levels off, or even falls slightly. This is accompanied by a reduction in the plasma radius below what is expected, such as may be accounted for by the magnetic surfaces near the separatrix being open.

In conclusion, we find the measured decay time agrees with the classical diffusion time in magnitude, and in scaling with B and ι, except for $\iota < 0.1$ and $\iota > 1.4$ radians. The variation of τ with B is incompatible with Bohm diffusion.

One characteristic of the plasma profile is worth mention. Typically, the maximum of the plasma density is not co-incident with the magnetic axis, but is displaced away from the major axis. Fig. 1 shows an example. L marks the position of the limiter, and S the calculated position of the outermost closed magnetic surface inside the limiter: in this case the separatrix. The outward displacement of the plasma is 11 mm. This phenomenon may be associated with the breakdown of the condition that the flow velocity around the torus necessary for equilibrium does not exceed the sound speed[4]. Near the centre of the confinement region, where ι is very small in $\ell = 3$ stellarators, this condition is difficult to satisfy. The profile can be made more symmetrical by applying a vertical field such as to move the magnetic surfaces towards the major axis. This also removes the zero in ι at the magnetic axis, but there is no significant change in confinement time.

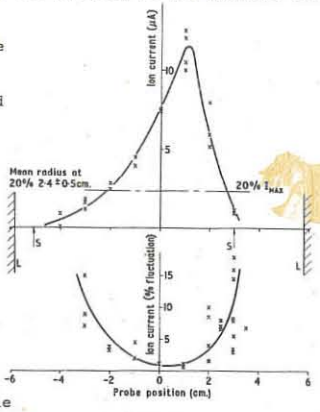

Fig.1.

Comparison with theory

As noted above, it is difficult to do scaling experiments in which only one parameter is varied. Very often density and temperature variations and changes in plasma profile accompany changes in B and ι. However, an overall picture can be obtained by allowing for these unwanted variations.

Figure 2 shows a plot of the ratio of τ to the Pfirsch-Schlüter confinement time (assuming a Bessel function profile, and ignoring variations in ι and B across the plasma column) against a parameter, α, equal to the ratio of connection length to the electron-ion mean free path.

Fig.2

X CLASP

O PROTO-CLEO

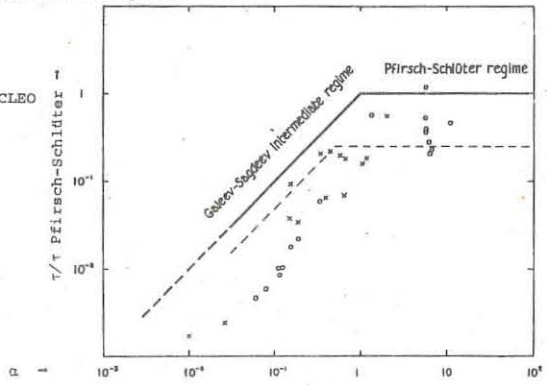

The solid lines show the theoretical confinement time, and the experimental points are those from the experiments described above, and from another stellarator experiment, PROTO-CLEO, which uses a gun-injected H_2 plasma with $T_i \sim 20$ eV, $T_e \sim 5$ eV and $n_e \sim 10^{10}cm^{-3}$.

All the experimental points are within a order of magnitude of the theoretical curve and show a similar trend with α. If an average value for ι instead of the maximum value, is inserted in the expression for the Pfirsch-Schlüter confinement time, the dotted curves represent the theoretical values, and show better agreement with the experiments.

References

1. A. Gibson, J. Hugill, G.W.Reid, K.B.Axon "Plasma confinement in CLASP", submitted to 'Nuclear Fusion'.
2. K.M.Young, S. Yoshikawa, R.M.Sinclair, Phys.Fluids 9 1447,1966.
3. A.A.Galeev,R.Z.Sagdeev, ZETP 53, 348, 1967.
4. D. Pfirsch, A.Schlüter, Max Planck Inst.Rep.MPI/PA/7/62,1962.

CONTAINMENT OF STEADY-STATE, ELECTRON-CYCLOTRON HEATED PLASMA IN A STELLARATOR

by
K. M. Young and W. Stodiek
Plasma Physics Laboratory, Princeton University
Princeton, New Jersey, 08540, USA

Abstract: Low density steady state hydrogen plasmas created by low power electron cyclotron heating in the C stellarator show containment times close to the Bohm value. The relative containment increases by about a factor three with helical transform, similar to results obtained for gun-produced and Ohmic heated plasmas.

Under conditions for which the electron mean free path was longer than the axial length around the C stellarator, modest improvements in containment over the Bohm value have been reported. [1, 2] The relative containment (defined as the ratio of the containment time to the Bohm value obtained from the magnetic field and temperature) increased with the transform up to a value about four. [1, 2] We describe here a study of low-density steady-state hydrogen plasmas produced by electron cyclotron resonance heating, the resonance region being located in the divertor. [3] The plasma has typically an electron temperature of 7 eV with an electron mean free path of ten machine lengths. The electron density is about 1×10^{9} cm^{-3} in a neutral background of 3×10^{10} cm^{-3} for a power input of a few watts. The confining field strength is 10 kG and the radius is 5 cm. Although the primary heating of the electrons takes place in the divertor, measurements of total light and the effects of insertion of large probes into the plasma at points outside the divertor mirror demonstrate that ionization takes place all around the machine.

The plasma confinement time and its dependence on the helical field has been investigated for these discharges. The confinement time is determined from measurements of flux and density during the steady state and from the decay after the power is shut off. The electron density is determined from 8 mm microwave interferometers, ion saturation current of Langmuir probes, and low amplitude, low frequency (500 Hz to 10 kHz) impedance measurements. The density determinations, from the interferometer and Langmuir probes are in fairly good agreement and the interpretation of the result is not very sensitive to a correct knowledge of the density profile. But for the determination of the density from plasma impedance measurements, the correct density profile must be considered. The flux was determined by flux collectors in the divertor and from the consumption of the neutrals. The temperature was determined from Langmuir probes, an energy analyzer, and the low frequency impedance. Within the experimental error, the temperature measurements are in agreement, but the energy analyzer also indicates the existence of a higher energy tail. During the density decay after the power is shut off, a comparison of the density decay time and the time obtained from flux and density measurements indicates that plasma production continues for at least 30 milliseconds. The light observed by a detector viewing the divertor throat has only decayed to about 25% of the steady value in this time. This level is inconsistent with recombination or with uniform ionization at the observed "temperature" of 2 eV. From this result we conclude that about 10% of the electrons have an energy as high as 600 eV, so as to survive as long as 30 milliseconds as ionizing particles, when the power is switched off. Although the falsification of the electron temperature of the bulk plasma by this tail may be small, ionization rates computed from this "temperature" can be underestimated by orders of magnitude.

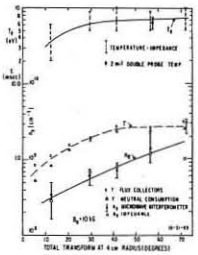

Fig. 1. Containment time, density and electron temperature as a function of $t = \frac{1}{q}$ total transform for constant power input.

Instigated by the investigation of gun-produced plasmas, the main emphasis of these experiments with long mean free path plasmas was on the dependence of the confinement on helical transform. Figure 1 is a summary of data from various series of scans of the helical field currents with closely the same input power. As the helical field current is increased, the most obvious effect is the increase in density, and neutral consumption. We note that the measured temperatures of the bulk of the plasma are not greatly different over our range and the observed change with transform in decay time is not greater than a factor of 4. The longest observed decay time gives τ/τ_{Bohm} not more than 3. Measurements of magnetic surfaces by Hosea and Sinclair [4] indicate a smaller effective aperture at high rotational transforms which would increase our values slightly. Because density and flux measurements refer essentially to the bulk of the plasma of about 7 eV so does the derived confinement time. The electron mean free path is about ten machine lengths under these conditions. Although the range covered for the electron cyclotron heating was quite small, no significant dependence of the confinement on the mean free path was observed. We cannot make a definite statement about the containment of the high energy tail of the electron distribution. The apparent contradiction between these results and those reported by Gorman et al. [5] can be removed by direct measurement of ionization rates rather than computing them from the conductivity temperature which is very inaccurate in the presence of a high energy electron tail providing most of the ionization. [6] All the containment results are then closely similar to previous work with gun plasmas. [1]

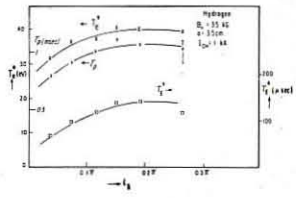

Fig. 2. Effect of the transform due to the $\ell = 2$ helical winding for constant Ohmic heating current discharges. τ_E^* and τ_E^* are the observed energy containment times and temperature and τ_p is the particle containment time.

On the basis of our present knowledge the scatter in the gun experiments can be attributed to ionization and heating by energetic electrons if their population varies irreproducibly from shot to shot. There is probably very little difference, if any, for the confinement properties of the bulk of the electrons in the gun-produced and microwave-produced plasmas in the C stellarator. Both show about a factor 3 longer confinement than the Bohm value with a weak dependence on the helical transform. The information about the dependence of confinement on helical transform in Ohmic heated discharges, at much higher density, is contradictory but the dependence could possibly be of the same order as observed in these discharges. [2, 7] An example is given in Fig. 2. The physical reason for the observed dependence of the confinement on the helical field is not clear. It is also not known whether the dependence is on transform or on shear. No sudden change in containment is observed which would be related to the suppression of an instability at a critical value of transform.

This work was performed under the auspices of the U. S. Atomic Energy Commission.

1. D. J. Grove, E. B. Meservey, W. Stodiek, K. M. Young, Plasma Physics and Controlled Nuclear Fusion Research, Conference Proceedings, Novosibirsk, 1-7 Aug. 1968 (IAEA, Vienna, 1969), Vol. 1, p. 479.

2. I. G. Brown, D. Dimock, E. Mazzucato, M. A. Rothman, R. M. Sinclair and K. M. Young, Plasma Physics and Controlled Nuclear Fusion Research, Conference Proceedings, Novosibirsk, 1-7 Aug. 1968 (IAEA, Vienna, 1969), Vol. 1, p. 497.

3. W. Stodiek, D. J. Grove, and J. O. Kessler, Plasma Physics and Controlled Nuclear Fusion Research, Conference Proceedings, Culham, 6-10 September, 1965 (IAEA, Vienna, 1966), Vol. II, p. 687.

4. J. C. Hosea, G. V. Sheffield, R. M. Sinclair and T. Tamano, Princeton Plasma Physics Laboratory Report MATT-785 (1970).

5. J. G. Gorman, and J. Orens, Bull. Am. Phys. Soc. 13, 1538 (1968), J. G. Gorman, I. G. Brown, G. Lisitano, J. Orens, Phys. Rev. Letters 22, 16 (1969).

6. K. M. Young, W. Stodiek and J. G. Gorman, Princeton Plasma Physics Laboratory Annual Report MATT-Q-27 (1970).

7. R. M. Sinclair, S. Yoshikawa, W. L. Harries and K. M. Young, Princeton Plasma Physics Laboratory Annual Report MATT-Q-21 (1964).

ION CYCLOTRON RESONANCE HEATING EFFICIENCY IN THE MODEL C STELLARATOR

by

J. C. Hosea, R. M Sinclair, and T Tamano
Plasma Physics Laboratory, Princeton University
Princeton, New Jersey, 08540, USA

Abstract: In an attempt to elucidate the cause of the reduced ICRH heating efficiencies previously observed on Model C, we have measured this efficiency over a broader range of density than hitherto [$10^{10} \leq n(cm^{-3}) \leq 10^{13}$]. We find that the efficiency is very strongly dependent on density, suggesting a density dependence of wave absorption in the beach and/or wave attenuation along the plasma column.

Diamagnetic pressure measurements taken previously on the Model C stellarator show that under optimum conditions, at a density of 6×10^{12}, only about 20% of the power delivered to the plasma at the Stix coil is transferred into ion energy. [1] We have recently demonstrated that the coil loading attributable to the plasma is caused by ion cyclotron waves alone and thus that extraneous losses in the coil circuit cannot be invoked to explain the reduced heating efficiency. [2] Therefore, wave attenuation along the plasma column or incomplete absorption of the wave at the magnetic beach would appear to be responsible for the mysterious loss of power.

In an attempt to explain this last unresolved feature of ion cyclotron resonance heating (ICRH) in the Model C stellarator, we have performed a series of heating experiments which cover a wide range of operating parameters. The effect of the magnetic field, for several axial field patterns, [1, 3] has been studied using deuterium plasma, formed at several background pressures, with plasma densities over a broader range than hitherto [$10^{10} \lesssim n(cm^{-3}) \lesssim 10^{13}$]. For diagnosing the effect of the ion cyclotron waves on the plasma, we have employed diamagnetic loops, neutron counters, and parallel conductivity measurements in addition to the coil loading and density diagnostics.

First, we have observed neutrons due to heated ions in the plasma over the entire range of plasma density quoted above. The hot ions appear to have been confined primarily to the mirror regions in the ICRH straight section [1] of the stellarator racetrack where a horizontal scan with a collimated neutron counter indicated (marginally) that the neutrons were coming from the plasma volume as opposed to the vacuum vessel wall. Secondly, both (1) direct ion heating under the coil and (2) wave heating in the beach occurred for $\Omega = \omega/\Omega_i$ (coil excitation frequency divided by the cyclotron frequency) equal to or less than the value 1 respectively. Neutron and diamagnetic pressure measurements combined to prescribe an ion temperature of a few keV in the straight section of the stellarator for both types of heating [(1) and (2) above] over a wide range in density with the power incident to the coil for 1 msec set at 1.5 MW. (This power also supplies coil losses and the power actually delivered to the plasma decreases as density decreases. [3]) And finally, it was possible to utilize the ion cyclotron waves to produce the plasma, rather than an Ohmic heating current. Complete ionization was obtained with a 1 msec power pulse for a gas pressure of 2×10^{-5} Torr ($n_{max} \sim 6 \times 10^{12} cm^{-3}$) and for the lowest pressure considered, 1×10^{-6} Torr, the ion cyclotron waves developed a plasma even though the breakdown oscillator preionization was imperceptible.

Heating efficiency was investigated over an extended gas pressure interval (2×10^{-6} to 3×10^{-5} Torr) for the magnetic field configuration of Fig. 1(a). A breakdown oscillator produced a moderately ionized plasma and then a 1.5 MW, 1 msec, 25 MHz ICRH power pulse was applied. By varying the magnetic field level it was found that for the higher gas pressures the diamagnetic pressure was maximized when the field level was sufficiently elevated to place the magnetic beach in the U-bend as was the case in Ref. 1. The line for $\Omega = 1$ at this diamagnetic pressure maximum is indicated in Fig. 1(a), and the axial profile of diamagnetic pressure in the stellarator straight section is presented in Fig. 1(b). (The U-bend diamagnetic pressure was typically one-half or less of the minimum recorded for the profile segment of Fig. 1(b).) When the gas pressure was sufficiently reduced ($\lesssim 5 \times 10^{-6}$ Torr), peak diamagnetic pressure was observed for a lower magnetic field level (larger Ω) and, consequently, for a magnetic beach in the straight section. However, the pressure profile retained the form of Fig. 1(b).

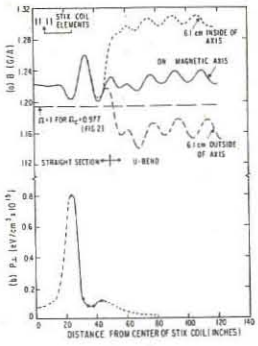

Fig. 1(a). Flat magnetic field configuration. (b)Diamagnetic pressure profile ($n = 3.7 \times 10^{11} cm^{-3}$).

The final heating efficiency found for the maximum diamagnetic pressure condition is plotted in Fig. 2 versus plasma density at the end of the ICRH pulse, along with the rf energy delivered to the ion cyclotron waves at the Stix coil, the diamagnetic pressure in the mirror region adjacent to the coil, and the neutrons emitted from this same mirror region. This efficiency is for the time just preceding the end of the heating pulse and is equal to the percentage ratio of the power sustaining the perpendicular plasma energy $P_\perp^*$ to the power actually delivered to the plasma at the Stix coil (exclusive of copper losses), with

$$d\int p_\perp dV/dt = P_\perp^* - \int p_\perp dV/\tau_c \qquad (1)$$

where we assumed τ_c is equal to the cooling time constant immediately following the pulse. Figure 2(a) shows that the efficiency for wave heating of the plasma decreased rapidly with decreasing density and was anomalously low even at the highest density considered. The level of efficiency is somewhat uncertain (~factor 2), since we did not have diamagnetic loops under the Stix coil, but the relative dependence of efficiency on density should not be affected by this uncertainty since the diamagnetic pressure profile was the same for all the densities studied.

The final efficiency obtained for the "long beach" magnetic field case in Ref. 1 is also plotted in Fig. 2(a) for $n = 6 \times 10^{12}$ cm^{-3}. Lastly, the efficiency for the "10% beach" field configuration, [4] obtained in the present study for an ohmically heated plasma, is also plotted for $n = 10^{13} cm^{-3}$. These data combine with the flat field data to demonstrate that the low heating efficiencies are not attributable to the magnetic field profile but result from a density dependence of wave absorption in the beach and/or of wave attenuation along the plasma column. [The efficiency for B66[6] (49% for $n = 2.5 \times 10^{13} cm^{-3}$) also falls in line with those of Fig. 2(a).] The reduced wave absorption interpretation requires that wave energy not be absorbed by the plasma beyond the beach. If wave attenuation is to be the explanation, there must be an enhanced heat transfer from the plasma during the ICRH pulse.

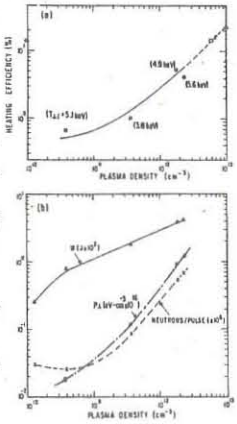

Fig. 2(a). Final efficiency of ICRH. (Field profile: ●-Fig. 1; ■-Ref. 1; ▲-Ref. 4.) (b) RF energy supplied to plasma W, max. diamagnetic pressure $p_\perp$, and neutrons emitted from the magnetic well adjacent to Stix coil.

An earlier attempt to observe ion heating at lower densities [5] apparently failed due to the very low heating efficiencies in conjunction with the reduced coupling at the coil because of the axial nonuniformity of the magnetic field configuration employed. [3]

[1] M.A. Rothman et al., Phys. Fluids 12, 2211(1969).

[2] J.C. Hosea and R. M. Sinclair, PPL Annual Report (1969).

[3] J.C. Hosea and R. M. Sinclair, Phys. Rev. Letters 23, 3 (1969).

[4] I. G. Brown et al., Phys. Fluids 12, 1318 (1969).

[5] I. G. Brown et al., Plasma Physics and Controlled Nuclear Fusion Research (IAEA, Vienna, 1969), Vol. I, p. 497.

[6] W. M. Hooke et al., Phys. Fluids 8, 1146 (1965).

NEW DATA ON PLASMA CONFINEMENT IN THE HIGH-SHEAR "URAGAN" STELLARATOR

Diky A.G., Zalkind V.M., Konovalov V.G., Pavlichenko O.S., Pavlova G.P., Souprunenko V.A., Tonkopryad V.M., Tolok V.T.

Physical-Technical Institute of Academy of Sciences of Ukr.SSR, Kharkov, USSR.

Abstract: The results of measurement of charged particle confinement on "Uragan" stellarator are given in this report. The recycling effect has been excluded by a spectroscopical procedure. Results reported earlier in Dubna [1] are confirmed.

The results of measurement of charged particles and energy confinement times in ohmically heated plasma in the high-shear "Uragan" stellarator were reported in Dubna in 1969 [1]. It was shown the confinement times of particles and energy to increase significantly with increase of transformation angle and shear, and to reach the value of $30\tau_s$ and $4\tau_s$, respectively (τ_s - is so-called Bohm time). Some assumptions were made about mechanism of particle and energy losses.

In these experiments the plasma confinement time was determined from escape rate of charged particles over an active discharge phase. Possible contribution of ionization of gas delivered into plasma during the discharge (recycling) was estimated in indirect manner on a basis of data obtained on "C" stellarator [2]. It was of some interest, however, to make a direct account of recycling influence, especially because there exists a procedure developed [3]. In the report given the results of measurement of the charged particle confinement time with allowance made for recycling are presented.

The experiments were made on ohmically-heated helium plasmas in the racetrack-stellarator "Uragan". Conditions of the experiment and plasma parameters are illustrated by Table 1.

The charged particle confinement time can be defined from the particle balance equation for electrons which takes the following form for helium plasma:

$$\frac{dn_e}{dt} = n^{\circ} n_e Q_i^{\circ} + n^{+} n_e Q_i^{+} - \frac{n_e}{\tau_n} \qquad (1)$$

where n_e, n°, n^{+} - are electron, neutral and single-ionized helium densities, $Q_i^{\circ,+}$ - ionization rate coefficients of neutral and single-ionized helium respectively. Densities of neutral and single-ionized helium can be obtained from measurements of absolute intensities of spectral lines. If corona model is applicable, equation (1) will take the form:

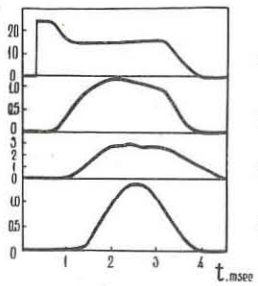

Fig.1

$$\frac{dn_e}{dt} = \frac{I_{km}^{\circ} \sum A_{kl} Q_i^{\circ}}{h\nu_{km} A_{km} \delta_e^{\circ}} + \frac{I_{np}^{+} \sum A_{ns} Q_i^{+}}{h\nu_{np} \delta_n^{+}} - \frac{n_e}{\tau_n} \qquad (2)$$

where $I^{\circ,+}$ are intensities of spectral lines HeI and HeII, $\delta^{\circ,+}$ - corresponding excitation rate coefficients.

In experimental conditions on "Uragan" stellarator, the applicability of corona model for description of population processes of excited levels of neutral helium atoms must be confirmed additionally. It should be noted, however, that corona model gives the lower limit of excited level population and therefore the upper limit of atom (or ion) density $n^{\circ,+}$ determined from spectral line intensity. With allowance made for this fact, we perform an upper extimation of ionization rate in equation (1) by measuring absolute intesities of spectral lines HeI 5015,7 Å ($2s^1S-3p^1P^{\circ}$) and HeII 4685,7 Å ($3d^2D-4f^2F^{\circ}$) on a basis of corona model.

Plasma radiation from discharge was recorded side-on on the racetrack plane through the window an a straight section by the two-channel monochromator calibrated with a standard radiation source. The electron density was measured by the microwave interferometer (λ = 8 mm), and the electron temperature was estimated from plasma conductivity.

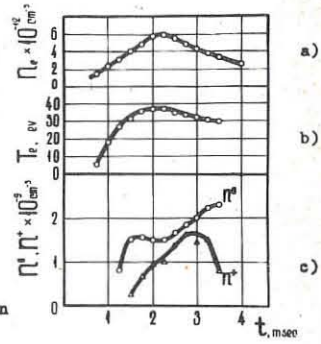

Fig.2

Fig.1 shows typical traces of voltage across the bypass (a), discharge current (b), intensity of spectral lines HeI 5016 Å in 10^{12} photon/cm^3 sec units (c) and HeII 4686 Å in 10^{13} photon/cm^{3}sec units (d). In Fig.2 one can see the history of temperature (b) and densities (a) of electrons, neutral atoms, and single-ionized atoms (c). Fig.3 illustrates the dependence of confinement time τ_n, reduced to a constant plasma diameter, upon parameter $\varepsilon = \frac{h_3}{H_z}$ obtained earlier without recycling corrections (h_3 is the first harmonic of helical field). Data corrected on ionization are marked with dots. The ionization account is seen to lead to a correction in τ_n which doesn't exceed 10%.

Thus, in the present communication the results obtained earlier about collisional plasma confinement in the high-shear stellarator are confirmed.

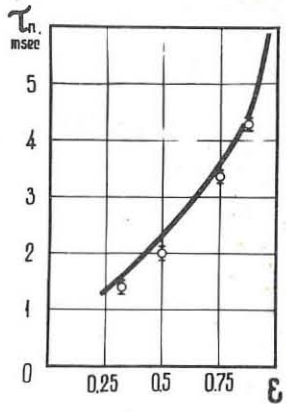

Fig.3

Table 1

Magnetic field	-	4,8 koe.
Shear θ_{max}	-	0,085.
Pressure	-	$1{,}4\cdot10^{-4}$ torr.
Electron density	-	$1\div6.10^{12}$ cm^{-3}.
Electron temperature	-	10 ÷ 40 eV.

References

[1]. Vishnevetsky V.N. et al. International Symposium on Closed Confinement Sytems. Dubna (1969).

[2]. Harries W.L. et al. Phys.Fluids, 7, 151 (1964).

[3]. Hinnov E. and Bishop A., Phys.Fluids, 9, 195 (1966).

THE EFFECT OF THE DIVERTOR MAGNETIC SURFACE ON TOROIDAL DRIFT OF A PLASMA

V.G.Zykov, V.I.Karpukhin, N.I.Rudnev, V.T.Tolok.
Physical-Technical Institute of the Academy of Sciences of the Ukr.SSR.
Kharkov, 108, USSR.

Abstract: It is shown that divertor magnetic field decreases the toroidal drift of a plasma. This is caused by the fact that polarisation electric field is removed by current which flow along magnetic lines of force and are shortened through the annular region of the divertor where the magnetic field equals zero.

It was shown recently [1,2], that when a plasma is injected into a stellarator through divertor magnetic slits a stable cylindrical plasma surface is formed in a region adjacent to annular line of magnetic field zero, i.e. in the region of divertor magnetic aperture. The stability of a plasma at the divertor surface is connected with the fact that the latter is a bottom of a magnetic well where $H = 0$ and potential $U = -\int \frac{dl}{H}$ has its minimum [3]. The stability of divertor or "heliotron" configuration was shown also in [4]. It was of interest to make clear the influence of that configuration on plasma toroidal drift in closed magnetic traps. One end of the stellarator "Syrius" divertor [1] was joined to a half-toroid, the large radius of which being 40 cm and inside of the tube - 7 cm (fig.1).

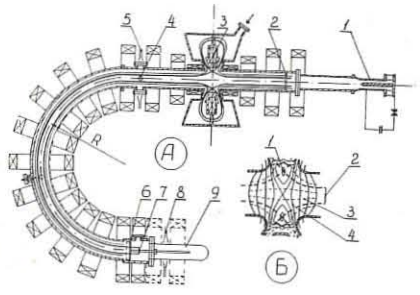

Fig.1. A. The principal scheme. 1 - plasma gun, 2 - diafragma, 3 - central coil of the divertor, 4 - electrostatic probe; 5,8 - horns of microwave interferometer, 6 - probe-collector, plasmascope, 7 - magnetic aperture, 9 - glass tube. B. 1 - point were H=0, 2 - magnetic aperture, 3 - lines of force, 4 - lines H=const.

A coaxial plasma gun injecting plasma along the magnetic field of the device was placed at the another end of the divertor. Plasma stream cross-section at the entrance to the divertor was limited by a diafragma whose diameter (3,5 cm) exeded slightly the magnetic aperture in this cross-section in order plasma to fill the divertor surface. Changing the current direction in the central coil of the divertor it was possible to create both divertor and solenoidal configuration of magnetic field.

Plasmagramms of the plasma stream cross-section relating to the plasma going along the half-torus are shown in Fig.2 (top - in divertor configuration of the magnetic field, bottom-solenoidal one).

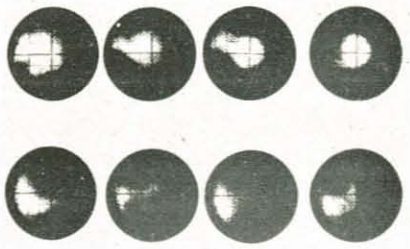

Fig.2. From left to right: H=2; 4; 6 and 7 koe.

If the plasma stream drifts entirely to the external wall of the half-torus in solenoidal configuration then in the divertor configuration the picture essentially different. For the last case the central "kernel" with the diameter equal the diameter of magnetic aperture, and narrow plasma jet ("tongue") from the surface of that "kernel" to the external wall of torus are cleary observed. The drift of the "kernel" with respect to the axis is practically absent and the total light of plasma "tongue" grow weak when the magnetic field strength increases.

An electrostatic probe collector placed at the entrance and at the exit of the half-torus was used to measure relative losses of the plasma charged particles passing the half-torus (Fig.3; curve I -divertor configuration; curve 2 - solenoidal configuration).

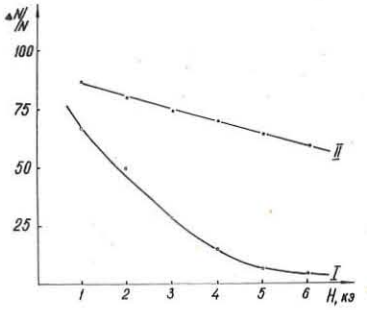

Fig.3. The coefficient of plasma losses vs magnetic field strength.

It is seen from Fig.3 that the losses are considerably less at the divertor configuration then at solenoidal one.

Thus divertor magnetic field, which has its own potential well at the divertor surface, considerably decreases toroidal drift and plasma losses in toroidal magnetic field configuration.

References

1. В.Г.Зыков, Н.И.Руднев, ЖТФ, 39, 1223 (1969).
2. В.Г.Зыков, В.И.Карпухин, Н.И.Руднев, В.Т.Толок, УФЖ, 14, 59 (1969).
3. Б.Б.Кадомцев в сб."Физика плазмы и проблемы управляемых термоядерных реакций", т.4, изд.АН СССР, М.,1958г.,стр.353.
4. K.Uo, R.Itatani, A.Mohri, H.Oshiyama, S.Ariga, T.Uede; Third Conference of Plasma Physics and Controlled Nuclear Fusion Research (Novosibirsk, 1968).CN-24/B-4.

DIRECTIONAL ION FLUXES IN A PLASMA CONFINED IN A TOROIDAL MAGNETIC TRAP.

M.S.Berezhetsky, S.E.Grebentshikov, I.A.Kossy, I.S.Shpigel.
P.N.Lebedev Institute of Physics, Academy of Sciens, Moscow, USSR.

Theoretical studies [1-4]; dealing with equilibrium of plasma column in a toroidal magnetic traps, predict the existence of closed axial ion and electron fluxes. We are not aware, however, of any experimental work, which have registered this kind of motion of plasma compononts.

Earlier [5] we have described the method of measurement with double flat and multielectrode probes of small longitudinal ion fluxes with $v_{oz_i} \ll \bar{v}_{T_i}$ (where v_{oz_i} is the velocity of ion motion directed along the longitudinal axis of a toroidal chamber; and $\bar{v}_{T_i}$ is the velocity of thermal motion). In this paper the analysis is made of the data on experimental measurements of the directional motion of ions, received by the method, described in [5]. The measurements were made at the stellarators "L-I" [6] and "Tor-2" [7] at the Lebedev Institute (Moscow, USSR).

The main measurement results are as follows:

I. The existance of longitudinal ion currents $j_{oz_i} = n_i v_{oz_i} e$ was observed both in "L-I" and "Tor-2".

2. The direction of an ion current depends on the direction of the main magnetic field H_z (the sign change caused the reversal of the velocity direction).

3. With the unchanged H_z the velocity (v_{oz_i}) direction is determined by the sign of the angle of rotational transform of magnetic limes of force ι_m (which is defined by the direction of a helical winding of a stellarator). The dependance on the sign ι_m was established at the "Tor-2" - stellarator; its design features enable to change the direction of the rotational transform.

4. Radial measurements (in two mutually perpendicular directions) show that the direction of the velocity vector remains unchanged across the chamber (i.e. the averaged directional motion of ions increases toward the periphery of the chamber, reaching the maximum at $r \approx 25$mm (Fig. I).

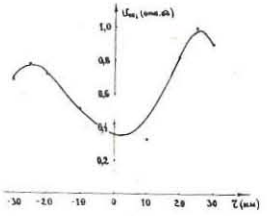

Fig.I.

5. The value of the directional velocity of ions v_{oz_i} depends on ι_m. The measurements made at Tor-2 show that at $\iota_m < 0{,}2\pi$ the directional flux can not be registered. When $\iota_m > 0{,}2\pi$ the increase of the angle of rotational transform causes a considerable growth of v_{oz_i} (see fig.2).

6. The ratio $\frac{v_{oz_i}}{\bar{v}_{T_i}}$ at the maximum of radial distribution /Fig.I/ is estimated to vary within 0,I - 0,5. This corresponds /at $T_i \simeq 30$ eV and $n_i \simeq 10^{10}$ cm^{-3}/ to the ion current density along the chamber axis approximetly I - 4 $\frac{mA}{cm^2}$.

7. The directional flux is quasistational and it is registered within the time periods, which are greater than relaxation time for the ion component.

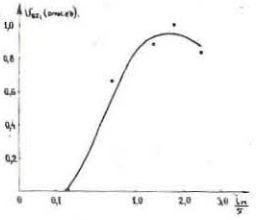

Fig.2.

The observed phenomenon may be analyzed qualitatively in the frame-work of the hypothesis, developed in [1] and based on taking into account the influence of the radial electrical field E_z on the motion of charged particles in a toroidal magnetic trap. Ions mooving along one of the axsial directions in a torus are characterized by the existance of the "resonance" group [8] of particles for which electrical rotational transform compensates the magnetic rotational transform. The resonance longitudinal velocity is given by the relation $v_{oz} = \frac{v_E}{\theta}$ /where $v_E = c \cdot \frac{E_z}{H_z}$, $\theta \equiv \frac{\iota_m \cdot r}{2\pi R}$ /.

For typical conditions of the experiment at L-I, when a substantial radial electrical field is formed [6], the value of deviation of resonance ions from magnetic surface (estimated on the basis of the results, obtained in [4,9]) is found the same order as the chamber radius. In that way their orbits should be intersect the wall of the chamber. It results in the formation of the "cone of losses" in the velocity space and the distribution function assumes the shape shown in fig. 3. In practice the development of instabilities [4] may lead to smoothing out the "gap" and to an effective displacement of the distribution function. These kinds of asymmetry of the distribution function result in the appearance of a longitudinal ion flux.

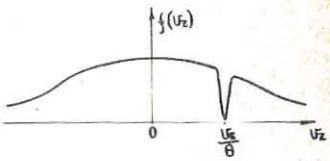

Fig.3.

The experimental data do not contradict to the discussed mechanism. Really, with the decrease of ι_m the resonance velocity shuld shift in the "tail" of the maxwellian ion distribution. The result of this - the decrease of the axial flux- is qualitatively confirmed by the results shown in fig.2.

The sign of the directional velocity observed in the experiment coinsides with that predicted by the hypothesis on the dominant role of the escape of resonance ions into the "losses cone". The radial distribution shown in fig.I does not contradict to the suggested nature of phenomena.

If we assume that ion distribution in space corresponds to that shown in fig.3, then it will be possible to estimate the ion flux into the "losses cone". This problem is similar to that solved for the traps with magnetic mirrors [10]. The flux estimated in this manner is found to be close to the longitudinal experimental flux.

The phenomenon observed by us cannot be explained qualitatively and quantitatevely by the equilibrium fluxes calculated in papers [2,4], as well as by the friction between passing and localised ions [3].

The analysis of the experiment shows that the longitudinal motion is not associated with the initial conditions of a plasma or with the existenee of vortex electrical fields.

The final conclusion about the dominant role of the considered mechanism of resonance particle losses requires additional theoretical and experimental studies.

The authors wish to thank M.A.Ivanovsky, L.M.Kovrizhnikh, I.S.Sbitnikova, A.P.Popryadukhin and S.N.Popov for their valuable advice and useful discussions.

References

[I] BishopA.S., Smith C.G.; Phys. Fl., 9, I380, (I966).
[2] D.Pfirsch, A.Schluter, Rept. Max-Plank Inst., Munich, MPI/PA/7/62, (I962).
[3] A.A.Galeev, R.S.Sagdeev, DAN SSSR, I89, 6, I204, (I969).
[4] H.L.Berk, A.A.Galeev, Phys. Fl., I0, 44I, (I967).
[5] M.S.Berezhetsky, at all, Pros. of Meeting of Plasma Diagnost. Sukhumi, USSR, (I970).
[6] M.S.Berezhetsky at all, IAEA, Vienna, v.I, 529, (I969).
[7] "Stellaratory FIAN SSSR", preprint FIAN No 57, Moscow, (I969)
[8] A.P.Popryadukhin, preprint FIAN, Moscow, (I966).
[9] A.P.Popryadukhin, preprint FIAN, No 99, Moscow, (I968).
[I0] G.I.Budker, "Plasma Phys. and Nucl. Fus. Problems", v.III, 3, Academy of Science of USSR, (I958).

Influence of superimposed shear on the confinement properties of the Wendelstein $\ell = 2$ Stellarator (WII a)

G. Grieger, D. Eckhartt, J. Eisert, G. v. Gierke, W. Ohlendorf, G.H. Wolf.
Institut für Plasmaphysik, 8046 Garching near Munich, Federal Republic of Germany

Abstract: The effect of shear on the confinement properties of the Wendelstein Stellarator was studied and a strong influence observed.

The WII a stellarator is equipped with $\ell = 2$ helical windings producing a large rotational transform, ι, ($\iota = 1$ corresponds to 360°) on the magnetic axis and very low shear. For MHD stability the magnetic field has a mean magnetic well, typically of a few per cent. Minima of the confinement time had been observed whenever the rotational transform was a rational fraction of not too high an order /1/.+) Whatever their cause, they are related to rational surfaces, being established over a large part of the plasma cross section simultaneously. Introducing some shear affects this state and might cause these minima to disappear.

Equally directed currents in three additional coils, as sketched in Fig. 1 enable us to vary the shear over a limited range. These coils

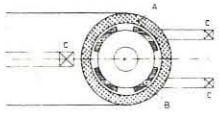

Fig. 1: arrangements for the coils
A: main magnetic field
B: Helical windings, $\ell = 2$
C: additional coils producing B_s

are arranged coaxially with the device; their magnetic field, B_s, vanishes on the magnetic axis /3/. Calculations of the corresponding combined magnetic field configuration have shown that the mean-minimum-B properties are only slightly affected by varying the shear in this way, but that too large values of B_s lead to destruction of the magnetic surfaces.

The major and minor radii of the WIIa stellarator are 50 cm and 5 cm respectively. The toroidal magnetic field B_o of 4.5 kG was maintained throughout the whole experiment. A barium plasma was generated by contact ionization on a tungsten sphere. The ion-density and its radial profile were measured by resonance fluorescence /1/.

In Fig. 2 the dependence of the steady state density on iota for $B_s = 0$ and for $B_s > 0$ is shown, with the input ion flux, ϕ, and the superimposed meridional field B_s kept constant. In both cases the magnitude of the shear ($\frac{\Delta\iota}{\iota}$) is a function of iota as shown on the top curves of Fig 2, with

$$\frac{\Delta\iota}{\iota} = \frac{\iota\,(r=4\text{cm}) - \iota\,(r=0)}{\iota\,(r=0)}.$$

In those regions where the shear is noticeably increased over the value for $B_s = 0$ the confinement time (which is proportional to the steady state density) is considerably reduced. For

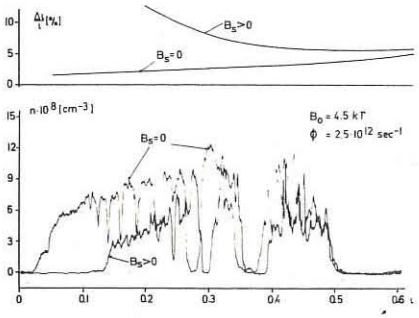

Fig. 2: top curves: $\frac{\Delta\iota}{\iota}$ vs. ι for two cases, $B_s = 0$ and $B_s > 0$
bottom curves: n vs. ι for the two cases shown in the top curves.

iota less than 0.14 extremely poor confinement is achieved; we are inclined to attribute this particular fact there to the break up of the magnetic surfaces as indicated by computations. However, it should be noted that our present knowledge of the magnetic field structure for $B_s \neq 0$ is based on calculations only. There is therefore still a slight possibility that the observed reduction of confinement time beyond iota = 0.14 might also be caused by the above mentioned destruction of the magnetic surfaces rather than by the effect of shear.

Consequently, another experiment was conducted where the direction of the additional field B_s was reversed so that the weak shear originally inherent in the $\ell = 2$-field could be compensated in the average. The corresponding results are shown in Fig. 3 . In this case one observes an improvement in the confinement time for any applied average shear, which is smaller than the value for $B_s = 0$. This improvement approaches an optimum for $\frac{\Delta\iota}{\iota} \approx 0$. Here again, however, the magnetic surfaces seem to break up when the value of iota crosses a lower limit, i.e. for $\iota < 0.1$.

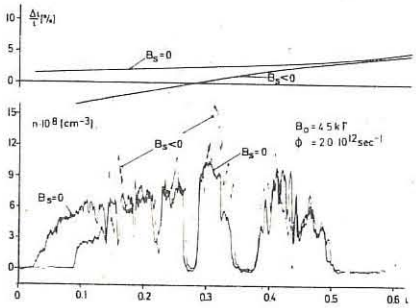

Fig. 3: top curves: $\frac{\Delta\iota}{\iota}$ for two cases $B_s = 0$ and $B_s < 0$
bottom curves: n vs ι for the two cases shown in the top curves

It should be noted at this point that the superposition of B_s also leads to a small change of iota. Since the iota scale presented on the curves in Figs. 2 and 3 is obtained by means of an on-line anologue computer which accounts only for the main and the helical field currents, it is slightly incorrect for $B_s \neq 0$. However, the true iota scale can easily be obtained by following the displacement of the individual maxima and minima.

Summarizing one may conclude that already for rather moderate values of additional shear the amplitude between the minima and maxima is reduced, but so is the confinement time itself. By analysing these data one can find a gross relation as plotted in Fig. 4, where the relative dependence of the maximum confinement time (steady state density) on $\frac{\Delta\iota}{\iota}$ is plotted. This figure shows a reduction of the confinement time with increasing shear, provided that a destruction of the magnetic surfaces can be excluded. Our results do not rule out, however, that higher values of shear eventually will improve the confinement properties.

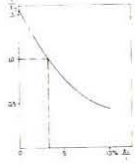

Fig. 4: Relative variation of the confinement time τ vs. shear being represented by $\frac{\Delta\iota}{\iota}$

Such experiments will become possible with our next stellarator, WII c, which will be equipped with two sets of helical windings, $\ell = 2$ and $\ell = 3$, so that iota and $\frac{\Delta\iota}{\iota}$ can be varied independently of each other.

/1/ E. Berkl, D. Eckhartt, et.al. Proc.3rd.Int.Conf.on Plasma Phys. and Contr.Nucl.Fusion Res. Novosibirsk (1969) Bd. I, S. 513
/2/ M.C. Berecheski, et.al. Proc.3rd.Int.Conf.on Plasma Phys. and Contr.Nucl.Fusion Res. Novosibirsk (1969) Bd. I, S. 529
/3/ This arrangement is very similar to the one used by Hartman; private communication

Work performed on association with Euratom.

+) Similar results were observed in the L - 1 stellarator at the LEBEDEV-INSTITUTE /2/, but there the minima in confinement time were obviously connected with destruction of the magnetic surfaces.

Confinement of Photo-Ionized Plasma in the Wendelstein $\ell = 2$ Stellarator (W IIa)

D. Eckhartt, J. Eisert, G. v. Gierke, G. Grieger, W. Ohlendorf, H. Wobig, G.H. Wolf

Institut für Plasmaphysik, 8046 Garching near Munich, Federal Republic of Germany.

Abstract: Photoionization of a neutral barium beam provides a steady state point like plasma source for the W IIa stellarator. The resulting confinement properties equal essentially those obtained with contact ionization on a tungsten sphere present in the confinement volume.

The previous experiments (1,2) in our stellarator were carried out using a Barium plasma, generated by contact ionization on a hot tungsten sphere of 3 mm diameter. This sphere, suspended by 2 wires, each 10 µm thick and positioned on the magnetic axis, was heated by laser radiation to 2.300°K. We now wish to report on the confinement of the same type of plasma, but generated by Photo-ionization. Several reasons made it necessary to change the production mechanism to this method: Up to now, for example, it could not be ruled out completely, that the presence of the hot sphere within the plasma might have damped instabilities by line-tying for example, thus being responsible for the long confinement times observed. Secondly, it was impossible, to decide whether the observed minima in the iota-dependence of the confinement time are a particular stellarator quality or if they are generated by the sphere-suspending wires which could originate convective cells, for instance. In addition to this the presence of the electron emitting sphere inhibits a heating of the plasma due to the very intense thermal coupling between sphere and plasma. For the benefit of better comparison with the former experiments we imposed several conditions on the new plasma source: Barium-plasma should be produced again, d.c.-operation would be desirable, the source region should approach a point source on the axis and the interaction between the ionizing mechanism and the plasma already produced, should be negligible. These requirements rule out any ionization by electron impact, for example, and therefore the application of r.f.-fields. However, crossing a beam of neutral Barium-vapor with an intense light beam provides a plasma source with the desired qualities. When looking for a d.c. light source of sufficient intensity in the relevant spectral range, two possibilities of approach have to be considered. At first, one could excite the metastable levels of a certain percentage of the Barium atoms by running the beam through a gas discharge, before entering the stellarator, or as suggested by E. Hinnov, by resonant charge exchange between neutral Rubidium atoms and Barium ionbeam. In this case the threshold wavelength for ionization is about 3.200 Å (3,4) and it is easy to find an intense light source in this region, a Xenon high pressure arc, for instance. The other possibility is the ionization from ground state. Here the threshold wavelength is 2.380 Å and most of the d.c.-light sources show only poor emission in this spectral range. Therefore one would be inclined to chose the ionization via an enhanced metastable population. But since the generation of this enhanced population, too, turned out to be technically not easy, ionization from ground state was selected as a first attempt.

The light source used was a Maecker-type high power cascade arc (5) running in Argon. (Fig. 1). Typical operating conditions were 1 Atm. Argon pressure, 900 Ampères and 110 Volts, resulting in 10 kw/cm arc length.

Fig. 2 gives a schematic drawing of the stellarator W IIa. The important changes are: no probes used anymore, the sphere being removed, and the heating lamp replaced by the cascade arc. Also the measuring circuit for the ion input flux had to be changed slightly. After having removed the sphere the two retractable spoon probes were used as a double probe. If they are aligned with respect to the source volume by virtue of a magnetic field they represent the only essential plasma sink and under those conditions the ion input flux can be deduced from their saturation current. It was checked that the ion collecting spoon did not emit any measurable amount of secondary electrons by photon-bombardement. Unfortunately, it turned out that the saturation of the ion current was not as satisfactory as expected so that there remained a slight uncertainty of about ± 30 % in the magnitude of the ion input flux.

A low base pressure is required, otherwise the ions are cooled down to room temperature due to ion-neutral collisions. This cooling would increase the classical diffusion rate, resulting in a lower peak density, as compared to the earlier measurements. However, the peak density will be reduced anyway because of the increased cross section of the source region. In addition, the Bohm loss rate is decreased due to the lower temperature. The difference between Bohm and classical loss rate is therefore reduced by one or two orders of magnitude. Fig. 3 shows a prelivinary plot of the ion density, as obtained with photo-ionized Barium, versus the angle of rotation transform . For an input ion flux of 10^{11} ions/sec. one would expect a density of 10^6 cm^{-3} from Bohm-diffusion, whilst from classical theory one estimates 3.10^7cm^{-3}. This measurement yielded a density of $1{,}6 \times 10^7$cm^{-3}, one order of magnitude more than the Bohm value and in fair agreement with classical theory. Qualitatively one observes the well known behaviour of the density as a function of iota; i.e., strongly pronounced minima of the confinement time at the rational values of ℓ. This strongly supports the conclusion, that our previous results with the sphere do indeed reflect general properties of our stellarator and are not caused by the sphere. Furthermore, those plasma loss processes connected with the rational values of ℓ, are investigated and which reduce the peak density for some orders of magnitude. Because of the short confinement time in this case, probe measurements do induce negligible further losses and thus can be used for obtaining detailed information of the flow pattern.

/1/ E.Berkl, et.al. Proc. Int.Conf.on Plasma Phys. and Contrl. Nucl.FusionRes. Novosibirsk (1969)

/2/ Paper presented at this conference

/3/ L. Haser, Proc.of the NATO Adv.St.Inst.,Keele, Engl.Aug.1966

/4/ S.Drapatz, MPI-PAE/Extraterr.13/67, Nov. 1967

/5/ H.Maecker, S. Steinberger, Z.angew.Phys. 23,456 (1967)

Work was performed on association with Euratom.

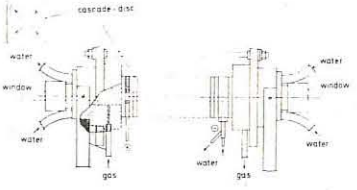

Fig. 1: Cascade arc arc-diameter 10 and ← 15 mm

Fig. 2: Schematics of the experimental setup →

Fig. 3: Density vs iota Base-pressure $p \approx 8.10^{-6}$ input-flux ca. 10^{11} ions/sec.

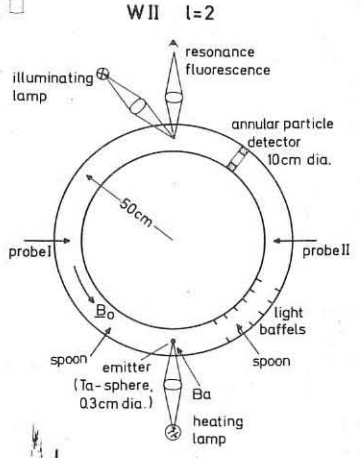

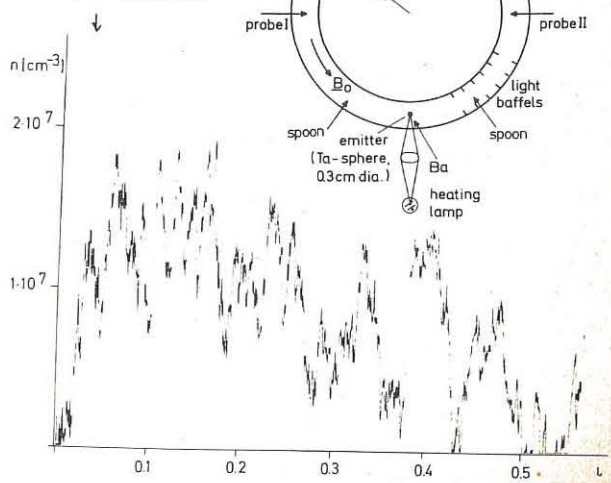

ECR-Generated Noble Gas Plasmas in the Stellarator W IIa

R.A. Ellis, Jr.[+] and D. Eckhartt
Institut für Plasmaphysik GmbH, 8046 Garching near Munich, Federal Republic of Germany

Abstract: Argon and xenon plasmas were produced by electron cyclotron resonance in the W IIa stellarator. Densities ranged from $3\cdot10^{8}$ to $2\cdot10^{11}cm^{-3}$ and electron temperatures from 4 to 12 eV. The confinement time was estimated to be five to ten times the Bohm time. The general features of the density versus rotational transform curves were similar to those observed with barium plasmas produced by contact ionization except for some cases with xenon.

The confinement of contact ionized barium plasmas in the W II stellarator has been interpreted as approaching the classical collisional limit for axisymmetric fully ionized plasmas and exceeds the Bohm value by about two orders of magnitude [1]. The present paper describes preliminary experiments with noble gas plasmas generated by low power electron cyclotron resonance. The aim of these experiments was to get an estimate of plasma confinement at higher electron temperatures and hence longer electron mean free paths than those in contact ionized barium plasmas and to see whether or not the sudden decreases in density for particular values of the rotational transform observed in barium plasmas were related to the presence of the solid plasma source and its supports. Wendelstein IIa is a circular stellarator with major diameter $2R_o$=1 m and plasma diameter $2r_o$= 10 cm. It has continuously wound $\ell = 2$ helical windings which produce a nearly shear-free stabilizing field. Technical details have been given elsewhere [1]. In our experiments the microwave power was radiated from an open X band wave-guide which is flush with the inner surface of the vacuum vessel.

[+] Permanent address: Plasma Physics Laboratory, Princeton University, Princeton, N.J., U.S.A.

Various magnetrons and klystrons with frequencies around 9.8, 13.3, and 15.7 GHz were used with output powers ranging from the minimum value required of 20 to 40 mwatts up to 7 watts. The magnetic field strengths for resonance are 3.28, 4.74, and 5.5 kG. For these values the main magnetic field and the helical windings could be operated in a steady state up to values of $\iota = \iota/2\pi$ of about 0.6. Operating pressures of argon and xenon ranged from 10^{-6} to 10^{-4} torr. The base pressure was usually a few times 10^{-7} torr. Plasma density and electron temperature were measured using cylindrical Langmuir probes with tips 4mm long and 0.1 mm thick. The probes could be moved in radial direction. The probe data were evaluated using the theory for infinitely long cylindrical probes by Laframboise [2]. The microwave power could also be switched off suddenly in order to observe the subsequent decay in particle density by means of the probes.

Depending on neutral gas pressure and microwave power, the peak particle density n_{eo} attained values between a few times 10^{8} and $2\cdot10^{11}cm^{-3}$. The electron temperature ranged from 4 to 12 eV. The degree of ionization thus varied between 10^{-4} and 0.6. Rough measurements of the space potential in a few cases indicated that the plasma was charged positively which implies that the electrons have a higher intrinsic loss rate. As indicated from the time decay in the afterglow, the mean plasma life time was of the order of milliseconds. This time is short compared to the time of equipartition between electrons and ions. Moreover, the ions are strongly coupled to the neutral atoms via resonant charge exchange collisions. The ion temperature, therefore, is practically equal to the neutral gas temperature.

The question of plasma confinement was studied by computing the mean particle life time τ, for a number of steady state discharges in argon, where τ is the ratio of the total particle number N, and the production rate $\dot{N}$. The rate coefficients have been taken assuming Maxwellian distribution of electron energies. This assumption is questionable for lower electron densities since the electron-electron collision times are too long. On the other hand, one can estimate the total production rate from the microwave power absorbed and the energy required to produce and to heat an electron to the observed temperatures. Taking the latter energy equal to 50 eV and assuming that all the power entering the discharge tube (i.e. about half the output power, W) is absorbed, the two estimates for the production rate agree reasonably well as seen from the Table below. (The lower numbers $\dot{N}$ refer to the μ-power estimates.) The mean particle life times are given in the same Table. The plasma decay times were usually found to be somewhat higher. A proper interpretation of these decay times which are taken from the ion saturation current traces requires a determination of T_e during the afterglow which has not been done. From the plasma life time an effective diffusion coefficient is deduced, $D_{eff} = (r_o/2.4)^2/\tau$. This value is compared with various theoretical estimates. The Pfirsch-Schlüter value, D_{PS}, is by far too small to account for the observed life times. Next we computed the values, D_K^A, (at max. T_e and n_e) from the theory of Kovrizhnikh [3] for weakly and strongly ionized axisymmetric plasmas which takes the self-consistent radial electric field into account. (The numbers in brackets refer to the respective values for both weakly and strongly ionized plasmas as neither of the criteria given by Kovrizhnikh strictly apply to these discharge conditions). The coefficient D_K^{St} from Kovrizhnikh for an $\ell = 2$ stellarator, which should reflect the influence of particles trapped in the helical mirrors, is given next. Finally, we quote the values of the Bohm diffusion coefficient D_B. Except for the case with high neutral pressure the effective diffusion coefficients range between D_K^A and D_B. As the electron temperature decreases radially outwards and D_K^A depends stronger on electron temperature than D_B, the departure from the Kovrizhnikh value becomes still more pronounced. For discharges with higher microwave frequencies and correspondingly higher magnetic fields the peak densities become somewhat higher at the same power level.

The plasmas in our ECR discharges exhibit relative density fluctuations generally of the order of 10 to 20 %. Measurements with the spectrum analyzer indicate strong activity in the frequency range of the drift waves which is not surprising since the $\ell = 2$ helical windings produce only weak shear.

W_{Par}	B_o / ι	n_{eo} / T_e [eV]	$\dot{N}$ [s^{-1}]	τ [ms]	D_{eff} x10^{-3}	D_{PS}	D_K^A x10^{-3}	D_K^{St}	D_B x10^{-3}
40mw	3.2	3.8×10^{8}	1.3×10^{15}	1	4.3	0.43	0.7	1.75	16.8
6×10^{-6}	0.125	8.6	2.5×10^{15}	2	2.2				
400mw	4.62	6.3×10^{9}	4.8×10^{16}	0.79	5.5	1.36	(0.16)	1.03	10
7×10^{-6}	0.2	7.4	2.5×10^{16}	1.5	2.9		(0.008)		
7watts	3.28	2.4×10^{11}	1.6×10^{18}	0.3	15	32	(0.51)	0.1	23
4.6×10^{-6}	0.328	12	0.5×10^{18}	1	4.5		(0.06)		
400mw	4.62	2×10^{9}	1×10^{16}	0.1	43				
2×10^{-4}	0.2	4.4	2.5×10^{16}	0.04	133	0.56	0.24	1.8	6

The dependence of the particle density on rotational transform ι in argon was found quite similar to that observed in contact ionized barium plasmas. An analogous pattern is observed with the annular grid-plate particle detector which encloses the plasma and measures part of the radially outstreaming particle flux. This indicates that at the particular values of ι the total plasma production rate is reduced. At higher pressures and microwave power levels the density decreases become less pronounced. With high enough power it is possible to maintain the discharge at all values of ι. In contrast to these results we found a different behaviour in xenon for a wide range of discharge parameters. Superimposed to the general appearance of broad minima there are pronounced density peaks at rational values of ι.

[1] Berkl, E., et.al. Proc. Novosibirsk Conf., 1, 513 (1969) Wien
[2] Laframboise, J.G., UTIAS Report No. 100
[3] Kovrizhnikh, L.M., ZhETF, 56 (1969) p. 877

This work was performed under the terms of agreement between the Institut für Plasmaphysik GmbH, Munich-Garching, and Euratom to conduct joint research in the field of plasma physics.

THE TORSATRON WITHOUT TOROIDAL FIELD COILS AS A POSSIBLE SOLUTION TO THE DIVERTOR PROBLEM

by

C. Gourdon, D. Marty, E. Maschke, J. Touche

ASSOCIATION EURATOM-CEA
Département de la Physique du Plasma et de la Fusion Contrôlée
Centre d'Etudes Nucléaires
Boite Postale n° 6 - **92 Fontenay-aux-Roses** (France)

Abstract : A stellarator type configuration, with only helical conductors and no toroïdal field coils is investigated by numerical calculations. Interesting properties are found for the configurations with high aspect ratio ($R/a \sim 10$) (ι up to 4, and $P/L_s \simeq 1$). This configuration (Torsatron) is particularly well suited for the construction of a divertor.

Introduction : In earlier numerical studies [1] a systematic comparison has been made between stellarator configurations of the classical type (2ℓ helical conductors which alternately carry currents + I and - I) and a new type called Torsatron (ℓ conductors only which all have currents +I and a compensating vertical field). This study has shown certain advantages of the Torsatron configurations, in particular the possibility to have simultaneously shear and average magnetic well. In the present work, configurations of the Torsatron type are investigated in a regime in which the toroïdal field is not created by separate field coils, but is due to the helical currents. The properties of this configuration have been investigated by numerical integration of the field lines. The study has shown interesting properties for the configurations with high aspect ratio ($R/a \sim 10$) and numerous field periods (~ 30). It is shown that a particular form of the separatrix allows the construction of an efficient divertor.

Numericaly investigated properties : In the Torsatron without toroïdal field coils the multipolar field and the azimuthal field are both created by the helical winding and the relative strength of the two fields is fixed when the pitch of the helical winding is fixed. We have chosen helical winding with $m = \frac{d\theta}{d\varphi} = \text{const.}$ where φ is the angular position around the z axis and θ the angular position around the circular axis of the torus. $\varepsilon = m\,a/R$ is then the mean value of the tangent of the pitch angle. The parameters of the study are $A = R/a$ and ε. We define ν^* as the volume enclosed in the last closed magnetic surface (separatrix) and normalized with respect to the volume of the toroïdal chamber ($2\pi R a^2$). On the picture number 1 we have represented ν^* against ε. We observe that for a given value of ε the curvature effect yields to a significant reduction of ν^* for $R/a < 8$.

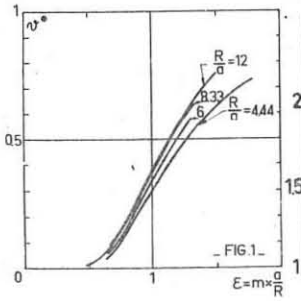

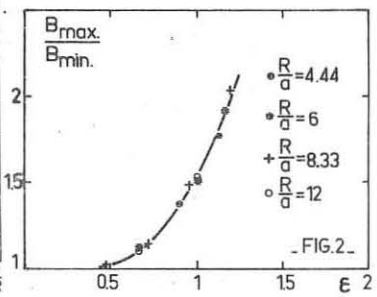

We have calculated the ratio of the two extreme values of the magnetic field encountered on the last closed magnetic surface. The figure 2 shows that this mirror ratio is independant of R/a (at last for $R/a > 4$). The picture number 3 gives the maximum value of the mean rotational transform ($\iota = L/2\pi$) on the last closed magnetic surface. We found that the value of ι per field period is, (for $R/a \geq 8$), a little greater than the value ($\iota/m\ell \approx 1/12$) given by A. GIBSON [2] for the classical stellarator.

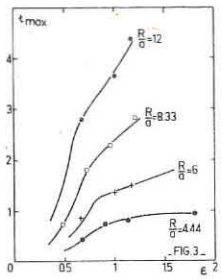

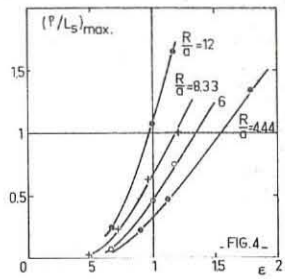

The picture number 4 gives the value of P/L_s on the edge of the volume ν^*. We define P by $\nu^* = (P/a)^2$ and $1/L_s = P/R \times \frac{d\iota}{dP}$. If we will choose A and ε for a realistic experiment (or reactor), we have to take account of the real size of the windings and to provide the distance between the winding and the separatrix according to the thickness of the required screens.

We are then limited to little values of (ν^*). We give on the table the values of the parameters for an experimental machine and for a reactor scale experiment.

Parameters	Experimental	Reactor scale
R/a	12	13
m	10	10
ε	0.83	0.77
ν^*	0.24	0.16
R	245 cm	32,5 m
a	20,4 cm	2,5 m
B	20 KGs	10^5 Gs
δ	4000 A/cm^2	2000 A/cm^2
P plasma	10 cm	100 cm
ι	3.5	3.5.
P/L_s	0.6	0.5
Bmax / Bmin	1.28	1.19

Schematic description of a divertor : If we study the escape from the configuration, of magnetic lines started just outside the last closed magnetic surface we observe that all these magnetic lines leave the configuration through a narrow helical region between the windings and then go around the windings. The picture number 5 gives the schema of a divertor taking advantage of this behaviour. One helical slit through the wall, allows the charged particles to leave the internal chamber. These particles are received on massive targets in the external chamber wich is provided with large pumping surfaces.

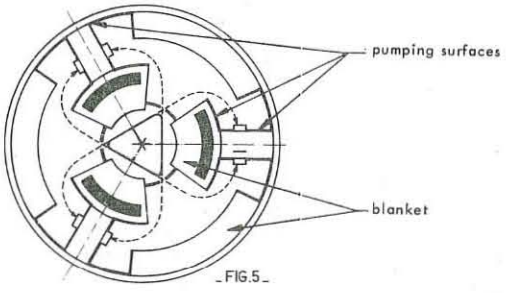

A realistic calculation made for the reactor size experiment given above, with $n \simeq 10^{14}$, $\tau \sim 1$s. gives an equilibrium pressure in the external chamber of about 5.10^{-6} Tor with the assumption of a 10 $\ell.s^{-1}.cm^{-2}$ pumping speed for the active surfaces.

[1] C. GOURDON, D. MARTY, E.K. MASCHKE, J.P. DUMONT
Proceedings of the Conference on Plasma Physics and Thermo nuclear Research, Novosibirsk, 1968, Paper CN 24 / F-2.

[2] A. GIBSON, Phys. Fluids 10 (1967), 1953.

Drift Waves and Plasma Diffusion in a Straight Stellarator

by

P.E. Stott and J. Burt

U.K.A.E.A. Culham Laboratory, Abingdon, Berks., England.

Abstract: The effects of magnetic shear on unstable drift waves are studied in a straight ℓ=3 stellarator. Increasing the shear reduces the amplitude of the instability and also the cross field diffusion coefficient.

It is well known that unstable drift waves supported by a density gradient may seriously weaken the containment of a low β plasma in a stellarator. We have investigated the effects of magnetic shear produced by an ℓ=3 helical winding on the drift instability and on plasma diffusion. A straight stellarator was used for these experiments, since in a toroidal device it is difficult to vary the shear significantly without disturbing the toroidal equilibrium.

The essential features of the experimental apparatus (STAMP) are shown in Figure 1.

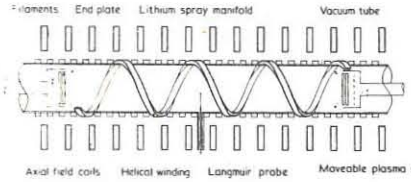

Fig.1. Schematic of the STAMP experiment. For clarity, only one of the helical conductors is indicated.

Lithium or sodium plasmas are produced by thermally ionising a beam of neutral atoms sprayed onto a rhenium plate (diameter 7.5 cm) heated to over 2000°K. The basic principles of Q-machines are well known and the detailed design of the sources used on STAMP has been reported previously[1]. Two identical sources which can be moved axially produce a plasma whose length may be varied between 40 and 400 cm. The axial magnetic field is variable up to 4000 Gauss and at that field the Larmor radius of lithium ions a_i = 0.3 mm. The periodicity of the ℓ=3 helical winding is 80 cm and the maximum current is 48,000 Amps.

Computations of the helical magnetic fields are in good agreement with measurements using an electron beam to trace out field lines onto a fluorescent screen. The magnetic field lines lie on a nested set of trefoil shaped cylinders. The rotational transform ι has a nearly parabolic radial dependence and at the separatrix the transform per winding period is 2π. It is convenient to express the magnetic shear in terms of the shear length $L_s = [(2\pi/80)r\, d\iota/dr]^{-1}$ which varies roughly as the inverse square of the radius and is about 7 cm at the separatrix.

When the current in the helical winding is zero, we observe spontaneously occuring oscillations of the plasma density $\tilde{n}$ and potential $\tilde{\varphi}$ which we have previously identified as collisionless drift waves[2]. At a density of 10^8 cm^{-3} the electron-ion collision length λ_{ei} = 600 cm, and electron-ion encounters within the length of the column are too infrequent to generate collisional drift waves. The density and potential oscillations have peak rms amplitudes n_1 and φ_1 close to the radius r_1 where the density scale length $\Delta \approx [d(\log n_o)/dr]^{-1}$ is smallest. Typically $n_1/n_o = e\varphi_1/kT$ = 10-20%. We observe that the amplitude of the unstable drift waves is reduced as the current in the helical windings is increased.

Typical radial profiles of n_o and n_1 with and without shear, are shown in figure 2. In this case the effective shear was Δ/L_s = 0.05.

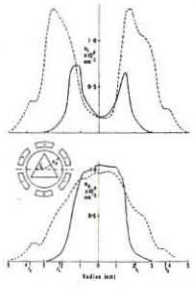

Fig.2. Radial profiles of mean density n_o and rms level n_1 compared for a shear free plasma (dashed curves) and for a helical current of 30,000 Amps (full curves). In the shear case, the profiles were measured parallel to the base of the separatrix triangle (see inset diagram) which lies just inside the diameter of the endplates. The length of the column was 200 cm and the axial field 1300 Gauss.

Krall and Rosenbluth[3] have calculated that the normal mode of a drift wave should be stable if $\Delta/L_s > a_i/\Delta$. An additional stability criterion due to Rutherford and Frieman[4] requires that $\Delta/L_s > (m_e/m_i)^{\frac{1}{3}}$ to prevent the local growth of non thermal fluctuations. For lithium plasma $(m_e/m_i)^{\frac{1}{3}} = 1/20$ which is fairly easy to satisfy and usually in our experiments the normal mode condition is the more stringent. In figure 3 n_1/n_o is plotted against $s = \Delta^2/L_s\, a_i$.

Extrapolating the experimental results suggests that n_1/n_o would reduce to zero in the vicinity of s = 1.

There is a corresponding decrease in the rate of cross-field diffusion. This results in a slight increase in the central plasma density but only amounts to 10% or so since recombination losses at the endplates exceed the radial losses in this plasma. The radial plasma flux can be calculated from the cross-correlation of the density and potential oscillations

$$\vec{j}\,(\text{wave}) = \langle \tilde{n}\, \tilde{E}_\theta/B \rangle = (1/rB)\, d\langle \tilde{n}\, \tilde{\varphi} \rangle/d\theta.$$

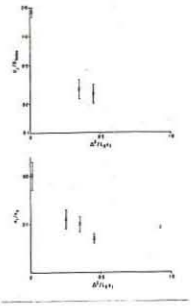

Fig.3. n_1/n_o and $D_\perp$ (normalised to $D_{Bohm} = ckT_e/16eB$) plotted against $\Delta^2/L_s\, a_i$. The theoretical threshold of stability is at $\Delta^2/L_s\, a_i = 1$.

We have measured $\langle \tilde{n}\, \tilde{\varphi} \rangle$ using two probes with a variable separation and we observe that $\tilde{n}$ leads $\tilde{\varphi}$, typically by a phase angle of 20 degrees. This results in an outward plasma flux which is a maximum close to the peak amplitude in n_1. At small radii $\vec{j}$ (wave) agrees well with values of the radial flux estimated from the small axial gradient in the central plasma density. The radial flux at the outside edge of the plasma was measured on a ion-biased cylindrical collector positioned just outside the radius of the endplates. The total flux measured in this way is equal to the peak value of $\vec{j}$ (wave). Close to the edge of the endplates, $\vec{j}$ (wave) falls off, indicating an additional loss mechanism in this region. This is probably due to convective plasma motions caused by slight asymmetries of the endplate temperature[5]. Asymmetries as small as 10°K would be sufficient to provide the observed loss rate at the edge of the plasma column. Thus our measurements of plasma diffusion are consistent with transport due to unstable drift waves in the body of the plasma assisted by convection close to the edge of the column.

The radial diffusion coefficient $D_\perp$ has been calculated from these flux measurements. In a uniform field $D_\perp$ is nearly inversely proportional to the field strength and is of the order of $D_{Bohm} = ckT/16\, eB$. This is roughly two orders of magnitude higher than the coefficient of diffusion due to binary collisions. We have not investigated in detail the dependence of $D_\perp$ (with shear) on either the axial magnetic field or the column length.

The main limitation in extending the measurements closer to the theoretical threshold of stability at s = 1 is that the density gradient steepens rapidly as the helical winding current is increased. This reduces the effective shear across the density gradient to much less than the total shear between the centre of the tube and the separatrix. The plasma density profile is determined by the spray of lithium atoms onto the end plates and ideally this should match the trefoil shape of the magnetic surfaces. We are modifying the spray pattern in order to make the density gradient less steep and thus improve the effectiveness of the magnetic shear. We are also improving the circular symmetry of the end plate temperature in order to reduce the convective losses at the edge of the endplates.

References

1. J. Burt, P.F. Little, P.E. Stott, Plasma Physics 11, 789-793 (1969), also Culham Laboratory Report CLM-R98.
2. P.E. Stott, P.F. Little and J. Burt, Proc. 3rd European Conference on Controlled Fusion and Plasma Physics, Utrecht, (1969) p.125.
3. N.A. Krall and M.N. Rosenbluth, Phys. Fluids 8, 1488-1503 (1965).
4. P.H. Rutherford and E.A. Frieman, Phys. Fluids 10, 1007-1016 (1967).
5. D. Mosher and F. Chen, Matt 691, Princeton University (1969).

HIGH β THEORY - A REVIEW OF PINCH PLASMA STABILITY[+)]

by

W. Grossmann

INSTITUT FÜR PLASMAPHYSIK

8046 Garching b. München, Germany

Abstract: This report attempts to outline progress towards understanding instabilities in high β plasmas and to compare theoretical results wherever possible with experiment.

It is not feasible to review all high β instability investigations, in fact one would not even want to do so. We concentrate here on those instabilities which appear to be the most dangerous and which have either been identified in an experiment or are suspected to be present in an experimentally produced high β plasma. The particular instabilities discussed here are classified in the following categories: 1. unstable behavior due to lack of equilibrium, 2. mirror like instabilities, 3. long wave length Kruskal Shafranov modes, 4. tearing modes, and 5. rotational instabilities. Most of these instabilities have importance for both straight and closed systems. The stability analysis for all the above mentioned instabilities was carried out for a straight system and one must use caution in applying the stability criteria to closed or toroidal systems.

[+)] This work was performed as part of the joint research program between the Institut für Plasmaphysik, Garching and Euratom.

REQUIREMENTS FOR THE STABILITY OF CYLINDRICAL AND TOROIDAL PINCH DISCHARGES

by

D.C. Robinson

U.K.A.E.A., Culham Laboratory, Abingdon, Berks., England

Abstract: The essential features for a stable diffuse pinch configuration are derived from the hydromagnetic energy principle. It is shown that for stability the pitch (length) must never possess a minimum and the $\overline{\beta_\theta}$ (i.e. average β with respect to the axial current) must always be less than unity. Stable configurations with $\beta \approx 40\%$ exist with reversed axial field outside the plasma provided the axial flux has the same sign everywhere. Without field reversal stable configurations with a[illegible]e β are only possible when currents flow outside the plasma.

Introduction: From the hydromagnetic energy principle[1] necessary and sufficient conditions for stability can be obtained. Here we shall consider the non-localised displacements or kink modes and obtain various necessary conditions for stability.

Pressure and Current Driven Instabilities: The energy integral can be written, in cylindrical geometry,

$$W(\xi) = \frac{\pi}{2}\int_0^a \left[f\left(\frac{d\xi}{dr}\right)^2 + g\,\xi^2 \right] dr \quad \text{where} \quad f = \frac{r(K_T B_z + B_\theta)^2}{1 + k^2 r^2} \qquad \ldots (1)$$

$$g = \frac{2k^2 r^2}{1 + k^2 r^2}\frac{dp}{dr} + \frac{k^2 r\, B_\theta^2}{(1 + k^2 r^2)^2}\left((kP + 1)(kP(3 + k^2 r^2) + k^2 r^2 - 1\right)$$

for m = 1, where ξ and k are the displacement and wavenumber, a the radius of the conducting wall, P being the pitch $\frac{rB_z}{B_\theta}$, the other symbols have their usual meaning. The maximum potential energy available to drive an instability is given by the lower bound on g which is made up of a pressure gradient term $2\frac{dp}{dr}$ and a current term $-B_\theta^2/rm^2$. Current driven modes are stronger for m = 1. Ignoring the pressure gradient term we see that the stability for current driven modes can be determined if the the pitch variation is known. Fig.1 shows all possible classes of toroidal pitch variations if we include a pitch going to infinity near or on the axis. Choosing a wavelength and displacement as shown in Fig.1(b) and (d), then as g can always be made negative for these regions and choosing ε small enough the energy integral is negative and therefore the configurations are unstable. Fig.1(b) corresponds to a linear TOKAMAK configuration where m = 1 is possible and (d) to a skin current or ordinary diffuse pinch with a vacuum outer region. Hence configurations with a minimum in the pitch are always unstable (for $\frac{dp}{dr} \leq 0$). Fig.1(a) and (c) can be stable. If we consider Fig.1(c) and wavelength λ_5, and a displacement as in (b), then a necessary condition for stability, i.e. g > 0, is that $P(r) > -3P(0)$, where P(r) is the pitch at the conducting wall. A more restrictive necessary condition for such a wavelength is that $\int_0^a g\,dr > 0$. Fig.2 shows the maximum degree of field reversal for stability as a function of the compression ratio of the plasma. It can be shown that this condition is almost sufficient for such configurations[2]. Stable configurations of this class are possible with β about 40% for example see Fig.3. Type (a) can also be stable but there is a limiting β obtained by combining the Suydam criterion with the condition $\int_0^{r_s} g\,dr > 0$, where r_s is defined by $kP(r_s) = -1$. Integrating W (Eq.(1)) by parts with a wavenumber such that kP(a) = -1, and then applying the condition $\int_0^a g\,dr > 0$ gives the necessary criterion for stability

$$\overline{\beta_\theta} < 1$$

where $\overline{\beta_\theta}$ is defined by the Bennet relation $\overline{\beta_\theta} I^2 = 4\pi \int_0^a r\,p\,dr$. Application of these criteria to a diffuse screw pinch configuration, Fig.4(a), gives the stability diagram shown in Fig.4(b), where the maximum β is 5%. If an appreciable current flows outside the plasma then stability is possible for β's up to about 30%.

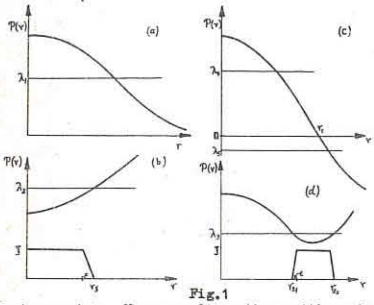

Fig.1

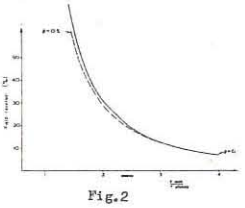

Fig.2

Currents below the Kruskal-Shafranov Limit in Toroidal Geometry: Considering only the cylindrical energy integral, then for a plasma with a vacuum outer region m = 1, kink instabilities are no longer possible when $q = \frac{rB_z}{RB_\theta} > 1$[3] (R = L/2$\pi$ where L is equivalent cylindrical length). Instabilities with m = 2 are possible but very local in charcter because g is only negative over a small distance, Δ, given from (1) by

$$\frac{\Delta}{q}\frac{dq}{dr} = \frac{2}{q}\frac{r}{R}\frac{\beta_\theta^{\frac{1}{2}}}{(m^2 - 1)^{\frac{1}{2}}}, \qquad \beta_\theta = \frac{r}{B_\theta^2}\frac{dp}{dr}$$

where β_θ is small then weak current driven instabilities become possible, depending upon the radial pitch variation. Such a localisation is believed to be the reason why the toroidal equivalent of Suydam forms a necessary and sufficient criterion in a TOKAMAK, i.e. q > 1 gives stability to all modes. However if β_θ is small near the magnetic axis it has been shown[4] that q > 1 is not sufficient, the further requirement being $\frac{dq}{dr} > 0$.

Conclusion: The stability to current driven instabilities is determined by the radial variation of the pitch. Conditions are given which show that limiting values of beta of 30-40% are obtainable when the axial magnetic field reverses outside the plasma or when there are appreciable currents flowing in that region.

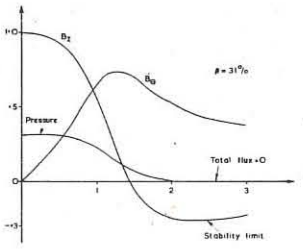

Fig.3.

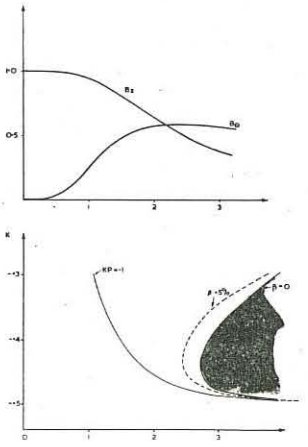

Fig.4.

References

(1) Bernstein, I.B. et al. Proc. Roy. Soc. A244 (1958) 17.

(2) Robinson, D.C. to be published.

(3) Shafranov, V.D. Zh. Tech. Fiz. 40, 241 (1970).

(4) Robinson, D.C. Dubna Conference on Toroidal Confinement Systems, September (1969).

EXPERIMENTS WITH A LINEAR (ℓ = 1) - HIGH - BETA - STELLARATOR [+)]

by

M. Kaufmann, E. Fünfer, W. Lotz, J. Neuhauser

INSTITUT FÜR PLASMAPHYSIK
D- 8046 Garching bei München, Germany

Abstract: This paper describes a linear (ℓ=1)-Stellarator experiment with a helically shaped coil, preparatory to a future toroidal experiment with a major diameter of 2.7 m. Stability is found to be comparable with a pure linear theta-pinch or with an (ℓ=1)-Stellarator using a pair of conductors.

Recent theoretical work suggests stable equilibria for a toroidal (ℓ=1)-Stellarator with high beta.[1-3] In order to separate the problems of stability and equilibrium, we tried to test possible toroidal configurations by doing linear experiments with a pair of helical conductors.[4] In this paper we describe experiments with a straight (ℓ=1)-Stellarator where the magnetic surfaces are formed by a helically shaped coil (Fig. 1) instead of the pair of helical conductors. For technical reasons, a shaped coil would be more convenient than helical conductors.

The inner surface of this coil is not exactly helical but is approximated by excentric cylinders of 23 cm diameter and 3 cm width. The period length is 60 cm, 9 periods fitting within the coil length of 5.4 m. The amplitude of the helix is 1.5 cm, the rotational transform in vacuum is 0.01 per period.

Fig. 2 shows stereoscopic smear-camera pictures of a discharge in 10 mTorr of Deuterium at a bank-energy of 1.5 MJ. After about 14 µs we see the onset of instabilities, which is within a few microseconds the same onset-time that we observe in a straight theta-pinch of equal parameters. Fig. 3 shows that with 3 % added oxygen instabilities set in much earlier, an effect which we observed in the straight theta-pinch as well but do not understand yet. Fig. 4 shows stereoscopic pictures of a discharge in 40 mTorr at 0.5 MJ (low impurity level).

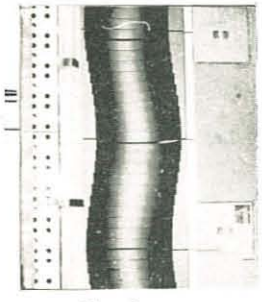

Fig. 1

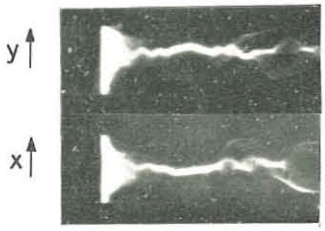

Fig. 2

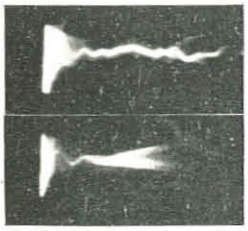

Fig. 3

a) 0.2 % impurities
b) 3 % oxygen

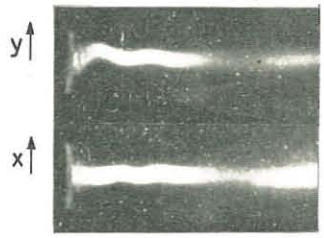

Fig. 4

The displacements of the plasma to be seen in Fig. 2 are resolved (slightly smoothed) in Fig. 5 in a plane perpendicular to the axis. It turns out that the plasma tends to drift into the equilibrium position near the magnetic axis at x = 0, y = 15 mm off the axis of the vacuum vessel. This is shown more clearly in Fig. 6 as position y versus time. The Figures shown are only examples for a typical set of parameters. Changing the parameters does not alter the overall behaviour of the plasma.

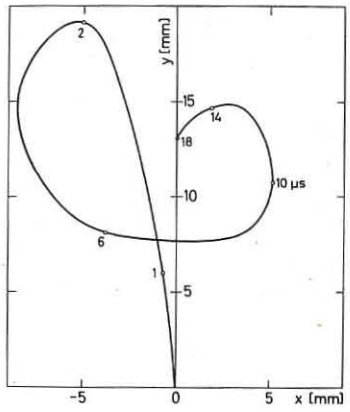

Fig. 5

In contrast to our experiments with a pair of helical conductors, we were not able to vary the time difference between the main field and the helical field.[4] But, obviously, this turns out not to be essential for successful experiments.

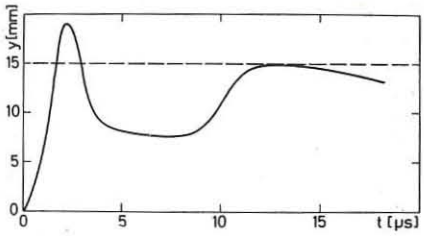

Fig. 6

The parameters of the experiments were: bank energy up to 2.6 MJ, bank voltage up to 40 kV, magnetic field up to 31 kG, rise time (quarter cycle) 7 or 9 µs, coil length 5.4 m, inner coil diameter 23 cm, inner vacuum-vessel diameter 10 cm, temperatures between 20 and 500 eV, densities between 10^{16} and 10^{17} per cm^3.

At the time of completion of this paper we displaced the vacuum vessel out of the axis of symmetry of the coil, in order to test the restoring forces that should be present after the initial implosion.

References:

1) H. Grad, H. Weitzner, Phys. Fluids 12, 1725 (1969).

2) J. Nührenberg, Rep. IPP 6/77, Institut für Plasmaphysik, Garching b. München (1969).

3) J.P. Freidberg, B.M. Marder, Rep. LA-DC-11350, Los Alamos Scientific Laboratory, Los Alamos, N.M. (1970).

4) M. Kaufmann, E. Fünfer, J. Junker, J. Neuhauser, Bull. Am. Phys. Soc. 14, 1037 (1969).

+) This work was performed as part of the joint research program of the Institut für Plasmaphysik and Euratom.

Helical Equilibrium and Stability Experiments in a 3-Meter Linear Theta Pinch

by
W. E. Quinn, F. L. Ribe, and R. E. Siemon
Los Alamos Scientific Laboratory, University of California
Los Alamos, New Mexico 87544 USA

Abstract: Helical $\ell = 1$ fields on a high-β plasma column are observed to produce a helical equilibrium and to induce I_z currents in the plasma. The $m = 1$ instability growth rates are reduced by applied I_z currents.

It may be possible to use helical fields to contain a toroidal high-β plasma column. [1] The $\ell = 1$ system [2-6], has been found theoretically to have the most favorable stability properties against the predominant $m = 1$ mode. The Scylla IV experiment [7] has been modified to have a 3-meter compression coil and a 120-μsec crowbar [B_z(max) = 60 kG]. Experiments with added helical $\ell = 1$ fields have been carried out in preparation for the Scyllac toroidal theta-pinch experiment [8].

Case I - Operation Without Helical Fields With a coil of uniform inner diameter (10.5 cm) Scylla IV-3 produces a stable plasma as indicated by the streak photographs of Fig. 1. Filling with 10-mtorr deuterium and no bias field gives a peak density of 3×10^{16} cm^{-3} (interferogram) and ion temperature of about 1.0 keV (neutrons). A rotating $m = 1$

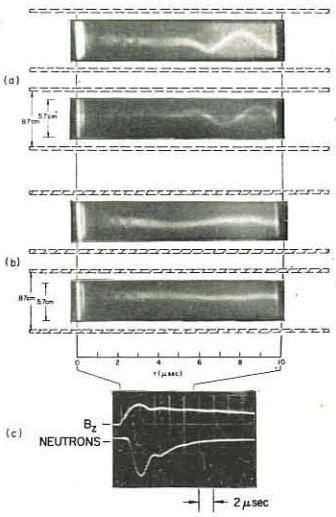

Fig.1. Operation without Helical Fields

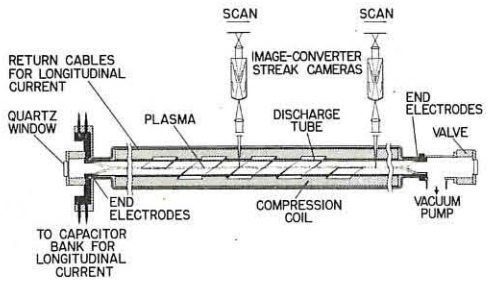

Fig. 2. Diagram of $\ell = 1$ coil arrangement with end electrodes

displacement with an amplitude which varies between discharges (Fig. 1) sets in after an Alfvén transit time of 5.0 μsec and is thought to be due to the onset of plasma rotation [9] resulting from end-shorting. [10]

Case II - Superimposed Helical Fields and Opposing Current I_z (Shorted End Electrodes) An $\ell = 1$ field, 9 periods long, with a wavelength of 30 cm was introduced by shaping the inner surface of the compression coil, using helical grooves of rectangular cross section (1.6-cm deep) as shown schematically in Fig. 2. Except for the different coil and externally shorted end electrodes to observe plasma-induced I_z, the theta pinch was operated under the same conditions as Case I and gave results shown by the streak photographs in Fig. 3A. The column moves quickly sideways on every discharge and hits the wall 2.2 ± 0.5 μsec after the start of the main field (growth rate $\gamma_1 = 3.0 \pm 0.4$ MHz). The observed I_z is interpreted as an axial current arising because of the plasma's high conductivity, which opposes the establishment of a rotational transform characteristic of the helical equilibrium [11]. I_z opposes a rotational transform whose direction corresponds to the vacuum fields of the right-handed helix.

Case III - Superimposed Helical Fields with Applied I_z In order to embed the rotational transform in the body of the plasma, I_z was generated by a

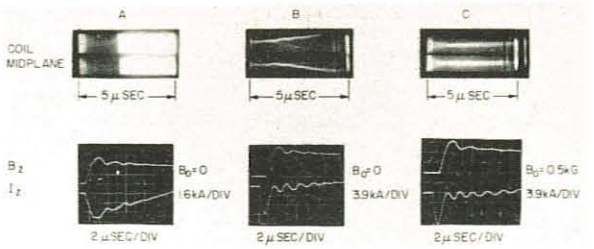

Fig. 3. Operation with Helical Fields. Case II (A) and Case III (B and C)

separate capacitor circuit which applied a current as shown in Figs. 3B and 3C. A noticeable improvement in stability was observed, which depended critically upon the timing of I_z relative to B_z, its magnitude, and the waveform of I_z (although not its sign). The more stable condition shown in Fig. 3B ($\gamma_1 = 0.6 \pm 0.1$ MHz) required that I_z reach its peak at the initiation of B_z and then quickly return to zero. With a $4\frac{1}{2}$-period groove in the center portion of the 3-meter coil, applied I_z stabilized the plasma.

Figure 3C shows the stable configuration resulting from a small bias field, $B_o = +0.5$ kG. We conjecture that in this case the transform is embedded by the bias field before the implosion, as is borne out by the observation that the opposing I_z (observed with shorted end-electrodes) is one-half that of Case II.

By means of end-on holographic interferograms [7] the integrated density $\int n_e dz$ was measured at peak field as shown in Fig. 4. Case III, which corresponds to Fig. 3B, gives clear evidence for the helical equilibrium (streak photographs show a 1.3-cm column). Case II (no I_z) is intermediate with a smaller helical displacement, while Case I (no helical groove) has none. All profiles show conservation of deuterons from the filling pressure of 10-12 mtorr. In Case III both the fractional helical distortion ($\delta \approx 1.3$) and the growth rate ($\gamma_1 = 0.6$ MHz) agree reasonably well with the theory. [3,4].

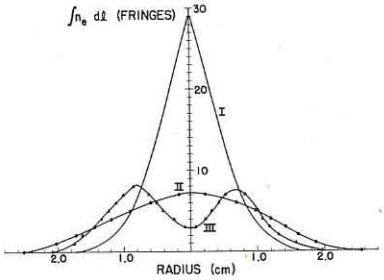

Fig. 4 Profiles of $\int n_e dz$

References

[1] F. L. Ribe and M. N. Rosenbluth, Phys. Fluids 13, to be published.

[2] A. A. Blank, H. Grad, and H. Weitzner, Plasma Physics and Controlled Nuclear Fusion Research, Novosibirsk Conference Proceedings 1968 (IAEA, Vienna, 1969). Vol. II, p. 607.

[3] M. N. Rosenbluth, J. L. Johnson, J. M. Greene, and K. E. Weimer, Phys. Fluids 12, 726 (1969).

[4] F. L. Ribe, Los Alamos Scientific Laboratory Report LA-4098 (1969).

[5] H. Grad and H. Weitzner, Phys. Fluids 12, 1725 (1969).

[6] H. Weitzner, Phys. Fluids 13, to be published.

[7] R. F. Gribble, E. M. Little, W. E. Quinn, and R. E. Siemon, J. Appl. Phys. 41, to be published.

[8] H. Griem, H. Grad, H. Grove, C. Hartmann, R. Kilb, N. Lazar, and F. Ribe, USAEC Report TID-23705 (1966).

[9] J. P. Freidberg and J. A. Wesson, Phys. Fluids 13, 1117 (1970).

[10] K. S. Thomas, Phys. Rev. Letters 23, 746 (1969).

[11] H. P. Furth, Princeton Plasma Physics Laboratory Report MATT-759 (1970).

THE m=0 TEARING-MODE INSTABILITY IN A LINEAR THETA PINCH WITH TRAPPED REVERSE MAGNETIC FIELD

L. Könen, P. Noll, F. Waelbroeck and H. Witulski

Institut für Plasmaphysik, KFA-EURATOM Assoziation, Jülich, Germany

Introduction. The stability of a current sheath has been investigated in several experiments /1-5/. In some cases /2,3/ the plasma behaviour is in disagreement with predictions for the resistive tearingmode instability /6,7,8,9/. In our previous experiments /4/, the stability of collisional theta pinch plasmas with trapped reverse magnetic field was studied in a coil of 10.5 cm diameter and 120 cm length. The growth rates of the m = 0 mode were observed to be about two times faster than expected; it was not possible to vary the plasma radius a sufficiently to derive experimental scaling laws. In the following we present new results obtained in a coil of 21 cm diameter and 120 cm length.

Experimental details. Deuterium gas was preheated by a low energy theta discharge and permeated by a slowly rising magnetic bias field B_o, and then compressed by a magnetic field of opposite polarity. In most experiments we had B_{max} = 28 kG, $\tau/4$ = 10.5 /usec, $\tau_{1/e} \approx 300$ /usec after crow-bar at B_{max}.
The plasma evolution was followed by simultaneous streak pictures made at 8 windows in the central region of the coil (spacing 8 cm) and by measurement of the diamagnetism $\Delta\phi$ along the axis with 16 compensated magnetic loops. The average electron temperature T_e was derived from X-ray absorption measurements and from the occurence of impurity lines. The radial distribution of the magnetic field in the midplane z = 0 was measured by a magnetic probe of 2 mm outer diameter.

Experimental results. Pure m = 0 modes growing to large amplitudes were observed for example for p_o = 50 mTorr and B_o = -600 G. Shortly after the start of the main discharge the plasma is essentially homogeneous ($\partial/\partial z \approx 0$) in the central coil region. After t = 4-5 /usec the plasma constricts radially at two axial positions. The growth time and the axial wavelength of this m = 0 instability are, resp., τ = 3 /usec and $\lambda \approx 33$ cm. τ is derived, independently from the relative perturbation $\delta\varphi$ of $\Delta\phi$ (see fig. 1a, τ = 3.1 /usec) and from the relative perturbation $\delta r_{1/2}$ of the halfwidth $r_{1/2}(z,t)$ of the radiation profile (τ = 3 ± 1 /usec). $\delta\varphi$ is defined by $1-2\Delta\phi_{min}/(\Delta\phi_1 + \Delta\phi_2)$ where $\Delta\phi_{min}$ is measured at the position of a constriction and $\Delta\phi_{1,2}$ are the neighboured maxima. $\delta r_{1/2}$ is analogously defined. At t = 4 /usec, the beginning of the instability, we have T_e = 90 eV, B_e = 15 kG, $n_e \gtrsim 3 \times 10^{16}$ cm^{-3} at the B = 0 neutral zone assuming $T_i \lesssim T_e$, and a B(r) profile as given in fig. 1b.

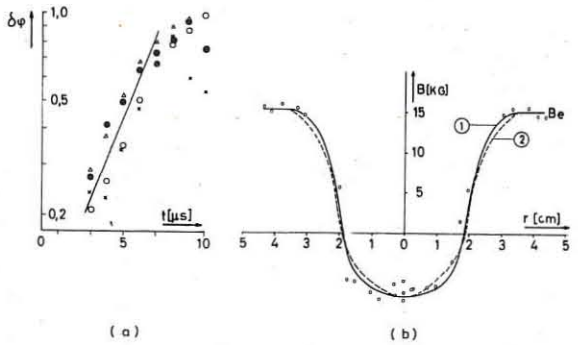

Fig. 1 (a) relative perturbation $\delta\varphi(t)$ of the diamagnetic signal $\Delta\Phi$ for 4 discharges with p_o = 50 mTorr, B_o = -600 G. $\delta\varphi$= 1 corresponds to a complete constriction a→0. End effects are expected to play a role after about 8 /usec.
(b) B(r) at t = 4 /usec. Curve 1: from magnetic probe at z = 0 (open circles), curve 2: average from Abel inversion of light profiles at z = -8, 0, +8 cm, whereby we assumed $\partial T_e/\partial r = \partial T_i/\partial r = 0$.

It should be remarked that strong deviations from axisymmetry (m ≳ 1 modes) occur when B_o > 1 kG and that the amplitude of the m = 0 modes is usually small when $p_o \lesssim 30$ mTorr.

Discussion. τ and λ can be compared with theoretical predictions for the resistive tearing-mode instability /6,7,8,9/. Numerical calculations for an imcompressible axisymmetric fluid model have been performed by Kaleck /4/. When B(r) is parabolic with a smooth transition to the outer region B_e and $-B(0)/B_e = 0.5 \ldots 1$, the growth time τ_m of the fastest growing m = 0 mode and the corresponding axial wavelength λ_m can be fitted by, resp., $\tau_m = 0.58\ s^{1.47}\ T_e^{0.44}$ /usec and $\lambda_m = 7.3\ s^{1.16}\ T_e^{0.32}$ cm. The characteristic thickness of the current sheath $s = B_e/(\frac{dB}{dr})_{B=0}$ is in cm, T_e is in eV, classical resistivity transverse to a strong magnetic field is assumed.

In the previous experiments with a 10.5 cm coil B(r) was deduced from light profiles only and approximated within the limits of error by a parabola. The result $\tau_m \approx 2\tau_{obs}$ can possibly be attributed to an overestimation of the skinlayer s.

In the 21 cm coil the plasma radius is about two times larger than in the smaller coil and the initial unpertubed period lasts longer. For this reason is was possible to obtain more accurate light profiles and to use a magnetic probe as a second independent method, i.e. to determine B(r) with better accuracy. Fig. 1b shows that both methods yield approximately the same B(r)-profiles. B(r) cannot be approximated by a parabolic distribution which fits B(r) at r = 0 and r = a (≈2.6 cm); the current is strongly concentrated in a relatively narrow sheath. Using the above mentioned formulas (i.e. an osculating parabolic fit at r_o where B = 0) we obtain τ_m = 2.8 /usec and λ_m = 23 cm. τ_m is in good agreement with the experimental value, the value of λ_m is probably not of much significance since the minimum of the computed $\tau(\lambda)$ relationship is broad. The error caused by the deviation of the applied fit from B(r) in the central region r ≈ 0 is estimated to be unimportant: the discontinuity $\Delta' = (\psi'/\psi)_+ - (\psi'/\psi)_-$ of the field perturbation calculated for the applied parabolic B(r) distribution increases only by about 10% when the parabola is cut-off by a flat bottom B = const. which fits the experimental B(r) near r = 0. Theoretically, Δ' should scale as $\Delta'^{-4/5}$ /7/.

For t < 4 /usec the radial oscillations resulting from the implosion are rather large in amplitude. The fact that long wavelength m = 0 modes grow only after $t \approx 4$ /usec may be attributed to acceleration effects /7/: from the observed oscillation amplitudes we estimate for the gravitational term $G \gtrsim 0.1$ for t < 4 /usec. Thus, the condition $G\ S^{2/5} < 1$ for purely growing tearing modes is possibly violated ($S = \tau_R/\tau_H \approx 3000$ is the ratio the resistive diffusion time to the hydromagnetic transit time).

Conclusion. The growth time of the observed m = 0 instabilities are in good agreement with values predicted for the resistive tearing-mode on the basis of a simplified model.

The authors thank Dr. H. Kever for useful discussions on theoretical aspects and Mr. G. Giesen for his help in the evaluation of the light profiles. The assistance of Mr. J. Schwarz during the experiments is gratefully acknowledged.

References:

/1/ H.A.B. Bodin, Nucl. Fusion 3 (1963) 459
/2/ A. Eberhagen, H. Glaser, Nucl. Fusion 4 (1964) 296
/3/ M. Alidierès, R. Aymar, P. Jourdan, F. Koechlin and A. Samain, Plasma Physics 10 (1968) 841
/4/ A. Kaleck, L. Könen, P. Noll, K. Sugita, F. Waelbroeck, K. Watanabe, H. Witulski, Plasma Physics and Controlled Nuclear Fusion Research, IAEA, Vienna 1969, Vol. II p. 581
/5/ O.A. Anderson and W.B. Kunkel, Phys. Fluids 12 (1969) 2099
/6/ P.H. Rebut, Plasma Physics (J. Nucl. Energy Part C) 4 (1962) 159
/7/ H.P. Furth, J. Killeen, and M.N. Rosenbluth, Phys. Fluids 6 (1963) 459
/8/ B. Coppi, J.M. Greene, and J.L. Johnson, Nucl. Fusion 6 (1966) 101
/9/ J.A. Wesson, Nucl. Fusion 6 (1966) 130

THE INITIAL BEHAVIOUR OF TOROIDAL DISCHARGES WITH PARALLEL MAGNETIC FIELD

by

G. Malesani[/], W.R. Ellis[*] and A.A. Newton[x]

/ Centro Gas Ionizzati C.N.R. - Universita di Padova, Italy

* Los Alamos Scientific Laboratory, New Mexico, U.S.A.

x U.K.A.E.A., Culham Laboratory, Abingdon, Berks., England.

Abstract: In a study of preionization by the "current trapping" technique[1] the experimentally determined times for current growth suggest a two stage multiplication process. Results in H_2 and D_2 at 10 to 40 mtorr in parallel fields ≤ 4 kG are presented and discussed.

Introduction: Measurements of breakdown have been made at Culham in a quartz vacuum vessel of 32 cm major radius, 4 cm minor radius with a superimposed quasi-steady magnetic field, B, parallel to the circular axis. An aluminium shell surrounds the vessel carrying a current parallel to B driven by a voltage $V(t) = V \sin(2\pi t/T)$, applied across a cut in the shell ($T = 7$ μsec). During the first microsecond an additional decaying high frequency voltage $< \pm 10\% \hat{V}$ due to circuit transients is also present. More detail is given in reference(1).

Two electric field components are present: an induced $E_z(t)$ and a conservative $E_s(t)$ in the region of the voltage feedpoints. The latter has been reduced by a guard ring inside the shell. In some cases a further reduction is made by covering the vessel with a resistive material (250 Ω/□) everywhere except at pumping ports. Its response time (evaluated by the method of reference(2)) is a few tens of nsec.

The breakdown time, τ, is defined as the interval between applying V at t = 0 and the sudden rise of current in the gas I_g, which is taken, for consistency, as the time when I_g reaches 3 kAmps. Values of τ have been measured for various B, $\hat{V}$ and pressures, p, with and without resistive screening for both gases.

Results: Figure 1 shows τ plotted against B_z for p = 21 mtorr H_2 at three values of V_M; typical results for the resistive screen are

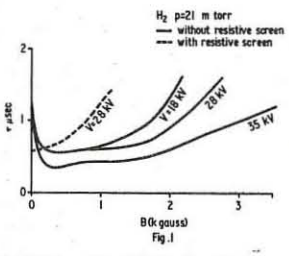

Fig.1

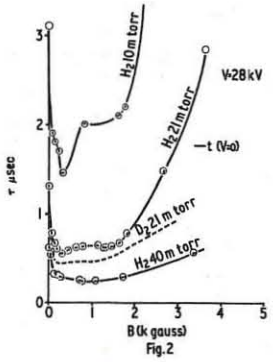

Fig.2

included. The effect of variations in p is shown in Figure 2. For low values of τ the product (pτ) is approximately constant for fixed $\hat{V}$,B but when $\tau \sim t$ (V = 0) precise values of τ are hard to measure.

Discussion: Since during τ the electric fields vary with time we discuss only data with $\tau \leq 1$ μsec. As B is increased from zero τ falls from τ_o to a minimum τ_{min}. This is interpreted as a reduction of electron loss to the walls (e.g. see (3)) and can be represented by

$$\tau^{-1} \propto \nu \left[1 - aD/\nu(1 + b\omega_{be}^2/\nu_{em}^2) \right] \qquad \ldots (1)$$

where ν is the growth rate of ionization without losses[1], D is a diffusion coefficient when B = 0, ω_{be} is the electron gyro frequency, ν_{em} is the total electron-molecule collision rate, b is the ratio of ion and electron mobility[4], and a is a geometrical factor. For H_2 $\nu_{em} = 5 \cdot 10^9$ p sec^{-1} and $b = 1/40$[5]. In figure 3 results are compared with equation (1) and agreement can be obtained with $aD/\nu \sim 0.5$ to 0.6. With the resistive screen $\tau = \tau_{min}$ when B = 0 suggesting that radial components of E_s are responsible for the above losses.

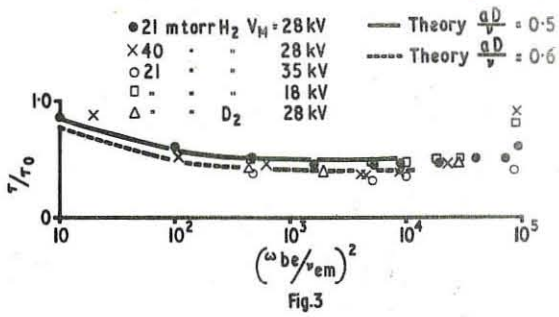

Fig.3

Since τ_{min} is roughly independent of screening and (pτ) ≈ constant, we infer that τ_{min} is determined mainly by volume processes. Then the electron density at breakdown, n_b, is related to the initial electron density, n_o, by $n_b = n_o \exp(\beta\tau_{min})$, where β is the ionization rate. Extrapolating measured values of electron drift velocity[6] to our E/p we estimate $n_b \sim 10^{12}$ cm^{-3} when $I_z = 3$ kA. Using known values of β[7] we find $n_o \sim 10^6$ to 10^7 cm^{-3}.

This initial density must be produced in times $\ll \tau$. One possible fast mechanism is ion induced secondary emission from the walls which can occur if the electrons do not screen E_s from the vessel[8] (i.e. if $n_o < 10^8$ cm^{-3}). The radial component of $E_s \sim 10^3$ v/cm is sufficient for this mechanism. The electrons liberated produce more ions by collision and the generation time is determined by the ion motion. The secondary emission coefficient, γ, is thought to be in the range 1 to 10[8]. After N generations the electron density is increased by $\gamma^{N-1}(e^{\alpha d} - 1)^N$ where α is the first Townsend coefficient and d is the distance travelled by the electrons. At high E/p the value of α is weakly dependent on E/p and $\alpha \sim 10p$ for H_2. We estimate a generation time of 20 nsec at 20 mtorr so that substantial multiplication is possible within the screen response time.

The rate of this process increases with $\hat{V}$ and decreases with B. In the latter case the ions are prevented from reaching the wall because B limits the amplitude of their cycloidal motion to $m_i E_r/B^2$. On this model τ increases when B exceeds a critical value which is an increasing function of p, $\hat{V}$ and m_i. The effect of the resistive screen (see Fig.1) can be interpreted in a similar manner.

Essentially the same behaviour is observed in deuterium but with an erratic shot to shot variation superimposed. The influence of ion mass at large B is seen when averaged values of τ for the two gases are compared.

Conclusion: We infer that current grows in two distinct phases; initially by ion induced wall secondary emission driven by the conservative electric fields, and subsequently by volume processes due to currents driven by the induced electric field. Large values of axial field inhibit the first process by limiting the ion motion and small values of axial field aid the second process by reducing electron loss to the wall.

It is a pleasure to acknowledge L. Firth and M. Holloway for assistance in the laboratory.

(1) W.R. Ellis. Culham Laboratory Report CLM-PR 12 p.B.51.

(2) M.R. Barrault, J. McCartan. Brit.J.Appl.Phy. 16, 1532 (1965).

(3) D.J. Rose, M. Clark. Plasmas and Controlled Fusion. Ch.4.7 - M.I.T. Press (1961).

(4) S.C. Brown. Introduction to Electrical Discharges in Gases. Ch.4., Wiley (1966).

(5) H. Beerwald. Julich Rep., Jul 480 PP(1967) also CTO/444.

(6) H. Schlumbohm. Z. Physik, 182, 317 (1965).

(7) E. Gerguoy, G.W. Stuard. Phys. Fluids, 3 1008 (1960).

(8) A. von Engel. Ionized Gases. Ch.3.8. Oxford Univ. Press (1965).

Preionization Studies for Toroidal High-Beta-Experiments[+)]

by

A. Eberhagen

Institut für Plasmaphysik, Garching, Germany

Abstract: Preionization is achieved in toroidal geometry by induced azimuthal currents. Favourable breakdown properties down to filling pressures of 3 mTorr D_2 and suitable preionization plasmas were established by application of a rf- predischarge and superposition of small azimuthal magnetic fields with only 10 kV potential difference around the 2 meter long torus circumference.

In the present studies preionization of deuterium was investigated in toroidal geometry for subsequent high-β experiments. A torus vessel with a major radius R = 30 cm and a smaller radius r = 5 cm was used. It was surrounded by a 1 mm thick copper shell, which was to simulate the current leads in case of a toroidal high-energy experiment. The preionization of the gas was achieved by azimuthal currents which were induced inside the torus by primary currents (I_z-currents) in two current belts. These two belts encircled the circumference of the torus outside the copper shell on the outer and the inner major radius, respectively. Shortening of induced currents in the copper shell was prevented by corresponding insulated slits. The primary I_z-currents in the belts were supplied by a bank of 16 kvolts charging voltage, which corresponds to 10 kvolts potential difference along the 200 cm long belts around the torus. This relatively low value was chosen to reduce the danger of adverse coupling of the preionization circuit to subsequent discharge circuits. The quarter period used was correspondingly relatively long. It had a value of 10 µsec and enabled sufficient breakdown in the same quarter period with delaytimes of up to 7 µsec. In addition to the induced currents azimuthal magnetic fields of up to 5 kGauss could be generated inside the torus by separate meridional windings and the corresponding B_z-bank. Finally,it was possible to investigate the breakdown behaviour of deuterium in the presence of a preceding 8-MHz-rf-predischarge. It was coupled into the torus by 8 pairs of loops around the smaller diameter of the torus vessel, which were equidistantly distributed along its circumference. The average peak to peak voltage of these rf-oscillations was 10 kV.

A) Breakdown properties of the toroidal discharges.

The distribution of the electric fields inside the torus vessel before breakdown corresponds to the equivalent situation in the thetapinch geometry, which was discussed, e.g., by Chodura et al. (1). It results from the superposition of the curl-field due to the increasing I_z-currents and of the electric potential field from the charges on the surface of the electric lead outside the torus vessel, which in the present arrangement is the copper shell rather than the current belts. The azimuthal curl-field contribution, which provides a longer path for the charges inside the torus for further ionization, is established only after the potential field is screened on the inner vessel surface by charge carriers initially formed.

The breakdown characteristics of the discharges investigated, i.e. the relationship between deuterium filling pressure p_o (mTorr) and delay time Δt (µsec) between start of the I_z-currents and actual breakdown, are summarized to a first approximation by the relationship:

$$p_o \cdot \Delta t = \text{const.}$$

In this representation any correction is omitted such as proposed by Malesani and Newton(2). The experimental results are shown in the diagram. The plotted values connected by the solid line refer to the case where no rf-predischarge was applied. They indicate:

(i) The hyperbolic relationship cited gives a suitable representation of the results, which were obtained for filling pressures from 50 mTorr on downwards.

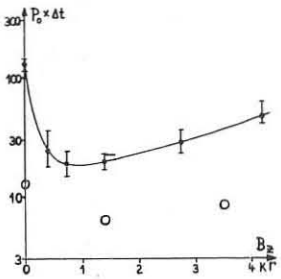

(ii) At complete absence of superimposed magnetic fields breakdown with delay times $\Delta t \leq 7$ µsec could only be achieved for filling pressures $p_o \geq 15$ mTorr.

(iii) Application of small B_z-fields improved the breakdown behaviour considerably: At B_z = 700 Gauss breakdown occured for $p_o \geq 3$ mTorr D_2. This can be understood from an extended presence of accelerated charge carriers inside the torus volume before they are lost for ionization processes by wall contact.

(iv) At higher B_z-fields the breakdown behaviour worsened again. This is attributed to the fact that screening of the electric potential field on the inner vessel surface by charge carriers is increasingly impeded by the higher azimuthal B_z-fields.

Also shown in the diagram are some results where the discharge was preceded by the 8-MHz-rf of 10 µsec duration. A substantial improvement was observed in this situation, e.g. even in the absence of any B_z-field breakdown did now occur for $p_o \geq 5$ mTorr. The duration of the rf-predischarge had only a minor effect on this improvement when longer than 2 µsec. The simple hyperbolic relationship cited, however, is no longer valid: At higher filling pressures breakdown occured together with the start of the I_z-currents, whereas at low p_o-values breakdown rapidly failed. Since only small amounts of impurities were found liberated by the rf-discharge the observed improvement in the breakdown properties is interpreted as an enhanced screening of the potential field by additional charges formed in the rf-oscillations.

B. Properties of the toroidal preionization plasmas.

Without superimposed B_z-fields the plasma was compressed after breakdown to a current channel of about 2 cm diameter which became unstable after 2 µsec. After this moment the impurity level rapidly exceeded values of 1 %. In order to avoid this undesired behaviour of the plasma two measures have been taken:

(i) A crowbar in the primary I_z-current circuit 1 µsec after achieved breakdown provided a limitation of the rapidly increasing plasma current to values between 15 and 20 kAmps.

(ii) As was indicated already, it was tried to reach a stable equilibrium position of the toroidal preionization plasma by superposition of azimuthal magnetic fields.

Probe measurements of the B_z- and B_θ- fields in the plasma gave evidence that even small superimposed fields of B_z = 400 Gauss were sufficient to attain a stable plasma in the torus when the crowbar in the primary I_z-circuit was used. In this case the plasma current flowed fairly homogeneously across about 2/3 of the diameter of the discharge vessel such that the copper walls could support stabilization of the toroidal plasma column. The ionization degree achieved was derived from the $D\beta$(4860) - line profile and was found to be α = 0.7 at 15 µsec after breakdown for p_o = 15 mTorr. The plasma temperature was then estimated to be below 1 eV from the electron density values obtained and from the absolute intensity of the $D\beta$- line. The impurity level from carbon and oxygen contaminations was of the order of 0.1 %. Application of a preceding 8-MHz-rf predischarge did not alter the above findings, except that the impurity level increased to about 0.2 % at 5 µsec rf-duration and 0.8 % at 20 µsec rf-duration.

(1) Chodura,R., Keilhacker,M., Zs.Naturf. 17a, 977 (1962)

(2) Malesani,G., Newton,A.A., Paper on this conference (1970)

[+)] This work was performed as part of the joint research program between the Institut für Plasmaphysik, Garching and Euratom.

NON-LINEAR (IN)STABILITY THEORY OF PINCH.

by

D.K.Callebaut

Instituut voor Nukleaire Wetenschappen

Rijksuniversiteit,Proeftuinstraat,40.Gent.Belgium.B-9000.

Abstract. The oscillation and instabilities of a mhd pinch are studied to second order in the amplitude of the perturbation. The stability critiria of the linear theory are not directly affected. Limits for the linear theory appear; Singularities in the second order coefficient do occur.

I. Introduction. The method for studying finite perturbations investigated extensively by the author for liquid, plasma and gravitational cylinders[1)2)] is exposed here for a simple pinch. The aim is to treat the non-linear behaviour, to look for the influence on the stability critiria, to set limits on the linear theory and to have a guiding model in the study of dynamic stability.

2. Model. At equilibrium the column is an infinitely long cylinder of radius R_o. The plasma is homogeneous, isotropic, of zero resistivity and incompressible. The magnetic field in it is homogeneous and parallel to the axis (z-axis) of the cylinder: $\bar{H}_o = H_o(0,0,1)$

The surrounding field is a vacuum field $\bar{H}_o^{vac} = H_o(0, \frac{\alpha R_o}{r}, \alpha)$ where α and β are parameters. A metallic concentric cylinder of arbitrary radius qR_o may be present ($q>1$). Extensions are given at the end.

3. Hierarchy of higher order systems. Consider first in the linear theory a single Fourier component. At the surface the corresponding perturbation is $R_o \varepsilon \cos(kz+m\varphi)$ where k and m have their usual meaning and where

$$\varepsilon = \epsilon e^{\sigma t} \qquad (1)$$

is dimensionless, as well as ε, the relative (i.e. divided by R_o) initial amplitude. σ is the corresponding time constant given as a function of m, k, κ, β and q by the dispersion relation of the linear theory[3)]. σ^2 may be positive (instability) or negative (oscillation) in the following.

To make a series development in ϵ seems quite logical in the case at hand; however, to make a series development in $\epsilon e^{\sigma t}$ may seem to be looking for a very particular case; moreover, when $\sigma > 0$ the divergent character of the terms when t grows large seems disastrous. Nevertheless we argue the necessity of this development as follows:

a. Mathematical argument. Substitution of the first order solution in the non-linear terms of the equations generates second order terms in ϵ^2. We infer that the remaining second order terms which are related to the particular first order perturbation under consideration also depend on time like ϵ^2. Similarly for higher orders.

b. Physical argument. As initial amplitude we may choose (within some limits) ε at any time instead of ϵ. Since a series development in the initial amplitude seems legitimate the development in ε is equally legitimate (within the same limits).

As to the convergence when $\sigma > 0$ we point out

a. Mathematically. 1) Although $e^{n\sigma t}$ grows infinitely large for n large, ε^n approaches zero when $\epsilon < 1$. 2) The series is useful up to the radius of convergence.

b. Physically. When $\sigma > 0$ the cylinder usually breaks for a finite time; and then the basic system has to be changed.

Substitution of $X = X_0 + \varepsilon X_1 + \varepsilon^2 X_2 + \varepsilon^3 X_3 + \cdots \qquad (2)$

where X denotes any quantity p, $\bar{H}$, $\bar{u}$ or $\mathcal{R}$ (= the r-coordinate of the surface) in the basic set of equations leads, for each power n of ε, to a system of equations. These systems are all independent of time; they are coupled; however any system contains only quantities of its own order or of lower order.

From the nature of this series in ε it becomes clear that an instability (resp. oscillation) of the linearized theory will remain an instability (resp. oscillation) to all higher orders and that the dispersionrelation is unchanged as long as ε is smaller than the radius of convergence.

4. System of second order. It can be shown (with a minor restriction in the case of oscillations) that the velocity field $\bar{u}_2$ is a gradient. (This feature is lost for compressible plasma). Moreover the solution can be shown to be based essentially on the second "harmonics" i.e. if the first order solution corresponds to $\mathcal{R}_1 = R_o \varepsilon \cos(kz + m\varphi) \qquad (3)$

then the second order solution has to contain $I_{2m}(2kr)$ and $K_{2m}(2kr)$ (these being the modified Bessel functions) and moreover cosines of 2kr and $2m\varphi$ or constants. Solving the second order system and applying the boundary conditions leads to the expressions of p_2, $\bar{u}_2$, $\bar{H}_2$, $\bar{H}_2^{vac}$ and

$$\mathcal{R}_2 = R_o \left[a - \tfrac{1}{4} + \tfrac{1}{2}\left(1 + \frac{m^2}{\kappa^2}\right) J_m(\kappa) \right] \cos(2kz + 2m\varphi) - \frac{R_o}{4} \qquad (4)$$

where $\kappa = k R_o$ and where

$$\left\{ \frac{(m+\epsilon\kappa)^2}{\kappa^2} \left[\mathcal{L}_{2m}(2\kappa) - \mathcal{L}_m(\kappa) \frac{J_{2m}(2\kappa)}{J_m(\kappa)} \right] + \left[1 - \frac{J_{2m}(2\kappa)}{J_m(\kappa)} \right] \right\} a$$

$$= \left[1 + \frac{3\kappa^2}{4 J_m(\kappa)} - \frac{3}{4}\left(1 + \frac{m^2}{\kappa^2}\right) J_m(\kappa) \right] + \frac{m(m+1\kappa)}{2\kappa^2} \left[2\mathcal{L}_m(\kappa) + \mathcal{L}_{2m}(2\kappa) \right]$$

$$+ \frac{(m+\epsilon\kappa)^2}{4\kappa^2} \left\{ \begin{array}{l} \left[-3\kappa^2 + \mathcal{L}_m(\kappa) \left[\dfrac{3\kappa^2}{J_m(\kappa)} + \left(1 + \dfrac{m^2}{\kappa^2}\right)\left(\kappa - J_m(\kappa)\right) \right] \right] \\ \left[+ 2\mathcal{L}_{2m}(2\kappa) \left(1 + \dfrac{m^2}{\kappa^2}\right) \left[\mathcal{L}_m(\kappa) - J_m(\kappa) \right] \right] \end{array} \right\} \qquad (5)$$

in which we have used the abbreviations $\epsilon = \alpha/\beta$, $J_m(\kappa) = \frac{\kappa I_m(\kappa)}{I'_m(\kappa)}$ and

$$\mathcal{L}_m(y) = \frac{\kappa \left[I_m(y) K'_m(q\kappa) - K_m(y) I'_m(q\kappa) \right]}{\left[I'_m(\kappa) K'_m(q\kappa) - K'_m(\kappa) I'_m(q\kappa) \right]} \qquad (7)$$

The coefficient a has been investigated extensively. We mention that when $\kappa \to 0$ singularities do occur (also in the higher order terms). Similarly when $\kappa \to \infty$. The linear theory is limited by the requirements $\varepsilon \ll 1$, $\varepsilon\kappa \ll 1$ (or $\varepsilon\kappa^2 \ll 1$ in some cases) and $\epsilon/\kappa \ll 1$, while we can roughly say that the nonlinear series will become useless when ϵ, $\epsilon\kappa$ (or $\epsilon\kappa^2$) or $\epsilon/\kappa = 1$. This can be interpreted physically.

5. Extensions

(a) The calculations are easily extended to the case when a force-free field surrounds the plasma cylinder.

(b) When compressibility is taken into account the calculations are more involved but similar. See also ref.4.

(c) Including higher orders gives no principal difficulties. In the case of the liquid jet we performed the calculations up to fourth order and verified them in various ways.

(d) The same calculations ($q = \infty$) were performed adding self-gravitation.

(e) Interference between two or more Fourier terms of the linearized theory leads to no principal difficulties. This is important (a) for the dynamic stabilization (b) for the generality of the method.

References.

1. D.K. Callebaut, Plasma Phys., 10, 440 (1968)
2. D.K. Callebaut, Aggregation Thesis (1970) (Rijksuniversiteit Gent)
3. S.Chandrasekhar. Hydrodynamic and magnetodynamic stability. Oxford (1961) p.565 etc.
4. W.Schuurman. Rijnhuizen report 68-48. (Ass.Euratom-Fom, the Netherlands.)

DYNAMICS OF A Θ-PINCH WITH A SUPERIMPOSED AZIMUTHAL MAGNETIC FIELD

by

T.A. El-Khalafawy, A.M. Youssef,

V.G. Diatlov+ and Ya. F. Volkov+

PLASMA PHYSICS AND ACCELERATORS DEPARTMENT,

Atomic Energy Establishment, Cairo, U.A.R.

Abstract: A magneto-hydrodynamic steady flow model, on the assumption of ideal plasma conductivity, has been used. The theoretical calculations of the discharge radius and the period of magneto-hydrodynamic oscillations are confirmed by experimental results.

I. Theoretical Consideration: In supposition of an ideal conductivity of plasma a magneto-hydrodynamic model is used. It is supposed that a thin ideal conductive current layer is confined between internal and external magnetic fields. If the kinetic pressure of the plasma is low the balance of magnetic pressures registrating the change of magnetic fields during the discharge can be written as follows

$$-B_{oz}^2 \frac{\alpha^4 \sin^2\tau}{(\alpha^2 - X_o^2)^2} + B_\varphi^2 \frac{a^2 - X_o^2}{X_o^2} + B_o^2 \frac{1}{X_o^4} = 0 \qquad (1)$$

where

$X_o = \frac{z}{z_o}$; $\tau = \omega t$; $\frac{R}{z_o} = \alpha$, $\beta = \frac{R_1}{z_o}$; $a = \ell n \frac{1}{\beta} / \ell n \frac{X_o}{\beta}$; B_{oz}, ω are the amplitude and frequency of the external magnetic field; B_φ is the value of the azimuthal field on the initial radius z_o; B_o is the initial value of the 'trapped' axial field; z is the radius of the discharge; R is the

+ On leave from the Atomic Energy Committee USSR.

radius of the external magnetic field coil; and R_1 is the radius of the axial rod, the current of which gives an azimuthal field.

For simplicity the second term of the equation can be approximated with enough accuracy by $0.5\,B^2\,(\frac{1}{X^4} - 1)$. The solution of equation (1) in X_o allows to evaluate the discharge radius. This solution for typical discharge parameters (B_{oz}=15 KG; B_φ = 2 KG; B_o=1 KG; α =1.3; ω =$2.10^5 sec^{-1}$; z_o=6 cm) is displayed in fig. 1 (curve a). The approximated equation for a minimum discharge radius is

$$X_{omin} = \alpha \left(\frac{\sqrt{B_o^2 + 0.5\,B^2}}{\alpha^2 B_{oz} + \sqrt{B_o^2 + 0.5\,B^2}} \right)^{1/2} \qquad (2)$$

In supposition that all the particles are 'trapped' by the current layer the equation of motion is written as follows

$$\frac{d}{d\tau}\left(\omega^2 M \frac{dX}{d}\right) = \frac{X}{4}\left[-B_{oz}^2 \frac{\alpha^2 \sin^2\tau}{(\alpha^2 - X^2)^2} + 0.5\,B_\varphi^2 \left(\frac{1}{X^4} - 1\right) + B_o^2 \frac{1}{X^4} \right] \qquad (3)$$

where M is the linear mass of the current layer

$$M = \left(1 + \frac{\mu_o}{\mu} - X_o^2\right) = \mu\,(\gamma - X_o^2)$$

where μ_o is the initial linear mass of the current layer.

μ is the aggregate linear mass of the discharge.

The qualitative consideration shows that the current layer is compressed while making oscillations round the equilibrium position which is determined by equation (1). The estimations of oscillations amplitudes based on the characteristics of a potential pit and maximum kinetic energy of the current layer show that for typical working conditions the amplitude does not exceed $\delta = \pm 0.1$. For small amplitudes it is possible to find the solution of equation (3) in every point of the equilibrium radius in supposition of the frequency of oscillations being high in comparison with the frequency of the external field. In this case the frequency of oscillations is

$$\omega_o = \left(\frac{0.5\,B_\varphi^2 \left[\alpha^2(3 + X_o^4) + X_o^2(1 - 5\,X_o^4)\right] + 4\alpha^2 B_o^2}{4\omega^2 \mu X_o^4 (\alpha^2 - X_o^2)(\gamma - X_o^2)} \right)^{1/2} \qquad (4)$$

For typical conditions of the discharge the period of oscillations is about $T = 0.1\,\mu sec$. Such radial oscillations of the plasma are of magneto-hydrodynamic nature. A simpler consideration of similar oscillations in a Θ-pinch for a no-azimuthal magnetic field case was given in paper (1).

II. Experimental Set-Up: The experiments were performed with the aid of the set-up described in paper (2). For measurements of radial velocity of a Θ-pinch with an azimuthal magnetic field plasma an axial electric polarization field method has been used. This field appears due to radial plasma motion in an azimuthal magnetic field. Knowing the value of the polarization field it is possible to calculate the radial velocity V_z using the expression

$$V_z = 10^8 \frac{E_z}{B_\varphi}$$

The discharge radius was graphically calculated using the data of the radial velocity. The measurements of the magnetic field B_φ was performed with the aid of a magnetic probe and that of the polarization fields with a double electric probe. High speed camera measurements have been taken too. Fig. 1 shows the time dependence of the radius of a Θ-pinch discharge with an azimuthal magnetic field, obtained by different methods: a) by magnetic pressure balance method, b) by a high speed camera method, c) by an axial polarization field method. The dotted curves show the shifts of inner plasma layers, calculated according to the axial polarization measurement. As the figure shows, all the methods used give similar results.

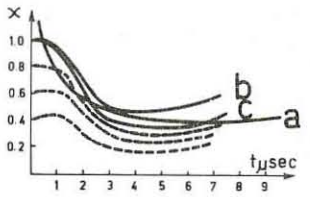

FIG.1

In Fig. 2 a typical oscillogram of the axial electric polarization signal is presented. This signal has a high frequency component which is caused by magneto-hydrodynamic oscillations. The oscillations period is close to the calculated one.

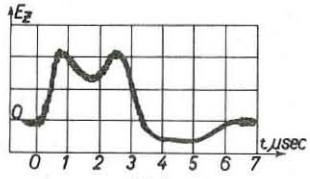

FIG.2

If the period of magneto-hydrodynamic oscillations is of the order or shorter than the ion-ion self-collision time, such oscillations can contribute to plasma heating. As the amplitude of radial oscillations is small, such oscillations cannot actually affect the plasma confinement.

References:

1. Niblet G.B.F. and Green T.S., (1959) Proceedings of the Physical Society, vol. 74, pt. 6, No. 480, p. 737.
2. El-Khalafawy T.A., Youssef A.M., El-Hak L.G., Hafez, L.A. and Volkov Ya. F., (1969) Proceedings of the 9th International Conference on Ionization Phenomena in Gases, Boucharest, Panel 3.1.8, No.3, p.211.

Invited Lecture

SURVEY OF SCREW PINCH STUDIES

by

P.C.T. van der Laan

Association Euratom-FOM
FOM-Instituut voor Plasma-Fysica
Rijnhuizen, Jutphaas, The Netherlands

Abstract

In many types of experiments the plasma column is confined by a helical magnetic field; in the screw pinch the two field components B_z and B_θ are applied simultaneously and with a similar time history. The first pinch of this type was studied in Livermore by Colgate et al.[1] in 1958. At present many laboratories study the screw pinch; these various investigations will be described.

Already short delays (e.g. 0.2 μs) between the application of the two field components lead to a considerable modification of the screw pinch. Longer delays and a different time behaviour for B_z and B_θ are used in the older stabilized pinches, in the new high β toroidal experiment at Culham and in the Tokamaks where the strong quasi-stationary B_z field prevents the plasma from pinching.

In most cases the programming of the fields determines the field distribution outside the pinch because of the presence of a well-conducting low-density plasma which fills the region between the main column and the wall. If this plasma has zero resistivity and if end effects are absent the pitch of any moving helical field line remains constant. The limitations of this model will be discussed. More general MHD-code calculations have been carried out at Culham for five different pinch configurations. Measurements carried out in a toroidal device will be compared to the computer results; the agreement in the outside region is good. The calculations also explain why the low-density plasma is present; if the pre-ionization is not complete neutrals are left behind in the outside region and are ionized later.

Calculations on the equilibrium and the stability of a pinch surrounded by a constant-pitch field[2] suggest two favourable regimes for toroidal confinement, namely at $q \simeq 3/4$ and at $q \simeq 2$, where q is the ratio of the pitch of the field to the circumference of the torus. Experimental results confirming this theory qualitatively will be presented. Two screw pinch devices are being fitted with better copper shielding of the torus so that fewer field and current lines will intersect with the quartz wall.

A calculation on kink instabilities in toroidal geometry (Schuurman, Bobeldijk) shows no effect in first order of the toroidal curvature on the growth rate of a kink; however, the basic mode in the torus consists of a triplet of modes with mode numbers m+1, m and m-1 where m is the azimuthal mode number of the equivalent mode in the cylinder.

Especially for the experiments at $q > 1$ the construction of the primary z-circuit should be such that the longitudinal plasma current increases when the plasma ring moves to its eccentric equilibrium position close to the metal wall. This increase of current can also be found in a second order equilibrium calculation.

This work was performed under the association agreement of Euratom and FOM with financial support from ZWO and Euratom.

References

1) S.A. Colgate et al. Proc. 2nd UN Int. Conf. PUAE 32 (1958), 140.

2) R.F. de Vries, R.J.J. van Heijningen, C. Bobeldijk, J.P. Goedbloed, P.C.T. van der Laan and W. Schuurman, Contributions III Eur. Conf. Contr. Fusion & Plasma Phys., p. 88, Utrecht, 1969, and earlier references quoted therein.

STABILIZATION OF PINCH INSTABILITIES BY FORCE-FREE MAGNETIC FIELDS

by

J.P. Goedbloed

Association Euratom-FOM/FOM-Instituut voor Plasma-Fysica
Rijnhuizen, Jutphaas, the Netherlands

Abstract

Stability of pinch experiments is discussed from the point of view that the outer region is approximately force-free.

It has been firmly established by now that the outer region of a pinch discharge is of great importance for its stability[1]. This is one of the reasons why sharp-pinch theory fails to account for the observed stability of screw pinches. If this theory is modified by replacing the vacuum by a pressureless plasma with a magnetic field of constant pitch, this failure is removed. On the other hand, completely diffuse models for the high-beta toroidal-pinch experiment, under construction in Culham, are predicted to be stable against all ideal MHD modes. In this paper some common features and some differences of the two models are discussed from the point of view that the outer region of the pinch has a low density and pressure and therefore approximately must be force-free.

The stability criteria for a dense plasma surrounded by a tenuous plasma with a force-free magnetic field, defined by $\nabla\times\underline{B}=\alpha(r)\underline{B}$, read:

1) The following inequalities should be valid at the plasma boundary:

a) If there is no singular point ($k+\mu m=0$) in the surface layer,

$$(1-\beta)k\frac{I_m(kr)}{I'_m(kr)} > \frac{\mu^2 r}{1+\mu^2 r^2} + \frac{\alpha r\,(k+\mu m)(k\mu r^2-m)}{(m^2+k^2r^2)(1+\mu^2r^2)} + \frac{r^2(k+\mu m)^2}{(m^2+k^2r^2)(1+\mu^2r^2)}\frac{(rQ_r)'}{rQ_r},$$

where Q_r is the radial magnetic-field perturbation.

b) If there exists a singular point:

$$L > \frac{k^2 r}{m^2+k^2r^2}\left[1-\beta\frac{(B^t)^2-(B^s)^2}{(B^t)^2-(B^p)^2}\right] > R,$$

where L and R are the expressions of inequality 1)a) and B^s, B^p, and B^t are the magnitudes of the magnetic field at the singular point, and at the inner and outer boundary of the surface layer.

2) The solutions to the marginal-mode equation for Q_r,

$$(rQ_r)''+\frac{1}{r}\frac{m^2-k^2r^2}{m^2+k^2r^2}(rQ_r)'+(\alpha^2-k^2-\frac{m^2}{r^2}+\frac{2km\alpha}{m^2+k^2r^2}-\frac{1}{r}\frac{m-k\mu r^2}{k+\mu m}\alpha')rQ_r=0,$$

should not have more than one zero in the outer region or the independent subintervals of it.

Violation of the three criteria yields: kink modes, resulting in a displacement of the dense plasma column; surface-layer modes, being of importance as limiting cases of instabilities possible in diffuse pinches; instabilities of the outer region itself. It was shown that a force-free field of constant pitch effectively stabilizes the dangerous kink instabilities, thus providing an explanation for the observed stable behaviour of the screw pinch.

In some respect the constant-pitch force-free field is rather peculiar. In particular the division which is usually made between localized interchange modes and non-localized kinks no longer makes sense. Because of the absence of shear interchange modes are not localized in a constant-pitch field. Moreover, in a force-free field of constant pitch it is not clear at all whether interchange modes can occur because Suydam's criterion is marginally satisfied. In the limit $k+\mu m\to 0$ the last term of Eq.2) blows up and, as a result rapidly oscillating solutions appear[2], showing that the constant-pitch force-free field is in fact unstable. The unstable region can be visualized by a plot of L and R as a function of k. Every time rQ_r has a zero point R blows up. Therefore, for the parameter values of Fig.1 the force-free region of the pinch is unstable for k-values from 18.4 to 20 m^{-1}.

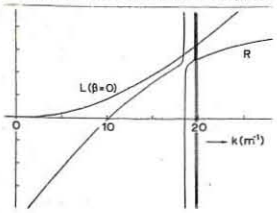

Fig.1.Stability diagram for μ =const. m =1, r_o =0.03 m, r_1 =0.06 m, μ =- 20 m^{-1}

The instabilities of the force-free field with a constant pitch arise in the situation that Suydam's criterion degenerates, and so one expects the growth rates to be small. In the local approximation with $kr\gg 1$ and $k_\parallel \ll k$ the equation of motion gives unstable solutions for $k_\parallel r = O(kr)^{-1}$ and the maximum growth rate is given by: $\rho\omega^2 = -27B_z^4B_\theta^{12}/(4\mu_o k^4 r^6 B^{14})$. This expression strongly depends on the value of μ. Indeed, for local values of $\mu r\sim 0.1$ (the Jutphaas experiment) this growth rate is negligible for the tenuous plasma. For local values of $\mu r\sim 1$ (the Culham experiment) the growth rate of these instabilities would be rather limiting. However, for the Culham experiment the constant-pitch model does not apply because the fields are programmed in such a way as to have a high shear.

The growth rate given above also strongly depends on the assumption of zero-pressure gradient and therefore it is more realistic to look at constant-pitch fields in the presence of a small pressure gradient. From Suydam's criterion one knows that these fields are unstable. On the other hand, it was argued by Ware[3] that the instabilities which develop are not important because the growth rate is so small that finite Larmor radius effects will stabilize them. However, this argument is based on an expression for the growth rate which is only valid if $k_\parallel r\to 0$. Again in the local approximation the maximum growth rates occur for $k_\parallel r = O(1)$. Then $\rho\omega^2$ is given by:

$$\rho\omega^2 = -\mu_o\left(\frac{2\gamma pB_\theta^2}{rB^3}\right)^2\left[1-\sqrt{\frac{rB^2}{2\gamma pB_\theta^2}\left(p'+\frac{2\gamma pB_\theta^2}{rB^2}\right)}\right]^2,$$

which for small negative p' reduces to: $\rho\omega^2 \simeq -\mu_o(p'/2B)^2$. These growth rates are not small at all and therefore Ware's argument does not apply. For practical values of ρ and B growth rates in a tenuous plasma will be very high, even for modest pressure gradients. The fact that for most of the instabilities that occur the assumption of locality is invalidated makes the situation even worse. Indeed, from the equation of motion it can be shown that the instabilities having the largest growth rate are never local and their growth rate is always higher than that given by the expressions above.

Instabilities of the outer region of the pinch can be avoided by dropping the restriction of constant pitch. For force-free fields with a constant α for example the last term of Eq.2) vanishes and oscillating behaviour of rQ_r is absent, at least if α is not too large. So the outer region of the pinch is stable. Moreover, one has a free parameter to fit experimental data. In Fig.2 L and R are plotted for three values of α: α=0 (the vacuum field); α=-24.6 m^{-1}, corresponding to a field which is on the average close to a constant pitch field; α=-50 m^{-1}, giving a high shear field. The α=-24.6 field conserves the beneficient effect of the constant-pitch field with respect to kink modes. Moreover, the small shear of this field is sufficient to remove the instabilities present in the constant-pitch field. A draw-back of the α=-24.6 field is that it has a minimum in the shear. So a small negative pressure gradient will again produce instabilities. Fields with a higher absolute value of α have more shear and the stability diagram of Fig.2 becomes optimal. The value α=-50 m^{-1} gives a field profile which can be regarded as a limit of the diffuse profiles of the Culham experiment. For this value of α the pinch is completely stable for a β up to 20%. For the much lower values of $\mu(r_o)$ of the Jutphaas experiments the optimal value of α gives a field which is close to a constant-pitch field. Instabilities in this case can be avoided by the introduction of enough shear so as to satisfy Suydam's criterion.

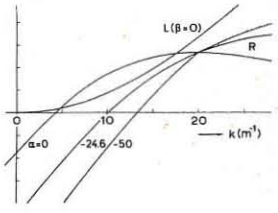

Fig.2.Stability diagram for α =const. m =1, r_o =0.03 m, r_1 =0.06 m, $\mu(r_o)$ =-20 m^{-1}

The author thanks Dr. M.P.H. Weenink, Dr. W. Schuurman, Dr. C. Bobeldijk, and Dr. P.C.T. van der Laan for helpful comments.

This work was performed under the Euratom-FOM association agreement with financial support from ZWO and Euratom.

References

1. See references in: J.P. Goedbloed, Phys.Rev.Lett. 24 (1970) 253.
2. Also noticed by J.P. Freidberg, H. Weitzner, and D. Weldon.
3. A.A. Ware, Phys.Rev.Lett. 12 (1964) 439.

NUMERICAL CALCULATION OF SCREW PINCH STABILITY[+)]

by

W. Grossmann

INSTITUT FÜR PLASMAPHYSIK

8046 Garching b. München, Germany

Abstract: A calculation of the M = 1 MHD long wavelength Kruskal-Shafranov mode of instability is presented for experimental conditions corresponding to the Garching toroidal and linear screw pinch experiments.

The Method used, first introduced by Freiberg / 1 /, involves solving the linearized dynamical equations of MHD for diffuse magnetic field and density profiles. A particular eigenvalue problem along with boundary conditions must be solved by numerical means yielding the growth rate and the form of the plasma perturbation as a function of radius. Results for growth rates, from the analysis based on a straight plasma column, agree to within 10 percent with experimental values obtained from the toroidal experiment. The calculated form or shape of the disturbance also seems to agree with what is observed experimentally. We conclude that the method is applicable for the calculation of the m = 1 type of instability. Information concerning growth rates for the higher m numbers is being obtained using this method and will be presented.

Finally we are using the method to study a family of magnetic field and density profiles which can be produced in the Garching device. These profiles are parametrised with β in an attempt to find more stable plasma configurations to the m = 1 mode of instability. These results will also be presented.

References:

/ 1 / J.P. Freidberg, Los Alamos Rep. LA-DC-10793

+) This work was performed as part of the joint research program between the Institut für Plasmaphysik, Garching and Euratom.

Plasma confinement in a toroidal screw pinch at reduced β - values[+)]

by

P. Grossmann, R. Wilhelm, H. Zwicker

Institut für Plasmaphysik, Garching, Germany

Abstract: The stability behaviour of a toroidal screw pinch plasma with trapped parallel and antiparallel B_z- fields is investigated. For trapped parallel field of B_{zo} = 1 kΓ improved m = 1 stability was found as compared to the case B_{zo} = 0. The lifetime of the plasma is limited by instabilities starting in the pressureless plasma region surrounding the dense plasma column.

Earlier investigations of a toroidal screw pinch with β - values of about β = 0,75(T_e + T_i between 100 eV and 1 keV) /1/ had shown, that the equilibrium position and the m = 1 growth rates can be represented by the constant pitch model./2/. As a second step of these experiments the influence of superimposed B_z - fields was studied. For negative bias fields the lifetime of the plasma was clearly reduced compared to the pure screw pinch with the same temperature.

Fig. 1 shows the radial field-distribution at the moment of the first compression for B_{zo} = -1 kΓ. The plasma temperature is about 150 eV. From these measurements, the radial distribution of the pitch $\mu(r) = B_\theta/rB_z$ was evaluated. This can be compared with the time behaviour of the pitch $\mu(t)$ at the inner surface of the compression coil which is determined by the programed time behaviour of the fields B_z and the current I_z. The result is shown in Fig. 2. One recognizes that the radial distribution $\mu(r)$ represents directly the time-behaviour $\mu(t)$ at the wall. This gives experimental evidence that a wanted special field distribution can be produced simply by correct time programming of the outer currents.

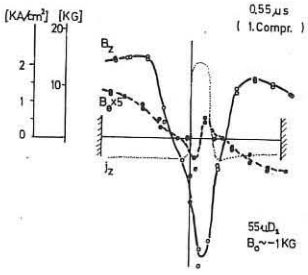

Fig. 1

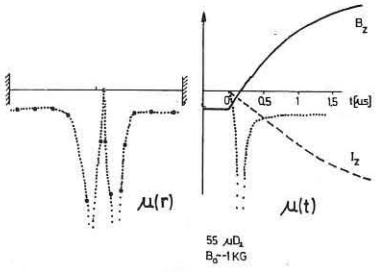

Fig. 2

For the case with positive bias field the m = 1 growth rates were strongly reduced and the lifetime of the plasma ($n_e \approx 10^{16}$ cm^{-3}, T_e;T_i ~ 70 eV) was improved compared to the case without bias field. This should be mainly a consequence of the decreased value of β which for our conditions was reduced typically from 0.75 down to about 0.25. Fig.3 gives a typical streak picture taken from above of the torus and showing that the dense column remains more or less stable for at least 10 µsec. The radial pitch distribution µ (r) at various times is shown in fig.4, as it follows from the measured field distributions.

The constant pitch is maintained only in the regions of the pressureless plasma which are directed towards the inner wall of the tube while in the opposite region of the pressureless plasma the pitch increases towards the wall and passes over a maximum which is shifted towards the wall.

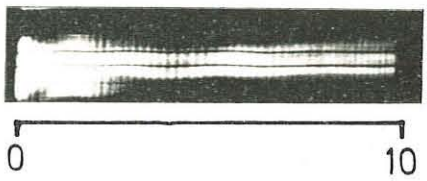

Fig. 3

For the same conditions as in fig.3 the stability behaviour of the toroidal plasma column is shown in a longer time scale in fig.5. One sees, that after about 6 µsec the pressureless plasma becomes luminous and that in the following the dense column starts to drift toward the outer wall and is destroyed. This seems to indicate that at a stable stage of the dense column the pressureless plasma becomes unstable with the consequence that the equilibriumposition is lost. Measurements of the plasma current I_z(t) show that at the time when the luminosity in the pressureless plasma appears the plasma current I_z which flows mainly in the pressureless plasma regions is strongly damped. Therefore it seems to be not unlikely that there is a connection between the instabilities in the outer plasma regions and the strong damping of I_z(t) which of course destroys the toroidal equilibrium. So far detailed reasons for the observed instabilities are not quite clear. Measurements in a linear screw pinch showed however, that for comparable conditions instabilities in the outer plasma regions do not occur. Therefore it seems that the instabilities in the pressureless plasma are due to the necessarily asymmetric distributions of the currents in a toroidal screw pinch equilibrium. Stability calculations including the pressureless plasma are being made by a new MHD code developed by W.Grossmann /3/. Comparisons with the experimental results will be given.

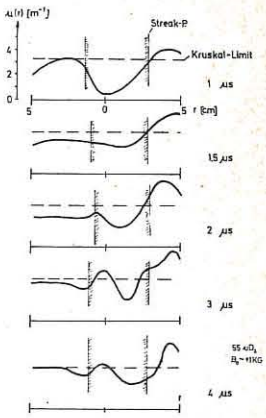

Fig. 4

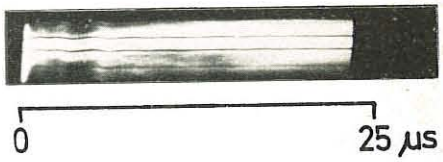

Fig. 5

/1/ P.Grossmann, R.Wilhelm, H.Zwicker, Z.Phys., 197o, to be published

/2/ W.Schuurman, et al., Plasma Physics, 11, 495 (1969)

/3/ W.Grossmann, Paper presented at this conference.

+) This work was performed as part of the joint research program between the Institut für Plasmaphysik, Garching and Euratom.

Absolute Measurement of Radiation Losses from a Theta Pinch Plasma in the Wavelength Region from 10 to 200 Ångstroms +)

by

W. Engelhardt, W. Köppendörfer, M. Münich, J. Sommer

Institut für Plasmaphysik, Garching, Germany

Abstract: A calibration procedure of a grazing-incidence spectrograph is described to allow for measurement of the radiation losses from a theta pinch plasma. The losses turn out to be small compared to both the electron energy content and to heat conduction losses.

1. Introduction There is lots of experimental evidence for the limitation of the electron temperature in linear theta pinches by energy losses /1/. One of the possible loss mechanisms are radiation losses by impurities within the plasma. According to the plasma temperature most of the radiation is emitted in the grazing-incidence region from about 10 to 200 Å. Because of the little knowledge of ionization and excitation cross sections, especially for more complicated ions, predictions on radiation losses from such a plasma are only possible within one order of magnitude accuracy. In order to get more accurate information the radiation from the plasma has to be measured.

Measurements therefore were performed on a linear theta pinch device (Isar II) having a stored energy of 200 kJ, a maximum magnetic field of 52 kG, and a 2.75 µsec quarter period. Coil length and diameter measured 100 cm and 10 cm. Typical plasma parameters were: $n_e = 1\text{-}4\cdot10^{16}\,cm^{-3}$, T_e= 200-300 eV, T_i = 0.5-3keV.

2. Calibration procedure of the Spectrograph The spectral resolution was obtained by use of a grazing-incidence spectrograph with either photographic plates or scintillator/multiplier combinations as detectors. For relative calibration of the instrument advantage was taken from ratios of lines from hydrogen-like ions such as CVI, NVII, OVIII being emitted from the plasma. Within either the Balmer series (76-182 Å) and the Lyman series (15-34 Å) line ratios were calculated by assuming corona equilibrium. The relative sensitivity of the apparatus was gained in these two wavelength intervals from the measured photographic densities. The intervals were then connected by branching ratios. For that the first Balmer line and the second Lyman line were suited since both start from the same level n = 3. A difficulty was the fact that the sublevels of level n = 3 showed deviations from statistical population which the branching ratios had to be corrected for. The correction was enabled by measurement of the intensity ratios of the fine structure components of the Balmer line. The relative calibration of the instrument, thus gained, could be well confirmed (within 20 % accuracy) by checking with known intensity ratios of lithium-like ion lines emitted by the plasma. The branching ratios 2S-3P/3S-3P of these ions finally allowed to hang the grazing-incidence spectrograph absolutely on a monochromator absolutely calibrated for the 3S-3P OVI line at 3811 Å. Usually the lines used were optically thin, with few exceptions, which could be corrected by extrapolating their optical thickness by seeding impurities of known amount.

3. The Results of Radiation Loss Measurements, Using the calibrated instrument the time integrated total energy losses were measured for different added impurities at filling pressures of 40 mtorr deuterium. Normalized to 1 % seeded impurity concentration the following radiated energies were obtained: carbon 27.7 J (CVI:24.9 CV:2.8), nitrogen 14.1 Joule (NV:0.95 NVI:5.1 NVII:8.0), oxygen 21.1 J (OVI:4.4 OVII:14.1 OVIII:2.6). No distinct dependence on the kind of the seeded impurity became evident. The distribution of the radiated energy on the different ionization stages of the atoms however showed characteristic features. The lighter the atom, the higher is the ionization stage by which most of the energy is radiated. Comparing these total energy losses, for example at 40 mtorr filling pressure, with the energy content of the electrons ($n_e=4\cdot10^{16}\,cm^{-3}$, T_e=200eV) they turn out to amount to 6 % only. Thus radiation cooling does not affect the electron temperature as long as the impurity concentration does not exceed 5 %.

Values for radiation losses from discharges without seeded impurities for different filling pressures and cases with bias field included are summarized in table 1. For 40 mtorr filling pressure and zero bias field the natural contamination is 0.085 % oxygen, 0.095 % carbon, and 0.0025 % nitrogen. For other pressures it is of the same order of magnitude and in any case smaller than 0.5 %. Only for low filling pressures and with bias field the more intense wall contact at the beginning of the discharge leads to unreproducible contamination and therefore often to larger energy losses. The contribution of free-free and free-bound continuum radiation to the losses is way below that of the line radiation.

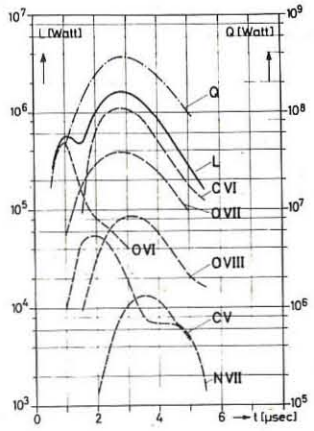

Figure 1 Radiation losses L and thermal conduction losses Q (p_o= 40 mtorr, B_o= 0G, no impurity added)

In fig. 1 the time dependence of the radiated power is displayed as determined photoelectrically. Absolute calibration stems from comparison of the time integrated power of a line with its photographic density on the plate. Losses by the thermal conduction estimated according to a model proposed by Green et al. /1/ are included in fig. 1. They exceed the radiation losses by a factor of 100 throughout the discharge. Except for impurity concentrations larger than 5 % the power radiated can exceed thermal conduction, predominantly by the ion OVI. These results agree essentially with measurements of Bodin et al. /2/.

References:

/1/ T.S. Green et al., Culham-Report CLM-P 124 (1966)

/2/ H.A.B. Bodin et al., Culham-Report CLM-P 198 (1969)

P_o mtorr	B_o G	oxygen	nitrogen	carbon
		Energy in Joule		
11	0	1,3	-	0.14
	500	19.0	0.017	0.035
17	0	5.0	0.012	1.3
	500	55	0.025	0.15
40	0	1.8	0.046	2.4
	500	14	0.025	0.73
80	0	1.0	0.056	2.3
	500	28	0.097	0.64

Table 1 Radiation losses under different initial conditions. No impurity added.

+) This work was performed as part of the joint research program between the Institut für Plasmaphysik, Garching and Euratom.

On the Influence of Ion Collisions on the Population Distribution of Atoms in a Theta Pinch Discharge[+)]

by

W.Engelhardt, W.Köppendörfer, M.Münich, J.Sommer

Institut für Plasmaphysik, Garching, Germany

Abstract: Line intensities of the Balmer series as emitted in the early phase of a theta pinch discharge show unexpected deviations from thermal equilibrium conditions. Because of the high ion temperature ($\frac{T_i}{T_e} \approx 10$) ion collisions can compete with electron collisions in populating levels with quantum numbers $n \gtrsim 3$.

1. Introduction. Line intensity measurements on a plasma frequently provide datas from which important plasma parameters can be deduced such as electron density and electron temperature. Usually lines are chosen starting from levels which are supposed to be thermally populated. Criteria for estimating whether local thermal equilibrium (LTE) exists have been reported by several authors /1,2/. Measurements on hydrogen or deuterium plasmas produced by fast theta pinch discharges /3/ however have shown considerable deviations from thermal equilibrium population distributions, although all criteria for LTE were fullfilled. Spatial and time resolved absolute intensity measurements of the first three members of the Balmer series of hydrogen have been carried out in the early phase of a fast theta pinch discharge. All necessary plasma parameters were additionally measured. Several possibilities which may be responsible for the departure from a thermal equilibrium population distribution have been discussed leaving the influence of ion collisions on higher lying levels as the most likely cause.

2. Experimental Results. The plasma investigated has been produced by a theta pinch discharge of 52 kG maximum field and 2.75 µsec quarter period. The discharge coil measured 100 cm in length and 10 cm in diameter. The filling pressures used ranged from 10 to 80 mtorr. Two axial current pulses of 1 µsec duration each served for preionization providing an about 40 percent ionized plasma at the time when the main discharge is fired. The electron temperature of the plasma was measured by Thomson scattering of laser light, the ion temperature was calculated from the neutron emission rate and from diamagnetic measurements. The electron density was gained from free-free continuum radiation measurements from Thomson scattering and from Mach-Zehnder interferometry. The radiation emitted in the visible from the plasma has been investigated by scanning the plasma radially with an absolutely calibrated monochromator. The emission coefficient of the observed lines was then obtained as a function of radius by Abel's inversion. Thus the emission coefficients for H_α, H_β, and H_γ, were determined in discharges of 11,17,40 and 72 mtorr filling pressure.

The lines peak rather independent of filling pressure at 0.3 to 0.4 µsec after the ignition of the main discharge. Afterwords they fall off rapidly in intensity and are essentially vanished after 1 µsec. They are approximately homogeneously emitted over the whole discharge volume with slightly increasing intensity towards the wall of the vessel. The relative radial distribution does not alter during the whole time this radiation is observed. The intensity ratios of $H_\alpha : H_\beta : H_\gamma$ for all filling pressures are typically 100:10:1 with deviations not larger than 30 % for either of the ratios. Using the Boltzmann factor this would yield an electron temperature of 0.4 to 0.6 eV. Quite different temperatures result if the absolute value of the emission coefficient and the electron density (at a distinct radius and time) is taken and the temperature calculated via the Saha equation again assuming LTE. Temperatures determined this way are usually by a factor of 10 to 100 higher than those evaluated from line ratios. Hereby H_α yields a lower temperature than H_β, and H_β a lower temperature than H_γ. The by Thomson scattering reliably measured electron temperature is at 0.5 µsec 100 eV for 11 mtorr, 70 eV for 17 mtorr, 45 eV for 40 mtorr and 20 eV for 72 mtorr filling pressure. All these findings indicate that the relative population density decreases much more rapidly towards increasing quantum numbers than as given by the Boltzmann factor. The absolute population density however exceeds at least for n=3 (H_α) the density as given by the Saha-equation.

3. Discussion of the results. Estimates considering relaxation effects for the population of the levels $n>2$, transport of radiation by resonance charge exchange or lack of LTE by inhomogeneities do not reveal that any of these processes is responsible for the observed anomaly. The strongest deviation from thermodynamic equilibrium is the difference in electron and ion temperature. The ratio of ion to electron temperature as determined from the neutron yield, diamagnetic measurements and from laser scattering is $8 \leq \frac{T_i}{T_e} \leq 12$ during the first microsecond and depends only weakly on the filling density since both electron and ion temperatures decrease at higher filling densities. Drawin /4/ has mentioned that under such circumstances higher lying levels might be influenced by ion collisions.

Therefore the stationary rate equations, as described by Mahn /5/ for a limited number of levels with collisional rate coefficients for ions included have been solved numerically for a set of the parameters n_e, T_e and T_i. To calculate the ionic rate coefficients the same cross sections as functions of the relative velocity of the colliding particles have been taken for the ions as for the electrons. The results show two effects.

1) Overpopulation of low lying levels $n \lesssim 3$ for electron densities $n_e < 3.10^{14} cm^{-3}$ and high electron temperatures ($T_e > \chi_H = 13.6$ eV).

2) Depopulation of high lying levels $n \gtrsim 3$ by proton collisions if $\frac{T_i}{T_e} \gg 1$.

Altough these solutions are well in the direction of the experimental observations they do not quantitatively meet the measured population densities. The observed anomaly still exceeds the calculated one. Possible causes for this discrepancy may bee: the crossections used for the ions in the calculations, the non Maxwellian velocity distribution of the ions in the plasma and relaxation effects for levels $n \lesssim 3$. The last possibility will be checked by solving the time dependent rate equations.

We thank Mr.R.Wunderlich for having written the computer programme.

References:

/1/ R.Wilson, J.Quant.Spectros.Radiative Transfer 2, 477 (1962)

/2/ H.R.Griem, "Plasma Spectroscopy" Mc.Graw-Hill, 150 (1964)

/3/ U.Schumacher, Laboratory Report, Institut für Plasmaphysik, Garching, Germany, IPP 1/93 (1968)

/4/ H.Drawin, Zeitschrift für Physik, 211, 404 (1968)

/5/ C.Mahn, Laboratory Report, Institut f.Plasmaphysik, Garching, Germany, IPP 3/52 (1967)

[+)] This work was performed as part of the joint research program between the Institut für Plasmaphysik, Garching and Euratom.

STUDY OF A NON CYLINDRICAL Z-PINCH BY HOLOGRAPHIC INTERFEROMETRY AND U.V. SPECTROSCOPY

A. BERNARD, J.C. BUGES, A. JOLAS, P. GENTA, J.P. WATTEAU
Commissariat à l'Energie Atomique, Centre d'Etudes de Limeil
B.P. 27, 94 - Villeneuve-Saint-Georges - France

Abstract - The electron density and electron temperature of a non-cylindrical Z-pinch are studied experimentally by means of the double exposure holographic interferometry technique and the ratio of two oxygen lines in the vacuum U.V. . Comparison are done with computations.

I - EXPERIMENT - The linear Z-pinch is known for the rapid rise of instabilities when the plasma sheath reaches the axis. To increase the sustainment time of the column a few authors /1,2/ have considered a curved rather than a straight pinch. The present experiment is aimed at verifying the influence of the initial curvature discharge on the final plasma. The two quantities studied here are the density and the electron temperature.

The experiment vessel is glassmade, axisymmetric with a narrowed central part (Fig. 1) filled with 0.1-1 Torr deuterium or hydrogen. It is energized by a fast capacitor bank of 25 kJ-120 kV.

We foresee to study the plasma theoretically by using a two-dimensional magnetohydrodynamic (MHD) model, as that written by POTTER /3/, but in the present report we used two available programs. One is a two dimensional snowplough model /4/ that is useful for comparison with the density front obtained experimentally by holographic interferometry. The other, a one dimensional MHD program /5/, is used fot the measurements done in the symmetry plane. For instance at t = 640 nsec the profiles of density and electron temperature are given by N_{MHD} and T_{MHD} in Fig. 2. From such graphs the curves N_{MHD} and T_{MHD} functions of time are plotted in Fig. 6

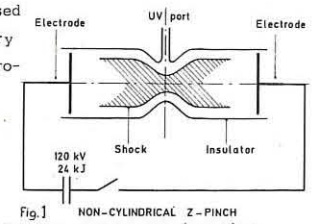

Fig. 1 NON-CYLINDRICAL Z-PINCH

2 - DENSITY MEASUREMENTS - The density measurements use the technique of double exposure holographic interferometry /6/, required in the experiment because of the poor quality of the chamber glass. The first exposure is taken without plasma. The second is taken at various times of the discharge dynamics. A hollow wedge, filled with a gas for the second exposure, gives a background of straight fringes - Fig. 3 shows a typical interferogram (at time t = 760 nsec) at 0.5 Torr hydrogen filling pressure. The dotted line indicates the location of the shock as given by the two dimensional snowplough model. The computed sheath velocity is seen to be smaller particularly on the sides of the central part. It is tried to obtain the density profile in the shock front from an Abel inversion. From the ID-MHD model and assuming a simpler rectangular density profile the maximum value $\int_o^{l} N_e \, dl$ has been calculated in the symmetry plane. For instance at t = 640 nsec we use the profile $Ne = 4 \times 10^{17}$ cm^{-3} for $1 < r < 1,7$ cm and $Ne = 0$ elsewhere giving $(Ne\ l)_{Max} = 1,1 \times 10^{18}$ cm^{-2} or a 3,5 fringes shift at 6943 Å. Comparison is made with a hologram taken at the same pressure as in the computation and at a time when the front is at the same distance from the axis. The maximum shift is 4 fringes which is in fairly good agreement with the computed value, but the actual front thickness - 4 mm - is smaller than that from the program, which might be caused by the choice of the viscosity coefficient. A hologram taken 100 nsec later shows (Fig. 4) larger shifts with matter not regularly located on the axis.

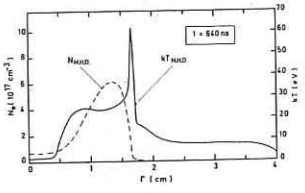

Fig. 2

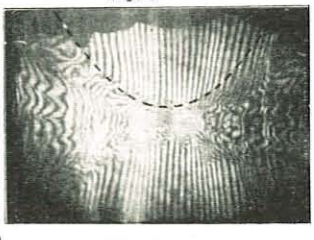
Fig. 3


Fig. 4

3 - ELECTRON TEMPERATURE MEASUREMENTS - The plasma radiates mainly in the U.V. region of the spectrum. The usual difficulties of observation are increased here by the experiment itself : the U.V. port oscillates to tens kilovolts and the solution found was to isolate the whole detection line (from the port to the oscilloscope).

The electron temperature is obtained from the measurement of the ratio R of two lines intensities. The lines from oxygen added in small amount (5×10^{-4} T) are OVI (1032 Å) and OV (1371 Å) as indicated by GRIEM /7/.

The plasma evolution being fast (characteristic time about 50 nsec) a quasiequilibrium cannot be reached between the two ions OV and OVI and a transient model has to be used - (Contrariwise there is a quasiequilibrium between the upper level of each line and the corresponding ground state). The population densities are solution of a diffential equations system and the measured ratio R is a function of temperature, density and past evolution. Drawing the temperature from R measurements assumes that the density is independently known. Short of experimental results at this time the curve N_{MHD} (Fig. 6) has been used. Then from the R measured values - dots on Fig. 5 - the curve kT_{SPECT} is deduced (Fig. 6). Actually for computational simplicity the curve kT_{SPECT} is assumed and the computed R is compared to the dots. The curve kT_{SPECT} of Fig. 6 is that giving the best fit between the computed and the experimental

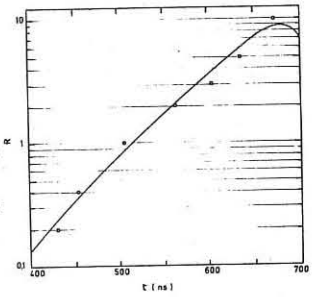

Fig. 5

R values. It is checked by varying the curves kT_{SPECT} and N_{MHD} that R is very sensitive to the temperature while very much less to the density.

The comparison between kT_{SPECT} and kT_{MHD} of Fig. 6 shows good agreement between the spectroscopic measurements and the MHD program.

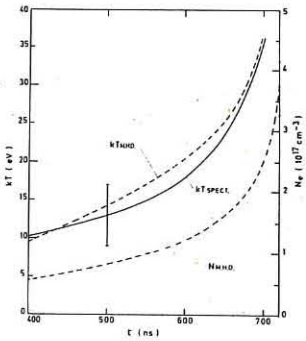

Fig. 6

REFERENCES

/1/ WATTEAU (J.P.) D. Sc. Thesis, University of Paris (1968)

/2/ COMISAR (G.G.) Phys. Fluids 12, (1969) 1000

/3/ POTTER (D.E.) Thesis Imperial College, London

/4/ BASQUE (G.), JOLAS (A.) WATTEAU (J.P.) Phys. Fluids 11 (1968) 1384

/5/ HAINES and ROBERTS ID-MHD Code, Culham Laboratory Abingdon Berks. (1970).

/6/ JAHODA (F.C.) , JEFFRIES (.R.A.) and SAYER (G.A.) Appl. Opt. 6 (1967) 1407

/7/ GRIEM (H.R.) Plasma Spectroscopy Mc Grawhill , New-York

/8/ BERNARD (A.), GENTA (P.), JOLAS (A.), MORIGNOT (S.) C.R.Acad.Sc. (to be published).

Z-Pinch Driven By Magnetic Energy Storage*

J. N. DiMarco and L. C. Burkhardt

Los Alamos Scientific Laboratory, University of California

Los Alamos, New Mexico, U.S.A.

Abstract: This experiment attempts to achieve a high temperature (keV) z-pinch by shock heating. The low inductance energy source uses the technique of magnetic energy storage. Voltages of ~ 60 kV and currents of ~ 200 kA at a rate of 2×10^{12} A/sec are obtained with deuterium at 20 mTorr; shock velocities of 4.2×10^{7} cm/sec are measured. The plasma column, grossly stable for 8 μsec, has an initial temperature of 1 keV as determined by pressure balance.

Description of Experiment: A schematic representation of the experiment is shown in Fig. 1

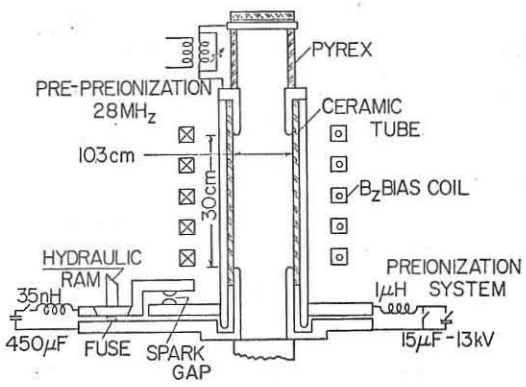

Fig. 1

*Work performed under the auspices of the U.S. Atomic Energy Commission.

Gas is preionized with a 25 kA axial current pulse. The primary energy storage is a 450 μF capacitor bank, charged to 12.5 kV. The electrostatic energy is then transferred into the magnetic energy storage inductance of 35-nH. The fuse[1] which consists of a copper foil 2.54×10^{-3} cm thick 14-cm wide, and 15-cm long, is vaporized by joule heating. The large voltage developed across the fuse fires an air gap switch which transfers the current to the z-pinch. The resulting large $\dot{B}$ causes a shock to form in the plasma.

Experimental Results: Typical voltage, current, and $\dot{I}$ is displayed in Fig. 2. Voltages of 40-60 kV are developed across the discharge tube.

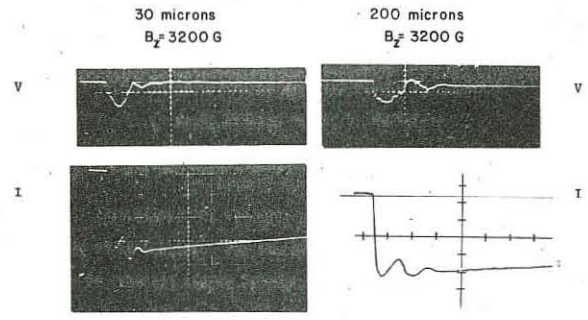

Voltage: 49 kV/div, Current: 60 kA/div
Sweep Time: 0.5 μsec/div

Fig. 2

The large $\dot{I}$ permits 80% of the current to transfer in ~ 0.1 μsec. A B_θ probe signal shows that the current sheath moves off the wall. Assuming a symmetrical current distribution, at least 90% of the current is flowing in the pinch inside the probe radius.

Shock generation is indicated by smear photographs which show luminous fronts propagating with velocities of 4.2×10^{7} cm/sec, through deuterium at 20 mTorr. This corresponds to an Alvén mach number of ~ 3 at 3000 G bias field. A shock structure similar to that seen by others[2] is obtained from the B_z and B_θ probes.

In a previous[3] fast z-pinch experiment a secondary breakdown is observed along the wall of the tube which is not detected in this experiment. A secondary breakdown would have prevented flux from escaping from the pinch tube and the oscillation of the voltage in Fig. 2 would not have been observed. In addition, the streak pictures do not show a secondary breakdown on the wall of the tube. This breakdown is inhibited by the use of a magnetic energy storage system. Such a system maintains a constant current so the voltage across the discharge is small at the time of peak compression when $\dot{L} = 0$. However, if a low-inductance capacitor bank were used, at the time of maximum compression almost the full capacitor-bank voltage is across the pinch. The discharge tube is then required to hold off a high voltage while exposed to the radiation of the hot pinched plasma. Figures 3 and 4 present the current obtained, by calculation, from the B_θ signals of two probes placed on a diagonal equidistant from the axis. Also plotted is the total current in the z-pinch. Current symmetry is maintained for ~ 8 μsec for the case of 30 mTorr D_2 and 3200 G bias field. Conversely, when the filling density is increased by a factor of 6.6 to 200 mTorr with an implied reduction of the plasma temperature, it can be seen from Fig. 4 that the current symmetry is lost in ≤ 5 μsec. It should be noted that for low value of bias B_z field the symmetry is lost within 1 μsec of pinch formation.

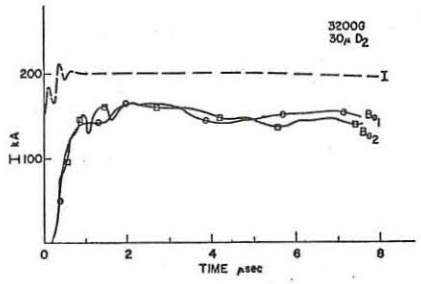

Fig. 3

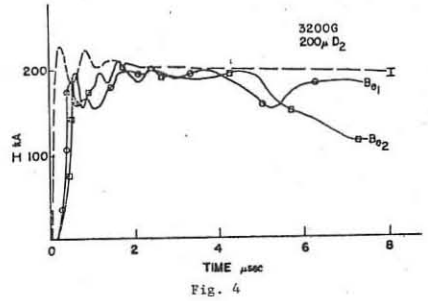

Fig. 4

References:

1. Los Alamos Scientific Laboratory Controlled Thermonuclear Research Program, LA-4075-MS, p. 3, 1968.
2. J.W.M. Paul, et. al., "Nature", 208, 133 (1965).
3. H.A.B.Bodin, A. A. Newton, and N.J. Peacock, "Nuclear Fusion", 1, 54 (1960).

INSTABILITY OF ELECTROSTATIC WAVES IN COLLISIONLESS SHOCKS

by

J. J. Sanderson

Department of Applied Mathematics, University of St. Andrews, Scotland, U.K.

and

S. P. Gary

Department of Applied Mathematics, University College of North Wales, Bangor, North Wales, U.K.

Abstract: This paper presents a linear analysis of electrostatic wave instability in collisionless shocks propagating perpendicular to an applied magnetic field. $\underline{E} \times \underline{B}$, ∇B, and ∇n drifts are included and the maximum growth rates are compared with those of the zero magnetic field ion acoustic instability.

Drift wave theory [1] has been used in a number of recent papers to find linear growth rates for the instabilities giving rise to the fluctuations observed in collisionless shock wave experiments. The model is well known; one considers perturbations of an equilibrium configuration in which the electrons experience an $\underline{E} \times \underline{B}$ drift (v_0) and other drifts due to inhomogeneities of the type $\underline{B} = B_0(1 + \varepsilon x)\hat{z}$ whereas the ions are effectively unmagnetized because the shock thickness << ion Larmor radius.

The linear dispersion relation for electrostatic waves in a Vlasov plasma has been solved numerically for both cold and warm ions including $\underline{E} \times \underline{B}$ and ∇B drifts [2,3]. The results of these calculations are summarized in the figure which shows the growth rate γ as a function of θ, the angle between the wave vector $\underline{k}$ and $\underline{B}_0$, the applied magnetic field. The parameter values chosen are those appropriate to the Culham Tarantula experiment [4]; $v_0/(T_e/m_e)^{\frac{1}{2}} = 0{\cdot}10$, $T_e/T_i = 10$,

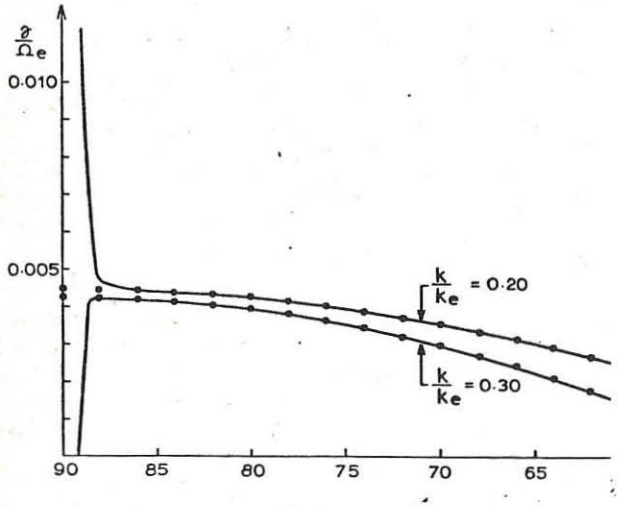

$\omega_e/\Omega_e \equiv (4\pi n_0 e^2/m_e)^{\frac{1}{2}}/(eB_0/m_e c) = 68$, $m_i/m_e = 1836$ and $\beta_e \leq 0.360$. At $\theta = \frac{\pi}{2}$ the instability is due to the coupling of electron Bernstein modes (which show a $\underline{k}.\underline{v}_0$ Doppler shift) with the ion acoustic wave. In this case the maximum growth rate can be substantially larger than that for the $\underline{B} = 0$ ion acoustic instability (represented by the dotted lines), in contrast with the results of Krall and Book [5]. For oblique propagation the Bernstein waves are strongly damped and no coupling occurs; the dispersion characteristics are then the same as for the $\underline{B} = 0$ ion acoustic instability and an appropriate non-linear theory should resemble the Kadomtsev-Sagdeev approach [6].

These results may be extended to include a ∇n drift by choosing for the equilibrium electron distribution function $f_e^{(0)} = n_0(m_e/2\pi T_e)^{\frac{3}{2}}(1 + \varepsilon'(x - \hat{y}/\Omega_e))\exp\{-m_e(\underline{v} - \underline{v}_0)^2/2T_e\}$. For $k \gg \varepsilon'$ this then leads to the dispersion equation [7]

$$1 + K_e + K_i = 0$$

$$K_e = \frac{k_e^2}{k^2}\left\{1 + \frac{2(m_e/2T_e)^{\frac{1}{2}}}{k\cos\theta}(\omega - k(v_0 - v_n)\sin\theta)\sum_{\ell}\int_0^{\infty} u\,du\,\exp(-m_e u^2/2T_e)\right.$$
$$\left. J_\ell^2(ku\sin\theta/\Omega_e)Z\left[\frac{(m_e/2T_e)^{\frac{1}{2}}}{k\cos\theta}(\omega + \ell\Omega_e - k(v_0 - v_B)\sin\theta)\right]\right\} \qquad (1)$$

$$K_i = -(k_i^2/2k^2)Z'[\omega(m_i/2T_i)^{\frac{1}{2}}/k]$$

where k_e, k_i are the electron and ion Debye wave numbers and $v_n = \varepsilon' T_e/m\Omega_e$, $v_B = \varepsilon u^2/2\Omega_e$ are the ∇n and ∇B drift velocities. Since v_n occurs only in the term $(v_0 - v_n)$ in eqn.(1) the extension of the above results is a simple matter. An approximate analytic expression for the growth rate is at $\theta = \frac{\pi}{2}$,

$$(\gamma/\Omega_e) = [m_e(k(v_0 - v_n) - \omega)^2/8m_i\beta_e\Omega_e k v_0]^{\frac{1}{3}}/(1 + \frac{k^2}{k_e^2}).$$

Since $v_n/v_0 \sim \beta_e$ the conclusion is that for a low β plasma the effect of the ∇n drift is negligible. One can contrast this with the ∇B drift for which we also have $v_B/v_0 \sim \beta$. For $\theta = \frac{\pi}{2}$

$$K_e = \frac{k_e^2}{k^2}\left\{1 - \frac{m_e}{T_e}(\omega - k(v_0 - v_n))\sum_{\ell}\int_0^{\infty}\frac{u\,du\,\exp(-m_e u^2/2T_e)J_\ell^2(ku/\Omega_e)}{\omega + \ell\Omega_e - k(v_0 - v_B)}\right\}$$

and the presence of v_B in the denominator of the integral produces a significant change due to a "smearing out" of the resonance; for the parameters chosen the ∇B drift reduces the growth rate by a factor of about 2 compared with that for the $\underline{E} \times \underline{B}$ drift alone. Since ∇T_e drifts give rise only to additional terms in the numerator of the integral one expects the effects of such terms to be negligible for a low β plasma also.

References

[1] Krall, N.A. "Drift Waves" in Advances in Plasma Physics Vol.1, A. Simon and W. B. Thompson, Eds. Interscience Publishers, New York (1968).

[2] Gary, S.P. and Sanderson, J.J. J. Plasma Physics (1970). (to be published)

[3] Gary, S.P. J. Plasma Physics (1970). (to be published)

[4] Paul, J.W.M., Daughney, C.C. and Holmes, L.S. Nature 223, 822 (1969).

[5] Krall, N.A. and Book, D.L. Phys. Rev. Letters, 23, 574 (1969).

[6] Sagdeev, R.Z. Proc. Sym. in App. Maths. XVIII, 281 (1967).

[7] Krall, N.A. and Rosenbluth, M.N. Phys. Fluids 6, 254, (1963).

COLLISIONLESS SHOCKS AND TURBULENT HEATING

COLLISIONLESS SHOCK WAVES AND ANOMALOUS ELECTRON HEATING AT VERY LOW DENSITIES

K.H. Dippel, K. Köthker, E. Hintz
Institut für Plasmaphysik, Assoziation KFA-EURATOM, Jülich, Germany

Detailed studies of the structure of hydromagnetic shock waves (at medium Alfvén Machnumbers M_A) by means of Thomson (see for example ref. 1) as well as cooperative scattering have confirmed the notion, that collective processes are predominantly responsible for energy dissipation in the shock front. It appears that mainly electrons are heated by scattering from non-thermal collective fluctuations which are the result of ion sound instabilities.

Reliable measurements of electron temperature and -density distribution by the light scattering method have so far been done in a very narrow range of plasma parameters. Besides, the plasma properties (electron density n_e, - temperature T_e, magnetic field B etc.) were such that the shock transition was not truly collisionfree, i.e. the ratio of the rise time of the shock τ_s to the electron-ion collision time $1/\nu_{ei,1}$ was much larger than one. (The subcripts 1 and 2 refer to the plasma state ahead of and behind the shock.) Shocks were also investigated at very low densities, where $\tau_s \nu_{ei,1} \leq 1$, however in this case information on shocks has mainly been obtained by magnetic probe measurements. This means that the knowledge about heating rates and turbulent resistivities is rather indirect. The purpose of experiments reported here was to extend the scattering measurements on shock waves to initial densities as low as it was possible with existing light sources. Since the shock width Δ increases with decreasing density this would also permit a better spatial resolution of the shock front and result in more accurate determination of plasma properties in the shock, e.g. of current densities and drift velocities.

Shocks were generated in a deuterium plasma by means of a theta pinch (2). The diameter of the discharge tube was 20 cm, the coil length 45 cm.

Electron temperature and electron density at a distance r=3,5 cm from the tube axis were obtained by 90°-Thomson scattering measurements using a 500 MW giant pulse ruby laser. For the determination of the electron temperature the Doppler-broadened scattered laser line was spectrally resolved by tilting a narrow bandwidth interference filter ($\Delta\lambda 1/2 = 5$ Å, typically). The electron density could be obtained from a direct integration of the entire scattered profile. This was possible because the stray light level could be kept down to values equivalent to $n_e \approx 10^{13}$ cm^{-3}. The magnetic field profile in the shock was measured with small, open loop magnetic pick up coils. These measurements also yielded the shock velocity.

The properties of the initial plasma were the following: Electron density $n_{e,1} = 1{,}7 \cdot 10^{13}$ cm^{-3}, electron temperature $T_{e,1} = 2{,}5$ eV, and magnetic field $B_1 = 600$ G; this corresponds to $\beta_1 = (8 \cdot 2 n_{e,1} k T_{e,1})/B_1^2 \approx 1 \cdot 10^{-2}$, $\alpha = (\omega_{ce}/\omega_{pe})^2 \approx 2 \cdot 10^{-3}$, and $\omega_{ce,1}/\nu_{ei,1} \approx 120$, where ω_{ce} and ω_{pe} are the electron cyclotron and electron plasma frequency, respectively. In contrast to former measurements the initial magnetic field B_1 and the compressing field were parallel. This way heat flow from the piston region to the shock front and to the initial plasma by electron heat conduction parallel to the field lines (this is possible for antiparallel fields) should be avoided. Furthermore it was still an open question whether shock waves could be generated at all at parallel fields and low electron densities.

The shock wave investigated had a velocity of $v_s = 4{,}1 \cdot 10^7$ cm/sec, corresponding to an Alfvén Machnumber of $M_{A,1} = 1{,}8$. The rise time of the shock front was $\tau_s \approx 25$ nsec. This corresponds to a width of the shock front of $\Delta \approx 1{,}1$ cm. With $\tau_i \nu_{ei,1} = 2{,}2$ a value was reached which lies considerably below those values (50-100) at which scattering measurements have been performed till now. The observed shock is nearly collisionfree. The density and magnetic field in the shock are shown in Fig. 1. The measured density jump is $\eta = n_{e,2}/n_{e,1} = 2{,}2$; for the electron temperature behind the shock we obtain $T_{e,2} = 140$ eV and this yields a temperature jump of $T_{e,2}/T_{e,1} = 56$. The measured values are in good agreement with those resulting from the shock relations for $\gamma = 5/3$, if only the electrons are heated. At these low densities the shock thickness is again $\Delta \approx 10\ c/\omega_{pe}$. Since $\tau_s/\tau_{ei,1} \approx 1/100$ energy dissipation must be chiefly due to collective interactions. The classical heating of the electrons obtained as the sum of Joule heating with the resistivity given by Spitzer and adiabatic heating amounts to less than 10% of the measured heating. It is noteworthy that the spectral profile of the scattered light does not show the deviation from a Gaussian distribution in the form of a pronounced peak in the neighbourhood of $\Delta\lambda = 0$ as it was observed for shock waves with antiparallel bias field for higher Machnumbers (3).

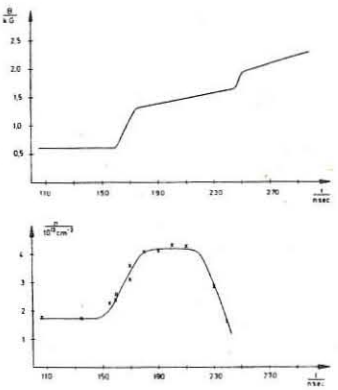

Fig.1 Measured profiles of n_e and B

The effective collision frequency as determined from the power balance equation is $\nu_{eff} \approx 0{,}8 \cdot 10^9$ sec^{-1}, while the calculated collision frequency for binary collisions behind the shock front is $\nu_{ei,2} = 4{,}8 \cdot 10^5$ sec^{-1}. For the electron drift velocity in the shock front we obtain $v_d \approx 10^8$ cm sec$^{-1} \approx 0{,}2\ v_{the}$, where v_{the} is the mean electron thermal velocity. At higher initial electron density for comparison a value of $v_d \approx 0{,}1\ v_{the}$ is reported (1). Considering the differences in the experimental conditions and in the measured ν_{eff} this variation goes in the rigth direction. From the measured distributions of B, n, and T it follows that pressure equilibrium exists approximately across the plasma-magnetic piston contact surface. Near the piston the density drops sharply. Previous investigations on shocks in theta pinches had shown in contrast (4) that the plasma pressure in the piston region may increase by a large factor.

With regard to the scaling of the effective collision frequency the values given here can only be compared with those obtained by (1); only these measurements have been performed under comparable conditions ($\beta_1 \ll 1$, $M_{A1} < M_{Acrit}$) and include a direct determination of the temperature. The densities in the two cases differ by a factor of about 40, the ion plasma frequencies by a factor of about 9. Since the effective collision frequencies differ only by a factor of 4 it appears that a simple scaling with ω_{pi} does not exist. On the other hand the observed scaling agrees quite well with the scaling proposed by Sagdeev (5): $\nu_{eff} \sim (T_e v_d \omega_{pi})/(T_i \cdot c_s)$ (c_s = ion sound speed), if the measured values of T_e, n_e, and v_d are inserted and if one assumes that the ions are heated adiabatically only.

Conclusions: Shock waves at $M_A \approx 1{,}8$ were generated under conditions where $\tau_s/\tau_{ei,1} \approx 2$, i.e. at maximum two binary collisions occur in the shock front. $\eta \approx 2{,}2$, $\Delta T_e \approx 138$ eV, and the energy of the drift motion corresponds to 2,8 eV. An effective collision frequency ν_{eff} $0{,}8 \cdot 10^9$ sec^{-1} is derived. According to these results and those of (1) the scaling contained in Sagdeev's formula for ν_{eff}, which was calculated for ion sound turbulence, seems to be right. It is furthermore shown that also at low initial densities and in case the compressing magnetic field is parallel to the initial field a fast rising piston is formed and nearly stationary shocks are generated.

References:

/1/ Paul, J.W.M., Goldenbaum, G.C., Jiyoshi, A., Holmes, L.S., Hardcastle, R.A., Nature 216, 363, 1967

/2/ Hintz, E., Proc. 3rd Conf. on Plasma Phys. and Contr. Nucl. Fusion Res., Novosibirsk (1968), Vol. 1, p. 69

/3/ Dippel, K.H., Hintz, E., Conf. on Collision-Free Shocks in the Laboratory and Space, Frascati (1969), unpublished

/4/ Keilhacker, M., Kornherr, M., Steuer, K.H., Z.Phys. 223, 385 (1969)

/5/ Sagdeev, R.Z., Proc. Symp. Appl. Math., New York 1965, Vol. 18, p. 281, AMS Providence, (1967)

COLLISIONLESS SHOCKS AND TURBULENT HEATING

On the Mechanism of Energy Dissipation in Collisionless Shock Waves[+)]

by

R.Chodura, M.Keilhacker, M.Kornherr, H.Niedermeyer, K.-H.Steuer

Institut für Plasmaphysik, Garching, Germany

Abstract: In shock waves with Mach numbers $M \lesssim M_{crit}$ strong electron heating is observed indicating a suprathermal level of fluctuations. Collective scattering of laser light shows that within the shock ion wave fluctuations are up to a factor 10 above the thermal level, whereas electron waves are thermal. For $M > M_{crit}$ non-adiabatic ion heating takes place.

This paper deals with the investigation of collisionless plasma heating by shock waves. The shock waves are produced by the fast rising magnetic field of a theta pinch discharge (0.5 µs rise to 12 kG in a coil of 15.8 cm diameter and 60 cm length) /1/. They propagate into a high β (β_1 = 0.3 - 5) hydrogen or deuterium plasma of density 2 - 5 x 10^{14}cm^{-3} formed by a theta pinch preionization/2,3/. In contrast with similar experiments at other laboratories, the ion temperature in the initial plasma is larger (T_{i1} = 20 - 50 eV) than the electron temperature (T_{e1} = 3 - 8 eV) and remains higher during the shock heating process. By properly choosing the initial conditions and the voltage of the shock bank almost stationary collision-free shock waves with magneto-sonic Mach numbers M ranging from 1.5 to 5 can be produced /2,3/.

Electron heating for $M \lesssim M_{crit}$

As reported previously /2/, in shock waves with intermediate Mach numbers ($M \approx 2 - 3 \lesssim M_{crit}$) strong electron heating is observed yielding an effective collision frequency about two orders of magnitude higher than the frequency for binary collisions. To gain an insight into the nature and magnitude of the collective fluctuations causing this effective collision frequency, two diagnostic techniques were employed that are sensitive to fluctuations of electric field and density respectively: Observation of satellites of forbidden lines and collective scattering of laser light.

As pointed out by /4/, strong oscillating electric fields can cause satellite lines disposed symmetrically in pairs about forbidden atomic lines, their total intensity being proportional to $\langle E^2 \rangle$ and their distance from the forbidden line being equal to the frequency of the electric field. In our experiment we used the He I line at 4922 Å, the profile of which was recorded with high time resolution using an 8 channel photomultiplier arrangement. The plasma to which 15 % He was added was viewed end-on through an annular diaphragm (r = 3.5 cm, Δr = 1 cm).

Fig.1 shows typical measured line profiles at different times within the shock. Owing to the relatively high plasma density the forbidden line already shows up as a result of the microfield of the ions (c.f. line profile in front of shock), thereby reducing the sensitivity of this method to fluctuating fields. Therefore only an upper limit can be placed on the amplitude of fluctuating electric fields, this being $\sqrt{\langle E^2 \rangle}$ = 6 kV/cm averaged over the observed plasma annulus. This value would be about two orders of magnitude above the thermal level.

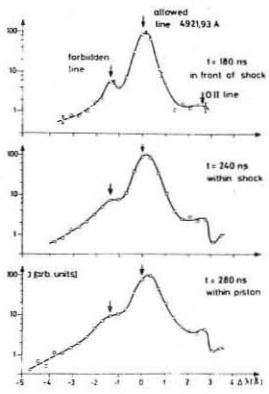

Fig. 1

The experimental arrangement for the laser forward scattering measurements is shown in fig.2. The scattering angle is 4°, giving $\alpha = 1/k\,\lambda_D = 1.5$ for the mean conditions in the shock. The scattering vector k is collinear with the azimuthal current within the shock. The bandwidth of the interference filter is chosen to transmit both the electron and ion lines, whereas the first F.-P. transmits only the ion line, which is then spectrally resolved by the second F.-P.. At the same time the density and electron temperature of the plasma at the point of observation are measured by 90° laser scattering.

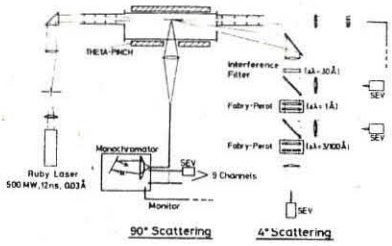

Fig. 2

Fig.3 shows the measured level of fluctuations within the ion feature of the scattered light (absolute calibration was obtained by comparison with Rayleigh scattering from H_2). Within the shock the fluctuations are clearly enhanced, being up to an order of magnitude above the thermal level which was calculated using the measured plasma parameters. On the other hand, electron waves do not seem to be enhanced, as indicated by measurement of the total scattered light (electron plus ion line). Measurements of the spectral profile of scattered light are currently under way and will be presented at the conference together with a discussion of the possible nature of instabilities involved.

Ion heating for $M > M_{crit}$

Since the shock waves are almost stationary the total shock heating $(T_e + T_i)_2$ can be derived from the steady state conservation relations /3/. As T_{e2} is measured by laser scattering, the ion temperature behind the shock T_{i2} can be calculated separately. In fig.4 the ratio of observed total ion heating to calculated adiabatic ion heating $T_{i2} / T_{i2\,ad}$ is plotted as a function of $M - M_{crit}$. For $M \lesssim M_{crit}$ the ions are only heated adiabatically, but for $M > M_{crit}$ additional non-adiabatic heating takes place that increases with Mach number. This indicates that above M_{crit} a collisionless dissipation process that heats the ions sets in.

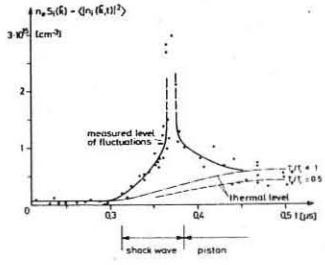

Fig. 3

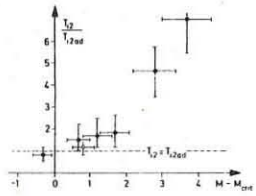

Fig. 4

/1/ R.Chodura et al., Plasma Physics and Contr. Nuclear Fusion Research, Vol.I, 81 (1969)

/2/ M.Keilhacker et al., Z.Physik 223, 365 (1969)

/3/ M.Kornherr, Z.Physik 233, 37 (1970)

/4/ M.Baranger and B.Mozer, Phys.Rev. 123, 25 (1961)

+) This work was performed as part of the joint research program between the Institut für Plasmaphysik, Garching and Euratom.

COLLISIONLESS SHOCKS AND TURBULENT HEATING

MEASUREMENT OF SPECTRUM AND ANISOTROPY OF TURBULENCE WITHIN A COLLISIONLESS SHOCK BY SCATTERING OF LIGHT

by

Daughney, C.C., Holmes, L.S., Paul, J.W.M., Summers, D.D.R.
U.K.A.E.A., Culham Laboratory, Abingdon, Berks., England.

Abstract: Scattering of light from the shock reveals a spectrum of ion waves with highly random phases and a sharp cut-off for $k > 1/\lambda_D$. This turbulence is highly anisotropic about the direction of the driving electron current. The significance of these results for non-linear kinetic theory is discussed.

Introduction

We have shown previously[1,2,3] that collisionless shock heating results from plasma micro-turbulence. The nature of such turbulence is also of current interest for the development of non-linear kinetic theory.

We have now measured the frequency (ω) spectrum[2,3], the wave number (k) spectrum[3] and the anisotropy of the turbulence within a collisionless shock. The level of turbulence is measured using the technique of scattering ruby laser light[2]. This yields the Fourier transform of the density fluctuations $S(\omega,\bar{k}) = \langle \delta n_e^2(\omega,\bar{k}) \rangle / n_e$ with $S(\bar{k}) = \int S(\omega,\bar{k})\, d\omega$ and $S_k(\omega) = S(\omega,\bar{k})$ for constant $\bar{k}$.

Experiment

The shock is produced by the radial compression of a magnetized plasma by a linear z-pinch ($n_{e1} = 6.4 \times 10^{20}$ m^{-3}, $T_{e1} = T_{i1} = 1.2$ eV, $B_{z1} = 0.12$ wb m^{-2}). The shock[4] is in a steady state with velocity $V_s = 240$ km s^{-1} (Alfven Mach number $M_A = 2.5$), width 1.4 mm and compression ratio 2.5. The electrons are shock heated to 44 eV, which requires about 100 times the classical resistivity. The level of turbulence $S(k)$ for $k \sim 1/\lambda_D$ is more than 100 times thermal and has $\omega \sim \omega_{pi}$ corresponding to ion waves[1].

The scattering experiments reported here have geometries which define mean wave vectors $\bar{k}_m$ with $|\bar{k}_m| \sim 1/\lambda_D$ and $\bar{k}$ in the (r,θ) plane at various angles φ ($0 < \varphi < \pi/2$) to the intersection with the tangent plane to the shock. For $\varphi = 0$, $\bar{k}$ is collinear with the azimuthal current in the shock front.

Wave Number Spectrum $S(\bar{k})$

We have measured $S(k)$ for $\varphi = 0$ by varying the scattering angle. The spectrum is shown in Fig.1 together with the form predicted by Kadomtsev[5]. The agreement is good, but within the observed range the logarithmic cut-off is important. This cut-off is observed for $k > 1/\lambda_{Dm}$ (mean shock conditions).

Similar cut-off phenomena have been observed at constant $\bar{k}$ by varying λ_{Dm} through changing B_{z1} (hence M_A and T_{e2}) or n_{e1}. In both cases the cut-off occurs for $\lambda_{Dm} \sim 1/k$.

Measurement of $S(\bar{k})$ as a function of φ shows a cut-off for $\varphi > \varphi_c \sim 45^\circ$. This corresponds to a cone of turbulence which is much smaller than the cone of linear instability for the mean shock condition (i.e. Cerenkov cone $\varphi_o \sim 75^\circ$).

Frequency Spectrum $S_k(\omega)$

We have measured $S_k(\omega)$ by spectrally analysing the scattered light using a Fabry-Perot interferometer (resolution 20 mÅ). The incident ruby line of width 20 mÅ (Fig.2a) is broadened, by the scattering, to $\delta\lambda = 55$ mÅ and also the peak is shifted to the red by $\Delta\lambda = 70$ mÅ (Fig.2b).

The direction of shift corresponds to scattering from plasma waves moving in the same direction as the azimuthal electron current (drift velocity $\bar{v}_D$) in the shock front. The direction of $\bar{v}_D$ can be reversed, without affecting the plasma behaviour, simply by reversing B_{z1}. This results in a reversal of the shift as shown in Fig.2c. This anisotropy with respect to electron current direction indicates that this current drives the turbulence.

The shift $\Delta\lambda$ corresponds to a wave frequency $\omega = 28$ GHz which together with the effective $k_m = 7.1 \times 10^5$ m^{-1} fits the ion wave dispersion curve for the mean shock condition. This identification of the fluctuations as ion waves is further verified by a scaling experiment in deuterium. This shows that $\Delta\lambda$ scales with ω_{pi} for constant $k\lambda_D$ and M_A.

The width of the shifted line is interpreted as measuring the lifetime (τ) of the mode (ω_o, k_m). For $\delta\lambda = 55$ mÅ, $\tau = 0.2$ns, which is comparable with the period ($2\pi/\omega_o$). There is appreciable randomness of phase.

Discussion

Apart from the broad frequency spectrum, $S_k(\omega)$, and the narrow cone ($\varphi_c < \varphi_o$), the results are consistent with Kadomtsev's[5] model of current driven ion wave turbulence. This model is based on the scattering of ion waves by ions.

Recently Tsytovich[6] has shown that this scattering process produces appreciable angular diffusion in k-space and is inconsistent with the observed anisotropy. He suggests an alternative non-linear process; ion wave decay. This can occur for a broad $S_k(\omega)$. He has shown that this process does lead to strong anisotropy.

References

1. Paul, J.W.M., Daughney, C.C., and Holmes, L.S., Nature 223 822, 1969.
2. Paul, J.W.M., et al., Contrib. to Proc. of Study Group on Collisionless Shocks ESRO Report SP.51, 1969.
3. Daughney, c.c., Holmes, L.S., and Paul, J.W.M., Subm.Phys. Rev. Lett. 1970 (Culham CLM-P235).
4. Paul, J.W.M. et al., Nature 208, 133, 1965 and 216, 363, 1967.
5. Kadomtsev, B., Plasma Turbulence, Academic Press 1965.
6. Tsytovich, V.N., Private communication, Subm. Plasma Physics.

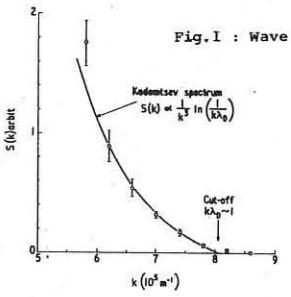

Fig.I : Wave no. spectrum S(k)

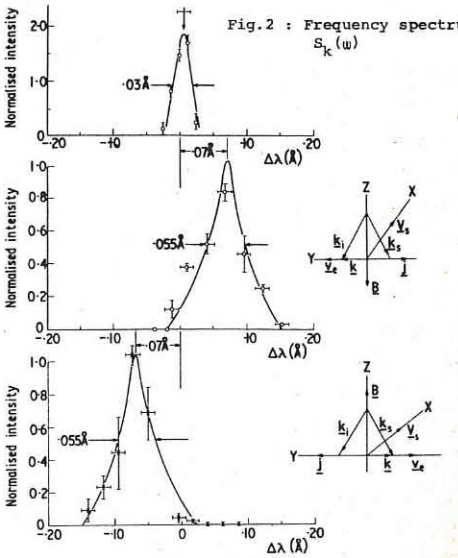

Fig.2 : Frequency spectrum $S_k(\omega)$

COLLISIONLESS SHOCKS AND TURBULENT HEATING

ELECTRON TEMPERATURE MEASUREMENTS IN OBLIQUE AND NORMAL COLLISIONLESS SHOCKS IN MAGNETIZED PLASMAS

by

J. Sheffield, G. Decker, A. B. Macmahon, and A. E. Robson

The University of Texas at Austin, Austin, Texas, U.S.A.

Abstract: Measurements are presented of the electron temperature behind shock waves in magnetized plasmas for Alfven Mach numbers in the range $M_A \simeq 2 \rightarrow 6$ and at angles of $55^o \rightarrow 90^o$ to the magnetic field. Below $M_A \simeq 2.5$ only the electrons are heated, while at higher M_A an increasing fraction of the available energy goes to the ions. The results are compared with the predictions of a theoretical model.

Introduction: The conversion of flow energy to thermal energy by a shock wave in a magnetized plasma can be calculated by applying conservation relations across the shock without reference to the dissipative mechanisms. However to determine the division of the energy between electrons and ions requires a knowledge of the internal processes in the shock front. The measurement of the electron temperature through the shock should throw light on the nature of these processes.

We have previously reported measurements of the magnetic and electric structure of shocks generated in the University of Texas oblique shock experiment[1]. A curved shock front is generated by a short θ-coil around the midplane of a 50 cm diameter glass tube. We are able to study shocks moving at angles from 90^o to 40^o to the magnetic field. Initial conditions are B_{zo}(250-1000 gauss), $n_{eo}(2.5\text{-}6 \times 10^{14} cms^{-3})$; $T_{eo} \sim T_{io} \sim$ lev; $\beta_o \leq 0.3$. Changes in M_A are effected by varying both B_{zo} and the shock coil voltage (70→ 180kv). Shock velocities $v_s(1.3\text{-}2.5 \times 10^7 cms/sec)$ are determined from time of flight measurements with two accurately spaced electric probes. These show that the shock is close to stationary conditions at around 8 cms radius.

Measurements of T_e: We have measured T_e using the Thomson scattering of light from a ruby laser (6943A°, 100 MW, 2 Joules) on both oblique (55^o, 75^o) and normal (90^o) shocks in hydrogen and deuterium for M_A in the range 2-6. A schematic diagram of the collection system for scattered light in relation to the shock apparatus appears in Figure 1. Accurate positioning and timing were achieved using the combination periscope and electric probe. The light was analyzed by a 5 channel diffraction grating polychromator, which allows a single shot temperature measurement to be made. The variance of the channel signals from a best-fit Gaussian was typically ±10%. A typical set of temperature measurements is shown in Figure 2 with the shock potential profile for reference. In Figure 3 the dimensionless ratio of the measured T_e to the flow energy per ion is plotted as a function of M_A for an oblique shock ($\alpha = 75^o$). Similar results were obtained for a 55^o shock[2]. Results for a normal shock ($\alpha = 90^o$), including those of other experiments[3],[4] are plotted in Figure 4. Shown on these diagrams is the total temperature $T_e + T_i$, computed from the conservation relations, and also the predictions of two theoretical models.

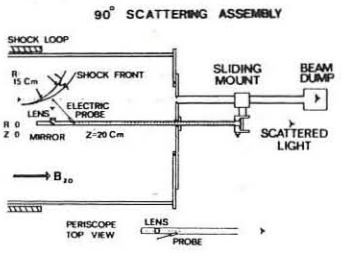

FIGURE 1

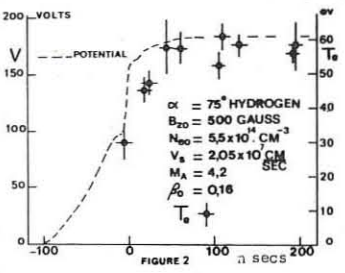

FIGURE 2

Discussion: It is well known that below a critical Mach number ($M_A \leq 2.7$) steady continuous shock solutions of the fluid equation exist with resistivity as the only dissipative mechanism.

For higher M_A a nonmagnetic dissipation (e.g. viscosity) or dispersion (e.g. charge separation) is necessary in order to obtain continuous solutions. If the scale length of this mechanism is small, it acts only within a narrow region which may be treated as a gas subshock (B = constant). The additional assumption that the electrons are compressed adiabatically (model 1) in the subshock permits us to calculate the final temperature ratio from the conservation equations[5]. Model 1 describes the small viscosity limit of the two fluid equations which, with "anomalous" resistivity and viscosity, give good agreement with the observed electric and magnetic structure[1]. It can be seen that the observed T_e lie close to predictions of this model.

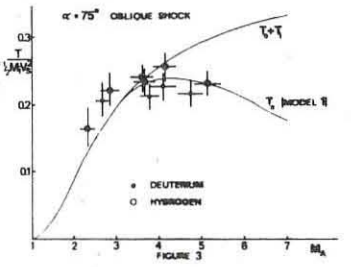

FIGURE 3

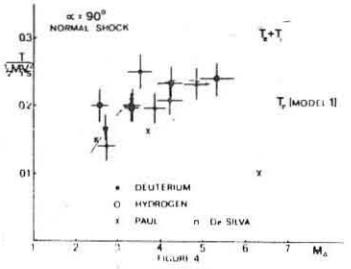

FIGURE 4

In our experiment the plasma behind the shock is contained by the curved shock front while in Paul's apparatus it is in contact with the metal electrodes. It appears likely that the difference between our measurements at high M_A (broader shocks) is connected with this. Note that while Paul observes a decrease in temperature behind the shock, in our case the temperature remains constant.

In our model no assumption is made about the actual mechanism by which the ions are heated. Recent numerical experiments by Lindmann[6] show the growth of an ion acoustic wave subshock at the back of supercritical shocks. Ions may be reflected from this wave train and after a single looping orbit carry significant internal energy into the downstream flow. This is a possible collisionless mechanism consistent with our model.

Acknowledgements: We are indebted to J. E. Goebel for his contribution to the engineering of this apparatus, and to M. Mahalek and P. Phillips for their assistance with the experimental work.

References:

1. Robson, A. E. and Sheffield, J. I.A.E.A. conference Novosibirsk, Paper CN-24/A-6.
2. Sheffield, J., Decker, G., Robson, A. E. Bull. Am. Phys. Soc. 14, 1057, 1969.
3. Paul, J. W. M. et al. Nature 216. 363, 1967.
4. DeSilva, A. W. and Stamper, J. A., Phys. Rev. Letters, 1027, 19,1967.
5. Macmahon, A. B., Bull, Am. Phys. Soc. 13, 1518, 1968.
6. Lindmann, E., Bull. Am. Phys. Soc. 14, 1058, 1969. Also see Robson, A. E., Proc. of ESRIN Study Group on Collision-Free Shocks, ESRO SP-51. Frascati, 1969.

PLASMA HEATING IN LOW-β COLLISIONLESS SHOCK WAVES

M. Martone and S.E. Segre

Laboratori Gas Ionizzati (Associazione EURATOM-CNEN), C.P. 65 - 00044 Frascati, Rome, Italy

Abstract: Measurements of electron density and temperature (by 90° laser scattering) and magnetic field in the radial implosion of transverse shocks (or different Mach number) and in the oscillations following the implosions confirm the excistence of a critical Mach number above which also ions are heated by collisionless phenomena.

Low-β cylindrical shock waves are produced by compressing a well ionized magnetized plasma by means of the fast rising magnetic field of a theta-pinch discharge:diameter 18 cm, length 80 cm / 1 /. The distributions of magnetic field, electron density and temperature in the initial plasma measured by magnetic probes and double electric probes / 2 / are reasonably uniform. Measurements on the compression have been made mainly by magnetic probes and 90° laser scattering.

Changing the initial conditions, shocks of different Alfvén-Mach number M_A have been produced, where the shock is well separated from the magnetic "piston" and it is stationary over a few cm . Fig. 1 shows the magnetic field profile at radius 3 cm for $M_A = 3.6$.Figs. 2 and 3 show the electron temperature T_e across the shock, for $M_A = 3.1$ and 3.6. As the jump in magnetic field, electron density and temperature across the shock are thus known and the shock is stationary, it is possible to use the conservation equations to determine the ion temperature behind the shock. The table summarizes the results.

M_A	n_o (cm^{-3}) x 10^{-14}	H_o (kG)	v_s ($\frac{cm}{\mu s}$)	T_e (eV)	T_i (eV)	d (mm)
3.1	5.2	0.78	23	54	0	5.3
3.6	5.2	0.78	27	55	30	6.0
3.8	4	0.68	28	61	35	6.3
4.25	4	0.68	31.5	77	54	6.8

It is therefore found (cfr. / 3 /, / 4 /) that below some critical Mach number M_A^* the ions are not heated. Furthermore the measured shock thicknesses and temperatures are not consistent with classical collisional dissipation. Below M_A^* ion wave turbulence is indicated.

Measurements on the axis of magnetic field, electron temperature and density confirm that above M_A^* the ions are heated appreciably. Indeed the radial oscillations following the first implosion / 5 / give rise to oscillations of T_e and n_e on the axis (see Figs. 4÷7); for $M_A = 3.6$, although the compressing magnetic field is stronger, the peak compression is weaker than for $M_A = 3.1$, i.e. the peak electron density,temperature and magnetic field are weaker. This indicates that the ion temperature should be appreciable, however the ions are certainly not heated by electron collisions since the equipartition time is about 6 μs.

REFERENCES

/ 1 / L. Marchegiani et al.: Laboratori Gas Ionizzati, Frascati, Internal Report, LGI No. 69/13 (1969).

/ 2 / M. Martone, S.E. Segre: Laboratori Gas Ionizzati, Frascati, Internal Report,LGI No. 69/15 (1969).

/ 3 / J.W.M. Paul et al.: Nature 216, 365 (1967).

/ 4 / M. Martone, S.E. Segre: Plasma Phys. 12, 205 (1970).

/ 5 / G.B.F. Niblett, T.S. Green: Proc. Phys. Soc. 74, 737 (1959)

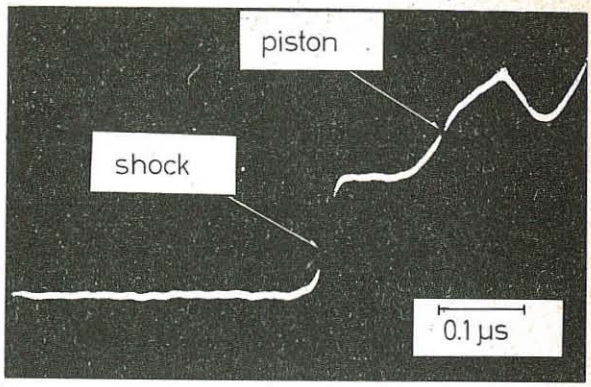

Fig. 1

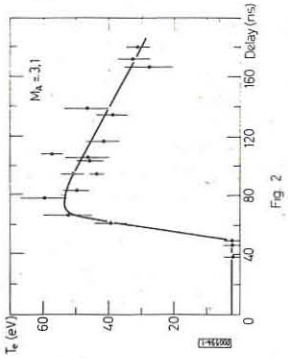

Fig. 2

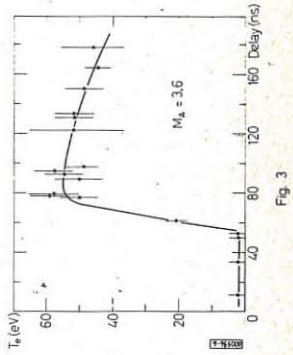

Fig. 3

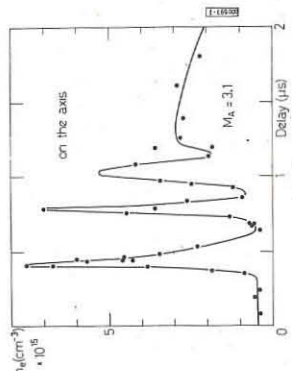

Fig. 5

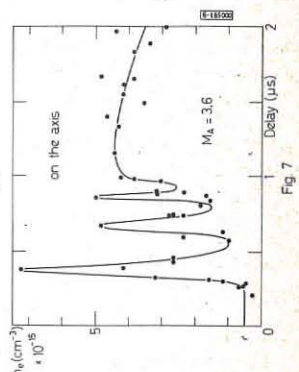

Fig. 7

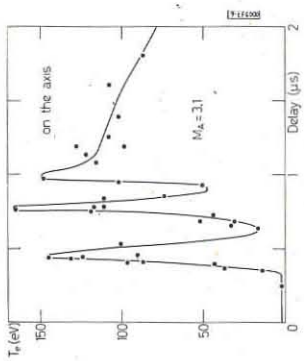

Fig. 4

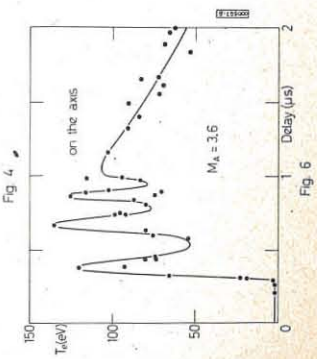

Fig. 6

COLLISIONLESS SHOCKS AND TURBULENT HEATING

SHEATH FORMATION AND PLASMA HEATING IN LOW DENSITY THETA PINCHES WITH ZERO INITIAL MAGNETIC FIELD

K.J. Dietz and E. Hintz

Institut für Plasmaphysik, KFA-EURATOM Assoziation, Jülich, Germany

The rates at which electrons and ions are heated during the implosion phase of a theta pinch and the eventual formation of a shock wave depend to a large degree on the width and on the structure of the plasma-magnetic field interface. If for example a shock shall develop the transit time T_p of the piston across the radius R ($T_p \approx R/U_p$; U_p = piston velocity) must be short compared to the magnetic field penetration time $T_d \approx R^2 \omega_{pe}^2 / c^2 \nu_{eff}$ (ω_{pe} = electron plasma frequency; ν_{eff} = effective electron-ion collision frequency). For the low density, magnetic field free plasmas, discussed here the mean free paths and the ion cyclotron radius are larger than the radius of the discharge tube and a comprehensive theory of the plasma sheath does not exist. Results of collisionless shock wave research have suggested (1,2) that current driven ion sound instabilities which provide a strongly enhanced resistivity may dominate the sheath structure, at least in the early phases. The resulting fast magnetic field penetration may inhibit the development of shock waves ($T_d \leq T_p$).

The experiments reported here were made with the following chief objectives: a) to examine whether collisionless shock waves can be generated in a fully ionized plasma at densities between 10^{12} cm^{-3} and 10^{13} cm^{-3}; b) to determine the magnetic field penetration rates at different electron densities, ion masses and piston velocities, in order to learn something about the scaling of the effective collision frequencies; c) to gain experience on the behavior of high voltage theta pinches at very low gas pressures, i.e., on the achievable temperatures, compression ratios and β-values.

The experimental setup consists essentially of a large diameter theta pinch. Coil length = 80 cm, coil diameter = 42 cm; i.d. of the tube = 40 cm. Bank characteristics: Energie = 14.4 kJoule; max. voltage = 120 kV; internal inductance = 20 nH. The initial plasma is generated by first preionizing the gas and then starting an electrodeless discharge, by which nearly full ionisation is achieved. Filling pressures of 1 mTorr (deuterium) and 0.5 mTorr (argon) were used. The compression pulse was applied during the afterglow phase at times where trapped fields had almost disappeared and electron density distributions across the radius were constant to within 10%. Initial electron densities could be varied between 10^{13} cm^{-3} and 10^{12} cm^{-3}. Magnetic fields and electron densities were measured with high time and space resolution by means of small, open loop, pick up coils and 2 mm (4 mm) fast microwave probes (3), respectively.

Results. The fast magnetic compression of low density plasmas was studied for various initial conditions. Table 1 gives a survey of the cases investigated together with a summary of the results. Most measurements were done under the conditions of case 1, where it was thougth that collisionless shock waves might be generated.

Case	Gas	$n_{eo}/10^{13}$ cm^{-3}	$u_p/10^7$ cms^{-1}	B_p/kG	$\nu_{eff}/10^8$ s^{-1}	$\bar{\beta}$
1	Deuterium	1	4.0	2.1	8.9	0.75
2	Deuterium	1	5.6	2.9	11.0	0.50
3	Deuterium	0.25	7.4	2.1	4.4	0.40
4	Argon	1	2.2	4.5	1.8	0.88
5	Argon	0.5	2.8	4.8	1.3	0.80

Table 1 $\bar{\beta}$ = average $\beta = (B_p^2 - \bar{B}_i^2)/B_p^2$
$\bar{B}_i$ = average magnetic field inside the plasma

Fig. 1a shows radial magnetic field distributions at various times. As in the other cases, the driving magnetic field B_p and the piston velocity u_p soon reach nearly stationary values. The most noteworthy observation is that the piston is rather diffuse, the width Δ of the current sheath reaching almost 10 cm at later times. Under such circumstances a shock should not be formed. Indeed, the temporal behavior of the magnetic field profiles could only be explained by shocks if γ would approach one or if a strong heat sink (e.g. electron heat conduction to the ends) would be present. This conclusion is confirmed by space resolved electron density measurements. They show the development of an electron density perturbation travelling ahead of the magnetic piston (see Fig. 1b). The risetime of the front is strongly time dependent reaching 200 nsec near the axis. At later times a density of about 10^{14} cm^{-3} is observed on the axis, i.e. an $\eta = n_{e\,final}/n_{eo}$ of about 10. Using this value in the pressure equilibrium relation one arrives at a temperature $T_m = T_e + T_i \simeq 7.5 \times 10^6$ °K. The shock relations together with the adiabatic expansion law ($\gamma = 5/3$) give in contrast $T_m = 2.6 \times 10^7$ °K and $\eta = 3,4$.

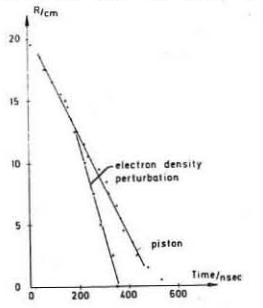

Fig.1b Space-time curve of piston and of electron density perturbation. (case 1)

For comparison the fast compression of argon was studied at the same initial electron density. The measured radial magnetic field profiles are shown in Fig. 2. The width of the current sheath is considerably smaller. At later times (800 nsec) when pressure equilibrium is reached, the plasma diameter is about 9 cm. Using the radial compression ratio and assuming that only ions are heated (electron temperature should be limited due to heat conduction to less than one hundred eV) one obtains an ion temperature of almost 10 keV in agreement with the value obtained from shock relations.

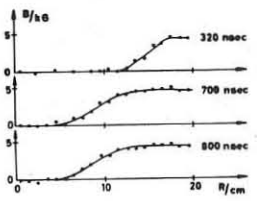

Fig. 2 Radial magnetic field distributions at various times (case 4)

Investigations were extended to even lower densities (see Table 1). The dynamic behavior of the fast compression can best be described by the relation $B_p = u_p \sqrt{\gamma+1} \sqrt{8\pi \rho_o}$. This is demonstrated in Fig. 3 for $\gamma = 5/3$.

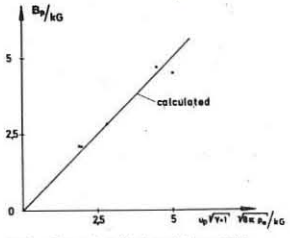

Fig. 3 Observed scaling law of B_p, u_p and β_o in comparison with theory

It is possible to get an estimate of the effective collision frequency from $\nu_{eff} = \Delta^2 c^2/\omega_{pe}^2 t$ (t = time of observation). When n_{eo} and m_i are varied it is found, that the scaling can best be described in the following way (see Table 1): $\nu_{eff} \sim \sqrt{n}\ 1/\sqrt{m_i}$. It seems that the effective collision frequency is proportional to the ion plasma frequency. The value of ν_{eff} for case 1 is in reasonable agreement with that obtained from microwave measurements under the same conditions.

Conclusions. Because of an anomalously fast magnetic field penetration shock waves cannot be formed during the fast compression of a collisionless deuterium plasma. The observed broad plasma sheath is explained by an anomalous resistivity resulting from ion sound instability. The effective electron-ion collision frequency scales as $\nu_{eff} \sim \sqrt{n}\ 1/\sqrt{m_i}$. This leads in case of an argon plasma to a considerably reduced sheath thickness. From pressure equilibrium follows that the mean energy of the argon ions should be of the order 10 keV.

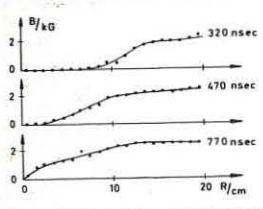

Fig.1a Radial magnetic field distributions at various times (case 1)

1.) E. Hintz, Plasma Phys. Contr. Nucl. Fusion Res., Proc. Cont., 3rd, Novosibirsk, 1968, Vol. 1, p. 69, IAEA Vienna 1969

2.) H.A.B. Bodin et al., Plasma Phys. Contr. Nucl. Fusion Res., Proc. Cont., 3rd, Novosibirsk, 1968, Vol. 2, p. 533, IAEA Vienna, 1969

3.) H. Hartwig, KFA Report , Jül-473-PP, KFA Jülich 1967

COLLISIONLESS SHOCKS AND TURBULENT HEATING

A TURBULENT HEATING EXPERIMENT

by

H. de Kluiver, A.M.J. Paans, H.W. Piekaar and H. Schrijver

Association Euratom-FOM
FOM-Instituut voor Plasma-Fysica
Rijnhuizen, Jutphaas, The Netherlands

Abstract

Results of turbulent plasma heating by a current in a straight hollow cathode arc situated in a magnetic mirror are presented. The duration of the turbulent heating is controlled by short-circuiting the discharge capacitor at a preset time. Heating efficiencies are proven to be in the order of 3 to 4%.

Experimental procedure

In a linear geometry a 20-100 A arc with a length of 60 cm is run between a tantalum or tungsten hollow cathode and a copper anode (Fig. 1).

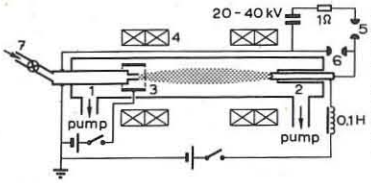

Fig. 1
Diagram of the apparatus
1 cathode
2 anode
3 auxiliary anode
4 coils
5 spark gap
6 crowbar spark gap
7 gas feed

The inner diameter of the cathode is 9 mm. Gases used are Ar, He and H_2. The vacuum system consists of a 15 cm diameter pyrex tube that is evacuated to a few times 10^{-6} Torr. During arc operation the gas pressure is between 10^{-4} and 10^{-3} Torr. The arc is struck by means of an auxiliary ring anode in an E × B discharge. When the cathode is heated sufficiently, the main anode takes over. The magnetic configuration is a magnetic bottle with a mirror ratio of 2 and a 0.4 T peak induction; the electrodes are situated just outside the mirror. The electron density of the plasma prior to the turbulent state is determined by a 2-mm microwave interferometer bridge, and is a function of arc current and gas feed. The plasma column has a density of 10^{19} to $10^{20}/m^3$, and a temperature of about 1 eV.

The turbulent state is excited by discharging a capacitor of 1.86 μF at 20-40 kV across the length of the plasma arc by means of a spark gap. The coaxial current paths ensure a low self-inductance. An auxiliary spark gap enables us to short-circuit the capacitor at a chosen time. A resistance of 1 Ω in series with the arc provides critical damping and dissipation of the superfluous capacitor energy after crowbarring.

Thus far the heating has been investigated by means of diamagnetic loops, X-ray scintillator counters, Rogowsky loops, spectroscopy, an image converter, and a 2-mm microwave interferometer.

Results

Heating by turbulence is observed when the capacitor voltage exceeds a critical value depending on the plasma density. In our experiments this critical value appeared to be 20 kV. After initiating the discharge the current rises to 2 or 3 kA depending on the voltage of the capacitor. The turbulent state is characterized by a high resistivity, in general around 10 Ω, and may last in excess of 4 μs. Following this highly resistive phase the plasma breaks down with a subsequent current rise up to 15 kA. If the capacitor is crowbarred the current surge can be avoided. The results refer to heating times of 1-2 μs (Fig. 2).

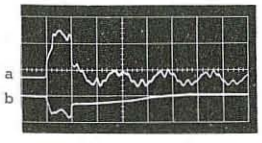

Fig. 2a
The voltage across the arc vs time.
Vertical scale 20 kV/div.
Horizontal scale 1 μs/div.

Fig. 2b
The current through the arc.
Vertical scale 5 kA/div.

It has been verified with the 2-mm interferometer that the anomalous resistance is inversely proportional to the square root of the plasma density. The absolute value of the resistivity agrees with the value calculated for the two-stream instability, for which the conductivity is given by[1]:
$\sigma = 1.4\ \varepsilon_o \omega_{pe} (M/m)^{1/3}$.

From the intensity of the light emitted by the plasma at wavelengths of 4686 Å(He II) and 3889 Å(He I) across the width of the discharge vessel, the diameter of the plasma column is determined to be about 3 cm (Fig. 3). By observing the rise time of the spectroscopic signal the speed of expansion of the plasma column is found to be nearly 10^5 m/sec. Similar results have been obtained with the image converter.

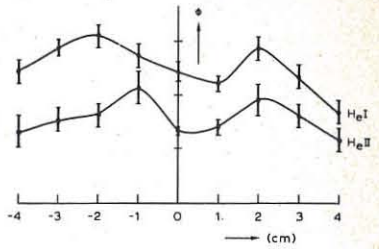

Fig. 3
Scanning of the intensity of a He I and a He II line at t = 4 μs, relative to the axis of the vessel.

The Bremsstrahlung has been measured in the afterglow. Scintillation counters with organic and inorganic scintillators are used for photon energies between 4 and 60 keV. During turbulence there is a short X-ray burst from 20-25 keV electrons. After a period of 20 μs of low intensity, there is a quick rise to a considerable radiation with a maximum around 40 μs after turbulence, followed by a slow decrease (Fig. 4).

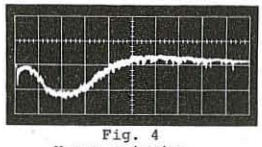

Fig. 4
X-ray emission.
Time scale 20 μs/div.

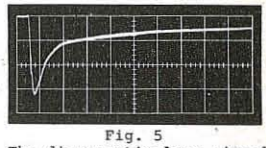

Fig. 5
The diamagnetic loop signal.
Time scale 5 μs/div.

Impurity gases have a characteristic time of 40 μs to reach the axis and may be responsible for the increase in the Bremsstrahlung emission. Pulse height analysis leads to the conclusion that the X-rays seem to arise from a Maxwellian electron distribution with a temperature of 12 ± 3 keV. This is confirmed by a statistical analysis of the results with the organic scintillator in a region of heavy pile-up.

From the diamagnetic loop signal (Fig. 5) the following conclusions are drawn. The signal decays to 40% in approximately 4 μs, followed by a much slower decay. Half of the fast decrease can be attributed to direct loss-cone depletion whereas the other half may be due to scattering of electrons into the loss-cone. This agrees with a leakage current of 1 kA during 3 μs (Fig. 2b). From the ambipolar diffusion time along the magnetic field an electron temperature of 500 eV is calculated. If we apply Berger's expression for the transverse expansion velocity, $\sqrt{kT_e/M}$, to our result of 10^5 m/sec, the same electron temperature is found[2]. The remaining loop signal can be explained by the 12 keV electrons, being lost at a much slower rate.

We are thus lead to an electron distribution at the moment of crowbarring which consists of $10^{18}/m^3$ of a temperature of 12 keV and $5.10^{19}/m^3$ at a temperature of 500 eV. The energy content of our plasma is 3 Joule for a capacitor voltage of 35 kV. This corresponds to 5.10^{22} eV/m^3. Up to 25 kV the energy content is proportional to the capacitor voltage. Beyond this value the energy content increases proportional to the third power of the voltage. Related to the energy dissipation, I × V × t, an efficiency of 3 to 4% is attained.

Many thanks are due to Messrs. B. de Groot, K.L. Buisman and Dr. W. Strijland for their enthusiastic assistance.

This work was performed under the association agreement of Euratom and FOM with financial support from ZWO and Euratom.

References

1) O. Buneman, Phys. Rev. 115 (1959) 503.
2) N.K. Berger et al., Soviet Physics JETP, Vol. 29 (1969) 784.

PLASMA TURBULENT HEATING IN "VIKHR - 3" TOROIDAL DEVICE.

B.A.Demidov, S.D.Fanchenko.

I.V.KURCHATOV INSTITUTE OF ATOMIC ENERGY, Moscow, USSR.

Plasma turbulent heating and loss mechanisms in "Vikhr-3" closed magnetic trap were studied. The plasma was confined in a longitudinal magnetic field B_z and outward-rising quadrapole field B_φ combination [1]. A twice repeated current pulse technique has been developed to test the dependance of heating and losses upon initial conditions.

I. Experimental arrangement. Fig.1 shows the "Vikhr-3" layout with a quartz vacuum chamber 1 (10 cm minor and 150 cm major radius toroid), 30 longitudinal-field magnetic coils 2 and four conductors 3 with anti-parallel currents wound around the torus and producing a quadrupole B_φ field.

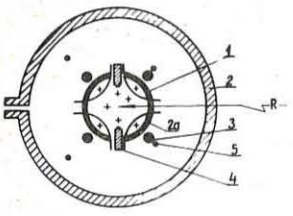

Fig. 1.

The effective mirror ratio $R = \sqrt{1 + 4\frac{B_\varphi^2}{B_z^2}}$ was equal to 2.2. Twelve titanium-hydride plasma guns were used to get a 10^{12}cm^{-3} density prei-onization plasma. Special windings 5 served to apply around the torus a E = 50 v/cm pulsed electric field of $\tau \lesssim 1$ μsec duration. Two low-inductance condenser banks were provided, each independantly dischargable through widndings 5 via a separate spark gap. The electric field applied, which was much in excess of the Dreicer limit, drew a plasma current producing turbulent heating. The plasma density was measured with λ = 8mm and 3cm microwave diagnostics.

II Experimental results. The pre-ionization plasma column effective diameter was measured to be about 2cm for n $\simeq 10^{12}$cm^{-3}. This less than 10 % ionization degree plasma would decay exponentially as shown by the broken-line curve in fig. 2.

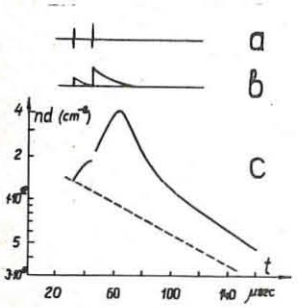

Fig. 2.

With the pulsed electric field applied (see fig.2a) n and nT behaved as shown in figs.2a,2b. It is evident from fig.2 that during the period of observable diamagnetic signal the density of the plasma would smoothly rise due to neutral gas ionization by turbulent heated electrons [1]. Hence, if the second electric field pulse was sufficiently delayed relative to the first one, it would act upon a higher ionization-degree plasma with a presumably uniform density distribution. With the strong electric field applied one was able to observe anomalous plasma resistivity and hyper-thermal microwave radiation peculiar to turbulent heating [2,3]. The effective electric conductivity of 1.10^{12}cm^{-3} hydrogen plasma during the turbulent heating was measured to be around 2.10^{12} CGSE units.

The diamagnetic signal traces of fig.2b indicate that after current cut-off some thermal energy was left accumulated in the plasma. In typical heating conditions with n = 1.10^{12} and E = 50 v/cm the hot plasma pressure at current cut-off amounted to nT $\simeq 1.10^{15}$ ev/cm^3. The exponentially decaying diamagnetic signal could be observed for 30–40 μsec. The nT e-fold decay-time versus turbulent-heated-plasma temperature is plotted in fig. 3.

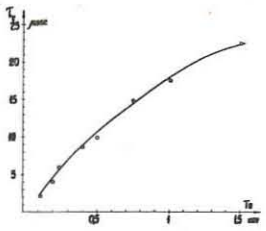

Fig. 3.

Tests were made with higher neutral gas pressure in the discharge chamber, demonstrating τ_c decrease with increasing neutral atom concentration.

III. Discussion. New experimental data on the energy confinement time of a partially ionized turbulent-heated plasma in a hydride-field toroidal trap have been obtained over a wider Te range than previously, supporting the ionization loss mechanism.

Since some speculations have been put forward concerning the possible importance of large-scale plasma and magnetic field inhomogeneity as a cause of anomalous resistivity, it is of interest to compare the effective plasma conductivity data of "Vikhr-3" with the results obtained elsewhere (see the Table). The table lists the σ_{eff} value for the first electric field pulse in "Vikhr-3". For the second electric field pulse acting on a plasma presumably homogeneous along the column lenght, σ_{eff} was found to have nearly the same value. Note, further, that in both "Vikhr-2-B" and "Vikhr-3" the plasma current was clear off the walls while the field corrugation ratio differed by at least two orders of magnitude.

Device	B_z	n, cm^{-3}	E, v/cm	CGSE	Ref.
Vikhr-1	quasiuniform	10^{12}	50	1.10^{12}	2
Vikhr-2-A	quasiuniform	10^{12}	40	1.10^{12}	3
Vikhr-2-B	$\frac{(B_z)_{max}}{(B_z)_{min}}=20$	10^{12}	40	1.10^{12}	3
Vikhr-3	quasiuniform	1.10^{12}	50	$2,5.10^{12}$	Present work
Twist	quasiuniform	10^{12}	50	1.10^{12}	4
R - 0	quasiuniform	4.10^{12}	100	$10^{12} + 10^{13}$	5

The data provide string evidence in favour of small-scale turbulence as the main cause of anomalous resistivity.

References

1. B.A.Demidov, S.D.Fanchenko. Intern. Symp. on. Plasma Conf. in Closed Traps. Dubna, USSR, 1969.
2. S.D.Fanchenko et al. JETP, 46, 497 (1964); 48, 454 (1965).
3. B.A.Demidov et al. Doklady Akad. Nauk SSSR, 174, 327 (1967).
4. S.M.Hamberger et al. Phys. Lett., 19, 350 (1967).
5. R.A.Demirkhanov et al. "Conf. Plasma Phys. and Contr. Nucl. Fusion Res". Culham (IAEA, Vienna Austria, 1966) vol.2, p.327.

TURBULENT HEATING OF IONS BY THE CURRENT OF A LINEAR DISCHARGE

V.S.Koydan, A.G.Ponomarenko

Institute of Nuclear Physics, Siberian Division of the USSR Academy of Sciences, Novosibirsk, USSR

The investigation of the mechanism of ion heating in a turbulent linear discharge is one of the important problems /I,2,3/. In this paper the dynamics of ion heating was investigated and the ion distribution function had been determined by means of the multichannel analyser of charge exchange neutrals.

Fig.I shows the principal scheme of arrangement on which the experiments were carried out. The initial plasma ($n_e \simeq 2 \cdot 10^{13}\,cm^{-3}$, $T_e \sim 2 \div 5 eV$) was produced by a discharge of the Penninge-type in a metallic chamber of ϕ 6,3 cm at the pressure of hydrogen $p_o = 5 \cdot 10^{-4}$ mm Hg. The basic discharge current flowed between electrodes of ϕ 3 cm placed in the distance of 80 cm from each other in the mirrors of quasi-stationary magnetic field H_o=I2 kOe ($H_{max}/H_o \simeq 2$). Under typical conditions the initial voltage between electrodes was U_o= 50 kv.

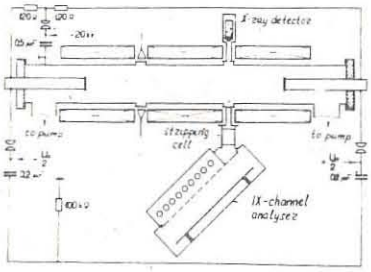

Fig.I.The principal scheme of arrangement.

The energy distribution function of the heated ions at the different stages of current was defined by our nine - channel analyser of the fast charge exchange neutrals. The using of ion-electron converters together with scintillator detectors for ion registration provided the analyser sensitivity of $\sim 5 \cdot 10^{-11}$A at time resolution of $\sim 10^{-8}$sec. The analyser can register the charge exchange neutrals in the range of $150 \div 2 \cdot 10^4$ eV with energy resolution of 3÷30 %.The calibration of analyser was made by means of proton beam. Simultaneously with the ion analysis there carried out the measurements of electron temperature T_e and its variation dT_e/dt (by X-ray two-channel detector), plasma density and microwave radiation at λ = 0,8 cm, plasma turbulence degree by means of external ion beam /4/ etc.

As in the previous experiments /5/, the shape of the current pulse in the discharge and the energy absorbed in the plasma depended essensially on the parameters of the initial plasma.The flowing of the current (Fig.2) was characterized by the intense absorption of energy, by the excitation of powerful microwave oscillations of the Langmuir's frequency ω_{pe} and by the heating of electrons and ions of plasma.The signals of analyser showed that in some time after the beginning of current the fast (during the time of 300÷500nsec) and intense heating of ions is observed.Fig.3 shows the distribution function of the heated ions $dn_i/dE = f(E)$ drawn for the moment when signals from the analyser reach its maximum value.At $E \gtrsim$ I,0keV the experimental points coinside satisfactorily with the Maxwellian function at $T_i \simeq$ 800eV.At low ion energies the disagreement of experimental points and Maxwellian is observed.This disagreement may correspond to the presence of the cold ion group in plasma. Besides,the distortion of experimental dependence $dn_i/dE = f(E)$ is possible because of the inaccurate knowledge of changing of stripping cross-section of hydrogen atoms at low energies. The absolute density of ions with $T_i \simeq$ 800eV was defined from the absolute value of neutral flow registered by the analyser.At the calculations the analyser sensitivity and geometry of experiments was taken into account and isotropic distribution of neutral flow was supposed.The density of heated ions determined by such method is $n_i \simeq I \cdot 10^{13} cm^{-3}$.This value shows the high efficiency of ion heating in the turbulent discharge.

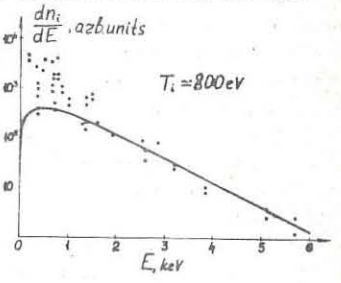

Fig.3.Energy distribution function of heated ions.Solid curve is the calculated Maxwellian with T_i=800 eV.

Fig.2 shows that the electron component (Fig.2c) is being heated faster than ions (Fig.2d).It was determined by means of X-ray detector that on the stage of increasing current the electrons are heated till T_e=3÷5keV for $\sim 10^{-7}$sec.At this moment the stopping of the current increase is observed and the quasi-stationary regime is established at which the resistance of discharge gap approaches to the doubled characteristic resistance of the discharge circuit.Assuming that the current is transfered by all plasma electrons then the current velocity at this moment $V_{cur} \simeq 2 \cdot 10^8 \frac{cm}{sec}$ is higher than the velocity of ion sound at $T_e \simeq$ 3÷5keV.Thus,the ion heating observed experimentally may occur as a result of excitation of ion-acoustic instability as Kovrizhnikh/6/ shows.However the presence of microwave radiation at the frequency ω_{pe} and the formation of fast electrons with $E_{eff} \sim$ 200keV (Fig.2e) indicates the possible plasma heating due to two-stream instability.

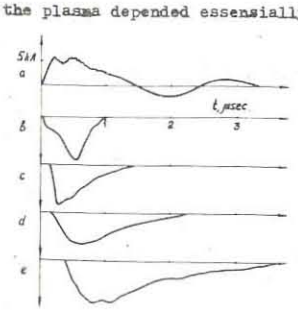

Fig.2.Typical oscilloscope traces: a)discharge current; b)microwave radiation at $\lambda \simeq$ 0,8cm; c)soft X-ray radiation, $T_e \simeq$ 3÷5 kev; d)signal of charge exchange atoms with energy E= 3,8 keV; e)hard X-ray radiation, $E_{eff} \sim$ 200kev.

The authors thanks greatly to R.I.Soloukhin for the displayed interest,A.J.Rogosin and N.K.Berger for their assistance.

REFERENCES

I.E.K.Zavoiskii et al.ZhETF Pis.Red.6, 95I, I967.
2.E.A.Sukhomlin et al. Ukr.Fiz.Zh.,I2, 507, I967.
3.T.H.Jensen,F.R.Scott,Phys.Fluids,II, I809, I968.
4.V.S.Koydan et al.Dokl.Akad.Nauk SSSR,to be published.
5.N.K.Berger et al.Zh.Eksp.Teor.Fiz.,56, I463, I969.
6.L.M.Kovrizhnikh.Zh.Eksp.Teor.Fiz.,52, I406, I967.

COLLISIONLESS SHOCKS AND TURBULENT HEATING

Microwave Scattering from Density Fluctuating during Turbulent Heating

by L.E. Sharp and S.M. Hamberger

U.K.A.E.A., Culham Laboratory, Abingdon, Berks., England.

Abstract: The spectral distribution of density fluctuation is studied for the case of current driven turbulence using the collective scattering of 2 mm microwaves. Preliminary results show short fluctuations at frequencies above the ion plasma frequency and characteristic of ion-electron streaming instability.

.....

The density fluctuation spectrum which occurs during the turbulent heating of a toroidal hydrogen plasma column has been investigated via the radiation scattered from a 2 mm wavelength microwave probing beam. The heating current pulse lasts ~ 300 nsec, is produced by electromagnetic induction of a strong electric field (~ 400 V cm^{-1}) parallel to the axial confining field (3 kG) of a stellarator (TWIST), and rapidly raises the mean particle energies to $\geq$ keV[1].

Fig.1 shows typical waveforms for: (a) applied electric field E_φ, (b) induced current, (c) λ = 3 cm microwave emission, indicating the time of maximum turbulence, (d) mean electron density $\bar{n} = \int n \, d\ell$ measured by 2 mm interferometer, (e) the direct transmission of 2 mm radiation across a plasma diameter. Trace (d) shows $\bar{n}$ is essentially constant during the heating pulse. Since $\omega \gg \omega_{pe}$, and binary particle collisions can be neglected, the attenuation shown in (e) during the pulse cannot be due to absorption and must therefore be attributed to the collective scattering of the microwave energy out of the received beam by the density fluctuations. Since the fraction S_o of the power scattered from the main beam is related to the mean square density fluctuation spectrum $< \delta n^2(\omega,k) >$ by $S_o = n^2 \ell \sigma_T \int < \delta n^2/n^2(\omega,\vec{k}) > d\vec{k} \, d\omega \, d\Omega$, where σ_T is the Thompson cross-section, $|k| = 4\pi/\lambda_o \sin \theta/2$ we estimate the r.m.s. level (for all scattering wave vectors not accepted by the forward receiver) to be $\delta n/n \sim 0.1$.

To resolve the wavelength and frequency spectrum we use the arrangement shown in Fig.2: the incident beam of 2 mm waves is focussed on to a non-reflecting "dump" to minimise unwanted specular reflections, and the signal scattered in various directions by the plasma received by a set of lens-horn antennae, each of which is connected to a low noise balanced crystal mixer. The local oscillator signal is derived from the primary microwave generator, so that the difference frequency output corresponds directly to the frequency ω of the scattering fluctuations[2]. Three scattering wave-vectors $\vec{k}$ $(H_1 - H_3)$ in the (horizontal) plane of the torus and four $(V_1 - V_4)$ in radial directions can be simultaneously observed, each with a bandwidth of 1000 MHz. Each wavelength channel can be subdivided into eight equispaced, 50 MHz wide bands between 10 and 500 MHz, or by heterodyning, into eight similar bands between 400 - 900 MHz.

Fig.3 shows the (rectified) scattered signals received by one antenna (H_3, $|k| = 40$ cm^{-1}) time resolved into various frequency bands. The gain of each trace shown has been adjusted for equal noise amplitude (i.e. they have unequal sensitivity). These semi-quantitative results show that large collective density fluctuations, with frequencies of the order shown, occur during the current pulse. Similar but weaker scattering is also seen on the six lower frequency channels (not shown).

The presence of fluctuations at frequencies > $f_{pi} \sim 300$ MHz is probably associated with an ion-electron streaming instability, with characteristic frequency $f^* \sim \frac{1}{2} (M/m)^{1/6} f_{pi} \sim 500$ MHz. Similar frequencies are seen in the potential spectrum using electric probes[3]. The lower frequencies may be associated with current-driven ion sound turbulence.

Although the system has not yet been sufficiently calibrated to compute absolute and time-resolved density spectra, it is apparent from Fig.3 that various "dominant" frequencies occur on occasions together, within the volume observed (V ~ 10 cm^3); since $v|k|^3 \sim 6.10^5$, many possible independent oscillations could co-exist, so that the fluctuation spectrum may be concentrated in several localised large-amplitude waves, with correlation times of the same order as our resolution time i.e. ~ 15 nsec, or several periods.

References

1. Adlam, J.H., et al. Conference Proceedings, Novosibirsk (1968).
2. Little P.F. & Hamberger S.M., Nature, 209, No. 5027, March (1966).
3. Jancarik, J., & Hamberger, S.M., Proceedings 4th European Conference Controlled Fusion and Plasma Physics, Rome, 1970.

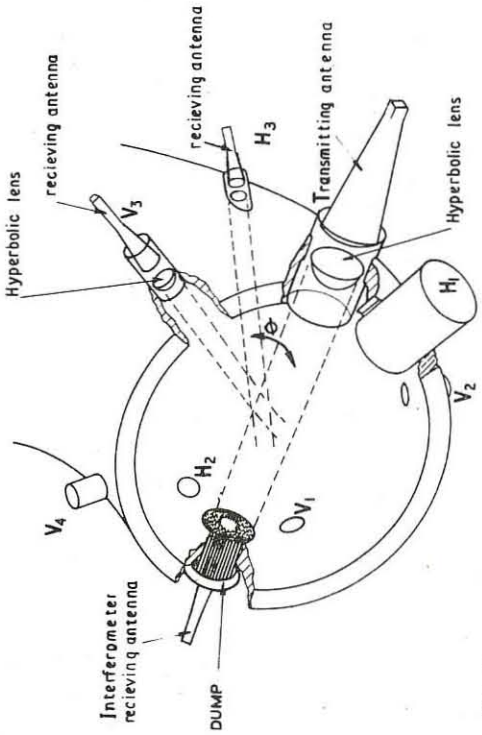

Fig 2.

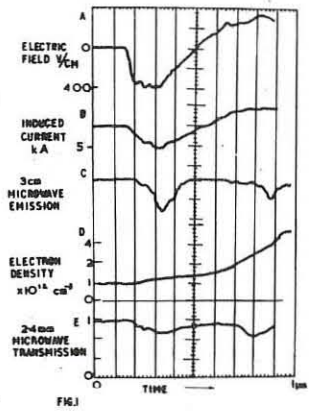

FIG.1

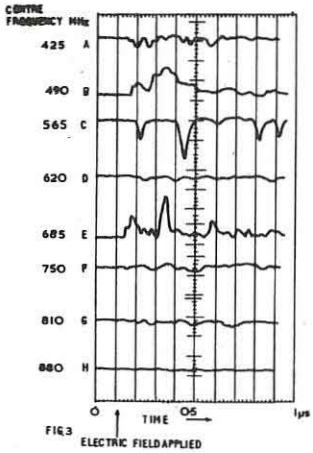

FIG.3

COLLISIONLESS SHOCKS AND TURBULENT HEATING

ELECTROSTATIC POTENTIAL FLUCTUATIONS MEASURED DURING CURRENT DRIVEN TURBULENCE

by J. Jančařík and S.M. Hamberger

U.K.A.E.A., Culham Laboratory, Abingdon, England.

Abstract: Results are presented of the fluctuation spectrum for a turbulently heated plasma, and show that three distinct types of spectrum can be seen depending on initial conditions. The 'anomalous' conductivity is shown to be related to the particular type of instability present.

We report a more detailed study of the frequency spectrum of collective electrostatic fields excited in a toroidal magnetically confined plasma during turbulent heating by a large induced axial current[1,2]. Applied electric fields (1 MHz ringing) between 100 and 500 V cm^{-1}, and hydrogen plasma densities $\sim 10^{11} - 10^{13}$ cm^{-3} are used in this investigation. The spectra are obtained by numerical computation from oscillograms of signals received (10MHz - 2GHz) from a calibrated differential electric probe with small (1mm) electrode spacing, and in this paper are evaluated for various time intervals during the first current pulse. The first current peak occurs between ~100 nsec and ~400 nsec, depending on the plasma impedance, which in turn depends on operating conditions, and varies from purely resistive to mainly inductive. The probe can be oriented to receive different signals parallel to or across the axis.

The type of spectrum observed depends primarily on the density and applied electric field, and may change with time during a single pulse. Typical examples which we use to characterise three main regimes are shown in Figs.(1-3):

Regime A (Fig.1) the fluctuation spectrum is concentrated at frequencies $\omega < \omega_{pi}$. It appears when the drift velocity $v_d \lesssim (2\text{-}3) \times 10^8$ cm sec^{-1}, and applied field $E_\varphi \lesssim 40\ E_o$ (E_o is the critical field for runaway $\approx 2 \times 10^{-12}\, n/T_{(eV)}$ ($V\,cm^{-1}$)). We interpret this as a spectrum of ion-sound turbulence. For small v_d the fluctuations are seen only in the parallel direction, the transverse components increasing with v_d until they are undistinguishable from the parallel for $v_d \approx 3 \times 10^8$ cm sec^{-1}.

Regime B (Fig.2) occurs for larger fields, $E_\varphi \gtrsim 40\ E_o$ and $v_d \gtrsim (2\text{-}3) \times 10^8$ cm sec^{-1}. The spectrum includes strong components at frequencies $> \omega_{pi}$ and characteristic of ion-electron streaming instability[3] i.e., $\omega^* \sim \frac{1}{2}(M/m)^{1/6}\, \omega_{pi}$. A detailed examination shows that this condition is preceded by a large amplitude low frequency ion-sound spectrum occurring during the current rise ($v_d \lesssim 2 \times 10^8$ cm sec^{-1}). This is immediately followed by a short (~20-40 nsec) burst of very intense signal $\sim \omega^*$, which then decreases to a much smaller steady level which persists until the current decreases. Somewhat similar bursts have been observed by Suprunenko[4]. The signal observed does not depend on the probe orientation. The microwave emission in this regime is much more intense than in A.

Regime C (Fig.3) is the least explored and occurs at largest E_φ and least n ($E_\varphi \geq 10^3 E_o$); much higher frequencies $\sim \omega_{pe}$ are observed, which may arise from electron-electron interaction (from runaway electron beam). Notice this regime has $\omega_{ce} > \omega_{pe}$. The early stages are as B.

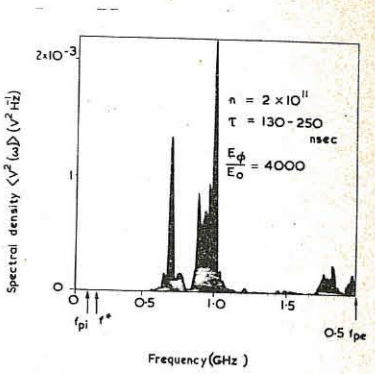

Fig.3

Fig. (4) shows the relation between measured electrical conductivity σ and drift velocity for various regimes, plotted separately according to the class (A,B,C) of spectrum observed at peak current, i.e., when the measurement of σ was made. The solid lines show the semi-empirical predictions of Buneman[3] and Sagdeev[5] for the respective cases of two-stream and ion-sound excited turbulence. Fig.4(b) shows the correlation time x frequency (i.e., the number of distinct periods of oscillation observed) for the three regimes. For A and B the trend is towards shorter correlation times, i.e. towards stronger turbulence, with increasing v_d.

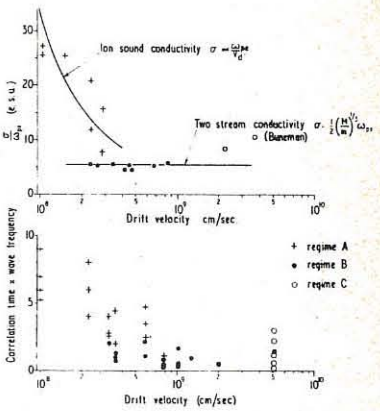

Fig.4.

Fig.1(b) shows a typical ion-sound spectrum plotted logarithmically. Assuming the maxima to be true wave potentials, we obtain the spectral distribution shown in Fig.5 (for four separate shots). The solid curve has the shape first predicted by Kadomtsev[6] for steady-state ion-sound turbulence in a current-carrying plasma.

References

1. S.M. Hamberger et al, Proc.3rd Europ.Conf.Contr.Fusion and Plasma Physics, Utrecht, 1969.
2. L.E. Sharp & S.M. Hamberger, Proceedings 4th Europ.Conf.Contr. Fusion and Plasma Physics, Rome, 1970.
3. O. Buneman, Phys.Rev. 115, 503 (1959).
4. V.A. Suprunenko et al, to be published in Plasma Physics.
5. R.Z. Sagdeev, Proc. XVIII, Symp. Appl.Math., 1967, p.281.
6. B.B. Kadomtsev, Plasma Turbulence, Academic Press, 1965, p.71.

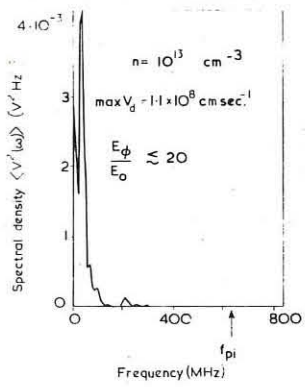

Fig.1(a)

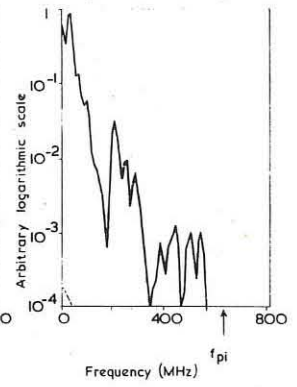

Fig.1(b)

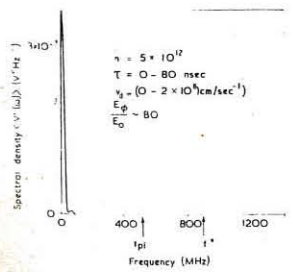

Fig.2(a)

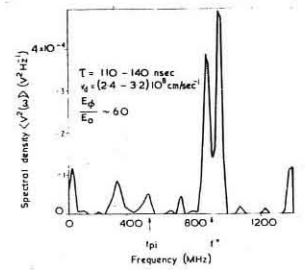

Fig.2(b)

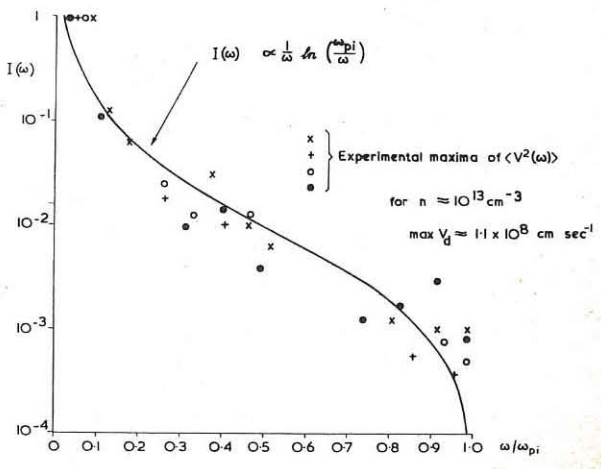

Fig.5.

TURBULENT CONDUCTIVITY OF PLASMA IN MAGNETIC FIELD WITH ZERO LINE

S.I.Syrovatsky, A.G.Frank, A.Z.Khodshaev

P.N.Lebedev Physical Institute, Moscow, USSR

Abstract: In the experiments described, the properties of current flow in plasma placed in a magnetic field with zero /neutral/ line were determined. The current distribution in such a field was obtained. The current region is rather broad in spite of the presence of a strong transverse magnetic field. Plasma conductivity is shown to be turbulent.

It is known that the appearance of accelerated particles in solar flares is connected with solar plasma motion in the vicinity of zero /neutral/ lines of magnetic field. It has been shown by Syrovatsky [I, 2] that two-dimensional plasma flow near zero lines produces magnetic energy cumulation and acceleration of charged particles along a zero line.

We have investigated experimentally phenomena taking place in the vicinity of a magnetic zero line. Our installation has a quadrupole magnetic field with 5.10^3 Oe/sm gradient. The vacuum chamber, 7 sm in diameter and 80 sm long, is surrounded by conductors producing a magnetic field with zero line along the chamber axis. A plasma source is placed at the end of the chamber inside the quadrupole field. Plasma from this source flows along the chamber axis and fills the chamber in about 10 μsec. The plasma has the shape of a cross in the transverse plane with rays directed along magnetic force lines /see fig. Ia/. The transverse dimension is about 4 sm in the direction of the quadrupole field conductors, and the maximum plasma density near the zero line is about 10^{13} cm^{-3}. Besides a magnetic quadrupole field there is an electrical induction field E_z applied along the zero line, its value being up to 500 v/sm.

This field induces plasma motion in the plane /X,Y/ which is perpendicular to the zero neutral line /Z-axis/. Plasma motion towards the zero line, for example along the Y - axis, is accompanied by its motion from the zero line along the X -axis /see fig. Ia, the directions of flow are shown by arrows/. As has been shown experimentally [3] plasma motion is actually of such a nature.

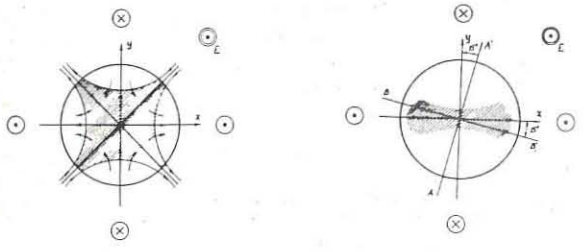

a/ b/

Fig.I.

If the magnetic field is frozen in /is carried over with plasma/ then the magnetic field distribution must change significantly near the zero line. Here the field gradient increases and a current sheet appears. Under such conditions we can expect the generation of energetic particles.

The electric field is produced by a discharge of low-inductive capacity C=0,I μF through conductors arranged parallel to the vacuum chamber tube as in the case of the quadrupole field conductors. The electric field frequency is about I MHz whereas the process is studied during the first quarter of period ~ 0,25 μsec when the electric field does not change direction.

In this work we are interested in the current produced by this electric field in the plasma which is placed in the quadrupole magnetic field. Fig 2. shows oscillograms of applied voltage and plasma current. Their phase relation shows that resistance of the plasma column is rather large. It depends on the magnetic field gradient and plasma density and varies from 2,5 to I5 ohms. The resistance is measured at the instant when plasma current is a maximum and hence dI/dt =0. Plasma current rises linearly with applied voltage, this means that plasma resistance does not depend on the electric field when the latter changes from 80 to 300 v/sm. To investigate the nature of plasma resistance we have changed the plasma column length. For half the length we obtain half the resistance /see table/. This means that the resistance is nearly uniform along the column and is not dependent on electrode phenomena.

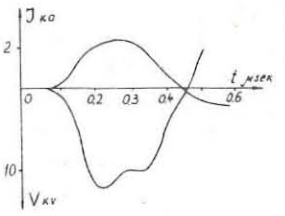

Fig.2

The current distribution was determined in two ways: with magnetic probes which measure the magnetic field of the current and with small Rogowsky coil. Magnetic probes are moved

Table:

l \ h	10^3 Oe/sm	2.10^3 Oe/sm
60sm	4,5± I,2 Ω	6,2± I,2 Ω
30sm	I,8± I,4 Ω	3,0± I,2 Ω

inside the glass tube of outer diameter 2,8 mm, the probe dimensions being smaller than 2 mm. The probes are moved in two directions AA' and BB' at an angle of 15° to the Y and X axes, respectively /see fig.I b/. The field component which is perpendicular to the displacement direction is measured. Fig 3 shows the magnetic field for the instant of plasma current maximum. We see that the width of current distribution /along the X-axis/ is definitely more than its thickness /along the Y-direction/. These dimensions are about 30 and I0 mm respectively. The same result was obtained in measurements with a Rogowsky coil. The magnetic field strength is small compared with the initial field hence there is no significant change of quadrupole field. The measurements allow to calculate the average plasma conductivity It equals 3.10^{12} CGSE. With this value of conductivity the magnetic field can be frozen in a region of I sm only for a period of about $\tau \sim 4.10^{-8}$ sec, i.e. ~5-I0 times shorter than the duration of the process.

The obtained conductivity is much smaller than the collision conductivity and is the result of generation of plasma instability in a strong electric field /ion-sound or Buneman instability/. This prosess should be followed by plasma heating, as it takes place in a number of experiments [4,5]. Current distribution measurments show that there is current practically everywhere where the plasma exists inspite of the presence of a strong transverse magnetic field. The nature of current across a strong magnetic field can be explained only as a result of rapid plasma heating due to instability. In fact the measured current is a diamagnetic plasma current which shows that plasma temperature is about $(T_e + T_i) \sim 1$ kev.

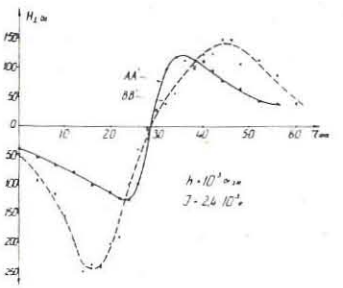

Fig.3.

References

I.S.I.Syrovatsky, Astron. J.43, 340,/I966/, JETF, 50, II33 /I966/.

2.V.S.Imshennik, S.I.Syrovatsky, JETF, 52,990 /I967/.

3.S.I.Syrovatsky, A.G.Frank, A.Z.Khodzhaev. Proceedings of the Symposium on Charged Particles Accelerators I968, Moscow, I970, v.2 p.538.

4.E.K.Zavoisky et al. Plasma Phys. and Contr. Nucl. Fusion Res. IAEA, Vienna, v.2, p.679 /I969/.

5.S.M.Hamberger M.Friedman, Phys.Rev.Lett, 2I, 674 /I968/.

EXCITATION OF LANGMUIR OSCILLATIONS IN AN ION BEAM-PLASMA SYSTEM

G.J. Brakenhoff and J.M. Houtkooper
Association EURATOM-FOM
FOM-Instituut voor Atoom- en Molecuulfysica, Kruislaan 407, Amsterdam/Wgm., The Netherlands

ABSTRACT: We report the observation of spontaneously excited Langmuir waves with frequencies between ω_{pi} and ω_{pe} and with phase velocities a factor 2.5 to 4.1 higher than the ion beam velocity. From the radial amplitude dependence of this wave it is identified as a Langmuir wave on a plasma column with the diameter of the ion beam. The mechanism to explain this excitation appears to be wave coupling in the end-sheaths of the Langmuir wave with the unstable slow ion beam wave and slow secondary electron beam wave.

1. INTRODUCTION: Spontaneously excited Langmuir waves have been observed previously in experiments with electron beams [1], and ion beams [2]. In this paper we compare the spontaneous wave with a wave excited in the system by a probe. This latter wave turns out to be even faster than the spontaneous wave and can be explained as a Langmuir wave on the broader diffusion plasma column around the ion beam. Typical parameter values of the system are: $n_e = 5 \times 10^7 - 5 \times 10^8$ cm/s; $T_e = 4.5 \pm 0.5$ eV, $v_{Te} \approx 0.85 \times 10^8$ cm/s; He^+ ion beam 20 keV, $V_b = 10^8$ cm/s.

2. THEORY: Consider a beam-plasma column of radius a with uniform densities of the constituents, in a cylindrical metal waveguide of radius b, in a homogeneous axial magnetic field. We take the dispersion for b >> a, [3]:

$$\{1 - \omega_{pb}^2/\left((\omega-kv_b)^2 - \omega_{cb}^2\right)\} Ta\ J_o'(Ta)/J_o(Ta) = ka\ K_o'(ka)/K_o(ka) \qquad (1)$$

$$T^2 = -k^2\left(1-\frac{\omega_{pe}^2}{\omega^2}\int \frac{f(v)}{(\omega-kv)^2}\,dv - \frac{\omega_{pb}^2}{(\omega-kv_b)^2}\right)/\left(1-\frac{\omega_{pb}^2}{(\omega-kv_b)^2-\omega_{cb}^2}\right) \qquad (2)$$

We take for f(v) the Maxwellian velocity distribution for the electrons. Further assumptions are: Quasi-static approximation, $\omega_{pe} >> \omega_{ce}$, no contribution from the plasma ions. We can separate the treatment of the dispersion equation in two parts:

I. Dispersion of Langmuir waves: $\omega/k >> v_{Te}$:
Since in our system, the thermal electron velocity is of the same order as the ion beam velocity, the Langmuir waves are far from synchronism with the beam waves, so that the beam contribution in (1) and (2) become negligible. Equation (2) can be simplified to:

$$T^2 = -k^2\{1 - \frac{\omega_{pe}^2}{\omega^2}\left(1 + \frac{3k^2v_{Te}^2}{\omega^2}\right) + j\sqrt{\frac{\pi}{2}}\frac{\omega_{pe}\omega}{(k\,v_{Te})^3}\,e^{-\omega^2/2k^2v_{Te}^2}\} \qquad (3)$$

If we consider $\omega \lesssim \omega_{pe}/\sqrt{2}$ and $\omega/k > 3\,v_{Te}$, we get a simple expression for the wave dispersion:

$$\omega_{pe}^2/\omega^2 = T^2/k^2 \qquad (4)$$

Using (4) for the wave dispersion we can derive from the imaginary part of (3) an expression for the spatial Landau damping of Langmuir waves:

$$k_i/k_r = \sqrt{\pi/4}\,\alpha^3\,e^{-\alpha^2/2}, \text{ with } \alpha = \omega/k\,v_{Te} \qquad (5)$$

II. Growth of the beam waves: $\omega/k \approx v_b \approx v_{Te}$:
To calculate the wave growth of the beam wave, by the resistive type of interaction with the plasma electrons, the set of equations (1) and (2) was solved by means of a computer program. This gives growthrates of the beam wave of about $k_i/k_r = 10^{-2}$ at our values of the parameters.

3. EXPERIMENT: The He^+ ion beam energy, 20 keV, current 0.5 mA, is injected through an entrance tube into the interaction vessel (fig. 1). The slightly diverging beam passes through the plasma, created by the beam itself through collisional ionization of the gas in the interaction space. The length of the interaction space, bounded by high transparancy grids, is variable. In the homogeneous (± 1/2%) magnetic field in the interaction space the beam plasma column has a nearly constant diameter of about 1.5 cm. Measurements were performed by means of movable probes (Langmuir probe, R.F. interferometer and spectrum analyzer) and a microwave cavity for density measurements. The measurements presented in this paper were done at a magnetic field of 0.26 Wb/m^2 and at helium gas pressures in the interaction space up to 1.3×10^{-4} torr. A typical spectrum of the spontaneously excited oscillations received on a probe in the system is shown in figure 2 for a pressure of 1.3×10^{-4} torr. Very noticable are the sharp spikes on the low frequency side of the spectrum. Changing the distance between the grids that limit the interaction space shifts the frequency of the spikes, but does not influence the shape of the envelope, indicating a resonance phenomenon connected with the finite system length. When we move a probe axially and record the intensity of the oscillations at a fixed frequency we find a standing wave pattern (see figure 3). From standing wave patterns the phase velocities of the detected waves can be determined, the distance between two maxima being equal to $\lambda/2$, as the intensity of the oscillations is recorded. We have measured the phase velocities in a range of the plasma density which scales with the gas pressure. We found at the lowest pressure $p = 3.5 \times 10^{-5}$ torr ($\omega_{pe} = 72$ MHz) the phase velocity to be 2.5×10^8 cm/s, while at the highest pressure $p = 2.7 \times 10^{-4}$ torr ($\omega_{pe} = 130$ MHz) the phase velocity is 4.2×10^8 cm/s. These waves are faster than the velocity of the ion beam (10^8 cm/s) which excludes direct excitation by the beam of these waves. Our next step was to compare these results with measurements with an R.F. interferometer on probe excited Langmuir waves. Figure 3 shows at the same frequency the standing wave pattern of the spontaneous wave and the interferometer pattern of the probe excited wave. We see that the probe excited wave has a phase velocity about twice that of the spontaneous wave. Subsequently we measured at the same conditions the radial dependence of both waves, beam density and plasma density, shown in fig. 4. We see that the probe excited wave follows the plasma profile, while the spontaneous wave is restricted to a much more narrow profile, corresponding with the beam cross section.

4. DISCUSSION: I. The observed difference in the phase velocities of the spontaneous wave and the probe excited wave, can be explained using (4). The values of T differ by a factor of 2, so do the diameters of the ion beam profile and the plasma profile. The result is that T.a values can be calculated in both cases to be about 1, as is expected from (1) in the range $0.15 < k.a < 0.5$ as is the case for the waves studied here. II. The influence of secondary electrons. The measurements presented here are obtained with the electrodes of the collector grounded, in order not to apply D.C.-voltages over the plasma. Then a current of secondary electrons of the order of 200 μA flows from the collector into the plasma. The velocity of the electrons, as estimated from the plasma potential, is 2×10^8 cm/s, too slow to be able to account for the observed phase velocities. When we suppress the secondary electrons we observe the spontaneous oscillations to diminish in amplitude by a factor of about 5, retaining the previous characteristics. III. The possible waves in the system are: Langmuir waves, ion beam waves and secondary electron beam waves. Of these, only the first propagate fast enough to be identified with the observed waves. However, they are stable, unlike the other waves. We propose the following mechanism: Noise will be amplified by the ion beam as it traverses the plasma. When arriving at the sheath in front of the grid, this signal will be reflected, as a Langmuir wave and possibly the secondary electron beam wave. The latter will increase in amplitude travelling to the other grid, while the Langmuir wave will be damped by Landau damping. At the other grid both waves will be reflected, exciting now the unstable ion beam wave and the Langmuir wave. Dommaschk [2] has made calculations on this type of wave coupling and found that the Langmuir waves could become unstable. IV. Landau-damping. If we consider the wave excitation by wave coupling, neglecting the secondary electrons, a minimum condition for the existence of the waves is that the spatial Landau damping of Langmuir wave is smaller than the spatial growthrate for the slow ion beam wave. We calculated from this condition, using (5) respectively (1) and (2), a condition for the phase velocity of the Langmuir wave. The observed spontaneous waves fulfill this condition.

REFERENCES:

[1] Etievant, C., (1964) CEA-R2456.
[2] Dommaschk, W., (1968) Conf.on Plasma Phys. and Contr.Nucl.Fusion, Novosibirsk, CN24/L-9.
[3] Trivelpiece, A.W. (1967) Slow wave propagation in plasma waveguides.

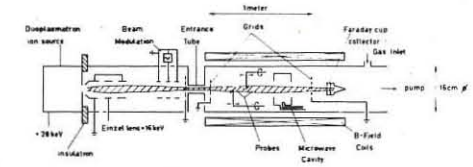

Fig. 1.

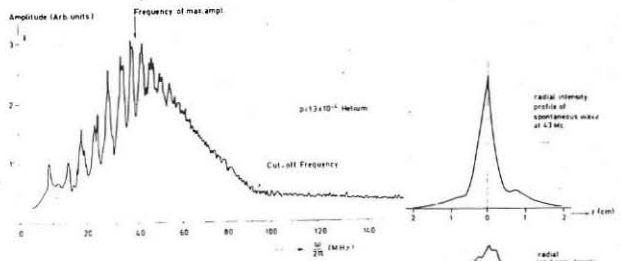

Fig. 2.

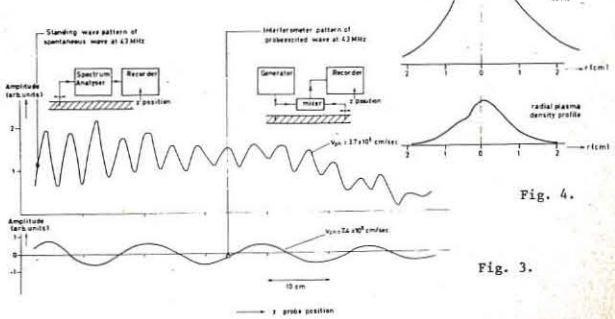

Fig. 4.

Fig. 3.

BEAM - PLASMA INTERACTIONS

ION HEATING BY BEAM PLASMA INTERACTION

F. Bottiglioni.

ASSOCIATION EURATOM-CEA
Département de la Physique du Plasma et de la Fusion Contrôlée
Centre d'Etudes Nucléaires
Boite Postale n° 6 - **92 Fontenay-aux-Roses** (France)

ABSTRACT : A powerful electron beam is injected longitudinally in a magnetic mirror configuration. By ionisation of the H_2 gas, a plasma is produced which is heated by interacting with the beam itself. The hot plasma density and the ion temperature are respectively a few $10^{11}\,cm^{-3}$ and a few hundred of eV.

INTRODUCTION : The production of ions, with energy exceeding several KeV has been observed in some particular regimes of low pressure discharges, confined by a magnetic field (1)(2)(3)(4), when an intense beam of uncupled energetic electrons (a few hundred of eV up to several KeV) is produced. The critical parameters of the electron beam to heat the ions are not yet well defined. Several different explanations have been proposed (5)(6)(7)(8) but anyone doesn't fit the whole of the experiments. We describe here only our experimental observations made on a plasma which is heated by interacting with a powerful electron beam. The plasma is produced by the ionisation of the beam on the H_2 gas.

EXPERIMENTAL APPARATUS. (Fig.1).

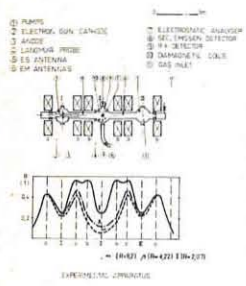

Fig. 1 : Experimental apparatus.

An electron beam (I_{Max} = 1A ; V_{Max} = 10 kV ; Ø = 1 cm ; beam pulse : 10 ms up to 2 s) is injected in a magnetic mirror configuration with a mirror ratio R changeable from 2 to 8 and with a maximum field strength at the mirrors of 0.6 T. Experiments are performed at R = 2 . In the mid plane between the mirrors an electrostatic analyser measures the energy of the ions obtained by stripping the fast atoms moving radially out of the plasma Fig.2. Fast atom radial flux, measured by secondary emission detectors, are used to estimate the hot plasma density. The oscillations are detected by an electrostatic antenna and the plasma diamagnetism is measured by a two diamagnetic loops. The H_2 gas is injected in steady-state through a gradient pressure system, opposite to the electron gun. The pressure inside the configuration is about (1-4) x 10^{-5} torr.

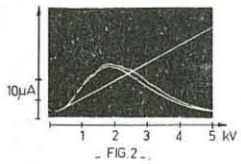

_ FIG.2 _

Fig.2 : Energy spectrum of fast atoms measured by the electrostatic analyser.
Hor. Units: 1 KeV/division
Vert. Units : 10 μA/division
Sweep time : 10 ms.

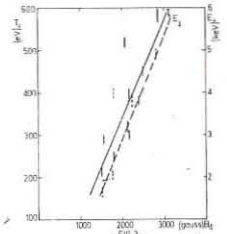

_ FIG.3 _

Fig. 3 : T and E of fast atoms versus B_4, the magnetic field strength in the middle plane between the mirrors

PLASMA PROPERTIES: The hot ions are confined near the middle of the magnetic configuration in a volume of about 200 cm^3. The longitudinal density profile , approximatively parabolic, drops of a factor 2 at about 2.5 cm from the center . The ion transverse temperature $T_\perp$ is deduced from the slope of the fast atoms energy spectrum. $T_\perp$ and the maximum transverse energy of the fast atoms $E_\perp$ depend on the magnetic field as shown in fig. 3. $T_\perp$ and $E_\perp$ decreases slowly (of a factor 1.5) when the pressure increases from 7 10^{-6} torr to 7 10^{-5} torr. The plasma diamagnatism growths with the magnetic field. The transverse energy density of the plasma, averaged on a diameter of 10 cm, is in the range of 10^{14} eV cm^{-3}. The radial flux of the fast atoms I_N exhibits two important characteristics : it increases with B, as plotted on Fig.4, and with the ratio B_4/B_o , where B_4 is the magnetic field in the midplane between the mirrors and B_o is the magnetic field at the electron gun. I_N doesn't change , in spite of what one would expect , in a rather wide range of the pressure (10^{-5} - 5 10^{-5}). Moreover, the mean hot ion density n_i, deduced on the basis of the charge exchange between the fast protons and the H_2 gas, doesn't fit

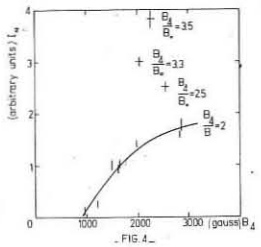

_ FIG.4 _

Fig.4 : Fast atom flux I_N versus B_4 for several values of B_4/B_o

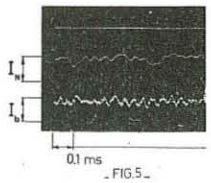

_ FIG.5 _

Fig. 5 : Modulation of the current of the collected beam and of I_N.
Hor. Units =0.1 ms / division
Vert. Units = I_b =1A/ division
Vert. Units I_N = 0.2 mA/division

the density of (2-5) $10^{11}\,cm^3$, inferred from diamagnetic and energy measurements unless the base pressure greatly increases owing to an important outgasing of the liner . Nevertheless a satisfactory agreement is found if the charge exchange of fast protons on H(9) or H_2^+(10) of the cold plasma are considered . As the whole gas ought to be in the atomic state, the charge exchange reaction on the H_2^+ could be the most effective one in producing the energetic atoms.

At the edge of the plasma region ($\Phi \simeq 6$-8 cm) is observed a strong emission in the band 50-120 MHz, in correlation with the ion heating. This is the range of the ion plasma frequency, for a plasma density of about 10^{11} cm^{-3} .

BEAM PROPERTIES. The current I_b of the primary electron beam is collected, after passing through the plasma, out of the mirrors. In the heating regime I_b is modulated with an amplitude reacting 30 % at a frequency of about 20 Kc/s. The modulation of I_N is well correlated in frequency, phase and amplitude with the beam modulation Fig.5. It has been observed that the longitudinal energy spectrum of the beam $f(W_{//})$, before interacting with the plasma, spreads out with increasing the ratio B_4/B_o . When $B_4/B_o \leq 1$ $f(W_{//})$ is a δ function, while for B_4/B_o = 3,5 $f(W_{//})$ has an half height width of about 700 eV and its maximum at 3,8 KeV. (Acceleration voltage ~ 4,7 KV).

REMARKS: The heating regime is obtained only if several physical conditions are fulfilled. For a given current and power of the beam, the ion heating occurs if the initial cold plasma density exceeds a threshold value and if the gas pressure is lower than a given value. These two limits are respectively in the range of a few 10^{10} cm^{-3} and 10^{-4} torr, in the present experiment. By injecting the gas through a pressure gradient system, in the high pressure region out of the mirrors is produced a plasma dense enough which diffuses into the magnetic configuration where the pressure is lower. The threshold on the plasma density is likely to be connected with a necessary condition for the starting of the oscillations which heat the plasma, whereas the pressure limit seems rather to be connected to the energy imput in beam-plasma system. The high frequency emission so as the low frequency modulation of the beam are strictly related with the heating regime. The observed dependence of I_N on the spread of $f(W_{//})$ of the beam affects mostly the heating efficiency (11) , which in our case is about 1 %.

REFERENCES.

(1) M.V. NEZLIN et al. JETP 45,840,(1963).
(2) I.ALEXEFF et al. Conf. IAEA Vol 2, p. 693, (1968) Novosibirsk.
(3) B.I. KANAEV et al. Conf. IAEA , special supplement p.169 (1969) Novosibirsk.
(4) M. FUMELLI et al. Plasma Physics (à paraitre)
(5) G .GUEST et al. Phys of Fluids 5, p.503 (1962).
(6) I. ALEXEFF et al. Phys. Rev. 129,516, (1963)
(7) A.B. MIKHAILOWSKII. Sov. Phys. Tech. Phys. 10 , 1490 (1966), Atomnaya Energya 20 , 103, (1966), Plasma Physics 8 , 705 (1966).
(8) M.V. NEZLIN , JETP, 26 , 693 (1968)
(9) E.W. Mc DANIEL , Collision phenomena in ionized gases , John Wiley 1964 p. 253.
(10) ORNL-3113 p. 11.
(11) B.S. AKSHANOV et al. Sov. Phys.Techn. Phys. 11, 446, (1966).

MEASUREMENT OF THE TRANSVERSE VELOCITY DISTRIBUTION FUNCTION OF THE BEAM ELECTRONS IN A BEAM-PLASMA EXPERIMENT

J.A. Cabral, H.J. Hopman, J.H.A. van Wakeren
FOM-Instituut voor Atoom- en Molecuulfysica, Kruislaan 407, Amsterdam
The Netherlands

ABSTRACT: We present measurements of the beam transverse energy as a function of the beam-plasma parameters. The transverse energy is seen to increase with the increase in the total radiated microwave power. It has been proved that the beam transverse energy is acquired at the cost of an axial deceleration of the beam electrons. With a simple model for the electron movement inside the analyser we could determine the beam transverse velocity distribution function.

1. INTRODUCTION: As it is well known, theory predicts that the development of any beam-plasma instability leads to an increase of both the parallel ($\delta T_{\parallel}$) and the transverse ($\delta T_{\perp}$) beam temperature. In case of excitation of Cerenkov instabilities $\delta T_{\parallel} >> \delta T_{\perp}$ [1]. On the contrary, during the instabilities caused by the anomalous Doppler effect, the energy lost by the beam goes over essentially to the increase of its transverse temperature and so $\delta T_{\perp} >> \delta T_{\parallel}$. Although there is a relatively large number of theoretical papers concerning this subject [2], only recently some experimental ones presented measurements on the beam transverse energy [3] [4].

2. EXPERIMENTAL DETAILS: Our beam-plasma experiment, described in a former publication [5], consists essentially of a cylindrical (ϕ = 8 cm) interaction chamber with a length of 73 cm. The background pressure amounts to 3×10^{-7} torr. The interaction chamber is filled with Helium at a fixed pressure p = 4.8×10^{-4} torr. The axial magnetic field is constant along the experimental tube (within 1%) and can be varied from 0.01 to 0.1 Wb m^{-2}. An electron gun injects continuously a beam of 1500 eV and a current variable up to 20 mA. The injection is parallel to the magnetic field and the beam is collected on the external wall of a specially designed electrostatic energy analyser. This analyser permits the measurement of the transverse velocity of the beam electrons and its first part is of conventional design, having a small entrance hole (ϕ = 0.2 mm) and two electrodes for the reflection of the ions and the application of the retarding potential. A third electrode can be used to modulate the parallel electron velocity. The electrons which pass the potential barrier strike a first collector which also has a hole (ϕ = 0.2 mm) in its centre. Electrons which pass through this hole are collected on a second collector. The assembly of these two internal collectors can be moved in the transverse direction over a maximum distance of 9 mm. This transverse scan of the second hole of the analyser is accomplished by 200 turns of a motordriven axis equiped with a helipot for X-Y recording. This permits a very precise measurement of the Larmor radius in a direct way. If $2r_M$ is the extension in the transverse direction where we can collect electrons in the second collector, then there are at least some electrons which possess a Larmor radius equal to $r_L = \frac{1}{2}(2r_M - \delta_1 - \delta_2)$. Here δ_1 and δ_2 are the diameters of the two holes in the analyser. The leak current between the two collectors ($\sim 10^{-10}$ A) sets a limit to the accuracy of the measurements.

3. EXPERIMENTAL RESULTS: Measurements were only done at the beam centre as only there is the expression for the Larmor radius valid (rotational symmetry). We began by measuring the "maximum" transverse energy of the beam electrons as a function of the beam current for different values of the magnetic field. For these measurements we assumed that we collected electrons if the current on the second collector was a factor 2 higher than the value it had in the absence of the electron beam. The axial retarding potential was continuously swept (50 Hz) from -100 V (to reflect the plasma electrons) to -2000 V (to reflect the whole beam). In this way the helical electron path inside the analyser (length about 10 cm) varies periodically in pitch. Thus we can, in first approximation, expect that, when the beam electrons arrive at the first collector (second hole), they will have the same probability of being at any particular position of their transverse circular orbit. This means that, no matter what their parallel velocity is, there will be moments at which the beam electrons will strike the first collector at their maximum distance from the analyser axis. Only so are the measurements of the maximum transverse energy trustworthy. Figure 1 presents the obtained results. We verify:

a) For all values of B the transverse energy begins to increase with the beam current i_b, attains a maximum and then decreases with a further increase in the beam current.
b) The value of i_b associated with the maximum transverse energy is some 20% lower than the one corresponding to the so-called 1^{st}-2^{nd} regime transition [3] [5].
c) The higher the magnetic field the higher the transverse energy.
d) The dependence on i_b of both the transverse energy as well as the total radiated microwave power (measured with a bolometer) is similar.

With the largest values of the beam current the plasma is, for every value of B, deep in the second regime. The beam axial velocity distribution function is then a plateau (f(v) = C) in an energy range extending from 0.1 to 1.3 times the beam initial energy. Looking for a relationship between the transverse and the axial energy of the beam electrons, we measured the "maximum" transverse energy possessed by the fraction of the beam which has an axial energy equal or greater than $U_{\parallel}$, for constant sets of beam-plasma parameters. This is simply done by sweeping the axial retarding potential of the analyser from (U/e) to -2000 V. In this way we reflect electrons possessing axial energies smaller than U = eV. Figure 2 presents the results. We verify:

a) For all values of the magnetic field the electrons which possess the highest transverse energy are the ones which are strongest decelerated. So, the transverse energy seems to be acquired at the cost of a decrease in the axial energy. This result is also referred by SCHUSTIN et al. [4].
b) Electrons which are accelerated to velocities greater than the beam initial velocity have very small transverse energies.

If we make a plot, on an X-Y recorder, of the current on the second collector (j) as a function of the radial distance (r) over which the assembly of the two collectors has been displaced, we obtain a curve j = j(r) peaked at r = 0 and monotonously decreasing with |r|. The position r = 0 represents the situation in which the two holes of the analyser are aligned with the magnetic field lines and with the axis of the retarding field structure. From j = j(r) we can determine the beam transverse velocity distribution function $f(v_{\perp})$. Due to the parallel velocity modulation (sweep of $U_{\parallel}$) and by rotational symmetry it is easy to find that

$$f(v_{\perp}) \sim \frac{\frac{d}{dr}[r.\, j(r)]}{r^{\frac{1}{2}}} \qquad (1)$$

Here $v_{\perp} = \frac{1}{2}\omega_{ce} r$ (r is the Larmor diameter). Figure 3 presents the obtained distribution functions for the case of B = 0.027 Wb m^{-2}. From identical measurements, made for other values of B, we can say:

a) For all values of B the shape of the distribution function is similar.
b) Every distribution is constituted by a cold bulk of electrons and a "hot" tail which is found to be Maxwellian.
c) The temperature of the "hot" tail increases with the beam current.
d) The ratio η between the number of "heated" electrons and their total number increases with i_b and, for a given beam current, with the magnetic field. This ratio seems to be related to the discontinuous character of the plasma radiation which, as is well known, occurs in bursts.
e) The fact that we found Maxwellian distributions probably reveals the stochastic nature of the beam-plasma instabilities.
f) For i_b = 20 mA we got the results: - (B = 0.0270 Wb m^{-2}, η = 10.9%, T_e = 11.2 eV); (B = 0.0385 Wb m^{-2}, η = 17.5%, T_e = 15.6 eV); (B = 0.0540 Wb m^{-2}, η = 45%, T_e = 22.2 eV). Therefore both η as well as T_e increase with B.

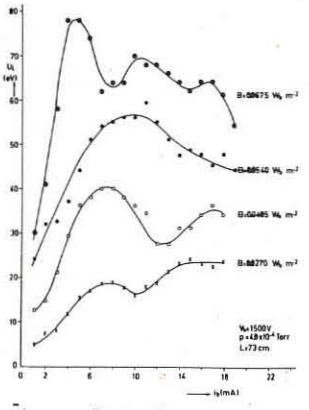

Figure 1: "Maximum" transverse energy of the beam electrons, as a function of the beam current, for different values of the magnetic field.

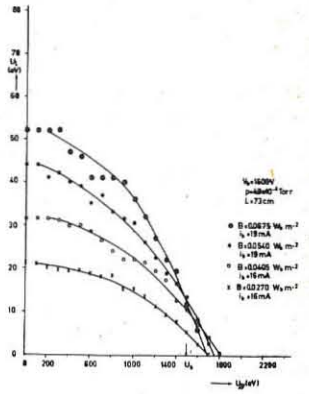

Figure 2: Plot of the "maximum" transverse energy possessed by the fraction of the beam which has an axial energy equal or greater than $U_{\parallel}$.

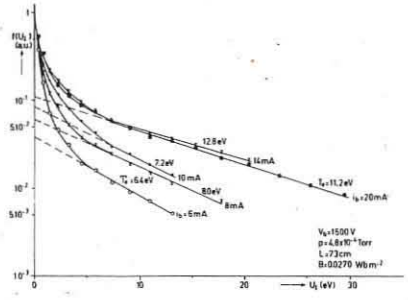

Figure 3: The influence of the beam current on the transverse energy distribution function of the beam electrons for a given value of the magnetic field.

REFERENCES:

[1] - Shapiro, V.D.; Shevchenko, V.I. - Soviet Physics JETP 15, 1053,(1962).
[2] - Shapiro, V.D.; Shevchenko, V.I. - Soviet Physics JETP 27, 635 (1968).
[3] - Cabral, J.; Hopman, H.J.; Insinger, F.G.; Ott, W. - "Plasma Physics and Controlled Nuclear Fusion Research", Vienna, 749 (1969).
[4] - Schustin, E.G.; Popovich, V.P.; Kharchenko, I.F. - Ninth Int.Conf. on Phenomena in Ionized Gases, Bucharest, 565 (1969).
[5] - Hopman, H.J.; Matitti, T.; Kistemaker, J. - Plasma Physics, 10, 1051 (1968).

PLASMA OSCILLATIONS IN AN AXIAL INHOMOGENEOUS BEAM PLASMA SYSTEM

by

H. Renner

SEKTION PHYSIK der UNIV. MÜNCHEN, Lehrstuhl Prof.Rollwagen

8000 München 13, Schellingstr. 2 – 8, Germany

Studying phenomena in the negative glow (NG) of an abnormal glow discharge we are interested on the importance of collective processes compared to binary collisions. As a model of NG beam scattering and the production of HF energy are investigated in a beam plasma system at corresponding experimental parameters [1]: Plasma H_2 gas 10^{-3} – $5\ 10^{-2}$ Torr pressure, n_p plasma density $3 - 8\ 10^9$ cm^{-3}. Beam $\varnothing$ 3 mm, current I_b = 0,5 – 2 mA, voltage U_b = 500 – 1500 V. B = 0 no magnetic field.

EXPERIMENT

As Fig.1 shows, the electron beam running in the axis of a cylindrical metal tube ($\varnothing$ 30 cm, 30 cm length) produces a plasma. The plasma density can be influenced by a cross burning glow discharge. The static parameters n_p and electron temperature T_e at the point z are deduced from Langmuir probe measurements. The beam density $n_b(z)$ and the energy distribution after interaction path z can be determinated by an electrostatic energy analyzer (E/ΔE = 600). Also with a movable HF probe and a registrating spectrum analyzer the HF energy in the interaction regime is detectable.

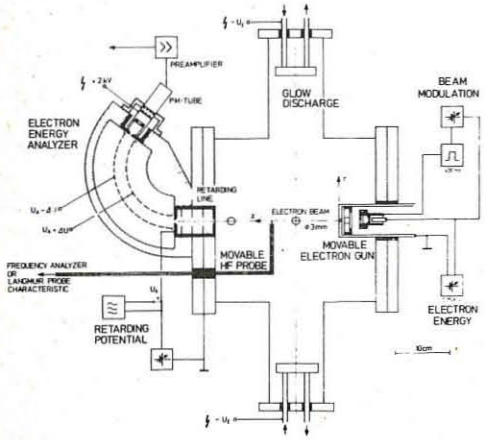

Fig.1 Schematic of Apparatus

THEORY

Starting from the linear theory of a homogeneous beam plasma -as done by SELF [2]- we get a dispersion relation $D(\omega, \gamma)$, where $\gamma = \alpha + i\beta$ gives the wave vektor. $D(\omega, \gamma) = 0$ represents for real ω to $\beta > 0$ plasma oscillations, which lead to instabilities of the system. At our exp. parameters we found $\beta = (\omega_p/2\, \nu_c)^{1/2}$, ν_c collision frequency belonging to $\omega \approx \omega_p$. The convective instability for an axial inhomogeneous plasma is described, if we define β_{eff} [3] along the interaction length z as a WKB approximation:

$$\beta_{eff} = \frac{1}{\Delta z} \int_0^{\Delta z} \beta(z)\, dz$$

$\beta(z)$ computed from local parameters at point z.

RESULTS

a. Parameters

Fig.2 presents the relative axial plasma density $n_p(z)$ and the measured beam density $I_b(z) \sim n_b(z)$ at various pressure:

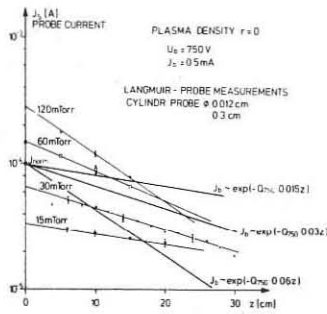

Fig.2 Axial Density

The simple scattering relation $I_b(z) = I_b(0) \cdot \exp(Qpz)$ is satisfied. Q is the total cross section. Also to $p < 60$ mTorr the same exponential function is valid for $n_p(z)$, so that ω_p / ω_b is a constant at fixed p and U_b. Electron temperature is always measured to 650°K.

b. Oscillations

The HF probe indicates spatially growing oscillations along z. Analyzing the received signal at various z one is able to determine $\beta(\omega)$ and compare the exp. value with the theory. Fig.3 demonstrates the agreement with the theor. predictions. The at z measured max. amplitude to ω_{max} is found

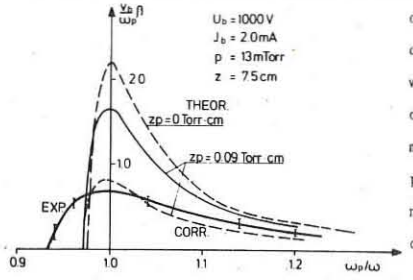

Fig.3 Growth Exponent

near $\omega_p(z)$. As $n_p(z)$ decreases with growing z, as decreases ω_{max}. In Fig.4 one can find spectra at various p and z. The saturation of the amplitude is caused by the axial inhomogenety of the system. The amplifikation to ω is only effective in regions ω near ω_p. Analyzing at z longer than z_{max} one receives not higher amplitudes. Estimations of the effective interaction length for growing amplitude experimentally could be verified.

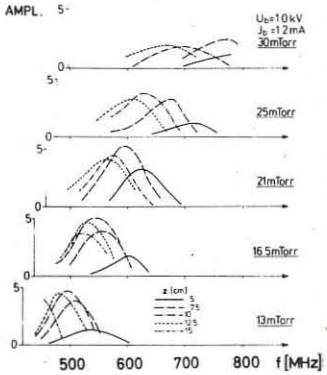

Fig.4 Oscillation Spectra

In contrast to the axial homogeneous system of LEVITINSKII [4] even at large z the amplitude is restricted. Therefore in our system electron heating and beam scattering caused by collective processes could not be observed.

REFERENCES

[1] Renner H., A.Heisen, J.Witt VII. Intern.Conf. PIIG Belgrad 1965, Vol. 1, 384

[2] Self S.A. III.Europ.Conf.Pl.Ph. Utrecht 1969, 32

[3] Ginzburg V.L. "The Propag. of EM Waves in Plasmas" Perg.Press, New York 1964

[4] Levitinskii S.M., J.P.Shashurin JETP 25, 227 (1967)

LOW FREQUENCY INSTABILITIES, DIFFUSION AND ION HEATING IN A BEAM-PLASMA SYSTEM

by

V.T.Astrelin, N.S.Buchelnikova, A.M.Kudryavtsev

INSTITUTE OF NUCLEAR PHYSICS, Novosibirsk, USSR

The experiments were performed on a Q-machine. Plasma column diameter $2R=4$ cm, its length $L=80$ cm, $H \sim 800$ G, $n\text{-}10^9 - 10^{10}$ cm^{-3}, $T_e \sim 0{,}2\text{-}40$ ev. The electrons were heated by high-frequency ($\sim$ 100–1000 Mc/sec) plasma oscillations being excited by electron beam /I/. The experiments were carried out in the electron sheath regime. The plasma density and density oscillation amplitude were measured by Langmuir probe, the electron and ion temperature – by two-grids analysers. The diffusion coefficient was found through direct measurement of the plasma flux from the column or through measurement of plasma decay time.

The instability. In cold plasma ($T_e \sim 0{,}2$ ev) there is practically no oscillations. When increasing T_e the oscillations are excited.

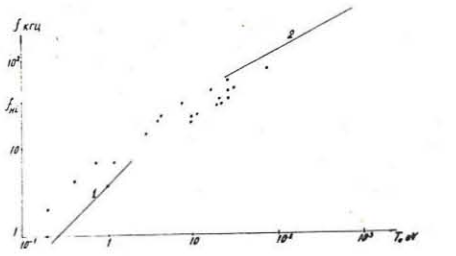

Their frequency and amplitude increase with T_e. In case $T_e \lesssim 7$ ev the oscillation frequency $f \sim T_e$, $f \sim H^{-1}$ and in absolute value is near to the drift frequency $f^* = \frac{K_y}{2\pi} V_D \approx \frac{1}{2\pi R} \frac{cT_e}{eH} \frac{1}{n} \frac{dn}{dz}$, where V_D – electron diamagnetic drift velocity (Fig.1, curve 1). When increasing T_e above 7 ev the dependence of frequency on T_e, H is getting not so strong, being in limit ($T_e \gtrsim 40$ ev) $f \sim T_e^{1/2}$, $f \neq f(H)$ and in absolute value is near to the ion-sound frequency $f_{is} = \frac{K_y}{2\pi} C_s \approx \frac{1}{2\pi R} \sqrt{\frac{T_e}{M}}$ where c_s is ion sound velocity (Fig.1, curve 2). In all cases the oscillations are asimuthal waves propagating in the electron diamagnetic drift direction. Taking into account that change of T_e is equivalent to change of relation V_D/C_s one can state that in agreement with theory /2/ in region $V_D/C_s < 1$, $f < f_{Hi}$ drift instability is excited, in region $V_D/C_s > 1$, $f > f_{Hi}$ – ion-sound instability is excited.

Turbulent plasma state. When $T_e \lesssim 20$ ev only one mode is excited usually. The oscillations are regular (the correlation time $\tau_c \sim$ 15–50 T – periods of oscillations) and correlated in space. When increasing T_e the second and higher modes are excited stochastically and so correlation time decreases. When $T_e \gtrsim 40$ ev the amplitude is high ($\frac{\tilde{n}}{n} \sim 1$) and the turbulence is developed. In this case $\tau_c \lesssim T$, asimuthal and radial correlation length $l_c \sim 1$ cm. Along the magnetic field the oscillations are correlated and so the turbulence is anisotropic.

The heating of ions. When oscillations are absent the ion temperature is $\sim 0{,}2$ ev. The excitation of oscillations causes increase of transverse ion temperature T_i. T_i increases when oscillation amplitude increases or correlation time decreases. When turbulence is developed ($T_e \gtrsim 40$ ev, $\frac{\tilde{n}}{n} \sim 1$, $\tau_c \lesssim T$) the maximal $T_i \sim 6$ ev. Because of dependence of T_i on correlation time one can suggest that heating mechanism is of stochastic type. In such a case the heating can be described by formula /3/ $\frac{dT_i}{dt} \sim \frac{e^2}{2M} \frac{E^2 \tau_c}{1+(\omega-\omega_{Hi})^2 \tau_c^2}$. Taking into account that the energy is carried out to the wall of the machine by ions with large larmor radii ($\rho_i \gtrsim 10$cm) one can compare calculated and experimental values of T_i (Fig.2). It is seen that experimental dependence of T_i on oscillation parameters is in good agreement with calculated one, the absolute values of T_i are agreed in order of magnitude. It is worth to note that energy flux connected with diffusion is much lower than energy flux carried to the wall by high energy ions. So in our case the value of T_i is limited only by low dimensions of the machine but not by diffusion.

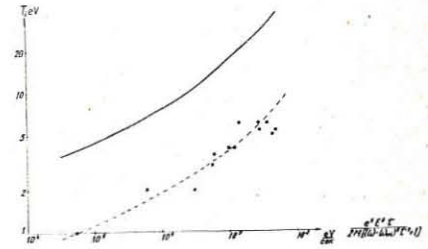

The diffusion across the magnetic field. When oscillations are absent the diffusion coefficient D is near classical one. The excitation of oscillations causes increase of diffusion. D increases with increasing of $\frac{\tilde{n}}{n}$ and T_e. In case of low T_e ($T_e \lesssim 3$ ev) D depends linearly on parameter $m(\frac{\tilde{n}}{n})^2 T_e$ (m-mode number) (Fig.3) and can be described by formula $D \sim \frac{1}{dn/dz} \frac{c}{H} \langle \tilde{n} \tilde{E}_y \rangle \sim \frac{m}{2} \frac{1}{n} \frac{dn}{dz} R \left(\frac{\tilde{n}}{n}\right)^2 \frac{cT_e}{eH} \sin\psi$ where ψ is $\tilde{n} - \tilde{\varphi}$ phase shift, suggested slightly depending on T_e. In case $T_e > 3$ ev the dependence of D on parameter $m \left(\frac{\tilde{n}}{n}\right)^2 T_e \sim \frac{\tilde{n}}{n} \tilde{E}_\varphi$ is weaker (Fig.3). It is found that in case $T_e > 3$ ev the drift velocity cE_y/H is more than ion-sound velocity. This fact can explain low dependence of D because the real plasma drift velocity cannot exceed c_s and so in this region D doesn't depend on $\tilde{E}_\varphi$. The maximal D is observed in case $T_e \sim 40$ ev, $\frac{\tilde{n}}{n} \sim 1$: $D \sim 2 \cdot 10^4 \frac{cm^2}{sec}$ ($D_{ei} \lesssim 1 cm^2/sec$), $D \sim 1/H$. It is worth to note that this value of D is an order lower than Bohm diffusion coefficient ($D \sim 4 \cdot 10^5 cm^2/sec$). The diffusion mechanism is of convective type.

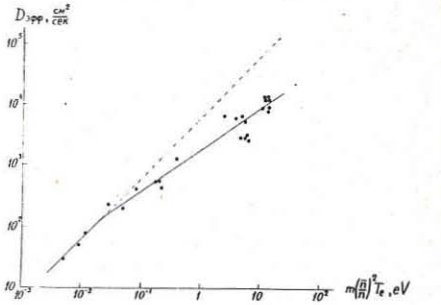

References.

1. V.T.Astrelin, N.S.Buchelnikova, A.M.Kudryavtsev, Third European Conf. on Contr. Fusion and Plasma Physics, Utrecht, 1969, p.92.
2. B.B.Kadomtsev, Plasma Turbulence, ch.IV, Academic Press, London, 1965.
3. F.G.Bass, Ya.B.Fainberg, V.D.Shapiro, Zh.Eksp. Theor. Fiz. (USSR), 49, 329, 1965.

Coupling of Electron cyclotron Harmonic Waves with Electron-beam induced Plasma Waves near the Upper Hybrid Frequency

A. Clinckemaillie, V. Piffl[+)]
Institut für Plasmaphysik, 8046 Garching near Munich
Federal Republic of Germany

In several experimental works dealing with electron-beam - plasma interaction, the observations of energetic plasma electrons and the presence of high-frequency instabilities associated with the "cold-theory" plasma waves have been shown to be related in frequency ranges near the electron cyclotron harmonics /1,2 /. On the other hand it has been shown experimentally that noise-emission from a quasi-Maxwellian plasma is strongly enhanced near the electron cyclotron harmonics when a small electron beam is fired through the plasma /3/; these results have been ascribed to the presence of longitudinal electron cyclotron harmonic plasma waves (Bernstein waves). The present investigations have shown that the wave phenomena quoted above, can appear simultaneously and are in fact coupled with each other under the condition that the upper hybrid frequency is close to the second electron cyclotron harmonic.

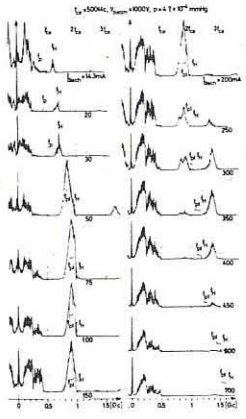

Fig. 1

The plasma is produced in the positive column of a low-pressure Argon glow-discharge /4/ and a separate continuously generated electron-beam ($\varnothing$ = 6 mm, 1 kV, 10 mA) is injected axially and parallel to the homogeneous magnetic field. The emission signals are detected with small cylindrical antennas outside the beam region, and received with a Spectrum Analyser and a Radiometer.

Emission spectra measurements were performed with a fixed magnetic field and constant electron-beam conditions, with the discharge current($\sim$ plasma density) as variable parameter (fig. 1, emission amplitude in log.scale vs.frequency). At low- and for increasing discharge currents, the emission peak (f_H) is shifted progressively to higher frequencies and as far as $f_H \ll 2f_{ce}$ can be identified with the upper hybrid frequency branch of the beam-induced plasma waves /1,3 /. Moreover, when the emission signals appeared just below the 2nd harmonic, ion-saturation current measurements showed a relative increase of the plasma density of 50 % and more; this suggests that the beam-induced emission is accompanied by an additional heating, which in our plasma system corresponds to an extra-ionization. Therefore we have limited the analysis of the emission spectra to the case when: $f_{ce} < f < 2f_{ce}$.

With measurements of the radial amplitude dependence of the noise-emission, we could verify that in this frequency range the beam-generated wave-signals have dispersion properties wich are identical to the well known Bernstein waves which propagate perpendicularly to the magnetic field /5/. These results are summarized in fig.2 together with the transmission-comparision measurements /4/.

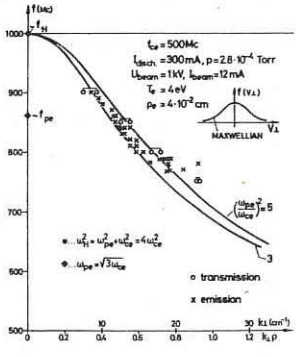

Fig. 2

Spatial phase correlation measurements were also performed between two antennas movable in the r- and z-direction. The emission signal detected by each antenna is mixed through an interferometric-like system (fig.3), one arm of which is used as reference signal and the other arm is connected to the antenna which is swept and the frequency is selected at the receiver. The measured phase differences are a function of the distance between the r- and z-antenna. Typical results (fig.3a) appear when the r-antenna is fixed and the z-antenna varied parallel to the beam. The parameter Δ l corresponds to the variable coaxial delay-line inserted between both arms. We see that the parallel wavelengths satisfy the Cherenkov-synchronism relation ($\omega = k_{//} v_{beam}$). In the other case when the r-antenna is moved and z-fixed (with the position of the z-antenna as parameter as shown in fig. 3a) we can conclude from these measurements: (fig. 3b, 3c)

1) the "parallel" and "perpendicular" phase-components of the observed waves are linearly correlated;
2) the "perpendicular" phase velocity component of the Beam-generated Bernstein waves is directed towards the axis of the beam-plasma system;
3) the "perpendicular" phase component is space dependent in the outer region of the plasma profil, until the limit layer corresponding to the local upper hybrid frequency is reached (fig. 3c); wheras, close to the beam-axis no variation of the phases can be observed when varying the external delay-line (Δ l);
4) the phase correlation measurements, perpendicular to the magnetic field, corroborate the results of the radial amplitude dependence of the emission signals: the beam-induced, Bernstein waves propagate across the radially density-inhomogeneous plasma profile with wavelengths which are only determined by the local plasma parameters (density, temperature).

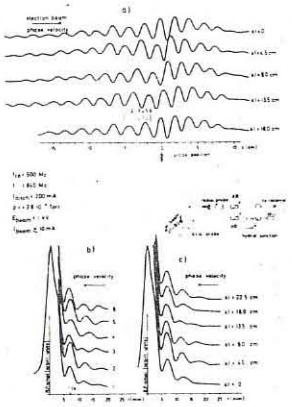

Fig. 3

So far our experimental results agree with the theoretical predictions, in /6/, about the coupling conditions between the Upper Hybrid and the Bernstein wave modes. However, the enhanced plasma heating which has been observed in the same frequency range, is believed to be a consequence of the coupling of both waves parallel to the electron beam, because Bernstein waves with a wave component parallel to the static magnetic field are Landau damped /7/.

/1/ M. Seidl, P. Sunka, Nuclear Fusion 7 (1967) 237
/2/ J. Jancarik, V. Piffl, M. Seidl, Phys. Lett. 28 (1968) 331
/3/ T. Idehara, K. Ohkubo, S. Tanaka, Journ. Phys.Soc. Japan 27 (1969) 187 (see also the Ref. given in /1/ and /3/)
/4/ A. Clinckemaillie, Inst.f.Plasmaph.Report II/84 Nov. 1969, Garching near Munich
/5/ R.S. Harp, Appl. Phys. Lett. 6 (1965) 51
R.S. Harp, Proc. 7th. Int.Conf.Phen.Ioniz.Gas. Belgrad 1965, Vol. 2, pg. 294
/6/ V. Kopecky, J. Preinhaelter, J. Vaclavik, J. Plasma Phys. 3 (1969) 179
/7/ I.B. Bernstein, Phys. Rev. 109 (1958) 10

This work was performed as part of the agreement between the Institut für Plasmaphysik GmbH, Garching near Munich, and Euratom to conduct joint research in the field of plasma-physics.

+) on leave from Institute of Plasma Physics, Prague 9, Nademlynska 600

BEAM – PLASMA INTERACTIONS

THE INFLUENCE OF ELASTIC COLLISIONS ON BEAM PLASMA AMPLIFICATION IN THE ION PLASMA FREQUENCY RANGE

R. Leven and J. Wisliceny

SEKTION PHYSIK/ELEKTRONIK, UNIVERSITÄT GREIFSWALD, DDR

Abstract: Beam plasma interaction is considered taking into account elastic collisions. The dispersion equation is found and solved for the case of drifting electrons. As an example the amplification curves are plotted for electron-ion collisions. It is shown, that for sufficient high collision frequencies the amplification is disturbed.

We start from the system of Vlasov-equation, including a simple collision term, the hydrodynamic equations for ions and neutrals, the equations of continuity and Poisson-equation. All equations are used in their one-dimensional form, since we look for longitudinal waves only.

$$(1)\quad \frac{\partial f_e}{\partial t} + v\frac{\partial f_e}{\partial x} - \frac{e}{m_e}E\frac{\partial f_e}{\partial v} = -\frac{1}{\tau_{en}}(f_e - f_{en}^*) - \frac{1}{\tau_{e+}}(f_e - f_{e+}^*)$$

τ_{en}, τ_{e+} - relaxation times. The f_{ik}^* should be chosen as simple as possible, but so, that the conservation of particle number and momentum is guaranted:

$$(2)\quad f_{ik}^* = n_i\,\delta(v - V_{ik}^*)$$

with

$$V_{ik}^* = (\varrho_i v_i + \varrho_k v_k)(\varrho_i + \varrho_k)^{-1}$$

v_i is the hydrodynamic velocity of the i-th component, ϱ_i the mass density.

$$(3)\quad \frac{dv_+}{dt} - \frac{Z n_+ e}{m_+}E = -\varrho_e\beta_{e+}(V_+ - V_e) - \varrho_n\beta_{+n}(V_+ - V_n)$$

$$(4)\quad \frac{dv_n}{dt} = -\varrho_e\beta_{en}(V_n - V_e) - \varrho_+\beta_{+n}(V_n - V_+)$$

where $\beta_{ik} = [\tau_{ik}(\varrho_i + \varrho_k)]^{-1}$. We suppose, that the β_{ik} are not depending from the ϱ_i, ϱ_k (see [1]).

$$(5)\quad \frac{d\varrho_i}{dt} + \varrho_i\frac{\partial v_i}{\partial x} = 0 \qquad i = +, e, n$$

(in the case i = e, (5) follows from (1)).

$$(6)\quad \varepsilon_0\frac{\partial E}{\partial x} = e(Z n_+ - n_e)$$

Now we linearize, taking all perturbation terms in the form

$$(7)\quad G_1 = G_{10}\exp\{i(\omega t - kx)\}$$

Taking into account, that (2) gives

$$(8)\quad f_{ik1}^* = n_{i1}\,\delta(v - V_{iko}^*) - n_{io}\frac{\partial\,\delta(v - V_{iko}^*)}{\partial(v - V_{iko}^*)}V_{ik1}^*$$

and allowing $E_o \neq 0$, $v_{io} \neq 0$ we obtain from (1)

$$n_{e1} = \int f_{e1}\,dv = \frac{e}{m_e}E_1\int\frac{\partial f_{eo}/\partial v}{i\omega - ikv + \gamma_e}\,dv + \gamma_{en}\int\frac{f_{en1}^*\,dv}{i\omega - ikv + \gamma_e} +$$

$$(9)\quad + \gamma_{e+}\int\frac{f_{e+1}^*\,dv}{i\omega - ikv + \gamma_e} + \frac{e}{m_e}E_o\int\frac{\partial f_{e1}/\partial v}{i\omega - ikv + \gamma_e}\,dv +$$

$$- \beta_{e+}(\varrho_{e1} + \varrho_{+1})\int\frac{(f_{eo} - f_{eno}^*)\,dv}{i\omega - ikv + \gamma_e} - \beta_{en}(\varrho_{e1} + \varrho_{n1})\int\frac{(f_{eo} - f_{eno}^*)\,dv}{i\omega - ikv + \gamma_e}$$

where

$$\gamma_{ek} = \beta_{ek}(\varrho_{eo} + \varrho_{ko}) \qquad \gamma_e = \gamma_{e+} + \gamma_{en}$$

Now we suppose, that the dc-field E_o is so weak, that the term with E_o is negligible. We also neglect the last two terms in (9), assuming them sufficiently small. After this we are able to exclude all variables from (9) and the linearized equations (3) - (6) except the n_{i1}. With the assumptions $\varrho_{eo} \ll \varrho_{no}$, $V_{+o}, V_{no}, \frac{m_e}{m_+}V_{eo}, \frac{\varrho_e}{\varrho_n}V_{eo} \ll \frac{\omega}{k}$ we get the coefficient determinant of the equation system for the n_{i1} in the form

$$(10)\quad \Delta = \begin{vmatrix} 1 + \frac{1}{k}\omega_p^2 I & \frac{i\gamma_e}{\omega - i\gamma_e} & -\frac{1}{k}\omega_p^2 I + \frac{i\omega\gamma_{e+}}{(\omega - i\gamma_e)^2} & \frac{i\omega\gamma_{en}}{(\omega - i\gamma_e)^2} \\ \frac{Z\varrho_{+o}\Omega_p^2}{\omega} + i\alpha_{e+} & & -\frac{Z\Omega_p^2\varrho_{+o}}{\omega} + \omega\varrho_{+o} - i(\alpha_{e+} + \alpha_{+n}) & i\alpha_{+n} \\ i\alpha_{en} & & i\alpha_{+n} & \varrho_{no}\omega - i(\alpha_{en} + \alpha_{+n}) \end{vmatrix}$$

with

$$\omega_p^2 = \frac{n_{eo}e^2}{m_e\varepsilon_o} \qquad \Omega_p^2 = \frac{m_e}{m_+}\omega_p^2 \qquad \alpha_{ek} = \varrho_{eo}\varrho_{ko}\beta_{ek}$$

$$I = \frac{1}{n_{eo}}\int\frac{\partial f_{eo}/\partial v}{\omega - kv - i\gamma_e}\,dv$$

The condition $\Delta = 0$ is the dispersion relation for our problem. From (10) we see, that this equation can be written in the form

$$(11)\quad \frac{\omega_p^2}{k}I = (C + iD)$$

where C and D are functions only of ω and the parameters, but are not dependend on the wave number $k = k_r + i\gamma$. Assuming the electron distribution function f_{eo} as a Maxwellian with a small drift velocity ($v_{eo}^2 \ll v_{eT}^2$), we can approximate the integral I as was shown in [2]. After this it is easy to find k_r and γ as functions of ω and the parameters.

The figure shows the increment $\gamma' = \gamma V_{eo}/\omega$ for the case of electron-ion collisions for $v_{eT} = 5\,v_{eo}$, $m_+/m_e = 7500$. The curves (1) - (4) correspond to the following values of the frequency ratio γ_{e+}/Ω_p : 0; 10^{-3}; 10^{-2}; 2.10^{-2}. We see, that for collision frequencies $\gamma_{e+} \lesssim 10^{-3}\Omega_p$ the influence of the electron-ion collisions is not essential. With increasing collision frequencies the increment γ' decreases, and for $\gamma_{e+}/\Omega_p \gtrsim 3.10^{-2}$ no amplification takes place.

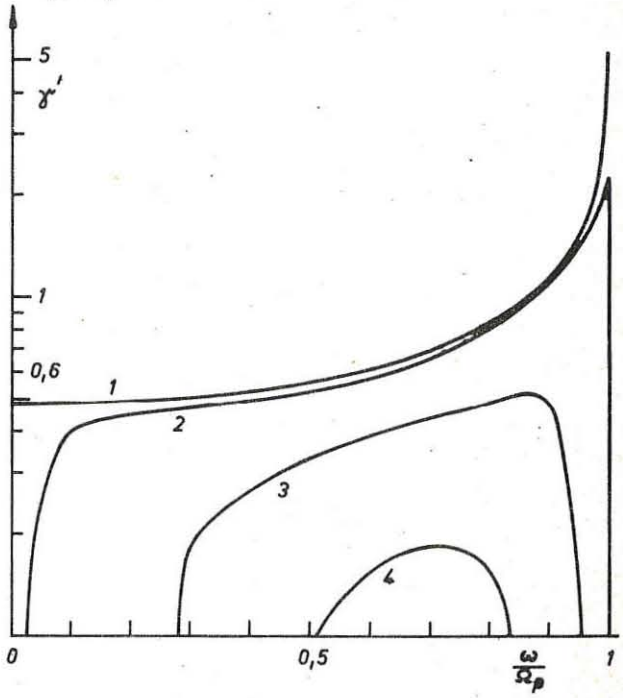

[1] J.Wilhelm, J.Wisliceny, Beitr.Plasmaphys. 6, 89 (1966)

[2] R. Leven, Beitr. Plasmaphys. 10 (1970)

ON THE THEORY OF BEAM-PLASMA INTERACTION

by

B. B. Kadomtsev*, O. P. Pogutse*

International Centre for Theoretical Physics, Trieste, Italy.

Abstract: Using as the simplest case the Langmuir wave excitation by an electron beam, a new theory of beam-plasma interaction is proposed in which the generation of waves by bunched electrons is taken into account. This fact naturally leads to a final distribution function similar to two-Maxwellians as was shown by many numerical calculations.

It is well known that the interaction of a beam with a plasma is determined by co-operative phenomena related to beam-plasma instabilities. At the early stage of investigations this interaction was considered qualitatively in terms of bunching of beam electrons. But later this argument was replaced by a more formal quantitative theory, so-called quasilinear approximation. In quasilinear theory the beam-plasma interaction is described as some sort of diffusion in velocity space which leads to the plateau on the beam distribution function. But this result seems to be in contradiction with many numerical calculations which give, as a rule, two-Maxwellian distribution. We shall show that this discrepancy can be overcome if we take into account the beam space charge fluctuations - which are analogous to the bunching effect.

Let F be the distribution function of the beam and plasma electrons. Its temporal behaviour is determined by the Vlasov equation

$$\frac{\partial F}{\partial t} + v \frac{\partial F}{\partial x} = \frac{e}{m} E \frac{\partial F}{\partial v} \quad , \tag{1}$$

where the electric field E is given by

$$\frac{\partial E}{\partial t} = 4\pi \int e v F \, dv \quad . \tag{2}$$

We suppose that F is one dimensional and that ions are at rest. Due to instability, the thermal fluctuations exponentially increase with time so that F may be written in the form

* On leave from Kurchatov Institute of Atomic Energy, Moscow, USSR.

$$F = f_0 + f \quad , \tag{3}$$

where $f_0 = \langle F \rangle$-average over x of F . Supposing that $\langle E \rangle = 0$, we find from (1) by averaging:

$$\frac{\partial f_0}{\partial t} = \frac{e}{m} \frac{\partial}{\partial v} \langle Ef \rangle \quad , \tag{4}$$

$$\frac{\partial f}{\partial t} + v \frac{\partial t}{\partial x} = \frac{e}{m} \frac{\partial}{\partial v} \left(Ef_0 + Ef - \langle Ef \rangle \right) \quad , \tag{5}$$

$$\frac{\partial E}{\partial t} = 4\pi \int e v f \, dv \quad . \tag{6}$$

In the quasilinear approximation the last two terms on the right-hand side of Eq. (5) are neglected. But at the final stage, when $\partial f_0 / \partial v$ becomes very small, this approximation is definitely not good. We shall use another approach. Let f be a sum of two terms $f = f_1 + f_2$, where f_1 corresponds to the linear approximation in (5):

$$\frac{\partial f_1}{\partial t} + v \frac{\partial f_1}{\partial x} = \frac{e}{m} E \frac{\partial f_0}{\partial v} \quad . \tag{7}$$

If we substitute the solution of Eq. (7) in (6) neglecting the slow dependence on time of the function f_0 , we obtain the following equation for E :

$$\frac{\partial}{\partial t} \hat{\varepsilon} E = 4\pi \int e v f_2 \, dv \quad , \tag{8}$$

where $\hat{\varepsilon}$ is the usual dielectric operator. The distribution function f_2 is coupled with chaotic motion of trapped particles and can be considered as weakly correlated with electric fields E . Therefore the term on the right-hand side of Eq. (8) can be considered as some external source which generates plasma waves. From the equation for the two-point correlation function it is possible to show that the external source intensity is proportional to f_0 . This leads to an equation of the quasilinear type but with an additional friction term which corresponds to the wave generation by bunched electrons. Taking into account the spread of electric field spectrum with respect to frequencies, it is possible to show that the distribution function will tend to two-Maxwellian type distribution. The details of this theory will be published elsewhere.

ACKNOWLEDGMENTS

The authors are grateful to Professor Abdus Salam, the International Atomic Energy Agency and UNESCO for hospitality at the International Centre for Theoretical Physics, Trieste.

SHOCK WAVE GENERATED BY A DISCHARGE PLASMA
APPROXIMATE DETERMINATION OF HOMOLOGICAL PARAMETERS

by

Rybowski (L.) and Renneboog (J.)

UNIVERSITY OF BRUSSELS

Ave. F. Roosevelt, 50 - 1050 Bruxelles - Belgium

Abstract : The Legendre representation of the experimental propagation law of a shock wave allows a fast and rather accurate calculation of the homological parameters. Results are given for different experimental conditions (gas, pressure and discharge voltage).

Introduction : The homological theory [1] describes the movement of an intensive, non-stationary and plane shock wave spreading in rest medium by the law

$$\theta = t_o + K(x-x_o)^{\lambda} \qquad (1)$$

where : - $(\theta - t_o)$ is the time spent by the shock-front to travel through the distance $(x-x_o)$

- K, λ, t_o, x_o are the characteristic constants of the movement
- K depends on the pressure and on the initial energy
- λ the homological exponent, is a function of adiabatic exponent.

An experimental law for the shock wave propagation along the expansion chamber of an electromagnetically driven shock tube can be deduced from the photographs of the luminous fronts (wave and discharge plasma), taken by means of the smear camera. This yields

$$t(x) \simeq \sum_i \alpha_i P_i(x) \qquad (2)$$

where $P_i(x)$ is the Legendre polynomial of $i^{\underline{th}}$ degree.

If $\theta(x)$ represents a good approximation of t(x) its associated Legendre development

$$\theta(x) = \sum_n h_n P_n(x)$$

must be nearly identical with the right side of relation (2).

Consequently

$$\alpha_n \simeq h_n = \frac{2n+1}{2} \int_{-1}^{+1} \theta(x)\, P_n(x)\,dx$$

Calculation of the homological parameters.

When $n \gg 1$ it is easy to show that

$$\frac{\lambda+n+2}{2n+3} h_{n+1} - x_o h_n - \frac{\lambda-n+1}{2n-1} h_{n-1} = -\delta_n^1 t_o \lambda \qquad (3)$$

where δ_n^1 is the Kronecker delta.

Relation (3) gives :

$$(\frac{\alpha_3}{7} - \frac{\alpha_1}{3})\lambda - \alpha_2 x_o + \frac{4}{7}\alpha_3 + \frac{\alpha_1}{3} = 0 \qquad (n=2) \qquad (4)$$

and

$$\frac{3(\lambda+3)\alpha_2}{5\alpha_1} - 3x_o - \frac{\lambda(\lambda+2)M_o}{(\lambda+1)M_1 + x_o M_o} = 0 \qquad (n=1) \qquad (5)$$

where

$$M_n = (1-x_o)^{\lambda+1} - (-1)^n \cdot (-1-x_o)^{\lambda+1}$$

The resolution of equations (4) and (5) gives x_o and λ, and the principle of least squares leads to

$$K = \frac{2\alpha_1}{3} \frac{(\lambda+1)(\lambda+2)}{x_o M_o + (\lambda+1)M_1} \qquad (6)$$

and to

$$t_o = \alpha_o - \frac{\alpha_2}{5} + \frac{5\alpha_1 x_o - 3\alpha_2}{5\lambda} \qquad (7)$$

so, from (4) and (5) we obtain

$$\boxed{\frac{1 + F(\lambda)}{1 - F(\lambda)} - \left(\frac{1 - m\lambda - p}{-1 - m\lambda - p}\right)^{\lambda+1} = 0} \qquad (8)$$

where

$$F(\lambda) = -\frac{\lambda+1}{(m\lambda+p) + \frac{\lambda(\lambda+2)}{(3m-r)\lambda+3(p-r)}}$$

$$m = \frac{3\alpha_3 - 7\alpha_1}{21\alpha_2} \quad , \quad p = \frac{5\alpha_3}{7\alpha_2} - m \quad , \quad r = \frac{3\alpha_2}{5\alpha_1}$$

The resolution of equation (8) by an iteration method finally gives λ. Hence by means of relations (4), (6) and (7), we can calculate x_o, K and t_o, which determine completely the function $\theta(x)$ and allow us to check the homological exponent λ preliminarly found.

Experimental results

The shock tube (similar to the one used by Kolb [2]) and the experimental arrangement are described in [3].

The values deduced from (8) for our experiments are summarized in the following tables. We have considered only the experiments which give a shock-wave front separated from the plasma one.

Helium			
Pressure (Torr) \ Discharge voltage (kV)	7	8,5	10
2	1.64		
4	1.65	1.47	1.43
6	1.67	1.55	1.48
10	1.65	1.62	1.60

$\langle\lambda\rangle = 1.60$

Hydrogen			
Torr \ kV	7	8,5	10
4	1.66		
6	1.69	1.64	1.60
10	1.63	1.61	1.64

$\langle\lambda\rangle = 1.64$

Conclusion

The results obtained by the calculation method developed here, show that the law of propagation of electromagnetically-driven shock wave (separated from the plasma one) agree with the homological standard theory.

References

[1] Häfele (W.) Zur analytischen Behandlung ebener starker, instationärer Stosswellen
Z. Naturforschg. 10a, 1955, pp. 1006-1016.

[2] Kolb (A.C.) Magnetically Driven Shock Waves
Magnetohydrodynamics, 1957, pp. 76-91, edited by Landshoff (R.K.M) Stanford University, California.

[3] Renneboog (J.) and Rybowski (L.) Study of the Propagation of a Discharge Plasma and the Associate Shock Wave in an Electro-magnetically Driven Shock Wave. Ninth International Conference on Phenomena in Ionized Gases, 1969, Bucharest Romania, p. 59.

SOME ASPECTS OF PLASMA FLOW IN AN ELECTROMAGNETICALLY DRIVEN SHOCK TUBE

by

J. BENSIMON and A. LASEK

Laboratoire d'Electrodynamique de Gaz Ionisés
Faculté des Sciences
quai Saint-Bernard
Paris Ve

Laboratoire d'Aérothermique
Centre National de la Recherche Scientifique
92 - Meudon

F R A N C E

An experimental study of plasma flow in an electromagnetically driven shock tube is reported. Special consideration is given to the behavior of the contact surface between shock wave compressed gas and the discharge plasma. Comparison with the theory of stability is made

The experiences aimed to obtain a sample of gas at a very high temperature (1) are often accompanied by a very rapid gas flow The phenomena which are related to the stability of these flows have a particular importance.

We studied (2) these phenomena in electromagnetically driven shock tubes : one with a conical discharge chamber, the other with a T-form discharge chamber of the type described in (3). The T-tube has two distinct gas arrivals at the two ends, and a gas pumping exit situated on an annulus at a distance of 5.5 cm from the electrodes . As driver and driven gas, we used respectively the combinations He-He, He-A, A-He and A-A; the pressures were between 1 mm Hg and 4 mm Hg, the discharge tension - 25 kV.

The flow of the plasma column satisfies the relation given by Sedov (4) :

$$x = \alpha t^{\beta}$$

It is possible to evaluate the theoretical value Δx of the distance of the shock wave front and the contact surface which separates at the abscissa x the plasma from the shock heated gas

$$\frac{\Delta x}{x} = \frac{\gamma-1}{\gamma+1} + \frac{2}{\gamma+1}\,\frac{\beta}{2-\beta}\,\frac{1}{M^2} \qquad (M = M(x))$$

If one compares (Fig.1) the theoretical curve obtained by this formula with the experimental results obtained with a streak camera, one observes that the experimental distance Δx is inferior to the theoretical limit. This discrepancy may be due to the phenomena of ionisation and of instability of the front of the plasma column.

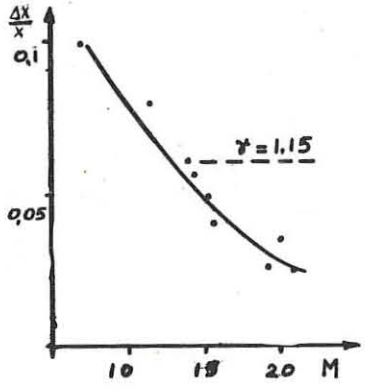

Fig. 1

In fact, the velocity of the gas diminishes along the tube axis and the gas is submitted to the action of a variable acceleration

$$\ddot{x} = \alpha\beta(\beta-1)\,t^{\beta-2}$$

which changes in time and space. This acceleration acts on two gas columns separated by a contact surface; the discharge plasma is heated in a volume V_o and is expanding along the tube axis. Its initial density being ρ_{1o} the density of the plasma at the abscissa x is

$$\rho_1(x) = \rho_{1o}\,\frac{V_o}{V_x}$$

Between the same contact surface and the shock wave front, we find the gas heated and compressed by the shock wave. If the initial density of this gas was ρ_{2o} its density behind the shock wave is

$$\rho_2(x) = \rho_{2o}\left(\frac{\gamma+1}{\gamma-1+\frac{2}{M^2}}\right)$$

In this situation where the gas of two different densities separated by a contact surface are submitted to an acceleration, there is a possibility of the existence of a Rayleigh-Taylor instability (5) in a somehow generalised form because : the gas is compressible, the acceleration is variable in time, the densities on both sides of the contact surface are varying with time.

Some particular cases (compressible gas with constant acceleration) have been treated (6) and prove that in general the results of Taylor should be qualitatively valid.

In fact, the A-He combination discharge (A - driver gas, He - driven gas) proves stable at lower pressure (Fig.2) but, at a higher pressure, important instabilities appear. Their evolution velocity is high as compared with the flow velocity. In the A-A discharge, the situation is the same, but the evolution velocity of the instability seems less important. In the He-A discharge, the contact surface is instable at all pressures experimented (Fig. 3); the evolution velocity of the instability seems small. The He-He discharge case seems analogous to the A-A case. The photographs compared were taken with the same time lag after the beginning of the discharge.

Fig. 2

The initial discharge form could have an influence on the development of the instabilities; it is less stable in Helium than in Argon (Fig.4). The initial form of the discharge does not seem to influence the stability of the contact surface in the He-He discharge case, but it could eventually have more influence in the He-A case.

Fig. 3

There seems to exist some discrepancy between the stability theory and the phenomena we are observing. We believe that this discrepancy may be due to a particular variation of the acceleration which characterises the electromagnetically driven shock tubes.

Fig. 4

Bibliography :

1. A. Kontrowitz (1962) Avco Everett Res. Laboratory; Res. Report 141.
2. J. Bensimon, A. Lasek, J. Laurent and B. Lesigne (1970) C.R.Acad.Sc. Paris, t.270, p.790-793.
3. M. Cloupeau (1963) Phys.of Fluids Vol. 6 No 5.
4. L. Sedov (1959) Similarity and Dimensional Methods in Mechanics. Academic Press.
5. G. Taylor (1950) Proc. Roy. Soc. (London) A201, 192.
6. M. Mitchner and R. Landshoff (1964) Phys.of Fluids Vol. 7 No 5.

On the Steady-State Current Sheet Speed in a Magnetically Driven Shock Tube

by
C. T. Chang
Danish AEC Research Establishment Risö
Roskilde, Denmark

Abstract: The discrepancy between the predicted and the measured steady-state current sheet speed is examined by taking into account of the effect of impurity, finite compressibility and finite conductivity.

Introduction. A simplified analysis based on the snow-plough model has indicated that a current sheet moving at a constant speed can be produced in a magnetically driven shock tube, when a constant voltage bank is chosen as an energy source[1]. Subsequent experiments carried out in a shock tube consisting of parallel planar electrodes showed good agreement with the prediction in the experimental range of discharge voltage and pressure used (7 to 18 kV.; 0.1 to 10 torr); after a short acceleration phase, the current sheet moved essentially at a constant speed. However, the observed speed was much lower than that predicted theoretically[2]. For examination of the discrepancy we report in the following some recent investigations concerning the possible effect of impurities, finite compressibility and finite conductivity on the steady-state current sheet speed.

Speed of the Current Sheet. According to the snow-plough model, the current sheet speed, $\hat{u}$, is at the steady state related to the driving current, $\hat{I}$, and the initial density, ρ_1, of the filling gas, expressed as

$$\hat{u} = \left(\frac{L_1}{2\rho_1 bd}\right)^{1/2}\hat{I}, \qquad (1)$$

where L_1 is the inductance per unit length of the electrodes, b is the width and d the gap of the electrodes. Fig. 1 gives a comparison with the measured value deduced from the onset time of the self-field.

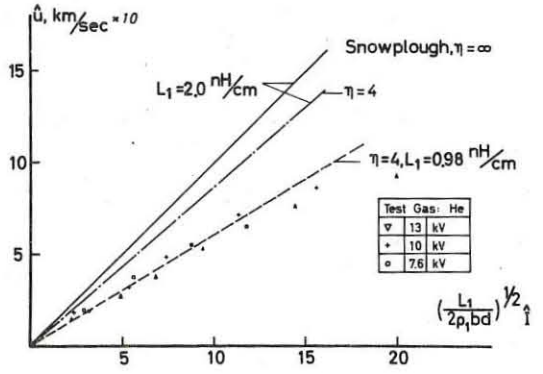

Fig. 1. Variation of the current sheet speed, $\hat{u}$, with the driving current, $\hat{I}$, and the initial gas density, ρ_1.

Impurity Effect. In a magnetically driven shock tube impurities can be introduced through cathode sputtering, hot spots, desorption, or ablation of the insulator material. Among these ablation of the insulator material is probably the most important. The introduction of insulator material into the discharge can have two effects: a) increase of the apparent density, ρ_1, of the plasma, b) formation of a standing arc near the driving end of the shock tube and thus reduction of the effective driving current[3]. Spectroscopic investigation of the plasma together with magnetic and current probe measurements taken near the insulator plate indicated that this could not be the main cause when a high-purity alumina plate (99.9% Al_2O_3) is used as insulator plate[4].

Finite Compressibility and Finite Conductivity Effect. The usual snow-plough model assumes that all the swept-up mass as well as all the delivered current are confined within a thin sheet; these assumptions in turn imply that the shock and the current sheet are indistinguishable, and the region behind the current sheet is a vaccum.

By application of the conservation laws across a strong shock it can be shown that when finite compressibility is considered, eq. (1) should be replaced by

$$\hat{u} = \left(\frac{\eta-1}{\eta}\right)\left(\frac{L_1}{2\rho_1 bd}\right)^{1/2}\hat{I}, \qquad (2)$$

where $\eta = \rho/\rho_1$ is the compression ratio, and ρ is the density of the compressed gas. For comparison, eq. (2) is also shown in fig. 1 with $\eta = 4$, corresponding to an ideal monatomic gas. Note that finite compressibility tends to lower the expected current sheet speed, but not sufficiently so to account for the experimental departure.

From fig. 1 it is seen that most of the experimental data fit reasonably well into a straight line with a slope much lower than expected. An additional possibility, besides those already examined, is that the inductance gradient, L_1, under actual running conditions might be much lower than that determined by the short-circuit method. Since a detailed account of this effect will be published soon[4], it is sufficient to state that this is possible when, instead of being confined within a thin sheet as originally assumed in the theoretical model, the current is distributed over a layer growing with time.

References:

1) C. T. Chang and O. Kofoed-Hansen, Plasma Physics 10, 137 (1968).
2) C. T. Chang, M. Popović and U. Korsbech, Proc. of the 7th Int. Shock Tube Symposium, 23-25 June, 1969, Toronto, Canada (Univ. of Toronto Press, in press).
3) J. Keck, Phys. of Fluids, Suppl. 7, S 16 (1964).
4) C. T. Chang, M. Popović and U. Korsbech, Plasma Physics (to be published).

Invited Lecture

RF-ELECTRON PLUGS AND THEIR POSSIBLE APPLICATION IN THERMONUCLEAR RESEARCH

by

E. Canobbio, O. De Barbieri, and S. Giuffré.

ASSOCIATION EURATOM - CEA
Département de la Physique du Plasma et de la Fusion Contrôlée
Service I.6n Centre d'Etudes Nucléaire
Cedex 85, 38 Grenoble Gare (France)

Abstract : The feasibility of increasing plasma lifetime in mirror machines by using resonant RF-electron plugs is examined (for comparison the case of RF-ion plugs is also briefly considered). An investigation into the basic physical mechanisms involved shows that a net thermonuclear power yield would require efficient plugging of 100-150 KeV electrons over several hundred electron mean deflection times.

In a steady state mirror machine, in which losses are balanced by injection, a negative ambipolar potential eV_o develops in the absence of cold plasma, if the electron plugging is efficient enough. Thus an ion distribution which is isotropic up to the energy $|eV_o|$ can be confined inside a two sheet hyperboloid which replaces the ion loss cone in velocity space for this case. If $|eV_o|$ is larger than kT_i the ion lifetime τ_i is the Spitzer energy relaxation time τ_s (at the temperature T_i) multiplied by the factor $(2/3)\exp\{|eV_o|/kT_i\}$ /1/ which is only implicitly dependent on the mirror ratio R and is also much larger than $\log_{10}R$. The electron lifetime τ_e is the same as the ion lifetime because of charge neutrality and eV_o is therefore determined by the equation

$$\tau_i(T_i, n, V_o) = \tau_e(T_e, n, V_o, \mathcal{E}_{RF}) \qquad (1)$$

In the absence of the plugs, the condition $eV_o < 0$ implies very high temperatures : $T_e > (m_i/m_e)^{1/3} T_i$. RF-electron plugs basically should result in $\tau_e = m\tau_s$ with $m \gg 1$ without overly increasing T_e during such a long time /2/.

On the basis of numerical single particle calculations, it can be shown that an electron suffering random small angle elastic deviations can be reflected by plugs situated in the two mirror regions before it crosses the exact gyroresonance surface $\omega = \omega_{ce}(\vec{r})$. In this case, efficient confinement of a steady state anisotropic $(T_\perp / T_\parallel > 1)$ electron distribution can be achieved in a mirror trap without appreciable heating. However, over time intervals larger than $\tau_s \ln\Lambda \equiv \tau_{\pi/2}$, large angle collisions shoot the electron through the gyroresonance well inside the loss cone . Then, in order to mantain particle confinement, the increase of perpendicular energy on a single crossing of the resonance, $\Delta E_\perp$ must be such that

$$|eV_o| + E_\parallel < (\bar{R}-1)\Delta E_\perp \equiv eV^* \qquad (2)$$

where $\bar{R}$ is the ratio between the maximum and the gyroresonance B value. Inside the trap, the kinetic energy is assumed to be $E_\parallel$ only. If the $\vec{B}$ profile at the resonance is smooth enough, $\Delta E_\perp$ can be taken to be as large as the relativistic limit $m_e c^2 (\mathcal{E}_{RF}/B)^{2/3}$ which is independent of particle energy /2/. The energy of a particle which crosses the gyroresonance in a mirror trap (several times) increases rapidly until a value of the order of a few times the relativistic limit is reached. A subsequent increase of energy is then usually observed only in the presence of collisions. This latter effect is, however, an extremly slow stochastic process resulting in a very moderate temperature increase unless the confinement time becomes too large. Assuming that $e(V^* - |V_o|)$ can really be made much larger than kT_e, the electron lifetime is roughly $\tau_{\pi/2} \simeq \frac{2}{3}\exp\{e(V^* - |V_o|)/kT_e\}$. Fig. 1 shows eV_o/kT_i (dashed lines) and $m\ln\Lambda = \frac{2}{3}\exp\{e(V^* - |V_o|)/kT_e\}$ (solid lines) versus T_e as given by the solution of Eq. 1 for two different values of both T_e/T_i and for $eV^* = 9 \cdot 10^3 g^{2/3}$ KeV , with $\bar{R} = 10$. In order to have $eV_o > kT_i$, large values of R (≈ 10) are required which in turn, imply $m\ln\Lambda \gtrsim 10^2 \div 10^3$. Space dependence has been neglected by supposing a uniform confinement region much longer than the mirror regions. Moreover, both the electron and ion distributions have been taken as isotropic. A few complementary results for a more elaborate model are given in Fig. 2, with $R(z) = 1 + g\sin^2(\frac{\pi}{2}z)$, $V^*(z) = z \cdot V^*$, $0 \le z \le 1$. The quantity $\alpha(z) = T_{e\perp}(z)/2T_{e\parallel}(z) - 1$ (solid lines) is plotted as a function of z for some values of $\alpha(z)$ at $z = 0$, assuming charge neutrality. The other set of curves represent $\frac{1}{n(0)}\int_0^z dz' n(z')$ for the same $\alpha(0)$ values. Curves 1 correspond to an electron isotropic Maxwellian distribution.

Now, if we consider a possible D-T reactor, positive power yield requires

$$\eta\left(P_{DT} + \tfrac{3}{2}nk(T_e+T_i)/m\tau_s\right) > \tfrac{3}{2}nk(T_e+T_i)/m\tau_s + P_B + P_S \qquad (3)$$

Here η (≈ 0.25) is the efficiency of conversion from thermal to plasma particle power. P_{DT} is the thermonuclear power density release. We have assumed no α particle heating. Also, $T_e > T_i$ since the e-i equipartition time is longer than $m\tau_s$ if $m\ln\Lambda \lesssim 3 \cdot 10^3$. P_B is the e-e and e-i Bremsstrahlung loss which is relativistically correct up to first order /3/. P_S is the Synchrotron loss taking self-absorption and wall reflection ($R_W = 0.9$) into account. The Black-Body portion of the Synchrotron emission W^- is reduced by the factor $1 - R_W$ and can be less than the "transparent" portion, W^+, (relatively unaffected by the wall) at high T_e and large plasma thickness, L /4/. The relative importance of $\eta(1-\eta)^{-1}P_{DT}$, P_B, and P_S is shown in Fig.3 for a typical case. Condition (3) can be transformed to find the critical m value as a function of T_e, with B, β , T_e/T_i, and L as parameters. This m value is plotted in Fig.4 for B = 50 (dashed lines) and 100 KG (solid lines), L = 100 cm, β = 0.5 and 1, and T_e/T_i = 2 and 5. The corresponding values of $|eV_o|/kT_i$ are plotted in Fig. 5. It is seen that $|eV_o|$ is large enough to make the truncation of the ion distribution above that energy irrelevant with respect to the evaluation of P_{DT}. It appears that in order to have $m\ln\Lambda$ less than a few 1000's in the useful T_e interval (50-150 KeV) the β factor has to be close to 1. At such β values stability of a plasma with isotropic ions ($\omega_{pi} \gg \omega_{ci}$) and anisotropic electrons ($\omega_{pe} \lesssim O(\omega_{ce})$) in the presence of imbalance between n_e and n_i (not enough to have diocrotron instability /5/), shear flow and finite Larmor radii effects /6/, is still an open question.

In conclusion, remembering that the plug efficiency depends critically upon $\Delta E_\perp / E_\parallel$ (Eq.2) which is a decreasing function of m, we infer that the reactor requirements are difficult to achieve. This adds a supplementary physical difficulty to the well known technological handicaps of this approach. Most of these difficulties do not appear when the case of the resonant RF-ion plugs is considered since, in principle, m values of less than a few tens would be sufficient in this case /7/. However, an overly high temperature increase is unfortunately still possible at such m's because of the ineffectiveness of the relativistic energy limitation in the case of the ions.

References :

/1/ W.M. MacDonald, M.N. Rosenbluth, and W. Chuck, Phys. Rev. 107, 350(1957)
/2/ T. Consoli, Plasma Phys. and Controlled Fusion, Vienna 1969, Vol. II.
/3/ J.B. McBride, and A. Pytte, Phys. Fluids, 12, 1130 (1969).
/4/ E. Canobbio, and S. Giuffré, Nuclear Fusion, 10 , N°2 (1970).
/5/ R.H. Levy, J.D. Daugherty, and O. Buneman, Phys. Fluids 12, 2616 (1969).
/6/ A. Simon, and M.N. Rosenbluth, Phys. Fluids, 8, 1300 (1965).
/7/ L.G. Kuo-Petravic, et al., Fusion Reactor Conf., Culham 1969, paper 2-4.

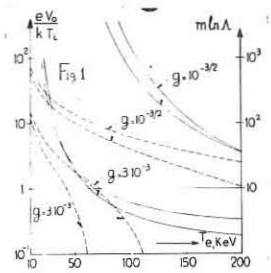

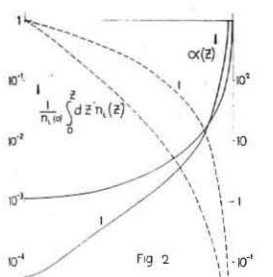

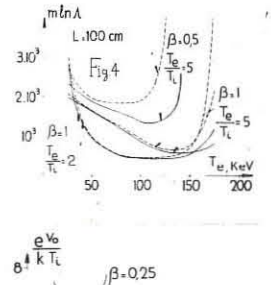

In Fig. 3 :
β = .5, T_e/T_i = 5, B = 100 KG.

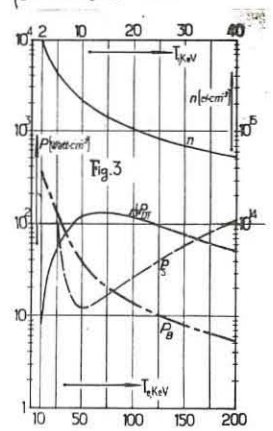

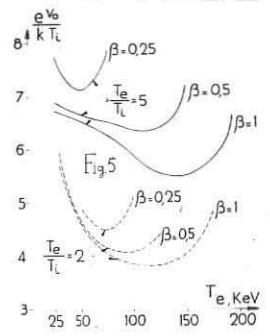

RECENT RESULTS FROM THE PLEIADE MIRROR DEVICE

by

R. GELLER - B. JACQUOT - C. JACQUOT -

ASSOCIATION EURATOM-CEA
Département de la Physique du Plasma et de la Fusion Contrôlée
Service I.Gn. Centre d'Etudes Nucléaire
Cedex 85. 38 Grenoble Gare (France)

Abstract : In this experiment energetic electrons ($W_i^- \gg W_i^+$) are trapped in a magnetic mirror and energetic ions ($W_a^+ \gg W_a^-$) are confined by electrostatic potentials. The energetic particles have lifetimes of several milliseconds with $n k T_\perp \geq 10^{13}$ eV cm^{-3} and $W_\perp^- \simeq W_a^+ \simeq 1$ KeV

Description : On the left side of the device (fig. 1) the preionization is created in a capillary tube (Ø = 8 mm p = 10^{-3} torr) by the RF leakage field of a cavity. The energetic electrons are generated at the resonance $\omega_c^- = \omega_{RF}$ obtained with a continuous standing wave (2500 MHz, P_{RF} = 500 W) inside the RF cavity (working pressure $\sim 10^{-5}$ torr) located in the steady state gradient of a magnetic mirror. As a result of this gradient, the spiraling electrons are driven towards the decreasing magnetic field, and hydrogen ions are accelerated in the same direction by an ambipolar space charge field + E along the axis. The electron energy $W_\perp^- \sim W_a^+ \sim W$ is given by :

$$W = mc^2/2\,(1-\delta z)^{-2/3} - 1 \; ; \quad \delta = 1/8\,(\Delta B/\Delta z)\,c/\omega \; ; \quad g = eE_{RF}/m\omega$$

The ion energy W_a^+ equals a potential ϕ which is roughly determined by

$$(\omega P_{RF})^{1/2} \; ; \; Q(G_0 n_0 - Q)^2 = P_{RF}^2/n_e^2 \; ;$$

where G_0 and Q represent the unloaded cavity Q's, n_e being the density of preionized cold plasma. In the present case $W_\perp^- \sim W_a^+ \sim 1$ KeV is expected.

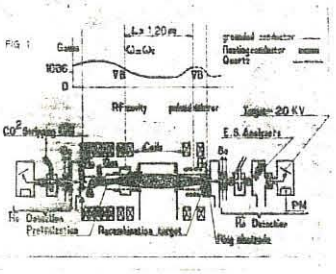

FIG 1

On the right side of the device a pulsed magnetic field is established by a 50 kA rectified current. This mirror reflects the energetic electrons ($W_\perp^-/W_a^+ \gg 1$) and their reflection creates a symmetrical space field -E for the ions which in turn are also reflected. In this manner, during the existence of the mirror, spiraling electrons and axially accelerated ions are reflected and accumulated inside the magnetic bottle. /1/.

The ultimate vacuum pressure inside the magnetic bottle is 10^{-9} torr and the available working pressure $p \geq 10^{-8}$ torr. This performance is obtained by a continuous pumping of $\sim$ 70000 l/s at $p \simeq 10^{-6}$ torr due to the addition of a turbomolecular pump (10000 l/s) and 2 liquid nitrogen cooled titanium evaporation pumps (40000 l/s) /2/.

Diagnostics : A calibrated diamagnetic loop, resonant frequency shift of a microwave cavity and X rays provide information on hot electron energy and density. The presence of a cold plasma in the bottle has to be avoided, and therefore the monitoring of the H_β line was necessary to determine the presence of cold plasma. Pyrometric and RF probes measure the energy flux and RF noise in the plasma. Floating probes measure the electro static potential build up in the mirror region. Measurements of energetic H^+ ions : Due to charge exchange on the residual gas, fast neutrals are created in the bottle. These leaking particles are reionized in stripping cells on both sides ($\overleftarrow{Ho}$,$\overrightarrow{Ho}$) of the magnetic bottle. After passing through an E.S. analyzer they provide informations on ion energy W_a^+, and consequently on the ion transit time $T = L/v_a^+$ between the mirrors. The rise time of the stripped H^0 signal during the mirror pulse is assumed to be the ion life time in the bottle $\langle \tau^+ \rangle$. The ratio of the saturation flux of H^0 during the time the mirror is on with respect to the flux obtained before the mirror is established, gives the ion accumulation ratio A. By multiplying (A T) we obtain an other check of $\langle \tau^+ \rangle$.

Effects of the recombination target and floating walls on the plasma stability.

We have already pointed out that the E.S. potentials measured in the reflecting region which have the same order of magnitude as the particle energies ($W \sim \phi \sim 1$KeV) are related to the stable reflection regime. The establishment of these potentials should not be hindered by the following wall effects :

1) Because of wall backdiffusion of leaking particles on the wall behind the mirror a large amount of these particles (loss-cone diffusion and cold plasma) are backdiffused into the magnetic bottle where they form an undesirable plasma component. A significant improvement with stable acceleration and accumulation behavior is observed when these leaking particles are deflected from the axis towards a titanium target where they are absorbed or recombined.

2) Forced wall potentials : In the mirror region when the accumulation regime is stable, potentials are developed with respect to ground (+ V). When a floating ring electrode is introduced in the vicinity of the mirror region, collision limited electron and ion accumulation is obtained, and E.S. potentials are present. In this case, r.f. probes detect only very low frequency noise. If the reflecting region is close to a grounded wall, or whenever the ring electrode is connected to ground, the E.S. potentials are destroyed, the ion accumulation is perturbed and a wide noise spectrum is detected where a strong peak at ω_c^+ is observed. The reason for the suppression of the instabilities by the floating walls is not clear as yet. One might assume that when a conducting wall in the vicinity of those E.S. potentials, is forced to ground potential, a short circuit of the potential is possible. It can be triggered by a low density cold plasma existing in this area or by the leaking particles. It could represent a strong perturbation mechanism (arcs, undesirable E fields, currents and noise emission) the effect of which may strongly influence the plasma behaviour inside the magnetic bottle, and generate all kind of instabilities /1/. One might also imagine that due to the onset of an instability, particles of one polarity are suddenly chased towards the floating wall, they electrically charge the wall and this potential creates an opposing field stopping the leakage of the particles. We have also suggested that the floating walls might suppress the external completion of a positive feedback circuit /4/.

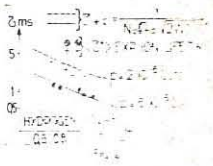

Recent experimental results : Accumulations ratios of A $\sim 10^3$ are obtained in the range of 10^{-6} torr working pressure. They are determined by measuring the leaking fast neutrals on the axis with a digital counting system. /5/ By keeping the plasma injection flux and energy constant, we could check the dependance of the energetic ion life-time $\langle \tau^+ \rangle$ and the accumulation ratio A with neutral pressure p in the magnetic bottle. It was shown that both vary as expected like 1/p. The results show also that stable accumulation is possible during the entire mirror pulse (7 milliseconds) and that charge exchange is the limiting loss mechanism for the energetic ions. /6/ The life-times of several milliseconds with energetic particle densities $n \geq 10^{10}$ are availables.

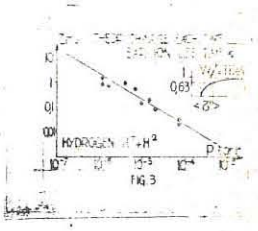

In figures 2 and 3, the absolute experimental ion life times are compared to the the theorical charge exchange collision-time for different ion energies and various neutral pressure. The agreement looks very good. The measured diamagnetism in the $10^{10} < n k T_\perp < 8 \cdot 10^{13}$ eV cm^{-3} ..In the stable accumulation regime, the rise time of the diamagnetism is similar to the fast neutral rise-time, indicating that the energetic electrons and ions are accumulated at the same rate in the magnetic bottle.

REFERENCES

/1/ 2ème Coll. Interm. Interact. Ch. Gas. Plasmas SACLAY Vol.2 P. 643-69 (1969)
/2/ R. GELLER Bull. Inform. Sci. Techn. CEA N° 142 p.29 (1969)
/3/ R. GELLER - B. JACQUOT - C. JACQUOT - 9th Int. Conf. Phenomena in Ion. Gases BUCHAREST p. 509 1969)
/4/ R. GELLER Phys. Letters 31 A 8, (1970)
/5/ R. GELLER - B. JACQUOT - C. JACQUOT C.R. Ac. Sc. Paris 269 p. 697 (1969).
/6/ R. GELLER - B. JACQUOT - C. JACQUOT Phys. Letters 30 A,2 p.80 (1969)

AMBIPOLAR POTENTIAL EFFECTS ON COULOMB SCATTERING INTO THE LOSS CONE

by

M. Brambilla and F. Werkoff

ASSOCIATION EURATOM - CEA
Département de la Physique du Plasma et de la Fusion Contrôlée
Service I.Gn. Centre d'Etudes Nucléaire
Cedex 85. 38 Grenoble Gare (France)

Abstract : The Fokker-Planck equation describing Coulomb scattering into the loss cone in the presence of an ambipolar potential has been written in a velocity coordinate system in which the loss hyperboloid is a coordinate surface..The equation is numerically solved for the case of ion-ion collision.

A large body of literature has been devoted to the collisional losses from open-ended magnetic traps /1/. BenDaniel and Allis /3/ considered only losses from ion-ion collisions, and simplified the Fokker-Planck equation by assuming the isotropy of the diffusion coefficients (Rosenbluth potentials /4/) and searching for a separate variable solution $f(v,t) = U(v,t)\Phi(\mu)$, where $\mu = v_{//}/v$. Φ was shown to relax in a time much shorter than Spitzer time to the most isotropic eigensolution of Legendre's equation

$$\frac{\partial}{\partial\mu}\left[(1-\mu^2)\frac{\partial P_j}{\partial\mu}\right] + \lambda_j P_j = 0 \qquad (1)$$

satisfying $P_j(\mu) = 0$ on the loss cone boundary $\mu = \mu_c = \sqrt{1-1/R}$, where R is the mirror ratio. The role of the ambipolar potential and collisions involving electrons was first investigated by Fowler and Rankin /4/. They maintained the separability assumption but allowed the eigenvalue λ in Eq. (1) to depend on the particle energy to take into account that the loss region for the ions in velocity space becomes a one-sheet hyperboloid in the presence of a potential well /5/. Fowler and Rankin model is remarkably simple, while its assuptions are made plausible by the previous single-species investigations. Since however these calculations are critical for the future of open-ended traps as thermonuclear reactors /2/, a mathematically more rigorous approach seems of some interest. We limit ourselves here to ion-ion collisions only. As a first step to solve the problem in the presence of the potential V_0 , we transform the independent variables from (v,μ) to ($u = \sqrt{v^2+\alpha^2}$, $\xi = \mu v/\sqrt{v^2+\alpha^2}$) where $\alpha^2 = eV_0/2m_i(R-1)$. In the new coordinates, the loss hyperboloid coincides with the coordinat line $\xi = \mu_c$. On the other hand, the transformed F.P. equation is no longer diagonal in the eigenfunctions of the Legendre equation, P_{m_j} Thus, if a development of the form $f(u,\xi) = \sum_j U_j(u,t) P_j(\xi)$ is used, coupling between the different modes "j arises". This coupling is clearly handled much more easily in this way than by trying to satisfy a "non-diagonal" boundary condition in the original variables.

The partial distribution U_j satisfy the following system of equations :

$$\begin{aligned}
\frac{N_j}{\Gamma}\frac{\partial U_j}{\partial t} &= 4\pi\sum_i\sum_k \gamma_{ikj}\, U_i U_k - \frac{1}{2u^3}\frac{\partial g}{\partial u} m_j(m_j+1) N_j U_j + \\
&+\frac{\alpha^2}{2u^2}\left[-\frac{3u^2+\alpha^2}{u^4}\frac{\partial^2 g}{\partial u^2} + \frac{2u^2+\alpha^2}{u^5}\frac{\partial g}{\partial u}\right] N_j U_j + \frac{1}{2u^2}\left[\frac{\alpha^2(u^2+\alpha^2)}{u^3}\frac{\partial^2 g}{\partial u^2} + \frac{2u^4-\alpha^4}{u^4}\frac{\partial g}{\partial u}\right] N_j\frac{\partial U_j}{\partial u} \\
&+\frac{\alpha^2}{2u^2}\left[\frac{(u^2+\alpha^2)^2}{u^2}\frac{\partial^2 g}{\partial u^2} - \frac{\alpha^2(u^2+\alpha^2)}{u^3}\frac{\partial g}{\partial u}\right] N_j\frac{\partial^2 U_j}{\partial u^2} + \\
&+\frac{\alpha^2}{2u^2}\left[\frac{3u^2-\alpha^2}{u^4}\frac{\partial^2 g}{\partial u^2} - \frac{4u^2-\alpha^2}{u^5}\frac{\partial g}{\partial u}\right]\sum_i X_{ji} U_i + \\
&+\frac{\alpha^2}{u^2}\left[-\frac{u^2+\alpha^2}{u^3}\frac{\partial^2 g}{\partial u^2} + \frac{\alpha^2}{u^2}\frac{\partial g}{\partial u}\right]\sum X_{ji}\frac{\partial U_i}{\partial u} \\
&+\frac{\alpha^2}{2u^2}\left[\frac{\alpha^2}{u^4}\frac{\partial^2 g}{\partial u^2} + \frac{u^2-\alpha^2}{u^5}\frac{\partial g}{\partial u}\right]\sum Y_{ji} U_i + \frac{N_j}{\Gamma} S_j(u)
\end{aligned} \qquad (2)$$

Here g (u) is the Rosenbluth potential as defined in /3/ Eq. (59), in which the isotropic part of the distribution function, $U_0 = C\, u\, \Sigma_j I_j U_j/\sqrt{u^2+\alpha^2}$ must be used (C is a normalisation coefficient such that $4\pi\int U_0(u)\, u^2\, du = n$, the density). m_j (m_j+1) is the J-th eigenvalue of Eq. (1), and

$$N_j = \int_0^{\mu_c} P_{m_j}^2(\xi)\, d\xi \qquad I_j = \int_0^{\mu_c} P_{m_j}(\xi)\, d\xi \qquad X_{ji} = \int_0^{\mu_c} P_{m_j}\frac{\partial}{\partial\xi}(\xi P_{m_i})\, d\xi$$
$$Y_{ji} = \int_0^{\mu_c} P_{m_j}\frac{\partial^2}{\partial\xi^2}(\xi^2 P_{m_i})\, d\xi \qquad \gamma_{ijk} = \int_0^{\mu_c} P_i P_j P_k\, d\xi \qquad (3)$$

This system, truncated at the 5-th term, was solved numerically by a well-known implicit unconditionally stable scheme /6/. The results are shown in Fig. 1 to 3. Fig. 1 shows the evolution of the density n and of the mean energy E for various values of α^2. and for R = 10.2[illegible]. The source was very peaked in v with a mean energy E_S of 100 Kev. This choice allows comparison with the results of Bing and Roberts /7/ in the case when $\alpha^2 = 0$. The accumulated density was found to agree to within a few percent with the "unseparated" case of Ref. /7/ for injected currents ranging from 10^8 to 10^{16} particles/cm³sec. All the results presented here are for $J = 10^{16}$. Time is measured in units of $\tau_0 = 10^5 A^{1/4} E_S^{3/4}/J^{1/2}$ (A = 2 for deuterium, $\tau_0 = 3{,}76\cdot10^{-2}$ sec for the parameters chosen here).

It is seen from Fig. 1 that n lowers and E increases when α^2 increases. The presence of the repulsive potential enhances the losses of the greater part of the ion population; on the other hand the life time increases with the energy. The curve marked F.R. was obtained by solving an equation equivalent to that of Fowler and Rankin for the ions only, with $\alpha^2 = 0$. We found that the discrepancy is due to inaccuracy in the representation of the f^2 term (the first in Eq. (2)) rather than in the representation of the loss term (the second of Eq. (2)).

Fig. 2 represents the velocity distribution at various times for $\alpha^2 = 0$ and $\alpha^2 = 0.2$. Fig. 3 shows the asymptotic angular dependence of the distribution function. When $\alpha^2 = 0$, the angular distribution is almost independent of v, and quite close to the most isotropic Legendre eigenfunction, as expected. The same is true when $v^2 \gg \alpha^2$ in the general case; however, for $v^2 \lesssim \alpha^2$ the distribution is much less isotropic.

Definite conclusions cannot be reached until the collisions with the electrons will be taken into account. Indeed, the relatively weak dependence of our results on α^2 (note that for a mirror ratio of 10 values of α^2 in excess of 0.2 are hardly conceivable) proves that the effects of collisions with the electrons is much more important than the enlargement of the loss region due to the potential. This gives indirect support to the model of Fowler and Rankin.

As our next step we will, of course, introduce the electrons, and evaluate the potential in a self-consistent way. Note that the terms of the F.P. equation which contain the angular derivatives of Rosenbluth potentials can also be treated as "coupling" terms. This would afford a means of verifying the "isotropy" approximation introduced by BenDaniel and Allis without facing the difficult problem of solving the F.P. equation in two dimensions, as was done recently by Marx and Killeen /8/.

/1/ Rosenbluth M.N., McDonald W.M., Judd D.L., Phys. Rev. 107,1,1957.
/2/ For a more complete bibliography see Kuo Petravic , L.G. Petravic M., Watson C.J.H., Nuclear Fusion Reactor Conf., Culham 1969,paper 2-4.
/3/ BenDaniel D.J., Allis W.P., Plasma Physics 4,31,1962.
/4/ Fowler T.K., Rankin M., Plasma Physics 4,311,1962.
/5/ BenDaniel D.J., Plasma Physics 3,235,1961.
/6/ Ritchmeyer R.D., Morton K.W., Difference Methods for Initial-Value Problems, Interscience 1967.
/7/ Bing G.F., Roberts J.E., Phys. Fluids 4,1039,1961.
/8/ Killeen J., Marx K.D., Methods in Computational Physics, 1969,Ch. 9.

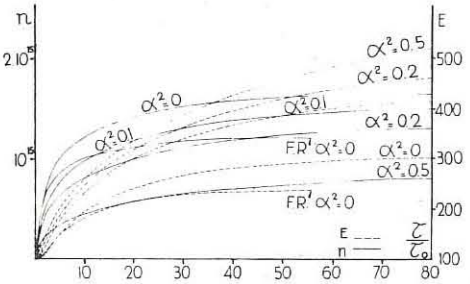

FIGURE 1

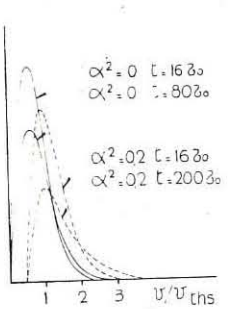

FIGURE 2

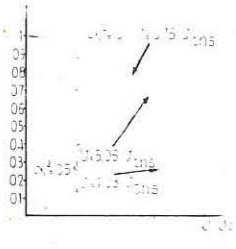

FIGURE 3

QUASIPERIODICITY PROPERTIES OF PARTICLE MOTION IN RF SUPPLEMENTED TRAPS

by

C. Ichtchenko

ASSOCIATION EURATOM - CEA
Département de la Physique du Plasma et de la Fusion Contrôlée
Service I.6n Centre d'Etudes Nucléaire
Cedex 85, 38 Grenoble Gare (France)

Abstract : Plasma confinement in a RF supplemented magnetic trap is studied in the single particle approximation. The condition for quasi-resonant and for exact resonant interaction are determined. The mean energy exchange between particles and field is computed as a function of the initial velocity. The influence of elastic collisions on particle confinement is studied by introducing random deflections of the velocity vector.

A particle injected into the symmetry plane of a RF supplemented magnetic bottle, is reflected -even if it is initially inside the "loss-cone"- provided its parallel velocity V_z is sufficiently small. Let V_z/c be the normalised initial velocity and α , a normalised perpendicular velocity :

$$\alpha = (V_x + iV_y)/(c\sqrt{b}\sqrt{1-\beta^2}) \qquad |\alpha|^2$$

is the usual relativistic invariant (In the absence of the HF field, i.e., the magnetic moment). In the above expression, $b = \frac{\omega_c}{\omega}$ is the static magnetic field normalised to its resonance value and β is the total speed divided by c. Then, in a confinement diagram (Fig. 1), a limiting zone may be defined between the initial representative points of particles that are reflected before and after a given value of the confining magnetic field /1/. The finite thickness of this zone is due to the fact that the reflection point depends upon the azimuthal direction of the initial velocity. As already pointed out in '1' and '2', a particle reflected before crossing the resonance plane undergoes no net change in energy. This is true as long as the representative point is located on the left of a curve parallel to the "loss-curve" which corresponds to reflection at the resonance plane. The point V_0^2/c^2 where this curve crosses the $|\alpha|^2 = 0$ axis can be obtained by considering the relativistic equation for the transverse motion in the following integrated form /3/:

$$\alpha = \alpha_0 + \int_0^t (g/\sqrt{b}) \exp(i\varphi(t))\, dt \qquad (1)$$

where $g = E/B$ characterises the RF space-independent electric field at frequency ω .

and $$\varphi(t) = \int_0^t (\omega - \omega_c(t))\, dt \qquad (2)$$

$$\frac{d^2 z}{dt^2} = \frac{1}{2} |\alpha|^2 c^2 \frac{db}{dz} \sqrt{1-\beta^2} \qquad (3)$$

determines the axial motion. In the non relativistic limit, V_0 can be found such that $V_0^5/c^5 = g^4/\frac{c}{\omega}\frac{db}{dz}$ which is in good agreement with the numerical results. Consider now the reflection of an electron with a given initial normalized magnetic moment $|\alpha_0|^2$ as a function of its initial phase in the azimuthal plane. Integrating the equations (1) to (3) numerically by a Runge-Kutta method, we obtain as a result, the representative points of the particles after they have come back to the symmetry plane (fig. 2 and 4). These points are distributed around a parallel to the loss line which passes through the representative point of the initial conditions (indicated by arrays). The dispersion is maximum when the initial point is close to the b = 1 "loss-line".

Figure 6 shows the representative point of an electron in a mirror trap at each crossing of the symmetry plane. The motion is followed for a few hundred back and forth oscillations. The large dispersion in $|\alpha|^2$ observed is mainly due to the beats between the RF field and the cyclotron motion. These beats are particularly large when the speed approaches the relativistic limit c. A function which describes the "distribution" of $|\alpha|^2$, that is, the number of occurences of $|\alpha|^2$ which appears in an interval $\Delta|\alpha|^2$ centered about $|\alpha|^2$ may be plotted as shown in fig. 7. As a result of the quasiperiodicity of the motion /4/, this distribution tends to an equilibrium function when the confinement time is long enough.

Obviously, this property disappears in the presence of a "randomizing" effect like collisions or turbulence. In order to simulate the effect of elastic collisions, we introduce a random variation in both the "pitch" and the azimuthal "phase" angle, when the particle crosses the symmetry plane. More precisely, we write : $\Delta\Pi = \varepsilon\, Q_{max} \sin A_\varphi$ where A_φ is a random value choosen by the computer in the interval $[-1, +1]$, $\Delta\Pi$ is the variation of the pitch angle, and ε is an amplitude factor for the deflection. The variation of the azimuthal phase angle is treated in the same way. The results show, for low ε values, a diffusion of the representative points outside the loss cone (fig. 8) associated with a widening of the distribution function (fig. 9). When the deflection approaches 90°, one observes simultaneously a reduction of the distribution width (fig. 11) and a penetration of the representative points well inside the loss cone (fig.10). The latter effect leads to particle losses if an upper limit is assigned to the static magnetic field strength..

References :

/1/ F. Brami, T. Consoli et G. Ichtchenko, Rapport C.E.A. R 3115, (1967)

/2/ C.J.H. Watson and L.G. Kuo-Petravic. Physical Rev. Lett. 20 1231 (1968)

/3/ E. Canobbio. Nuclear Fusion, 9 , 27, (1969)

/4/ E. Canobbio and G. Ichtchenko. Phenomena in Ionised Gases. Bucharest (1969) p. 384.

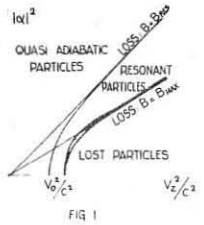

FIG 1

For all the figures :
$g = 10^{-3}$
$\frac{c}{\omega}\frac{db}{dz} = .02$
$B_0 = .8$

$|\alpha|^2$ as a function of the initial phase angle (Polar representations)

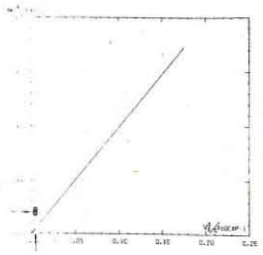

$|\alpha|^2 = 10^{-2}$
$V_z^2/c^2 = 4\ 10^{-4}$

Fig. 2

Fig. 3

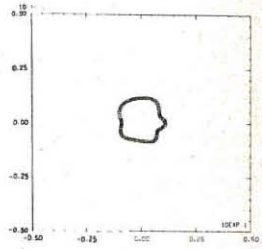

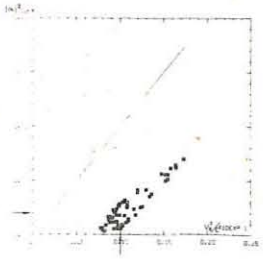

$|\alpha_0|^2 = 10^{-2}$
$V_z^2/c^2 = 10^{-2}$

Fig. 4

Fig. 5

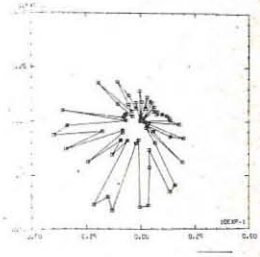

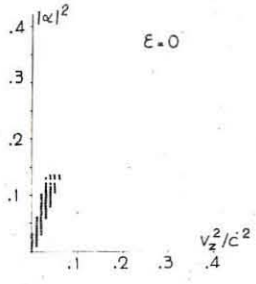

Fig. 6

Fig. 7

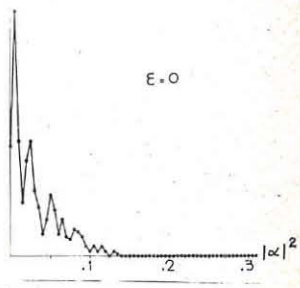

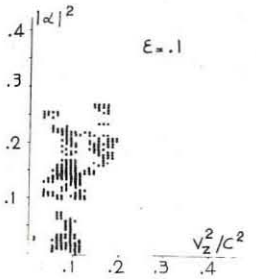

Fig. 8

Fig. 9

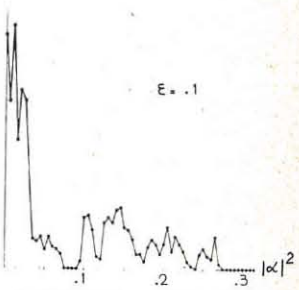

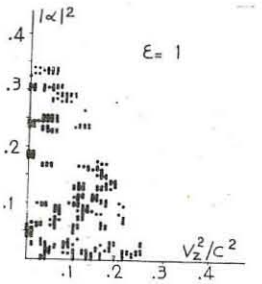

Fig. 10

Fig. 11

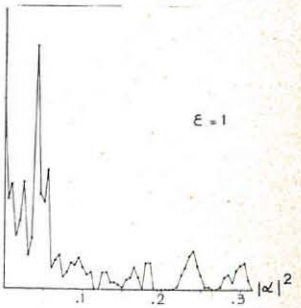

SIMULATION OF RADIOFREQUENCY HEATING AND CONFINEMENT OF A PLASMA (COMPUTER - FILM)

by

J. L. SHOHET*

ASSOCIATION EURATOM - CEA
Département de la Physique du Plasma et de la Fusion Contrôlée
Service I.Gn. Centre d'Etudes Nucléaire
Cedex 85. 38 Grenoble Gare (France)

Abstract : A computer model of a plasma has been used to demonstrate electron cyclotron heating and confinement by means of electromagnetic waves. The basic problem is to solve Poisson's equation for the self-consistent electric field and then add in the external r.f. field. The particles making up the plasma are then moved by solving their equations of motion simultaneously by means of a finite difference scheme. Heating and confinement can be shown effectively.

Experimental research has shown that effective heating of a plasma is possible by means of electron cyclotron resonance. When the r.f. heating field is oriented perpendicularly to a uniform d.c. magnetic field, highly anisotropic plasmas are produced. Theory to explain the heating mechanism is largely based on three assumptions. They are (1) at any instant of time, it is equally likely for a particle to be decelerated as it is to be accelerated, (2) since a net heating occurs, some sort of collisional process must "throw" the electrons into the proper phase to produce a net heating effect, and (3) after heating, a non-Maxwellian velocity distribution, which usually has a collection of "hot" and "cold" particles, is often the result.

It is the purpose of this paper to show that a computer simulation of a plasma in the resonance (heating) plane will satisfy the above three assumptions. In addition, the same model, in the absence of a d.c. magnetic field, can be used to demonstrate the r.f. confinement of a plasma.

The basic problem which is solved is to follow the motion of a large collection of "super-particles" in a 2-dimensional rectangular region. A super-particle is essentially a cloud or group of real particles, and has the same charge-to-mass ratio as that of a real particle. The present work uses both "super-ions" and "super-electrons".

The rectangular region may be immersed in a d.c. magnetic field. The external a.c. electric field used for either heating or confinement may be made uniform or into a section of the TE_{111} mode of a rectangular microwave cavity.

The solution is obtained by initially placing all the particules where desired in the region. From their initial positions, Poisson's equation may be solved[1] to obtain the self-consistent electric field of the particles. The initial velocities of the super-particles are given a Maxwellian distribution, corresponding to a given initial temperature, which was typically about 10 EV.

Each super particle was assumed to obey the following finite difference equation, which includes a relativistic mass correction. In components, the equations of motion are:

$$V_{j+1,x} = \frac{\beta\delta + \gamma}{1+\beta^2} \qquad \text{and} \qquad V_{j+1,y} = \frac{-\beta\gamma + \delta}{1+\beta^2}$$

where

$$\beta = \frac{q}{m_o}\frac{\Delta t}{2} B_o \alpha \qquad \alpha = \left(1 - \frac{V_{j,x}^2 + V_{j,y}^2}{c^2}\right)^{1/2}$$

$$\gamma = V_{j,x} + \frac{q}{m_o}\Delta t \alpha E_{j,x} + \beta V_{j,y} \qquad \delta = V_{j,y} + \frac{q}{m_o}\Delta t \alpha E_{j,y} - \beta V_{j,x}$$

m_o is the rest mass, B_o is the d.c. magnetic field, Δt is the time step, and q is the charge. $V_{j,x}$ and $V_{j,y}$ are the components of velocity in the x and y directions at the time t. The subscript j+1 refers to the vqlues of quantities Δt units of time later. The electric field in the above expressions, $E_{j,x}$ and $E_{j,y}$ is the sum of the self-consistent field plus the external r.f. field. Once the new velocities are determined, the change in position may be easily computed to produce the changes in position of the particles, by using the average of the old and new velocities. After each calculation, the new average values of kinetic and potential energy of the particles is computed, and the velocity distribution itself may be examined in detail to observe changes. In addition, the positions of the super-particles were recorded on motion-picture film after each time step.

The specific problem consisted of a collection of 900 super-ions and 900 super-electrons of equal and opposite charge. The d.c. magnetic field was 3000 gauss and the r.f. field amplitude was 100,000 volts per meter. By varying the number of real particules per super-particule, the plasma frequency could be changed. Results of the case when $\frac{\omega_{pe}}{\omega_{ce}} \approx .01$ are shown in Figure 1.

Computations were made up to 11 cyclotron periods. The total kinetic energy of the electrons increases with time, as long as heating was applied, and becomes asymptotic to a heating rate of 1.75×10^9 per second. The ions do not increase in energy, and, when the heating is removed, the electron kinetic energy remains constant. This can be seen from Figure 1 for heating turn-off at two different times. Figure 2 shows the velocity distribution of the electrons before, during, and after heating. Each set of points corresponds to a different time of observation. The solid lines are Maxwellians whose temperatures are fixed by the relation $1/2\ m \langle v^2 \rangle = kT$, where $\langle v^2 \rangle$ is the average value of the square of the velocity at the time the distribution was plotted. A close fit to a Maxwellian is seen for all three cases. It must be noted that the self-consistent field is necessary for this result, otherwise the velocity distribution rapidly becomes non-Maxwellian, with a drift velocity. Heating of this type occurred in both the uniform and TE_{111} field configurations, as long as the collisional effects are included.

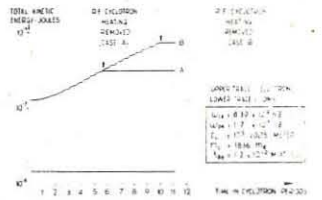

Figure 1

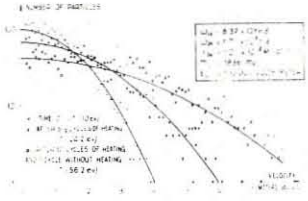

Figure 2

When the plasma frequency was increases, the velocity distribution became non-Maxwellian, and the ions were heated as well. A further increase in density resulted in the plasma becoming unstable. Under these conditions, the collisional effects have begun to dominate[2] and are over-emphasized from reality, by about the ratio of the number of real particles per super-particle. In order to observe heating at higher plasma frequencies, it is necessary to increase the number of super-particles, thereby lowering the number of real particles per super-particle for a given value of plasma frequency. The instability can then be controlled in this manner.

By eliminating the d.c. magnetic field, and using the TE_{111} mode, the theoretical model of r.f. confinement[3] of a plasma can be observed. It produces a striking constriction and compression of the plasma in accordance with the theory. It was found that confinement did occur in short times when the ion mass was lowered to about 5 electron masses. Otherwise, if the correct value is used, the heavy ion mass slows down the rate of confinement due to the ionic space charge field acting on the rapidly moving electrons. The lower mass permitted confinement to be observed within 20 r.f. periods. (40 minutes of CDC 6600 time) The following motion picture shows the results of the confinement simulation. The electrons are represented by a ⋈ and the ions by a ✳ . The theoretical region of confinement is a rectangular region in the center of the plasma. The particles are seen to effectively coalesce in this area as time progresses.

* Permanent address: The University of Wisconsin, Madison, Wis. (USA)

1. R.W. Hockney, Phys. Fluids 9, 1826 (1966)
2. R.W. Hockney, Proc. Conf. of Computational Physics, Culham (1969)
3. G. Schmidt, Physics of High Temperature Plasmas (Academic Press, Inc;, New York, 1966)

INTERACTION OF PLASMA BUNCHES WITH COMBINED VHF - MAGNETOSTATIC MIRROR IN THE RANGE OF ELECTRON CYCLOTRON RESONANCE.

K.S. Golovanivsky, V.D. Dougar-Jabon

Plasma Physic Laboratory, Patrice Lumumba University, Moscow W-302, USSR.

Abstract: It is shown experimentally the possibility of setting aside the cone-loss leakage in a mirror confined plasma using a VHF field near electron - cyclotron resonance.

1. Deficiency of principal of the right mirror traps is an inevitable particles leakage through cone-loss. The object of this paper is to limit this losses by creating in the mirror an electrostatic barrier for the ions. This barrier is formed by giving a transversal energy to the electrons with a velocity vector inside the cone-loss range from standing VHF wave near electron cyclotron resonance. In this case electrons leaves the cone-loss and are holded by the mirror-trap. Space charge of this electrons creates an electrostatic barrier which reflects the ions leaving the cone-loss. Essentially this mechanism is opposite with relation to plasma accelerating mechanism in the Pleade system [I].

2. Block scheme installation is shown on fig.1. Plasma generating by a coaxial gun has the shape of two bunches propogating with a residual pressure of 10^{-5} - 10^{-6} torr-within a glass tube with a ϕ 30mm and 1.2m long. Energy and density of the particles passed through the mirror are registrated by an electrostatic analyser of energy. In the zone of the mirror where field magnitude becomes 848 oersted and its gradient 53 oersted/cm a cylindrical cavity was situated being excited on a mode TE_{111} by a magnetron oscillator with a regulating power from zero to 2.5 kW (λ =12.5cm). Cyclotron electron resonance takes place in the middle plane of the cavity. Transversal pressure before cavity was appreciated by the mean of a diamagnetic signal. Plasma density determined by cutting off the microwave signal (λ = 3cm).

Parameters of the plasma bunches reaching magnetic mirror are the following : (potential of a capacitor is 2ϐ kV) :

	density	velocity	longitudinal ion energy
1st bunch	$10^{11}cm^{-3}$	$2\cdot10^{7}cm\cdot sec^{-1}$	> 3 kev
2d bunch	$10^{12}cm^{-3}$	$0.7\cdot10^{7}cm\cdot sec^{-1}$	~1 kev

The velocity of plasma and longitudinal ion energy are founded independently by a transit time and by the analyser data.

3. The results of the initial experiments are given. Decrease of longitudinal leakage of the plasma in a transition from magnetostatic mirror to combined fields in the range of electron cyclotron resonance is demonstrated. The essence of the experiments is reduced to investigate the plasma parameter modifications before and after VHF power feed to the cavity. For registration of passing plasma through the mirror the electrostatic analyser of energy is used, a signal from which is shown on an oscilloscope. The secondary electron emission is suppressed by means of giving -100V on an earthed grid. The current of the collector without external fields (magnetostatic and VHF) is shown on fig 2. The shape of this signal which doesn't change when a maximum transversal magnetic field of 1000 oersted is created near the analyser and it is independent of sign and value of the grid analysing potential (to 2.5 kV). So plasma gun generates together with a plasma the rapid neutrals which is the cause of the secondary emission from earthed grid. Without external magnetic field the plasma scatters by ambipolar diffusion on the tube walls without reaching the analyser, while rapid neutrals incident on the collector. When the magnetic mirror is working a radial plasma diffusion is limited by magnetic field. In this case the collector signal essentially is changed by plasma passing through cone-loss as it's shown on middle fig. 2. Lower oscillogramme corresponding to combined mirror is identical to the upper oscillogramme. Thus the collector signal in the case of combined mirror is conditioned mainly by the rapid neutrals. Oscillogrammes on fig. 2 are obtained as the potential feed were about 2.8 kV and VHF power 700 W. Simultaneously with plasma leakage elimination through the mirror a plasma density increase is observed in front of mirror when the VHF field is put in. We can see it on oscillogramme of cutting off the microwave signal (λ = 3cm) presented on fig. 3. If the maximum density of plasma in 27cm from the middle plane cavity in case of the ordinary magnetic mirror is lower than full cut off level, then while putting in the combined mirror, the accumulate plasma density exeeds $10^{12}cm^{-3}$.

1. T.Consoli, VIII Intern. conference, Vienna, 1967.

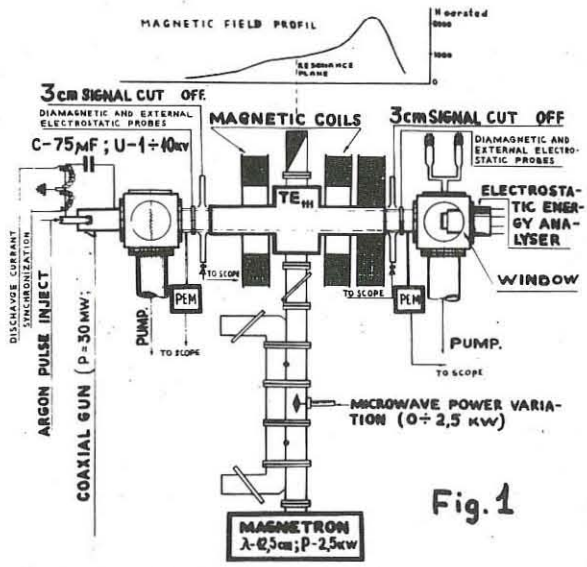

Fig.1

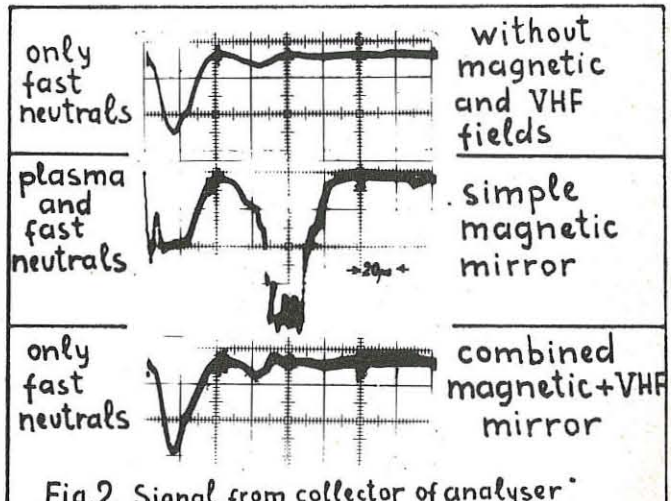

Fig.2 Signal from collector of analyser

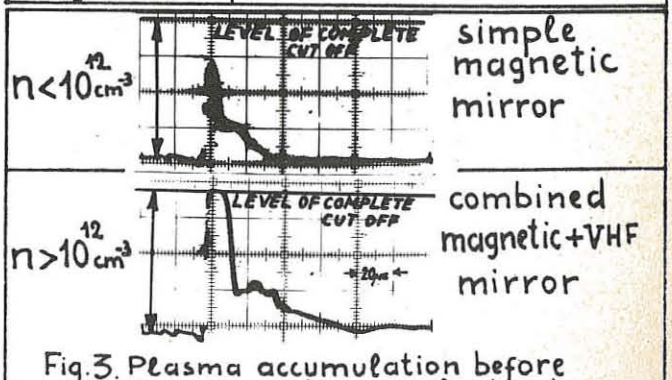

Fig.3. Plasma accumulation before the mirror (3cm signal cut off)

ON THE STABILITY OF MICROWAVE-HEATED PLASMAS*

by

G. E. Guest and D. J. Sigmar

OAK RIDGE NATIONAL LABORATORY

Oak Ridge, Tennessee, U.S.A.

Abstract: Magnetically-confined plasmas, created and heated by electromagnetic fields near the electron gyrofrequency, can support several modes of instability driven by inherent temperature anisotropy or possible loss-cone effects. If $T_\parallel \ll T_\perp$, both electrostatic and electromagnetic waves can grow in time; while if $T_\parallel \to T_\perp$, electrostatic waves at the hybrid frequency can be driven unstable by the loss-cone effect. Here we review the relevant known criteria and develop several new criteria to describe the stabilization of the temperature-anisotropy modes as $T_\parallel \to T_\perp$. We also report the results of a detailed analysis of the electrostatic loss-cone mode, for which temporal growth rates greater than anticipated electron bounce frequencies are obtained only for electron densities near microwave cut-off.

Microwave-heated plasmas confined in magnetic mirror traps have been observed to support various modes of instability which limit the charged-particle lifetimes. These include interchange modes in simple mirror traps and electrostatic and electromagnetic microinstabilities. Under some conditions, however, it has been possible to stabilize all instabilities in dense, energetic microwave-heated plasmas.[1] In this report we review the known stability criteria applicable to these plasmas and develop additional criteria for the occurrence of two electrostatic modes, one driven by temperature anisotropy of the heated electrons, the other by the loss-cone effect inherent in mirror confinement. Here we summarize briefly the modes considered and the associated stability criteria.

*Research sponsored by the U.S. Atomic Energy Commission under contract with the Union Carbide Corporation.

A. Electrostatic temperature-anisotropy modes[2] in the frequency range $0.5 \leq \omega/\Omega \leq 1$, where Ω is the electron gyrofrequency, can occur if $T \equiv T_\parallel/T_\perp \leq 1/6$ and $\omega_p^2 \geq \Omega^2/4$, where ω_p is the plasma frequency corresponding to the total electron density.

B. Electrostatic loss-cone modes[3] in the frequency range $\Omega < \omega < (\omega_{pc}^2 + \Omega^2)^{\frac{1}{2}}$, where ω_{pc} is the cold-electron plasma frequency can occur in anisotropic plasmas if $\omega_{pc}^2/\Omega^2 \leq T_\parallel/T_\perp$. As $T_\parallel \to T_\perp$ this criterion becomes inapplicable and detailed stability boundaries must be obtained by numerical solution of the complete electrostatic dispersion relation. For densities below microwave cut-off instability growth rates (in time) are very slow, and the mode may be stabilized by effects neglected in the model used for the present computations: infinite, homogeneous, collisionless plasma with mirror confinement simulated by "loss-cone" distribution functions.

C. Electromagnetic waves propagating in the "whistler" mode[4] can grow rapidly in time if[5] $T_\parallel/T_\perp \leq (8\,\beta_\perp/27)^{\frac{1}{2}}$, where $\beta_\perp$ is the perpendicular plasma pressure relative to the magnetic field pressure. If the anisotropy is less extreme, the growth is convective and decreases rapidly with further increases in $T_\parallel/T_\perp$.

D. Mirror instabilities[6] are expected to occur under similar circumstances, namely, $T_\parallel/T_\perp \leq \beta\,(1 - T_\parallel/T_\perp)$.

E. Interchange modes in simple mirror traps are apparently stabilized only by line-tying, through cold electrons, to the conducting cavity wall. Although relatively small densities of cold electrons are expected to provide adequate line-tying, it is difficult in practice to utilize this stabilization technique at low ambient gas pressures because of the tendency of the plasma to charge negatively and expel all cold electrons.

Other slowly growing microinstabilities such as negative-mass modes seem likely to be stabilized by the electron-microwave interactions which occur at twice the electron bounce frequency.

We note that for typical microwave-heated plasmas the critical values of temperature anisotropy predicted for electrostatic, electromagnetic, and mirror modes are similar in that if $T_\parallel/T_\perp \approx 1/6$, (the critical value for electrostatic modes), whistlers are stable up to cut-off for $v_\perp/c \approx 0.3$ and mirror modes are stable up to $\beta \approx 0.2$. Since mirror confinement in a trap of mirror ratio R permits equilibria such that $T_\parallel/T_\perp \leq R - 1$, temperature-anisotropy modes need not occur if $R > 7/6$. However, microwave-heating can cause heated electrons to turn near the "resonant surface" (on which the local gyrofrequency equals the applied microwave frequency), giving rise to equilibria in which density and anisotropy are maximum near the resonant surfaces. Such configurations, which are likely to exhibit the instabilities discussed above, can be avoided in simple mirror traps by applying small amounts of off-resonant power at frequencies well above the gyrofrequency to smooth the distribution of electron turning points.[1] Magnetic-well configurations require special care in design to minimize regions in which the field lines are tangential to the resonant surface.

REFERENCES

[1] R. A. Dandl, Bull. Am. Phys. Soc. 15, 60 (1970).

[2] A. V. Timofeev, Sov. Phys. - JETP 12, 281 (1961).

[3] L. S. Hall, W. Heckrotte, and T. Kammash, Phys. Rev. 139, A1117 (1965).

[4] R. N. Sudan, Phys. Fluids 8, 153 (1965).

[5] C. L. Hedrick, private communication.

[6] S. Chandrasekhar, A. N. Kaufman, and K. M. Watson, Proc. Roy. Soc. (London) A245, 435 (1958).

PLASMA TRAPPING AND MICROINSTABILITIES IN THE PHOENIX II EXPERIMENT

by

E. Thompson, D.R. Sweetman, E.G. Murphy and M.J. Church.

U.K.A.E.A., Culham Laboratory, Abingdon, Berks. England.

Abstract: The existence of plasma trapping in a high energy neutral injection experiment has been demonstrated. An estimate of the observed ion lifetime against loss due to microinstabilities has also been made and found to be independent of ion density.

Introduction: The plasma containment region in the Phoenix II magnetic mirror experiment is a "minimum B" or magnetic well configuration.[1] A plasma with ion energy of several keV and density of up to 5×10^9 ions cm^{-3} is produced by Lorentz ionization of a beam of neutral atoms. By improving the ion source used on the Phoenix injector we have been able to double the injected current of neutral atoms to 40 mA equivalent whilst reducing the energy from 20 to 8 keV. The most significant feature of the preliminary results obtained using this improved injector is the strong evidence for the contained plasma making a contribution to the trapping of the injected beam.

The equation governing the ion density n in a neutral atom injection experiment is given by

$$\frac{dn}{dt} = F\frac{I_o}{V} + \frac{I_o}{V} n \sigma_t L - \frac{n}{\tau_{ox}}$$

where F is the fraction of the total beam I_o which is Lorentz ionized, V is the plasma volume, σ_t is the cross-section for trapping of the injected beam by the plasma, L is the trapping length and τ_{ox} the ion lifetime against charge exchange which is assumed to be the only loss mechanism. The equilibrium density is given by

$$n = \frac{F I_o' \tau_{ox}}{1 - I_o' \tau_{ox} \sigma_t L} \qquad \ldots(1)$$

where $I_o' = \frac{I_o}{V}$. The possibility of plasma trapping due to collisional ionization of excited states has been known for some time and earlier measurements on Phoenix II showed enhanced trapping.[1] However the observed trapping was rather small and confined to a small region so that effects due to plasma redistribution could not be entirely ruled out.

Results from the present experiments are shown in the figures which show the measured density plotted against the product $I_o \tau_{ox}$. The graph on the left relates to the central axial density determined from the cold ion current through the mirrors whilst the other curve was obtained using a fast neutral emission detector sensitive to the whole plasma volume. If Lorentz ionisation was the only trapping mechanism the density should follow the dashed line, but as can be seen the effect of plasma trapping is quite pronounced and its contribution can equal, or even exceed Lorentz trapping.

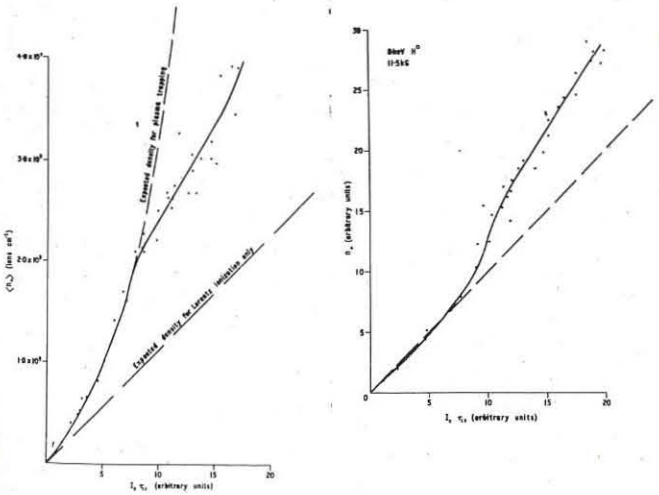

By fitting a curve of the form given by equation (1) to the measurements of the axial density we calculate $\sigma_t \approx 2.8 \times 10^{-15}$ cm^2 which is consistent with a theoretical estimate by Berkner and Riviere.[2] The theoretical model considers collisional excitation and upward cascade of excited states, as well as the ground state, into levels which are Lorentz ionized. The unusually high value of the cross-section is primarily due to the contribution of the excited states.

The deviation of the measured density from that predicted is due to plasma losses associated with the microinstability which is still observed to be present. Although detailed measurements have not yet been made, the RF emission is in general similar to that reported earlier[3] in that it appears at harmonics of the ion cyclotron frequency - the higher harmonics occurring as the density is increased.

By taking the predicted density variation with $I_o \tau_{ox}$ we can estimate the average ion lifetime (in the region being observed) against loss due to the microinstability. This lifetime is found to be of the order of 200 msec - comparable to that found for 20 keV injection - and appears to saturate at this value and does not decrease as the density is increased.

Because of the sensitivity of the equilibrium plasma density to the dominator of equation (1) even these relatively long loss times have a significant effect on the density. However the density is still rising with increasing $I_o \tau_{ox}$ due to the effect of plasma trapping. These results are much more encouraging than those obtained with lower current 20 keV injection which showed a saturation in ion density with increasing $I_o \tau_{ox}$.

References

1. Bernstein et al. Plasma Physics and Controlled Nuclear Fusion Research. 2 p.23. 1966.
2. Berkner and Riviere. Private Communication.
3. Cordey et al. Plasma Physics and Controlled Nuclear Fusion Research. 2 p.267. 1969.

INVESTIGATION OF PLASMA DECAY IN THE PR-6 DEVICE

Yu.T.Baiborodov, Yu.V.Gott, M.S.Ioffe,
R.I.Sobolev, E.E.Yushmanov.
I.V.Kurchatov Institute of Atomic Energy, Moscow, USSR

Abstract. Disappearance of ions of various energies was measured during the decay of plasma with the initial density of $10^{12}cm^{-3}$. The results obtained indicate that non-classical mechanism of losses should exist in the initial stage of the decay.

In the experiments on the magnetic well mirror trap plasma confinement conducted in the PR-5 device[1] it was found that the decay of plasma occured anomalously. During the first 100-200 μsec after the injection the density of plasma quicly dropped from its initial value $n \sim 10^{11}cm^{-3}$ down to a level of $5.10^{9}cm^{-3}$, after which a stage of significantly slower decay set in. At that second stage the plasma confinement was stable during many milliseconds, and the decay times were close to the charge-exchange.

The foregoing experiments in the PR-6 device[2] showed that the anomalous plasma loss at the initial stage of decay could not be attributed to the drift-loss cone instability though its presence could be expected in those experiments.

Investigations of other possible sources responsible for anomalous plasma loss led to an assumption that during plasma decay there should appear an ambipolar electric field, which could greatly decrease the mirror confinement of the main fraction of ions. The basis of this assumption is as follows. Measurements of the ion energy distribution carried out earlier could be performed with sufficient accuracy only beginning with 400-500 ev, and it is not excluded that the energy of most ions is lower than the above values. In this case the positive plasma potential set at the initial stage of the decay due to Coulomb electron scattering may be sufficient for pushing out low energy ions. The six-bar magnetic field configuration may cause the ions to disappear mainly through relatively weak radial mirrors.

The pattern of plasma decay observed as a function of perpendicular-mirror ratio $\alpha_\perp$ supports this point of view. Upon increase $\alpha_\perp$ the initial drop of density is reduced, and the density of stable plasma increases correspondingly.

The above considerations can be directly checked by measuring the disappearance of various energy ions. If the plasma potential is positive in the centre region of the trap (with respect to the mirrors) the minimum energy of the ions confined $E_{i\ min}$ is related with φ through $E_{i\ min} = \frac{\varphi}{\alpha - 1}$ where α is the mirror ratio along the considered tube of the magnetic lines of force. Such a potential should not influence the confinement of higher energy ions. Thus, observing the variation of ion life-time as a function of energy it is, in principle, possible to determine the potential and its variation with time.

An analyzer with threshold of energies measured reliably reduced to 200 ev has been used in such measurements. The analyzer was placed in the central cross section of the trap. A charge-exchange neutral flux entering the analyzer was collimated at an angle $\pm$ 2.5° with respect to the trap radius. Therefore, the perpendicular energy component was essentially measured.

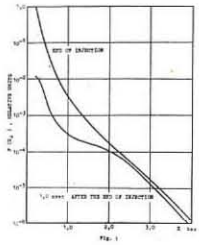

To make the analyzer signals sufficiently large the initial plasma density was increased up to $10^{12}cm^{-3}$ due to forcing the injection regime. The ions were heated by r.f. pulses as in Ref./1/. The plasma decay pattern recorded by the radiointerferometer was of the previous character. The only exeption was that the density of the stable plasma increased up to $10^{11}cm^{-3}$. Fig.1 (the upper curve) shows the energy distribution of ions at the moment when the injection was ceased. Fig.2 illustrates oscillograms of the analyzer signals for four energy values during injection and subsequent decay of the plasma.

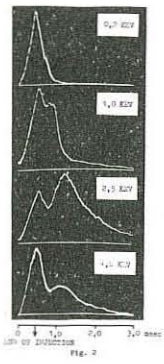

We can see that the plasma decays in a more complicated way than according to our idealized model. The most unexpected is the peak appearing in the oscillograms during the decay. When considering such oscillograms for a large number of descrete energy values, we may see a lot of other characteristic features, namely, a) the most fraction of low energy ions (up to 0.8kev) disappears during 400 μsec after injection; b) for the ions of intermediate energies (0.8-2 kev) the initial phase of the decay is covered appearance of the peak. After this the decay occurs with two time constants due to two diffrent mechanisms of loss of such ions; c) after the peak, the high energy ions (> 2 kev) suffer an exponential decay with time close to charge-exchange. At present we are not able to interpret all these features unambiguosly. However, if we do not enter into details one may resume as follows. The behavior of ions of various energies does not contradict roughly the idea of the ions being pushed out by an electric field. Indeed, at the initial stage, when the density sharply drops, low energy ions constituting the main fraction of the entire ion density escape from the trap. (See Fig.1). The high energy fraction of the ion distribution exhibits rather complicated evolution at this period of time. It, however, remains within the trap and continues being confined during a long period of time.

It is, however, important to emphasize that the totality of the phenomena occuring in the initial phase of decay cannot be attributed only to pair Coulomb Collisions. It concerns, in particular, the nature of the electric field as well as the peaks mentioned above. The latter are, most probable, associated with certain collective phenomena which exist for an appreciable period of time after the stage of fast decay and cause deformation of the high-energy tail in the ion distribution.

References

1. Yu.V.Gott, M.S.Ioffe, E.E.Yushmanov. "Plasma Physics and Controlled Nuclear Fusion Research", v.I, p.35, Vienna (1966).
2. Yu.T.Baiborodov, Yu.V.Gott, M.S.Ioffe, R.I.Sobolev, ibid, v.II, p.213 (1969).

PLASMA CONTAINEMENT IN A CIRCULARIZED QUADRUPOLAR MAGNETIC WELL : DECA II B.

D. Launois, P. Lecoustey, M. Nicolas, J. Tachon.

ASSOCIATION EURATOM-CEA
Département de la Physique du Plasma et de la Fusion Contrôlée
Centre d'Etudes Nucléaires
Boite Postale n° 6 - **92 Fontenay-aux-Roses** (France)

ABSTRACT : The focalization of magnetic lines out of a quadrupolar well reduces the wall plasma interaction. Such a trap confines a 500 eV hydrogen plasma with an initial density of 10^{12} cm^{-3} . The decay time is 400 μsec.

The confinement of the compressed plasma in DECA II was limited by charge exchange with the desorbed gas from the walls [1] . In order to reduce the plasma wall interaction the magnetic well configuration is circularized so that the magnetic line is bended towards the axis out of the mirrors (Fig.1).

PRINCIPLE OF THE EXPERIMENT : As the previous experiment [2] , the plasma is injected along a longitudinal magnetic field by a thetatron gun. After a five meters path, the plasma goes into the confinement stage. The magnetic quadrupolar trap is created by circular coils and rectangular windings. This static trap is opened during a short time by a pulsed coil which cancels one of the mirrors.

REALIZATION OF A "CIRCULARIZED QUADRUPOLAR WELL" : The configuration was optimized to adjust two conflicting properties of the magnetic lines :

1) Good curvature to suppress the flute instability.
2) Weak concavity to minimize the radial extension of the circularized flux tube.

The quadrupolar field distribution along the magnetic bottle was adjusted to obtain the same energy well for all the particles. If E is the particle energy , J (r,E) the second adiabatic invariant, we define the depth of the energy well as:

$$\frac{\delta E}{E} = \frac{1}{J(0,E)} \cdot \frac{\partial J(r,E)}{\partial r} \cdot \frac{B_M - B_o}{B_o}$$

where B_M is the magnetic field modulus where the particle is reflected, B_o the intensity of the field at the well center.

Fig. 2 shows the claculated distribution $\eta(u)$ of the quadrupolar field between the mirrors to verify the stabilization criterion.

To perform such a distribution, we have divided the quadrupolar windings in five groups of four coils each, as shown on fig.3.

The first three groups, one central winding and two reinforcing coils, create the quadrupolar well. The focalization of the magnetic lines is ensured by four circularizing coils on each side of the well. The current flows in this coils in the opposite direction of the stabilizing current. The effective quadrupolar field distribution $\eta(u)$ obtained is shown fig.2. We have also plotted the depth of the energy well for a 5 cm radius.

The main characteristics of the magnetic configuration are :

- Intensity at the well center : 3500 gauss
- Axial Mirror Ratio 1.84 . Distance between Mirrors 130 cm.
- Transverse depth of the well : r_o = 4 cm $R_\perp$ = 1.004
  r_o = 20 cm $R_\perp$ = 1.07

To maintain the quality of the circularization during the plasma injection, the pulsed coil have to simultaneously reduce the longitudinal and the radial field. A double base ball coil around a glass chamber carries out this purpose. Fed by a 43 μF - 15 kV condenser bank, it produces 3.5 kGs on the axis with a 10 μsec rise time.

In the final static configuration the flux tube without any wall contact is 7 cm in diameter, measured in the median plane.

EXPERIMENTAL RESULTS.

The plasma gun operates to produce an hydrogen plasma with 10^{13} cm^{-3} density and 200 eV of mean longitudinal energy. The useful flux tube is defined by a 6 x 4 cm diaphragm, placed at 1.5 m from the median plane.

The confined plasma is investigated by microwave interferometer (λ = 4 mm) and two fast atoms detectors. One of them is a secondary emission type one, the other uses a reionization gas cell (Air pressure = 5.10^{-3} torr, length = 10 cm) and an electrostatic analyzer [1].

Fig. 4 shows the signals without and with quadrupolar field. In the latter, the plasma lifetime is much longer. The neutral signal suggests an increasing of the pressure during the confinement.

We can generally adjust two exponential decays : from 500 μsec to 900 μsec $\bar{\tau} \simeq 400$ μsec and from 900 μsec to 1600 μsec $\bar{\tau} \simeq 300$ μsec.

The electron density is maximum during the injection. At t = 100 μsec the density is $\bar{n}_e \ell = 10^{13}$ cm^{-2} and decreases with an e-folding time of 400 μsec. If the characteristic length "ℓ" is taken as the diameter of the last flux tube $\bar{n}_e \simeq 10^{12}$ cm^{-3}.

A fast atom spectrum was measured along a direction which is inclinated 10° with the normal to the magnetic axis. The neutrals are counted during 2 msec. Fig.5 shows this spectrum, taking into account the reionization efficiency [3]. The mean energy is 500 ev which is compatible with the energy of the injected plasma. We have also measured the angular dependence of the neutral flux (for E = 600 ev). The flux presents a minimum for the normal direction and increases by a factor of 5 from 0° to 10°. That indicates an anisotropy $\frac{E_\perp}{E_{//}} < 10$.

CONCLUSION.

The circularization of a quadrupolar well allows to confine a 500 ev plasma with a 300 μsec decay time. The total density of the plasma at the beginning of the confinement is about 10^{12} cm^{-3}. However , the plasma lifetime is probably limited by charge exchange. To improve the vacuum, we are going to place a liquid nitrogen-cooled wall with titanium evaporation.

Références :

[1] Etude de l'importance du phénomène d'Echange de charge dans DECA II. Lecoustey.P, Renaud.C. Plasma Physics 9 (1967) 527.

[2] Chauffage et Confinement de plasma dans le puits magnétique de DECA II. Biguet A et al Proc. Conf. Culham 1965) 1, IAEA, Vienna (1966)69

[3] Method of investigation of the flux of atoms Emitted by a plasma V.V.Afrosimov et al Soviet Physics, Technical Physics Vol 5, N° 12 June 61

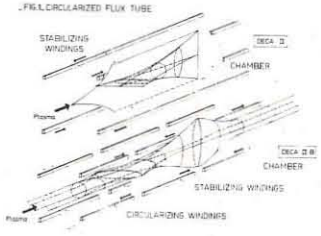

FIG.1 CIRCULARIZED FLUX TUBE

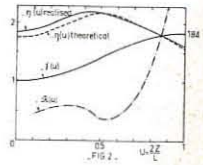

FIG 2

$$\eta(u) = \frac{L}{2r_o} \frac{B(r_o,u)}{B(0,o)} \quad , \quad \gamma(u) = \frac{B(o,u)}{B(0,0)}$$

$$\mathcal{R}(u) = \left(\frac{L}{2r_o}\right) \frac{\delta J}{J} \frac{B_M - B_o}{B_o}$$

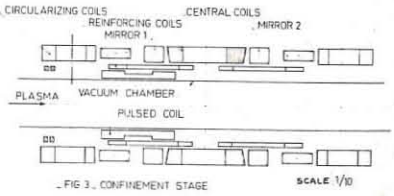

FIG 3 . CONFINEMENT STAGE SCALE 1/10

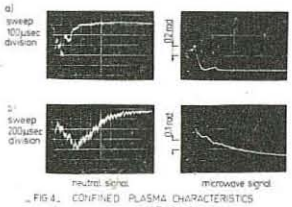

FIG 4 . CONFINED PLASMA CHARACTERISTICS
B_o = 3 kGs
a) without quadrupolar field
b) with quadrupolar field (B = 32kGs at the wall

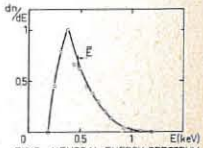

FIG.5 . NEUTRAL ENERGY SPECTRUM

BOUNCE EFFECTS IN THE NEGATIVE MASS INSTABILITY.

D. Launois , G.Laval, R. Pellat, J.Tachon.
ASSOCIATION EURATOM-CEA
Département de la Physique du Plasma et de la Fusion Contrôlée
Centre d'Etudes Nucléaires
Boîte Postale n° 6 - **92 Fontenay-aux-Roses** (France)

ABSTRACT: Unstable modes at bounce harmonic satellites of the ion cyclotronic frequency exist for any density. The thermal spreading reduces slightly the unstable domain. The decreasing of ion bounce frequency does not stabilize dilute plasma.

In different magnetic mirror traps [1], one can observe a same kind of "Flute type" instability, at ion cyclotronic frequency ($\omega \sim \Omega_{ci}$) ; the perturbation, mainly electrostatic, is constant along the line of force ($k_{//} \simeq 0$) and has a long radial wavelength compared with the mean ion Larmor radius ($k_\perp a_i \ll 1$). A recent theory proposed independently by Kadomtsev and Pogutse [2] and Clarke and Kelley [3] seems to fit with the observations. These authors have supposed that the ion bounce frequency (ω_t) is much larger than the spread of ion cyclotronic frequency. In that case, with no spread in the pitch angle distribution function, the instability has a rather low density cut-off. More recently Callen and Horton [4] have shown that thermal effects introduce a density threshold. Our paper presents the effect of a finite bounce frequency. We find new unstable modes and an unstable density domain larger than the previous one.

1) With a monoenergetic distribution function, peaked at some value of the pitch angle, the dispersion relation is

$$k = \sum_n \left\{ \frac{\omega' - \frac{\eta}{2}}{(\omega' - n)^2} J_n^2(\eta) + \frac{\omega' - 2\eta}{\omega' - n} J_n(\eta) \cdot J_n'(\eta) \right\} \qquad (1)$$

where $k = \frac{4\Omega_{ci}\omega_t}{\omega_{pi}^2}$; $\omega' = \frac{\omega - <\Omega>}{2\omega_t}$; $<\Omega>$ is the bounce averaged cyclotronic frequency, as given by $<\Omega> = \Omega_{ci}\left(1 + \frac{\lambda^2}{2L^2}\right)$ where L is the axial characteristic length for the magnetic field ; $\omega_t = \frac{v_\perp}{L}$; λ is the axial excursion of the ion. $\eta = \frac{\Omega_{ci}\lambda^2}{4\omega_t L^2}$ is the argument of Bessel functions.

Unstable roots are found near each value of n. With n = 0, the result is Kadomtsev's one :

With n > 0, there is instability if $\left(\frac{\omega_{pi}}{\Omega_{ci}}\right)^2 \gtrsim \frac{n}{\eta}\frac{\lambda^2}{L^2}$; with n < 0 , the unstable domain extends to any density. The maximum growth rate is $\sim \frac{3}{2}\eta\omega_t$ for $n = \pm 1$.

2) To demonstrate that the instability is not due to our first choice of distribution, we consider two cases : a Gaussian distribution function in pitch angle centered around λ_o , then a centered parabolic distribution function which vanishes for $\lambda \geq \lambda_o$, which is of course much relevant of experimental situations.

A- Gaussian distribution function :

Let $f_o = \frac{L}{4\pi^{5/2} v_o^2 \Delta}\delta(v_\perp - v_o)\exp -\left(\frac{\lambda - \lambda_o}{\Delta}\right)^2$, the dispersion relation, derived for n = 0 , in the limit $\eta \ll 1$ and a weak dispersion $t = \frac{\lambda_o}{\Delta} \gg 1$, is given by :

$$1 + \frac{Kt}{4}\left\{ Z(\xi)\left[3 - t\xi - \xi^2\right] + Z(\xi')\left[3 - t\xi' - \xi'^2\right]\right\} = 0$$

with $K = \frac{1}{k\eta} = \frac{\omega_{pi}^2}{\Omega_{ci}^2}\frac{L^2}{\lambda_o^2}$; $\xi = \frac{a - \lambda_o}{\Delta}$; $\xi' = -\frac{a + \lambda_o}{\Delta}$; $a = L\left[\frac{2(\omega - \Omega_{ci})}{\Omega_{ci}}\right]^{1/2}$ and $Z(\xi)$ is the plasma dispersion function.

We find again the δ function results in the case of $\xi > 1$ and $|\xi'| > 1$. There is instability if $\frac{\omega - <\Omega>}{2\omega_t} < \eta$. Now, with $\xi < 1, |\xi'| > 1$, we find stabilization for $K \lesssim 4/t^2$

That corresponds to the very low density range and this result is similar to Callen and Horton's one [6].

B- Centered parabolic distribution function :

Let : $f_o(v_\perp, \lambda) = \frac{L}{\pi^2 v_o^2 \lambda_o}\delta(v_\perp - v_o)\cdot\left[1 - \left(\frac{\lambda}{\lambda_o}\right)^2\right]$

Expanding the Bessel functions we obtain the equation, by picking up the $n = 0 ; \pm 1$ terms :

$$1 + K\left\{ (3 - 4X)\,\mathrm{Log}\left|1 - \frac{1}{X}\right| - 4 + \frac{\eta_o^2}{2}\left[\frac{Y^2}{2}(1 - 2Y)\left(1 - \frac{2}{\eta Y}\right)\right.\right.$$
$$\left.\left. \mathrm{Log}\left|1 - \frac{1}{Y}\right| + \frac{2Y}{\eta} - Y^2 + \frac{Z^2}{2}\left(1 - 2Z\right)\left(1 + \frac{2}{\eta Z^2}\right)\mathrm{Log}\left|1 - \frac{1}{Z}\right| - \frac{2Z}{\eta} - Z^2 - \frac{1}{6}\right]\right\} = 0$$

Where : $X = \frac{a^2}{\lambda_o^2}$; $Y = X - \frac{1}{\eta}$; $Z = X + \frac{1}{\eta}$; $a^2 = 2L^2\frac{\omega - \Omega_{ci}}{\Omega_{ci}}$

The figure 1 shows the unstable ranges for the density and the δ function limits. The main effects we find are that the thermal spreading : 1) displaces the δ function limits (cut-off for n = 0 , threshold for n = 1) ; 2) introduces a density threshold for n = 0 and a density cut-off for n = 1 . 3) The unstable domain disappears for n = -1. The growth rate is always of the same order : $\gamma \sim 0.4\eta\omega_t$

3) The physical situation where $\eta \gg 1$ has been solved only for a rather dilute plasma.

Let us consider the following distribution function :

$$f = \frac{L}{2\pi^2\lambda_o v_o^3 <y^2>}\theta(x - 1)\, g(y)$$

with $x = \left(\frac{\lambda}{\lambda_o}\right)^2$, $y = \frac{v}{v_o}$, $<y^n> = \int y^n g(y)\,dy$

the dispersion relation is :

$$0 = \left(\frac{\sqrt{2}\lambda_o\Omega_{ci}}{L\omega_{pi}}\right)^2 + 1 + \frac{\eta_o}{<y^2>}\sum_n\left\{\iint \frac{y^3 dx\, dy\, J_n^2\left(\frac{\eta_o x}{y}\right)\frac{\partial g}{\partial y}}{\omega' + (1 - x)\eta_o - ny} + \left(1 - \frac{\omega'}{\eta_o}\right)\int \frac{y^2 dy\, J_n^2\left(\frac{\eta_o}{y}\right)\cdot g(y)}{\omega' - ny}\right\}$$

with : $\eta_o = \frac{\Omega_{ci}\lambda_o^2}{4v_o L}$, $\omega' = \frac{\omega - \Omega_{ci}\left(1 + \frac{\lambda_o^2}{2L^2}\right)}{2v_o/L}$

When $\omega' \ll 1$, the n = 0 second term between brackets gives the main contribution in computing the real part of ω' . One gets :

$$\omega' \simeq -\frac{<y^3>}{\pi <y^2>}\left[1 + \left(\frac{2\lambda_o\Omega_{ci}}{L\omega_{pi}}\right)^2\right]^{-1}$$

Our assumption is valid if $\frac{\omega_{pi}}{\Omega_{ci}} < \frac{\sqrt{2}\lambda_o}{L}$. The main contribution to the imaginary part comes from the resonant term of the first integral between brackets ;

$$\delta\omega' \sim \frac{\pi}{<y^3>}\omega'^2\sum_n\int y^3 dy\, J_n^2\left(\frac{\eta_o}{y} - n\right)\frac{\partial g}{\partial y}$$

with $0 < n < \frac{\eta_o}{y}$, which shows that $\delta\omega' \sim i\omega'^2 \mathrm{sig}\frac{\partial g}{\partial y}$ a result independant of η_o .

For that value of the density ($\frac{\omega_{pi}}{\Omega_{ci}} < \sqrt{2}\frac{\lambda_o}{L}$) , we get an instability if $\frac{\partial g}{\partial y} < 0$. That result shows that increasing η to values larger than one does not stabilize dilute plasmas. When density increases ($\frac{\omega_{pi}}{\Omega_{ci}} > \sqrt{2}\frac{\lambda_o}{L}$) it is likely that the plasma remains unstable with $\mathrm{Re}\,\omega' \sim \mathrm{Im}\,\omega' \sim 1$.

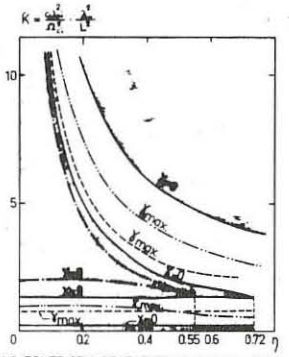

FIG 1. ZONES OF UNSTABLE DENSITIES VERSUS η
δ FUNCTION ——— $\gamma = 0$
——— γ max
PARABOLIC FUNCTION — $\gamma = 0$
--- γ max

REFERENCES :

[1] B.I. KANAEV, E.E. YUSHMANOV,
Conference Proceedings (H-9) Novosibirsk 1968.

J.F.CLARKE, G.G. KELLEY, J.F. LYON, R.F. STRATTON,
Conference Proceedings (H-6) Novosibirsk 1968.

P. BROSSIER, P. LECOUSTEY, C. RENAUD, J. TACHON
Conference Proceedings (H-7) Novosibirsk 1968.

[2] B.B. KADOMTZEV, O.P. POGUTSE,
Conference Proceedings (G-10) Novosibirsk 1968.

[3] J.F. CLARKE, G.G. KELLEY,
Instabilities due to magnetic field spatial variations,
Phys. Rev. Letters, Vol. 21, n°15 oct. 1968.

[4] J.D. CALLEN , C.W. HORTON,
Negative Mass Instabilities
Phys.of Fluids Vol.13, N°3 , Jan.1970.

LOSS CONE MODES IN INHOMOGENEOUS MEDIA

by

H. L. Berk,* L. D. Pearlstein,* J. G. Cordey**

Lawrence Radiation Laboratory, Livermore, Calif., USA.

Abstract: A general treatment of standing wave loss cone modes is presented in a spatially inhomogeneous medium. Critical scale lengths for stability are found.

As is now well known, the intrinsic nature of the loss cone distribution in a mirror machine is a strong instability source even for a collisional mirror distribution. Post and Rosenbluth[1),2)] showed that a rapidly growing convective instability always exists at high density, and they estimated the permissible axial length that could be tolerated. They also found that limitations on the permissible cross-sectional length exist due to a drift cone mode. Subsequently, it was found that unstable standing waves exist in a sufficiently long system[3),4)]. These waves can be classified as either an absolute instability[3)] or as negative energy waves that are destabilized in a spatially varying system due to a radiative-like dissipation mechanism[4)].

Recently we have developed a model that follows these loss cone modes as a function of axial scale length to the stable regime[5)]. We find that all the above modes are related to each other and, at the scale lengths needed for stability, none of the above classifications is particularly unique.

The equation we use that describes a wave,

$$\phi(\underline{r}) = \phi(s)\exp(il\theta)\,J_l(k_\psi\psi)\exp(-i\omega t)$$

along a field line in an axially symmetric system is:

$$\frac{B(s)}{\omega_{pe}^2(s)}\frac{d}{ds}\frac{\tilde{\omega}_{pe}^2(s)}{B(s)}\frac{d\phi}{ds} = -k_{\perp o}^2\frac{\omega^2}{\omega_{ci}(s)\,\omega_{ci o}}\frac{m}{M}\left[\frac{\omega_{ci}^2(s)}{\omega_{pi}^2(s)} - \frac{l}{n}\frac{\partial n}{\partial\psi}\frac{B_o}{k_{\perp o}^2}\frac{\omega_{ci}}{\omega} + \frac{m}{M}\sum_N H_N(s)\right]\phi(s) \qquad (1)$$

where $k_{\perp 0} = k_\psi/r(0)\,B(0)$ and $H(s)$ is an integral operator defined as:

$$H_N(s) = -\left[F_N(b(s)) + \frac{l}{k_{\perp o}^2}\frac{B}{n}\frac{\partial n}{\partial\psi}G_N(b(s))\right] \qquad (2)$$

$$\cdot\, i\int_0^\infty dv_\parallel f(v_\parallel)\int_{-\infty}^{\infty}\frac{ds'}{v_\parallel}\exp\left[i\int_{s'}^{s}(\omega - N\omega_{ci}(s''))\frac{ds''}{v_\parallel}\right]\theta(s-s').$$

With $f(v_\perp^2) = \frac{v_\perp^2}{4v_{th_i}^4}\exp\left(-\frac{v_\perp^2}{2v_{th_i}^2}\right)$ we have

$$F_N = \frac{8\omega\omega_{ci o}^2}{B_o k_{\perp o}^2}\int_0^\infty dv_\perp^2\frac{\partial f}{\partial v_\perp^2}J_N^2\left(\frac{k_{\perp o}v_\perp}{\omega_{ci o}}\left(\frac{B(s)}{B_o}\right)^{1/2}\right) = -\frac{d}{db}\left(I_N(b)e^{-b}\right),$$

$$G_N = \int_0^\infty dv_\perp^2 f(v_\perp)\,J_N^2\left(\frac{k_{\perp o}v_\perp}{\omega_{ci o}}\left(\frac{B(s)}{B_o}\right)^{1/2}\right) = \frac{d}{db}\left(bI_N(b)e^{-b}\right),$$

$$b = \frac{k_{\perp o}^2 v_{th_i}^2}{\omega_{ci o}^2}\frac{B(s)}{B_o}, \qquad \theta(s) = \begin{cases} 1, & s>0 \\ -1, & s<0 \end{cases},$$

$$\tilde{\omega}_{pe}^2 = \frac{\omega_{pe}^2(s)\,k_{\perp o}^2 c^2\,B(o)}{k_{\perp o}^2 c^2 B(s) + \omega_{pe}^2(s)\,B(o)}.$$

In Eq. (1) the electrons are treated in a fluid approximation and the integral operator describes ions whose guiding centres have constant speed. This approximation can be justified when $(\omega - N\omega_{ci0})\Delta\tau_B >> 1$, where $\Delta\tau_B$ is the spread in the ion bounce frequency. We have also included electromagnetic effects due to electron motion along a field line. The boundary conditions for these equations are outwardly propagating waves.

Under many conditions the integral operator is accurately approximated by a relatively simple expression; namely when

$$M_{ax}\left[\left|\frac{k_\parallel v_{th_i}}{\omega - N\omega_{ci}}\right|, \left|\frac{k_\parallel^2 v_{th_i}^2}{N\omega_{ci}'}\right|^{1/2}, \left|\frac{k_\parallel^3 v_{th}^3}{N\omega_{ci}'}\right|^{1/3}\right] < 1 \qquad (3)$$

where $k_\parallel \simeq \phi'/\phi$ and the primes indicate the spatial derivative. In this case we find

$$H_N(s) = -\frac{1}{\omega - N\omega_{ci}(s)} \qquad (4)$$

and Eq. (1) becomes a relatively simple second-order differential equation.

The simple form for $H_N(s)$ also breaks down if two resonance points tend to coalesce at the centre (or ends) of the machine. The additional resonance condition that must be satisfied is:

$$\left|\frac{\omega - N\omega_{ci o}}{\omega_{ci o}}\right|^3 > \frac{v_{th_i}^2}{L_M^2\,\omega_{ci o}^2} \qquad (5)$$

When the simplest differential equation can be used, we can usually solve the problem through a WKB analysis where we study how waves can propagate through regions where $k_\parallel(s) \to \infty$, when $N\omega_{ci}(s) \to \omega$. In stable positive energy systems this singular behaviour in $k_\parallel$ leads to wave attenuation, such that for real frequencies

$$|\phi_i|^2 > |\phi_t|^2 + |\phi_r|^2$$

where ϕ_i, ϕ_t and ϕ_r are the amplitudes of the incident, transmitted and reflected waves, respectively. However, in a negative energy system we find that the singularities induce wave amplification, and therefore

$$|\phi_i|^2 < |\phi_t|^2 + |\phi_r|^2$$

Since the incident signal is amplified at the singular points, standing waves can arise even though the signal convects away from the central regions.

The rough critical scale length criterion that arises as a result of the WKB analysis is

$$L \lesssim 10\left(\frac{N}{\beta}\right)^{1/2}\left[1 + 3N^2\left(\frac{m}{M\beta}\right)\right]^{-1/2} \qquad (6)$$

where L is the magnetic scale length in ion gyroradii and N the harmonic number, as long as

$$N \lesssim \left(\frac{\omega_{pi}}{\omega_{ci}}\right)^{3/4}$$

which results from violating Eq. (3). This result is more pessimistic than previous estimates[1),2)].

In addition, we find a mode that tends to resonate at the central cyclotron frequency which is never stabilized in the simple differential equation approximation. However, the critical length for this case occurs from ion transit effects that are important when Eq. (5) is violated. Unfortunately, the dependence of the frequency shift to density and scale length is very model sensitive so that it is difficult to ascertain the proper scaling of the resonant mode in a realistic mirror machine.

* Temporary address: ICTP, Trieste, Italy.

** Permanent address: Culham Laboratory, Abingdon, Berks, England.

REFERENCES

1) M.N. Rosenbluth and R.F. Post, Phys. Fluids 8, 547 (1965).

2) R.F. Post and M.N. Rosenbluth, Phys. Fluids 9, 730 (1966).

3) H.L. Berk, T.K. Fowler, L.D. Pearlstein, R.F. Post, J.D. Callen, C.W. Horton and M.N. Rosenbluth, "Plasma Physics and Controlled Nuclear Fusion", Vol. II (IAEA, Vienna 1969) p. 151.

4) H.L. Berk, L.D. Pearlstein, J.D. Callen, C.W. Horton and M.N. Rosenbluth, Phys. Rev. Letters 22, 867 (1969).

5) H.L. Berk, L.D. Pearlstein and J.D. Cordey, in preparation.

PLASMA CONTAINMENT IN THE MAGNETIC WELL M.T.S.E. II

by

D.E.T.F. Ashby, E.L. Bydder, J.W. Hill, M.H. Hughes & D.W. Mason
U.K.A.E.A., Culham Laboratory, Abingdon, Berkshire, England

ABSTRACT M.T.S.E. II is a large pulsed magnetic well, filled by injection from a plasma gun. Experiments show that ion scattering is not caused by Coulomb collisions although the energy transfer between ions and electrons does appear to be classical. Electric fields of ~ 1v/cm are observed at frequencies up to ω_{ci}.

INTRODUCTION The results to be described have been obtained since the Novosibirsk Conference[1]. Several extra diagnostics are now employed including a diamagnetic loop, an 8 mm interferometer, an atomic beam using Kr or Xe for determining T_e[2] and double electric probes for measuring fluctuating electric fields. In addition titanium getters have reduced the background pressure in the vacuum system and desorption from the walls of the vacuum chamber; as a result the duration of fast atom emission has increased by a factor of 3-4. Finally a new divertor system has reduced considerably the amount of cold plasma which drifts along the injection line and into the trap after the initial filling stage; in the past the presence of this cold plasma[2] confused the measurements of $\int n d\ell$ and T_e.

EXPERIMENTAL RESULTS Typical parameters are as follows: B_z = 1.8kG, mirror ratio R=1.7, well depth = 1.3-1.1, ion energy $W_i \simeq 1.5$ keV, $T_e \simeq 15$ eV and the initial plasma density $n_o \simeq 4 \times 10^{12}$ cm^{-3}. The contained plasma shows a rapid initial decay for ~ 200μsec, when 70% of the plasma is lost, followed by a steady loss lasting for ~ 1.5 msec. This rapid loss is associated with the initial velocity space distribution which peaks near the loss cone angle θ_c; hence small angle scattering causes ions to move into the loss cone and escape. The distribution has been estimated experimentally by comparing the initial trapped diamagnetism at different mirror ratios and hence at different values of θ_c.

The measured values of $\int n d\ell$ and diamagnetism have been used to deduce W_i and n. The behaviour of W_i shows that the ions are cooled by the trapped electrons. The electron temperature deduced from dW_i/dt compares with T_e measured by the attenuation of the Kr and Xe beams as follows:
$T_e(Kr)/T_e(cooling) = 1.9 \pm 0.7$ (standard deviation of 23 obs.);
$T_e(Xe)/T_e(cooling) = 2.8 \pm 0.9$ (standard deviation of 13 obs.).
From this result it is concluded that the energy transfer rate between ions and electrons is essentially classical.

The measured plasma loss rate has been compared with theory using the equation $(\tau/n)\ (dn/dt)=1$, where τ is the time for an ion to be scattered into the loss cone. Classical behaviour predicts that $\tau \simeq \tau_{ii} \log_{10} R$, where τ_{ii} is the ion-ion collision time given by Spitzer. When the values of W_i and n, deduced from diamagnetism and $\int n d\ell$ measured at 200μsec, are substituted into the above equations

$(\tau/n)\ (dn/dt) = 32 \pm 22$ (standard deviation of 26 obs.);
this result shows that τ is an order of magnitude smaller than the classical value and does not have the $W_i^{3/2}/n$ dependence characteristic of Coulomb collisions. (The latter fact is demonstrated by the large standard deviation). The behaviour of density with time suggests that the ion-scattering time τ is constant; this is shown by evaluating $(1/n)\ (dn/dt)$ for the previous data, i.e.

$(1/n)\ (dn/dt) = \tau^{-1} = (4.71 \pm 0.95) \times 10^3$ sec^{-1}.

The behaviour of $(\tau/n)\ (dn/dt)$ is shown more completely in the two figures. The curves show the expected behaviour as the initial angular distributions A, B and C, assume steady profiles; they were obtained by numerically solving the diffusion equation on the assumption that the ions are monoenergetic.

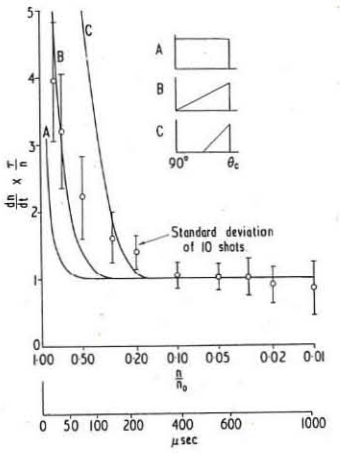

Fig. 1
$(\tau/n)\ (dn/dt)$ against n/n_o for τ=250μsec. The solid curves show the effect of the three initial angular distributions A,B,C.

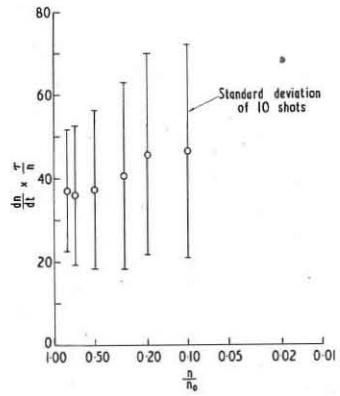

Fig. 2
$(\tau/n)\ (dn/dt)$ against n/n_o for $\tau = \tau_{ii} \log_{10} R$ where τ_{ii} is the Spitzer ion-ion collision time. If the plasma loss were classical the experimental points would behave like the solid curves in Fig. 1.

The behaviour of fast atom emission from the confined plasma also suggests that Coulomb collisions are not responsible for the ion scattering. The signals from three detectors, viewing the plasma from different angles (+ 68°, 90°, - 68° with respect to horizontal axis) differ initially, while the velocity space distribution is changing, and then decay smoothly. The time at which the smooth decay commences (~400μsec) is the same for both 1keV and 4keV emission; if Coulomb collisions caused the ion scattering the 4keV ions would take six times longer to reach a steady distribution.

Double electric probe measurements show the existence of fluctuating electric fields of ~ 1v/cm at frequencies up to ω_{ci}. Measurements across the plasma diameter show potential fluctuations of ~50V between r = ± 15 cm. Together these two measurements show there is probably no more than one complete wavelength around the plasma circumference. Simple calculation shows that fluctuations of 1v/cm are capable of causing the plasma to escape with the observed e-folding time of 250μsec; however it has not been possible to identify the instability responsible for the fluctuations and plasma loss.

(1) G. Francis, J.W. Hill, B. McNamara and D.W. Mason Proc. 3rd Conf. Plasma Phys. and Controlled Fusion, Novosibirsk (1968) CN-24/H3 II 239, Pub. IAEA Vienna (1969).

(2) M.H. Hughes, J.W. Hill and B.D. Cooper, 3rd Eur. Conf. Controlled Fusion & Plasma Phys. Utrecht (1969). Gromingen, Wolters-Noordhoff 13, (1969).

HOT IONS AND DIFFERENTIAL ROTATION IN A NON-MAXWELLIAN PLASMA WITH A STATIC PARALLEL ELECTRIC FIELD

by

Hopfgarten, N., Johansson, R.B., Nilsson, B.H. and Persson, H.

Division of Plasma Physics,
ROYAL INSTITUTE OF TECHNOLOGY,
Stockholm 70, Sweden.

Abstract: Energetic ions of a Penning discharge in a strongly inhomogeneous magnetic mirror field are investigated. The measurements strongly suggest a fast rotational drift with violation of the isorotation law, and non-Maxwellian velocity distributions. An explanation involving both parallel and transverse electric fields is proposed. In one of the mirror regions a shock-like structure is observed.

We have studied a Penning discharge in a strongly inhomogeneous magnetic mirror field, with two cathodes in the mirrors, and a ring-shaped anode in the midplane, [1]. The aim is to investigate a) whether a significant electric field component $E_{\parallel}$ is established along the magnetic field, b) whether energetic ions are produced in such a discharge, c) the energy distribution of such ions, and d) the role played by the parallel electric field for the ion heating.

Theoretical investigations show that electric fields - of other origin than v x B polarization, or classical resistivity - can be produced by a) a longitudinal magnetic gradient, [1+ref. cit., 2, 3], b) sheath (shock) structures, [4+ref. cit., 5], or c) turbulent resistivity, [6, 7]. None of these possibilities can be a priori ruled out in the present experiment.

Among the consequences and applications of a parallel electric field we wish to mention the following:

1. The frozen-in condition, (with the special case the isorotation law), will no longer be valid. Thus any heuristic description in terms of magnetic field lines moving with the plasma will be doubtful.
2. In nuclear fusion research $E_{\parallel}$ has been suggested as a mechanism for ion heating, [8, 1], as a natural constituent of the loss-production balance in mirror devices, [3], and as an important feature of practically any plasma under fusion conditions.
3. $E_{\parallel}$ is believed to be essential in geophysics and cosmogonic theory.

Hydrogen gas of $(1.5\text{-}50)\cdot10^{-4}$ Torr pressure is used in the discharge, [1]. The mirror ratio of the magnetic field can be varied between 20 and 100. The burning voltage was found to be 0.5-15 kV, and the current 1-10 A/cathode.

Two modes of the discharge were found to exist, with the pertinent mode determined by the magnetic field strength in the anode plane. In the high magnetic field mode energetic ions are moving perpendicular to the magnetic field, and the discharge is burning unsymmetrically, i.e. the cathode voltages are different even with equal cathode resistors. The high magnetic field mode appears when the gyro radii of ions with sufficiently large magnetic moments to be axially confined are smaller than the radial dimensions.

The classical mean free path for energetic ions, determined by charge exchange, (2 m at the lowest pressure), is larger than the dimensions. Electron gyro radii and Debye length are negligibly small. From measurements of the cathode heating the density and energy of the current-carrying ions are estimated to 10^{10}-10^{11} cm^{-3}, and 1-5 keV, respectively. The degree of ionization becomes 10^{-3}-10^{-2}.

The present report concerns the high magnetic field mode, in particular the properties of the emission of fast neutral particles. Their velocity distribution faithfully reflects that of the ions. Two instruments have been used; one is a scintillator with a photomultiplier, in the other the particles are stripped in a gas cell and then electrostatically analysed. Both instruments accept particles from a line segment through the plasma. A determination of the local velocity distribution is not possible in this case, since the angular dependence of the emission is not a priori known. The measurements discriminate between different models of the plasma, and suggest a unifying interpretation of all types of measurements. The analyser provides energy spectra, but is complex to use. Often detailed information from energy spectra is not needed, and the scintillator detector can be used. The signal from this detector is proportional to the excess energy above the threshold 2 keV.

Measurements with different position and orientation of the instruments reveal a remarkably high reproducibility, and - concerning measurements perpendicular to the magnetic field - a high azimuthal symmetry as well.

The results can be summarized as follows:

A. Energetic ions, (3-8 keV), moving perpendicular to the magnetic field, are found mainly in front of the low-voltage cathode, while no such ions are observed in the opposite half of the apparatus.

B. The detector signal, with the detector oriented perpendicular to the magnetic field, is shown in Fig. 1 as a function of axial distance z and the distance r (with sign) between the line of sight and the axis. In the lower part of the figure the cathode is indicated. Clearly, the signal is highly unsymmetric with respect to the axis. (Qualitatively the same phenomenon is observed with the analyser.) The sense of the asymmetry is changed with the direction of the magnetic field. The low-signal side is opposite to what one would expect on the basis of a plasma without rotation, or a rotation much slower than the gyrational motion. This suggests the explanation that the plasma is rotating with a velocity of the order of the total velocity. This conclusion holds, even if very special distributions of gyro centra are considered.

Fig. 1

C. Fig. 1, taken at $3\cdot10^{-4}$ Torr, exhibits oscillating structures both in the r and z directions. With increasing pressure the structure becomes less pronounced; the radial structure disappears, and the curves become symmetric with respect to r at $9\cdot10^{-4}$ Torr. The axial variation persists as far as $4\cdot10^{-3}$ Torr. Thus, no rotation, (item B above), takes place at high pressures, which may be due to neutral gas drag. Incidentally, a structure similar to the axial variation is found, when the detector is fixed, and the magnetic field is varied.

D. Analyser measurements reveal an essentially monoenergetic ion distribution for a line segment with r=0. For some values of z the peak of the spectrum is split into two for $r\neq0$. It is remarkable that such pronounced deviations from Maxwellian distributions occur in a gas discharge without any external injection, and this may be a result of an acceleration mechanism that involves $E_{\parallel}$.

Using the picture of ions with given energy of rotational drift in the cathode region (in our case 5 keV), and different assumptions on the transfer of angular momentum along the inhomogeneous magnetic field, we can calculate the rotational energy in the anode region. With the angular velocity constant - isorotation - the energy would (in the present geometry) be increased by a factor equal to the mirror ratio (40), resulting in an energy of 200 keV. With the mechanical angular momentum constant, the energy would instead be decreased by the same factor, giving 125 eV ions in the anode region. All measurements favour the latter picture.

Thus, when the ions move into the funnel-shaped part of the magnetic mirror field, the velocity of rotation is not decreased like in an isorotating medium, but instead increased like in a free whirl.

From the energy of rotation the radial electric field can be estimated, and it is found that the magnetic field lines are not equipotentials.

The complicated structure in Fig. 1 may be due to some interference or shock phenomenon. The axial structure would then be associated with the linear momentum of the ions, and the radial variation with the angular momentum.

References

1. N. Hopfgarten et al., Phys. Fluids 11, 2272 (1968); 2. F.L. Hinton and C. Oberman, Report MATT-686, Plasma Physics Laboratory, Princeton Univ., New Jersey (1969); 3. D.J. BenDaniel, Plasma Physics 3, 235 (1961); 4. H. Persson, Report 69-05, Division of Plasma Physics, Royal Inst. of Techn., Stockholm (1969); 5. S. Torvén, Report 69-18, Division of Electron Physics, Royal Inst. of Techn., Stockholm (1969); 6. J. Adlam and L.S. Holmes, in Plasma Physics and Controlled Nuclear Fusion Research (IAEA, Vienna 1962), Part 3, p. 1121; 7. M.V. Babykin et al., in Plasma Physics and Controlled Nuclear Fusion Research (IAEA, Vienna 1962), Part 3, p. 1073; 8. T. Consoli, in Plasma Physics and Controlled Nuclear Fusion Research (IAEA, Vienna 1966), Vol. II, p. 483.

PLASMA INJECTION AND ADIABATIC COMPRESSION EXPERIMENT
(PIACE) BY FAST RISING MAGNETIC FIELD

by

K. Hirano, H. Kishimoto, M. Ushio and H. Itô

Plasma Physics Laboratory, Faculty of Engineering, Osaka University, Yamada-Kami, Suita, Osaka, Japan.

Abstract: High β plasmas from two conical theta-pinch guns are injected and collided with each other in the mirror field produced by four single turn coils. Observation by S.T.L. framing photographs shows that two plasma puffs seem to meet just at the center of the apparatus and stay about 16 μsec or longer. The main compression field, which rises to 3.0 Wb/m^2 within 1.4 μsec, is powered by 60 kV and 126 kJ fast condenser banks with crowbar circuit.

The aim of our experiment is to study fast collisionless adiabatic compression which seems one of the most efficient methods for heating high density plasmas. To realize such a compression, the temperature of the plasma to be compressed must be so high that the mean free path of ion-ion collision is much longer than the radius of the discharge tube. The fast rise of the compression field is also required, since the compression phase must be finished before considerable amount of energy is lost from the plasma. Taking account of these conditions, we have constructed the apparatus called "PIACE" (Plasma Injection and Adiabatic Compression Experiment). Since the detailed construction and performance of our apparatus will be reported in the coming symposium on fusion technology held at Aachen, we shall describe it only briefly here. Its schematic drawing is given in fig.1. As shown in this figure, it has a bisymmetric construction. It consists of a pair of conical theta-pinch guns on each end, plasma guiding parts and the main compression part equipped with four single turn coils. Each high β plasma produced by the gun is introduced into the main compression part through the guiding field which makes the plasma free from touching the wall of the discharge tube. Each compression coil is connected to its own condenser bank, so that compression field can be excited at any time with chosen polarities.

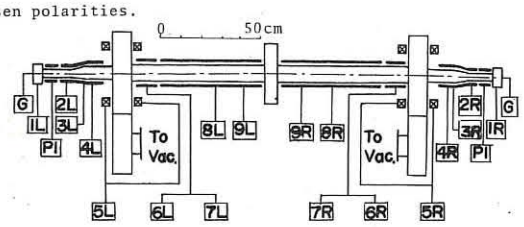

Fig. 1. Schematic drawing of the apparatus. G) Gas Reservoir 1) Gas Valve Bank PI) Pre-Ionization R.F.Power Source 2) Theta-Gun Main Bank 3) Pre-Heating Bank 4) Theta-Gun Bias Bank 5) Plasma Guide Bank 6) 1st Coil Main Bank 7) 1st Coil Bias Bank 8) 2nd Coil Main Bank 9) 2nd Coil Bias Bank

As a result, several field patterns are realized. It is noted that the first compression coils can be used as a gate coils to prevent the inflow of low temperature plasmas to the compression region. Characteristic parameters of our device are summarized in the table below.

	Charging Voltage (kV)	Stored Energy (kJ)	Field Rise Time (μsec)	Max. Mag. Field (Wb/m^2)	Max. Mag. Rise Speed (Wb/m^{2}sec)
Gun	60	18×2	1.1	3.3	4.5×10^6
1st Coil	60	15×2	1.2	2.7	3.5×10^6
2nd Coil	60	48×2	1.4	3.0	3.4×10^6

Table 1. Characteristic Parameters of the fast discharge system of the device.

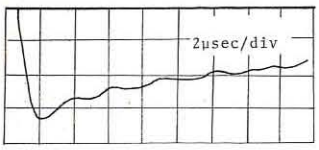

Fig. 2. Crowbared current wave form through the coil.

A typical current wave form through the compression coil is seen in fig.2. As the first stage of our experiment, we have studied the operating conditions of the gun using He gas. We have found some suitable conditions under which the guide field is completely excluded by streaming plasma along the axis of the discharge tube. A typical magnetic probe signal in the guiding part is seen in fig.3. The flight velocity of the plasma puff is about 2×10^7 cm/sec. We could make no big difference between the operating characteristics of the both guns. For the preliminary experiments, we tried to let two plasma puffs from the guns encounter in the central part of the device initially appling the mirror field. Field distribution along the axis is shown in fig.4.

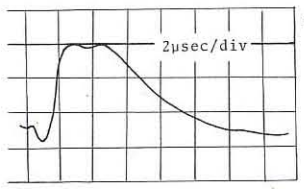

Fig. 3. A magnetic probe signal in the plasma guiding part.

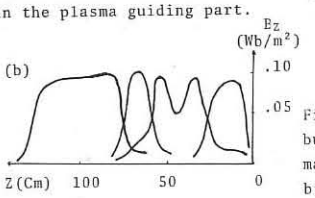

Fig. 4. Magnetic field distribution along the axis. (a): main compression field. (b): bias and guide field.

We have succeeded in encountering that two plasma puffs just at the central plane of the apparatus. Such a process can be seen from the S.T.L. framing photographs shown in fig.5.

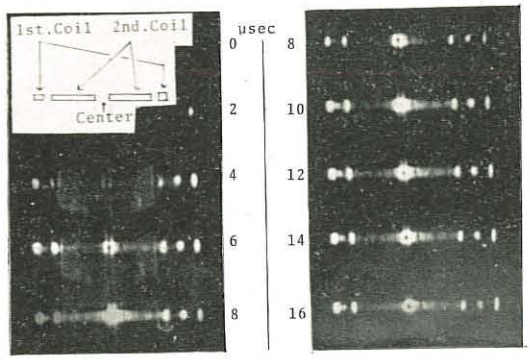

Fig. 5. S.T.L. framing photographs; plasma puffs are seen to encounter just at the center of the apparatus.

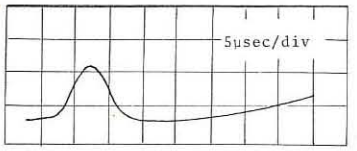

Fig. 6. Magnetic probe signal at the center of the apparatus.

The mirror ratio of our field is 1.7 , but the plasma seems to be very stable all the time before it fades out. On the magnetic probe signal shown in fig.6, high frequency oscillation does not appear, although the β value is greatly reduced from that in the guide field. This was due to the dip of the guide field formed by the pumping port. The exclusion of this dip was furnished by insertion of some correction coils into the vacuum tube. Consequently, we could obtain β=1 plasma at the central region of the apparatus. Experiments are now going on to realize the fast adiabatic compression of the high density plasmas.

Particle loss from the Polytron

J.D. Kilkenny and A.E. Dangor
Physics Dept., Imperial College,
London, England.

Abstract: Single particle calculations of the ion motion in the polytron configuration show that particles situated inside a volume close to the minor axis are contained indefinitely. Particles situated outside this volume are lost. Experimental confirmation of this loss region is presented.

The polytron experiment attempts to contain a high temperature plasma in a series of magnetic cusps arranged in the form of a torus. Leakage from the ring cusp should be prevented by accelerating the plasma in the toroidal direction by the application of a toroidal electric field E_ϕ. In previous experiments (1,2) it was found that a rapid leakage occurred about 1 μsec after the application of the electric field. Doppler shift measurements and spectroscopic temperature estimates indicate that the condition $V_d < V_H$ where V_d is the ion drift velocity in the toroidal direction and V_H is the thermal velocity of the ion is only marginally satisfied. This condition is thought to be necessary to avoid the normal thermal losses through the ring cusp. However a single particle calculation shows that $\underline{V}x\underline{B}$ forces on the particle can give rise to additional leakage, which is found to dominate experimentally.

The equation of motion of a particle is solved numerically, taking the actual vacuum magnetic field produced by the 36 toroidally placed cusp coils, and starting the particles at rest. The motion of ions fall into three categories. Firstly there are those particles located near the magnetic axis which are accelerated in the toroidal direction straight through the magnetic

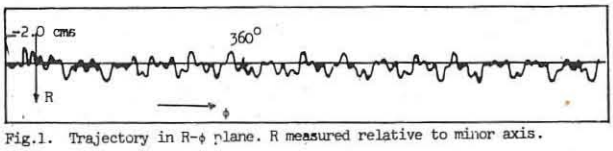

Fig.1. Trajectory in R-φ plane. R measured relative to minor axis.

cusps. Secondly, further away from the axis, the particles are reflected by the magnetic field towards the minor axis, whereupon reaching a region of smaller radial magnetic field they are accelerated and behave as particles in the first category. The third category of particles are still further off the magnetic axis. These particles are lost straight through the ring cusp. In all cases the instantaneous Larmor radius of the ions is comparable with or larger than the dimensions of the cusp field, and each coil acts as a focussing magnetic lens to the ions which are accelerated through.

In the toroidal configuration all of the ions which are accelerated initially are eventually lost, because of the dominance at high velocities of the centrifugal force. However when collisions are included we would expect a limiting ion velocity $v_d = \sigma E\phi/ne$. This is simulated in the model by making the toroidal electric field $E_\phi = E_o(1-v_\phi/v_d)$. With this modification the ions can be contained indefinitely as long as $5.0\ 10^6 V_c Z/A > v_d > 2.1\ 10^4\ V_c Z/A$ m/s for this geometry. Fig. 1 shows such an ion trajectory in the R-φ plane. The field strength is specified by V_c, the charging voltage of the cusp bank in kV : 1 kV is equivalent to an average radial field of .3tesla. Z and A are the ionic charge and atomic weight respectively. This can be compared with a Busch formula, fig. 2, for a magnetic lens

$$\Delta\psi = \frac{\delta}{f} = \frac{1}{4v_d^2}\left(\frac{\overline{eB_\phi}}{m}\right)^2 L\delta$$

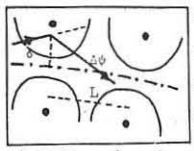

Fig.2. Focussing of particle by cusp field.

We require $\overline{\Delta\psi} = \frac{L}{R_o} = \frac{2\pi}{36}$ where R_o is the major radius. So a particle with a large δ undergoes a large deflexion. There is also a rotation of the particle about the minor axis of $\Delta\theta = \frac{1}{2}(\frac{e}{m})\frac{L}{v_d}$ which alternates in sign through successive cusps. In order that particles do not accumulate a large angle between their trajectories and the minor axis we require $\overline{\Delta\theta} < 1$ and as $\overline{\delta} < a$ (the tube radius) both conditions can be satisfied if $\frac{L}{2}\frac{eB_\phi}{m} < v_d < \frac{1}{2}\frac{\overline{eB_\phi}}{m}\overline{aR_o}$.

Numerical agreement is reasonable.

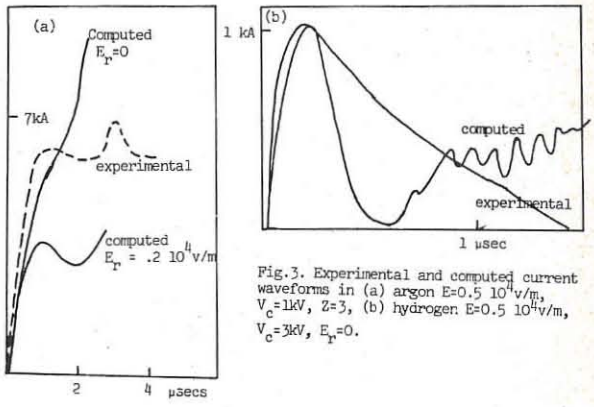

Fig.3. Experimental and computed current waveforms in (a) argon E=0.5 10^4v/m, V_c=1kV, Z=3, (b) hydrogen E=0.5 10^4v/m, V_c=3kV, E_r=0.

The number of electrons which belong to the first and second category is very small and originate very close to the magnetic axis. The radial loss of these electrons will be prevented by electrostatic fields and to allow for this a radial field is included in the calculation. To compare the particle motion and losses in this computational analysis with experimental results a reasonable number of particles (256), distributed uniformly throughout the region of the discharge vessel are taken. As particles reach the wall in the calculation they are removed. It is found that losses are limited to the ring cusp region, and shift in the direction of the applied electric field. Experimental evidence for this exists in framing camera photographs of the discharge which show that at the time losses are predicted the wall at the ring cusp becomes luminous. A shift in the E_ϕ direction is also observed. Ion probes measuring the flux of particles also give an appreciable signal at this time. Fig. 3 shows the calculated and experimental toroidal currents. The fall off in the current is caused by particle loss. Good experimental agreement is obtained by including a radial electrostatic field equivalent to a temperature of 70 eV.

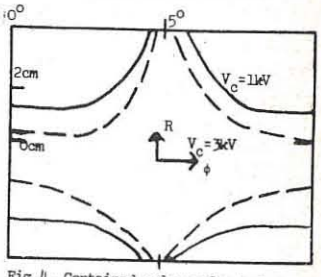

Fig.4. Contained volumes for hydrogen, E_ϕ=.5 10^4v/m. The ring cusp is at φ=5°.

The volumes from which lost and accelerated plasma originates are shown in fig. 4. The dependence of the contained volume on B, E_ϕ and e/m can be obtained as follows. Assuming cylindrical symmetry and using the constancy of canonical angular momentum and energy $|r^2\cos kz - r_o^2\cos kz_o| \leq |\frac{r}{E_o}(\frac{2zmE_z}{e})^{\frac{1}{2}}|$ where (r_o, z_c) specify the initial position of the particle. The field is taken as $B_z = B_o\cos kz$, $B_r = \frac{1}{2}kr\sin kz$. Since r<a, the tube radius, particles are lost if

$$r_o > \left(\frac{a}{B_o|\cos kz_o|}\left(\frac{\pi}{k}\frac{mE_z}{e}\right)^{\frac{1}{2}}\right)^{\frac{1}{2}}.$$

This dependence is in agreement with the calculations and the experiment.

Ref.: (1) Dangor et.al., 1968, Novosibisk, Vol.I, p.255 (IAEA).
(2) Dangor et.al., 1969, Utrecht, p.83 (Wolters-Noordhoff).

A QUIESCENT E.C.R. DISCHARGE, PRODUCED WITH A LISITANO ANTENNA IN A MIN. B-FIELD CONFIGURATION

By A.Goede and G.J.Brakenhoff

Association Euratom-FOM

FOM-Instituut voor Atoom- en Molecuulfysica, Kruislaan 407, Amsterdam. The Netherlands.

ABSTRACT: The stabilization of low frequency plasma instabilities in a min. B-field is well-known. Suchs fields are often produced by means of Joffe bars. Here we create such a field by adding to a magnetic mirror field the transverse field of permanent magnets. At not too high field strengths, this is a technically simple method to obtain a min. B-field configuration. In the E.C.R. plasma, in which the experiment is performed we get a decrease of density fluctuation level from about 10% to 0.2%.

The magnetic material we use is Philips Ferroxdure K6 in slab form (dim. 5 x 2 x 0.5 cm). The magnetization direction is perpendicular to the slab plane. The magnets are fixed in six strips of 120 x 2 x 1 cm, which are symmetrically mounted along the plasma column in a stainless steel frame. The arrangement of the strips is shown in the cross section fig. 1a. Also some field lines are sketched, which are similar with Joffe bars in a hexapole configuration. In fig. 1b the radial dependence of B_r and B_z along the cross sections I and II is given. The field strength increases with the square of the radius along the lines I and II. The coercive force of these permanent magnets is sufficient to withstand demagnetization by the main B_z-field. Superimposed on the B_z-field we get with this structure a radial mirror ratio $R_\perp$ = 1.1, when the field is adjusted for E.C.R., i.e. $|\vec{B}|$ = 876 Gauss. Plasma is generated by the electron cyclotron resonance

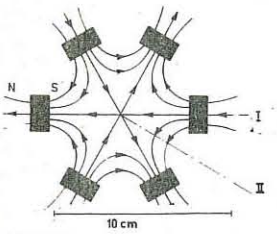

Figure 1a.

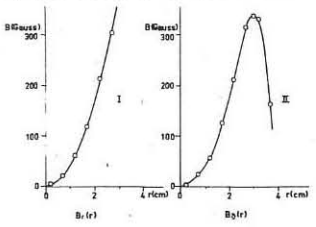

Figure 1b.

method (E.C.R.). The h.f. wave energy is coupled into the plasma with a so called Lisitano microwave antenna [1]. This is in fact a folded slot antenna, cut out in the surface of a cylindrical metal tube, which surrounds a short section of the plasma column. The structure is fed with typically 25-60 Watt C.W. R.F.-power at 2.45 GHz. For the measurements presented here, plasma is created in Helium gas, neutral gas pressure range: 3×10^{-4} torr to 3×10^{-3} torr. The B_z-field in our experiment consists of an axial homogeneous part ($\pm$ ½%) of 60 cm length, with magnetic mirrors at both ends, mirror ratio $R_\parallel$ = 1.8. The antenna can be moved axially along the system. When the antenna is positioned in the homogeneous part, in the beginning of the magnetic bottle, we get optimum plasma production.

The most important result of the addition of the min. B-field made with the permanent magnets is the reduction in fluctuation level by about a factor 50, compared with the magnetic mirror only. The radial dependence of this fluctuation level in both cases is given in fig. 2, in case of min. B measured at 3 values of the magnetic field. The increase of the fluctuations towards the plasma boundaries is not observed anymore with the minimum B-field. The plotted fluctuation level is the root mean square (r.m.s.) value of the fluctuations in the ion saturation current observed on a negarively biased Langmuir probe, divided by the total ion saturation current.

We should point out here, that the plotted fluctuation level is the net-value of the fluctuations, ignoring the changes in density caused by variations at the line frequency of the R.F. power and the main magnetic field. The contribution of this effect is without min. B much smaller than the real plasma fluctuations. With min. B the line frequency contribution amounts 0.3 to 1%, depending on conditions.

We will now consider the effect of addition of the min. B-field on plasma density and on electron temperature. We find that the electron temperature is nearly the same in both cases: about 10 eV.

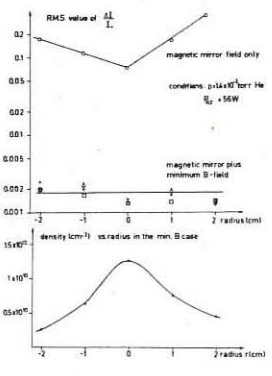

Figure 2.

The influence of plasma density is shown in Table I.

	Without min. B.	with min. B-field	
	P_{RF}=28 W; P_{refl}=5 W	P_{RF}=28 W; P_{refl}=17 W	P_{RF}=56 W; P_{refl}=33 W
n_o	2.6×10^{10} cm^{-3}	1.2×10^{10} cm^{-3}	2.2×10^{10} cm^{-3}

Table I. Conditions: gas pressure 7×10^{-4} torr Helium.

We see that the density is reduced with min. B added, but that because of the changed coupling conditions the power reflected back from the Lisitano antenna increases. If we increase the power level in such a way, that the absorbed power in the plasma attaines the same value as without min. B, then the density returns to about its previous level. The values for the plasma density in Table I are obtained from the ion saturation part of a Langmuir probe characteristic, using Langmuirs orbital-motion theory[2,3] . Data from the dispersion characteristics of the propagation of an electron plasma wave [4] give a 30% lower value for the densities, but with the same relative difference.

In fig. 3 we have plotted plasma density fluctuations as function of plasma density. Here we assume, that the variations in ion saturation current represent the fluctuations in plasma density. We see that the fluctuation level stays below 0.5% in the density range 5.10^9 cm^{-3} to 10^{11} cm^{-3}.

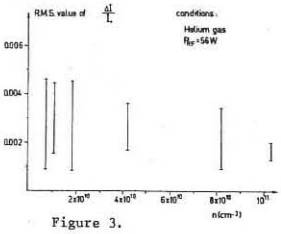

Figure 3.

The density of an E.C.R. plasma depends on the gas pressure, R.F. power and on the specific resonance conditions as determined by the value of the main B_z-field in the interval in which plasma can be produced. The fluctuation ranges as given in fig. 3 are those as observed at the specified densities, which are obtained however at various combinations of gas pressure and magnetic field. The lowest fluctuation levels observed, are somewhat below 0.1%. We found about the same values by using Argon as dischange gas. The frequency power spectrum of the fluctuations, monotonically decreasing towards higher frequencies, is mainly concentrated in the band 1 to 300 kHz.

DISCUSSION: We found that the plasma stabilized by the min. B-field has densities of about the same order as without min. B. This is somewhat surprising as one would expect that, with reduction of plasma losses connected with the suppressed instabilities, higher densities would be reached. However density limitations in min. B configurations depending on the value of $R_\perp$, have been encountered before [5]. At $R_\perp$ = 1.1 a density limitation of $n \approx 5.10^9$ cm^{-3} was found, set by an anomalously fast plasma loss in the decay. The cause for this is unknown. Now it is remarkable that we have plasma stabilization up to much higher densities (10^{11} cm^{-3}), without any instability present. So we tend to think that plasma loss in our case is not connected with fluctuations, but that other mechanisms play a role; for instance particle loss along the magnetic field lines, from which now end some on a conducting surface without passing the magnetic mirrors.

REFERENCES

[1] Lisitano, G. (1966) Proc. of the VII conf. on phenomena in ionized gases I, Belgrade, 464.

[2] Chen, F.F. et al. (1968) Physics of Fluids 11, 811.

[3] Cohen, A.J. (1969) MIT quarterly progress report 94, 106.

[4] Matitti, T. et al. (1969) Proc. of the IX conf. on phenomena in ionized gases I, Bucharest, 471.

[5] Baiborodov, Y.T. et al. (1968) Proc. of the Novosibirsk conf. Nuclear Fusion special supplement, 159 (1969).

THE BUILD UP OF A PLASMA IN A MAGNETIC WELL WITH A MULTI-ENERGY AND MULTI-ANGLE NEUTRAL ATOM INJECTION SYSTEM

by

R.Dei-cas, F.Hennion
ASSOCIATION EURATOM-CEA
Département de la Physique du Plasma et de la Fusion Contrôlée
Centre d'Etudes Nucléaires
Boîte Postale n° 6 **92 Fontenay-aux-Roses** (France)

Abstract : Numerical calculations of the plasma build up, anisotropy and energy distribution are presented for a neutral multi-injection system (10 injectors) in a quadripolar coil. With an equivalent current of 0,72 A ; $p_o \simeq 3.10^{-8}$ torr ; B_o= 10 KGs ; well depth R = 2, we can obtain a plasma having the following characteristics : $n_i > 10^{13}$ cm^{-3}, $T_i \simeq$ 5-10 KeV ; $\Delta E/E > 1$; $T_{//i}/T_{\perp i} \simeq 0,4$ in a volume of 30 liters.

The present experiments on fast neutral injection in a magnetic well (ALICE, OGRA 2, PHOENIX 2) are limited in density by the instabilities resulting from anisotropy of the distribution function due to the injection method. These instabilities cause a loss of particles and prevent the build up of the plasma. In order to suppress this kind of instabilities we have to spread the injection angles. At higher densities, when the ion plasma frequency is of the order of or exceeds the cyclotron frequency, the drift loss cone instability can develop ; an energy spread and a smooth density gradient will stabilize this instability. To satisfy these stability conditions, a multi-angle neutral injection experiment in a quadripolar configuration has been proposed [1]. The energy distribution and the isotropy of injection should be obtained by the help of ten injectors at different potential and located in a 50° sector in such a way that the Lorentz capture is optimum (fig.1). In the ALICE device the broadening of the distribution function should be obtained by collisional effects [2]. The object of this work is to study the density build up and the evolution of the distribution function as a function of time and space in realistic conditions [3]. Each injection line is divided into ten source elements, thus with ten injectors we have to follow the evolution of 100 partial densities ; at each ionisation point we know the first adiabatic invarant (μ) of the particle, so we can attribute a volume for each source element, that is to say we suppose that the particle fills uniformly the volume defined by the conservation. By different sommations of these partial densities we can obtain the local density, the anisotropy and the energy distribution.

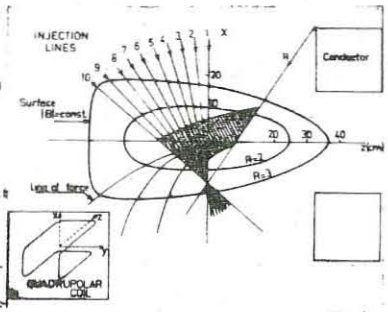

Fig.1 - Injection lines and capture zone (hatchured)
The injection plan is the xz plan in the fig.1 a

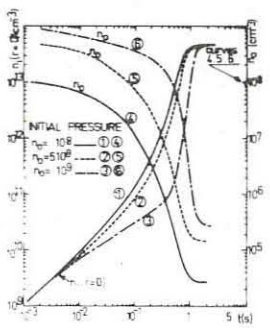

Fig.2 - Plasma build up. Curves 1,2,3 plasma density and 4,5,6 neutral density inside the plasma.

In our model we take into account the Lorentz trapping coefficient, the cascading effect, the variation of the residual pressure inside and outside the plasma, the wall desorption effects. We don't take into account the energy exchange between the hundred partial populations, which is a valuable approximation in our case for densities up to 10^{12} to 10^{13} cm^{-3}. The density build up depends on a number of parameters ; the figure 2 shows, for a typical case, the evolution of the plasma density and the residual pressure at the center, for different initial pressures. The main parameters are the following : equivalent current and energy are distributed from 125 mA, 20keV for the injector n°1 to 20 mA, 2 keV for the injector n°10; desorption coefficient γ = 0,2. The total injected current is 0,72 A eq. for a mean plasma volume of 30 liters and with an initial pressure in the range of 10^{-8} to 3.10^{-8} mmHg. That is comparable to the necessary conditions for a reactor : injected current of the order of 1 A for 25 lit. of plasma. In Fig.3 is shown the influence of the wall desorption coefficient under particle bombardment. In Fig.4 is shown an exemple of the energy spectrum at different radius. Fig.5 gives the density gradient and the mean anisotropy $\tau = T_{\perp i}/T_{//i}$ as a function of the radius ; we see that we can obtain a mean anisotropy of the order of $\tau \sim 0,4$-$0,5$.

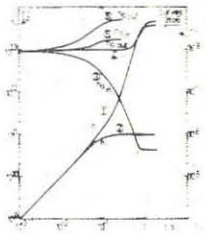

Fig.3 Effect of the desorption coefficient on the plasma build up. Curves 1,2: plasma density ; 3,5 : pressure inside the plasma ; 4,6 : pressure outside the plasma. γ = 1 for curves 1,3,5 and γ = 1,5 for curves 2,4,6.

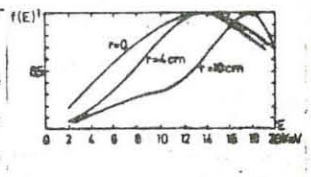

Fig.4 : Distribution function at different radius.

Above a density of 10^{12} cm^{-3} the plasma outside the capture zone will be opaque to the excited atoms and the Lorentz trapping becomes ineffective, the injection should be done along a line where the non trapping region is minimum for exemple along the line n° 11 (fig.1). For these densities the collisional effects will broaden the distribution function.

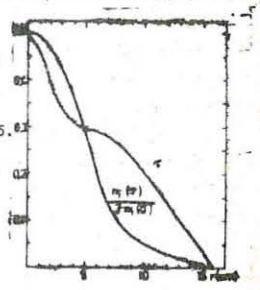

Fig.5 - Mean anisotropy $\tau = T_{//i}/T_{\perp i}$ and density profil.

In conclusion we can say that :

- this multi-injection system should allow to control the distribution functions which is important to understand their effect on the microinstabilities,
- with the anisotropy (fig.5) and the energy distribution obtained (fig.4) this plasma should be stable up to 10^{12} to 10^{13} cm^{-3} that is to say in the range of thermonuclear interest : $\omega pi/\omega ci \simeq 10$ to 30, mean energy 10 KeV, B_o = 10 KG; life time 0,1 to 0,2 s. These parameters are those of a plasma "model" for a thermonuclear plasma. If these values can be obtained, this will demonstrate the possibility to confine a thermonuclear plasma in an open ended system.

Références :

[1] Rapport annuel EUR-CEA - FC 420 (1966), R. DEI-CAS EUR.CEA FC 454 (1967)

[2] R.F. POST, C.C.DAMM, J.H. FOOTE.UCID15181 (1967)

[3] R. DEI-CAS, F. HENNION. NI 1057 (1969)-BAPS vol.11 (1969)

PLASMA FORMATION BY DISSOCIATION OF AN ACCELERATED HYDROGEN CLUSTER BEAM

F. Bottiglioni, J. Coutant, M. Fois.

ASSOCIATION EURATOM-CEA
Département de la Physique du Plasma et de la Fusion Contrôlée
Centre d'Etudes Nucléaires
Boite Postale n° 6 - **92 Fontenay-aux-Roses** (France)

ABSTRACT : The dissociation rate of an hydrogen cluster beam crossing an electron target is calculated with a model involving spontaneous breaking of multicharged clusters.

INTRODUCTION : Dissociation of accelerated condensed particles (clusters) appears to be an attractive way for hot ion plasma formation.

Since Becker and his co-workers have produced the first accelerated beam of condensed hydrogen [1], several similar clusters sources have been built in different plasma laboratories. The expected advantages of this method are :

- high accelerated flux with lower space charge problems
- velocity spread of protons produced by dissociation, due to initial mass dispersion of the clusters
- easy penetration in magnetic fields due to high mass-to-charge ratio

In Fontenay-aux-Roses, the INGRA device, recently achieved, can provide a beam of nitrogen or hydrogen clusters accelerated up to 600 kV. The first purpose of this experiment is to study the process of cluster dissociation in a plasma target, as a function of initial cluster mass. Interpretation of experimental results requires the working out of a dissociation model ; some preliminary calculations made with such a simplified model are presented in this paper.

2. DESCRIPTION OF THE MODEL. This model must take into account the following experimental facts :

- the cross-section for ionisation by electron impact increases with cluster mass [2]
- the mean mass of a cluster beam passing through an electron target decreases with increasing of electron density [3]. This is generally attributed to multiple ionisation : a multicharged cluster being instable breaks, giving rises to two lighter fragments.

The assumptions, this model is based on, are :

1) the reaction occuring when ionisation by electronic impact takes place is the following :

$$H_N^+ + e \longrightarrow H_N^{++} + 2e \longrightarrow H_{fN}^+ + H_{(1-f)N}^+ + 2e$$

-The same reaction can be written for ionic impact.

If the double-charged cluster is stable or if one of the fragments remains neutral, the reaction should be written in two steps

$$H_N^+ + e \longrightarrow H_N^{++} + 2e \qquad H_N^{++} + e \longrightarrow H_N^{+++} + 2e \longrightarrow H_{fN}^+ + H_{(1-f)N}^{++} + 2e$$

or

$$H_N^+ + e \longrightarrow H_N^{++} + 2e \longrightarrow H_{fN} + H_{(1-f)N}^{++} + e \qquad H_{fN} + e \longrightarrow H_{fN}^+$$

Anyway, final results should not be appreciably affected because these processes could be expected only for heavier clusters whose mean free path is very short.

2) the electronic ionisation cross-section of a cluster containing N atoms is taken as

$$\sigma(N, W_e) = A N^{2/3}\left[1 - \exp(-k N^{1/3})\right] \qquad W_e \text{ is the electron energy}$$

In this formula, the term into brackets is the probability of ionisation for an electron passing through the cluster, the density of which is assumed to be the solid hydrogen one's : the $N^{2/3}$ term represents the cluster geometrical cross-section.

The factor A, which depends, like k, upon the electron energy, is determined for each value of electron energy, by equaling the formula for N=2 with the corresponding experimental cross-section of H_2.

This formula does not take into account any recombination effect of secondary electrons inside the cluster; therefore one could expect over evaluated values for heavy clusters.

3) The velocity of the fragments remains always equal to the initial cluster velocity.

4) At a fraction ratio f is associated a probability density $p(f)$, which is an essential parameter of the model ; up to now $p(f)$ has been considered as independant of the cluster mass.

5) A fragment is considered fully dissociated when it's Larmor diameter becomes smaller than the vacuum vessel radius r_c since it will then cross several times the plasma target ; this defines a critical mass number N_c which is a function of magnetic field B, vessel radius r_c and fragment velocity. N_c is the second important parameter of the model.

CALCULATION RESULTS : For each set of parameters and a given mass number N_o of the initial clusters, the mass distribution function $F(N, N_o, \gamma)$ is calculated as a function of γ by solving a system of N_o integro-differentials equations. The computer gives also the capture ratio $K_{N_o, N_c}(\gamma)$ defined as

$$K_{N_c N_o}(\gamma) = \frac{1}{N_o} \sum_{N=1}^{N=N_c} F(N, N_o, \gamma) \qquad \gamma = \frac{x}{\lambda_o}$$

x : traversed length in the target ; λ_o : initial N_o cluster mean free-path

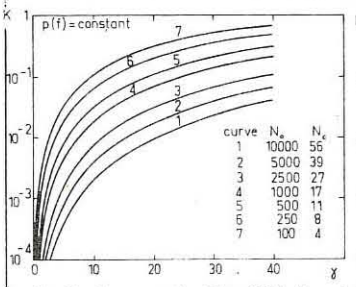

Fig. 1 : Capture ratio K for 600 keV clusters, as a function of γ, for several initial masses N_o. $W_{electrons} = 100$ eV.

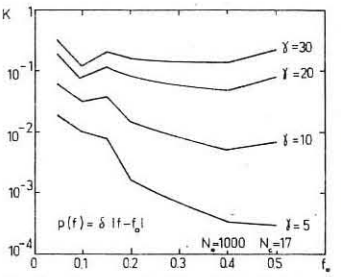

Fig. 2 : Capture ratio K for 600 keV clusters as a function of f_o, for several values of γ. $W_{electrons} = 100$ eV.

Fig. 1 shows for example the capture ratio K for 600 keV clusters and 100 eV electrons. The critical number N_c corresponds to B = 10 kG and r_e = 12,5 cm. In this case $p(f)$ is uniform i.e. the probability density is the same for all possible values of f.

Fig. 2 shows, for $N_o = 1000$, the capture ratio K as a function of f_o for $p(f) = \delta |f - f_o|$, and several values of γ.

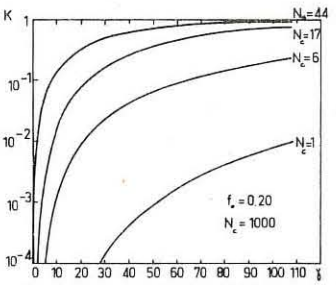

Fig. 3 : Capture ratio K for 600 KeV clusters as a function of γ for several values of N_c. $p(f) = \delta |f - 0.20|$ $W_{electrons} = 100$ eV.

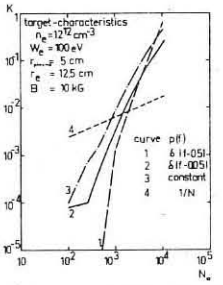

Fig. 4 : Capture ratio K for 600 keV clusters as a function of N_o for several values of f_o.

Fig. 3 shows K versus γ curves for several values of N_c ;

Fig. 4 gives the final capture ratio K on a typical plasma target as a function of initial cluster mass. It shows that K increases steaply with N_o. For $N_o > 10^3$, K is weekly dependent on the fraction rate except for $f_o = \frac{1}{N}$ corresponding to the case where the electronic collision would pull out only one proton. This case gives on the other hand a higher value of K for small clusters.

REFERENCES.

[1] W. HENKES, Zeitschrift fur Naturforschung 17 a, 9, (1962).

[2] O.F. HAGENA, W. HENKES, Zeits. fur Naturforschung, 20a, 10, (1965).

[3] J. COUTANT, M. FOIS, A.M.LE BIHAN, Note Interne EUR-CEA n° 1011 (1970).

HIGH INTENSITY ION BEAM FOR PLASMA INJECTION

by

E. Sindoni* and H. P. Eubank

PRINCETON PLASMA PHYSICS LABORATORY

Princeton, New Jersey USA

Abstract: We present an experimental investigation of electron cyclotron resonance plasma accelerators as a source of high intensity, low energy (keV) ions in which ion current and electron and ion energies are related to rf power and gas pressure.

Considerable interest has developed in fusion research toward achieving high current, low energy ion beam sources for injection, usually as neutral beams, into confinement devices. The desire for high currents at low (keV) energy is not particularly compatible with the space charge equation, it is apparent, however, that the plasma accelerators studied extensively both theoretically and experimentally by Consoli's group[1,2] embody many attractive features as an ion source in this regard. We refer to that general class of plasma accelerators which transfer rf energy to plasma electrons through electron cyclotron resonance in a magnetic field gradient. Efficiencies can be high in terms of plasma kinetic energy and input rf power but most important, ions can be accelerated to keV energies via an internal electrostatic sheath.

Experiment: The experimental apparatus is shown schematically in Fig. 1 with the plot of axial magnetic field. The magnetic field gradient is fixed and equal to 130 gauss/cm at the resonance plane. The microwave source is an X band generator at 10.5 GHz.

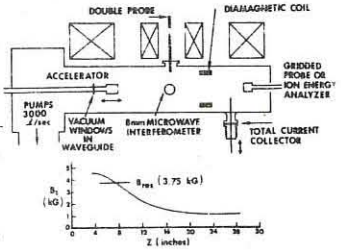

Fig. 1

Three basically different accelerating structures have been tried: (a) slotted lines or "Lisitano" coils[3] axially and radially fed from X band rectangular guide and having 1 and 2 cm ID and 2λ length, (b) a rectangular microwave cavity operated in the TE_{10} mode with a 1 cm diameter plasma aperture, and (c) standard X band rectangular guide with a 1 cm diameter aperture. In the first approximation all perform similarily in regard to variation in power and gas pressure and provided they have insulating liners to bound the discharge from the metal walls[4] will produce ions ~ 1 keV at about 1 ampere. In terms of ease of fabrication and absence of any resonant tuning requirements the waveguide has much to be said for it.

The radial profile of the plasma was made with a double probe by assuming constant temperature. Line density was obtained from an 8-mm microwave interferometer, a 100 turn diamagnetic loop served to indicate the electron pressure $T_{e\perp}$ since the ions should have negligible velocity perpendicular to B, and a multigrid retarding potential probe yielded $T_{e\parallel}$ for the electron motion parallel to B. The aperture size for this probe is less than the local Debye distance. Ion distributions were also made with this probe and with a 90° radial electrostatic analyzer located downstream of the magnetic field. The gridded probe yields absolute current densities although with some uncertainty due to the fact that the grid transparency is a function of the velocity distribution $v_{\parallel}/v_{\perp}$.

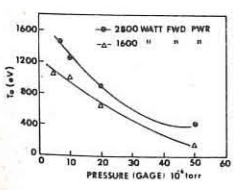

Fig. 2. $T_{e\parallel}$ versus Pressure.

All accelerating structures show mean ion and electron energies which decrease with increasing pressure as shown in Figs. 2 and 3. The total current increases slowly with pressure in this range, however, as does the electron density so that it becomes a matter of compromising somewhat between total current and mean ion energy.

At 10^{-5} Torr (pressures in the accelerating structure are about 250 times the gage values) mean ion energies of ≥ 1 keV at total currents of ≈ 1 ampere can be achieved with a beam radius of 1 cm.

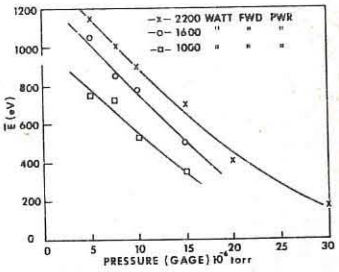

Fig. 3. Mean Ion Energy vs. Pressure.

Both mean particle energy and total current increase with input rf power up to a point, beyond a certain input power level, the exact value varies with the accelerating structure, abrupt decrease in beam output occurs which for the axially fed "L" coil could be traced to arcing across the slots and for the cavity and waveguide usually resulted from breakdown outside the Pyrex or quartz liners. The waveguide appears capable of handling the largest input power which for our case was about 4 kW. Normally all high power results are taken with 2 msec pulses at about 3 pulses/sec, but we have varied the pulse width from 0.1 to 8 msec. At the higher powers of ≥ 1 kW, plasma is pumped from the accelerating region at a rate in excess of the neutral gas feed, which in long pulse operation produces considerable change in ion energy over the pulse width because of the pressure dependence. This results in, for certain applications in plasma confinement experiments,[5] a nicely smeared energy distribution whose halfwidth is comparable with the mean energy (Fig. 4).

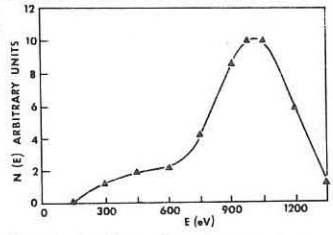

Fig. 4. Ion Energy Distribution.

One of the most interesting results of the experiment is the measurements of $T_{e\parallel}$ for the electrons (Fig. 5). In the simplified one-dimensional flow model, electron motion along the field is tightly coupled to the ions such that $T_{e\parallel} \ll T_{i\parallel}$. In reality we find a group of electrons for which $T_{e\parallel} \approx T_{i\parallel}$. Although the density of this group must be down from the total electron density by roughly $(M_i/m_e)^{1/2}$ these electrons constitute essentially the total electron current.

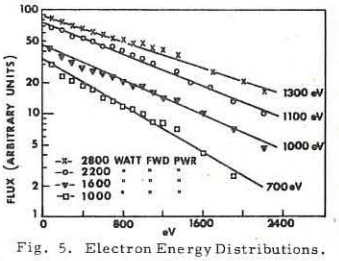

Fig. 5. Electron Energy Distributions.

Coulomb or gas scattering of the primary large $v_{\perp}/v_{\parallel}$ electrons cannot account for any large $v_{\parallel}$ group which constitute of the order of 2% of the density. We are led therefore to the conclusion that this 2% group of electrons must arise from a sheath rendered leaky by virtue of secondary or reflected cold electrons which flow back into the sheath region and provide partial neutralization. True adiabatic expansion of electrons from the cyclotron region would yield $T_{e\parallel} \approx 0.7$ the initial $T_{e\perp}$, a value comparable with the diamagnetic loop estimates of $T_{e\perp}$. To separate the pressure effects of sheath leakiness from the effect on the primary production is beyond our data at this time. We are pursuing this further as it may be crucial in any attempt to neutralize the ion beam.

This work was performed under the auspices of the U. S. Atomic Energy Commission.

---

* On leave from Istituto di Fisica, Universita di Milano.

1) T. Consoli and R. B. Hall, Nucl. Fusion 3, 237 (1963).

2) E. Canobbio, Nucl. Fusion 9, 27 (1969).

3) G. Lisitano, P. Caldirola, N. Barassi, M. Fontanesi, and E. Sindoni, Plasma Physics and Controlled Nuclear Fusion Research (International Atomic Energy Agency, Vienna, 1969), Vol. II, p. 415.

4) R. Geller, B. Jacquot, and C. Jacquot, EUR-CEA-FC-511 (1969).

5) R. F. Post and M. N. Rosenbluth, Phys. Fluids 9, 730 (1966).

"MICROBE": Microwave Ionization in a Crossed Beam Experiment

G. Cattanei, and J.-G. Wegrowe, Institut für Plasmaphysik GmbH, 8046 Garching near Munich, Federal Republic of Germany

Abstract: A new plasma source using microwave power focused on a neutral beam has been developed. Some results are presented.

Introduction: An adequate plasma source for various confinement and heating experiments in stellarators should possess the following characters:

- Small spatial extension compared to the dimensions of the vacuum vessel.
- Absence of electrodes, antennas, limiters etc. in the source region.
- Measurable intensity.
- Ability to produce continuously a quiescent plasma of high density with respect to the background gas density.

For this purpose a source was deviced using microwave power at the electron gyrofrequency focused on a collimated neutral-gas beam. The neutral and the microwave beams are perpendicular to each other and to the static magnetic field B_o.

The minimum neutral flux necessary for breakdown is inversely proportional to the lifetime of the plasma particles and to the ionization cross section. Even with the poor confinement of a straight device this flux is realizable by using alkali metals.

We present preliminary results obtained in such an experimental set-up.

Experimental set-up: Figure 1 shows a blockdiagram of the machine. The stainless steel vacuum vessel has a diameter of 17 cm and a length of about 1 m.

The magnetic field may be varied up to 6 kG and is homogeneous to within $5 \cdot 10^{-3}$ in the interaction region. The microwave power (up to 20 watts at 13.3 GHz) is fed through horns and ceramic lenses (12 cm in diameter) which are also used as parts of an 8 mm interferometer.

Further diagnostic tools are: a Langmuir probe, a diamagnetic coil and a contact ionization probe for neutral flux measurements.

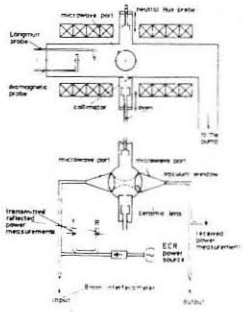

Fig.1 MICROBE Experimental set-up

Results: The plasma was produced using a collimated beam of Cs. The oven could be moved to vary the width of the beam on the axis of the device between 1 and 2 cm.

Fig. 2 shows the dependence of the ion saturation current of the Langmuir probe on the magnetic field for three different radial positions: on axis and 3 cm apart on each side.

For comparison, Fig. 3 shows the corresponding results obtained without Cs beam and filling the machine with Argon.

As may be seen a good spatial limitation of the plasma is obtained with the Cs beam. (a radial profile is shown in Fig.4). Half-width down to about 2 cm could be measured. This corresponds, as expected, to the dimensions of the interaction region between the microwave and neutral beams.

The density was evaluated from Langmuir probes and checked by the microwave interferometer. Peak densities up to some times $10^{12} cm^{-3}$ have been obtained.

The results obtained up to now indicate the feasibility of a source possessing the required properties. More quantitative measurements e.g. particles and power balance, are in progress.

This work was performed as part of the agreement between the Institut für Plasmaphysik GmbH, Munich-Garching, and Euratom.

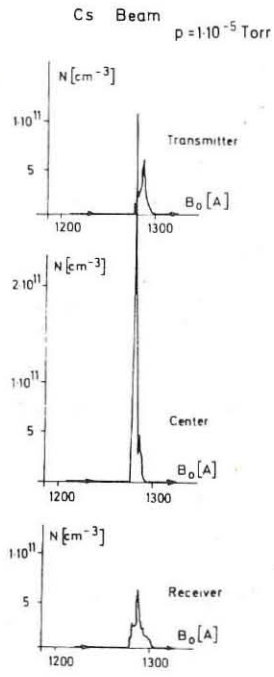

Fig. 2

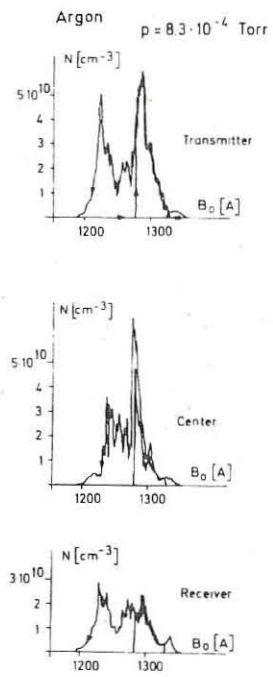

Fig. 3

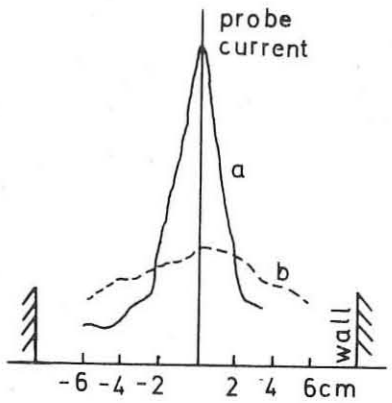

Fig. 4: Radial Profiles
a) Cs Beam
b) N_2 ($P = 4.5 \times 10^{-5}$ Torr)

DESCRIPTION OF WAVES TO ALL ORDERS IN ELECTRON AND ION TEMPERATURES IN A NONUNIFORM MAGNETIZED PLASMA .

J-L MONFORT* and P.E.VANDENPLAS

*Laboratoire de Physique des Plasmas***, Ecole Royale Militaire, 1040 Bruxelles, Belgium.*

*Laboratorium voor Plasmafysica***, Koninklijke Militaire School, 1040 Brussel, Belgium.*

Abstract. *A general description of waves (with the differential equation for the electromagnetic field) in a nonuniform magnetized plasma is given to all orders in the T_e electron and T_i ion temperature and permits the complete treatment of a bounded plasma. The influence of T_e and T_i on the waves occurring in the magneto-ion domain (including the region around the lower hybrid frequency) is investigated.*

New resonances in the magneto-ion domain of hot bounded plasmas have been predicted on the basis of the standard fluid model of a hot electron plasma in which the equations are closed by assuming $p_\alpha = \gamma_\alpha K T_\alpha n_\alpha$ ($\alpha = e$ or i) for the perturbed $\exp(-i\omega t)$ pressures [1] and experiments have confirmed their existence [2]. The basic character and the possible thermonuclear importance of these resonances render a complete description of the plasma in the magneto-ion domain necessary. We use an operator method to give a general description of waves in a non-uniform magnetized plasma to all orders in the electron and ion temperature and obtain the corresponding dispersion relation.

Consider a non-uniform plasma immersed in a uniform magnetic induction $\bar{B}_o = \bar{B}_o \bar{1}_z$. The rather general theory we develop concerning the waves in such a plasma is nonrelativistic and linear, i.e., the product of two perturbed quantities is neglected. The steady electric field $\bar{E}_o$ is neglected; this is warranted either when $r_{L\alpha} \ll L$ or when $r_{D\alpha}^2 / \lambda \ll L$ ($r_{L\alpha}$ and $r_{D\alpha}$ are respectively the Larmor and the Debye radius of particles, L the characteristic length of the density gradient and λ the local wavelength; $\alpha = e, i, \ldots$). The linearized Boltzmann equation for the $\exp(-i\omega t)$ perturbed distribution function f_α can be written as $[\partial/\partial\phi + P_\alpha(\phi)] f_\alpha = Q_\alpha(\phi)$ in which $P_\alpha(\phi)$ is a linear operator containing $\partial/\partial x$, $\partial/\partial y$ and $\partial/\partial z$; the velocity $v = [v_\perp \cos\phi, v_\perp \sin\phi, v_\parallel]$ and $\perp$ means perpendicular to $\bar{B}_o$. The collision term is represented by $-\nu_\alpha f_\alpha$. The use of a single ν_α although rather crude can be useful, among other things, in a practically collisionless plasma to remove the infinities that would otherwise appear in some integrals. The above operator equation can be interpreted and furnishes f_α under the form of an operator represented by a product of 10 infinite series and acting on the perturbed electric field $\bar{E}$ and on the nonuniform equilibrium distribution function $\langle F_\alpha \rangle$. This expression for $\langle f_\alpha \rangle$ enables one to calculate all the macroscopic quantities that are necessary to solve Maxwell's equations and to state the boundary conditions pertaining to a bounded plasma.

In particular, if $\langle F_\alpha \rangle$ is Maxwellian and centred on zero and if $\partial/\partial z \equiv 0$ (the wave vector $\bar{k}$ is thus $\perp$ to $\bar{B}_o$), the first of the 3 equations for the components of the electric field, to all orders in T_e and T_i, is of the form [3][4]:

$$\frac{c^2}{\omega^2}\left[\frac{\partial^2 E_x}{\partial y^2} - \frac{\partial^2 E_y}{\partial x \partial y}\right] + E_x + \sum_\alpha \sum_{P=0}^{\infty} \frac{1}{P+1} \prod_{l=1}^{P} \left[l^2 \omega_{c\alpha}^2 - (\omega + i\nu_\alpha)^2\right]$$

$$\left[K_{1,\alpha}^{2P} E_x + K_{2,\alpha}^{2P} E_y + U_\alpha K_{3,\alpha}^{2P+1} E_z\right] T_\alpha^P \omega_{p\alpha}^2 = 0 \qquad (1)$$

where T_α: absolute temperature, $\omega_{p\alpha}$: plasma frequency, ν_α: phenomenological collision frequency, $\alpha = e$ or i for electrons and ions. We shall see later that this leads to a convergent description when the cyclotron frequencies $\omega_{c\alpha} \neq 0$. K^{2P} is a linear differential operator of order $2P$ in x and y. This method is particularly interesting to use when one considers a nonuniform plasma with different species of particles, since it furnishes a temperature-ordered description.

The three equations of type (1) lead, when ∇^2 is replaced by $(-k^2)$, to the general electromagnetic dispersion equation, which is temperature-ordered, of an uniform plasma under the not too restrictive assumptions made. If, furthermore, the quasi-static approximation is made ($\bar{E} = -\nabla\phi$; note carefully that this is still more general than considering purely longitudinal waves, see e.g. pages 8-10 of [5]), the above dispersion equation leads to a simpler one:

$$k^2\left[1 + \sum_\alpha \sum_{N=0}^{\infty} (-k^2)^N \frac{(2N+1)!!}{N+1} \left(\frac{KT_\alpha}{m_\alpha \omega^2}\right)^N \frac{\omega_{p\alpha}^2}{\omega^2} \prod_{l=1}^{N} \frac{1}{(l^2 B_\alpha^2 - 1)}\right] = 0 \qquad (2)$$

which is equivalent to Bernstein's dispersion relation. Eq(2) has, however, attractive features: it consists of two infinite series ($\alpha = i$ and e) which are absolutely convergent when ω_{ce} and $\omega_{ci} \neq 0$. A sufficient condition for interrupting the series by retaining the terms up to order N in T_α is that $(N+1)^2 \omega_{c\alpha}^2 > \omega^2$ and that $|(2N+3) k^2 K T_\alpha / m_\alpha| \ll |(N+2)^2 \omega_{c\alpha}^2 - \omega^2|$. These conditions show that the power of N of the terms which must be retained cannot be a priori decided but depends on the values of $\omega_{c\alpha}$, ω, T_α, m_α, k^2 in the domain in which the wave is being investigated. For instance, when the magnetic field is low ($\omega_{c\alpha}/\omega \ll 1$), we must use a rather high N and introduce the first $(N+1)$ cyclotron harmonics for a detailed description of the phenomena. This does not necessarily mean, however, that a satisfactory description cannot be obtained when the above sufficient conditions are not met.

A systematic comparison between the k^2 given by the above general description [electromagnetic and quasi-static ($\bar{E} = -\nabla\phi$)] and the standard hydrodynamical k^2 obtained with the closure $p_\alpha = K T_\alpha n_\alpha \gamma_\alpha$ has been carried out. Because of lack of space, we only summarize the results in the magneto-ion domain. In this domain we mostly have $|k^2 c^2/\omega^2| \gg 1$. Fig.1 gives the dispersion relation for different values of $k^2 K T_i / m_i \omega^2$ in the region $\omega_{pi}^2 \sim \omega^2$ in which the waves are quasi-longitudinal (quasi-static approximation fully warranted); three approximations are considered: (a) T^∞, i.e. all orders in T_i and T_e (b) T^1, i.e. order 1 in T and (c) $p = \gamma n K T$. The electrons have no influence as soon as $\omega_{ci}/\omega \gg \sqrt{m_e/m_i}$. When $|k^2 K T_i / m_i \omega^2| < 1$, the T^1 and T^∞ descriptions agree except around the cyclotron harmonics; the same is true of the scalar pressure description when $|\omega_{ci}/\omega| < 1/2$.

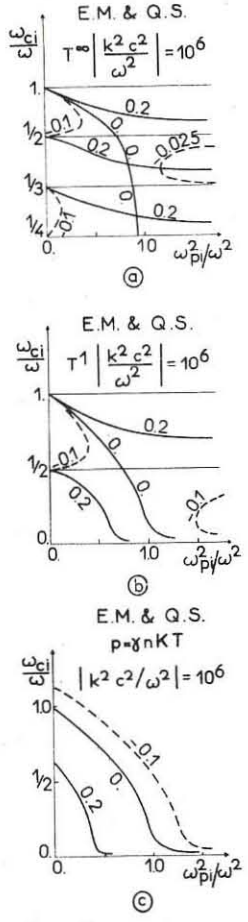

Fig.1. Dispersion relations of the quasi-longitudinal extraordinary ($\bar{k}$ and $\bar{E} \perp \bar{B}_o$) wave for three descriptions ((a) T^∞; (b) T^1; (c): $p = \gamma_\alpha n_\alpha K T_\alpha$. The parameter is $k^2 K T_i / m_i \omega^2$.

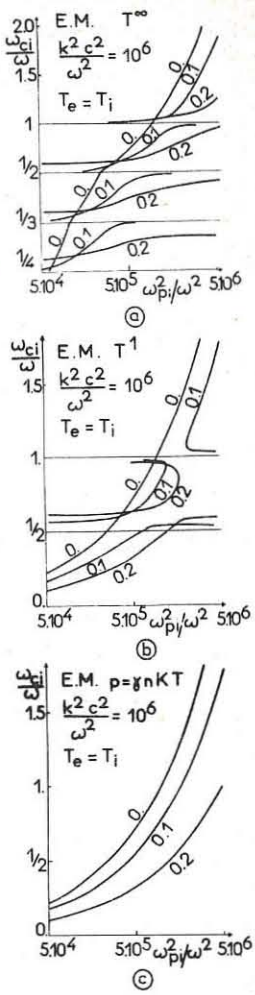

Fig.2. Dispersion relations of the extraordinary wave with elliptical polarization with respect to $\bar{B}_o$ ($\omega^2 \gg \omega^2$). The parameter is $k^2 K T_i / m_i \omega^2$.

Fig.2 gives the dispersion relation of the waves having elliptical polarization around $\bar{B}_o$, i.e. in the region $\omega_{pi}^2 \gg \omega^2$. This region can be very important for thermonuclear plasmas. Except, of course, around the cyclotron harmonics, the three descriptions are in satisfactory agreement especially when $|k^2 K T_i / m_i \omega^2| \ll 1$. The quasi-static approximation is generally warranted when $|k^2 L^2| \ll 1$.

1. P.E.VANDENPLAS, A.M.MESSIAEN, J-L MONFORT and J.J.PAPIER, Phys.Rev.Letters 22 (1969) 1243; Plasma Physics 12 (1970) 391.
2. A.M.MESSIAEN, P.E.VANDENPLAS, J-L MONFORT 4th European Conf. on Controlled Fusion and Plasma Phys. Rome (1970).
3. J-L MONFORT, D.Sc. Dissertation, Report n° 43, Lab.Phys.Plasmas, Ecole Royale Militaire, Brussels (1970). Complete references are given.
4. J-L MONFORT, P.E.VANDENPLAS, Phys.Letters 31A (1970) 11.
5. P.E.VANDENPLAS *"Electron Waves and Resonances in Bounded Plasmas"* Wiley - Interscience, London, New York, Sydney (1968).

* Chercheur agréé de l'Institut Interuniversitaire des Sciences Nucléaires. Presently at IBM Belgium, Brussels.

** Association Euratom-Etat belge.

HIGH FREQUENCY ION-ELECTRON RESONANCES AND ABSORPTION IN A STRONGLY MAGNETIZED PLASMA COLUMN

A.M.MESSIAEN*, P.E.VANDENPLAS and J-L MONFORT**
*Laboratoire de Physique des Plasmas**-Laboratorium voor Plasmafysica**
Ecole Royale Militaire-Koninklijke Militaire School; 1040 Brussels, Belgium.

Abstract. *We give the main results of a fluid description of a bounded hot ion-electron plasma which includes collision effects and a full electromagnetic treatment. The importance for rf absorption of the boundedness and of the hot character of the plasma is again emphasized. Experimental results agree satisfactorily with theory.*

I. INTRODUCTION AND THEORETICAL ANALYSIS. The possibility of *rf* energy absorption for $\omega \ll \omega_{ce}$ (ω_{ce}: electron cyclotron frequency) and more precisely at the lower hybrid frequency ω_{LH} has been investigated by several authors [1][2][3]. In particular, the importance of considering the boundedness of actual plasmas has been demonstrated[2][3]. In [2] we theoretically investigated a hot (T_e and $T_i \neq o$) uniform magnetized plasma column ($\bar{B}_o$ magnetic field // axis) submitted to a *rf* $\bar{E}$-field ($\bar{E}$ and vacuum wavevector $\bar{k}_o \perp \bar{B}_o$). The hydrodynamical equations for ions and electrons without collisions are closed assuming a perturbed scalar pressure and the quasi-static approximation ($\bar{E} \simeq -\nabla\phi$) is made. This theory predicts the existence of new resonances (and particularly of main resonances) in the magneto-ion domain which are due to the boundedness and to the hot character of the plasma. We also show that a theoretical treatment with $T_i = o$ but $T_e \neq o$ gives a good first approximation of the resonances existing when both T_i and $T_e \neq o$.

We now consider the same model with $T_e \neq o$ and $T_i = o$ but use the full electromagnetic treatment and introduce collision frequencies ν_e and ν_i for momentum transfer. The plasma column of radius a is excited by a *TE* wave (cylindrical coordinates r, θ, Z with $\partial/\partial Z = 0$) with magnetic field $H_Z = F_n J_{|n|}(k_o r)\, e^{i(n\theta - \omega t)}$. The ratio $\mathcal{D}_n = D_n H^{(1)}_{|n|}(k_o a) / F_n J_{|n|}(k_o a)$ between scattered and incoming H_Z field at $r=a$ is computed. One can easily show that

$$\frac{d P_{abs}}{d Z} = \frac{2\pi}{\omega \varepsilon_o |n|!\,|n-1|!} \left(\frac{k_o a}{2}\right)^{2|n|} |F_n|^2 \; Im\,\mathcal{D}_n$$

when $k_o a \ll 1$. (P_{abs} = absorbed power in the plasma, ε_o = permittivity of vacuum).

The calculations lead to the following conclusions: (1) The validity of the quasistatic approximation as discussed in [2] is fully confirmed. A typical curve of $|\mathcal{D}|$ versus ω is shown in Fig 1a ($n=-1$). The peak on the right hand side is the low frequency continuation of one of the two well-known magnetic main dipolar resonances which exists for $\omega \gtrsim \omega_{ce}$. The peak on the left hand side is one of the new main resonances. These two resonances satisfy the following equation:

$$\omega^2_{pe} = \frac{K\,(\omega - n\omega_{ce})\,(\omega + n\,\omega_{ci})\,(\omega + n\,\omega_\tau)}{\omega - \omega_\tau\, \omega_{ci}/\omega} \; ; \; n = \pm 1 \qquad (1)$$

with ω_{pe} : electron plasma frequency, ω_{ci} : ion cyclotron frequency, $\omega_\tau = (\gamma_e kT_e)^{1/2}/a$, K : geometrical factor depending on the outer medium, γ_e : pressure law constant. In the center of the figure, near ω_{LH}, the dashed region corresponds to a fine structure of narrow resonances (see (3)). (2) Fig 1b and 1c show the influence of the collision frequencies on the absorbed power. At high ν the main resonance on the left spreads out and disappears while a narrow absorption peak remains near ω_{LH}. (3) Fig 2a shows a typical fine structure of absorption peaks near ω_{LH} (due to real eigenvalues of the relevant k). The decisive influence of increasing temperature on P_{abs} even when $\nu \gg \omega$ is apparent on Fig 2b and 2c.

II. EXPERIMENTAL SETUP. A *rf* resonantly sustained plasma [4] is created in a glass tube placed across a waveguide (Fig 3) by a microwave signal of frequency ω_m ($\sim$3GHz). The density of the plasma can be easily ajusted by a small change of B_o when $\omega_{ce}/\omega_m \lesssim 1$ and the plasma is then practically quiescent. The plasma is furthermore excited at a frequency $\omega \ll \omega_m$: (i) either directly by a ω signal applied to a plane electode A inside the waveguide and received by probes B (ii) or by nonlinear mixing. The ω_m microwave signal is amplitude modulated at frequency ω and the nonlinear behaviour of the plasma provides a ω component which is picked up by A or B. The latter excitation is much easier at low ω. Experiments were performed in Hg ($p \sim 10^{-3}$ Torr, $T_e \sim 20000°K$, $T_i \sim 300°K$, $B_o \sim 1$ k G).

III. EXPERIMENTAL RESULTS FOR $\omega_{LH} \ll \omega \ll \omega_{ce}$. Using a continuity analysis from $\omega \simeq \omega_{ce}$, we followed the $n=-1$ main electron resonance down to the domain $\omega \ll \omega_{ce}$. Eq (1) is plotted on Fig 4 (with $\gamma_e = 2$, $T_e = 2$ eV, $K=3.1$, $n=-1$) and compared to the experimental points. We find good agreement especially concerning the existence of a cut-off value $\omega = \omega_\tau$ for which the resonance vanishes. The existence of this resonance when $\omega_{ce}/\omega \gg 1$ is also important in connection with the obtention of overdense *rf* plasmas. More details will be given in [5].

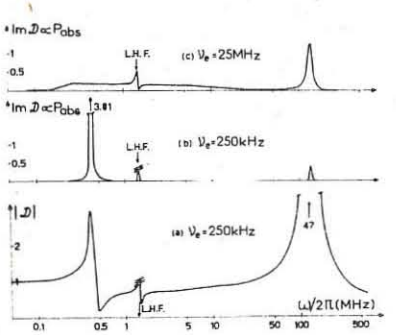

1) $|\mathcal{D}|$ *and normalized power absorption* P_{abs} *versus* ω. *Influence of* ν_e *on* P_{abs} ($N=10^{10}cm^{-3}$, $\gamma_e=2$, $T_e = 2$ *a* V, $a=0.38cm$, Hg, $\nu_i=3k$ Hz, $n=-1$, $B_o=920G$).

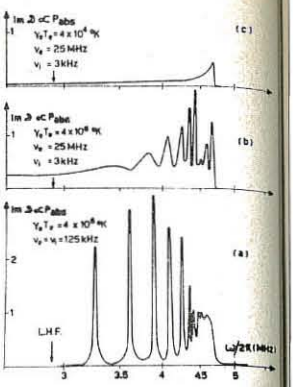

2) *Typical influence of* T_e *and* ν *on* P_{abs} *in the vicinity of* ω_{LH} ($N=10^{11}cm^{-3}$, $\gamma_e=2$, $a=0.38cm$, Hg, $B_o=800$ G).

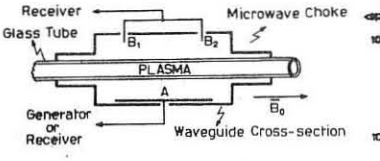

3) *Experimental set up*

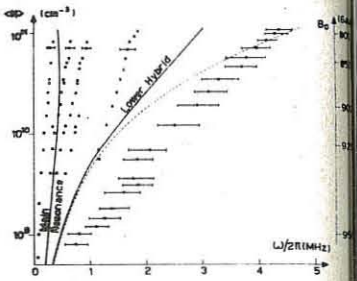

4) *Comparison of Eq (1) with the experimental data for* $n=1$ *and* $\omega \gg \omega_{ci}$.

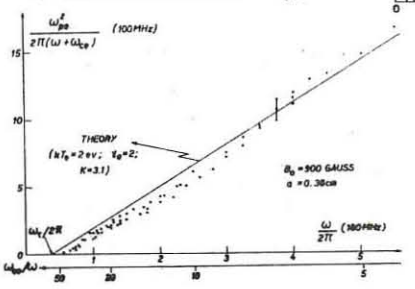

5) *Theoretical resonances (main and absorption region near* ω_{LH}) *compared to observed resonances* (<N> *density). Since* <N>$=f(B_o)$, *the value of* B_o *is also indicated.*

IV. EXPERIMENTAL RESULTS WHEN $\omega < \omega_{LH}$ AND $\omega \simeq \omega_{LH}$. Experimental data mostly obtained by nonlinear excitation are presented in Fig 5 and compared to the theoretical location of the main resonance and of the resonance region near ω_{LH} (positive k^2 between the solid line corresponding to ω_{LH} and the thin dashed line). The strongest effect observed is the resonance situated in the domain at the right of ω_{LH}. Since the experimental $\nu_e \simeq 25$ MHz $\gg \omega$, theory leads us to expect that the main resonance (left of Fig 1c) shall be strongly damped. In fact we observe in the vicinity of the theoretical location of this resonance, a series of small ones. A part of this series has already been observed by an indirect method [5]. It has not yet been possible to determine the exact nature of this series; it may be related to main resonances (possibly with values of $|n| \neq 1$, parametric effects, etc) or to non-uniformity phenomena.

CONCLUSIONS. We have observed most of the effects which are, in our present experimental conditions, predicted on the basis of hot uniform plasma theory. However, more experiments are needed with quiescent plasmas having lower ν and with a stronger coupling of the *rf* energy. The inclusion in the theory of nonuniformity is also desirable.

REFERENCES [1] See e.g. M.E.OAKES, H.SCHLUTER, Ann.Phys. 35,396 (1965); AGNELLO, P.FIEFFE-PREVOT, G.ITCHENKO, S.KULINSKI, P.LALLIA. Contributed papers of the IXth Int.Conf.Phen.Ion.Gases, Bucharest 1969, p.519; B.V.GALAKTIONOV, V.E.GOLANT, A.D.PILIYA, O.N.SHCHERBININ, Sov.Phys.-Tech.Phys.14,721 (1969).

[2] P.E.VANDENPLAS, A.M.MESSIAEN, J-L MONFORT, J.J.PAPIER, Phys.Rev.Letters 22,1243 (1969); Contributions "Third European Conf. on Contr.Fusion and Plasma Phys" p.98, Wolters Noordhoff Publ. Utrecht (1969); Plasma Phys. (1970) to be published.

[3] C.R.SKIPPING, M.E.OAKES, H.SCHLUTER, Phys.Fluids 12,1886 (1969).

[4] A.M.MESSIAEN, P.E.VANDENPLAS, Phys.Fluids 12,2406 (1969).

[5] A.M.MESSIAEN, P.E.VANDENPLAS, Phys.Fluids, to be published (1970).

[6] A.M.MESSIAEN, P.E.VANDENPLAS, J-L MONFORT, Phys.Letters 29A,573 (1969).

* Chercheur agréé de l'Institut Interuniversitaire des Sciences Nucléaires.
** Association "Euratom-Etat belge" - Associatie "Euratom-Belgische Staat".

NON LINEAR EFFECTS IN TRANSIT TIME MAGNETIC PUMPING

by

E. Canobbio

ASSOCIATION EURATOM - CEA
Département de la Physique du Plasma et de la Fusion Contrôlée
Service I.Gn. Centre d'Etudes Nucléaire
Cedex 85, 38 Grenoble Gare (France)

Abstract : The conditions for the validity of the collision-independent EM power absorption by Transit Time Magnetic Pumping as derived by the linear theory are investigated. In the case of very low collision frequency, non linear effects result in power absorption that is proportional to the ion-ion collision frequency.

By slightly modulating the toroidal component of a closed magnetic configuration at a low frequency ($\omega \ll \omega_{ci}$, the ion gyrofrequency) with a phase velocity of $v_\varphi \gtrsim v_\theta \equiv (2kT_i/m)^{1/2}$, which is the ion thermal speed, direct conversion of EM energy into thermal energy of the plasma ions appears. This results in a uniform heating which is independent of the density, without need for "beach" modifications of the $\vec{B}_0$ field /1/. This modified version of the original concept of Transit Time Magnetic Pumping (TTMP) i.e. a strong field modulation over a short section of the toroid /2/, is a potential method for overcoming the limitations of ohmic heating in toroidal traps both for present day experiments and for thermonuclear reactors /3/.

We consider the following situation. External azimuthal currents that flow through an array of coils (radius R) surrounding a uniform plasma cylinder (radius $r_p \ll R$) produce a modulation of the static field viz.

$$\vec{B}(t,\vec{r}) \approx \vec{e}_z B_0 \,(1 + b\cos(Kz - \omega t)), \qquad (1)$$

where the constant b will be independent of the presence of plasma provided that $v_\varphi \ll v_{Alfven}$. If $v_\varphi \gtrsim v_\theta$, this last condition will imply that $\beta_i \ll 1$. β_i is the ratio of ionic to magnetic pressure. We assume magnetic moment invariance, hence conservation of the magnetic flux within the plasma i.e. $Br_p^2 = \text{const.}$ and also neglect ion collisions ($\nu_i \ll \omega$). The opposite case ($\nu_i > \omega$) has been considered in ref. /4/. Ion dynamics can be described by the following linearized Vlasov equation ($b \ll 1$) for $f_1(t,z,v_z,v_\perp)$, for small departures from the equilibrium distribution function f_0 :

$$\partial f_1/\partial t + v_z \partial f_1/\partial z + \left(\frac{e}{m}E_{//} - \frac{v_\perp^2}{2B_0}\frac{\partial B}{\partial z}\right)\partial f_0/\partial v_z + \frac{v_\perp}{2B_0}\left(\frac{\partial B}{\partial t} + v_z\frac{\partial B}{\partial z}\right)\partial f_0/\partial v_\perp = 0, \qquad (2)$$

($v_\perp$ is the gyration velocity). If the electron collision frequency is larger than ω, the electron fluid can be considered in mechanical and thermal equilibrium : $-en_eE_{//} - kT_e\,\partial n_e/\partial z = 0$. By assuming plasma charge neutrality and using the ion continuity equation with Eq. (2), it can be shown that

$$eE_{//} = -\frac{kT_e}{B_0}\partial B/\partial z \cdot g_{f_0}(v_\varphi/v_\theta, T_e/T_i) \approx -\frac{kT_e}{B_0}\partial B/\partial z \,. \qquad (3)$$

The function g_{f_0} is given in ref. /1/ assuming a Maxwellian distribution function f_0. The approximated expression (which we shall use in the following) holds as long as $T_e \lesssim T_i$, so that ion sound wave excitation and electron heating can be disregarded /1a, 4/. TTMP both puts energy preferentially into the parallel component of ion velocity uniformly within the column and keeps the plasma as close as possible to thermodynamic equilibrium. Assuming f_0 to be an isotropic Maxwellian distribution, we may integrate Eq.(3) over $v_\perp$ and use Eqs. (1) and (2) to obtain an equation for $F_1(t,z,v_z)$. This is

$$\partial F_1/\partial t + v_z\,\partial F_1/\partial z + Kv_\theta^2(b/2)(T_e/T_i + v_\varphi/v_\theta)\sin(Kz-\omega t)\,dF_0/dv = 0, \qquad (4)$$

where $F_0(v) = \exp(-v^2/v_\theta^2)/v_\theta\sqrt{\pi}$. We notice that under the assumed conditions no supplementary enhanced collisional and/or turbulent cross-field diffusion should substantially shorten the plasma confinement time in a toroidal configuration during the heating phase. Eq. (4) is identical to the equation used to derive Landau damping, after the substitution

$$-\frac{e}{m}\mathcal{E} \longrightarrow Kv_\theta^2(T_e/T_i + v_\varphi/v_\theta)\,b/2 \qquad (5)$$

is made. Notice, incidentally, that this substitution is written incorrectly on p. 234 of ref. /5/. In order to obtain the expression for the power absorption per unit volume, we use the same procedure as when computing power absorption by Landau damping. That is, in terms of a given EM field and a given set of ω and K values, without using Poisson's equation. By using substitution (5) we obtain in our case

$$P = \sqrt{\pi}\,\omega(v_\varphi/v_\theta)\beta_i\left(T_e/T_i + v_\varphi/v_\theta\right)^2 \exp(-v_\varphi^2/v_\theta^2)\cdot\frac{(B_0 b)^2}{16\pi}. \qquad (6)$$

We will let 2γ be the absorption rate. Then, invoking conservation of energy we may write $P = 2\gamma W$, where W, the energy density of the wave, is $\frac{(B_0 b)^2}{16\pi}\cdot(1 + O(\beta_i^2, \omega^2/\omega_{ci}^2))$. In our case, we obtain for γ

$$\gamma = \tfrac{1}{2}\sqrt{\pi}\,\omega(v_\varphi/v_\theta)(T_e/T_i + v_\varphi/v_\theta)^2\beta_i\exp(-v_\varphi^2/v_\theta^2). \qquad (7)$$

For order-of-magnitude estimates we shall use the maximum γ value for the isothermal case ($T_e = T_i$), $\gamma_M \approx 1.3\,\omega\beta_i \ll \omega$. It occurs for $v_\varphi = v_\theta$.

The linear collisionless theory used to derive the above results holds under the following condition. The non linear distortion of the Maxwellian distribution produced by TTMP in the resonance region must be destroyed by ion-ion collisions sufficiently rapidly. The effects of like particle collisions on the distribution function in the resonance region can be described by the Fokker-Planck term /6/ shown below

$$3(2\tau_D(v_\varphi))^{-1}\frac{\partial}{\partial v_z}\left(\partial f/\partial v_z\, v_\theta^2/2 + v_z f\right), \qquad (8)$$

where $\tau_D(v_\varphi)$ is the Spitzer deflection time ($m^2v_\theta^3/8\pi e^4 n(\phi-G)\ln\Lambda$). Expression (8) is exact in the limit of a sufficiently narrow one-dimensional resonance region in velocity space which is far from the thermal velocity. It is correct to within an order-of-magnitude for all possible values of v_z.

In discussing non linear effects, as in the electrostatic case /6/, we will distinguish between narrow and broad wave packet modulations, depending on the phase velocity spread Δv_φ . We compare Δv_φ with the velocity interval $|(v - v_\varphi)| = \Delta v = v_\theta\,(b(T_e/T_i + v_\varphi/v_\theta))^{1/2}$. A resonant particle will be trapped in the EM wave under consideration when its velocity falls in this interval. If $\Delta v_\varphi \ll \Delta v$ (narrow packet) strong correlations among trapped particles occur and the spatial periodicity of F_0 in the resonance zone is important /7/. In the opposite case $\Delta v_\varphi > \Delta v$, no particle can be considered to be trapped in any one wave and F_0 is homogeneous in space, i.e. the basic assumption of the quasi-linear approach. In both case, a non linear treatment which takes account of the collision term (8), gives the following modification of the power absorption /6/ : $P_{NL} \approx P/(1 + \tau_1/\tau_2)$, where τ_1 is the characteristic time for remaxwellization in the resonance zone and τ_2 is the characteristic time for the non linear distortion of the distribution function in the resonance zone. The remaxwellisation condition will be satisfied if $\tau_1 \ll \ll \tau_2$. This inequality, when applied to the two cases, produces two different threshold values for ν_i/ω. In the monochromatic (narrow-band) case with insufficient remaxwellization $\tau_2 \ll \tau_1$, we may use the results of ref. /7/, and substitution (5) to obtain the following expression for the non-linear power absorption

$$P_{NL} = (3\sqrt{2\pi}/4\tau_D)(v_\varphi/v_\theta)^4 B_0^2 b^{1/2}(T_e/T_i + v_\varphi/v_\theta)^{-3/2}\exp(-v_\varphi^2/v_\theta^2). \qquad (9)$$

By equating the r.h.s. of equations (6) and (9), we obtain a critical value of ν_i below which (6) and (7) hold and above which (9) holds

$$\nu_{ic}/\omega \equiv (\tau_{Dc}\omega)^{-1} = (v_\theta/3\pi v_\varphi)\left(\tfrac{1}{2}b(T_e/T_i + v_\varphi/v_\theta)\right)^{3/2} \approx b^{3/2}/3\pi \,. \qquad (10)$$

In the broad-band case, but still considering insufficient Maxwellization, we can use the results of ref. /8/ in a similar way to obtain

$$P_{NL} = (3/16\sqrt{\pi})\nu_i\beta_i(v_\varphi/v_\theta)^3 B_0^2 \exp(-v_\varphi^2/v_\theta^2). \qquad (11)$$

This equation holds below the following critical value of ν_i

$$\nu_{ic}/\omega = (v_\theta/v_\varphi)^2\left(b(T_e/T_i + v_\varphi/v_\theta)\right)^2/3 \approx 4b^2/3 \qquad (12)$$

A comparison between Eqs. (10) and (12) shows that the critical ν_i value for the broad-band case is lower than that in the narrow-band case if $b \lesssim (4\pi)^{-2}$ It is interesting to notice /9/ that the behaviour of the absorption rate as a function of collision frequency as given by Eqs. (6), (9), and (11) is quite analogous to the corresponding behaviour of the equilibrium diffusion coefficient in a toroidal plasma at very low and intermediate collision frequencies /10/. It is also instructive to compare the collision term (8) to the forcing term in Eq. (4) for the perturbed distribution for the case when $\nu_i > \nu_{ic}$. Collisions dominate whenever the velocity is in the range $|v_z - v_\varphi| \lesssim \Delta u \equiv v_\theta(\nu_i/\omega)^{1/3}$.

We now compare Δu with the width of the resonance zone in the case of collisionless absorption ($\Delta v \approx \gamma/K \approx v_\varphi\beta_i$). We see that the velocity distribution of resonance particles is not collision dominated when $\Delta v > \Delta u$ i.e. $\beta_i > (\nu_i/\omega)^{1/3}$. Remember that $\nu_i > \nu_{ic}$. When this condition is included β_i must satisfy the following : $\beta_i^2 > b$. Even in the collisiondominated case ($\Delta v \ll \Delta u$) it is easy to show /9/ that the power absorption is still given by the collisionless formula (6) !

Equations (6),(9) and (11) give the power absorbed by δN resonant particles, $\delta N \approx n\,|dF_0/dv|_{v=v_\varphi}(\Delta v)^2/2 < n(\omega/kv_\theta)^2 \ll n$. Substitution (5) can no longer be used to calculate the collisionless power transfer to the main body of the ion distribution, using the electrostatic analogue, because wave dispersion is involved in this process. Assuming equipartition of energy between ions and electrons so that $P \approx 3nk\,dT/dt$ we find from Eq. (6) that $dT/dt \approx \omega\beta^2 T$. Hence, under the condition $\nu_i > \nu_{ic}$, $dT/dt < \nu_i T_0$ so that the heating of the main body ions is mainly collisional. When (9) and (11) are valid , then non linear processes would have to be considered to show complete thermalization.

References :

1. a) K.N. Stepanov, Soviet Phys. JETP, 18, 826 (1964).
   b) J.M. Dawson and M.F. Uman, Nuclear Fusion, 5, 242 (1965).
2. a) J.M. Berger et al., Phys. Fluids, 1, 301 (1958).
   b) H.U. Schmidt, Z. Naturforschg., 14a , 975 (1959).
3. D.J.H. Wort, Nuclear Fusion Reactor Conference, Culham 1969, Communication 5-7.
4. V.V. Nemov and K.N. Stepanov, Nuclear Fusion, 8, 133 (1968).
5. T.H. Stix, The Theory of Plasma Waves, McGraw-Hill, 1962.
6. R.Z. Sagdeev, Reviews of Plasma Physics, Consultant Bureau (1966) vol.4, p. 23.
7. V.E. Zakharov and V.I. Karpman, Soviet Phys., JETP, 16, 351 (1963).
8. A.A. Vedenov, E.P. Velikhov, and R.Z. Sagdeev, Nuclear Fusion 1, 82(1961).
9. T.E. Stringer, Private Communication.
10. A.A. Galeev and R.Z. Sagdeev, Soviet Phys. JETP, 26 , 233 (1968).

HIGH FREQUENCY HEATING OF A DENSE FULLY IONIZED PLASMA

by

B.Lehnert, J.Bergström, M.Bureš, and E.Tennfors

ROYAL INSTITUTE OF TECHNOLOGY

S-10044 Stockholm 70, Sweden

Abstract. A dense fully ionized plasma with a neutral gas blanket is confined in an internal ring device. High-frequency power of about 0.5 MW is absorbed by the plasma at the magneto-acoustic resonance. The plasma can be sustained when the power input exceeds a certain minimum level. The losses along the magnetic field affect the plasma balance at small fluid velocities, as expected from theory. There are indications that the plasma can be stabilized against flute disturbances by line-tying effects which are controlled by external means.

1. Experimental Aim and Arrangement. A dense fully ionized plasma with a neutral gas blanket can only be sustained when the heating power exceeds a certain minimum level P_{min}(1,2,3). For magnetic confinement in an internal ring device with magnetically screened supports, it is also necessary that the fluid motions are slow compared to the thermal particle velocities(4).

As a first step along these lines experiments have been performed with device F IIA in which an internal ring-shaped coil is suspended by unscreened supports. Only the fraction κ_w=0.061 of the confinement volume consists of field lines ending on a wall surface, i.e. on the supports. A rotating plasma of density $10^{21} m^{-3}$ is created by a discharge across a magnetic field of mean strength 0.44 Vsec/m^2 in the mid-plane of the device. High-frequency heating is imposed at the magneto-acoustic resonance of radial oscillations, at about 1.3 MHz. To study the effect of losses along the magnetic field, a glass plate can be made to cut the field lines passing through the area inside the internal coil. This corresponds to a change of κ_w from 0.061 to 1.

2. Large Rotational Velocities. The behaviour of the voltage ϕ_{12} between the electrodes of the rotating plasma and the corresponding current J_r are shown in Fig.1 for two superimposed shots. When the plasma is sustained by shear heating from the rotation only, the minimum power input is reached at time $t_m(0)$=0.8 msec., after which a transition takes place to a lowly ionized mode of high impedance ϕ_{12}/J_r. If high-frequency heating is superimposed by applying ϕ_0=15kV on the power supply of the high-frequency generator, the transition is displaced to $t_m(15)$=3.4 msec. The time t_m changes abruptly from about 1.2 to 2.4 msec. when ϕ_0 passes about 11.5 kV. That the plasma state makes a sharp transition is also seen from the azimuthal high-frequency current J_φ induced in the plasma (Figs.2a,b). Thus the required minimum power input has at least been passed at the observed transition, the heating being mainly due to an absorbed high-frequency power which can be estimated to about 0.5 MW. The decrease in J_φ at $t>t_m$ in Fig.2b is due to the decay of the power supply voltage ϕ_0.

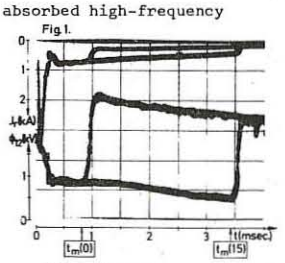

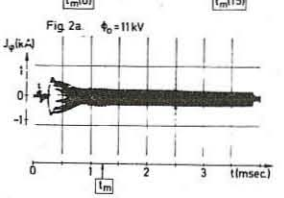

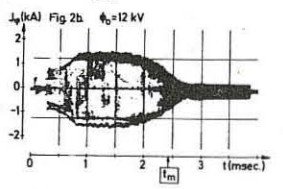

3. Small Rotational Velocities. The duration of the main rotating plasma mode has been shortened in the experiments of Figs.3a-e. The shear heating power from the rotation becomes less than 0.3 MW for times $t>t_r$=0.7 msec. and decreases to a value below 0.1 MW at t=1.3 msec. These levels are much lower than P_{min}. In the interval $t_r<t<t_J$ a slowly rotating holding mode is sustained by a small current J_r which drops to zero at $t=t_J$. During this mode part of the voltage ϕ_{12} arises from sheet potentials, and not from induced voltages due to the rotation. With κ_w=0.061 and a small high-frequency power input (ϕ_0=7.5 kV), J_r decreases rapidly to a low level at times $t>t_r$, i.e. when the shear heating becomes small and the plasma cools off and decays (Fig.3b). When ϕ_0 is increased to 15 kV, however, high-frequency heating is provided by a large current J_φ which sustains a fully ionized plasma also after the time t_r, all the way to $t=t_f$ where the plasma balance breaks down (Fig.3c).

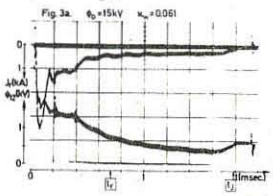

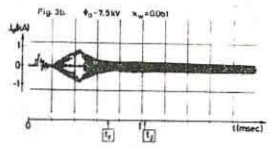

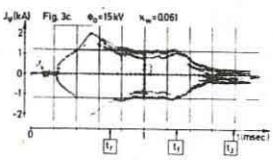

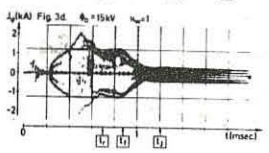

With the plate position corresponding to κ_w= 1 in Fig. 3d there is no change as compared to Fig.3c in the behaviour for t<0.5 msec. where there is a strongly developed rotation. At later times, however, the current J_φ becomes smaller and the plasma break-down at t_f occurs earlier. This is explained by the increase in longitudinal losses which occurs in a slowly rotating plasma when κ_w is being increased (1).

It is likely that the breakdown at t_f is not due to a sudden decrease in the available power input, but to a flute instability which arises when the current J_r has dropped below a certain level. This is supported by Fig.3e where the current J_r of the holding mode has been cut off instantaneously by a short-circuit at $t=t_J$. A possible explanation of these results is that the plasma is stabilized by the joint effects of line-tying and the finite Larmor radius (5), and that line-tying between the plasma boundary region and the electrodes is weakened when the electrode current J_r becomes small.

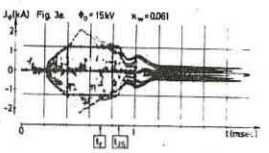

The authors are indebted to Mr. S.Holmberg, Mr. R. Ekman, Mr. D. Haslbrunner, Dr. B. Wilner, Mr. A. Brahme, Mr. P.Mattson, Mr. G. Hägerström, Mr. G. Kindberg, and Mr. L. Åsbrink for valuable help with the measurements and the development of the experimental equipment. The work has been supported financially by the Swedish Atomic Research Council and the Bank of Sweden Tercentary Fund.

References.

(1) B. Lehnert, Arkiv f. Fysik 38 (1968) 499.

(2) B. Lehnert, J. Bergström, and S. Holmberg, Third European Conference on Controlled Fusion and Plasma Physics, Utrecht, (1969), Wolters-Noordhoff Publ., p.57.

(3) B. Lehnert, J. Bergström, S. Holmberg, and E. Tennfors, Electron and Plasma Physics, Royal Inst. of Technology, Stockholm, Rep. 69-34 (1969).

(4) B. Lehnert, Plasma Physics 10 (1968) 263.

(5) B. Lehnert, Phys. Fluids 9 (1966) 1367.

H.F. PLASMAS AND HEATING

Ion Cyclotron Excitation and Extended Containment by RF Fields

M. L. Pool and Paul Arendt
Ohio State University, Columbus, Ohio USA

Abstract: By means of two-phase cyclotron excitation ions can be driven to arbitrarily chosen energy values in the thermonuclear range and maintained in energy in prescribed parking areas. The orbital guiding centers walk toward the central axis of the magnetic bottle. Small angle scattering losses in energy and in direction of motion are removed.

An inspiriting approach to a realistic thermonuclear reactor is now evinced through experimental results and through computer analyses. The former is secured by an auxiliary rotating electric field and a revolving magnetic field, both at the ion cyclotron frequency, impressed upon the main B_z magnetic field of the magnetic bottle employed. The latter is secured by submitting various pertinent boundary and operating conditions to a 360 IBM computer. The auxiliary rotating electric field is normal to the direction of the central axis of the magnetic bottle and is obtained from neighboring electric currents. The auxiliary revolving magnetic field is parallel to B_z[1].

The experimental results were obtained from a plasma produced by two 30-kW amplifiers operated at 4.225 MHz in quadrature and controlled by a crystal. The plasma was contained in a 10-cm diameter pyrex tube in a magnetic bottle. The action of the rotating electric field and revolving magnetic field accelerated the ions and prevented them from reaching the wall of the container. By means of a Faraday cup energies in the neighborhood of 1.0 keV were measured. Ion densities of 5×10^{12} cm^{-3} were obtained. The cyclotron resonance was sharp. The computation results have been carried out for a plasma to be produced in a 20-cm diameter container by two-phase excitation at 5.0 MHz for the deuteron and 3.4 MHz for the triton. Both two-phase frequencies are present at the same time in a deuterium tritium mixture.

As an example, the rotating and revolving fields can readily heat the tritons from an energy of a few electron volts to a maximum of 57 keV. From then on the ion's energy slowly oscillates between 7 keV and the maximum. Simultaneously in the same plasma the deuterons are energized to a maximum of 58 keV and then slowly oscillate in energy between this value and 20 keV. Even though the guiding centers of the low energy ion orbits may start many centimeters from the mirror axis, the centers gradually move to within 0.5 cm of the mirror axis and remain. Thus no ions are lost through energizing beyond controll. Motion in three dimensions also has been numerically analyzed. Although the magnetic mirrors tend to put the ion ahead in phase relative to the phase of the cyclotron frequency of the oscillator, the electric field impressed by the oscillator continually tends to rephase the ion in its orbit so that the gain in phase caused by the mirrors is nullified.

The effects of scattering on the motion of an ion have been considered at each 0.15 degrees of arc of the ion's orbit. Many small angle scatterings contribute to give a single large scattering angle. The rephasing action of the electric field during the mean free time reduces the net scattering angle. Consequently, nearly all the ions which initially have energies of even a few tenths of an electron volt, and therefore have many scattering experiences, reach energies in the keV range without being scattered out of the system. In most cases calculations were made where the small angles varied between 10 and 15 degrees of arc and where a scattering event occurred whenever the deflection probability reached or exceeded 40 percent. Ion diffusion losses across magnetic lines of force are thus effectively eliminated.

Scattering in more detail: The root mean square of the net deflection is related to the total number of individual deflections and to the root mean square average deflection in such a way that 81 random 10-degree scatterings are needed on the average to obtain a 90-degree deflection. Thus the mean deflection for a scattering angle of 10 degrees will occur approximately in a time $T_{10} = T_{90}/81$. The probability of deflection at a particular angle, b, for an ion at a constant speed depends on time in an exponential manner, $P_b = 1 - e^{-t/T}$. To take into account the cyclotron acceleration of the ions, the mean deflection time, T_b, was recalculated during each iteration of duration Δt, so that $P_b = 1 - \exp[-\Delta t (1/T_{b1} + 1/T_{b2} + \ldots)]$. Whenever the deflection probability equaled 0.40, a reasonably conservative criterion, a deflection was assumed to take place. These small angle scatterings were not varied in a random fashion. Scattering sequences were chosen which were more conservative than average. Also the deflections were not restricted to the plane perpendicular to the axis of the magnetic mirror. The calculation of the velocity of the ion after a deflection proceeded as if the ion encountered a stationary particle. The ion thus experienced a continuous loss of energy to its neighbors. In a plasma of density 2×10^{13} ions cm^{-3} with a 50-volt cm^{-1} accelerating electric field a deuteron with an initial energy of only 0.25 eV is shown to have a high probability of being accelerated into the keV energy range without being scattered out of the plasma volume. (2)

Energizing in more detail: For the numerical calculation of the motion on an ion, an orbit is partitioned into many small arc lengths. At the beginning of each small arc the ion's position, velocity, radius, and guiding center are known. The parameters of the ion halfway through the arc are determined as well as the DC magnetic induction and the electric field parallel and perpendicular to the direction of motion. These values are used as averages over the arc segment in calculating the new radius, velocity, guiding center, position and incremental phase change at the end of the segment. The above process is then repeated. A similar program for analyzing ion motion in a three dimentional mirror geometry has been used. The strength of the electric field increases with radius in order to force a drift of the guiding centers toward the symmetry axis. The strength of the magnetic field decreases with radius in order to force a phase lag as the ion energy increases. When the phase lag is $\pi/2$ relative to the impressed electric field, no additional energy will be given to the ion. Calculations have been made for ion motion in a plasma of density up to 10^{14} cm^{-3}. At these densities the depression in the magnetic field becomes significant. The positions of a deuteron after each of many rotations of the electric field is shown in the sketch. The positions oscillate about the phase lag angle of $\pi/2$ radians, and in so doing form a parking area as indicated. Since the ions are not lost by excessive energization nor by scattering, greatly extended containment time accrues through the above unique use of R F fields. (3)

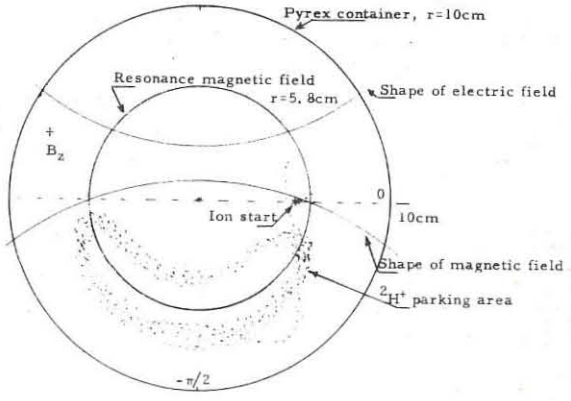

(1) John W. Snyder, Paul E. Weiler and M. L. Pool. Bull. Am. Phys. Soc. 13, 1509 (1968). Abdul Kabir Bashir, J.R. Springer, R. R. Kempple, Paul Arendt and M. L. Pool. Bull. Am. Phys. Soc. 14, 1020 (1969).

(2) B. Samuel Tanenbaum, Plasma Physics, McGraw-Hill Co. 1967.

(3) N.E. Andreev. Soviet Physics - Technical Physics, 14, 1171 (1970)

Work supported by a Grant from the U.S. AFOSR.

INVESTIGATION OF HIGH FREQUENCY WAVE ABSORPTION BY PLASMA BETWEEN ELECTRON CYCLOTRON AND LOW HYBRID FREQUENCIES

B.V.Galaktionov, V.E.Golant, V.V.Djachenko, O.N.Scherbinin

A.F.Ioffe Physico-Technical Institute, Leningrad, USSR

Abstract: In experiments described the conditions of hf wave absorption by plasma and efficiency of plasma heating were determined. The sharp boundaries of absorption and heating were revealed. Data on efficiency of electron and ion heating were obtained.

In recent experiments /I-3/ the absorption of hf waves by plasma was observed between the low hybrid frequency (ω_L) and the electron cyclotron frequency (ω_{eH}). In an inhomogeneous plasma the absorption can be accounted for by the linear transformation of electromagnetic waves into plasma waves possible in 3 separate transformation ranges /4/. For a one-dimensional plasma layer the boundaries of these ranges are determined by the angle α between the density gradient and the magnetic field. In our frequency band the transformation range extends from ω_{iH} up to ω_c, where

$$\omega_c^2=\omega_L^2\left(1+\frac{m_i}{m_e}\cos^2\alpha\right)=\omega_{eH}\omega_{iH}\frac{\omega_p^2+\omega_{eH}\omega_{iH}}{\omega_p^2+\omega_{eH}^2}\left(1+\frac{m_i}{m_e}\cos^2\alpha\right) \qquad (1)$$

(ω_p – plasma frequency for the maximal plasma density, ω_{eH}, ω_{iH} – gyrofrequencies of electrons and ions).

An analysis made by A.D.Pilija and V.I.Fedorov has shown that in a real plasma with axial symmetry the one-dimensional theory remains true qualitatively if the dependence of plasma parameters on one of coordinates is much stronger than on the others (for instance, if $\nabla_r n \gg \nabla_z n$). In the opposite case some peculiarities can arise. In particular, new transformation regions become operating near the flex points of lines of equal plasma density.

The results of two experiments are presented below which were obtained with an impuls device described in /3/. In the first experiment an argon plasma was used at pressures 2.10^{-4} – 10^{-2} mm Hg when the role of transverse diffusion in plasma formation was rather high ($\alpha \neq 90^\circ$). The boundary of effective absorption was found from studying the conditions under which plasma was maintained by hf power at frequencies much lower than electron cyclotron. The power of 50w generator (f = 100–300 Mhz) was delivered to a single turn 8cm diam. x 20cm long coil placed in the middle part of the device. Plasma behaviour was checked by integral light emission. The average density was measured by a resonator near the coil.

The plasma with $n = 10^{10} - 10^{11}$ cm^{-3} emerged at the strong enough magnetic fields and ceased when the magnetic field decreased below the critical value (H_{cr}). Fig.1 represents the dependence of light emission intensity on the magnetic field at a steady hf power level (f = 116 Mhz) for various pressures. It is shown that there are sharp drops of light intensity at some critical magnetic fields (H_{cr1}, H_{cr2}). The number of such drops increased with pressure and power level, whereas the values of the critical fields diminished.

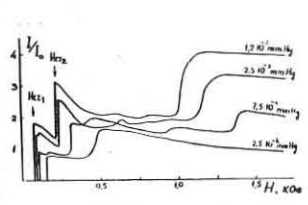

Fig.1.

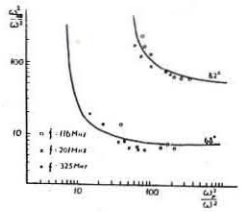

Fig.2.

Fig.2 shows the values of H_{cr1} (lower group of points) and H_{cr2} (upper group of points) for various operating frequencies and power levels (i.e. plasma densities) at pressure $p = 7{,}5.10^{-4}$ mm Hg. Both groups of the experimental points are close to theoretical curves culculated from eq.(1) for the angles α of 68° (H_{cr1}) and 82° (H_{cr2}). Of significance is the fact that the critical field values do not depend of wave frequency but on plasma parameters. So the dependence on pressure mentioned can be accounted for by larger longitudinal density gradients at higher pressures (and consequently by smaller α angles). It was observed also that the change of discharge structure (diameter) occured at the magnetic field equal to H_{cr2}. It might be related to "switch-off" of the additional transformation regions mentioned above.

The second experiment was carried out in hydrogen at $p = 5.10^{-4}$ mm Hg when the axial density distribution was practically uniform ($\alpha \approx 90^\circ$). Plasma with $n = 5.10^{11} - 5.10^{12}$ cm^{-3} was obtained by 3-cm microwave power under the cyclotron resonance conditions in mirrors. An impulse hf generator (f = 116Mhz, P = 3kw, τ = 2 μsec) was used for plasma heating. The power delivery remained the same. The change of transverse energy of charged particles measured by a diamagnetic probe in dependence on the magnetic field is plotted in fig.3. The efficiency of heating is shown to decrease abruptly at the magnetic field less than the value corresponding to the low hybrid frequency (marked by the arrow), i.e. at leaving the transformation range.

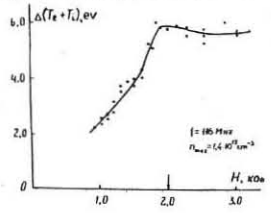

Fig.3.

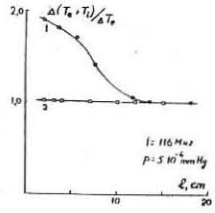

Fig.4.

The diamagnetic measurments of the temperature distribution (fig.4) disclosed that considerable part of absorbed power went to ion heating. Curve 1 shows the decrease of the summary temperature with the removal from the hf coil at the distance of order of the ion charge exchange path (for the conditions of the experiment $\lambda_i \approx$ 5cm). The flat part of the curve corresponds to the temperature of electrons for which the length of energy relaxation was much larger than the system dimensions. The uniform electron heating in these conditions was confirmed by the distribution of diamagnetic signal at applying a short pulse of microwave power to the middle part of plasma column (curve 2, fig.4).

It should be noted that the energy input efficiency decreased at the maximal plasma densities ($n > 10^{12}$ cm^{-3}). It might be due to the influence of evanescence region. The data obtained on the correlation between elelctron and ion heating are in agreement with the calculations of collisional damping of plasma waves. In the experimental conditions the effective collision frequencies determinant electron and ion parts of energy absorbed were the same order of magnitude ($\frac{\nu_e}{\omega} \approx \frac{\nu_i}{\omega} \approx 10^{-3}$).

REFERENCES

1. O.M.Shvets, S.M.Sotnikov, V.F.Tarasenko, S.S.Ovchinnikov, ZTF, 39, 610 (1969).
2. V.N.Budnikov, V.E.Golant, A.A.Obuchov, Phys.Lett., 31A, 76 (1970).
3. B.V.Galaktionov, V.E.Golant, O.N.Scherbinin, 9-th Int.Conf.on Phen. in Ionized Gases, 1969, Contributed Papers, Bucharest, 1969, 516.
4. A.D.Pilija, V.I.Fedorov, ZETF, 57, 1198 (1969).

H.F. PLASMAS AND HEATING

TWO-ION COLLISIONAL ABSORPTION OF LOW FREQUENCY ELECTROMAGNETIC WAVES IN A TOROIDAL HARD-CORE CONFIGURATION

by

J. Adam, F. Alvarez de Toledo and D. Feltin.

ASSOCIATION EURATOM-CEA
Département de la Physique du Plasma et de la Fusion Contrôlée
Centre d'Etudes Nucléaires
Boite Postale n° 6 - **92 Fontenay-aux-Roses** (France)

Abstract : The absorption of the fast hydromagnetic wave propagating in a two species plasma (H + D) has been investigated in a Levitron-type device. In agreement with the calculations, the wave could be excited for experimental parameters appropriate to the collisional absorption and the damping length outside the emission coil was found to be minimum for $\omega_{cH} > \omega > \omega_{cD}$.

Collisions between two ion species provide a simple way of thermalizing the ordered motions induced in a plasma by electromagnetic RF waves, with subsequent heating of the ion component.

An analysis of that process shows that the power transfered from the wave to the ions is given by

$$W = \frac{1}{8\pi\omega}\left(\gamma^{+}|E^{+}|^2 + \gamma^{-}|E^{-}|^2\right)$$

with
$$\gamma^{\pm} = \omega \xi \frac{\omega_{p_1}^2\,\omega_{p_2}^2}{\omega_{c_1}\,\omega_{c_2}}\left[\frac{\omega(\omega_{c_1}-\omega_{c_2})}{(\omega\pm\omega_{c_1})(\omega\pm\omega_{c_2})}\right]^2 \qquad (1)$$

and
$$4\pi e^2 c^4 \xi = \frac{m_1 \nu_{12}}{n_2} = \frac{m_2 \nu_{21}}{n_1}$$

$E^{\pm}$ are the rotating components of the RF electric field perpendicular to the magnetic field (the - sign corresponds to the ion gyration direction). The other symbols have their usual meaning . Examination of equation (1) and of the phase relations of the electric field shows that the efficiency of the heating mechanism is maximum for $\omega_{c_1} > \omega > \omega_{c_2}$. For these conditions, the ions motions of the two species are opposite in phase : the space charges generated tend to neutralize each other and especially large ion currents are allowed to develop in the plasma. Thermalization of these motions is achieved by ion-ion collisions, the efficiency of the process being larger for higher densities and lower temperatures.

That heating mechanism was checked in the hard-core configuration described below . Figure 1shows the radial profile of the heating rate computed in that configuration for the parameters indicated in the figure. An appreciable heating requires a high value of the RF electric field ($\geq$100v/cm). However a considerable amplification of that field can be expected if the conditions for maximum absorption can be made to coincide with the conditions for exciting the fast hydromagnetic wave. Fig.2 shows the dispersion relation of the fast wave computed by numerical integration /1/ for a hard-core geometry and a plasma containing 50 % H_2 and 50 % D_2 . For $\omega_{cH} > \omega > \omega_{cD}$, the wave should propagate for $n_H = n_D \cong 2.10^{14}$ cm^{-3}. These conditions actually coincide with the absorption conditions indicated in Figure 1 .

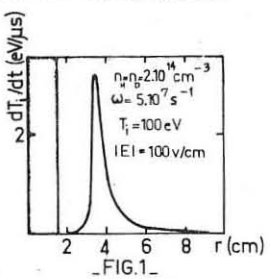

FIG.1

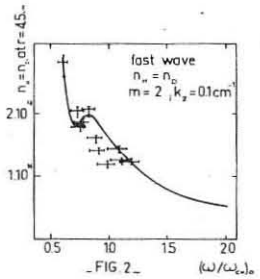

FIG. 2

The purpose of the experimental work was two-fold :

- To check the possibility of exciting the fast wave in the expected conditions.
- To investigate the damping of the wave.

Experimental Device.

Stator B is a toroidal Levitron-type device with supported ring. The major diameter of the ceramic vessel is 150 cm, the minor diameter 20 cm. The toroïdal and poloïdal fields rise-time is 300 µs. After crowbar , the fields decay with a time constant of 1 ms. The gas is ionized by the electric field associated with the time-varying magnetic fields and heated by the current induced in the plasma. The average density, measured by 2mm interferometry can be varied between 2.10^{13} cm^3 and 2.10^{14} cm^{-3}. Electron temperature deduced from the plasma resistivity reaches 10 to 20 eV.

The waves are generated by a helical coil,periodic along the toroidal (k_z=0,1cm^{-1}) and azimuthal (m = 2) coordinates. The coil is supplied by a power oscillator, the frequency of which can be varied from 5 to 12 MHz. The amplitude and profile of the wave field can be measured at different locations along the torus by a number of small magnetic probes.

Fast wave propagation.

The plasma density and the magnetic field both vary during the duration of the discharge. With the oscillator triggered at the breakdown-time, an amplification of the RF field is observed in the plasma, outside the coil, when the experimental parameters match the propagation conditions. The values of n and B , measured at the time when propagation occurs can then be plotted for comparison with the theoretical curves.

Figure 2 shows the result of that comparison in the case of a [50 % H + 50 % D] plasma. The agreement is satisfactory : as expected by calculations, the fast wave can be excited in a two-ion plasma at the parameters appropriate for collisional damping ($\omega/\omega_{cH} \sim 0,75$; $n_H = n_D \cong 1$ to 2.10^{14} cm^{-3} at the center of the plasma).

Wave damping.

Measurement of the RF power absorption via the increase in ion temperature was discarded for this experiment, owing to the short energy confinement time in Stator B ($\tau_E \leq 100$ µs). The damping of the wave could be demonstrated however by measuring its attenuation length outside the coil. The decay of the wave amplitude away from its emission source can be due to two differents causes : an actual damping or an evanescent character of the wave, if the experimental conditions are slightly different from the propagation conditions. Special care was taken to differentiate those two effects by comparing the wave behaviour in pure D_2 and in the mixture $H_2 + D_2$.

In the case of pure D_2, experimental conditions corresponding to negligible damping can be found for any value of $(\omega/\omega_{cH})_o$ (measured at 4.5 cm from the axis) between .5 and 1. In the case of the mixture ($H_2 + D_2$), similar measurements show that no-damping propagation is observed only for $(\omega/\omega_{cH})_o$ values larger than.85 or smaller than.55. Between those limits , the wave amplitude, 84 cm away from the coil , is 2 to 3 times smaller than it is in the corresponding experiments using D_2 . The measured values of the damping length as a function of $(\omega/\omega_{cH})_o$ are plotted in figure 3.

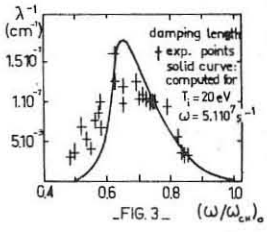

FIG. 3

The solid curve in that figure was computed on the basis of a model assuming cylindrical geometry, a given density profile consistent with independent measurements, and a uniform ion temperature of 20 eV. Although no direct measurement of T_i was made, that value is consistent with T_e deduced from the resistivity measurements. The reasonable fit between the curve and the experimental points gives confidence that the observed damping can be explained by the mechanism we have considered.

/1/ J.Adam, F. Alvarez de Toledo, P.H. Rebut and A. Torossian Plasma Physics, 11, 297 (1969)

HARMONIC ABSORPTION OF MICROWAVES IN MAGNETIZED LOW DENSITY PLASMA

by

R.Cano, I.Fidone, M.Schwartz, B. Zanfagna

ASSOCIATION EURATOM-CEA

Département de la Physique du Plasma et de la Fusion Contrôlée
Centre d'Etudes Nucléaires
Boite Postale n° 6 - **92 Fontenay-aux-Roses** (France)

Abstract : Increased ionization and temperature due to harmonic cyclotron absorption have been observed in a low density, warm magnetized plasma subjected to high power microwaves.

I. The absorption of high power microwaves in a low density, warm Argon plasma has been indirectly detected by increased ionization and temperature at the electron cyclotron frequency and its second harmonic. This differs from the direct measurements of Arunasalam et al, [1], in which absorption in a low power transmitted beam by a high density plasma was observed. The absorption was investigated as a function of microwave power, pressure and magnetic field. The average density was determined by interferometric measurement of the phase shift of the ordinary wave. Temperature was determined by a Langmuir probe placed perpendicular to the magnetic field.

The 17.6 GHz microwave beam, modulated at 500 Hz, was propagated in the extraordinary mode at an angle of 80° with respect to the applied DC magnetic field. Focussing of the beam at the center of the discharge was accomplished with teflon lenses. The power of the beam was variable from 3 to 100 watts.

II. In figures 1 and 2 the ion current to a negatively biased Langmuir probe is shown as a function of magnetic field for two different levels of input power. It is clear that relatively little power is required to initiate the discharge near the fundamental and second harmonic of the electron cyclotron frequency. If sufficient power is applied the discharge can be initiated throughout the frequency range $2f_c \geq f_i \geq f_c$, where f_c, f_i are the cyclotron and incident microwave frequencies respectively [2]. In figure 3 the thre shold power for discharge initiation is shown as a function of magnetic field. The minimum required power at $f_i = f_c$ can be accounted for by single particle resonance phenomena and is well known in the theory of microwave breakdown in a magnetic field [3]

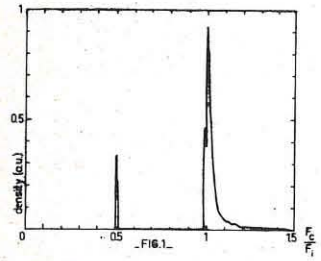

FIG.1

Ion saturation current of a Langmuir probe located in the center of the discharge vs. magnetic field.
F_i = 17,6 GHz, P_i = 10 W
$P_o = 10^{-3}$ torr.

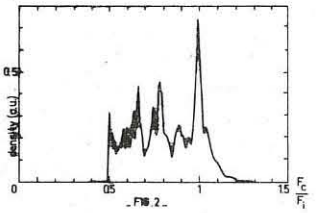

FIG.2

Ion saturation current of a Langmuir probe located in the center of the discharge vs. magnetic field.
F_i = 17,6 GHz ; P_i = 100 W
$P_o = 10^{-3}$ torr.

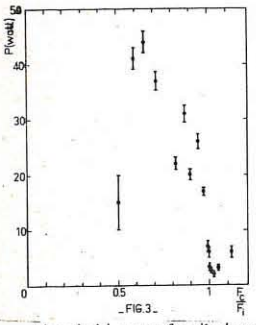

FIG.3

Thre shold power for discharge initiation as function of magnetic field.
F_i= 17,6 GHz $P_o = 10^{-3}$Torr

We speculate that the apparent resonance phenomena at $f_i = 2f_c$ represents a plasma assisted microwave breakdown. The high frequency microwaves may cause sufficient ionization, resulting in a low density, warm plasma that escapes detection by the relatively insensitive method used to detect breakdown. Cyclotron absorption (to be discussed shortly) then results in further coupling of power culminating in a clear breakdown condition.

III. We now turn our attention to the plasma aspects of the experiment. In figures 4 and 5 the measured temperature, T (eV), and density, n (cm^{-3}), at the fundamental and second harmonic are shown as a function of input power. The density is seen to vary linearly with power.

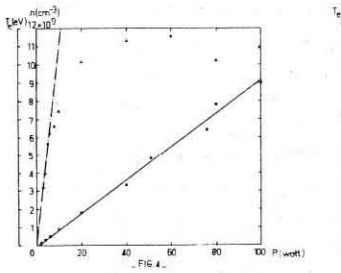

FIG.4

Measured temperature (▲) and density (•) vs. input power at the second harmonic. The dashed line is calculated from eq.(1)
$P_o = 10^{-3}$ Torr - F_i = 17,6 GHz

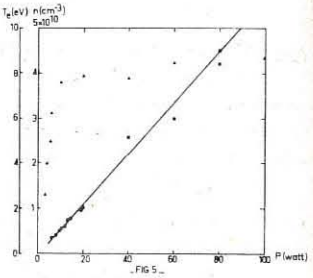

FIG.5

Measured temperature (▲) and density (•) vs. input power at the fundamental.
$P_o = 10^{-4}$ Torr - F_i = 17,6 GHz

The temperature exhibits linear behaviour for low power, but is constant for $P_i \gtrsim 20$ watts. For low input power the relatively low values of n, T suggest that only elastic, binary collisions are of importance. If we assume the dominant heating mechanism at the second harmonic to be cyclotron absorption followed by collisional thermalization we may write :

$$(1) \quad \frac{2}{3} \vec{J}.\vec{E} = n \delta \nu T$$

where δ = fraction of energy transferred per collision

ν = collision frequency for momentum transfer = $P_o P_c V_{th}$

P_o = pressure in Torr

P_c = collision probability (taken to be constant for simplicity)

V_{th} = thermal velocity

$$\text{Now } \vec{J}.\vec{E} = \frac{P_i}{V} c = \frac{P_i}{V} \frac{\pi^{1/2} \ell \gamma \left(\frac{kT_e}{m}\right)^{1/2} \omega \tan\theta}{2\sqrt{2}\, c^2}$$

where ℓ = geometrical path length of radiation through the plasma

$\gamma = \frac{\omega^2 p}{\omega_c^2}$

$\theta = 80°$, angle between the direction of propagation of the wave and D.C. magnetic field.

V = interaction volume.

We use the experimental values to separately calculate each side of (1). Thus for $T = 5eV, n = 3,6\ 10^9 cm^{-3}, P_i \sim 4,0W, P_o \sim 10^{-3}$Torr the collisional thermalization (RHS) = $2 \frac{erg}{sec\,cm^3}$ while cyclotron absorption (LHS) = $6 \frac{erg}{sec\,cm^3}$ in reasonable agreement.

The constancy of temperature for $P_i \gtrsim 20$ watts may be indicative of inelastic processes such as excitation, and ionization now dominating the plasma behaviour. The calculation of absorption near f_c is considerably more complicated as the wave must first travel through a cutoff region by tunneling, before reaching the resonance at the upper hybrid frequency, f_H . Here we make use of a simplified expression for absorption, due to Budden [4], to calculate $\vec{J}.\vec{E}$. In Budden's model the energy accumulated at the resonance in the limit of $\nu \to 0$ is determined. The introduction of a finite ν results in heating as in the case of absorption at the second harmonic. We can write :

$$(2) \quad P_i\, e^{-2\pi^2 \frac{\Delta x}{\lambda}} = \delta \nu T n V$$

where $\Delta x = \Delta x(n,B)$ = distance that wave must propagate beyond the cutoff to reach the upper hybrid resonance. We have separately calculated both sides of (2) with experimental values and find agreeement to within an order of magnitude. We believe better agreement would be illusory because of the difficulty of determining Δx, and its appearance in the exponential in (2).

References :

[1] V.Arunasalam et al. - Physics of Fluids Vol.11 n°5 - May 1968

[2] A.M.Messian - P.E.Vandenplas - Physics of fluids Vol.12 n°11 Nov.1969.(Some aspects of this experiment are similar to ours).

[3] A.D. Mac Donald, Microwave Breakdown in Gases - Wiley (1966)

[4] K.G.Budden., Radio waves in the Ionosphere - Cambridge University Press (1966).

THE INFLUENCE OF AN ELECTROSTATIC FIELD ON CYCLOTRON RESONANCE BEHAVIOUR OF A PLASMA

by

D.C. Schram, P. Manintveld and E. Oord

Association Euratom-FOM
FOM-Instituut voor Plasma-Fysica
Rijnhuizen, Jutphaas, The Netherlands

Abstract

The theoretically predicted influence of an electrostatic field on the energy gain of electrons at e.c.r. is confirmed experimentally by measuring the loss tangent of the plasma as a function of an applied D.C. voltage. The applicability of this effect as a heating scheme is discussed in general terms.

In a recent publication[1] the influence of an electrostatic field on the energy gain of charged particles at cyclotron resonance has been studied. Here a circularly polarized TEM wave (ω, k) was assumed to propagate along a uniform static magnetic field. In the following $g=eE^{\sim}/m\omega c$, $a=eE_o/m\omega v_p$, $\beta=eB_o/m\omega-1$, are parameters defining the e.m. wave, the e.s. field, and the static magnetic field resp.; $\alpha=n_e e^2/m\varepsilon_o\omega^2=\omega_p^2/\omega^2$, is a parameter for the electron number density, n_e. Close to the resonance even a weak external effect, here an e.s. field, has a considerable influence on the motion of single electrons, resulting in a change of the characteristics of plasma.

In the absence of an e.s. field, the so-called "undisturbed case", the energy of the particle is a periodic function of time, Fig. 1 curve "0", and an oscillation time t_{os} can be defined. This remains valid if the relativistic mass variation and axial velocity variation due to the Lorentz force are taken into account.[3]

In the presence of an e.s. field two regimes can be distinguished, depending on the time scale on which the e.s.field causes a certain change of the resonance function, $r(t)=(\omega-kv_z-\Omega(t))/\omega$[2]:

- "strong external effect", the particle is pulled out of resonance within the first oscillation period. A stepwise energy increase is found (curves "1.03", "2" of Fig. 1).
- "weak external effect", the particle remains close to resonance: a continuous increase in energy is added to the undisturbed oscillatory behaviour (Fig. 1, curves ".1", ".5").

At the transition, $a=a_{synchr.}$, defined as the synchronous case, a continuous increase in energy occurs (Fig. 1, curve "1").

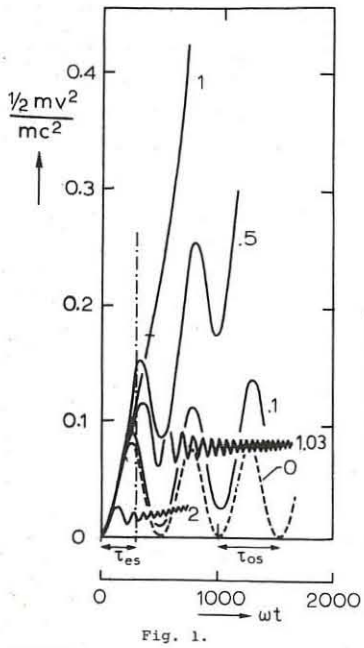

Fig. 1.
Numerically calculated gain of kinetic energy as a function of time; $c^2/v_p^2=0.75$, $g=2.10^{-3}$, $v(t=0)=0$, $\beta=0$, $a_{synchr.}=1.2\times10^{-4}$. The quantity $a/a_{synchr.}$ is curve parameter.

The reactive and resistive behaviour of the plasma has been studied for the "undisturbed case" in Ref. 3. Using the same calibration for the electric field strength of the e.m. wave as in Ref.3, we find for $\beta=0$ (at cyclotron resonance), $a=0$(no e.s.field):

$$\left.\frac{1-\varepsilon}{\alpha}\right/_{\beta=0,a=0} \overset{\sim}{=} 900\, P_{in}^{-1/3}$$

where P_{in} is the incident power of the e.m. wave in Watts. If an e.s.field is applied a part of the electrons is accelerated and a part is decelerated. This leads to resonance functions of opposite sign and, consequently, to dielectric currents of opposite phase. For high values of the e.s. field parameter a, the permittivity, ε, tends to the vacuum value 1.

The loss tangent of the plasma can be calculated if the time of escape of the particles is known. Experimentally[3]

$$t_{es} \approx 1/2\, t_{os}\Big/_{\beta=0,a=0} \quad \text{yielding} \quad \left.\frac{tg\delta}{\alpha}\right/_{\beta=0,a=0} \overset{\sim}{=} 620\, P_{in}^{-1/3}.$$

Evidently, the loss tangent will show a weak maximum for $a=a_{synchr.}$. For values of $a>a_{synchr.}$ the step in energy decreases with increasing a. Consequently, if the escape time is assumed to be independent of a, the loss tangent decreases.

The experimental facility shown in Figs. 9, 10 of Ref. 3 has been used for the measurements. Two electrodes were mounted on the axis and a negative D.C. voltage was applied. The magnetic field strength of the static magnetic field was chosen such that the cyclotron frequency was equal to the applied frequency ($\beta=0$). The loss tangent, the permittivity, and the density of the plasma were measured as functions of the applied D.C. voltage for several values of P_{in}. The result for P_{in}=20W are plotted in Fig. 2 (normalized to the density); the loss tangent shows a maximum at V=2.2.Volt, taken to be $V_{synchr.}$. Values of $V_{synchr.}$ for various values of P_{in} are plotted in Fig. 3.

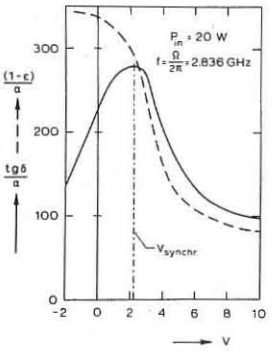

Fig. 2.
Measured loss tangent and dielectric constant as functions of the applied D.C.voltage. $V_{synchr.}$ is the value of V where $tg\delta/\alpha$ is max.

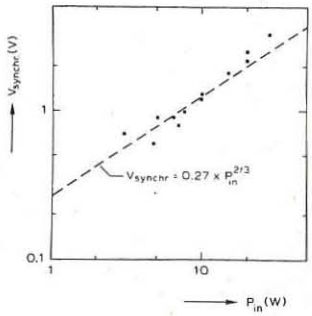

Fig. 3.
$V_{synchr.}$ as a function of P_{in}. The dashed line is the theoretically predicted curve for a Debye length $\lambda_D \sim 1$ cm.

As predicted in Ref. 1 we find $V_{synchr.} \propto P_{in}^{2/3}$. Taking the field calibration of Ref. 3, we find theoretically $a_{synchr.}=.92\times10^{-6}\times P_{in}^{2/3}$. The e.s. field is assumed to be constant over a shielding length λ_D of 1 cm, which corresponds to the measured $n_e=3\times10^{17}$/cc and the estimated parallel electron energy of 50 eV. The experimental result, $V_{synchr.}=.27\times P_{in}^{2/3}$, is in agreement with theoretical predictions.

Discussion

The mechanisms discussed here may, in more general terms, be applied to heat plasmas. A discussion of both cases, weak and strong external effects, may be of interest.

If the external effect is weak, the energy grows without any limitation but time. However, even if the density is small the plasma can become extremely reactive, while for higher densities cyclotron absorption will damp the wave before large energies are reached. As a heating scheme it is only attractive in very tenuous plasmas of large dimensions, e.g. extra terrestial plasmas.

In a strong e.s. field a quasi-collisional energy gain occurs. The reactive components of the current are relatively low and can be chosen zero by choosing a value of β slightly different from zero. The permittivity of the plasma is close to the vacuum value. This mechanism could be applied as a heating mechanism in which the heating rate can be chosen. It should be remarked that the external field need not be static: e.g. an e.s. field varying slowly with respect to t_{os} leads to repetitive heating. Such electrostatic waves can be introduced into the plasma.Frequency modulation is an attractive alternative as an external mechanism.

Acknowledgement

Discussions with Dr. L.Th.M. Ornstein and Ir. T.J. Schep have been of great help to the authors.

This work was performed under the association agreement of Euratom and FOM with financial support from ZWO and Euratom.

References

1) D.C. Schram and G.P. Beukema, Physica 42 (1969), 277-290.
2) D.C. Schram, W. Strijland and L.Th.M. Ornstein, Contributions III Eur.Conf.Contr.Fusion & Plasma Phys., p.71, Utrecht,1969.
3) D.C. Schram, Physica 46 (1970), 97-118.

Neutron Production by Vortex Annihilation in the "Plasma Focus"

W. H. Bostick, L. Grunberger, W. Prior, and V. Nardi

Stevens Institute of Technology, Hoboken, N. J. U.S.A.

Abstract: Image-converter photographs show that when neutrons are being produced in the "plasma focus" the hot dense plasma is not concentrated on the axis but is in the regions where plasma vortex filament annihilation is taking place. Analytical solutions for particle distributions and fields have been found which predict the existence of these plasma filaments.

Image converter photographs[1,2] of the continuum light coming from the plasma focus essentially provide the equivalent of time-resolved X-ray photographs. Figures 1 are 5-nanosecond I.C. axial-view photographs taken of a "plasma focus" (3.5 kj energy storage) operated near the threshold of neutron production. The center conductor (3.4 cm in dia.) is hollow and therefore the light which usually comes from the copper plasma with a solid center conductor does not interfere with the detail of the photographs. Figure 1a is taken at the moment of maximum compression (minimum radius) when the luminous plasma diameter is about 4 mm. and there are on the periphery of this 4 mm disk a series of bright dots which represent locally the beginning of the simultaneous annihilation of the several vortex filament pairs. Note that the photo is taken at the sharp minimum of the $\frac{dI}{dt}$, when there is maximum back emf due to I $\frac{dL}{dt}$, 40 n sec before the neutron pulse has started. Figure 1b taken about 30 ns later shows more clearly the bright spots at filament apexes where filament annihilation is occurring, but the neutron production is still essentially zero. Figures 1c and d are taken when neutron production is occurring and on the back slope of the $\frac{dI}{dt}$ signal. The bright spots in the region of vortex annihilation are quite clearly seen in figure 1d. Figures 1d and e are taken after the $\frac{dI}{dt}$ signal has essentially returned to normal and neutrons are being produced. Note

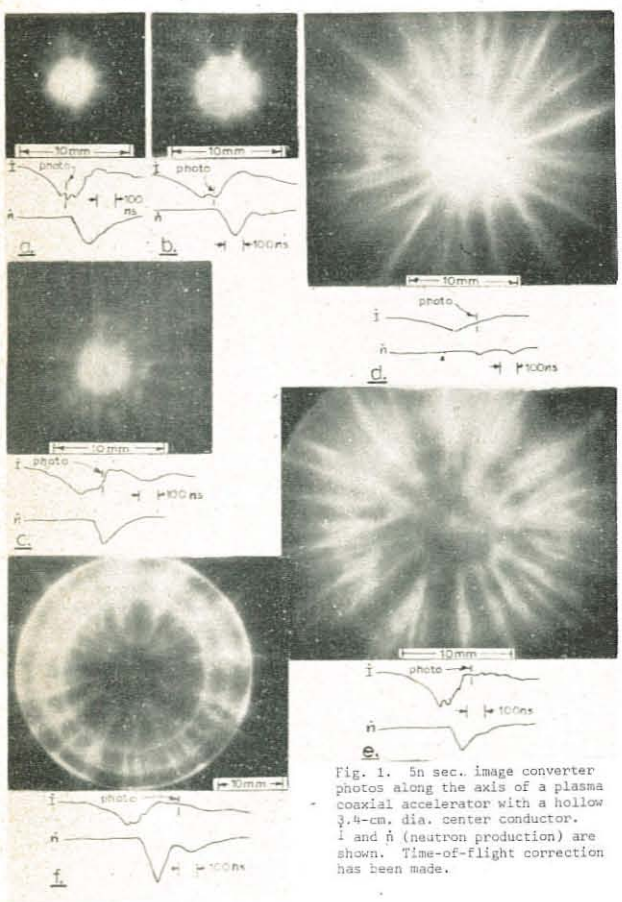

Fig. 1. 5n sec. image converter photos along the axis of a plasma coaxial accelerator with a hollow 3.4-cm. dia. center conductor. I and ṅ (neutron production) are shown. Time-of-flight correction has been made.

that in none of the photos, when neutrons are being produced, is there a marked plasma concentration on the axis, and in figure 1f there is no illumination at all from plasma in the vicinity of the axis. The maximum concentration of plasma on the axis has vanished 150 nsec before the peak of neutron production occurs.

With a hollow center conductor one has a "two ring circus": the configuration of plasma vortices and current sheath inside the center conductor is quite similar to that occurring outside the center conductor. Figure 2 taken obliquely shows the two hot areas representing the regions of vortex annihilation[1] proceeding in both directions along the axis, one inside the center conductor, one outside the center conductor. J.P.Baconnet[3] et al, with schlieren measurements and Thompson scattering measurements also observed that the plasma is not concentrated on the axis when neutrons are being produced. X-ray pinhole photographs by J. H. Lee[4] and by Mather[5] et al, show X-rays produced from an extensive halo pattern as well as from the region on the axis. All of these observations show that the moving boiler model which explains neutron and X-ray production on the basis of an adiabatic compression on the axis is incorrect, as indeed the product of d-d axial center of mass velocity (10^8cm/sec.) and neutron production time (1 to 2 μ sec.) has shown it to be. These observations also show that the traditional simple beam target model which assumes a single pinched current channel on the axis with an accelerating electric field produced by the I $\frac{dL}{dt}$ is incorrect: the neutrons come considerably after the peak of this electric field. Even Bernstein's[6] modified beam target model which assumes a single pinched channel, is untenable. The observations suggest that the deuterons gain energy from the electric fields ($\nabla \times \vec{E} = -\frac{\partial \vec{B}}{\partial t}$) in the region of vortex annihilation and that these deuterons are then projected forward into the as-yet-uncombined portion of the filament pairs. These stable vortex filaments act as particle guides (see bright portions of filaments in figures 1d,e, and f) and it is within these filaments that the accelerated deuterons encounter target deuterons. It must be recognized that the accelerated deuterons have complicated trajectories in the magnetic field of the filament. The model of neutron production can explain why neutron yield with a positive polarity center conductor is higher than with a negative center conductor. J. H. Lee[7] has measured an X-ray spectrum (> 100 kev) from the plasma focus and finds that it follows a power law as does the X-ray spectrum from solar flares. We believe that the vortex annihilation process observed in the laboratory plasma focus is essentially the solar flare process.

Figure 2

Solutions of the equations for the particle distributions account for the generation of these filaments in the current sheath and provides theoretical profiles of the magnetic fields, density, and mass flow within the filaments.

References:

1. W. H. Bostick, L. Grunberger, and W. Prior, Third European Conference on Controlled Fusion and Plasma Physics, Utrecht, June 1969, p. 120.
2. H. W. Jalufka and J. H. Lee, APS Meeting. Winnipeg, June 1970.
3. J. P. Baconnet, G. Casari, A. Coudeville, and J. P. Watteau, 9th International Conference on Ionization in Gases, Bucharest 1969, 4.4.6
4. J. H. Lee, et al, Meeting of the Plasma Physics Division of APS, Miami 1968.
5. J. W. Mather, Physics of Fluids, 8, 366 (1965)
6. M. J. Bernstein, Phys. Rev. Letters 24, 724 (1970)
7. J.H. Lee et al, Bulletin of APS, Washington, April 1970.KD8

Research sponsored by the Air Force Office of Scientific Research under AFOSR Grant No. AF-AFOSR-465-67.

Theory of Magnetic Bundles in Dense Flowing Plasma

V. Nardi

Stevens Institute of Technology, Hoboken, N.J., U.S.A.

Abstract: An exact theory of plasma filaments observed in coaxial accelerators (CA) is derived from a steady-state ($\partial/\partial t = 0$) description of the three dimensional flow of reacting deuterium plasma. Neutron and x-ray production at the muzzle of the gun is associated by this theory with the rapid variation with time of the magnetic structure of the filaments (bundles of helical field lines) in the final (focus) stage.

By considering shock-wave conditions for the current sheath (CS) in CA, it can be proved[1] that the plasma vorticity $\omega = \frac{1}{2}\nabla \times \underline{u}$ is large in the region of space where the filaments are located, immediately behind the shock front Σ (Σ can be considered, essentially, as the foremost luminous face of CS). Vorticity and filament axis have the same orientation[1] (parallel to the z-axis; see fig. 1; without a relevant loss of generality we take $\partial/\partial z \cong 0$, the filaments are considered as parallel cylinders). The existence of a large ω in a narrow region of space (containing the filaments) is not sufficient to conclude that vortex structures exist in that region. More stringently an analytic description of the plasma can be deduced which depicts the vortex nature of the filaments. We can show that a strong component B_z (2.10^3 gauss and larger) of the self-consistent magnetic field exists along the filament axis (orthogonal to $B_\theta \cong B_y$) inside the filaments. This fact was already pointed out by magnetic probe measurements[2]. The density in phase space for ion and electrons $f_\pm$ satisfies

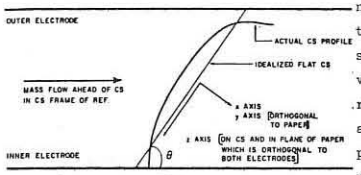

FIG. 1

[1] $\qquad df_\pm / dt = S_\pm$ where d/dt is the Vlasov's operator with self-consistent fields $\underline{E} = -\nabla\phi$, $\underline{B} = \nabla \times \underline{A}$; $\partial/\partial t = 0$ in the CS frame of reference (moving with a velocity $u_o \sim 10^7$ cm/sec in the lab. system); the source term S accounts for ionization and recombination reactions. The role of the neutral atoms is simply to affect the anisotropy in velocity of the newly-born charged particles and to function as a reservoir for ions and electrons. Neutral atoms are further disregarded. S is chosen ad hoc, according to the criteria: I) A solution of [1] can be obtained at a glance if a solution f_v of the Vlasov eq. $df_v/dt = 0$ is known; in our case $f_v = f_v(\varepsilon, p_z)$; the corresponding macroscopic quantities and their relevant derivatives are continuous functions. II) The solution f must generate specific mass and current flows [$m_+\rho_+u_+$ and $\underline{j} = e(\rho_+\underline{u}_+ - \rho_-\underline{u}_-)$] which are suggested by experimental evidence. This is conveniently accomplished by considering S as a collection of many (including a continuous distribution of) typical terms, i.e. $S = \sum_i \int S_{\gamma i}$. The particles are ejected on (by ionization), or removed from (by recombination) orbits which are defined as in the Vlasov theory and can be labelled by some constant of the motion. We chose $\mu_\pm(\varepsilon, p_z) = \mathcal{E}_\pm + \Gamma_\pm$ with

$$\mathcal{E}_\pm = [v_x^2 + v_y^2 + (v_z + c_\pm)^2]m_\pm/2 \quad , \quad \Gamma_\pm = \pm e(\phi + c_\pm A_z) \quad ,$$

$c_\pm$ = constants, $c_+ > 0$; the typical term $S_{\gamma i} = S_\gamma(\mu_i)$ is then depending on a specific numerical value μ_i of μ. As an example if

$$S = S_x(\mu_i) = f_v(\mu)\, L(\mu_i)\, d/dt\, [C(\Psi_{xi})\, C(D_{xi})]$$

where C is the Heaviside's unit function [the ionization spectrum $L(\mu_i)$ is a constant and $\Psi_{xi} = v_x - D_{xi}^{1/2}$, $D_{xi} = \mu_i - \Gamma_m^2 - v_y^2 - (v_z + c)^2$] then

$$f = f_v + f_s = f_v + LC(\Psi_{xi})\, C(D_{xi})\, f_v$$

gives a solution of [1]. For the non-linearity of [1], the self-consistent fields in d/dt, f, $S_{\gamma i}$ are always determined according to the total S. The complete theory is presented elsewhere; we list here some of the results for the case $f_{v\pm} = \text{const.}\, e^{-\alpha_\pm \mu_\pm}$, $\rho_{s+} = \rho_{s-}$, $j_z = j_{zv} + j_{zs} = -e(\rho_{v+}c_+ - \rho_{v-}c_-) + j_{zs}$,

$u_{z\pm} = -\rho_{v\pm}c_o/c_\mp(\rho_{v\mp} + \rho_{s\pm})$, c_o = speed of light, $u_{xs}, u_{ys} \neq 0$ (i.e. no contribution to the net charge comes from the source-controlled part f_s of f, etc.) and $\Gamma_+, \Gamma_- > 0$. A_z, ϕ (u.e.m. units) satisfy

$$\nabla^2 A_z = 4\pi e[\rho_{o+}(c_o^2/c_-)e^{-\alpha_+\Gamma_+} - \rho_{o-}(c_o^2/c_+)e^{-\alpha_-\Gamma_-}]$$

and similar equation for ϕ; ρ_{o+}, ρ_{o-} = constants > 0. We find the convenient solution

[2] $$\begin{cases} A_z = [e(c_- - c_+)]^{-1} \ln(F_1^{1/\alpha_+} F_2^{1/\alpha_-}) \\ \phi = c_+/e(c_+ - c_-) \ln(F_1^{c_-/c_+\alpha_+} F_2^{1/\alpha_-}) \end{cases}, \quad \begin{cases} \rho_{v+} = \rho_{o+}F_1 \\ \rho_{v-} = \rho_{o-}F_2 \end{cases}$$

with $F_1 = (4/\alpha_+ K_1^2)/\partial g_1/\partial\eta|^2[1 + |g_1|^2]^{-2}$, $F_2 = (4/\alpha_- K_2^2)|\partial g_2/\partial\eta|^2[1 + |g_2|^2]^{-2}$ where g_1, g_2 are arbitrary functions of the complex variable $\eta = x + iy$ and $K_1^2 = -e^2c_o^2\rho_{o+}(c_+ - c_-)\, 2\pi/c_-$, $K_2^2 = -c_-K_1^2\rho_{o-}/\rho_{o+}c_+$; $c_- < 0$ if the gun is operated with a positive center electrode. The conditions $\Gamma_\pm > 0$ imply $A_z > 0$ and, if $\phi > 0$, $|c_-| > c_+$, i.e. j_z is mainly carried by electrons. The magnetic field lines in the x, y plane,

$$F_1 F_2^{\alpha_+/\alpha_-} = \text{const.} = \tau \quad (\tau\text{-lines}) \quad ,$$

are in general different from the equipotential lines ϕ = const. (they become nearly coincident if $c_+ \sim c_-$; this case is consistent with a negative center electrode; different solutions must be considered if $c_+ = c_-$). In the particular case F_1 = const. F_2 the two systems of lines are coincident and the net charge density is proportional to the mass density (slightly positive plasma; some electrons are removed at the electrodes; $\phi \propto A_z$). g_1, g_2 are chosen according to physical conditions on ρ and on the fields, in particular to the periodicity of the filament arrangement (e.g. a simple period $\frac{2\pi}{m}$ on the y axis). Since ionization is high on CS and much smaller far from CS, we consider $\rho_\tau \to 0$ for $x \to \pm\infty$ where practically only neutral atoms exist, etc. For convenience we can take g_1, g_2 both of the same form $g = a + (1+a^2)^{1/2} e^{m\eta}$ (a_1, a_2 = constants > 0) already used in a known treatment[3] of the plasma filaments (that treatment was confined to $A_x = A_y = u_x = u_y = \rho_+ - \rho_- = 0$). The explicit expressions for $\Psi(\phi, A_z, ..)$ in S define functions Ψ of $\phi, A_z, ..$, locally, with x,y which play the role of the parameters determining the connections between successive branches. By taking $\Psi_{\tau i} = v_\tau - D_{\tau i}^{1/2}$ (the pair of orthogonal components v_τ, v_y replacing v_x, v_y) for $\mu_i \leq \mu_o$ we have a particle flow collinear with the τ-lines in some (x,y) region; with the spectrum $L = e^{\alpha\mu_i}(b_o + b_1\mu_i + ... + b_4\mu_i^4)$ we have $u_\tau = \beta_o[(\Gamma - \beta_1)(\Gamma - \beta_2)]^2$. Magnetic field lines and collinear flow

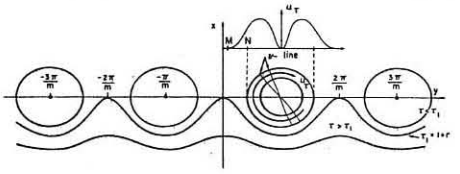

Fig. 2. E // y-lines; $F_2 \propto (\cosh mx + r\cos my)^{-2}$, $r = a(1+a^2)^{-1/2}$

on (x,y) are depicted in Fig. 2; β_1 β_2 are the values of Γ respectively on the filament axis (maximum of ρ) and on some close line $\tau_f = \tau_f(\mu_o)$ crossing in M the y axis (we have considered $\phi \propto A_z$ for simplicity). N is given by the τ-line which is best fitting the optical profile of the filament; for high currents across CA, M $\cong$ N can coincide with y = 0 (then CS has no filament structure but is optically a continuum; see Fig. 2). From the expression of J_τ we estimate B_z; the upper limit of B_z (maximum value on the filament axis) can be estimated, apparently, only by a stability analysis. Each filament is a bundle of helical magnetic field lines with a pitch increasing from the periphery to the axis of each filament. A filament on the CS can perform as a "corkscrew" device[4] (Sinel'nikov magnetic trap) for particles reaching CS with a large velocity component v_z. A cyclotron resonant transfer of kinetic energy occurs from z-direction (that we consider from now on as defined by the filament axis) into the Larmor rotation. At the dense focus stage, the CS is partially collapsed in the column but the filament still exist both in the column as well in the off-axis, still advancing, part of CS. Time-dependence as well as z-dependence become then necessary. It is possible, however, to see from the static solutions that even a small rearrangement in mass flow or net charge distribution can produce drastic changes in $\underline{j}$ and so large $\partial\underline{B}/\partial t$ and large $\underline{E}$-fields which can accelerate relatively few particles. The B_z variations are responsible in part for the acceleration of reacting deuterons which collide predominantly in the radial direction[5]; B_θ variations are responsible for the axial center-of-mass-velocity (2.10^8 cm/sec.) of reacting deuterons[5]. There is some evidence that the delay of the commencement of neutron production (with respect to the time of maximum of compression of the central column) corresponds to the relaxation time of the $\underline{u}$, ρ rearrangements which trigger the field decay at some point of the column. As an example, $|\nabla\rho|$ (by Schlieren) disappears[6] on the central column after the maximum compression but before the neutron commencement.

References

1. Bostick, W. et al.; Proceed. 9th Int. Conf. Phenom. Ionized Gases, Bucharest 1969, p. 66.
2. Bostick, W. et al.; Phys. of Fluids 2079, 9 (1966).
3. Komarov, N. et al.; Nuclear Fusion, 192, 5 1965.
4. Dreicer, H. et al.; Nuclear Fusion, p. 299, 1962 Supp. I.
5. Bernstein, M. J. et al.; Phys. of Fluids 193, 12 (1969).
6. Watteau, J. P., Baconnet, J. P., Cesari, G, Coudeville, A.; Onde Electrique (to be published).

Credits

Research sponsored in part by the Air Force Office of Scientific Research, Office of Aerospace Research, USAF under AFOSR Grant No. AFOSR-70-1842.

DENSE PLASMA FLOW FROM AN ELECTRODE CONIC SOURCE

by

T.A. El-Khalafawy, E.E. Nofal, M.F. El-Menshawy,

M.A. EL-Masry, M.S. El-Gwaily and Ya. F. Volkov+

PLASMA PHYSICS AND ACCELERATORS DEPARTMENT,

Atomic Energy Establishment, Cairo, U.A.R.

Abstract: Density, velocity and temperature of a plasma flow have been measured as a function of time, distance and intensity of the magnetic field. A change in the composition of the flow head-part has been investigated. Parameters of plasma which appears in the tube under the effect of fast electrons and discharge emission have been measured.

Experimental Set-up and Methods of Measurements: A plasma was injected from a plexiglass cone into a glass tube 80cm in length and 4cm in diameter. The tube was placed in a logitudinal magnetic field which could range from 0 to 8kG. The plasma was produced by discharging the capacitor bank of capacity of C=30μF, voltage of V=3:8kV, and current half cycle equal to 4.5μsec. The plasma density was determined from Stark-Broadening measurements of H_β spectral line. The monocromator was used to scann the H_β spectral line with very narrow exit slit. Relative time variations of the width of the spectral line during a single discharge can be obtained knowing the ratio of the total line intensity I_t to that at the line center I_{max} at every instant of time. The change in the plasma composition was investigated by measuring the ratio of H_β spectral line total intensity to the total intensity of impurity line. If the temperature changed are slight ($\Delta T_e \simeq 0.5$eV) the ratio of the total intensities equal to that of the density of the radiators. The electron temperature was determined from the Balmer-sprung measurements. The electron temperature in the source was estimated according to the plasma conductivity. To measure density of a plasma which appears in the tube before the plasma flow is formed, the microwave interferometer (λ=4mm) was employed. The flow velocity was measured with the high-speed camera. The arrangement of the main units are shown in Fig. (1).

+ On leave from the Atomic Energy State Committee, USSR.

Results and Discussion: As seen from Fig. (2a) the shock wave is formed at a distance of about 30cm from the source. Up to this moment the plasma flow existed, the density of which monotonically increases. Fig. (3) shows density variations with distance. The flow maximum density is taken for $0 < X \ll 28$cm and the density of the shock wave front is taken for $X \gg 34$cm. With the increase of the distance from the source, the density of a plasma falls off and the magnetic field starts to reduce particles scaping to the walls. With the increase of the magnetic field gas pick up of the shock wave begins to dominate over diffusion and recombination and density gradually increases with distance Fig. (3). For investigation of the changes in flow composition, the most bright line of the visible spectrum was chosen (Fe I 4271 Å). Fig. (3) illustrates the measured results. ($\frac{I_{H\beta}}{I_{Fe}}$) is the intensity ratio of the lines H_β and Fe I at the instant of time when the intensity line of iron is maximum. It coincides with the shock-wave front. The content of impurities decreases with distance due to the loss of fast impurity atoms on the tube walls and hydrogen is brought to the shock-wave front by the wave propagation along the gas, i.e. the snowplough model can be applied in this condition. Fig. (2b) illustrates temperature measurements. Knowing the degree of ionization, the temperature of a "foreplasma" was calculated from Saha's equation. The plasma temperature in the source proved to be equal to 4eV. It is possible that this value have been understated, for no-multiply charged ions was assumed when calculating. For $X > 30$cm the temperature of the wave front doesn't change with distance and it is independent of the magnetic field. As the plasma is injected into the magnetic field a deceleration of the flow is possible. The induced current can reach 400 A/cm^2 at the tube walls and the decay time can be equal to 2:3μsec. Generally if the shock wave propagated through a homogeneous longitudinal magnetic field the velocity change doesn't depend on the magnetic field intensity. In the present work the shock velocity change depends on the magnetic field, see Fig. (4). With the increase of the magnetic field the plasma velocity grows at any position up to $X \ll 35$cm from the source. At $X > 35$cm the velocity doesn't depend on the magnetic field and this phenomena can be observed more at higher capacitor bank voltages. From the snow plough model [1] the dependence of the shock wave on time is

$$X = P/m_2 \cdot t \qquad t \ll m_2^2/2P\, m_3 \qquad \dots \qquad (1)$$

$$X = (2P\, t/m_3)^{\frac{1}{2}} \qquad t \gg m_2^2/2P\, m_3 \qquad \dots \qquad (2)$$

where m_2 is plasma mass for X=0, m_3 is the increase of the mass of the plasma per unit of X, P is the plasma momentum. Measurements show that plasma density and velocity do not depend on the magnetic field for X=0, i.e. the quantities m_2 and P are independent of the magnetic field, It can be assumed that when the magnetic field increases the plasma flow is compressed and gas pick-up takes place not in all the cross-section of the tube, i.e. the quantity m_3 decreases. This indicates that the velocity time independence increases. In the course of the decay of the current which appeared in the plasma the flow fills in all the cross-section of the tube and the velocity rapidly decreases. The flow energy is dissipate in ionization, dissociation and gas pick-up.

References:

1 Cormack G.P., Canad. J. of Phys. 41 (1963)1591.

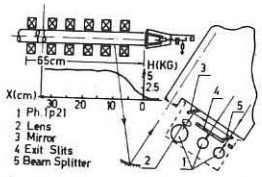

Fig. (1) Diagram of the experiment.

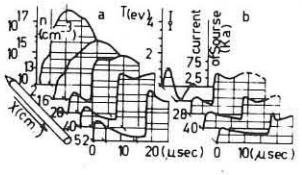

Fig. (2) Density (a) and temperature (b) as a function of time and distance. Voltage of the source V_s=5kV, P=200m.Torr, H=0.

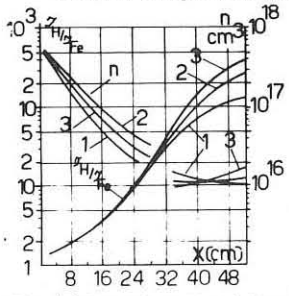

Fig. (3) Intensity ratio of lines H and Fe I and density as a function of distance (1)H=0,(2)H=3,(3)H=7kG.

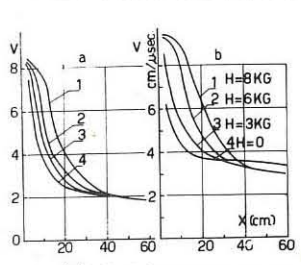

Fig. (4) The velocity as function of distance (a)V_s=5, (b)V_s=8kV.

Invited Lecture

REVIEW ON LASER-PRODUCED PLASMAS

A. Caruso

Laboratori Gas Ionizzati (Associazione EURATOM-CNEN) -

C.P. 65 - 00044 Frascati, Rome, Italy

FUSION BY LASER DRIVEN FLAME PROPAGATION IN SOLID DT TARGETS

J.L. BOBIN, G.F. TONON
Commissariat à l'Energie Atomique, Centre d'Etudes de Limeil
B.P. 27, 94 - Villeneuve-Saint-Georges - France

Abstract

After a review of plasma flow properties, inequalities analogous to Lawson criterion are derived and conditions for a positive energy balance are discussed.

Advances in the knowledge of laser created plasmas, allow us to set up a satisfactory description for the generated flow. In the high Temperature plasma fusion reactions can occur /1/ and higher temperature would yield a large amount of thermonuclear reactions.

Hydrodynamics under laser heating

The main features are described in /2/ and /3/ for non conductive (deflagration) and purely conductive regimes respectively. Further investigations taking into account electron heat conduction lead to the laser flux, temperature and density profiles displayed on fig. 1. ρ_c is the critical density for which the plasma frequency equals the incident laser flux frequency. For fusion conditions ($T_2 \sim 10$ keV and long pulses) it can be shown that the build up of the stationary deflagration structure occurs in the early stages of the interaction process both for Nd laser light and CO_2 laser light.

Reactor efficiencies will be evaluated with

(1a) $$T_2 = 8\,10^{-9}\left(\frac{\Phi}{\rho_c}\right)^{2/3} \qquad \text{(1b)} \qquad X_0 = \frac{4}{5}\frac{\gamma-1}{5k-1}\left(\frac{m}{k}\right)^{3/2} A\,\frac{T_2^{\,2}}{\rho_c}$$

where m is the ion mass, k the Boltzmann constant; $AT^{5/2}$ is the non-linear electron heat conduction coefficient. Φ is the incoming flux.

Criterion for a power producing reactor

Two parts of the plasma flow are interesting viz : the isothermally expanding plasma the characteristic length of which increases linearly with time, and the deflagration structure. Let η be the overall efficiency of the energy conversion process in the reactor : kinetic energy of escaping reaction products → thermal energy → electrical energy → laser light energy. Then following Lawson reasoning /4/, the reactor efficiency $\mathcal{R}$ reads

(2) $$\mathcal{R} = \frac{\int_0^\tau P_i(t)\,dt + \tau P_s}{\int_0^\tau R_i(t)\,dt + \tau R_s + \mathcal{E} + K} = \frac{6.2\times10^{-6}\, n_i \tau \langle\sigma v\rangle \left[\frac{N_i}{4} + N_s\right]}{1.42\times10^{-27} T_i^{3/2}\left[\frac{N_i}{4} + N_s\right] + 2\times3\, k\, T\left[N_i + N_s\right]} \longrightarrow \frac{1}{\eta} - 1$$

where P is the power emitted as escaping particles, R the radiated power, $\mathcal{E}$ and K the thermal and kinetic energies in the flow respectively, N the total number of particles involved during the cycle duration τ. Indices i and s refer to the isothermal expansion and the structure respectively. $n = \rho/m$ and the total energy in the flow is roughly twice the thermal energy of the interesting parts. For a given n_c (i.e. given laser light), $\mathcal{R}$ is a function of τ and T. A typical plot isshown for Nd glass laser light ($n_c \sim 10^{21}\ cm^{-3}$, $N_s \sim n_i X_0$, $N_i = n_i \tau \sqrt{kT/m}$) on fig. 2. The fuel is a 50 % DT mixture.

If a satisfactory cycle efficiency η could be achieved, then a successful reactor would operate with long laser pulses ($\tau > 100$ ns) and due to (1.a) only moderate fluxes. The CO_2 laser offer a promise of a cycle efficiency η of about 10 %. Roughly the same curves as in fig. 2 hold but with duration 10 to 100 times longer. Pulses over 10 µs in duration and fluxes of about $10^{13} - 10^{14}$ W/cm^2 would prove successful.

Condition for a positive energy balance

The above stated requirement are several order of magnitude greater than actual laser performances. A first interesting step would be achieved if the energy released by thermonuclear reaction W_F would exceed the invested laser beam energy W_L. Then instead of (2) one is to investigate the condition

(3) $$\mathcal{R}' = \frac{W_F}{W_L} > 1$$

In the flame propagation regime without electron heat conduction inequality (3) is fulfilled when the pulse duration τ is greater than /5/ :

(4) $$\tau_0 = 2.6\times10^{3}\,\frac{\lambda^2 T}{\langle\sigma v\rangle_{DT}}$$

λ being the laser light wavelength in µm, T is in keV. On Fig. 3 are plotted critical Nd glass laser charactéristics (energy, duration and flux impinging on the target) for fulfilement of inequality (3) as functions of the plasma temperature. It should be noticed that optimum values are

(5)
- $T = 8$ keV
- $\tau \gtrsim$ 300 nsec (target lengh $\sim$ 3 cm)
- $\Phi \sim 2.3.\ 10^{14}$ W/cm^2 (quite a reasonable value)
- $W_F \gtrsim 7.10^{7}$ joules/cm^2 or 7.10^{3} joules for a target of (100 µ)^2 cross section

Fluxes of about 10^{14} W/cm^2 are within the possibilities of present state laser technology and focusing lenses technology. However such fluxes have been so far associated only with nanosecond laser pulses. A power producing reactor using the laser driven flame propagation as a hot plasma generator would require reasonable fluxes but considerably longer pulses.

REFERENCES

/1/ FLOUX (F.) et alii - Nuclear fusion reactions in solid deuterium laser produced plasma. Physical Review - 1970. vol. 1 A n° 3. pp. 821 824

/2/ FAUQUIGNON (C.) - FLOUX (F.)
Hydrodynamic behaviour of solid deuterium under laser heating
Physics of Fluids - vol. 13 n° 2 - février 1970. pp. 386-391

/3/ BABUEL-PEYRISSAC (J.P.) - FAUQUIGNON (C.) - FLOUX (F.)
Effect of powerful laser pulse on low Z solid material. Physics Letters, vol. 30 A n° 5 3 novembre 1969 - pp. 290-291

/4/ LAWSON (J.D.) - Some criteria for a power producing thermonuclear reactor Proc. Phys. Soc. 70 B, 6. 1957, pp. 6-10

/5/ TONON (G.F.)
Le laser et la fusion thermonucléaire (Onde Electrique - à paraître)

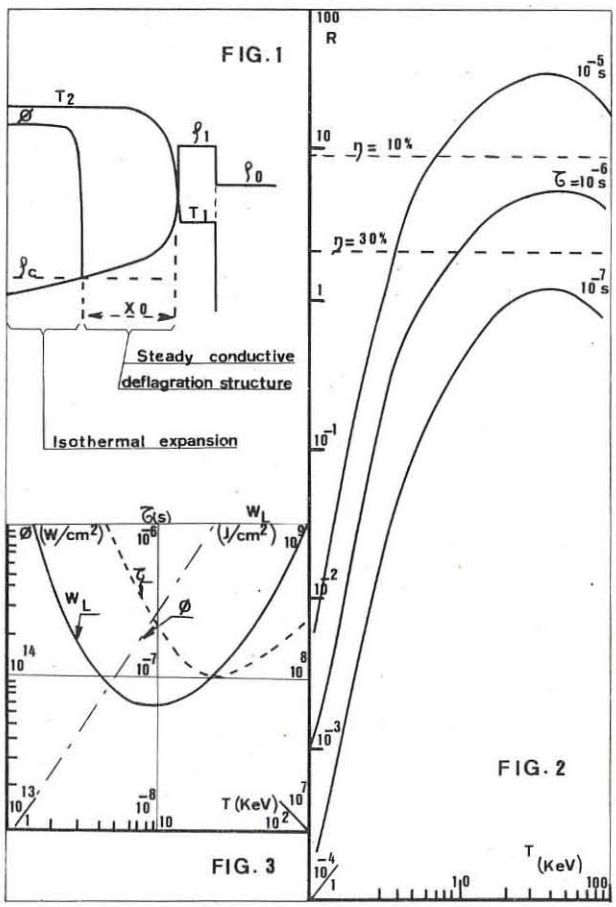

EXPERIMENTS ON A LASER-PRODUCED OVERDENSE PLASMA

J. Schlüter and W. Winkelmann

Institut für Plasmaphysik, KFA-EURATOM Assoziation, Jülich, Germany

Abstract. The optical thickness of a laser-produced plasma has been measured as a function of wavelength. For power densities $\geq 2\cdot10^{10}$ W/cm^2 the plasma becomes optically thick at wavelengths shorter than the wavelength of the ruby laser. It is concluded that the electron density is $\geq 8\cdot10^{21}$ cm^{-3}.

Introduction. It is generally assumed, that the rapid ionization and heating of solid materials in the focus of a giant pulse ruby laser should generate electron densities of the order of 10^{22}-10^{23} cm^{-3}, i.e. a medium where the plasma frequency is larger by a factor of about 10 than the laser frequency. In this medium, transport of radiation energy at the wavelength of the laser is not possible. Other mechanisms for the heat transfer have to be considered, if such "overdense" plasmas with $n_e > 2\cdot10^{21}$ cm^{-3} are to be generated. It has been calculated /1/ that in the case of hydrogen, heat conduction by the electrons may not be neglected, when the power density N of the laser is larger than $2\cdot10^{11}$ Watts/cm^2.

Experiment. The laser radiation was focussed with a lense of 10 cm focal length on thin foils of polythene, which were mounted in an evacuated vessel. The plasma radiation was measured at an angle of 20° (I_V) and 200° (I_R) to the direction of the incident laser radiation. Spectral resolution was achieved by interference filters. Fast photodiodes were used as detectors; the overall time resolution was about 2.5 nsec.

In Fig. 1 the ratio I_V/I_R measured at the maximum of the laser power is plotted against wavelength. If the plasma is optically thin for the wavelength concerned, this ratio should be one. If the plasma is optically thick, a ratio $I_V/I_R \neq 1$ should be expected, except if the temperature and density profiles are symmetric with respect to a plane parallel to the surface of the foil. Fig. 1 shows that for $N \gg 3\cdot10^{10}$ Watts/cm^2 this ratio is about 0.35 in the whole of the investigated wavelength domain. We conclude, that this value characterizes an optically thick plasma. This is further justified by the fact, that if the laser radiation is totally absorbed, the ratio I_V/I_R 0.3-0.4 is always obtained for $\lambda > \lambda_{ruby}$. The meaning of the absolute value of the ratio I_V/I_R in the limit of high laser powers is not yet clear; it may be influenced by radiation emitted from the periphery of the focal spot, where presumably the plasma is optically thin. The possibility of contributions of scattered light at the wavelength of the ruby was excluded by additional experimental tests.

If $N \leq 1.2\cdot10^{10}$ Watts/cm, the plasma is optically thick only for $\lambda \geq \lambda_{ruby}$. At a laser power of $2.7\cdot10^{10}$ Watts/cm, the transition from optically thin to an optically thick plasma occurs between 5000 and 4000 Å.

Fig. 2 shows the ratio I_V/I_R plotted against time for λ = 3960 Å and λ = 7500 Å. At the longer wavelength the plasma is optically thick ($I_V/I_R \approx 0.3$) during nearly the whole of the laser emission, whereas at $\lambda < \lambda_{ruby}$ the time during which the plasma is optically thick is much shorter.

Comparing the plasma radiation with the radiation of a carbon arc, the temperature of the absorbing layer is about 15 eV.

Discussion. We suppose that the observed jump of the optical thickness τ from $\tau \ll 1$ to $\tau > 3$ at the wavelength λ_c indicates directly the maximum of the electron density in the laser produced plasma, if we equate the corresponding frequency ν_c with the plasma frequency ν_p, we have

$$\nu_c \approx \nu_p = \frac{1}{2\pi}\sqrt{\frac{4\pi n_e e^2}{m_e}} \quad . \qquad (1)$$

It is experimentally known /2/, that the originally produced absorbing layer at the surface of the solid has a thickness $d = 10^{-4}$ cm. With a layer of this thickness, the absorption coefficient $\varkappa$ should be larger than 10^4 cm^{-1}, if $\tau = \varkappa d > 1$. Using the formula for the absorption coefficient (/3/, see also /4/)

$$\varkappa = \frac{8\pi}{3}\frac{Z^2 n_e n_i e^6}{c^2 (2\pi m_e kT)^{3/2}(1-\nu_p^2/\nu^2)^{1/2}}\,\bar{g}\,\Lambda \qquad (2)$$

it follows that for a given frequency ν, the condition $\varkappa > 10^4$ cm^{-1} is fulfilled when $\nu_p - \nu$ is very small or negative, that is when the plasma is (nearly) overdense.

According to this derivation, our investigated plasma becomes overdense at $N = 2\cdot10^{10}$ W/cm^2. From the observation, that plasma at higher power densities is optically thick at λ = 3960 Å, we conclude further, that the plasma frequency is then at least a factor of 2 higher than the laser frequency; this implicates $n_e = 8\cdot10^{21}$ cm^{-3}.

References.

/1/ A. Caruso and R. Gratton, report LGI 69/1 (1969)

/2/ W. Griffin and J. Schlüter
Physics Letters 26A, 241 (1968)

/3/ J.M. Dawson and C.R. Obermann
Phys. Fluids 5, 517 (1962)

/4/ H. Hora, report IPP/6/23 (1964)

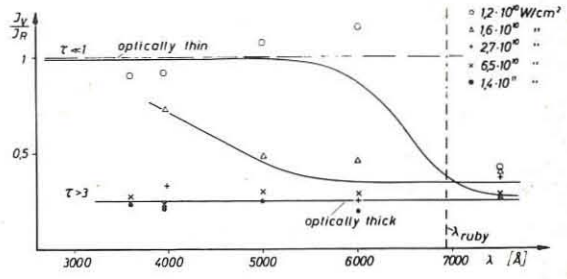

Fig. 1 Ratio of the plasma radiation emitted parallel (I_V) and antiparallel (I_R) to the direction of the laser light as a function of wavelength measured at the maximum of the laser-pulse.

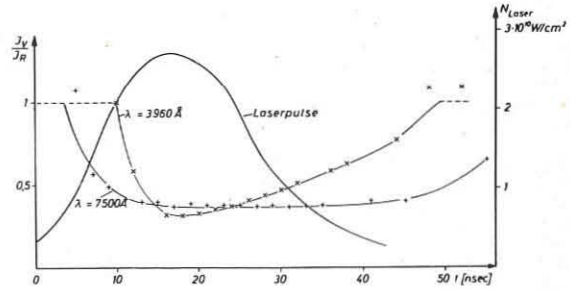

Fig. 2 The ratio I_V/I_R as a function of time for two different wavelengths. For comparison the power density of the laser radiation in the focal spot as s function of time.

INVESTIGATION OF LASER PRODUCED PLASMAS IN A MAGNETIC FIELD

by

F. Schwirzke

Naval Postgraduate School, Monterey, California 93940, USA

Abstract: The influence of finite conductivity on the dynamics of a laser produced plasma has been studied. The expanding plasma forms an elliptical shell of hot plasma due to enhanced resistive heating of the electrons at the plasma field boundary. The long lasting plasma shell could be utilized as a target plasma in neutral beam injection mirror machines.

High powered lasers are currently applied in the following four areas of the CTR program: 1) Production of a clean plasma within magnetic field configurations for basic studies of collisionless shock wave phenomena, stability and confinement. 2) Utilization of a laser produced plasma as a target in neutral injection mirror machines. 3) Scattering of laser light for plasma diagnostics. 4) Short time plasma heating for thermonuclear neutron production. Neutron emission has been obtained by focussing a giant laser pulse on a solid deuterium target. However, the power levels of the presently existing lasers are far too low to achieve a self sustaining fusion process. For this reason the other above mentioned laser applications seem to be more useful at the present time. The purpose of this paper is to discuss the interaction of a laser produced plasma with a magnetic field and the implications of the results for the creation of a target plasma.

Long confinement times in mirror machines have been achieved recently. In addition, a highly efficient method has been proposed [1] for regaining the energy of the particles which escape through the loss cone by direct conversion. These encouraging results provide the motivation for considering mirror machines as one of the prime types of possible fusion reactors. Estimates show that the ionization probability may be increased tenfold or more in comparison with Lorentz ionization if a laser produced target plasma is utilized [2]. Certainly, it would be highly desirable to keep the laser produced target plasma over a longer time localized within a small core volume of the mirror machine. Obviously the interaction of the expanding laser produced plasma with the magnetic field is of special importance if we want to create a target plasma.

A dense and hot plasma was created in the central region of a magnetic mirror field with a mirror ratio of 2:1 by focussing a 150 MW 20 ns pulse from a Q-switched neodymium laser on the tip of a 30μ pyrex fiber. It is advantageous to use a heavy ion plasma for the investigation of the dynamics of a laser created plasma expanding in a magnetic field because the macroscopic flow velocity is reduced and the behavior of the plasma can be more easily analysed by magnetic probes, Langmuir probes and high speed photography. During the initial expansion phase of the $\beta \gg 1$ plasma the temperature decreases rapidly according to the form $T_r = T_o(r_o/r)^2$ where T_o and r_o are the temperature and radius of the plasma when it becomes transparent. The

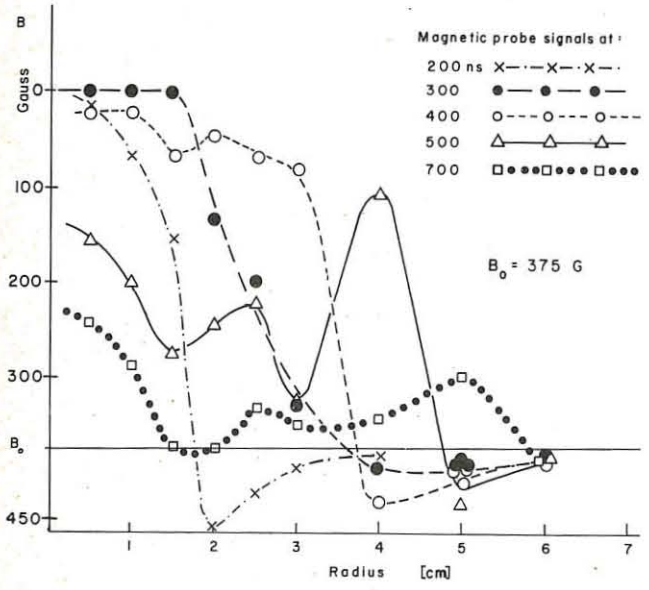

Fig. 1. Magnetic field profiles measured in radial direction across B_o. Parameter is the time elapsed from firing of the laser pulse.

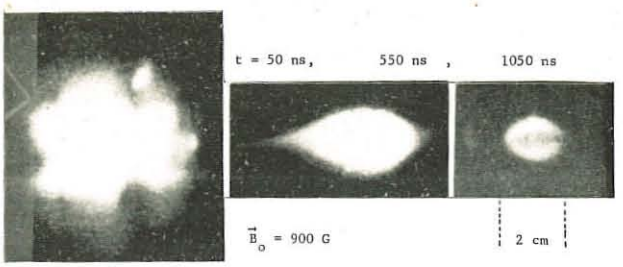

Fig. 2. Image converter photos of laser produced plasma.

rapid decrease of T_r implies that an asymptotic plasma expansion velocity V is reached in a rather short time while $\beta \gg 1$. Resistive effects, associated with surface currents in the front of the plasma expanding against a magnetic field, form the most effective means of rethermalization of the kinetic energy of expansion. The skin depth for which B penetrates into the plasma is determined by the effective resistivity. We would expect from Spitzer's formula for the conductivity σ that with decreasing T_r the width of the front of the expanding plasma, $d = c^2/4\pi\sigma V$, increases proportional to $d \propto T_r^{-3/2}/V$ or as function of the radius $d \propto r^3/V$. The measured magnetic field profiles of Fig. 1 do not show such a relationship between d and r. Furthermore, the magnetic probe measurements, Fig. 1, and the image converter photos of the expanding plasma, Fig. 2, clearly show the development of a shell structure in the plasma at $t \gtrsim 500$ ns.

Resistive heating becomes more efficient with decreasing T_r. Correspondingly, the temperature of the expanding plasma goes through a minimum. Computer calculations show that the minimum value of T_r and the time of its occurence is a function of B_o. With increasing B_o-field the minimum occurs earlier in time and it is less pronounced. The B - field penetrates the whole plasma if at low temperatures d becomes larger than the plasma radius. Later, with increasing conductivity this field will to some extent be "frozen" into the plasma. Even a weak B - field in the plasma reduces the transverse heat flow in the plasma considerably due to the $1/B^2$ dependence of the coefficient of thermal conductivity. Since the resistive heating of the electrons is mainly due to the surface currents, a reduced heat flow backwards into the plasma leads to an enhanced temperature increase in the outer shell of the expanding laser produced plasma. If the growth rate of the two-stream instability becomes larger than the electron - ion Coulomb collision frequency, turbulence developes in the wave front and contributes also effectively to the plasma heating [3]. Actually the half width of the shell structure in Fig. 1 at t = 500 ns corresponds to a Bohm-diffusion like heat transport. Later in time the shell remains almost stationary and the density decays relatively slowly. The experimental results indicate that the plasma losses along the field lines are considerably reduced probably due to a captured poloidal field. In conclusion, such a long lasting plasma ring produced by laser irradiation of a pellet would represent a useful target plasma for neutral beam injection machines.

Research sponsored by the Air Force Office of Scientific Research, Office of Aerospace Research, United States Air Force, under AFOSR Grant No. MIPR - 0004 - 69.

References

1. R. F. Post, Bull, Am. Phys. Soc., 14, 1952 (1969).
2. D. O. Hansen, W. Bernstein, B. D. Fried, Bull. Am. Phys. Soc., 14, 1022 (1969).
3. F. Schwirzke, R. Tuckfield, Phys. Rev. Letters, 22, 1284, (1969).

FORBIDDEN OPTICAL TRANSITIONS INDUCED IN DENSE LITHIUM PLASMAS

by

B. Ya'akobi

Department of Physics and Astronomy

UNIVERSITY OF MARYLAND

College Park, Maryland, U.S.A.

and

E. V. George, M. Pawlak and G. Bekefi

Department of Physics and Research Laboratory of Electronics

MASSACHUSETTS INSTITUTE OF TECHNOLOGY

Cambridge, Massachusetts, U.S.A.

Abstract: The line intensities and profiles of the forbidden 2P-3P transition of LiI and of its neighboring optical satellite (induced by collective electron plasma oscillations) are studied experimentally and theoretically. The plasma is produced in two ways, by exploding electrically a fine lithium wire and by illuminating a lithium surface with intense radiation from a CO_2 laser.

In a sufficiently dense plasma, transitions normally forbidden by the usual selection rules radiate as a result of the strong electric fields produced by the charges lying in the vicinity of the radiating atom. Thus a forbidden line adjacent to an allowed line can be made to radiate through the action of the essentially random, quasi-static electric field of the ions. In addition, the high frequency almost monochromatic field produced by collective electron plasma oscillations gives rise to optical satellites[1-5] flanking the forbidden line and separated from the latter by $\pm \omega_o$ where ω_o is the oscillation frequency of the collective mode.

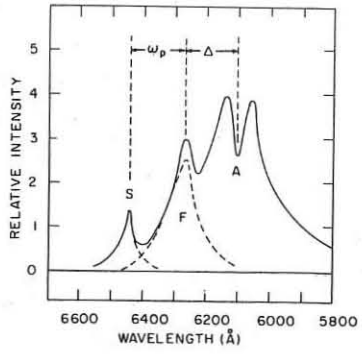

Fig. 1. Part of spectrum observed from an exploded lithium wire after subtraction of the continuum. A is the allowed line, F the forbidden line and S the plasma satellite. The dashed curve represents the unfolding of the partially overlapping lines.

In Fig. 1 is shown a section of the time integrated spectrum from a plasma produced by discharging a 50 J capacitor through a 0.05 mm O.D lithium wire. The plasma lasts for approximately 7 μ sec during which time the electron density N and temperature T have the following typical values: $10^{17} \leq N \leq 3\times10^{18}\,cm^{-3}$, $6\times10^3 \leq T \leq 2\times10^4$ K. The spectrogram exhibits the allowed 2P - 3D line (A) which is self reversed due to large spatial temperature gradients in the plasma; it also exhibits the 2P - 3P forbidden line (F) and one satellite (S). The other satellite is within the line width of the allowed line. The frequency separation ω_o between the satellite and forbidden line is very nearly equal to the plasma frequency $\omega_p = (Ne^2/m\epsilon_o)^{1/2}$ from which we deduce an electron density $N \approx 2\times10^{18}\,cm^{-3}$. This density occurs at approximately 2 μ sec after initiation of the breakdown and it is at this time that most of the emission from the neutral atoms occurs. At earlier times the plasma is highly ionized and the density of neutral atoms is low; at later times the electron density is low.

The intensity of the satellite is proportional to the square of the electric field[1] in the collective plasma oscillations. If the latter are of thermal origin, a determination of the strength of the satellite (relative to the allowed or forbidden line) yields the electron temperature. On the basis of our measurements we find[4] that the plasma is indeed close to being in thermal equilibrium with an electron temperature of $\sim$ 1 eV.

A study of the forbidden line itself can be used for diagnosing the plasma density. Figure 2 shows computations based on the work of Griem[6] of the profile of the allowed 2P-3D (6103 Å) line and of the neighboring forbidden 2P-3P (6241.5 Å) line of LiI. As the plasma density increases, two effects occur. First, the peak of the forbidden line moves away from the allowed line by very appreciable amounts ($\sim$25 Å as N changes from 10^{17} to $10^{18}\,cm^{-3}$). Secondly, the ratio of the peak intensity of forbidden to allowed line changes; for example, when $N = 10^{17}\,cm^{-3}$ the ratio is $\sim(200)^{-1}$ and when $N = 10^{18}\,cm^{-3}$ the ratio is $\sim10^{-1}$.

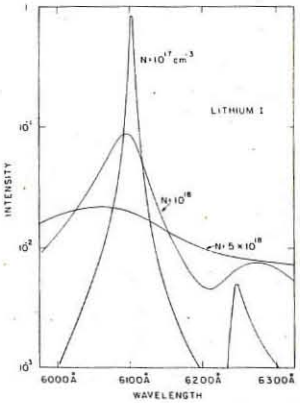

Fig. 2. Calculated profiles for the LiI 2P-3D allowed line and the 2P-3P forbidden line for various electron densities N. Self absorption is neglected.

However, to compare these computations with experiment, self absorption of radiation (not taken into account in Fig. 2) must be allowed for.

The laser-produced plasma is generated by means of a novel, high-power, high-repetition rate CO_2 laser described in a companion paper.[7] The laser radiation is focused by means of a 3.8 cm focal length lens onto a cylindrical post of lithium, housed in a cell containing helium as a buffer gas. The lithium post is rotated continuously to prevent excessive pitting of the surface by the laser pulses. The radiation from the intense plasma plume thus generated is studied by means of a 1.5 m spectrometer, focused on a small section of the plasma. Excellent spatial revolution of $\sim$0.1 mm is achieved so that the spatial plasma profile can be readily observed. To date, the 2P-3P forbidden line has been studied but the plasma satellites have as yet not been seen.

Acknowledgments. We are grateful to Prof. H. R. Griem for fruitful discussions. This work was supported in part by U.S. Atomic Energy Contract AT(30-1)-3980.

References

1. M. Baranger and B. Mozer, Phys. Rev. 123, 25 (1961).
2. H. J. Kunze and H. R. Griem, Phys. Rev. Letters 21, 1048 (1968).
3. W. S. Cooper, III and H. Ringler, Phys. Rev. 179, 226 (1969).
4. B. Ya'akobi and G. Bekefi, Phys. Letters 30A, 539 (1969).
5. G. Baravian et al, Phys. Letters 30A, 198 (1969).
6. H. R. Griem, Astrophysical J. 154 111 (1968)
7. E. V. George, Optical Production of High Density Plasmas with a Novel CO_2 laser (Paper in this conference).

NEUTRON PRODUCTION MECHANISMS IN THE PLASMA FOCUS

by

D. E. POTTER

Imperial College, Prince Consort Road, London, S.W.7, England.

INTRODUCTION

Results from the application of a two-dimensional magnetohydrodynamic code[1] to the plasma focus experiment[2] have provided good agreement with experiment in describing the dynamics and structure of the plasma focus[3]. The behaviour and parameters of the focus pinch produced in the numerical fluid model suggest two mechanisms for the production of neutrons. In this paper estimates of the neutron yield are determined for each mechanism, and the neutron properties on the basis of the calculations are compared with experiment.

The fluid model used and numerical methods applied in the two-dimensional magnetohydrodynamic code to describe the plasma focus have been discussed previously[1,4].

STRUCTURE OF THE PLASMA FOCUS

The calculation is initiated with a voltage of 40 kvolts. applied across the breach of a coaxial gun, with an initial filling pressure of 1 torr deuterium (n_e=4.5x10^{16} cm^{-3}). A steady state shock is established and driven between the coaxial electrodes[4]. At the end of the centre electrode an axisymmetric shock collapses radially to the axis. The structure of the shock just before it meets the axis is illustrated in Fig. 1. The peak shock velocity immediately prior to meeting the axis reaches 50 cms. μsec.$^{-1}$ and in consequence of this large shock velocity together with the low compression ratio in the imploding shock, the subsequent focus pinch formed on the axis attains very high temperatures. The axial dependence of the variables in the resulting pinch are illustrated in Fig. 2 at early times, 10 nanosecs. after the pinch has formed.

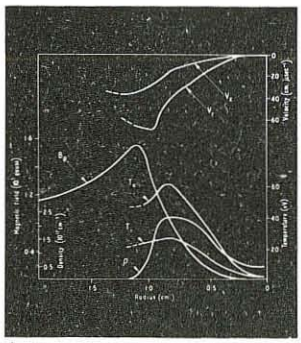

Figure 1. Structure of radially imploding shock prior to meeting axis.

Two features in the focus pinch in particular are clear. Firstly a hot pinch zone in which the parameters reach $T_i \sim 1.5$ keV. $n_e \sim 3\times10^{18}$ cms.$^{-3}$, $r \sim 0.2$ cms. (the high temperatures are achieved by adiabatic compression and viscous heating). Secondly a fast axial shock is produced where the density decays to $n_e \sim 10^{18}$ cms.$^{-3}$ and an axial velocity of 80 cms. μsec.$^{-1}$ is reached. The ion temperature in the shock is 600 eV.

At later times (Fig. 3) the hot pinch region is more than a centimetre long and axial flow occurs (V_z = 30 cms. μsec.$^{-1}$). The axial shock has moved downstream a considerable distance, while the pinch does not translate significantly. Though the pinch is stabilised by ion viscosity[3,4] the peak pinch is corrupted after long times (40 nanosecs.) by an m=0 instability.

NEUTRON EMISSION

On the basis of these results it is clear that two mechanisms are available for the production of neutrons. Neutrons will be emitted due to thermally reacting deuterons in the hot pinch region, where the yield may be estimated from,

$$N_1 = \pi r^2 \ell n^2 \tau \left(\frac{2.3\times10^{-14}}{T_i^{3/2}}\right) \exp\left(\frac{-18.76}{T_i^{1/2}}\right),$$

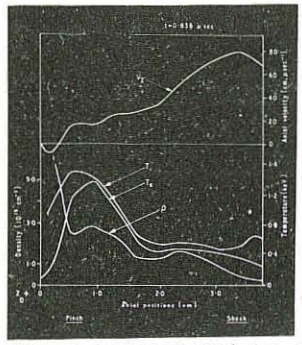

Figure 2. Axial dependence in the focus at early times: $t=t_{pinch}+10$ nanosecs.

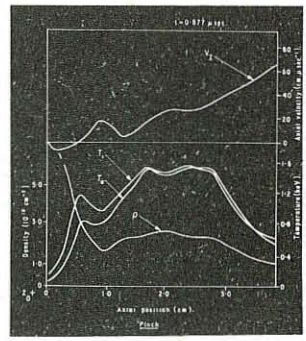

Figure 3. Axial dependence in the focus at late times: $t=t_{pinch}+49$ nanosecs.

where ℓ is the length of the hot pinch, r the radius, n the deuterium number density, T_i (keV) the ion temperature and τ the lifetime. Using the values given above (Fig. 3) then,

$$N_1 = 5\times10^9 \text{ neutrons.}$$

This value is rather smaller than that suggested by experiment. The yield however is a very strong function of ion temperature. Taking into account the uncertainty in the ion viscous coefficient, a fluid model certainly provides a thermal plasma capable of producing the neutron yields found experimentally. While the source remains relatively stationary with respect to the anode, flow occurs through the pinch (V_z = 30 cms. μsec.$^{-1}$) leading to a small anisotropy in the neutron energy flux[2].

A second neutron emission mechanism[5] exists as the result of the interstreaming of deuterons in the axial shock (Fig. 2) which attains very high velocities of 80 cms. μsec.$^{-1}$. While this mechanism would account for the anisotropy of the neutron energy flux[2], the yield N_2, estimated on the basis of the fluid calculations (Fig. 2) is very small[4],

$$N_2 = 2\times10^6 \text{ neutrons.}$$

Indeed to account for experimental yields a shock velocity well in excess of 10^8 cms. sec.$^{-1}$ would be required and no such velocity is apparent from the calculations. In addition the shock would translate the neutron source over considerable axial distances during the emission.

DISCUSSION

On the results of the calculations, neutrons would occur in the focus as the result of the first model (N_1) emanating from the hot pinch due to thermally colliding deuterons. The anisotropic properties of such emission do not however agree with experiment.

Since the ion-ion collision time ($\tau_{ii} \sim$ 20 nanosecs.) is of the order of the timescale of the pinch, the ion distribution function in the hot pinch will be non-Maxwellian. It is clear therefore, that a singular class of particles may be produced on the field free axis of the pinch, where particles not trapped by cyclotron orbiting, are freely accelerated by the axial electric field. While such singular particles are restricted to a small volume in space their extreme properties will produce a radical effect on the neutron emission. Two-dimensional particle calculations with a reversed magnetic field are in progress to determine the properties of such a singular class of particles.

REFERENCES

(1) ROBERTS, K.V. and POTTER, D.E. (1970). Methods of Computational Physics, Vol. 9, Academic Press.

(2) BOTTOMS, P.J., CARPENTER, J.P., MATHER, J.W., WARE, K.D. and WILLIAMS, A.H. Paper CN-24/G-5. IAEA Third Conference on Plasma Physics and Controlled Nuclear Fusion Research, Novosibirsk, Aug. 1968.

(3) MORGAN, P.D., PEACOCK, N.J. and POTTER, D.E. Third European Conference on Controlled Fusion and Plasma Physics, (p. 118), Utrecht, June 1969.

(4) POTTER, D.E. (1970) Ph.D. Thesis, University of London, England.

(5) DYACHENKO, V.F. and IMSHENNIK, V.S. (1969). Zh. Eksp. Fiz. 56(15), 1766.

SCALING LAWS OF PLASMA FOCUSES

Ch. Maisonnier, M. Samuelli, B. Robouch, F. Pecorella

Laboratori Gas Ionizzati (Associazione EURATOM-CNEN),
C.P. 65 - 00044 Frascati, Rome, Italy

Abstract: The variation of the neutron emission N_o of a Plasma Focus device as a function of the voltage (U) and capacity (C) of the condenser bank has been experimentally measured for $20 < U < 40$ kV and $30 < W < 120$ kJ. It is found that N_o varies as $U^{4.5}$ and $C^{2.5}$

Description of the experiment: Using the experimental device described in /. 1 / and whose sketch is represented in Fig. 1, a detailed investigation of the variation of the neutron emission as a function of the voltage U, the capacity C, and some geometrical parameters of the discharge chamber has been carried out. In particular, it has been possible to vary U from 20 to 40 kV, and C from 144μF to one quarter of this value, maintaining anyway a symmetrical distribution of the cables connecting the bank to the collector.

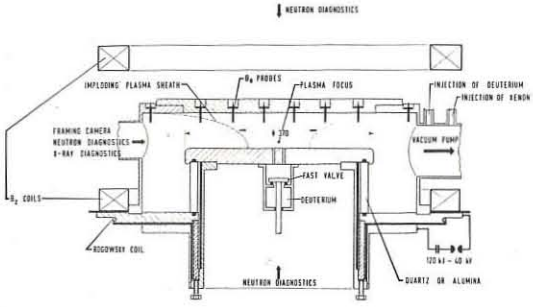

Fig. 1 Sketch of the experimental chamber

For each value of U and C, the static filling pressure p_o and the pressure p_1 behind the fast valve were varied in order to find the combination giving the optimum neutron yield. Fig. 2 and 3 show that this occurs always for about the same value of the collapse time.

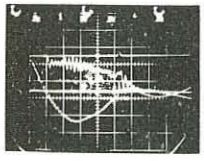

V_o=24 KV; p_o= 1000μ, p_1=12 atm.

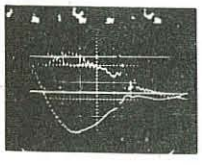

V_o=28 KV; p_o=1100 μ; p_1=12,5 atm.

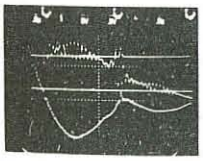

V_o=36KV; p_o = 1500μ ; p_1 13 atm.

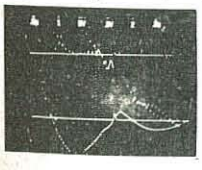

V_o=40KV; p_o=1500 μ ; p_1=12 atm.

Fig. 2
Optimization of the neutron yield at various voltages

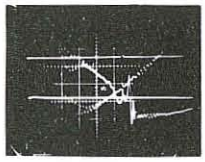

C=36 μF; p_o=400 μ; p_1=8,5 atm.

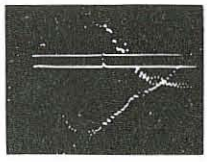

C=72 μF; p_o=1000 μ; p_1 = 8,5 atm.

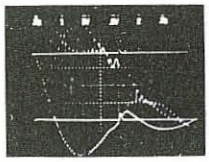

C=144 μF; p_o=1450 μ; p_1=11,5 atm.

Fig. 3

Optimization of the neutron yield at various capacities of the condenser bank.

When the device was working properly, a very good reproducibility of the neutron yield has been observed (Fig.4), so that it was possible to get well defined values of the mean neutron yield (mean yield of the good series). For each point (a given C and a given U) a few hundred discharges have been made.

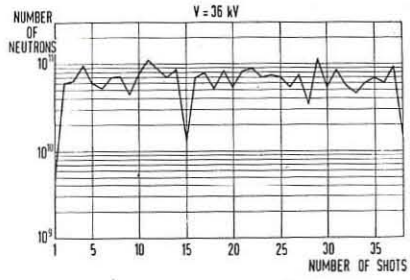

FIG.4-Neutron yield in 40 successive identical shots.

Experimental results.

The variation of the maximum and mean values of the neutron emission N_o as a function of U and C is shown on Fig.5 . N_o is found to vary as $U^{4.5}$ at constant capacity, and as $C^{2.5}$ at constant voltage in the range of parameters under consideration. It is seen that N_o varies roughly as the energy W of the bank to the power 2.3, indipendently of the fact that the variation of W is due to a variation of U or to a variation of C. This fact is of great pratical importance, as an extrapolation of the present devices in the MegaJoule range will not require to face the difficult technical problems linked with very high voltage large condenser banks.

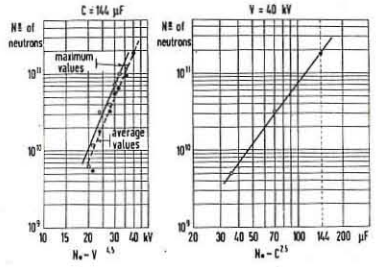

FIG.5-Scaling laws (experimental).

The influence on the neutron yield of some geometrical parameters, of the nature of the background gas (for instance the fast valve injecting deuterium in a hydrogen or argon atmosphere), of polarity, etc. as well as a confrontation of the experimental results with theoretical models / 2, 3, 4 / will be presented soon in another paper.

References.

1) Ch. Maisonnier et al, Plasma Phys. and Controlled Nuclear Fusion Research, vol.2, 77 (1969)
2) B. Robouch et al, Lab. Gas Ionizzati Internal Report L.G.I. 70/5 (1970)
3) V.F. Djachenko and V.S. Imshennik, J.E.T.P. 56, 1766 (1969)
4) D.E. Potter, PhD Thesis , Imperial College , London (1970)

DENSITY, TEMPERATURES AND NEUTRON MEASUREMENTS OF A PLASMA FOCUS

J.P. BACONNET, G. CESARI, A. COUDEVILLE, C. PATOU, J.P. WATTEAU
Commissariat à l'Energie Atomique, Centre d'Etudes de Limeil
B.P. 27, 94 - Villeneuve-Saint-Georges - France

Abstract : The plasma focus electron temperature and neutron emission are analysed in space and time. Density and ion temperature are studied by schlieren pictures and Thomson scattering respectively. Preliminary reports of recent studies with various capacitor banks are given.

Several diagnostics are used to know more about the plasma which focuses in front of a coaxial gun working at a high pressure regime. The operating data are : 50 mm inner electrode and 100 mm outer electrode diameters, 190 mm gun length ; 3 torr deuterium pressure ; 90 μF - 18 kV - 15 kJ capacitor bank. The maximum value of the current is 500 kA and the average neutron yield $1.5.10^9$. We choose as time origin the negative peak of the current derivative when the beginning of the main neutron emission /1/ occurs.

Schlieren pictures (Fig. 1) show the unstable /2/ plasma sheet pinching on the gun axis from which a very irregular filament originates. These schlieren pictures are quite different from the time-integrated X rays pictures on which the filament appears well defined /3/. When the polarity of the inner electrode is negative it seems that before the sheet reaches the axis, it breaks, or thickens near the inner electrode, the density gradients becoming less sharp. The soft X rays and neutron distributions along the gun axis z are indicated on figure 2-a. The 5 mm resolution is obtained by collimating the X rays beam with metal and the neutron beam with polyethylene and paraffin. A plastic scintillator with a photomultiplier are used as a detector and an aluminium thickness of 50 μ is placed in front of the X rays detector. The distributions are averaged over 15 discharges producing a $1.5.10^9$ neutron yield. We note the correlation in space of the soft X rays and neutron emissions which was also observed in time /4/.

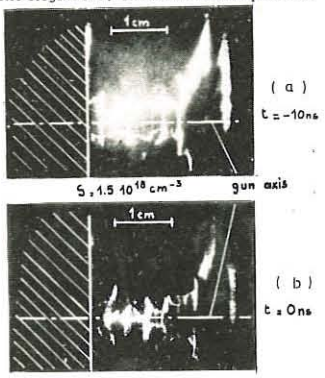

Fig. 1

Assuming a free-free bremsstrahlung continuum we deduced the electron temperature T_e with time (Fig. 3) from the absorbing foils technique. Four channels equipped with the previous detector are used with different absorbing materials and thicknesses. T_e measurements are delimited by two curves between which a dotted curve stands for the average value of T_e. Before the plasma sheet collapses on the axis and during the primary neutron emission /1/ T_e is of the order of 500 eV ; then it reaches such high values as 5 keV when the main emission is maximum. Fig. 2-b gives an example at time t = 50 nsec of the z variation of T_e ; it decreases away from the electrode as in the two-dimensional MHD model /5/. These temperature measurements have to be compared with those obtained from Thomson scattering /6/. A 90° scattering spectrum is shown on figure 4, 40 nsec before the main neutron emission it is symmetrical and its shift to the red may come from an axial plasma velocity of $1.7.10^7$ cm.sec^{-1} directed outwards from the electrode. From this spectrum the following values are deduced : Salpeter parameter β = 0,7; electron density $n > 3.10^{18}$ cm^{-3}; 135 eV < T_e < 220 eV and ion temperature T_i = 270 eV. T_e is lower than T_i like in a cylindrical shock wave before axis thermalization. Thomson values of T_e at differents times before the main neutron emission are drawn on figure 3 and lower than the X-rays values. It is not possible to do 90° measurements during the main emission because the signal to noise ratio is too low. This can be interpreted as a spread of the scattered spectrum due to a decrease of the Salpeter α - parameter, T_e increasing faster than n during the collapsing phase. Consequently to keep a collective behaviour of the plasma during the main emission it seems necessary to look forward. Attemps are made but at present the stray light is too high.

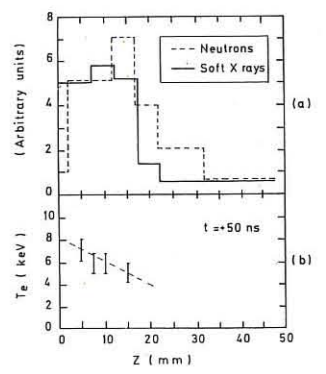

Fig. 2

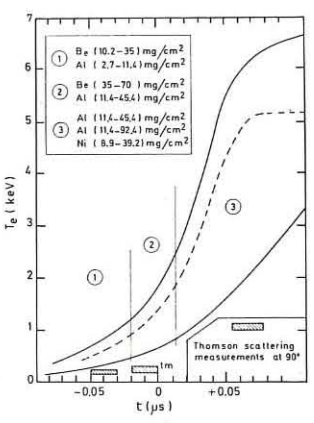

Fig. 3

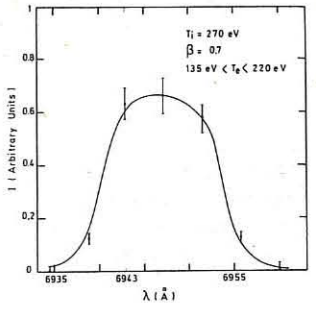

Fig. 4

The energy spectrum anisotropy results give an axial velocity of C.M. which is $v_{C.M.} = 1.2.10^8$ cm/sec when neutron yield is lower than 10^{10}. Neutron flux monotically decrease from 0° to 180° in agreement with the value of $v_{C.M.}$. This means that relative velocities of neutrons appear isotropic. We need to measure directly T_i by Thomson scattering in order to ascertain a thermal plasma, but the boiler model for instance accounts for present results.

Exp	R_2/R_1	P torr	V kV	E kJ	Imax MA	N_{10^9}
1	2	3	18	15	0.50	1.5
2	2	2	33	16	0.51	2.5
3	2	3	45	30	0.77	6.5
4	1.5	2.5	33	32	1	6.5
5	1.5	4	40	48	1.2	12

R_1 inner and R_2 outer electrode radius, P pressure, V charging voltage, E storage energy, I maximum current and N average neutron yield

Fig. 5

References

/1/ PATOU (C.), SIMONNET (A.) et WATTEAU (J.P.).- Journal de Physique t. 29 n° 11-12, 1968, pp. 973-984.

/2/ BACONNET (J.P.), CESARI (G.), COUDEVILLE (A.) and WATTEAU (J.P.).- Ninth International Conference on Phenomena in Ionized Gases, Bucharest, Romania, 1-6 September 1969.

/3/ PATOU (C.), SIMONNET (A.).- Note C.E.A. n° 1189, août 1969.

/4/ PATOU (C.), SIMONNET (A.).- Note C.E.A. n° 1188, août 1969.

/5/ POTTER (D.E.), ROBERTS (K.V.).- Magnetohydrodynamics calculations. Methods of computational physics. Academic Press (ed.) to be published.

/6/ BACONNET (J.P.), CESARI (G.), COUDEVILLE (A.) and WATTEAU (J.P.).- Ninth International Conference on Phenomena in Ionized Gases, Bucharest, Romania, 1-6 September 1969.

HIGH ENERGY DENSITY CONCENTRATION BY MEANS OF A CYLINDRICAL OR SPHERICAL COLLIDING PLASMA LINER

M. Haegi, R. Keller, J.G. Linhart and B.V. Robouch

Laboratori Gas Ionizzati (Associazione EURATOM-CNEN), C.P. 65 - 00044 Frascati, Rome, Italy.

Abstract: Experimental results are reported on the structure of snowploughed cylindrical shells and on the axial magnetic field compressed by them. These results compare well with numerical calculations showing that the model used for describing the processes is realistic.

Introduction: One of the main problems of applying a very high density plasma to CTR is to produce locally a high energy density / 1, 2, 3 /. We analyse the physical processes involved in the snowplough collapse of neon-plasma liners as one of these concentration experiments. The experimental device / 3 / is made of a 25 KJ, 40 KV low inductance condenser bank which can be used with an either cylindrical or quasi-spherical experimental chamber operated in the 0,1 torr range with neon as driving gas and supersonically injected deuterium as target gas.

In this report we will limit ourselves to the study of shape and structure of a snow-ploughing current layer in the cylindrical case with and without axial magnetic field, used instead of the deuterium target so as to measure the compression ability of the plasma liner.

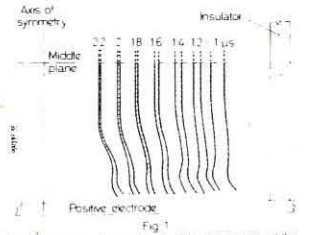

Fig. 1

Shape of a magnetic constant flux tube in the vicinity of the maximum of the trapped field at different instants in the case of a strong axial field (V_0 = 35 kV, 100 µ N_2)

Current-sheet dynamics: The following results have been obtained by means of triple magnetic probes which give simultaneously, for one point, the three components of the field. Without initial magnetic field and outside the perturbed zone near the electrodes, the current sheet assumes a cylindrical shape which follows well the numerical results based on a mean transparency of the magnetic piston of 60% to 95%. Applying an initial axial magnetic field to be compressed, introduces complexe but reproducible behaviour for the azimutal field / 4 /. The "snowploughed" axial field behaves quite simply (Fig. 1). The departure from the cylindrical symmetry is essentially due to 1) the magnetic field lines being "frozen" in the electrodes; 2) the coupling with the azimutal field dynamics. This departure increases with the initial axial field intensity.

Structure of the liner: Outside of the perturbed zone near the electrodes and excluding regions near $r = 0$ and $r = r_{initial}$, the magnetic field compression occurs in two different modes: 1) In very slow and resistive shots the compressed field increases nearly uniformly in the whole space in front of the piston. 2) In normal and rapid shots the magnetic field is no more uniform but "accumulated" in front of the piston (Fig. 2), in spite of the unperturbed medium having an Alfvén velocity an order of magnitude higher than the liner velocity. One can explain this fact as follows: Mass accumulates in front of the "snowploughed" axial magnetic field thus lowering the local Alfvén velocity and impeding the propagation of the increased axial field away from the liner front. The density needed therefore is equal to that found for the liner. The ratio of "snowploughed" to unperturbed axial field intensity can reach 50. Inside the liner the magnetic pressure is spatially uniform. Thus augmenting the initial axial field will increase the thickness of the "snowploughed" field rather than its intensity. The thickness of this field decreases with the radius. The liner is completely collision dominated: the collision mean free paths are some 10^{-3} cm and the Larmor radius 10^{2} times larger.

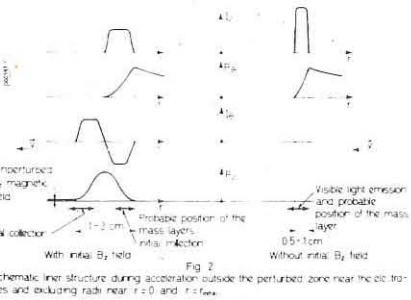

Fig. 2

Schematic liner structure during acceleration outside the perturbed zone near the electrodes and excluding radii near $r = 0$ and $r = r_{initial}$

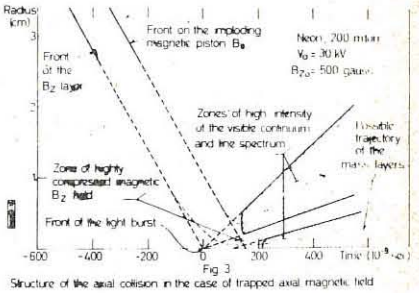

Fig. 3

Structure of the axial collision in the case of trapped axial magnetic field

The axial collision: We have already reported the results / 3 / obtained inserting destructive magnetic probes and microfuses in the axial region where the energy density reaches 10 KJ/cm^3. Time and space-resolved spectra of this region have been taken in the visible using a Kerr cell shutter. Presently, the full spectroscopical data are not yet worked out / 5 / but it can easely be seen that the observed transitions in Ne_I and Ne_{II} come from an electronic level population corresponding to temperatures $\gtrsim$ 40 eV. The spatial distribution of the global spectral intensity has been plotted against time in (Fig. 3). The expansion velocity being less than half of the implosion velocity indicates that about 80% of the kinetic energy of the liner has escaped from the axial zone as electromagnetic radiation.

Numerical model: The previous model / 3 / has been completed by introducing a finite constant thickness and a finite resistivity for the liner / 6 /. The magnetic field is supposed to be homogeneous in front of the liner.

For an optimum parameter-set one gets at the collapse: that of the stored energy 65% is transformed in heat by Joule effect and inelastic particle-pickup and 35% appears in the total magnetic energy 10% goes into the magnetic energy of the B_z field. This model allows maximum compressed field of about 10^6 gauss which is coherent with experimental data.

The authors want to thank M. Carinci, for technical support, S. Ortolani and G. Ramponi for their collaboration.

REFERENCES

/ 1 / J.G. Linhart, Nucl. Fusion 10, 3 (1970)

/ 2 / M. Haegi, Thèse No. 1474, Univ. de Genève, Suisse (1968)

/ 3 / M. Haegi, J.G. Linhart, III European Conf. on Controlled Fusion and Plasma Physics, Utrecht (1969) p. 115.

/ 4 / M. Haegi et al., (to be published)

/ 5 / R. Keller, Internal Report LGI (to be published)

/ 6 / B.V. Robouch, F. Moscatelli, Laboratori Gas Ionizzati, Frascati, Internal Report LGI No. 70/2 (1970)

A METHOD FOR THE DETERMINATION OF ELECTRONIC DENSITY AND TEMPERATURE IN AN INHOMOGENEOUS PLASMA

by

R. Vanhauwermeiren

UNIVERSITE DE BRUXELLES

Avenue F.D. Roosevelt, Brussels 1050, Belgium

Abstract : A method has been devised to give an estimate of the electronic density and temperature, as a function of the depth, in a hydrogen inhomogeneous plasma, by spectroscopic means. It is assumed that the plasma is in local thermal equilibrium.

Introduction : It is often difficult to give even an estimate for the electronic density and temperature in a plasma which is inhomogeneous along the line of sight. In many experiments, the large irreproducibility of the phenomena excludes the use of spectroscopic measurements under different angles, as required by the Abel inversion technique. The method presented in this paper makes use of the alteration of the line shape due to the inhomogeneity.

General method

As it is well known [1] , the outgoing intensity of radiation, at the wavelength λ may be written :

$$I_\lambda = \int_o^{\tau_o} B(\tau)\, e^{-\tau}\, d\tau \qquad (1)$$

where B is the block-body intensity and the optical depth

$$\tau(s) = \int_s^L k'(x)\,dx \qquad (2)$$

with k' , the absorption coefficient (cm^{-1}), function of the coordinate x through N(x) and T(x), the electronic temperature and density.

We approximate N(x) and T(x) using a Lagrange interpolation formula [2]

$$N(y) = \sum_1^n N(y_i)\, \frac{L_n(y)}{y-y_i}$$

where L_n is the Legendre polynomial of degree n and the y_i are the roots of this polynomial.

We now integrate (1) and (2) by the Gauss technique [2,3]

$$I_\lambda = \frac{\tau_o}{2} \sum_1^n B(\tau_o x_i)\, e^{-\tau_o x_i}\, \varpi_i \qquad (3)$$

$$\tau_{o\lambda} = \frac{L}{2} \sum_1^n k'(x_i)\, \varpi_i \qquad (4)$$

where the ϖ_i are the gaussian weights and the x_i are related to the roots y_i .

In eq. (3), we have

$$B(\tau_o x_i) = B(T_i) \quad \text{with} \quad T_i = T(z_i)$$

z_i being the root of the equation

$$\tau_o x_i = \tau(z_i)$$

If we give a fixed values for (n-1) couples $T(x_i)$, $N(x_i)$ and allow τ_o to vary, equation (3) is, for each value of τ_o , an equation with a single unknown T_x . When this equation is solved, equation (4) gives the corresponding N_x . We thus obtain two curves $T_x(\tau_o)$ and $N_x(\tau_o)$ for (n-1) given couples (N_i,T_i), or a function $T_x(N_x)$.

If we apply the same process for different wavelenghts, the curves $T_x(N_x)$ for different λ must intersect in a single point if the n couples (T,N) are correct. This fact gives rise to an iteration process, which is possible to be completed by means of an electronic computer.

The Parabolic approximation

As an example, we treat the simple case of the parabolic approximation. Let us assume that the plasma is a slab, symmetric around a median plane. We take for T(x) a parabolic approximation

$$T(x) = T_c + a\,(T_{ex}-T_c)(x^2-b)$$

where $T_c = T(.33L)$, $T_{ex} = T(.07L)$, and a and b are known constants.

Eq. (3) becomes

$$I_\lambda = \frac{\tau_o}{2}\,(pB(T_1) + qB(T_2)) \qquad (5)$$

p and q are known functions of τ_o .

$$T_1 = T(z_1) \quad \text{with} \quad .65214\,\tau_o = \tau(z_1)$$

$$T_2 = T(z_2) \quad \text{with} \quad .33001\,\tau_o = \tau(z_2)$$

In this case, for given N_c and T_c , $k'_{ex} = k'(N_{ex},T_{ex})$ is fixed for each τ_o .

The roots z_1 and z_2 are given by the equation

$$\frac{\tau(z)}{\tau_o L} = \frac{(1-z)}{2}\,(k'_c + (k'_{ex}-k'_c).1.59(.218 + \frac{z+z^2}{3}))$$

It is important to notice that the position of these two roots describes the inhomogeneity of the medium.

When, for given τ_o , T_c and N_c , T_{ex} has been determined from equation (5), N_{ex} follows from the knowledge of k_{ex} .

The iteration is thus to be performed on T_c and N_c for different wavelenghts.

Example

The line shape of the H_γ Balmer Line and the neighbouring continuum was calculated for a parabolic electronic distribution, the temperature being determined by the requirement that the total pressure should be constant, the geometrical depth was 3.67 cm.

The computer code used 49 points to calculate the integral

$$I_\lambda = \int_o^L \varepsilon\, e^{-\tau}\, ds$$

Three wavelengths were selected to apply the method 4340 Å, (center of the line), 4366 Å and 4600 Å (continuum).

For the correct values of T_c (=9089 °K) and N_c ($7.21\ 10^{16}\ cm^{-3}$), the curves $N_{ex}(T_{ex})$ intersect at the point T_{ex} = 8550 °K , N_{ex} = $4.70\ 10^{16}\ cm^{-3}$, the correct values being 8834 °K, $5.6\ 10^{16}\ cm^{-3}$.

The relative discrepancy is attributed to inaccuracy in the interpolation in the table of absorption coefficients.

References

1 H.R. GRIEM - Plasma Spectroscopy - Mc Graw-Hill - 1964

2 C. LANCZOS - Applied Analysis - Pitman & Sons - 1964

3 G. SZEGO - Orthogonal Polynomials - American Mathematical Society - 1939.

PLASMA DIAGNOSTICS USING LANDAU DAMPED LONGITUDINAL WAVES

by

Nguyen T.Dzoanh and Howard Pinsky*

Department of Electrical Engineering,University of Notre Dame

Notre Dame,Indiana 46556,U.S.A.

Abstract

A method of measuring accurately the plasma temperature and density,using the Landau damped electrostatic waves is reported. It is based on the analysis of the Landau damping length and dispersion relation of longitudinal waves propagating in collisionless plasmas. This method is particularly useful when a magnetic field is involved because the characteristics of the Langmuir probe is not reliable in this case.

There is considerable controversy about the accuracy of Langmuir probes when a magnetic field in plasma is present.[1,2] The measurements of electron temperature are somewhat in doubt and may differ from the actual values by a factor of three or higher depending on the case. An alternative and much more reliable method for measuring the temperature and density of a plasma is reported in this paper.It is based on the analysis of the experimental data concerning the Landau damping length and dispersion relation of electrostatic waves propagating in the direction of the magnetic field. The method consists of continuously exciting longitudinal electron waves in plasma by a high frequency electric field and recording the interferometric output of the wave amplitude versus the propagation distance.

The wave launching and interferometric detection system is shown in figl. The launching probe is connected to a R.F. generator and frequencies in the range of 15 to 40 Mhz are used.The detection probe is connected to a receiver which is tuned to the same frequency as the R.F. generator. The R.F.output from the receiver is fed into the Y axis of a XY recorder through a wave analyzer. The X axis of the recorder is connected to a gear down precision potentiometer mounted on the shaft which makes the detection probe moving along the plasma column.The output of the wave analyzer is amplified and used to modulate the R.F. signal launched by the probe. A reference signal taken from the R.F. generator is properly attenuated and mixed with the received signal before being applied to the receiver. Connected in this fashion,the system operates as an interferometer. When the refernce and received signals are in phase,an amplitude maximun will be seen on the XY recorder. The interferometric response of the plasma is shown in gig.2.Both the dispersion and Landau damping effects are readily apparent. From these wave patterns the wave length,the frequency and the Landau damping length can be obtained with accuracy. From the above data the phase velocity of the wave v_p can be computed. To ascertain the electron temperature T_e we compare the measured values of the Landau damping length with the theoretical values given by Landau[3] and corrected for finite temperature and finite size by Drummond [4].That is:

$$D_L = (1/k)\sqrt{2/\pi}\left[3/x^2 + (1 + 3x^{-2})/(2 + ka)\right] e^{x^2/2}/x^3$$

where a is the radius of the plasma column,k is the wave number and x is the ratio of phase velocity to thermal velocity v_p/v_e. A computer program is generated to calculate the Landau damping length as a function of both v_p^2 and k.The value of x can be decremented to the third significant figure until the theoretical value of D_L agrees with the experimental data. It is then a simple matter to solve for the electron temperature T_e since $v_e=(KT_e/m)^{1/2}$ The temperature so computed,together with the frequency and the wavelength will be used to derive the electron density from the dispersion relation:[5]

$$w^2 = w_p^2\left(1 + 3v_e^2/v_p^2 + \ldots \; -i(\pi/2)^{1/2} v_p^3/v_e^3 \exp -v_p^2/2v_e^2\right)$$

where $w_p = (Ne^2/m)^{1/2}$ = plasma frequency,N is the plasma density to be deduced.

The above procedure gives a very accurate value for density and temperature and is much more reliable than the probe measurements.

References

1-F.F.Chen Plasma Diagnostic Techniques Acad.Press (1965) Chapt 4

2-D.Bohm et al. Characteristics of the Electrical Discharges in magnetic Fields Mc Graw Hill (1949) Eds A.Guthrie and Warkeling.

3-L.Landau J.Phys.(USSR) 10,25,(1946)

4-W.E.Drumond et al. Plasma Phys. and Contr.Nucl.Fusion Vol 1,p.488,(1966)

5- B.S.Tanenbaum Plasma Physics Mc Graw Hill p.177 (1967)

* Graduate fellow from I.I.T. Chicago,Illinois.

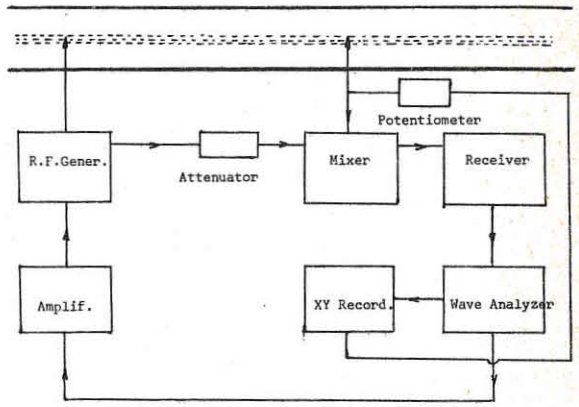

Fig.1

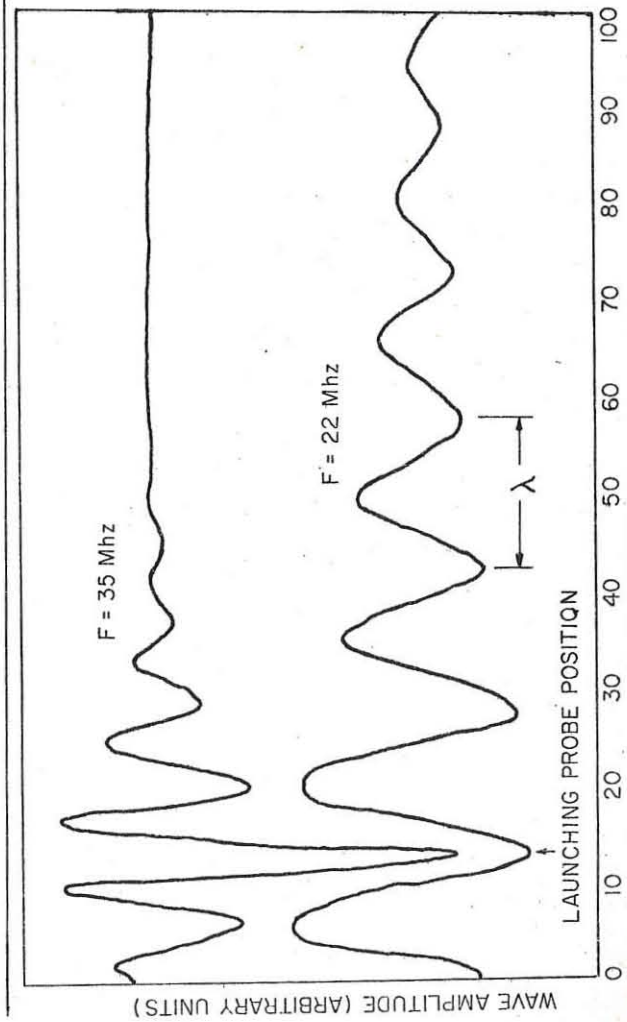

FIGURE 2. INTERFEROMETRIC OUTPUT OF THE ELECTRON WAVE AMPLITUDE VERSUS THE PROPAGATION DISTANCE. THE FIRST PEAK ON THE LEFT IS DUE TO THE NEAR-FIELD EFFECT. THE SECOND PEAK IS USED AS REFERENCE FOR MAXIMUM AMPLITUDE AND ZERO DISTANCE OF THE WAVE.

Comparison of Ion Temperatures Measured with an Ion Sensitive Probe and Spectroscopic Doppler Broadening

I. Katusmata[+)]
Research Institute for Atomic Energy, Osaka City Univeristy, Osaka, Japan
M. Otsuka and K. Ishii
Institute of Plasma Physics, Nagoya University, Nagoya, Japan
R. Ikee
Department of Physics, Hiroshima University, Hiroshima, Japan

A purpose of a present experiment is to test the reliability of an ion sensitive probe in high density plasmas. The probe was proposed by one of present authors as a method to measure the ion temperature of the plasma in magnetic field[1)]. The characteristics of the probe were experimentally studied and the results were fairly satisfactory as expected[2,3)]. In addition, a calibrating experiment was made using a cesium plasma in a Q-machine, since the ions in the Q-machine is in the quasi-thermal equilibrium with the plasma emitting plate if the plasma is in the ion rich regime. The good agreement was observed between the measured ion temperature and the temperature of the emitting plate as long as the plasma was in the ion rich regime[4)].

In the present experiment, the ion temperature measurement is made in helium plasmas, whose densities are $10^{13}\sim10^{14}/cm^3$, with the ion sensitive probe and the Doppler broadening of an helium ion spectrum line of 4686 Å by means of a Fabry-Perot interferometer.

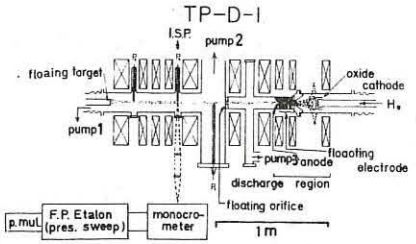

Fig. 1: The experimental arrangement in horizontal view.

The plasma is produced in a modified Duo-plasmatron which is shown in Fig. 1 as "discharge region"[5)]. The inner diameters of the anode and the floating electrodes are 8mm. In order to make the differntial pumping efficient, a floating limiter, whose orifice is 30 mm in diameter, has been set just before the vacuum connection to the pump 2. The helium gas is fed through a leak valve behind the cathode at the rate of 860 torr cm^3/sec and the pressure in cathode region is several torrs. The discharge tube is evacuated always by the pump 1 and the fine control of the pressure in the plasma region is made by opening of the valves of the pump 2 and pump 3. The pressure at the pump 1 is of the order of 10^{-4} torr and that of at the pump 2 is approximately 10^{-2} torr or less. The magnetic field is kept constant throughout the experiment, which is 1.8 kG at the anode and then increases gradually to 3 kG to the position of I.S.P..

The structure of the ion sensitive probe is shown in Fig. 2, which is specially designed for the use in the present experiment. Because the probe must be able to bear up against the large dissipation of power on it, in such a high density plasma as of the order of $10^{13}/cm^3$, it is cooled with the water which is supplied at the rate of 1 cm^3/sec. The upper limit of the power dissipation on the probe is limited by the thermal conduction of the guard electrode and the ceramic insulator jacket and is somewhat lower than 100 watts. The ion collector of the probe is a flat end of a tungsten rod 0.7 mm in diameter. The other electrode is a guard electrode to prevent the electrons to the ion collector. To make the electron current to the guard electrode small,

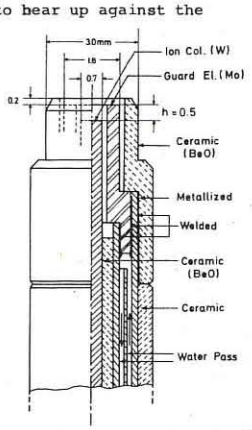

Fig. 2: Ion sensitive probe

the top of the guard electrode is lowered 0.2 mm from the top of the outer insulator. The depth of the ion collector, which is shown in Fig. 2 as h, is 0.5 mm from the top of the guard electrode.

The value of h is the most important parameter in the ion sensitive probe and it should be made larger than a critical value h_c to prevent the electron current to the ion collector, which is expressed as $10\bar{\rho}_e \leq h_c \leq 10\bar{\rho}_e + 10\lambda_D$. Where $\bar{\rho}_e$ is a mean Larmor radius of electrons and λ_D is a Debye distance. The equality at the left hand side holds for $10\lambda_D \gtrsim d$ (diameter of the probe) and that of the right hand side holds for $10\lambda_D \ll d$ [3)]. The plane of the ion collector should be arranged parallel to the magnetic field and the same voltage should be applied to both the electrodes.

The insturmental width of the Fabry-Perot interferometer is 0.0015 Å, which is good enough for the present measurement, because observed half-intensity breadths are larger than 0.2 Å. The seperation between two strong peaks, 0.099 Å, in the fine structure of 4686 Å line is used as the wave-length standard, which is produced in a hollow cathode discharge. The ion temperature is obtained from the half-intensity breadth of the line profile according to the calculation of K.E. Welmer[5)] in which the fine structure and the Zeeman effect are taken into account. The sprecrometer is arranged so as to observe 1 mm thick layer of plasma at its axis. A window of the discharge tube to the spectrometer is just opposit to the probe port of I.S.P..

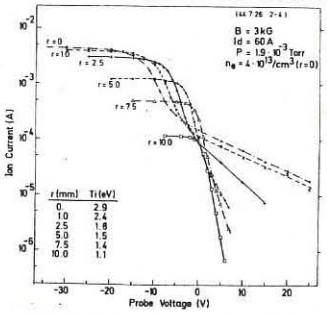

Fig. 3: Typical examples of ion current characteristics of the probe.

Fig. 3 shows typical examples of characteristics of I.S.P. taken at different radial positions in a plasma. The pressure indicated in the figures are the value at the position of I.S.P. It is clear in Fig. 3 that the energy distribution function of the ions is not Maxwellian near the axis of the plasma but it becomes good Maxwellian as going to outward. This is a characteristic feature of the plasmas in this experiment. This fact may be explained in terms of the deformation the distribution function of ions in the strong radial electric field (24 V/cm in the case of Fig. 3) near the axis of the plasma column. As a measure of the mean energy of ions, the steepest tangent on the low energy part of the curve is taken as the ion temperature. The results, thus obtained, are shown in Fig. 4 together with the results by the Doppler broadening measurements.

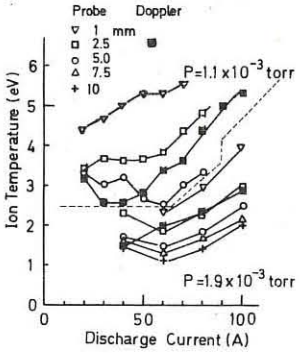

Fig. 4:

The plasma density is 9 x $10^{12}/cm^3$ at I_d = 20 A and increases to 8 x 10^{13} per cm^3 at I_d = 100 A on the axis of the plasma. Taking into account the radial intensity distribution of the spectrum line, which is well approximated, in mm unit, $\propto (r-4)^2$, one can conclude that the results of the ion temperature measurements with both the methods agree well each other.

1) I. Katsumata, M. Okazaki, Japan J.Appl.Phys. 6 (1967) 123
2) I. Katsumata, Annual Review of IPP Japan (April 1966-March 67) 76
3) I. Katsumata, "Collec. Pap.of Riken Synp.(Nov.20, 1968)" - in Japanese - Publ. March 5, 1969 by Inst.of Phys.and Chem.Res. Tokyo, Japan, 28
4) I. Katsumata, A.R. of IPP Japan (Apr. 1967-Mar. 1968) 59
5) M. Otsuka et.al. Proc. VIIth Int.Conf.Pheno.Ion.Gas,Beograd Aug. 1965, 420
6) K.E. Welmer, NYO-7885

+) Pres.Adr.:Institut für Plasmaphysik, 8046 Garching near Munich Federal Republic of Germany

Measurements of the Ion-Velocity Distribution Function in a Single-Ended Q-Machine

by

S.A. Andersen, V.O. Jensen and P. Michelsen

Danish A.E.C. Research Establishment Risö

Roskilde, Denmark

Abstract: An electrostatic energy analyser with a resolution better than 0.03 eV was constructed and used to determine the ion-velocity distribution function at different conditions in a single-ended Q-machine. The influence of a neutral gas on the distribution function was examined. Double-humped distribution functions were obtained.

1. Introduction: In recent years many experiments have been performed in order to study the propagation properties of density perturbations in single-ended Q-machines. In order to make quantitative comparisons between experimental results and theoretical predictions knowledge of the undisturbed ion-velocity distribution function is essential. To the best of our knowledge, careful measurements of this distribution function in plasmas in single-ended Q-machines have not been performed. A few attempts to measure the distribution function were reported recently [1,2]. In this paper we will describe the results of measurements of the distribution function under different working conditions. Details of the measurements will be reported elsewhere.

2. Experimental Set-Up: The experimental set-up is shown in Fig. 1. The Cs-plasma column is confined radially by a magnetic field and is terminated on an electrostatic ion-energy analyser movable along the axis. The analyser, which is similar to the one described by Buzzi et al. [2], consists of a collector electrode in front of which a copper mesh, 35 μm thick - 40000 25 μm x 25 μm holes/cm^2, is placed. The mesh is biased negatively (-6 to -10 V) with respect to the earth in order to reflect the electrons.

The distribution of ion energies parallel to the magnetic field is determined by measuring the current-voltage characteristic of the collector plate. The connection between the ion velocity distribution function f(v) and the collector current, I_c, is given by $dI_c/d\varphi_a \propto f\left(v = \sqrt{\frac{2e(\varphi_a-\varphi_{pl})}{m}}\right)$ where φ_a is the collector voltage, φ_{pl} the plasma potential and m the ion mass. The electrical circuit shown in Fig. 1 displays the collector current differentiated with respect to the collector voltage on a scope.

Experimentally the plasma-potential is found by introducing a small group of slow, cold ions, which is detected as a narrow peak when $\varphi_a \simeq \varphi_{pl}$ (see Fig. 2). This group of slow ions is produced by charge-exchange in a neutral Cs-cloud confined in the copper tube shown in Fig. 1.

3. Experimental Results:

(a) Low-Density Region ($n \lesssim 10^8$ cm^{-3}). In this density region the ion-ion mean free paths are long compared with the length of the machine. Fig. 2 shows a typical oscillogram of the distribution function. The main peak corresponds to the contribution of the main plasma, while the small left-hand-side peak is made up of ions formed by charge exchange in the neutral Cs-cloud in the copper tube. The sheath potential drop, φ_o, infront of the hot ionizer plate accelerates the ions to velocities corresponding to this drop. Experimentally we find good agreement between this acceleration and φ_o as calculated from a balance equation involving the formula for the Richardson electron emission.

(b) Medium-Density Region (10^8 cm$^{-3} \lesssim n \lesssim 5 \cdot 10^9$ cm^{-3}). In this region, where the ion-ion mean free path is comparable to the length of the plasma column, the velocity distribution function is expected to vary with the distance from the ionizer plate. Near the plate the distribution function is like that described under (a), and it changes along the column to approach a drifting Maxwellian. We find that this change agrees with a simple model based on conservation of mass-, momentum- and energy-flow.

(c) High-Density Region ($n \gtrsim 5 \cdot 10^9$ cm^{-3}). In this region the ion-ion mean free paths are short compared with the length of the plasma column. The distribution function is therefore always very close to a drifting Maxwellian. The temperature and drift velocity is determined by a physical process which is not present at lower densities. This process consists of charge exchange interaction between the neutral Cs-flux from the generating oven (A in Fig. 1) and the ion flux from the ionizer plate. Fig. 3B shows the drift velocity and ion temperature as a function of density for a fixed plate temperature. This variation agrees with a rough calculation of the rate of charge exchange processes taking place in front of the hot plate.

4. Shaping of the Distribution Function: We have used the analyser to examine the effect of introducing a neutral gas into the plasma column, a method used in the past for the purpose of ion cooling [3,4,5]. The oscillograms in Fig. 4 show the distribution function for increasing neutral Cs-pressure in the copper tube (Fig. 1). Note that a double-humped distribution function, suitable for the study of Landau growth, is obtained.

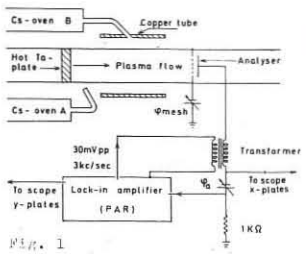

Fig. 1

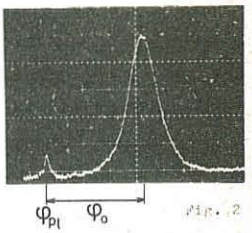

Fig. 2

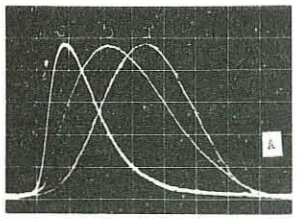

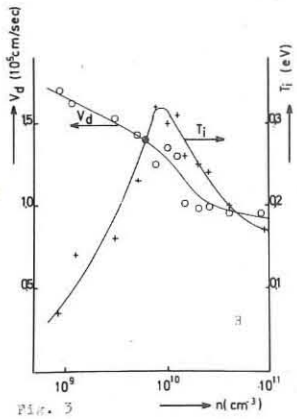

Fig. 3

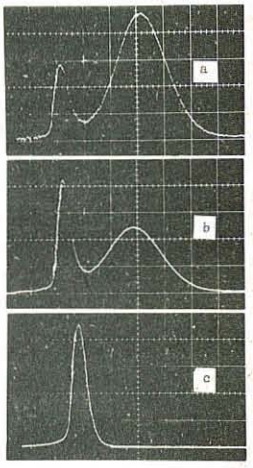

Fig. 4

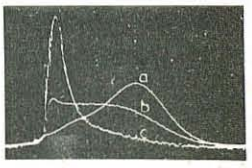

Fig. 5

When a neutral background pressure of an inert gas covers the full plasma column we find that the distribution function varies considerably with the distance from the ionizer plate. Fig. 5 shows this variation.

References:

1. H.K. Andersen, S.A. Andersen, V.O. Jensen, P. Michelsen and P. Nielsen, International Conference on Physics of Quiescent Plasmas, Paris, Sept. 8-13, 1969, 1 (Paris, Laboratoire de Physique des Milieux Ionises, Ecole Polytechnique, 1969) 55-60.
2. I.M. Buzzi, H.J. Doucet, and D. Gresillon, ibid. 2, 149-156.
3. F.P. Blau, E. Guilino, M. Hashmi, and N. D'Angelo, Phys. Fluids 10, 1116-17 (1967).
4. H.K. Andersen, N. D'Angelo, V.O. Jensen, P. Michelsen, and P. Nielsen, Phys. Fluids 11, 1177-80 (1968).
5. S.A. Andersen, Risö Report No. 188 (1969), Risö, Roskilde, Denmark.

Figure Captions

Fig. 1. Schematics of the experimental set-up.

Fig. 2. Typical example of differentiated analyser characteristic. Sweep 0.5 V/large div. Analyser positioned at x = 26 cm, Ta-plate at x = 0. $n \simeq 10^8$ cm^{-3}.

Fig. 3. (A) Examples of distribution functions measured at different densities. a) $n \simeq 3 \cdot 10^9$ cm^{-3}, b) $n \simeq 8 \cdot 10^9$ cm^{-3}, c) $n \simeq 3 \cdot 10^{10}$ cm^{-3}. $T_{hp} \simeq 2400^{\circ}$K. Analyser positioned at x = 62 cm. Sweep 0.5 V/large div. B) Experimental values of drift velocity and ion temperature as functions of density.

Fig. 4. Examples of distribution functions obtained at different neutral Cs-pressures in the copper tube. a) rather low Cs-pressure, b) medium Cs-pressure, c) high Cs-pressure. $n \simeq 1.5 \cdot 10^8$ cm^{-3}. Analyser positioned at x = 26 cm. Sweep 0.5 V/large div.

Fig. 5. Distribution functions at three positions along the column in partly ionized plasma. a) x = 26 cm, b) x = 56 cm, c) x = 106 cm. Argon background pressure $2 \cdot 10^{-4}$ torr. Plate temperature 2400°K. Sweep 0.5 V/large div. $n \simeq 10^9$ cm^{-3}.

CONSTRUCTION OF ELECTRON DISTRIBUTION FUNCTIONS FROM LASER SCATTERING SPECTRA

J. H. Williamson, UKAEA Culham Laboratory, Abingdon England
and M. E. Clarke

Abstract: The full three dimensional electron velocity distribution function of a low density plasma can be constructed from Thomson scattering spectra observed in several different directions. Most of the complications which arise at relativistic electron velocities can be avoided by placing a diffraction grating in the scattered laser beam.

Thomson scattering from electrons can be observed when a plasma is illuminated by a laser beam. The frequency of radiation scattered through an angle θ by an electron moving with a velocity $\underline{v}$ will be Doppler shifted by an amount $\omega = \underline{k}.\underline{v}$, where $\underline{k} = \underline{k}_s - \underline{k}_i$ and $\underline{k}_i$ and $\underline{k}_s$ are the wave vectors of the incident and the scattered waves, Fig. 1.

Fig.1

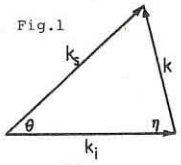

The contributions from each electron will combine incoherently[1] when collective effects can be neglected; i.e., when $\alpha = 1/kL_D \ll 1$ where L_D is the Debye length. The form of the spectral function is then

$$S(\underline{k},\omega) = \int f(\underline{v})\,\delta(\omega - \underline{k}.\underline{v})\,d\underline{v} \qquad \ldots (1)$$

where $f(\underline{v})$ is the electron velocity distribution function. Thus all the electrons with the same component of velocity, $\underline{v}.\underline{n} = \omega/k$ in the direction $\underline{n}$ ($=\underline{k}/k$), will contribute to a single point ω in the spectrum. The problem is to disentangle f from these spectra.

We first express (1) in terms of the parameters $R = \omega/k$ and $\underline{n}$. The spectrum as a function of R for fixed $\underline{n}$ is

$$S(R|\underline{n}) = \int f(\underline{v})\,\delta(R-\underline{v}.\underline{n})\,d\underline{v} = kS(\underline{k},\omega) \qquad \ldots(2).$$

The Fourier transform of the distribution function $f(\underline{v})$ is

$$\tilde{f}(\underline{p}) = \int f(\underline{v})\,\exp(-ip\,\underline{v}.\underline{n})\,d\underline{v}$$

where $\underline{p} = p\underline{n}$. If we now introduce a dummy integration over a δ-function with argument $(R-\underline{v}.\underline{n})$,

$$\tilde{f}(\underline{p}) = \int\int f(\underline{v})\,\exp(-ipR)\,\delta(R-\underline{v}.\underline{n})\,dR\,d\underline{v}$$
$$= \int \exp(-ipR)\,S(R|\underline{n})\,dR \qquad \ldots (3).$$

Thus $f(\underline{v})$ can be restored by taking the three dimensional Fourier transform of $\tilde{f}(\underline{p})$ which is itself the one dimensional Fourier transform of $S(R|\underline{n})$. In its simple form this method involves a large amount of computation and we now show that the number of integrations can be reduced.

The Fourier transform of Eqn.(3) can be written

$$f(v) = (1/8\pi^3)\int\int\int \exp(ipR - ip\,\underline{v}.\underline{n})\,S(R|\underline{n})\,dR\,p^2dp\,d\Omega$$

where $d\Omega$ is an element of solid angle, and where we have separated the radial and angular parts of the integral over $\underline{p}$. After integrating over p, we obtain finally

$$f(v) = -\frac{1}{8\pi^2}\int \left(\frac{d^2S}{dR^2}\right)_{R = \underline{v}.\underline{n}}\,d\Omega \qquad \ldots (4).$$

Thus $f(\underline{v})$ can be constructed by integrating over solid angle the second differential of each spectrum at the point $R = \underline{v}.\underline{n}$.

It may easily be shown, using Eqn.(4), that a spherically symmetrical velocity distribution f(v) is related to the spectrum S(R) by

$$f(v) = -\frac{1}{2\pi v}\left(\frac{dS}{dR}\right)_{R = v} \qquad \ldots (5).$$

It is important to note that these inversion formulae have been derived in terms of spectra for fixed directions $\underline{n}$. In practice a spectrum will be observed at a fixed angle θ. The direction $\underline{n}$ is given by the angle η (Fig.1) where

$$\eta = \tfrac{1}{2}(\pi-\theta) - \frac{\omega}{ck}\cos\tfrac{1}{2}\theta + O\left(\frac{\omega}{ck}\right)^2.$$

Hence there will be a small variation of the direction $\underline{n}$ with ω at a fixed angle θ. Usually ω/ck is very small and we can assume that a spectrum observed at fixed θ will be the same as a spectrum at fixed $\underline{n}$. If the assumption of constant $\underline{n}$ cannot be used in a particular experiment, there are several possible courses of action:

1. The dispersion effect can always be eliminated by performing back-scattering experiments in which $\cos\frac{1}{2}\theta = 0$.
2. The scattered light can be passed through a diffraction grating to correct for the dispersion. A grating with 6000 lines per cm gives perfect correction at 68° and 130° for $\lambda_i = 6943$Å
3. Brown and Rose[2] have shown how an expression equivalent to Eqn.(4) can be derived in terms $S(R|\theta)$. Their solution is very complicated and difficult to use.

It is implicitly assumed in this work that the Thomson scattering cross section σ_T is the same for all electrons. Although this is true in the non-relativistic limit, Brown and Rose have shown that in general the dependence of σ_T on v is $O(v/c)$. However if the direction of the incident electric vector is perpendicular to the direction of observation, as is usually the case in Thomson scattering experiments, any variation in σ_T is only of order v^2/c^2. The part of this due to the relativistic increase in mass is easily dealt with and the remaining errors are usually extremely small for electron energies up to 30 keV.

We have tested the inversion formula using a model loss-cone distribution function having azimuthal symmetry. The original $f(v,\theta)$ at $\theta = 37°$ and 80° is shown by the solid lines in Fig. 2, and its reconstruction by the circles. Only four spectra, two of which are shown in Fig. 3, were used but the resulting root mean square error in f was less than 1%.

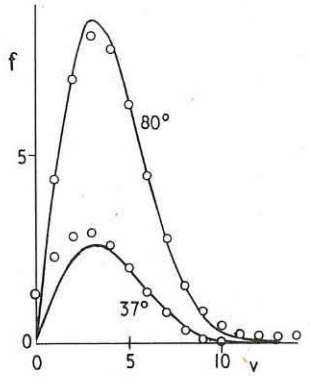

Fig. 2

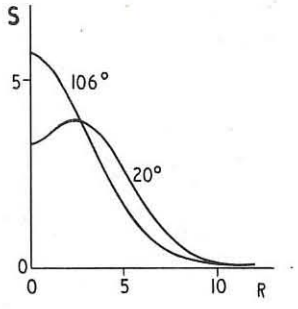

Fig. 3

References

1. Bekefi, "Radiation Processes in Plasmas", ch.8 (Wiley & Sons, New York, 1966).
2. Brown, T. S. and Rose, D. J., J.Appl.Phys. 37, 2709 (1966).

MAGNETIC FIELD MEASUREMENT BY LIGHT SCATTERING[+)]

by

L. Kellerer

INSTITUT FÜR PLASMAPHYSIK

8046 Garching b. München, Germany

Abstract: The conditions for measuring magnetic fields in plasmas by light scattering are discussed. In experimental observations of laser light scattered by a magnetized arc plasma we have measured deviations from the normal thermal spectrum. The observed spectrum fits best with the theoretical curve due to the probe measured magnetic field.

Local measurement of magnetic fields in hot plasmas is very important. Unfortunately, the methods used hitherto have marked disadvantages, e.g. changing the plasma parameters and yielding integrated values [1]. On the other hand, laser scattering offers a possibility of locally determining magnetic fields with negligible disturbance of the plasma, in addition to the usual measurement of temperature and density. This method is based on the fact that under certain circumstances the spectrum of the scattered light is influeced by the magnetic field within the scattering volume.

In theoretical papers (e.g. [1-3]) the scattering spectrum is calculated for $B_\perp k_s$ (Fig. 1). If, furthermore, $\alpha = 1/k_s D$ (D = Debye length) is lower than 1, only the electron spectrum is considered. It consists of lines whose separation equals the gyrofrequency of the electrons and whose envelope is nearly equal to the thermal scattering spectrum.

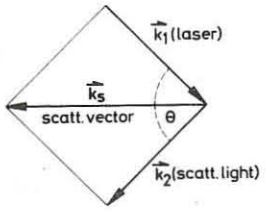

$$\vec{k}_s = \vec{k}_2 - \vec{k}_1 = \frac{4\pi}{\lambda_0} \sin \Theta/2$$

Fig. 1

In this paper first we specify the conditions for measuring such a modulated spectrum. We then describe a light scattering experiment which shows the influece of the magnetic field in a laboratory plasma on the spectrum of the scattered light.

The inequality $\alpha = 1/k_s D = \frac{n}{T \sin \Theta/2} \cdot \text{const} \ll 1$ (1) ensures that we have only the electron spectrum and that collective effects disappear. A second condition means that the modulation of the spectrum is well marked. This requires that the half-width $\lambda_{1/2}$ of a line is small enough compared with the separation $\Delta\lambda$ of two lines. $\frac{\lambda_{1/2\,\parallel}}{\Delta\lambda} = \frac{v_{th\,\parallel} \cdot k_s}{\lambda_c} \sim \frac{\sin \beta}{\alpha} \frac{\sqrt{n}}{B} \cdot \text{const}' \ll 1$ (2). The half-width is determined by the Doppler shift $\lambda_{1/2\,\parallel} = v_{th\,\parallel} \cdot k_s$ which, roughly speaking, is governed by the component parallel to the magnetic field, while the perpendicular component is responsible for the envelope of the spectrum. The separation is proportional to the electron gyrofrequency. β is the mean value of the angles between $\vec{k}_s$ and the perpendicular to the magnetic field. Therefore β is a measure of the divergence of laser light as well as of inhomogeneities in the magnetic field within the scattering volume. A third condition requires that the scattered light per channel L is sufficient to keep the statistical error small: $L \sim \alpha^2 B^2 \cdot \text{const}'' \ll 1$ (3).

Conditions (2) and (3) call for large α, as opposed to (1). In accordance with the general scattering theory we may have α to about 0.5 and then get 80 % and more of the whole scattered light into the part of the electron spectrum. Then condition (2) is satisfied by electron densities of about 10^{16} cm^{-3} and magnetic fields of about 100 kG and divergence angles β of a few 10^{-2} rad. Usual scattering experiments work with β values of about 10^{-1}. Therefore, the main difficulty in our experiment lies in the small apertures and hence small scattered signals. The scattered light intensity depends only on α and B. With $\alpha = 0.5$, B = 100 kG and 100 MW laser intensity in the scattering volume, the statistical error is about 20 %. Electron temperature and scattering angle can still be freely determined, but are related by the condition $\alpha = 0.5$. Therefore there exist the possibilities

T	2	5	100	(eV)
θ	180	90	20	(grad)

. For all pairs we have the same modulation and the same scattered signals.

For a first experiment [4] we chose 90°-scattering in order to keep the stray light sufficiently small. Therefore the parameters of this experiment should be: $n_e \approx 10^{16}$ cm^{-3}, $T_e \approx 5$ eV, $\alpha \approx 0.5$. The appropriate plasma is formed in a hydrogen arc in an axiparallel magnetic field B_z. The homogeneous magnetic field of 120 kG is produced by a pulse discharge via two parallel coils (Fig. 2). The arc burns parallel to the magnetic field lines. From normal 90°-scattering we get the parameters $n_e = 1.2 \times 10^{16}$ cm^{-3}, $T_e = 3.2$ eV and $\alpha = 0.6$. The giant pulse of a Ruby laser is focused in direction $\vec{k}_1$ into the plasma, when B_z has reached its maximum value. We observe the scattered light emitted in the direction $\vec{k}_2$. The scattering vector $\vec{k}_s$ is perpendicular to $\vec{B}_z$. Deviations in the planes $B_z k_1$ and $B_z k_2$ originate in the apertures around $\vec{k}_1$ and $\vec{k}_2$, both 0.02 rad, in the homogeneities of B_z and the magnetic field B_θ of the arc current. In spite of these deviations we expect a modulation greater than 80 %. Fig. 3 shows the scattering spectra both with and without magnetic fields. The crosses and circles are mean values of seven discharges each. We could not measure at the laser wavelength because of excessive stray light. The curve is the best fit according to the theory of Lehner [1].

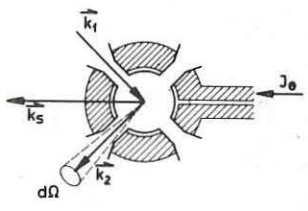

scattering geometry

Fig. 2

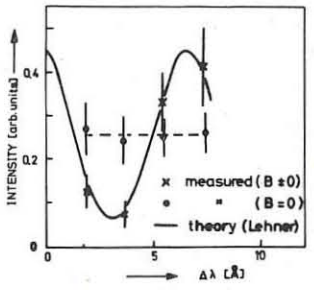

Fig. 3

From the separation of the laser wavelength and the wavelength of the first minimum we can determine the electron gyrofrequency which then gives a magnetic field of 150 ±20 kG. Deviations from an uniform modulation frequency have been calculated by Platzman et al. [5] for cases where the condition $\alpha \ll 1$ is not satisfied. With their numerical computations for cases, similar to ours, the magnetic field is lower, but by a factor less than 30%.

[1] G. Lehner, F. Pohl, Z. Physik 232, 405 (1970)
[2] Th. Laaspeere, J. Geophys. Res. 65, 3955 (1960)
[3] E.E. Salpeter, Phys. Rev. 122, 1663 (1961)
[4] L. Kellerer, Z. Phys. 232, 415 (1970)
[5] P.M. Platzman, P.A. Wolf, N. Tzoar, Phys.Rev.174,489 (1968)

[+)] This work was performed as part of the joint research program between the Institut für Plasmaphysik, Garching and Euratom.

OBSERVATION OF MAGNETIC FIELD MODULATION OF THE THOMSON SCATTERED LIGHT SPECTRUM IN A LABORATORY PLASMA

by

D.E. Evans, R. Peacock and P. Carolan

U.K.A.E.A., Culham Laboratory, Abingdon, Berks. England.

Abstract: A 2.7 Å band of the broad, nearly Gaussian spectrum of laser light scattered by a plasma in the presence of a 15 kG magnetic field has been isolated and passed through a 0.1 Å resolution interferometer. Magnetic modulation of the spectrum has been detected. There is close agreement between the field strength calculated from the modulation and that measured by Faraday rotation.

Introduction: Thomson scattering of laser light is favoured as a diagnostic technique for laboratory plasmas because of its many desirable features which include high spatial and temporal resolution, freedom from perturbing influence on the plasma, and applicability to a wide range of plasma conditions. The motivation for the present work is to bring magnetic field into the set of plasma parameters which can be measured by laser light scattering.

The effect of static magnetic field upon the spectrum of light scattered by a collisionless plasma has been calculated by a number of authors [1-5] who have shown that the presence of a magnetic field can be ignored unless the differential wave vector for scattering, $\underline{k}$, is nearly perpendicular to the magnetic field vector $\underline{B}$. When this condition is satisfied, the spectrum exhibits peaks at near-integer multiples of the electron cyclotron frequency ω_{ce}. The basic process from which the magnetic structure springs is the sinusoidally-varying Doppler shift experienced by light waves scattered by electrons which are performing gyrations at the Larmour frequency about the magnetic lines of force. If the vector $\underline{k}$ is not exactly parallel to $\underline{B}$, then the component of the motion of the electron along $\underline{B}$ introduces a Doppler broadening of the peaks proportional to the projection of the electron thermal velocity v_e along the $\underline{k}$ direction, namely $v_e \cos\phi$, where ϕ is the angle between $\underline{k}$ and $\underline{B}$ as shown in Fig.1. Should the resulting frequency line breadth, $2 k v_e \cos\phi$, approach the spacing between the lines, ω_{ce}, then serious smearing of the resonances will occur. Accordingly a necessary condition for the appearance of magnetic structure is that $2 k v_e \cos\phi < \omega_{ce}$.

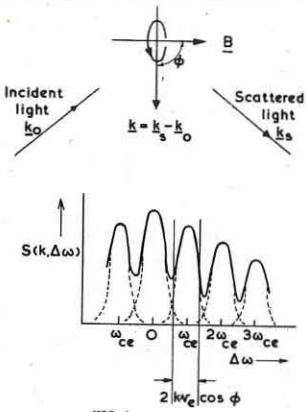

FIG.1

Experiment: An experiment designed to put this magnetic modulation in evidence has been constructed. A small pre-ionized theta pinch discharge (~3 KJ) which generates a magnetic field peaking in the neighbourhood of 16 kG is the plasma source. Light from a 100 MW ruby laser is directed through the centre of the theta coil at an angle of 15° to the direction of the magnetic field. Provision is made to detect and disperse light scattered in the plane containing the incident beam and $\underline{B}$, at an angle of 30° to the former and 15° to the latter. The scattering vector $\underline{k}$ is thus perpendicular to $\underline{B}$. The optics which bring the laser beam into the scattering volume and the detection optics are arranged in such a way that each point within the scattering volume is characterised by an identical cone of $\underline{k}$ vectors occupying a range of angle $\lesssim \pm 1°$ about the perpendicular to $\underline{B}$.

Scattered light passes through a narrow (2.7 Å) band dielectric interference furnished with a device to tilt it with respect to the incident light direction and so shift the wavelength of the passband. This facility permits us to build up, over a sequence of machine discharges, the spectrum of scattered light from which the plasma temperature and density are determined. It also serves to isolate a narrow band of the spectrum which is then further dispersed by a Fabry-Perot interferometer having a resolution of 0.1 Å. Pressure scanning is used for the latter, and the wavelength distribution of the fine structure of the scattered light spectrum is constructed from the results of a series of separate experiments. Fig.2 illustrates the experimental arrangement.

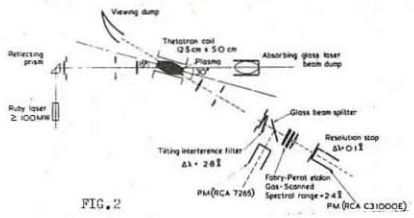

FIG.2

Results and Discussion: Preliminary measurements were carried out using the tilting filter apparatus alone. The total spectrum for the plasma formed from 45 millitorr of hydrogen was measured at the peak of the first half-cycle of the thetatron current and was consistent with an electron temperature $T_e = 20$ eV, and a density, confirmed by an independent Rayleigh scattering measurement of a few times 10^{15} electrons cm^{-3}. The corresponding correlation parameter α lies between 0.2 and 0.3.

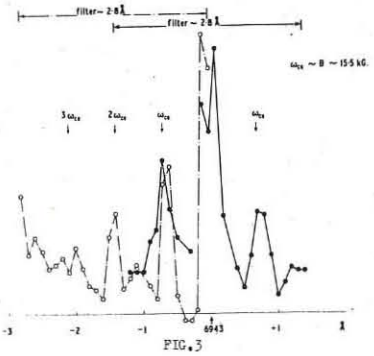

FIG.3

The spectrum of scattered light measured through the Fabry-Perot with the interference filter centred at the laser wavelength and then shifted by 1.3 Å is shown in Fig.3. The spectrum is split into a sequence of peaks each displaced from its neighbour by approximately 0.7 Å. Four such peaks counting the central one are resolved. Assuming that these arise from the magnetic field effect, their spacing corresponds to a field strength of 15.5 kG. This is nearly an order of magnitude smaller than the field for which a similar observation has recently been reported[6], and is in fact typical of fields commonly found in laboratory controlled fusion experiments.

An auxiliary field measurement using Faraday rotation of the plane of polarization of the beam of an He-Ne laser in a small cylinder of dense glass placed at the coil's centre gave a value of 16 kG. Thus, there is close agreement between the field calculated from the scattered light spectrum and that measured by Faraday rotation.

Conclusion

In an experiment in which the scattering vector $\underline{k}$ is almost perpendicular to the magnetic field $\underline{B}$, fine structure consisting of a sequence of peaks 0.7 Å apart has been detected in the nearly Gaussian spectrum of scattered laser light. The magnetic field calculated from the spacing of the peaks, 15.5 kG, agrees closely with that measured by Faraday rotation.

References

1. J.P. Dougherty, D.W. Barron and D.T. Farley. Proc. Roy. Soc. A 263 238 (1961)
2. J.A. Fejer. Can. J. Phys. 39 716 (1961)
3. T. Hagfors. J. Geophys. Res. 66 1699 (1961)
4. T. Laaspere. J. Geophys. Res. 65 3955 (1960)
5. E.E. Salpeter. Phys. Rev. 122. 1663 (1961)
6. L. Kellerer. Z. Physik 232 415 (1970)

DIAGNOSTICS FOR HOT-ELECTRON, MAGNETICALLY CONFINED PLASMAS

by

A. J. Lichtenberg, M. J. Schwartz and M. A. Lieberman

Department of Electrical Engineering and Computer Sciences

Electronics Research Laboratory

University of California, Berkeley, California U.S.A.

Abstract: Diagnostics have been developed for measuring the temperature, density, velocity distribution, axial and radial profiles, and decay rate, of a hot-electron (T_e between 20 and 200 keV) plasma confined in a magnetic mirror field. Comparison among a number of diagnostics is made. It is shown that measurements of temperature, density, and axial profile can be considerably in error if the experimental results are compared with Maxwellian velocity distributions, rather than self-consistent, mirror distributions.

I. Experiment: The experiment employs a magnetic mirror field which rises to a peak midplane value, typically 50 kG, with a rise time of 500 microseconds and decays with a time constant of τ = 10 milliseconds [1]. The mirror ratio $R_{max} = \frac{B_{max}}{B_0}$ is equal approximately to 1.4 at peak compression. A washer stack source injects plasma into the mirror region. At peak compression of 50 kG, the plasma parameters are typically kT_e = 60 keV in the tail of the Maxwellian, $n_e \simeq 5 \times 10^{12}$ cm^{-3}, length L ≃ 6 cm, and diameter D ≃ 0.5 cm.

Fig. 1 shows some of the diagnostics. Four radial ports sample synchrotron radiation, light, X-rays, and microwave radiation. The vacuum chamber itself can be made into a microwave cavity in which a resonance is perturbed by the plasma to obtain the density. A moveable light pipe with a 45° mirror at its end samples either synchrotron radiation or visible light emitted radially.

II. Measurement of Temperature and Speed Distribution: The energies of single X-rays are measured by deposition in a NaI crystal which emits light proportional to the X-ray energy. In Fig. 2 we compare the experimentally determined X-ray

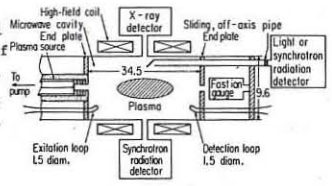

Fig. 1

heights, with the theoretical values for a loss cone distribution $v^s \exp(-mv^2/2kT)$, for the two values of s and kT that best fit the experiment. We see that it is impossible to determine kT independently of s from the X-ray data alone.

Synchrotron radiation is detected with a cryogenically operated, indium-antimonide photodetector [1]. The spectral distribution of the radiation is obtained with an echelette grating monochromator that has 10% bandwidth at the central frequency in each grating [1]. In Fig. 3 the experimental spectrum, somewhat smoothed, is compared with the theory using the loss cone distribution of the form used for X-ray calculations. For the distributions that bracketed the experiment from the X-ray data, we see that kT = 80 keV, s = 0, has neither the correct shift of the maximum nor the correct slope near $\omega = \omega_c$; kT = 60 keV, s = 4 has the correct slope but too large a shift in the peak. kT = 60 keV, s = 2 has the correct shift but slightly too steep a slope. Our best estimate, therefore is kT = 60 keV, s = 3, which is also consistent with the X-ray data. Collective plasma behavior may be responsible for the additional structure at lower frequencies.

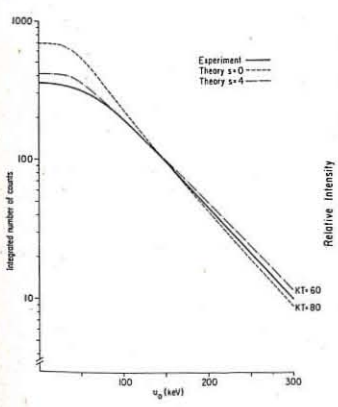

Fig. 2

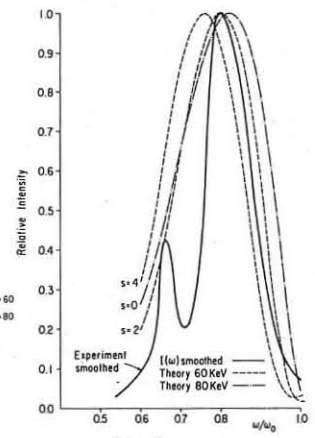

Fig. 3

III. Measurement of Diameter, Length, and Angular Distribution: A light pipe, as shown in Fig. 1, rotating about its own axis, is used to measure the radiation intensity as a function of angle. Depending on the detector, the radiation measured can be either synchrotron radiation in the infrared, or atomic transitions in the visible. Another method for determining the plasma radius is to detect fast electrons with an end loss camera. The radial profile can be obtained from each of these methods, but the accuracy is rather poor if the plasma radius is small. In Fig. 4 we compare the results of the radial profile as measured by the end loss camera (a) with that obtained from synchrotron radiation and light (b). The existence of a hot plasma core with a diameter less than a centimeter is confirmed by a comparison of the synchrotron radiation and end loss data. Both the light and the end loss measurement suggest the existence of an outer plasma shell.

The axial hot electron profile is determined from the synchrotron radiation intensity by sliding the light pipe axially along the plasma chamber. In mirror-confined plasmas, the angular velocity distribution can be

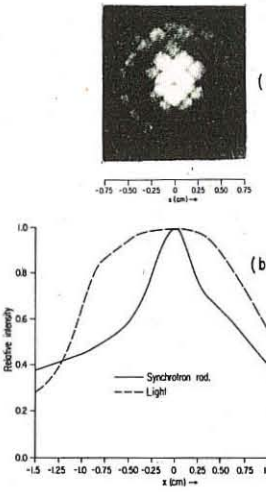

Fig. 4

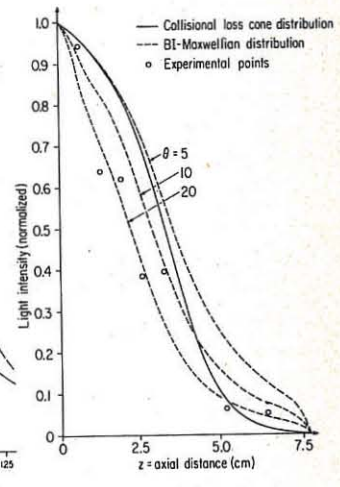

Fig. 5

determined from the axial profile. In Fig. 5 the profile measured using synchrotron radiation is compared with the theoretically predicted profiles. The theoretical profiles are calculated both from the collisional loss cone normal mode and from a bi-Maxwellian with anisotropy ratios $\theta = T_\perp/T_\parallel$. The experimental points are found to give a somewhat more anisotropic distribution than the normal mode. The results using visible light are in substantial agreement with those for synchrotron radiation.

IV. Measurement of Density: To determine the absolute intensity of radiation measured by the combined monochromator-detector system, the observed radiation is compared with radiation from a mercury arc lamp [2]. The line density of hot electrons can then be determined from a theoretical knowledge of the radiation per particle.

For our plasma, which is small and dense, the combined hot plus cold electron number has been measured using a microwave cavity perturbation technique [3]. The total number of plasma electrons when compared with the line density found from the absolute synchrotron intensity, indicates a plasma length of 12 cm, twice as long as the direct measurement of plasma profile from Fig. 5. The discrepancy is resolved by assigning the excess plasma to cold electrons, and this conclusion has been confirmed by other evidence [3]. A density decay constant of 5 msec. has been determined by both techniques.

Acknowledgement - The research was supported by AFAL contract AF 33 (615)-1078, NSF grants GP-2239 and GK-2978, and AFOSR grant 69-1754.

References

[1] Sesnic, S., Lichtenberg, A. J., Trivelpiece, A. W., and Tuma, D. T. (1968) Phys. Fl. 11 2025.

[2] Lichtenberg, A. J. and Sesnic, S. (1966) J. Opt. Soc. Am. 56 75.

[3] Lieberman, M. A. and Lichtenberg, A. J. (1969) Phys. Fl. 12 2109.

"WAVE PENETRATION IN A MAGNETOACTIVE PLASMA"

by

M. Moresco and E. Zilli

Centro Gas Ionizzati (C.N.R.), Istituto di Elettrotecnica e di Elettronica, Università di Padova (Italy).

Abstract: The anomalous penetration of an extraordinary wave in a magnetoactive plasma is studied. The effect of the ion motion is investigated in two cases: cold ions, hot ions with low collision frequency. The displacement current is not neglected in this analysis.

In a previous paper [1], the skin effect in a dense plasma in a d.c. magnetic field was studied, the case of the extraordinary wave ($\underline{k} \perp \underline{B}_o$, $\underline{E} \perp \underline{B}_o$) was considered. It was found that if the conditions:

$$(1) \qquad |k|^2 u_e^2 \gg \omega_{ce}^2 \quad , \qquad |k|^2 u_e^2 \gg \omega^2 + \nu_e^2$$

(u_e is the most probable electron speed, ν_e is their collision frequency, ω_{ce} their angular cyclotron frequency) are satisfied, then the penetration becomes anomalous and the skin depth independent of both collision frequency and magnetic field. In this paper, the anomalous penetration of an extraordinary wave is studied without neglecting the displacement current term in the dispersion relation, the solutions so obtained are valid for all densities. Ion motion is at first neglected, later it is included in two cases: cold ions, hot ions with low collision frequency. Attention is devoted to the cases where the anomalous penetration may be affected by ions. Maxwellian zero-order distribution functions are considered and all the oscillatory quantities are assumed to vary as $\exp[j(\omega t - \underline{k}\underline{r})]$, since the usual boundary condition (specular or diffuse reflection of the particles) is neglected. The conditions (1) for electrons are always assumed to be valid.

In the cases which are considered here, the dispersion relation can be written as:

$$(2) \qquad k^3 - Ak + jB = 0 \ ,$$

and the solution of eq. (2) as:

$$(3) \qquad k = \sqrt{\tfrac{3}{2}}\,(C_1 + C_2) - \tfrac{1}{2}\, j\,(C_2 - C_1) \ ,$$

where:

$$(4) \qquad C_1 = \left\{ \left[(B/2)^2 + (A/3)^3 \right]^{1/2} - B/2 \right\}^{1/3}$$

$$C_2 = \left\{ \left[(B/2)^2 + (A/3)^3 \right]^{1/2} + B/2 \right\}^{1/3} \ .$$

The skin depth is given by: $\delta = -1/\mathrm{Im}(k)$.

NEGLECTING ION MOTION.

In this case A and B are given by:

$$(5) \qquad A = \omega^2/c^2 \ , \qquad (6) \qquad B = \pi^{1/2} \omega_{pe}^2\, \omega / c^2 u_e \ ,$$

and C_1, C_2 are real positive quantities with $C_2 > C_1$. It follows that $\mathrm{Im}(k) < 0$ and $\mathrm{Re}(k) > 0$, this means that wave attenuation occurs even at low densities, the skin depth being:

$$(7) \qquad \delta = 2/(C_2 - C_1) \ ;$$

and at high densities there is no cut-off but a gradual transition between propagation and skin effect conditions. To separate these situations, a criterion can be established looking at the displacement current term in the dispersion relation (2): depending on whether this term is important or negligible, propagation or skin effect can be assumed to occur. The application of this criterion is straightforward using (3) and (4); it is interesting to notice that the skin effect condition:

$$(8) \qquad (A/3)^3 \ll (B/2)^2 \ ,$$

taking into account (5) and (6), becomes:

$$(9) \qquad \omega_{pe}^2 / \omega^2 \gg 0.2\ u_e / c \ ,$$

which is different from the one given by the cold plasma theory. If the condition (9) is valid, eq. (3) and (7) reduce to:

$$(10) \qquad k = \left(\sqrt{\tfrac{3}{2}} - 1/2\, j\right) \pi^{1/6} \left(\omega_{pe}^2\, \omega / c^2 u_e\right)^{1/3}$$

$$\delta = 2\, \pi^{-1/6} (c^2 u_e / \omega_{pe}^2\, \omega)^{1/3} \ .$$

COLD IONS.

In this case, B is given by (6), and :

$$A = \frac{\omega_{pe}^2}{c^2} \, \frac{(1 - j\,\nu_i/\omega - \omega_{pi}^2/\omega^2)^2 - \omega_{ci}^2/\omega^2}{(1 - j\,\nu_i/\omega)^2 - \omega_{ci}^2/\omega^2 - \omega_{pi}^2/\omega^2 (1 - j\,\nu_i/\omega)} \ .$$

If (9) holds, the effect of ions will be noticeable if :

$$(11) \qquad (|A|/3)^3 \gtrsim (B/2)^2 \ .$$

This can be expected to occur in resonance conditions, provided that ion collision fraquency is small enough. Actually, for $\omega = (\omega_{pi}^2 + \omega_{ci}^2 + \nu_i^2)^{1/2}$, condition (11) is verified if :

$$\frac{\nu_i}{\omega} \lesssim 0.36\, \omega_{pi}^2 / c^2 (c^2 u_e / \omega_{pe}^2\, \omega)^{2/3} (\omega^2 - \omega_{pi}^2)/(2\omega^2 - \omega_{pi}^2) \ ,$$

and the wave number and the skin depth are given by :

$$k \cong \frac{\omega}{c} \left(\frac{\omega^2 - \omega_{pi}^2}{2\omega^2 - \omega_{pi}^2} \right)^{1/2} (4 + \omega_{pi}^4/\omega^2 \nu_i^2)^{1/4} \, (\cos\theta/2 - j \sin\theta/2) \ ,$$

$$\delta \cong \frac{c}{\omega} \left(\frac{2\omega^2 - \omega_{pi}^2}{\omega^2 - \omega_{pi}^2} \right)^{1/2} \frac{(4 + \omega_{pi}^4/\omega^2 \nu_i^2)^{-1/4}}{\sin\theta/2} \ ,$$

where :

$$\theta = \tan^{-1} (\omega_{pi}^2 / 2\omega\nu_i) \ .$$

HOT IONS WITH LOW COLLISION FREQUENCY.

If the conditions for ions $|k|^2 u_i^2 \gg \omega^2$, $|k|^2 u_i^2 \gg \omega^2 \nu_i^2$ are verified (u_i being the most probable ion speed), it follows :

$$A = \omega^2/c^2 \ , \qquad B = \pi^{1/2} \omega / c^2 (\omega_{pe}^2/u_e + \omega_{pi}^2/u_i) \ .$$

If skin effect condition (8) holds, which in this case yields:

$$\omega_{pe}^2\, c/\omega^2 u_e + \omega_{pi}^2\, c/\omega^2 u_i \gg 0.2 \ .$$

we obtain :

$$k = \left(\sqrt{\tfrac{3}{2}} - 1/2\, j\right) \pi^{1/6} \left[\omega/c^2 (\omega_{pe}^2/u_e + \omega_{pi}^2/u_i) \right]^{1/3}$$

$$\delta = 2\, \pi^{-1/6} \left[(c^2/\omega) / (\omega_{pe}^2/u_e + \omega_{pi}^2/u_i) \right]^{1/3} \ .$$

Comparing this result with eq. (10), one notices that the skin depth can be affected by ion motion, when :

$$T_e/T_i \gtrsim m_i/m_e \ , \quad \text{or:} \quad R_e \gtrsim R_i \ ,$$

1. NEGLECTING ION MOTION

$$\delta = 2\, \pi^{-1/6} (c^2 u_e / \omega_{pe}^2 \omega)^{1/3}$$

2. INCLUDING ION MOTION

a) Cold ions:

$$\delta = \frac{c}{\omega} \left(\frac{2\omega^2 - \omega_{pi}^2}{\omega^2 - \omega_{pi}^2} \right)^{1/2} \frac{(4 + \omega_{pi}^4/\omega^2 \nu_i^2)^{-1/4}}{\sin\theta/2}$$

where: $\theta = \tan^{-1} (\omega_{pi}^2 / 2\omega\nu_i)$

if: $\omega = (\omega_{pi}^2 + \omega_{ci}^2 + \nu_i^2)^{1/2}$

and:

$$\frac{\nu_i}{\omega} \lesssim 0.36 \omega_{pi}^2 / c^2 (c^2 u_e / \omega_{pe}^2 \omega)^{2/3} (\omega^2 - \omega_{pi}^2)/(2\omega^2 - \omega_{pi}^2)$$

b) Hot ions with low collision frequency :

$$\delta = 2\, \pi^{-1/6} \left[(c^2/\omega) / (\omega_{pe}^2/u_e + \omega_{pi}^2/u_i) \right]^{1/3}$$

Table I.- Depths of penetration in anomalous skin effect conditions for electrons .

where $R_e = u_e/\omega_{ce}$, $R_i = u_i/\omega_{ci}$ are the mean cyclotron radii . The skin depths which have been calculated in the cases considered are summarized in Table I.

[1].- M.MORESCO, E.ZILLI - Proc. Int. Conf. Phys.Quiescent Plasmas, Paris, I, 175 (1969). See also: Lett.Nuovo Cimento, 3, 581 (1970).

PENETRATION OF A STRONG ELECTROMAGNETIC WAVE IN AN INHOMOGENEOUS PLASMA GENERATED BY ECR ON A MAGNETIC BEACH

J. Musil, F. Žáček

Institute of Plasma Physics, Czechoslovak Academy of Sciences,
Nademlýnská 600, Prague, Czechoslovakia

Abstract: This paper deals with the penetration of a strong RHCP /right-hand circularly polarized/ electromagnetic wave in a dense inhomogeneous plasma generated by electron cyclotron absorption of this wave on a magnetic beach. Experimentally was proved the existence, movement and overcoming of the evanescent region. The experimental results are in a good qualitative agreement with the theory.

The RHCP wave propagating in an infinite homogeneous magnetoactive plasma parallel to a static magnetic field is strongly absorbed at $\omega = \omega_{ce}$; ω is the frequency of the wave, ω_{ce} is the electron cyclotron frequency. The strong ECR absorption of the RHCP wave has been recently successfully used for the production of a dense plasma in which $\omega_0^2/\omega^2 > 1$; ω_0 is the plasma frequency. As the reflection on a plasma in a homogeneous magnetic field is too high it is better to generate plasma by ECR absorption of RHCP wave on a magnetic beach, where the efficiency of the energy transfer into plasma is much higher. This method is successfully used for generation of a dense plasma in magnetic mirror machines.

However, in a plasma generated by ECR on a magnetic beach electron density along magnetic field N(z) increases in the direction of decreasing magnetic field. Propagation in such an inhomogeneous plasma can considerably differ from propagation in a homogeneous plasma. The study of propagation under this conditions was carried out on the modified ER-2 device [1,2], see Fig. 1. The plasma is generated by ECR absorption of microwave

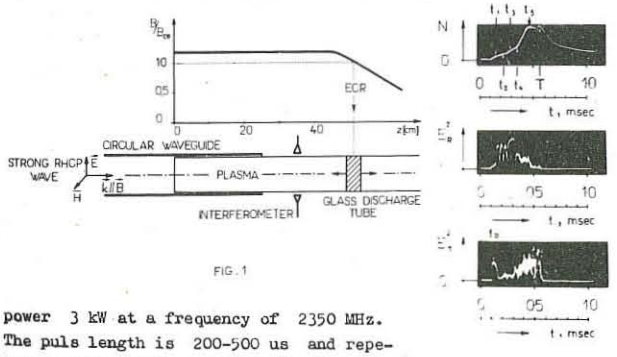

FIG. 1

FIG. 2

power 3 kW at a frequency of 2350 MHz. The puls length is 200-500 us and repetition rate 50 Hz. The typical time dependence of the electron density N measured with 8 mm interferometer at z = 35 cm is shown in Fig.2. It may be seen that the strong additional increase of N occurs at the time t_4. The new value of N_2 corresponding to $t \in \langle t_5, T \rangle$ is several times higher than N_1 corresponding to t_4 and depends on the power of the wave and on the gas pressure.

To explain the causes of this considerable increase of N we have measured the time dependences of the reflected power E_R^2 and the power transmitted into the plasma E_T^2, see Fig. 2. From Fig. 2 it may be seen that time display can be divided into two regions corresponding to time intervals $0\text{-}t_4$ and $t_4\text{-}T$, where T is length of the magnetron puls . In the first region where $N \leq N_1$ the E_R^2 periodically oscillates and its increase corresponds to the decrease of the E_T^2 and on the contrary. It is important that in the second region E_R^2 decreases and E_T^2 is approximately the same as at the beginning of the puls when $\omega_0^2 \ll \omega^2$ and wave freely penetrates . These facts show that in the time t_4 the qualitative change in the penetration of RHCP wave takes place. Fig. 3 shows the distribution of a saturated ion current $i_+(z) \sim N(z)$ from the movable langmuir probe along the axis at different times. It may be seen that N increases in the direction of the wave propagation. This situation can be well followed on dispersion curves of the RHCP wave propagation in a magnetoactive plasma for the propagation at a small angle $\alpha \neq 0$ to a static magnetic field [3], see Fig. 4. n is refractive index, indexes 1,2 and 3 mark the extraordinary, ordinary and plasma wave, $Y = \omega_{ce}/\omega$. To make the problem more simple we suppose that in an inhomogeneous plasma the wave propagates in the direction of density gradient. In Fig. 4 the time evolution of the plasma density distribution N(z) is given as well.

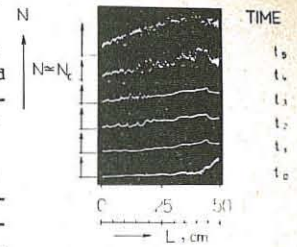

FIG. 3

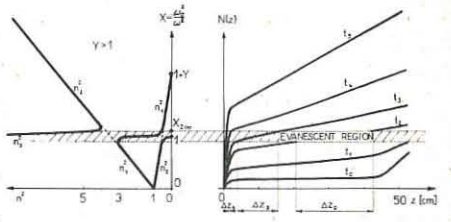

FIG. 4

The greatest significance for propagation of the RHCP wave at $Y > 1$ has the fact, that at $\alpha = 0$ the wave 1 (dashed line) freely passes through the inhomogeneous plasma but at small angle $\alpha \neq 0$ only a partial penetration into a region of $X_2 > X_{2\infty}$ takes place. This is consequence of the existence of the evanescent region in the vicinity $X_{2\infty}$ at $\alpha \neq 0$. It is clear that magnitude of wave penetration depends first of all on geometrical width Δz of this region. In our case plasma is produced in a waveguide and $\alpha \leq 45°$ at the density corresponding to the beginning of the evanescent region; details are given in [4].

From Fig. 4 it may be seen that the qualitative jump in the propagation have to occur in the moment t_4, when Δz achieves a critical magnitude at the beginning of the tube . From this moment the wave freely passes through this region and is absorbed in the point of ECR on the magnetic beach. This results in further very considerable increase of the plasma density. This model is in good agreement with measurements of the distribution $E_T^2(z)$ of the wave penetrating along the axis in different times, see Fig. 5. Moreover, from Fig. 5 it may be seen well the movement and overcoming of the evanescent region caused by the sudden change of the geometrical width Δz of this region at the beginning of the tube.

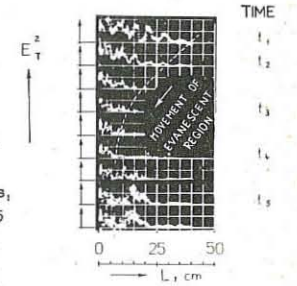

FIG. 5

So, the penetration of the RHCP wave into a dense plasma generated by ECR on a magnetic beach can be explain on the basis of properties of the RHCP wave propagation in an inhomogeneous magnetoactive plasma. The existence of the evanescent region has been verified experimentally. The free passage of the RHCP wave through this region results in a strong additional increase of the density; in our case N increases five times and is proportional to the wave power.

The authors wish to thank to Dr. V. Kopecký and Dr. J.Ďatlov for valuable discussions.

References:

[1] Ďatlov J., Musil J. and Žáček F. /1968/ Proc. 4th Czechoslovak Conf. on Electronics and Vacuum Phys., Prague

[2] Musil J., Žáček F. Czech. J. Phys. B20 /1970/

[3] Ginzburg V.L. /1960/ Propag. of Elmag. Waves in Plasma, Moscow

[4] Musil J., Žáček F. /1970/ Res. Rep. IPPCZ-141, to be published in Plasma Physics

REFLECTION AND DAMPING OF ELECTRON CYCLOTRON WAVES IN A HIGH DENSITY PLASMA

by

S.Bernabei, R.De Dionigi and M. Fontanesi

LABORATORIO DI FISICA DEL PLASMA DEL C.N.R. - Istituto di Scienze Fisiche - Milano - Italia

and by

G. Lisitano

INSTITUT FUR PLASMA PHYSIK - Garching - Germany

Abstract: Reflection measurements of an electron cyclotron wave propagating along a magnetic beach was made by means of a multi fringe interferometer.

It is generally assumed that the absorption by means of cyclotron damping of ion or electron cyclotron waves, propagating along a weakening magnetic field (magnetic beach), occurs when the local ion or electron frequency (ω_{be} and ω_{bi}) become sufficiently close to ω and the local wave number $k_{\parallel}$ is sufficiently large. The experimental results reported in this paper show that generally an electron cyclotron wave is progressively reflected by the increasing refractivity of the plasma, before reaching the gyromagnetic resonance region. However the reflection of the wave does not contradict to the well established phenomena of rf energy transfer to the plasma in electron or ion cyclotron heating devices (1-2). In these devices the energy absorption by means of cyclotron damping occurs either in proximity of the rf coupling system or in regions of cyclotron resonance, where the rf power, filling the whole device, is really available. In this experiment however the electron cyclotron wave, coupled to the plasma in a region where $\omega_{be} \gg \omega$, is reflected before reaching the resonance region. The amplitude and phase variation of the electron cyclotron wave in the frequency range from 1 to 2 GHz was measured, along a magnetic beach, for a wide range of parameters of an almost fully-ionized argon plasma, i.e. $3 < \omega_p/\omega < 30$; $1 < \omega_b/\omega < 10$; $T_e \div$ 3-10eV; $n_e \div 10^{12} - 10^{13}$ cm^{-3}. The plasma was produced in a magnetic mirror (mirror ratio 3:1) by non resonant absorption of rf power (at a fixed frequency of 2.4 GHz) coupled to the plasma by means of a retarding structure (3) which was placed at one end of the mirror. The electron-cyclotron wave has been launched into the plasma column, either by means of the same slow wave structure used to produce the plasma or by a second similar structure placed at the other end of the magnetic mirror. The wave was detected by a very thin screened radial probe, immersed in the plasma. The wave propagation path, between the wave coupling system and the probe, forms one branch of a variation (4) of the Wharton interferometer with a multifringe display of the phase angle of the wave. In Fig.1 the lower trace refers to the amplitude of the wave along 10 cm propagation path of a magnetic beach, the zero cm point to the left of the figure corresponding to the center of the mirror. The upper traces showing the multiple fringes refer to the phase shift of the wave along the same path. The fringe calibration is 2π/cm. The wave was launched from the right at a distance of 20 cm from the center of the mirror. Fig. 1a) shows that the electron cyclotron wave is almost completely reflected at the region of increasing plasma refractivity near the gyromagnetic resonance region rather than being absorbed. In the case of a collisional plasma we have observed a smooth damping of the wave (Fig.1b). The standing wave pattern (of the wave amplitude variation) is supported by the corresponding 180° phase change (nodes of the pattern) as indicated by the phase

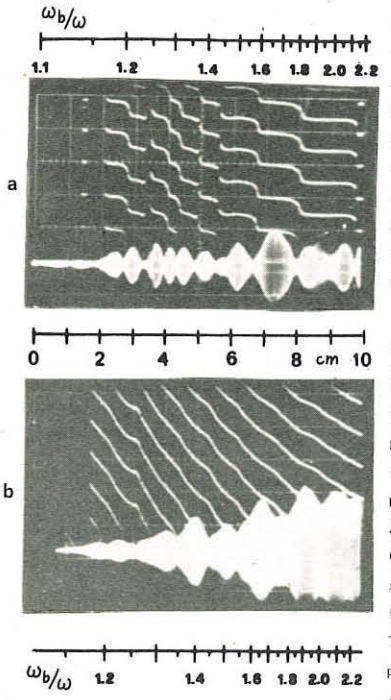

Fig.1

shift interferometer. We have always noted that the wave is reflected at values of $\omega_b/\omega > 1$. Depending on the discharge conditions we observed a shift of the reflection point which is qualitatively in agreement with the approximate dispersion relation (5-6)

$$n^2 = \left(\frac{\omega_p}{\omega}\right)^2 \Big/ \left(\frac{\omega_b}{\omega} + \delta - \beta - 1\right)$$

valid for $\omega_{p/\omega} \gg 1$

$\left(\delta = \frac{kT_e/m_e}{\omega^2/k_{\parallel}^2}\right.$ and $\left.\beta = \frac{4\pi kT}{B^2}\right)$

For our magnetic field profile along the measured propagation path was possible to assume

$$\frac{\omega_b}{\omega} - 1 = C\, e^{Kx}$$

where C and K are constant and x is the axial distance from the mirror center. The expression for the phase shift

$$\varphi = \frac{2\pi}{\lambda}\,\frac{\omega_p}{\omega}\, C \int_o^x e^{-\frac{Kx}{2}}\, dx$$

for the simple case of $\delta = \beta = 0$ gives us a linear relationship between $\ln\varphi$ and Kx. In Fig.2 this linear dependence is shown for two discharge conditions having the same K (that is the same test frequency and magnetic field profile). For values of δ and $\beta \neq 0$ the slope of this curve should give a dependence on the electron temperature.

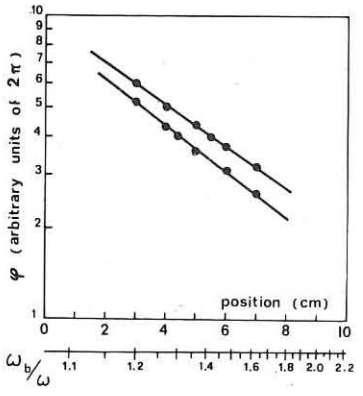

Fig.2

While the general properties of this linear relationship have been observed for all the data, we have not yet enough correlation measurements between the observed slope and the density and the temperature of the plasma. However the preliminary results presented in this work demonstrate that almost total reflection of cyclotron wave may occur in a magnetic beach for a large range of plasma parameters.

REFERENCES

(1) W.H.Hooke, M.A.Rothman - Nucl.Fusion-4, 33 (1964)

(2) R.A.Dandl, A.E.England, W.B.Ard et al.-Nucl.Fusion, 4, 344(1964)

(3) G.Lisitano, M.Fontanesi and E.Sindoni-Appl.Phys.Lett. 16, 122 (1970)

(4) E.Rossetti, A.Capitanio - to be published

(5) M.A.Heald, C.B.Wharton-Plasma diagnostics with microwaves - J.Wiley (1965)

(6) T.H.Stix - The tehory of plasma waves - McGrawHill (1962)

NUMERICAL SOLUTIONS OF THE FULL WAVE EQUATIONS IN AN INHOMOGENEOUS COLD PLASMA SLAB NEAR THE LOWER HYBRID RESONANCE

by

V. Agnello, D. Colombant, P. Pieffé-Prévost, G. Ichtchenko, S. Kulinski.

ASSOCIATION EURATOM - CEA
Département de la Physique du Plasma et de la Fusion Contrôlée
Service I.Gn. Centre d'Etudes Nucléaire
Cedex 85. 38 Grenoble Gare (France)

Abstract : The absorption of an E.M. wave in an inhomogeneous cold plasma slab is considered. For perpendicular incidence, the absorption coefficient presents sharp geometric resonances and depends strongly on the length of the region of evanescence. The case of oblique incidence is then discussed. In a second part, we compute the resistive loading of a coil imposing an axial wavelength so that the accessibility condition /1/ is fulfilled. It is shown that this resistance varies little with density gradient and that the lower hybrid resonance may be masked by coupling resonances.

1. In the first section, we calculate the reflexion, transmission and absorption coefficients of an inhomogeneous cold plasma slab (fig. 1) where the frequency of the E.M. wave passes through the lower hybrid resonance : $\omega_H^2 = \frac{\omega_{pe}^2 + \omega_{ce}\omega_{ci}}{\omega_{pe}^2 + \omega_{ci}^2}\,\omega_{ce}\omega_{ci}$
In this model the accessibility condition is not fulfilled. Since the W.K.B. method cannot be used near cut off and resonance, we solve numerically the full wave equations. Few collisions ($\nu/\omega = 10^{-3}$) have been included in order to facilitate computations near the resonance. The equations are integrated twice, starting in the vacuum from two different sets of initial conditions /2/. When $\theta_o = 0$ each initial condition excites one mode in the plasma independent from the other. In this case, only the extraordinary mode (initial condition A) possesses a resonance. We have plotted on fig. 2, the absorption coefficient A_1 of the extraordinary mode versus ℓ. Geometric resonances appear when :

$$\ell = m\,\frac{\Lambda_o}{\bar{N}} \qquad (1)$$

where m is a positive integer, Λ_o is the wavelength in the vacuum and $\bar{N}$ is the average refractive index in the slab. The absorption is negligible if condition (1) is not fulfilled. On fig. 3 A_1 is plotted versus ω_{ce}/ω for three values of the maximum density when condition (1) is satisfied. This figure shows that a condition exists for which the value of A_1 is maximum (50 %). This occurs when the length of the region of evanescence is such that the energy transmitted by tunneling is exactly equal to the energy reflected. If this length is too small, the tunneling is very efficient and most of the energy is transmitted. Conversely if it is very large the wave is principally reflected. In oblique incidence, the two modes are coupled in the plasma. The initial condition A gives rise to a component E_z of the E.M. field which is not absorbed by the particles. Similarly the initial condition B gives rise to a component E_y which may be absorbed by the same process as in perpendicular incidence. These remarks can explain fig. 4 where the absorption coefficients associated with initial conditions A and B are plotted versus θ_o.

2. In this section, the resistive loading of an oscillator coil inductively coupled to a finite plasma slab (see fig. 5) is computed near the lower hybrid resonance when the accessibility condition is met. These calculations follow those of Skipping and al. /3/ but differ in that the plasma is now treated as inhomogeneous. This approach insures that once the maximum plasma density is greater than the lower hybrid resonant density, the resonance will occur at some layer in the plasma and not over a whole plateau. After /3/, the resistance is defined as

$$R = \frac{|V|^2}{2P_d}$$

where V is the coil voltage amplitude and P_d the power dissipated in the plasma. Resonances are revealed by minima in R. Because of the accessibility condition, the fields are evanescent in the vacuum. Using the full wave equations and matching tangential components of the fields an their derivatives at the vacuum-plasma boundary and at the coils, R is found to be :

$$R = \frac{4Z_o L}{\pi^2}\,\frac{\left|\sum_{n\ odd} \frac{\exp(-N_x^o d\omega/2c)}{N_x^2\,n^2}\,\sin^2\frac{n\pi a}{2L}\;G\right|^2}{\sum_{n\ odd} \frac{\exp(-N_x^o d\omega/2c)}{N_x^o\,n^2}\,\sin^2\frac{n\pi a}{2L}\;Im(G)}$$

where

$$G = \exp(N_x^o d\omega/2c) - \exp\left[N_x^o\tfrac{\omega}{c}(\ell - \tfrac{d}{2})\right]\left\{\frac{(\mathcal{H}_y^1 - i\frac{E_x^1}{N_z^o})(i\mathcal{H}_z^1 - N_x^o E_y^1) - (\mathcal{H}_y^1 - i\frac{E_z^1}{N_x^o})(i\mathcal{H}_z^1 - N_x^o E_y^1)}{(\mathcal{H}_y^1 - i\frac{E_x^1}{N_z^o})(i\mathcal{H}_z^2 + N_x^o E_y^2) - (\mathcal{H}_y^1 - i\frac{E_z^2}{N_x^o})(i\mathcal{H}_z^1 + N_x^o E_y^1)}\right\}$$

$\mathcal{H}_y^{1,2}, \mathcal{H}_z^{1,2}, E_y^{1,2}, E_z^{1,2}$ are the field amplitudes at the vacuum-plasma boundary for modes 1 and 2, $Z_o = \sqrt{\mu_o/\epsilon_o}$, $N_x^{o\,2} = N_z^2 - 1$, $N_z = \frac{n\pi}{L}\frac{c}{\omega}$. The geometric paremeters a, d, l, L have been defined on fig. 5 and the current distribution in the coil has been assumed to be uniform. Since we are interested in the case a = L, the resistance has been computed for the Fourier component n = 1. However, higher order terms cannot be neglected when a ≪ L.

The variation of the resistance with density gradient is shown in fig. 6. This variation is small since, when the accessibility condition is met, the energy absorption is not dependent on a tunneling effect. In fig. 7, it has been assumed that the plasma expands steadily in the x direction and that its density decreases in order to conserve the number of particles. The figure shows the resistance due to the plasma as it fills the space up to the coils. At point A, the maximum density falls below the lower hybrid resonant density and therefore, none of the resonances after this point are lower hybrid ones. It is seen that in this case, the coupling resonances which are natural modes of the system, are more important than the lower hybrids ones. The importance of the lower hybrid resonance may be judged by comparison with the homogeneous case which appears as a dotted line.

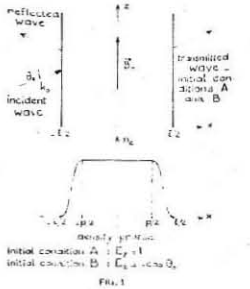

FIG. 1

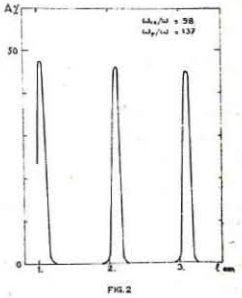

FIG. 2

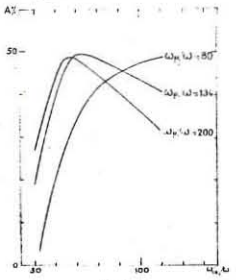

FIG. 3

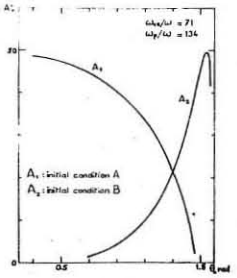

FIG. 4

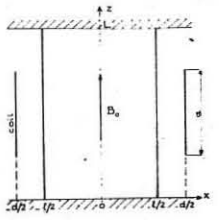

FIG. 5

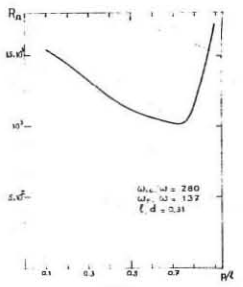

FIG. 6

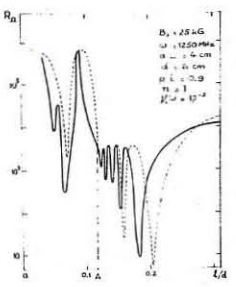

FIG. 7

REFERENCES

/1/ Stix T.H.. The Theory of Plasma Waves. Mc - Graw Hill (1962) P. 65

/2/ Budden K.G. Proc. Roy. Soc. A, 227, 516 (1955)

/3/ Skipping C.R.. Oakes M.E.. Schlüter H.. Phys. Fluids 9 , 1886 (1969)

BEAM INSTABILITY, TRANSFORMATION AND EIGENMODES IN AN INHOMOGENEOUS PLASMA

V. Kopecký

Institute of Plasma Physics,
Nademlýnská 600, Prague 9, Czechoslovakia

Abstract: In a hot anisotropic plasma with an inhomogeneity across the magnetic field, eigenmodes are a superposition of long waves of cold plasma and short-wave Bernstein modes. As a consequence, threshold currents of beam instability increase comparing with the case of homogeneous plasma.

As follows from the linear theory, in anisotropic plasma there exist a branch φ_c of potential waves of cold plasma for frequencies $\omega > \omega_c$ (ω_c is the electron cyclotron frequency) with the dispersion

$$\omega^2 = \frac{1}{2}\left\{\omega_0^2+\omega_c^2+\sqrt{(\omega_0^2+\omega_c^2)^2-4\omega_0^2\omega_c^2k_z^2/(k_z^2+k_\perp^2)}\right\},$$

where ω_0 is the plasma frequency and $k_\perp$, k_z are the transversal and longitudinal wave numbers respectively. $k_\perp$ approaches infinity as ω goes to the hybrid frequency $\omega_H^2 = \omega_0^2+\omega_c^2$. Apart of these waves in a hot plasma there exist wave branches φ_B propagating normally to the magnetic field - the so called Bernstein modes [1]; for them $k_\perp$ approaches zero as ω goes to the hybrid frequency. Influence of temperature on waves of cold plasma appears considerably only at $k_\perp >> k_z$ in such a way that this branch matches with the branch of the Bernstein modes in the region of the hybrid frequency.

Thus for frequencies $\omega > \omega_c$ there exist the region

(1) $$\max(\omega_c^2,\omega_0^2) < \omega^2 < \omega_0^2+\omega_c^2$$

in a hot anisotropic plasma, where two kinds of waves with the same frequency and same k_z but different $k_\perp$ can propagate (Fig. 1). However, in an inhomogeneous plasma these two kinds are not independent. Both wave types propagates in regions (1); at the same time the wavelength φ_c shortens when waves propagate from the region of greater density towards the hybrid resonance and the wavelength of the Bernstein modes lengthens (Fig. 1). In the region of the hybrid resonance, where the wavelengths are equal, a coupling of both wave types takes place [2] : $\varphi = \varphi_c^{\pm} - \varphi_B^{\pm}$, where the superscript sigh $\pm$ denotes a direction of the phase velocity.

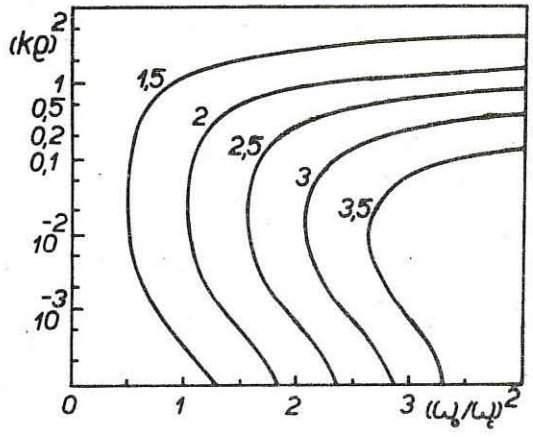

Fig. 1. Dispersion curves for potential waves in a hot plasma for $(k_z v_{Tp}/\omega_c)^2 = 10^{-3}$ and $(\omega/\omega_c)^2$ as a parameter.

In an inhomogeneous plasma eigenmodes must therefore be (in the WKB approximation) a combination of the short and long waves. Solutions satisfying transformation conditions in the region of the hybrid resonance ($x = \pm x_0$) are

$$\varphi = \varphi_c^- - \varphi_B^- e^{in\pi} \quad \text{or} \quad \varphi = \varphi_c^+ - \varphi_B^+ e^{in\pi}$$

or its combination. Here n is integer and it determines the quantum condition

$$\left(n-\frac{1}{2}\right)\pi = \int_0^{x_0}\sqrt{\frac{2(4\omega_c^2-\omega^2)[\omega_H^2(x)-\omega^2]}{3v_T^2\omega_0^2(x)}}\,dx - \int_0^{x_0}\sqrt{\frac{k_z^2(\omega^2-\omega_c^2)(\omega^2-\omega_0^2(x))}{\omega^2[\omega_H^2(x)-\omega^2]}-k_y^2}\,dx.$$

It thus appears that such combined eigenmodes can also be travelling waves, energy being transmitted by the wave φ_c in one direction and by the Bernstein mode in the opposite one.

Because in the region of harmonics of the electron cyclotron frequency a wave damping is mostly determined by the Doppler damping (being proportional to $(k_\perp v_T/\omega_c)^{2l-1}$) the short wave Bernstein modes are damped more intensively than waves of cold plasma. Therefore a damping of eigenmodes in inhomogeneous plasma will be more intensive than that of modes in homogeneous plasma. In this way also threshold currents of the beam instability increase.

The threshold current of a beam of the radius r in a homogeneous plasma of the radius R can be approximately determined by the relation $\gamma_b r - \gamma_c R = 0$, where γ_b is the instability increment and γ_c is the decrement of the waves φ_c. In the case of inhomogeneous plasma the condition of the threshold current has an approximate form

(2) $$\gamma_b r/v_{g\perp}^c - \gamma_B R/v_{g\perp}^B = 0,$$

where γ_B is the decrement of the waves φ_B, $v_{g\perp}^c$ and $v_{g\perp}^B$ are the group velocities in the direction of an inhomogeneity of the waves φ_c and φ_B, respectively. Because of $\gamma_B > \gamma_c$ and $v_{g\perp}^B < v_{g\perp}^c$ the increment of the beam instability in an inhomogeneous case must be greater and therefore the density or current of a beam must be greater. From accurate computations the following expressions for the threshold current of a beam in a homogeneous plasma layer of the width R is obtained

(3) $$I_h = \frac{2{,}7m\omega_{0max}^2 R\,v_{Tb}^2\omega^2(\omega^2-\omega_{0max}^2)(\omega^2-\omega_c^2)}{16\pi e\,v_{Tp}\,\omega_c^2\omega^2(\omega_{Hmax}^2-\omega^2)}\cdot \left\{\exp\left[-\left(\frac{\omega}{\omega}\frac{\omega_c}{\omega}\frac{v_0}{v_{Tp}}\right)^2\right]+\frac{\omega^2}{8\omega_c^2}\frac{v_{Tp}^2}{v_0^2}\exp\left[-\left(\frac{\omega}{\omega}\frac{2\omega_c}{\omega}\frac{v_0}{v_{Tp}}\right)^2\right]\right\}$$

and in an inhomogeneous layer with the parabolic course of density

$$I_i = \frac{2{,}7\,mR\,\omega\sqrt{4\omega_c^2-\omega^2}(\omega_{Hmax}^2-\omega^2)}{4\sqrt{3}\,\pi e\,\omega_c^2}\sqrt{\frac{(\omega^2-\omega_{0max}^2)(\omega^2-\omega_c^2)}{\omega^2(\omega_{Hmax}^2-\omega^2)}-k_y^2\frac{v_0^2}{\omega^2}}\cdot$$

(4) $$\cdot\frac{v_{Tb}^2\,v_0}{v_{Tp}^2}\left\{E\left(\frac{\pi}{2},\sqrt{\frac{\omega_{Hmax}^2-\omega^2}{\omega_{0max}^2}}\right)\exp\left[-\left(\frac{\omega-\omega_c}{\omega}\frac{v_0}{v_{Tp}}\right)^2\right]+\frac{(4\omega_c^2-\omega^2)(\omega^2-\omega_c^2)}{12\omega_{0max}^2\omega_c^2}\cdot\right.$$
$$\left.\cdot\left[\frac{\omega_{0max}^2}{\omega^2-\omega_c^2}E\left(\frac{\pi}{2},\sqrt{\frac{\omega_{Hmax}^2-\omega^2}{\omega_{0max}^2}}\right)-F\left(\frac{\pi}{2},\sqrt{\frac{\omega_{Hmax}^2-\omega^2}{\omega_{0max}^2}}\right)\right]\exp\left[-\left(\frac{\omega-2\omega_c}{\omega}\frac{v_0}{v_{Tp}}\right)^2\right]\right\},$$

where F and E are eliptic integrals of the first and second kind, respectively, v_0 is the beam velocity, $v_{Tp,b}$ is the thermal velocity of a plasma and beam, respectively. Expression (4) agrees approximately with estimation (2).

Comparing expressions (3) and (4) we see the thresholds current for frequencies near ω_c in an inhomogeneous case to be v_0/v_{Tp} times greater. For frequencies near $2\omega_c$ in the case of an inhomogeneous plasma the threshold current is of the same order as for frequencies near ω_c and therefore $(v_0/v_{Tp})^3$ times greater than in a homogeneous plasma. Also plasma heating increases together with an increase of threshold currents comparing with the homogeneous case.

References

[1] Bernstein I.B.: Phys. Rev. 109 (1958) 10
[2] Kopecký V. at al.: J. Plasma Phys. 3 (1969) 179
[3] Rabenstein A.L.: Arch. Rat. Mech. and Anal. 1 (1958) 418

EXPERIMENT ON THE EXCITATION OF BUCHSBAUM-HASEGAWA-RESONANCES

F. Leuterer
Institut für Plasmaphysik, Garching b. München, Germany

In a hot inhomogeneous plasma column in a magnetic field resonances known as Buchsbaum-Hasegawa-modes [1] can be observed at the low frequency side of the electron cyclotron harmonic frequencies. They are attributed to electrostatic electron plasma waves which can propagate perpendicular to the magnetic field (Bernstein waves [2]). If $\omega_p^2 > \omega_{pH}^2 = \omega^2 - \omega_c^2$ (= hybrid density), then for frequencies $\omega/\omega_c = n - \Delta$ (ω/ω_c), where the B-H-resonances are observed, these waves propagate as backward waves. This implies that in an inhomogeneous plasma column and for ω near $2\,\omega_c$, these waves can only exist in the dense core of the column bounded by the hybrid layer. Within this dense core these oscillations form a standing wave pattern, which manifests itself in the resonances whenever the phase condition

$$\int_{r_H}^{0} \hat{k}(r)\,dr = (n + \alpha)\pi \qquad n = 1, 2, 3 \ldots$$

is fulfilled [1,3,6].

It is generally assumed that the Bernstein waves, which lead to the oscillations, are coupled to the electromagnetic field at the hybrid layer [4]. This implies that in an inhomogeneous cylindrical plasma column the group velocity of the thus excited waves should be directed radially inward, from the hybrid layer towards the higher density region. However, Gruber and Bekefi [5] report the observation of just the opposite direction of propagation which would require another excitation mechanism instead of a local coupling at the hybrid layer. They propose a continous coupling throughout the volume where the waves propagate.

In a steady state experiment [6] where the waves have been excited by means of an externally applied high frequency capacitor field, we obtained results which are contrary to the findings of Gruber and Bekefi. In such a steady state experiment, however, the group velocity of a wave cannot be measured directly.

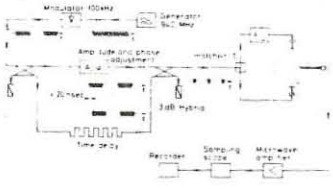

Fig. 1
Experimental arrangement

Therefore, a short microwave pulse (≈ 2o nsec, 94o MHz) was applied to the capacitor plates and the transient plasma wave response was observed with an antenna inside the plasma. Fig. 1 shows the experimental arrangement. Fig.2 shows a set of recorded probe signals for different probe positions between the axis of the column and the wall. We see, expecially for 4 mm < r < 8 mm, four clearly separated pulses arriving at the probe which indicate that the excitation is mainly a local one. The first one of the pulses is due to capacitive coupling from the capacitor plates to the probe. It is an electromagnetic signal which arrives without appreciable time delay. The second and third pulses are the Bernstein wave pulses which are excited on both sides of the plasma column in the region of the hybrid layer (at $r \approx \pm$ 12 mm). It is seen from fig. 2 that the wave pulses travel radially inward with a considerable time delay.

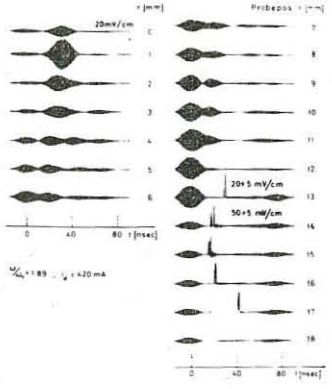

Fig. 2
Pulse records at various probe positions, ω/ω_c = 1.89; ω_{po}^2/ω^2=2.4; different sensitivities

This direction is identical to the direction of the group velocity of the excited Bernstein waves in a steady state experiment, i.e. away from the hybrid layer towards the higher density region. From the dispersion relation we can calculate the group velocity $v_{gr} = \partial\omega/\partial k$ as a function of density. The time delay assuming excitation at the hybrid layer then is:

$$t(r) \approx \int_{r_H}^{r} \frac{1}{v_{gr}(\rho)}\,d\rho$$

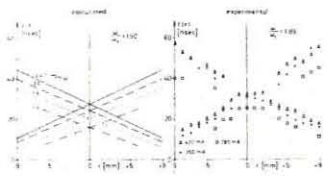

Fig. 3
Comparison between measrued and calculated timedelays

Fig. 3 shows a comparison between measured and calculated time delays. When the two wave pulses travel just once across the plasma column and reach the hybrid layer at the opposite side of the column they couple out to the electromagnetic vacuum field which we again detect at the probe without appreciable time delay. This is the fourth pulse we see in fig. 2. His time delay is just twice the time delay of the pulse at r = 0. With the probe situated outside the dense core, we could detect up to 4 coupled out pulses, which are due to mulitple reflection of the Bernstein wave pulses inside the dense plasma core. One set of measurements is presented in fig.4. We see how with increasing peak plasma density (or discharge current), the time delay of the coupled out pulses increases due to the increasing diameter of the hybrid layer in the column. From the relative amplitudes of successive coupled out pulses we can estimate the coupling coefficient:

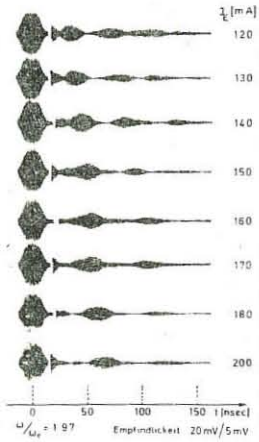

Fig. 4
Records of coupled out pulses for various densities, ω/ω_c=1.97

$$\alpha \approx 1 - 1/\sigma \cdot N_{n+1}/N_n$$

σ represents a damping of the pulse during one transit time from a hybrid layer to the opposite one.

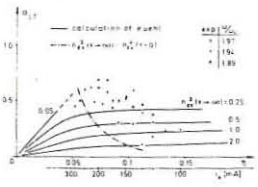

Fig. 5
Comparison between experimental and calculated coupling coefficients.

In fig. 5 the dots show experimental results neglecting damping, i.e. for σ = 1. The heavy lines in fig. 5 correspond to the results of Kuehl [7], who has calculated this coupling coefficient for excitation of the Bernstein waves by an extraordinary wave in an infinite inhomogeneous plasma. Taking Kuehl's parameter n_{ex}^2 ($x \to \infty$) (refractive index of the extraordinary wave for $x \to \infty$) equal to n_{ex}^2 (r = o) in our experiment, we obtain the dashed line in fig. 5, representing the coupling coefficients expected in our experiment. We find agreement within an order of magnitude. Matching our experimental results to this theoretical line would give a reasonable value of o.65 for the neglected damping term σ.

These observatious, together with the results in [6] show that Buchsbaum-Hasegawa-resonances can be well understood in terms of Bernstein waves excited mainly in the vicinity of the hybrid layer.

This work was performed as part of the joint research programme between the Institut für Plasmaphysik and Euratom.

References:

[1] S. J. Buchsbaum, A. Hasegawa: Phys. Rev. Lett. 12, 685, 1964 and Phys. Rev. 143, 303, 1966
[2] I. B. Bernstein: Phys. Rev. 1o9, 1o, 1958
[3] H. J. Schmitt, G. Meltz, P. J. Freyheit: Phys. Rev. 139, A 1432, 1965
S. Tanaka: J. Phys. Soc. Japan 21, 1804, 1966
[4] T. H. Stix: Phys. Rev. Lett. 15, 878, 1965
[5] S. Gruber, G. Bekefi: Phys. Fluids 11, 858, 1968
[6] F. Leuterer: 9th Inf. Conf. Phen. Ionized Gases, Bukarest 1969, paper 4.3.2.9 and IPP Report 3/1o2, 1969
[7] H. H. Kuehl: Phys. Rev.154, 124, 1967

LINEAR STABILITY OF EXPONENTIAL DENSITY PROFILES

by

R. Croci and R. Saison

INSTITUT FÜR PLASMAPHYSIK
8046 Garching bei München, Germany

Abstract: The exact dispersion relation for a plasma with density profiles n(x) exp (-ax) in a homogeneous magnetic field $B=i_z B_o$ is derived. As example, we consider the low-frequency drift instability.

The problem fo the linear stability of a Vlasov plasma whose equilibrium distribution function depends on space coordinates leads to an integro- differential equation for the Laplace transform of the electric potential φ. In general, considering only wavelengths much larger than the mean Larmor radius R. Then, in the further limit where the wavelengths are smaller than the inhomogeneity length, one applies the WKB method. The most severe of these two limitations is, of course, the first one.

In this paper we shall consider exponential density profiles $n(x) \sim \exp(-ax)$. The results have a physical meaning for profiles with $n'/n \sim -a$ over a length L if the considered wavelengths λ_x in the x-direction satisfy $\lambda_x < L$.

Since the density is a monotonic function of x with n'/n =Cte, the electrostatic waves cannot go back and forth in a finite region. Then it can be expected that in the dispersion relation the part of the density profile with $n \to \infty$ will play an important role. In other words, the dispersion relation can be expected to be very similar to that obtained in the approximation of quasi-neutrality. We will show that the exact dispersion relation is in fact the same as in the quasi-neutrality case. It follows that the proposed profile can always be used to get a dispersion relation valid also for $|k_x R| \gg 1$, if the approximation of quasi-neutrality is reasonable.

Let us consider a plasma inhomogeneous in the x-direction, in a magnetic field $\vec{B}=\hat{i}_z B_o$ with B_o= const. We treat the following case of equilibrium distribution functions:

$$f_{oj} = g_j(v_\perp^2, v_\parallel^2) \exp\left[-a\left(x + v_y/\omega_{cj}\right)\right] ; \left(j = e,i ; \omega_{cj} = e_j B_o/m_j\right)$$

where $\lim_{v_\perp \to \infty} (v_\perp^2, v_\parallel^2) \exp(\beta v_\perp) = 0$ for any positive constant β:.

We shall consider electrostatic perturbations, although the treatment could be extended to electromagnetic ones. If the initial perturbation decreases faster than $e^{-a|x|}$ for $|x| \to \infty$, the same will be true for the solution φ (electric potential) at all times t. Then

$$\int dx\, e^{i(K_x + ia)x} \varphi(x) = \varphi(K_x + ia)$$

and the integral equation for φ becomes

$$\left(K_x^2 + K_y^2 + K_z^2\right) \varphi(K_x) = G(\omega, K_x) + C(\omega, K_x + ia)\, \varphi(K_x + ia)$$

where G contains the initial conditions and

$$C(\omega, K_x) \equiv i \sum_{e,i} \frac{4\pi e_j^2}{m_j} \int d^3v \int_0^\infty du\, e^{-i\omega u}\, e^{i\vec{K}\cdot(\vec{r}-\vec{R})}\, e^{-a v_y/\omega_{cj}} \left(\vec{K}\cdot\vec{\nabla}_v \vec{g}_j - \frac{K_y a}{\omega_{cj}} g_j\right)$$

It can be shown that $\varphi(K_x)$ has poles in the complex k_x-plane at $K_x = K_o(\omega) + ina$ $(n = 0,1,2,\ldots)$ where k_o is a solution of

$$C(\omega, K_x ; K_y, K_z) = 0$$

with $\mathrm{Im}(k_x) > 0$ when φ lies in its convergence half-plane, which is the same as in the "quasi-neutral" approximation. The above condition is necessary and sufficient for the singularities.

As an example we give here the stability condition for the low-frequency drift instability for an isotropic Maxwell distribution g(and $T_i = T_e$). In the range $v_{ith} < \left|\frac{\omega}{K_\parallel}\right| \ll v_{eth}$ wich is the most unstable, and in the limit $1 < K_\perp R_i < (m_i/m_e)^{1/2}$ where the local approximation is expected not to be valid, one gets the following results:

$$\lambda_D/\lambda - 1 \simeq -2K_\perp R_i \sqrt{\pi} \quad ; \lambda = \frac{\omega}{K_\parallel v_{ith}} \; , \; \lambda_D = \frac{K_y a R_i^2 \omega_{ci}}{K_\parallel v_{ith}}$$

$$-2a K_x/K_\perp^2 - \left(\pi \frac{m_e}{m_i}\right)^{1/2} \left(\lambda_D + \lambda\right) > 0 \quad \text{for stability}$$

or:

$$|K_x/K_\perp| > \frac{1}{4}\left(\pi \frac{m_e}{m_i}\right)^{1/2} K_\perp R_i \left|K_y/K_\parallel\right|$$

with the restriction $1 < (4\pi)^{-1} \left|\frac{a}{K_\parallel} \frac{K_y}{K_\perp}\right| \ll \left(\frac{m_i}{m_e}\right)^{1/2}$

One sees clearly the stabilizing effect of k_x.

In the limit $|K_\perp R_i| < 1$, one obtains the known results (exept for corrections of the order of $|a/K_x|$) of the local approximation.

Acknowledgements:

We wish to thank Dr. D. Pfirsch for useful discussions.

* This work was performed under the terms of the agreement on association between the Institut für Plasmaphysik and Euratom.

CHANGE IN THE POLARIZATION OF AN E.M. WAVE IN A SHEARED MAGNETIC FIELD

R.Cano - C.Etievant - I.Fidone - B.Zanfagna

ASSOCIATION EURATOM-CEA
Departement de la Physique du Plasma et de la Fusion Contrôlée
Centre d'Etudes Nucléaires
Boite Postale n° 6 - **92 Fontenay-aux-Roses** (France)

Abstract : We describe an experiment showing that an extraordinary electromagnetic wave propagating across a plasma column confined by a slightly sheared magnetic field is partially converted into an ordinary mode at the upper hybrid resonance.

A 8,85 GHz microwave beam of few hundred mW power was propagated in the extraordinary mode into a low density ($n = 8.10^{10}$ cm^{-3}) Argon plasma produced by a Radio Frequency discharge. The beam was focussed in the center of the discharge by a system of teflon lenses.

The slightly sheared magnetic field was produced by superposing to the main magnetic field (Z direction), a small component in the x direction, obtained by two coils placed in the vacuum chamber close to the plasma discharge.

In fig.1 we show the measured components B_z and B_x along the direction of propagation of the incident wave (y axis). The asymmetric configuration for the main field was chosen so as to have a good accessibility to the upper hybrid resonance.

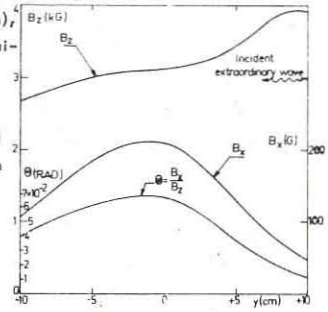

-Fig.1 - Variation of the magnetic field components along the direction of propagation.

In fig.2 we show (a) the transmitted power of the extraordinary mode and (b) the detected power of the ordinary mode when we vary B_z. In fig.3 we plot the power of the ordinary mode as a function of B_x for the value of B_z corresponding to the maximum value of the amplitude of the ordinary wave.

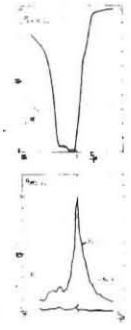

Fig.2 Received power of the extraordinary mode(a) and of the ordinary mode (b) Vs $\frac{Fco}{F}$ .Fco is the cyclotron frequency at the center.F=8,85Ghz $p_o = 10^{-3}$ torr $\bar{n}_e = 8.10^{10}$ cm^{-3}.

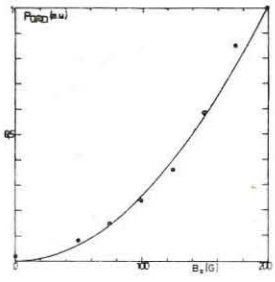

Fig.3 Measured power of the ordinary mode Vs. B_x.

We note that this maximum is very close to the minimum transmission of the extraordinary incident wave and the power of the ordinary mode is proportional to the square of B_x.

A tentative explanation of these experimental results may be found in the coupling of the principal modes at the upper hybrid resonance in a slightly rotating magnetic field [1]. At the condition of total extinction of the incident wave the amplitude of the ordinary electric field is given by :

$$(1)\quad \frac{|E_{ORD}|}{|E_{EXTR}|} = \Theta(y_o)\,\frac{\omega_c^2\,\omega_p^2}{\omega^3\sqrt{\omega_+^2-\omega^2}}\sqrt{\pi\,\frac{\omega}{c}\,a_o} = A(y_o)\,\Theta(y_o)$$

where

$\Theta = \frac{B_x}{B_z}$

ω = incident frequency

ω_c = electron cyclotron frequency

ω_p = plasma frequency

ω_+ = cut off frequency

$a_o = \dfrac{\omega_H^2(y_o)}{\left(\frac{d\omega^2 H}{dy}\right)_{y_o}}$ and ω_H = upper hybrid frequency.

E_{extr} = amplitude of the extraordinary incident wave.

In fig.4 we show, for a typical experimental condition, F_p^2, F_c^2, F_H^2 and F_+^2. We measured the density profile by Langmuir probe and the average density by phase shift of an ordinary wave.

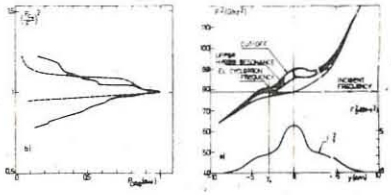

Fig.4

(a) variation of F_p^2, F_c^2, F_H^2, F_+^2 along the direction of propagation.

(b) Plot of the power of the ordinary mode Vs. $\left(\frac{Fco}{F}\right)^2$. Measured (solid line) and calculated (dashed line).

We also show the calculated (from eq.(1)) and the measured power of the ordinary wave Vs F_{co}^2/F^2 normalized to the maximum value.

By inspection of eq.(1) we note that the value of A (y_o) depends on the gradient of F_H^2 at $y = y_o$ and consequently for the case described in fig.4 the position of the maximum is shifted from the discharge center. The experimental width is larger than the calculated one and can be explained by radial inhomogeneity of the B_x field. Absolute measurement of the factor A gives for the conditions corresponding to the maximum, $(A\,\Theta)_{exp} = 0,20$, as compared to the calculated value from eq.(1) with the experimental density profile, $(A\,\Theta)_{calc.} = 0,22$. Experimental errors and the approximations involved in eq.(1) render the agreement rather illusory. Refinements in experiment and theory are required in order to have definitive confirmation.

Finally, this technique can be used to determine the local poloidal magnetic field in a toroidal Tokamak device.

Reference

[1] C.ETIEVANT - I.FIDONE -
"A proposal for measuring the poloidal field in a toroidal magnetic configuration".
Internal Report EUR-CEA FC 537 (1970).

AMPLITUDE AND DAMPING OF PLASMA WAVE ECHOES

by

M. Guillemot, G. Matthieussent*, J. Olivain, F. Perceval and A. Quémeneur

ASSOCIATION EURATOM-CEA
Département de la Physique du Plasma et de la Fusion Contrôlée
Centre d'Etudes Nucléaires
Boite Postale n° 6 - **92 Fontenay-aux-Roses** (France)

* Labo de Physique des Plasmas - Faculté des Sciences 91/ORSAY (France)

Abstract : A theory taking into account diffusion in velocity space shows that a spatial plasma echo exihibits new features when either the second wave amplitude or the distance between the transmitters are increased. Good agreement is found between this theory and experiment.

Plasma wave echoes have been predicted [1] and observed [2]. A more recent theory [3], taking into account the fact that the electron free trajectory is only slightly perturbed by the electric field, shows that the echo amplitude depends in a non symetric way on the amplitude of the two initial waves. However this theory does not take into account diffusion in velocity space [4]. If Φ_1 , Φ_2 and ω_1 , ω_2 are respectively the applied potentials and frequencies of the waves excited by the two transmitters separated by ℓ , then echoes appear at frequencies : $f_3 = n f_2 - f_1$. The amplitude of these echoes is given by :

$$E_{\omega_3}(z) = \frac{e}{2\epsilon_0 \omega_3} \int_0^\infty d\upsilon \, \frac{U_{-\omega_1}(\upsilon)}{\varepsilon(\frac{\omega_3}{\upsilon}, \omega_3)} \upsilon \frac{\partial f^{(0)}}{\partial \upsilon} J_n \left[\frac{\omega_1 \ell U_{\omega_2}(\upsilon)}{\upsilon^2} \right] \exp \left[j \left(\frac{n\omega_2 \ell - \omega_3 z}{\upsilon} + \varphi_{\omega_2} - \varphi_{\omega_1} \right) - K \right]$$

K is defined in ref [6].

If a resonant echo is considered (n = 2), $f_2 = f_1$, one obtains :

$$E_{\omega_3 max} \sim \Phi_1 J_2 \left[\beta \ell \Phi_2 \right] \exp - \left[D_2 (\frac{\omega_1}{k}) \frac{2}{3} \frac{\ell^3 k^5}{\omega_1^5} \right] \qquad (1)$$

β is calculated from plasma characteristics.

The machine used for the experiment is described in a previous paper [5]. The Landau damped waves are launched and the echo detected by probes. Fig.1 and 2 show the dependence of the peak echo amplitude E_{max} as a function of the two primary waves amplitudes for a quasi-resonant echo : for convenience sake the frequencies in experiment are chosen slightly different. At large amplitude of the second wave the peak echo amplitude reaches a maximum at $\Phi_{2\,max}$ and then decreases. As predicted by Eq (1) the maximum amplitude of the peak echo $\hat{E}_{max}$ is observed when : $\Phi_{2\,max}\, \ell = cst$. Fig.3 checks this result. Theory predicts that the maximum amplitude of the peak echo $\hat{E}_{max}$ decreases as $\exp - \frac{\ell^3}{\ell_0^3}$ (Fig.4). The experimental dependance of the peak echo amplitude as a function of the amplitude of the primary waves and transmitter separation length, is in agreement with theory.

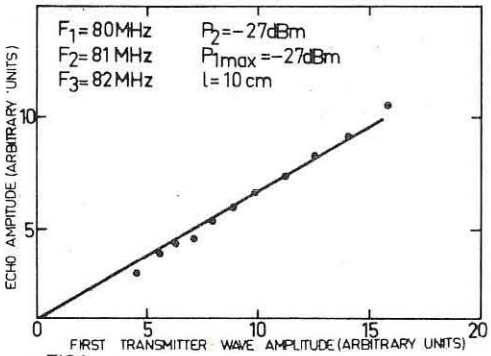

-FIG.1- QUASI-RESONANT ECHO AMPLITUDE VERSUS FIRST TRANSMITTER AMPLITUDE

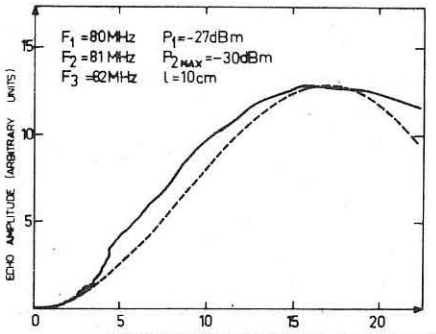

-FIG.2- QUASI-RESONANT ECHO AMPLITUDE VERSUS SECOND TRANSMITTER AMPLITUDE DOTTED CURVE IS THEORY

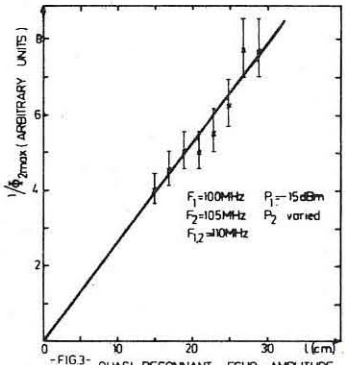

-FIG.3- QUASI-RESONNANT ECHO-AMPLITUDE Φ_{2max} VERSUS EMITTER SEPARATION FOR MAXIMUM PEAK ECHO AMPLITUDE

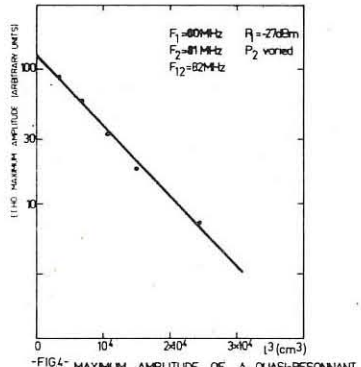

-FIG.4- MAXIMUM AMPLITUDE OF A QUASI-RESONNANT ECHO VERSUS l^3 (l is the distance between the two transmitters)

References

1. T.M. O'Neil, R.W. Gould, Phys. Fluids 11 , 134 (1968)

2. J.H. Malmberg, C.B. Wharton, R.W. Gould and T.M. O'Neil, Phys. Fluids 11, 1147 (1968)
M. Guillemot, P. Leprince, G. Matthieussent, J. Olivain et F. Perceval C.R. Acad. Sci. Paris 270 B, 317 (1970)

3. J. Coste, J. Peyraud, Journal of Plasma Physics 3 603 (1969)

4. T.M. O'Neil - Physic. Fluids 11 , 2420 (1968)

5. M. Perulli, Thèse, Rapport EUR-CEA n° R 3639 (1968)

6. T.H. Jensen, J.H. Malmberg, T.M. O'Neil
Phys. Fluids 12 , 1728 (1969).

TEMPORAL LANDAU DAMPING OF ION WAVES IN ARGON PLASMA

by

Nguyen T.Dzoanh and Robert S.Rohde *

Department of Electrical Engineering,University of Notre Dame

Notre Dame,Indiana 46556,U.S.A.

Abstract

Temporal Landau damping of ion plasma waves have been investigated experimentally by using standing waves which can be either self excited or externally excited by an electric pulse.The experimental results agree very well with the theory of Fried and Gould.That is,in a collisionless argon plasma,waves may decay exponentially by resonnant absorption.The decay rate in time depends closely on the ratio of electron and ion temperature T_e/T_i ,as predicted by the theory.

The damping by resonnant absorption of electrostatic waves in a collisionless plasma predicted by Landau in 1946 has been verified experimentally by Malmberg and Wharton [1] and other authors [2,3,4] For the case of longitudinal electron waves in space evolution.Spatial Landau damping of ion waves has also been observed by Wong,Motley and D'Angelo[5] in highly ionized cesium plasmas and later by Alexeff ,Jones and Montgomery [6]in zenon plasma. However,the temporal Landau damping has not been directly observed. Fried and Gould [7] have shown that ion oscillations could be damped in a collisionless plasma if the electron temperature approached that of the ions. In this paper the experimental results on temporal Landau damping of ion oscillations in collisionless plasma will be discussed. It shows a perfect agreement with the theory of Fried and Gould.

* Graduate fellow from I.I.T. Chicago

To observe the temporal damping,standing ion waves have been used instead of travelling a waves as in the case of spatial damping. Also argon gas has been chosen because of its relatively heavy mass. In this way the time change of ion waves is rather slow and therefore, more accessible to detection. The experimental set up is shown in fig.1. The argon plasma generated in a duoplasmatron is guided into a large drift tube by the combined action of an electric field E and a magnetic field B at the orifice of the duoplasmatron. The plasma terminates on a positively biased grid which reflects ions and absorbs electrons. The electromagnet is capable of producing a uniform field up to 3 kilogauss over a distance of 3 feet with a ripple of 0.1%. The boundary conditions are such that standing ion waves can be easily either self excited or externally excited by applying an electric pulse to the duoplasmatron. The background pressure is about 10^{-6} Torr and the density of the plasma is 10^{7} part./per cc. In this range the plasma cen be condidered as collisionless in the sense of theory. The sampling techniques together with the pulse time delay have been used to extract the signal from the noisy plasma. The experimental results are shown in fig.2. As we can see,it shows a very good agreement with the theory of Fried and Gould within the experimental error.Note that the experimental points have been normalized to the case of equal electron and ion temperatures $T_e = T_i$. For T_e/T_i smaller than 4.32,no experimental points could be recorded since the waves were heavily damped. This observation is also in agreement with the theory. Other interesting results related to this work will be presented and discussed at the conference.

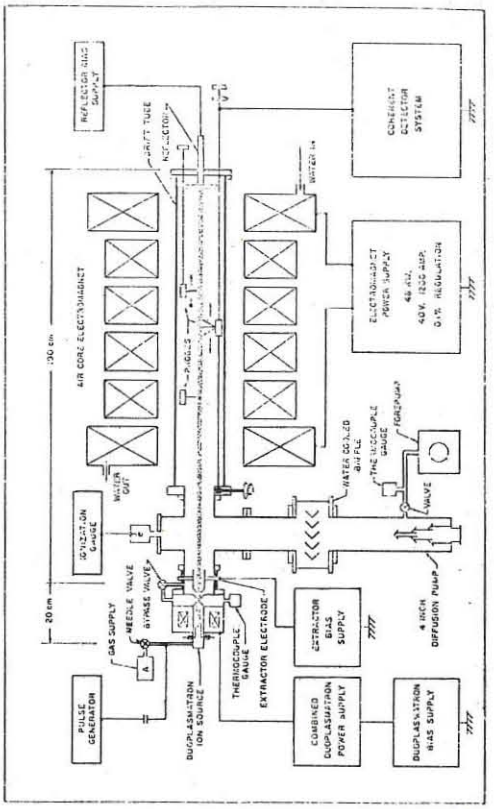

FIGURE 1. APPARATUS FOR LANDAU DAMPING AND PLASMA WAVE ECHO EXPERIMENTS

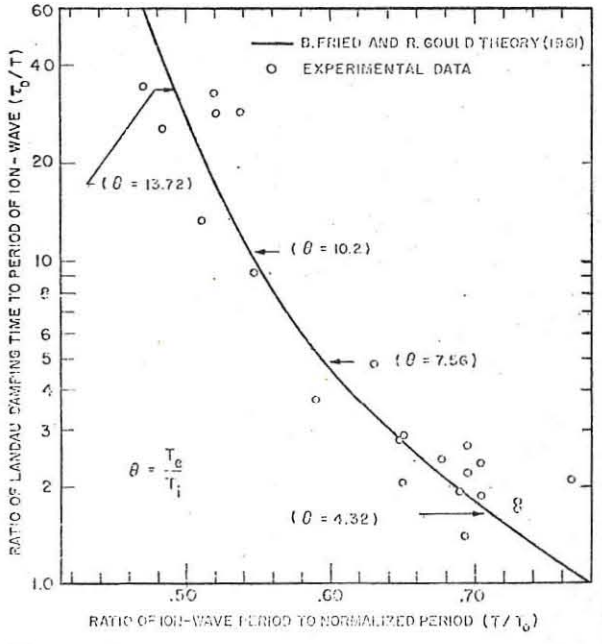

Figure 2 Dependence of the Landau damping time per period on the oscillation period of the waves. The abscissa is normalized to a constant period $T_o = 27\mu s$ which corresponds to the case of $\theta = 1$.

References

1-Malmberg and Wharton Phys.Rev.Lett. 13,184,(1964)
2-Malmberg et al. Plasma Phys. and Contr.Fusion Vol.1,485 (1966)
3-Van Hoven Phys.Rev.Lett. 17,169,(1966)
4-Derfler and Simonen Phys.Rev.Lett. 17,172,(1966)
5-Wong et al,Phys.Rev. 133,A436,(1964) 6-Alexeff et al.Phys.Fluid.11,167, (1968). 7-Fried and Gould Phys. Fluids 4,139,(1961)

TEMPORAL ION WAVE ECHOES IN A COLLISIONLESS ARGON PLASMA

by

Nguyen T.Dzoanh and Robert S.Rohde *

Department of Electrical Engineering,University of Notre Dame

Notre Dame,Indiana 46556,U.S.A.

Abstract

Recent experiments at the University of Notre Dame to verify the theory of Gould and O'Neil on the temporal evolution of plasma wave echoes are reported. The experimental results agree well with the theory.Two standing ion waves are excited separately in time and decay exponentially by the Landau process. A third wave called echo spontaneously appears at a time predicted by the theory.The relationshipsbetween the amplitudes of three waves are also satisfactorily checked.

A new phenomenon directly associated to the Landau damping of plasma waves,called echo, was recently predicted by Gould and O'Neil [1] .This phenomenon arises from the non linear nature of the plasma.This effect is universal and similar to other phenomena such as the spin echo[2] ,cyclotron resonance echo [3] and photon echoes [4]. In all the echo phenomena , macroscopic quantities such as the electric field and charge density are damped by the phase mixing of microscopic elements. This phase evolution can be reversed to yield a non linear macroscopic effect in the absence of collisions. The existence of spatial wave echoes has been confirmed experimentally by Malmberg et al. [5] for electron waves and by Ikezi et al. [6] and Wong et al.[7] for ion waves.The temporal evolution of plasma wave echoes have not been experimentally confirmed.It is the purpose of this paper to report recent results of the experiments done at Notre Dame,to verify the theory of Gould and O'Neil on temporal plasma echoes.

* graduate fellow from I.I.T. Chicago,Illinois

The experimental set up is very similar to that used in the temporal Landau damping experiment described in another paper of this conference.That is the plasma generated by a duoplasmatron is guided into a drift tube by a combined action of the electric and magnetic fields at the orifice of the duoplasmatron,and is confined along the axis by a longitudinal magnetic field. The plasma terminates on a positive biased grid which reflects ions and absorbs electrons.The background pressure is 10^{-6} Torr and the plasma density is 10^{7}part/cc. To produce in a short time,the cosine distribution in space of the electric field called for by the theory,we have made use of standing ion waves excited by applying square wave pulses to the duoplasmatron.Te standing waves are thus created over the entire plasma column. They were found to be damped in time and their frequency and damping time could be varied easily by changing the characteristics of the plasma. Once the boundary conditions and the characteristics of the plasma are determined the frequency of the standing waves is well defined and is independent of the excitation source.In this condition two standing waves launched separately in time shoudl have the same frequency ($f_1 = f_2$) or the same wave number ($k_1 = k_2$) since the phase velocity is the same. The echo,if it exists, would also have the same frequency and the same wave number as the previous waves. Thus on the light of the theory of Gould and O'Neil,only the 3rd order echo could be created. That is $k_1 = k_2 = k_3$ and m= 1 , n= 2 where the sum m+n is the echo order. The time t^* for the echo to appear is exactly twice the time from the launching of the first wave to that of the second wave. ($t^* = 2t$). The experimental results are shown in fig.1 and fig.2.They show good agreement with the theory.Other data will be shown at the conference.

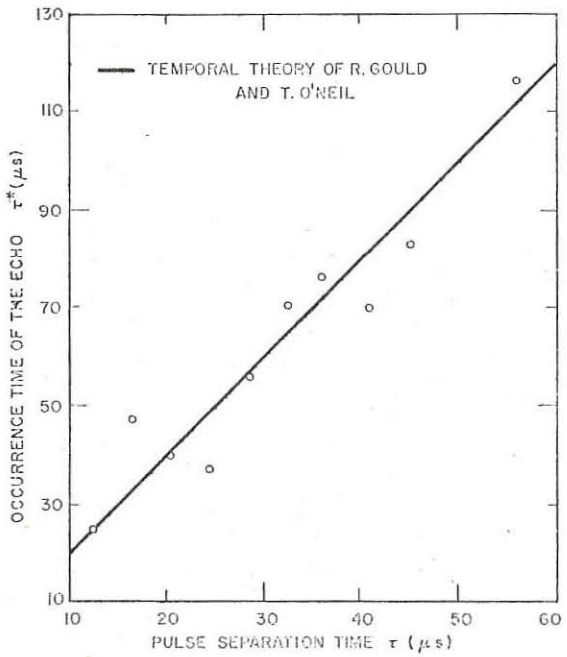

Figure 1 Occurrence time τ^* of the third order echoes versus the separation time τ between the two excitation pulses.

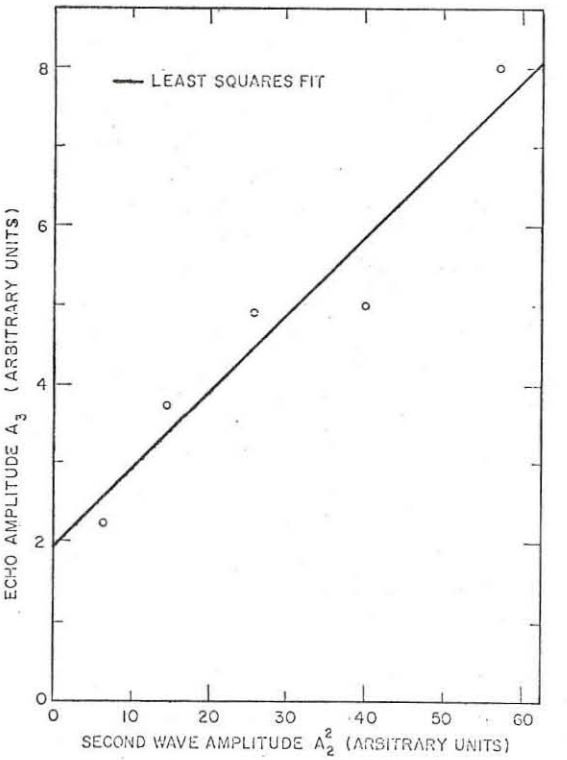

Figure 2 Echo amplitude A_3 versus the square of the amplitude A_2^2 of the second wave. The amplitude of the first wave A_1 is held constant. Third order echo theory predicts $A_3 \propto A_1 A_2^2$.

References

1-O'Neil and Gould Phys.Fluids 11,134,(1968) 2- E.I.Hahn Phys.Rev.80,580 (1950) 3- R.M.Hill and D.E.Kaplan Phys.Rev.Lett.14,1062,(1965) .4-I.D.Abella et al.Phys.Rev.141,391,(1966) 5-J.H.Malmberg et al. Phys.Fluids 11,1147,(1968) 6-H.Ekezi and Takahashi Phys.Rev.lett.20,140,(1968) 7-A.Y.Wong et al. Phys. Rev.lett.20,318,(1968)

NONLINEAR ECHO PHENOMENA IN PLASMA

A.G.Sitenko

Institute for Theoretical Physics,

Academy of Sciences of the Ukrainian SSR, Kiev, USSR.

Abstract: High-frequency and low-frequency echo oscillations appearing in plasma under the external perturbations are studied, those due to the oscillation transformation being analysed in detail.

As it is known oscillations of the macroscopic quantities in plasma exponentially decrease in time even in the absence of collisions whereas the distribution function deviations from the equilibrium value may experience undamped oscillations. The existence of the distribution function undamped oscillation is due to the fact that in plasma, without binary collisions, the equilibrium cannot be set under the effect of the self-consistent field only, since the latter does not change the enthropy of the system. In plasma these distribution function undamped oscillations may lead to the echo effects. The onset time and the shape of the echo oscillations in the collisionless plasma are determined by the delay time of external perturbations, by the nature of perturbations and the character of the arising echo oscillations.

While considering the echo phenomena in plasma we start from the nonlinear kinetic equation for the electron distribution function and the equation for the self-consistent electric field. The kinetic equation should be supplemented by the values of the distribution function perturbations for the moment $t = 0$ and for $t = \tau$ (jump of the distribution function). We choose the distribution function perturbations in the form of plane waves and the amplitudes of the initial and repeated perturbations in the form $g_1(v)$ and $g_2(v)$. Assuming the external perturbations to be small, one may apply the method of iterrative approximations.

With such perturbations that $g_i(v)$ are integral functions v (v is the velocity component parallel to the wave vector), the damping electric field oscillations with frequencies equal to plasma eigenfrequencies arise in plasma. The distribution function perturbations being nonintegral functions, singularities of the function

$$G_i(k,p) \equiv \int dv \frac{g_i(v)}{p + ikv} \qquad (I)$$

are added to those of the field amplitude $\vec{E}_{\vec{k}p}$, which are defined by roots of the dispersion equation. Location of these singularities depends on the form of the functions $g_i(v)$, i.e. on the nature of perturbations; it is not affected by the properties of plasma. Thus, in the general case, the field asymptotics may contain the oscillations with complex frequencies determined by the character of the external perturbation, apart from the eigenfrequencies of specific plasma oscillations. Taking into account the nonlinear (with respect to external perturbation) term in the kinetic equation, one obtains the following expression for the field amplitude in the second approximation

$$\vec{E}(\vec{r},t) = \frac{128\pi^5 e^3 (t-\tau)}{m k^2 k_2^2} (\vec{k}\vec{k}_2)\vec{k} \, e^{i\vec{k}\vec{r}} \int d\vec{v} \frac{G_2(k_2, -i\vec{k}_2\vec{v})}{\varepsilon(k,\vec{k}\vec{v})\varepsilon(k_2,\vec{k}_2\vec{v})} \left[g_1(\vec{v}) - \frac{4\pi e^2 \vec{k}_1 \frac{\partial f_0}{\partial \vec{v}}}{m k_1^2 \varepsilon(k_1,\vec{k}_1\vec{v})} G_1(k_1, -i\vec{k}_1\vec{v}) \right] e^{-i\vec{k}\vec{v}(t-\tau')}, \qquad (2)$$

$$\tau' = \frac{\vec{k}_2\vec{v}}{\vec{k}\vec{v}}\tau .$$

The wave vector of the quadratic signal is determined by the sum of the wave vectors of the succesive perturbations. For $t = \tau'$, the exponential factor in the integral turns to a unit and the field magnitude takes maximum value. If, however, t differs from τ', the fast oscillations of this factor result in zero value of the field since the integral over the velocities in (2) vanishes. Thus, inequality $\tau' > \tau$ governs the domain of the appearance of the echo. With the wave vector $\vec{k}_1$ parallel to $\vec{k}_2$, i.e. $\tau' < \tau$, the echo becomes impossible. The immediate calculation shows that for the echo to be possible the angle between the vectors $\vec{k}_1$ and $\vec{k}_2$ should differ from π by the value not greater than the angle $(ks\tau)^{-1}$, where s is the heat velocity of electron in plasma and $k_2 > k_1$.

The formula (2) completely defines the echo oscillations field. According to (2), in plasma there are echo phenomena associated both with the plasma specific oscillations and with the oscillations whose dispersion is determined by the character of the distribution function external perturbations. Using (2), one can study the high-frequency and low-frequency echo oscillations appearing in plasma under the influence of external charges, and the echo phenomena due to the transformation of plasma waves. As an example, we present an expression for the echo oscillation field in plasma where the perturbations are excited by external charges and all the three oscillations correspond to Langmuir frequencies [1,2]:

$$\vec{E}(\vec{r},t) = \vec{E}_0 \sin\varphi \, e^{i(\vec{k}\vec{r} - \gamma|t-\tau'|)} \cos[\Omega(t-\tau') + \varphi], \quad \vec{E}_0 = -\frac{32\pi^2 i}{3} \frac{e f_1 f_2 \Omega \tau}{m\omega_e^2 k^2} \vec{k} \qquad (3)$$

The field of the Langmuir echo oscillations, which arise because of the superposition of sound oscillations and those of Langmuir, is given by

$$\vec{E}(\vec{r},t) = \vec{E}_0 e^{i\vec{k}\vec{r}} \begin{cases} -\frac{3}{4} \frac{\alpha^4 k^6 v_s^2}{\Omega \gamma_s} e^{-\gamma_s(\tau'-t)} \cos[kv_s(t-\tau')], & t < \tau' \\ \sin\varphi \, e^{-\gamma(t-\tau')} \cos[\Omega(t-\tau') + \varphi], & t > \tau' \end{cases} \qquad (4)$$

In nonequilibrium plasma penetrated by the beam of charged particles and exposed to high damping short-wave perturbations, slowly decreasing or even increasing long-wave echo oscillations may appear.

Likewise, one may consider the echo oscillations which arise in plasma due to the superposition of the three succesive perturbations separated by the time intervals that are large in comparison with the characteristic time of the oscillation damping [3]. If the wave vectors of the succesive perturbations $\vec{k}_1$, $\vec{k}_2$ and $\vec{k}_3$ are not antiparallel in pairs, the echo effects are absent as a result of the superposition of some two perturbations. Yet, the echo phenomena turn out to be possible in consequence of three subsequent perturbations. In this case, the complanarity of wave vectors becomes the requirement which determines the possibility of the echo effectr. Then, the echo oscillation electrical field contains the longitudinal component as well as the transverse one. The onset time and the shape of the echo signals appear essentially sensitive to the delay times between the succesive perturbations.

The study of the echo phenomena in plasma seems rather interesting in connection with potential application of the echo effects for plasma diagnostics, for the investigation of plasma processes and for practical purposes in electronics and radiophysics.

References

1. R.Gould, T.O'Neil, J.Malmberg, Phys.Rev.Lett. 19, 219, 1967.

2. A.Sitenko, Nguen Van Chong, V.Pavlenko, Preprint ITF-69-68, Kiev, 1969.

3. A.Sitenko, Nguen Van Chong, V.Pavlenko, JETP 58, 1377, 1970.

Electrostatic waves for periodic inhomogeneous "Water Bag" and "Two streams" models

by

P. BERTRAND - G. BAUMANN - M.R. FEIX

Groupe de Physique théorique et Plasma

Université de Nancy - 54 - NANCY FRANCE

Abstract : In periodic inhomogeneous plasma the concept of dispersion relation $\omega(k)$ can be generalised into a relation $\omega(k, K)$ where K is the wavenumber of the periodic steady state. The solution in the two described models is easily obtained by introduction of a Lagrangian model. Results are presented and it is shown that in the two streams case while the long wavelength have a smaller growth rate an increased instability is found for $k/K = 1/2$.

I - Introduction : For one dimensionnal problem the "Water Bag" model has been extensively used in analytical and numerical work [1 - 3]. In this paper we deal with the problems of the longitudinal electrostatic oscillations in an inhomogeneous media. First we study a periodic Water Bag (W.B.) and we compute the new dispersion relation. Secondly the case of two cold electron streams is with a periodic modulation of density and velocity is studied and the growth rate are computed for different parameters of inhomogeneity.

II - Lagrangian formulation of the problem

For the two above mentionned problem, the dynamic is simply described :

- by the evolution of the two boundaries of the contour for the "Water Bag" i.e of the two streams with maximum energy.
- by the hydrodynamic equations of the two streams in the second problem. In both cases we note V_+ and V_- the velocities of the two streams. We have :

(1) $$\frac{\partial V_\pm}{\partial t} + V_\pm \frac{\partial V_\pm}{\partial x} = \frac{e}{m} E$$

(1) must be supplemented with the Poisson equation $\frac{\partial E}{\partial x} = 4\pi e \left[N(x) - N_i(x)\right]$

$N(x)$ and $N_i(x)$ being respectively the electron and ion densities. The ions provide a fixed neutralising background, homogeneous in the T.S. problem and inhomogeneous in the W.B. case. Now $N(x)$ is given by (2) $N(x) = A(V_+ - V_-)$ (W.B.)

(3) (T.S.) $N(x) = N_+ + N_-$ $\quad \frac{\partial N_\pm}{\partial t} + \frac{\partial}{\partial x}(N_\pm V_\pm) = 0$

The linearisation is performed around an inhomogeneous steady state characterised by $V_\pm = \pm W(x)$ and the electric field $E_0(x)$. Consequently (4) $V_\pm(x,t) = \pm W(x) + v_\pm(x,t)$

$$E(x, t) = E_0(x) + \mathcal{E}(x, t)$$

We introduce $\omega_p^2(x)$ the local plasma frequency and instead of x we consider the new Lagrangian variable θ with $d\theta = dx / W(x)$. The W.B. and T.S. equations take respectively simple form (5) and (6)

(5) $$-\frac{\partial^2 \mathcal{E}}{\partial t^2} + \frac{\partial^2 \mathcal{E}}{\partial \theta^2} = \omega_p^2(\theta)\,\mathcal{E}$$

(6) $$\left(\frac{d}{d\theta} \pm i\omega\right) W^2 \left(\frac{d}{d\theta} \pm i\omega\right)\mathcal{E} \pm (\cdot\theta) + \frac{4\pi e J}{m} W (\mathcal{E}_+ + \mathcal{E}_-) = 0$$

$\mathcal{E}_+$ and $\mathcal{E}_-$ being respectively the electric fields associated to the two streams and J the magnitude of the current carried by each stream (at equilibrium)

III - Solution : To solve (5) and (6) we use the Bloch Floquet transformation and seek solutions of the form

(7) $$\mathcal{E} = \sum_{n=-\infty}^{+\infty} \mathcal{E}_n \exp i\,(k_0 + nK)\,x$$

where K is the wavenumber of the steady state periodic solution. The interesting point in the study of periodic plasma is that we describe the situation by a wave of arbitrary wavenumber k_0. For a homogeneous plasma the eigenfrequencies are $\Omega(k_0 + nK)$ where Ω is the solution of the dispersion relation. In the Bloch Floquet expansion $\Omega(k_0 + nK)$ appear as the elements of a diagonalised matrix. The fact that the inhomogeneity is periodic allows a coupling between the different wavenumbers and introduces a shift in the eigenfrequencies For small inhomogeneity characterised by a parameter ϵ the diagonals next to the main diagonal of the eigenfrequency matrix are of order ϵ and we can expand the eigenfrequency shift in successive power of ϵ taking 3x3, 4x4 etc... determinants : Consequently the first terms of this expansion can be obtained analytically. Stronger inhomogeneity requires numerical calculations.

IV - Results : We present only the T.S. problem results. Knorr [4] has treated a somewhat related problem of counterstreaming ions and electrons. Rowlands [5] study this problem but treats only the small wavenumber case.

The steady state is described by $W(\theta) = a(1 + \epsilon \cos \omega_p \theta)$ and $N_\pm(\theta) = J / e W(\theta)$ where ω_p is the plasma frequency corresponding to the average value of the electron density. The wavenumber K of the steady state solution must be taken equal to ω_p / a and is independant of ϵ. It can be shown that K is exactly the maximum wavenumber of instability for the homogeneous ($\epsilon = 0$) case.

On Fig. 1 we show for $\epsilon = 0$ (the homogeneous case) and $\epsilon = .12$, the square of the growth rate normalised to ω_p^2 as a function of the ratio $k_0/K = k_0 a/\omega_p$. The apparition of a discontinuity at $k_0/K = 1/2$ is connected with a resonance coupling between 3 waves of respective wavenumbers $k_1 = k_0 = K/2$ $k_2 = K$ and $k_3 = -k_0 = -K/2$. The second wave is the stationnary inhomogeneity with a frequency equal to zero. The first and the third have a growth rate equal to $\gamma_0(K/2)$ (γ_0 being the growth rate for the homogeneous plasma. The 3 waves fulfill the Manley Rowe relation. For ϵ small enough the discontinuity is given by $\gamma^2(K/2) = \gamma_0^2(K/2) \pm \omega_p^2 \epsilon/4$ and for $\epsilon = .12$ the agreement with the numerical results is excellent. Fig. 2 gives a comparison between our results and those of ROWLANDS. While ours are obtained through a wave wave interaction formalism (with more waves needed for greater inhomogeneity), Rowlands makes no supposition on ϵ but study only the case $k_0 \longrightarrow 0$ For $k_0/K = .02$ and .04 the agreement is indeed excellent. The third curve shows the influence of finite wavelength on Rowlands theory.

BIBLIOGRAPHY

[1] K.V. ROBERTS and H.L. BERK - Symposium on Computer simulation of plasma and many body problem. NASA SP 153 1967

[2] Nonlinear effects in Plasma G. KALMAN M.R. FEIX Ed. Gordon and Breach 1969

[3] P. BERTRAND M.R. FEIX. Physics Letters 28A 68 1968
P. BERTRAND - G. BAUMANN M.R. FEIX Physics Letters 29A 489 69

[4] G. KNORR - The Physics of fluids 11 885 1968

[5] G. ROWLANDS - Journal of Plasma Physics 3 567 1969

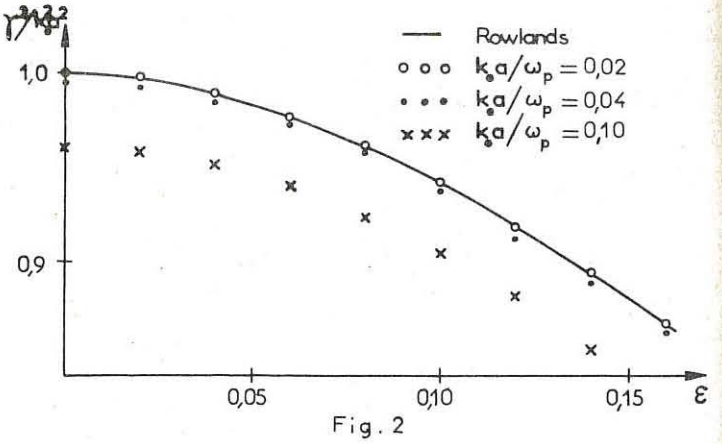

Fig. 2

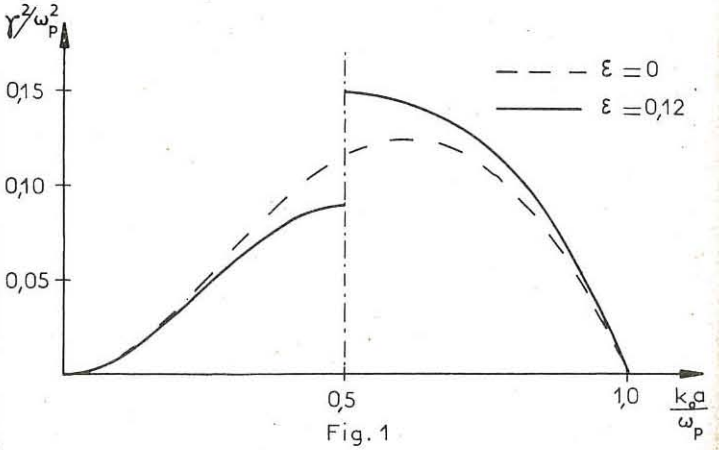

Fig. 1

TRAPS FOR THE FAST MAGNETOACOUSTIC WAVES IN THE TRAPS FOR PLASMA.

by

R.V.Deutsch, I.Grosu and D.Zoler

Politehnical Institute, Calea 23 August, Nr.11, Iaşi, Romania.

Abstract. It is shown that in the magnetic traps for plasma, used in the experiments for the termonuclear reactions achievement, exist ring-like traps, having as symmetry axis the axis of the trap, in which the magnetoacoustic waves can be concentrated. It is studied the structure and the fundamental properties of these domains for four particular models.

The methods of the geometrical optics can be applied to the study of the fast magnetoacoustic waves, when the plasma is dense enough in order that the magnetohydrodynamics methods may be used–the sizes of plasma being much larger than the wavelength, and the Alfvén velocity much greater than the sound velocity. By applying this method it results that a plasma column traversed by electric current, is at same time a wave guide for the fast magnetoacoustic waves/1/. Consequantly, in the plasma column from the toroidal systems(Zeta, Tokamak) the fast magnetoacoustic waves, whose wavelength is smaller than width of the plasma columns, are also expected to be guided by the column. In the systems with elicoidal symmetry(stellarator) for the ortogonality condition is not fulfilled, a permanent transformation of the three magnetohydrodynamic waves, which appear in the homogeneous plasma, is expected to take place, fact which can lead to the destruction of the magnetic surfaces /2/. The fast magnetoacoustic waves can propagate independent from other magnetohydrodynamic waves, into the magnetic traps, which present an axial symmetry, and into the multipolar fields as well. The study of the perturbations propagation, through the geometrical optics method, as far as the fast magnetoacoustic waves are concerned, is reduced to solving the Hamilton-Jacobi equation which in the case of the axial symmetry systems, can be written as it follows /1-3/:

$$\left(\frac{\partial S}{\partial r}\right)^2+\frac{1}{r^2}\left(\frac{\partial S}{\partial z}\right)^2+\frac{1}{r^2}\left(\frac{\partial S}{\partial \varphi}\right)^2=\left(\frac{1}{U}\right)^2 \qquad (1)$$

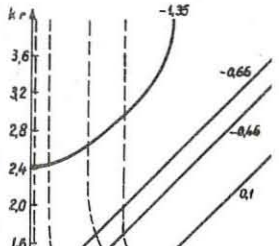

Fig.1

Because in the case of the magnetic traps with axial symmetry U=U(r,z), the coordinate φ is cyclic and from (1) results:

$$\frac{U}{r}=\alpha\frac{rd\varphi}{ds} \qquad (2)$$

ds being the length element measured along the ray, and α is constant for a ray. Having the inequality $rd\varphi \leq ds$, it results that the rays can be only in domains where:

$$\frac{U}{r}<\alpha \qquad (3)$$

On Fig.1-4 we represented graphically the surfaces $\frac{U}{r}$ =const, on which the reflexion of the rays with different values of the parameter α is produced, we limitted to only four field models when $rot\vec{B}=0$. On the Fig.1 we represented the surfaces:

$$\log\frac{J_o^2(kr)ch^2(kz)+J_1^2(kr)sh^2(kz)}{k^2r^2}=C \qquad (4)$$

corresponding to the traps characterized by:

$$B_r=B_oJ_1(kr)ch(kz) \text{ and } B_z=-B_oJ_o(kr)sh(kz) \qquad (5)$$

On the Fig.2 surfaces:

$$\log\frac{I_o^2(kr)\cos^2(kz)+I_1^2(kr)\sin^2(kz)}{k^2r^2}=C \qquad (6)$$

are represented (corresponding) to the traps with

$$B_r=B_oI_1(kr)\cos(kz) \text{ and } B_z=B_oI_o(kr)\sin(kz) \qquad (7)$$

On these figures we also indicated the field lines of the magnetic field. On Fig.3 and 4 the surfaces $\frac{U}{r}$=const for the field created by two (colinear) magnetic dipoles at the distance 2a. Fig.3 corresponds to the parallel, and Fig.4 to the antiparallel ones. The surfaces $\frac{U}{r}$ =const are characterized on these figures through the constant values of the expressions:

$$\log\frac{1}{r^2}\left\{\nabla(\vec{l}\nabla)\left(\frac{1}{\sqrt{r^2+(z-a)^2}}\pm\frac{1}{\sqrt{r^2+(z+a)^2}}\right)\right\}^2 \qquad (8)$$

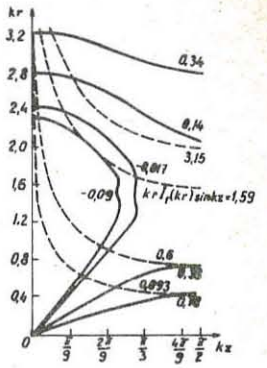

Fig.2

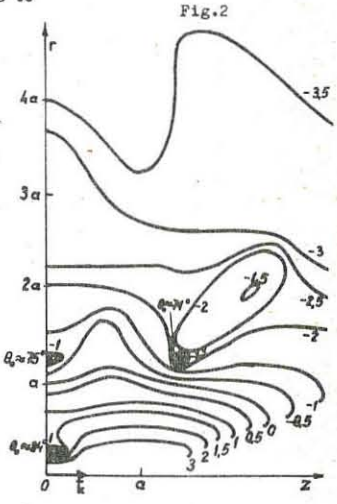

Fig.3

In the figures 2-4 can be seen that in the rOz plane there are domains which surround minimums of the $\frac{U}{r}$ values. The traps, having axial symmetry, these domains are ring-like, having as their axis, the symmetry axis of the trap. Let us consider the circle which links the minimum value points of α (α_{min}). From(2) it results that for the angle θ formed by the ray with the tangent to the circle α_{min} it results the condition: if $\theta<\theta_o=\arccos\frac{\alpha_{min}}{\alpha_{lim}}$ the ray can not leave the ring-like domain (through α_{lim} we marked the value for the limits of the closed domain). θ_o has the values indicated on the Fig.3 and 4 in the case of the two dipoles systems. So, in the magnetic traps for plasma exist ring-like traps for the fast magnetoacoustic perturbations. A qualitative study of the equations solution(1) shows that in the case $\theta>\theta_o$, a limitation of the perturbations propagation can appear, not only on the surfaces $\frac{U}{r}$=const but also in the direction of the oz axis /4/.

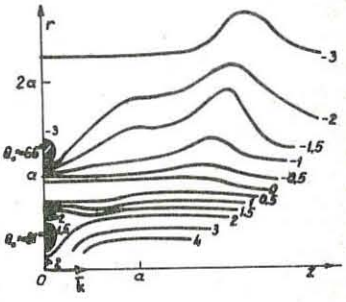

Fig.4

/1/ R.V.Deutsch, I.Grosu, Rev. Roum. Phys., 15, 63-71, (1970)

/2/ R.V.Deutsch, ... Plasma Physics and Controlled Nuclear Research, Conference Procedings, Novosibirsk 1-7 August, 1968, vol II pag. 181-194.

/3/ S.Masahisha, ... Radio Science Journ. of Research NBS/USNC-URSI, 69D, 8, 1133, (1965).

/4/ R.V.Deutsch, I.Grosu, D.Zoler, Beiträge aus der Plasmaphysik (to be published).

PROPAGATION OF NANOSECOND WAVES ON PLASMA COLUMNS

B.A. Aničin

Ion Physics Laboratory, Boris Kidrič Institute of Nuclear Sciences, Belgrade, Yugoslavia

Pulse measurements on wave supporting structures have the general advantage to give information on group velocities directly. Experiments with a wave packet in the dipolar surface wave mode have been reported recently /1/. The wave packet in these experiments was obtained by passing sub-nanosecond pulses through a band pass filter set at 2.2 GHz. It was proved experimentally that the wave is actually of the dipolar type and its group velocity was determined as a function of ω/ω_p.

This report deals with the propagation of nanosecond wave packets in the axially symetric TM mode on a positive column in mercury vapour. The experimental set-up is shown in figure 1. The tube diameters are 12.00 and 15.4_3 mm, the glass is pyrex ($\varepsilon_g = 4,8$) and the temperature of the mercury pool is controlled at 20°C. Waves are launched with a coaxial coupler, to prevent excitation of modes with higher azimuthal variation. In reception, a similar coaxial coupler was connected to a sampling oscilloscope, the vertical and time outputs of which are linked to a chart recorder. In contrast to the experiments described in /1/, nothing was done to select a specific frequency range from the 4 V, 3 nsec pulse. A typical record of waveforms is shown in figure 2. The general impression there is that the waveforms can be described well enough with a sine wave in a Gaussian envelope, which spreads gradually as the pulse progresses down the positive column. The frequency of the wave, measured at the maximum of the envelope, changes with discharge current, but the ratio of frequency and plasma frequency is nearly constant and varies between 0.14 and 0.19. We conclude that the launching and reception of a surface wave with couplers of the type sketched in figure 1. are strongly frequency sensitive processes, with a prominent resonance at $\omega/\omega_p = 0.16$ which selects a narrow frequency band from the broad spectrum of the 3 nsec pulse.

Time-space diagrams like the one in figure 2 have been taken at discharge currents of 12.5, 25, 50, 90 and 120 mA. The values of frequency, wavelength, phase and group velocity obtained from these diagrams are listed in the table below:

I mA	f_p MHz	f MHz	f/f_p	v_p cm/s	v_g cm/s	v_g/v_p	λ_g cm	βa	$\frac{\omega/\omega_p}{\beta a}$	$\frac{\partial(\omega/\omega_p)}{\partial(\beta a)}$
				x 10^9						
12.5	350	60	.169	1.0	0.64	0.64	17.6	0.214	0.76	0.49
25	490	80	.163	1.5	1.0	0.63	18.3	0.206	0.82	0.52
50	700	110	.163	2.3	1.5	0.63	22.7	0.167	0.88	0.56
90	930	140	.151	3.2	2.3	0.72	23.3	0.162	0.92	0.67
120	1080	160	.151	3.8	2.6	0.68	25.7	0.146	0.94	0.64

The ratio of group and phase velocity is nearly constant and has an average value of 0.648 for all discharge currents. The theoretical ratio v_g/v_p is 0.659, derived from the dispersion relation for $\beta a = 0.2$, a ratio of glass tube radii of 1.3 and pyrex glass ($\varepsilon_g = 4.8$). All other data in the table are also consistent with the dispersion properties of the n = 0 mode. The frequency data in the table are derived from waveforms recorded 35 cm from the launcher. There is a constant tendency of frequency to drop as the distance between receiver and launcher is increased.

Several auxilliary experiments were carried out. The linearity of the phenomenon was checked by reducing the pulse generator level to 2 and 1 V and comparing the resulting waveforms with the record obtained with 4 V. That the wave actually has no azimuthal variation was proved with a wire probe which produced the same signal irrespective of angular position. An attempt was made to launch the n = 1 mode with split cylinder couplers in transmission and reception, but the polarization effect was not observed and the time of flight was exactly the same as with the axially symmetric antennae. This is at variance with the result in /1/, where the sensitivity was not limited to 2 mV by the sampling oscilloscope, due to the use of TWT amplifiers. Transmission was attempted with the discharge tube switched off, and the near field was measurable 10 cm from the launcher and not further.

Several assumptions regarding the resonant phenomenon at $f/f_p = 0.16$ were tested. The first idea was to compute the amplitude of the surface wave from the residue of the surface wave pole in the complex wavenumber plane, working with a model magnetic current ring launcher, and see whether this exhibits any peaks in wavenumber or frequency. In fact a maximum was found, but not at the right value of wavenumber and too broad to account for the observed resonance. A second possibility, that the whole length of the guide is in resonance due to mismatch at the coronet absorbers, was eliminated by replacing the terminations with metallic reflectors, which proved not to affect the waveform. Waves were launched by applying the voltage pulse between the anode and a metallic sleeve around the glass tube, and two axially displaced copper rings. Compared with the coaxial couplers, these launching methods differ in efficiency, but the frequency remains basically the same. It was finally observed that the waveform changes when the length of the coaxial couplers is varied, which led to the assumption that the resonance is related with axial standind waves in the couplers themselves. This hypothesis is also supported by the observation that the waveforms depend on the relative axial displacement of inner and outer coupler electrodes and the fact that very short couplers lack the selective property when the distance from launcher to receiver is small. An important role seems also to be played by the combined effect of launching efficiency and attenuation, which tends to eliminate very low and very high frequencies from the spectrum. This effect is position dependent.

Thanks are due to Prof. K.E.Lonngren, from the University of Iowa for discussions of the subject and communication of data prior to publication, and to Dr.M.Vojnović and A.Šrebel from the Electronic Laboratory of this Institute, for the loan of a sampling oscilloscope and nanosecond pulse generator.

References

1. O.Demokan, H.C.S. Hsuan, K.E. Lonngren, A Time-of-Flight Study of Waves Guided by a Plasma Column - Abstract submitted for the Winnipeg Meeting of the American Physical Society, 22-24 June 1970.

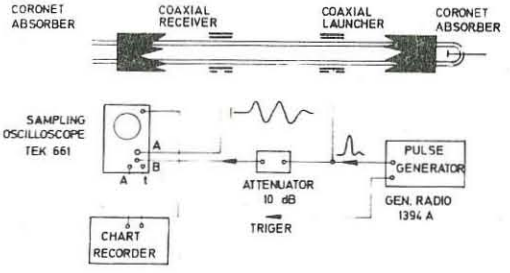

Figure 1.
The experiment

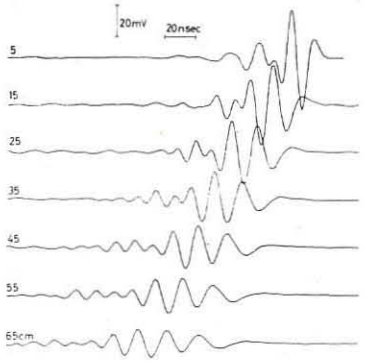

Figure 2.
Waveforms recorded at various distances from the launcher with a discharge current of 12.5 mA. Time runs from right to left. The parameter is the distance between launcher and receiver

INFLUENCE OF A COLLISIONAL PLASMA BACKGROUND ON THE TWO-STREAM INSTABILITY

Eryk Infeld and Andrzej Skorupski

Institute of Nuclear Research, Hoża 69, Warsaw, Poland

Abstract. The classification of the two stream instability into convective and absolute for two hot streams and a collisional plasma background is outlined. The case of cold streams is solved completely. The collisional background has the effect of quenching the absolute instability for some stream parameters.

We will give a method for finding the classification of the two-stream instability into convective and absolute when the effects of a collisional background are included. The whole point of the approach is that it can be used whenever the problem has been solved in the absence of the background. We will demonstrate our procedure by solving the problem for two cold streams. The same could easily be done for hot ones in the resonance model, as the required solution in the absence of a background is known [1].

Consider a cold plasma comprised of mobile electrons and immobile ions. If the effect of electron-ion collisions, which is more important than that of electron-electron collisions, is taken into account the dispersion relation usually used when charged streams are present is

$$D(k,\omega) = 1 - \omega_p^2 \omega^{-1} (\omega + i\nu)^{-1} - k^{-2} F(\omega/k) = 0. \qquad (1)$$

Here ω_p and ν are the plasma and collision frequencies of the plasma. (Recently this formula has been seen to be justified when the temperature of the electrons in the plasma is small, as can be shown using [2]).

We are on the borderline between absolute and convective instabilities if ω_c defined by

$$D(k,\omega) = 0, \quad \partial D/\partial k = 0 \qquad (2)$$

is real [3]. To find ω_c we solve the second equation first:

$$2F(\omega/k) + (\omega/k) F'(\omega/k) = 0 \qquad (3)$$

and get $\omega_c/k = f(p)$, where p stands for the parameters of the streams, and f is a function of p only. We obtained an equation in ω/k, even though (1) was not of that form.

Denote by ω_0 the value of ω_c when the background is absent. For this background - free case and two or more streams, from (1) and (3),

$$\omega_c^2 = f^2(p)\, F[f(p)] \qquad (4)$$

If we now express ω_c as a function of ω_0 we obtain from (1) and (3)

$$\omega_c = \omega_0 / (1 - \tfrac{1}{2} i\nu/\omega_c) \qquad (5)$$

Since we are on the borderline between absolute and convective instabilities when ω_c is real, we have reduced the problem of classification to that of finding ω_0 for no plasma background. The background moves the line of marginal absolute instability from the real ω_0 axis to the line (5) parametrized by ω_c real (strictly speaking only a part of (5) is relevant, i.e. for ω_c outside the interval $1/2 - \sqrt{1/4 - s^2}$, $1/2 + \sqrt{1/4 - s^2}$. This follows from an argument concerning branches).

As an illustration, for two counterstreaming cold beams in a collisional plasma background:

$$F(\omega/k) = \omega_{b_1}^2/(\omega/k - v_1)^2 + \omega_{b_2}^2/(\omega/k - v_2)^2 \qquad (6)$$

Introduce $\Omega_{b_1} = \omega_{b_1}/\omega_p$, $\gamma = \omega_{b_2}^2/\omega_{b_1}^2$, $y = -v_2/v_1 > 0$ which together with s, determine the problem. Solving (3) we get from (4) and (6)

$$\Omega_c'^2 = \Omega_{b_1}^2 \gamma^{-2} (1-y)^{-2} \left(\gamma - \tfrac{1}{2}\gamma^{3/3} y^{2/3} + i\tfrac{\sqrt{3}}{2}\gamma^{2/3} y^{2/3}\right)^3 \qquad (7)$$

Substituting this value of $\Omega_c'^2$ into (5) and eliminating Ω_0 we obtain an equation for the m.a.i. in parameter space. In Fig.1 this line is shown for $\gamma = 1$, $s = 0.01$. When collisions are absent ($s = 0$) this line is $y = 0$, as in the case of no background. Thus if there are no collisions adding a background leaves the classification unaffected (except for $v_1 = -v_2$, which we will not go into here).

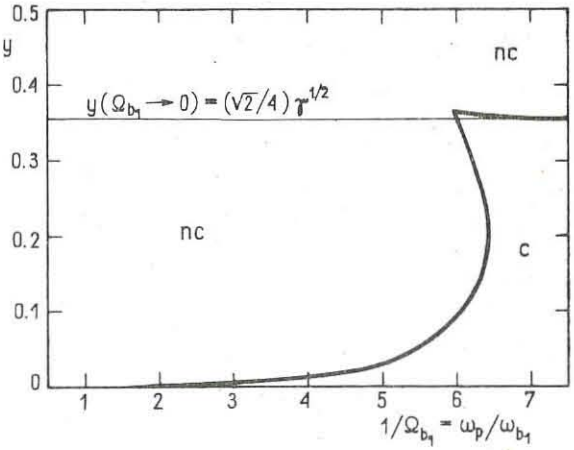

Fig.1 ($\gamma = 1$, $s = 0.01$)

References

1 E. Infeld, A. Skorupski, J.Plasma Physics, in print; Nuclear Fusion 9, 25 (1969).

2 L.P. Shkorofsky, Phys.Fluids 11, 2454 (1968); K.Matsuda 12, 1081 (1969) etc.

3 R.J. Briggs, Electron-Stream Interaction with Plasmas, M.I.T. Cambridge, Mass. (1964).

LINEAR WAVES AND INSTABILITIES II

DRIFT WAVES IN A COLLISONLESS PLASMA

by

P.Blanc, P.Brossier, P.Deschamps, R. Gravier,

R.Pellat, C. Renaud

ASSOCIATION EURATOM-CEA

Département de la Physique du Plasma et de la Fusion Contrôlée
Centre d'Etudes Nucléaires
Boite Postale n° 6 - **92 Fontenay-aux-Roses** (France)

Abstract : Pressure-gradient driven drift waves have been observed in a collisionless, low-density, 5.40 m long plasma. Comparisons with the theoretical predictions show a reasonable agreement.

Experimental apparatus and macroscopic parameters :The experimentshave been performed on the ODE device.An hydrogen plasma is created by two magnetron sources located 8.80 m apart at each end of the apparatus.The plasma diffuses through two cusp fields into a 5.40 m long central chamber immersed in an homogeneous magnetic field $B_z \leqslant 5000$ Gs.A differential pumping system ensures a base pressure $p_o = 10^{-6}$ mm Hg : the observed frequencies are larger than any collision frequency by at least one order of magnitude. Most of the measurements, were performed using spherical ($\Phi = 0.5$ mm) coaxially shielded Langmuir probes. The wave potential was detected with a high impedance capacitive probe.The ion temperature ($T_i \simeq 2$ eV) was measured either spectroscopically (Doppler broadening of H_β) or with gridded probe. On the axis n_o ranges from 10^8 to 10^{10} cm^{-3} and $T_e = 14$ eV. Both n_o and T_e exhibit a Gaussian radial profile with $\nabla n_o/n_o = \nabla T_e/T_e = 1$ cm^{-1}.Owing to the longitudinal symetry of the experiment, n_o, T_e, $\nabla n_o/n_o$ and $\nabla T_e/T_e$ are constant along the column and there is no current parallel to B_z. The plasma potential variations show the existence of a radial electric field E_o directed inward and increasing linearly with radius. At 2000 Gs, $E_o = 6$ V/cm (at r = 1 cm).

Characteristics of the waves expected in this experiment : As is well known, in such a collision-free, low-pressure ($\beta < m_e/m_i$) plasma, pressure-gradient driven drift waves can be unstable ; those waves have short transverse wavelengths and large but finite parallel wavelength. The dispersion relation in a plane geometry has been solved, using the measured macroscopic parameters. For $0.1 < k_\perp \rho_i < 1$, and when the parallel wavelength increases from 0.20 m (marginal stability) to 8.50 m, - the growth rate increases from 0. to a maximum of $\gamma \sim \omega \sim 4.10^5$ s^{-1}, - the phase difference $\Delta\varphi$ between the perturbed density n_1 and potential Φ_1 increases from 0 to 40° (n_1 leading) - the parallel phase velocity increases from 0.1 V_{Te} to 0.5V_{Te} ($V_{Te,i}$ =electron, ion thermal velocity).

The $\vec{E}_o \times \vec{B}_z$ rotation was ignored in this work; it has been shown, in a cylindrical geometry [1], that such a field slightly increases the maximum growth rate.

Instabilities : The fig.1 a shows a typical spectrum of plasma oscillation in the gradient. Hereafter we will distinguish the 50 kHz mode or 'flute mode", and the 100 and 150 kHz modes or "drift modes". The drift modes are much more sensitive to the experimental conditions than the flute mode. They can appear only when the base pressure is low enough ($p_o \leqslant 5.10^{-6}$ mm Hg) and when the sources are operated symetrically (fig. 1 b) . A common feature of the flute and drift modes is their radial position (maximum amplitude at r = 10 mm) and extension (about 12 mm). The flute mode is not affected by the variation of the magnetic field ($1500 \leqslant B_z \leqslant 3000$ Gs).Its frequency is equal to the calculated electric drift frequency.The azimuthal and radial phase and amplitude measurements show a pure m = 1 progressive azimuthal and stationnary radial mode.Using several probes carefully aligned along B_z, the phase and amplitude of the perturbed density were measured with a lock-in amplifier.The reference probe was located at 2 m from the median plane(fig.3 a). Those measurements yield a parallel wavelength $\lambda_{//} \gg 2$ L (L = plasma length= 5.40 m).Finaly the perturbed density and potential are out of phase by 180°. From these observations we conclude that this mode is created by the radial electric field.Furthermore $\vec{E}_o$ will Doppler-shift the higher frequencies observed in the laboratory frame by 50 kHz. The drift mode frequencies decrease when increasing B_z; substracting the 50 kHz Doppler-shift yields a $1/B_z$ dependance ($1500 \leqslant B_z \leqslant 3000$ Gs) as expected from the electron diamagnetic drift velocity (V_{DE}) variation.The two modes propagate along the V_{DE}direction with m = 1 (100 kHz) and m = 2 (150 kHz) azimuthal modes, and are stationnary along the radius (fig.2).Parallel measurements clearly show a node in the middle of the column (fig.3b and c).Both modes have a standing wave structure, with $\lambda_{//} \simeq 7.50$ m, which gives a parallel phase velocity $V_{ph} \simeq 4 \times 10^7$ cm/s, to be compared with $V_{Te} \simeq 1.8 \times 10^8$ cm/s.Moreover, the perturbed density n_1 and potential Φ_1 are out of phase by $\Delta\varphi = 10°$ ($\pm 10°$), n_1 leading). The detailed comparison of the experimental results : $0.15 < k_\perp \rho_i = \sqrt{k_r^2 + k_\theta^2}\,\rho_i < 0.25$, $\lambda_{//} \simeq 7.50$ m , f = 50 and 100 kHz, $V_{ph} \simeq 30\, v_{Ti} \simeq 0.4\, V_{Te}$, with theory lead us to condude that driftwaves develop in this collision free plasma.

It is a pleasure to thank P.Moyen for spectroscopic measurements and M.Occhionorelli for help in experiment.

Reference : [1] H.Luc - Rapport EUR-CEA-FC 428, 1967.

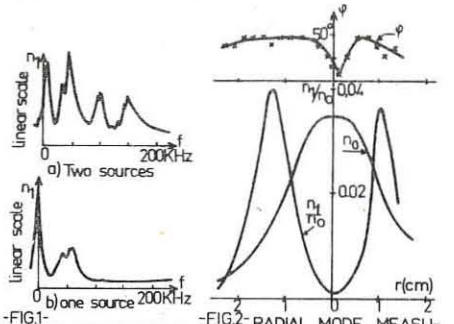

-FIG.1- DENSITY FLUCTUATIONS SPECTRUM $B_z = 2000$Gs - $n_o = 2 \times 10^{10} cm^3$

-FIG.2- RADIAL MODE MEASUREMENT FOR m=2 PHASE AND AMPLITUDE VARIATIONS VERSUS RADIUS F=150 KHz

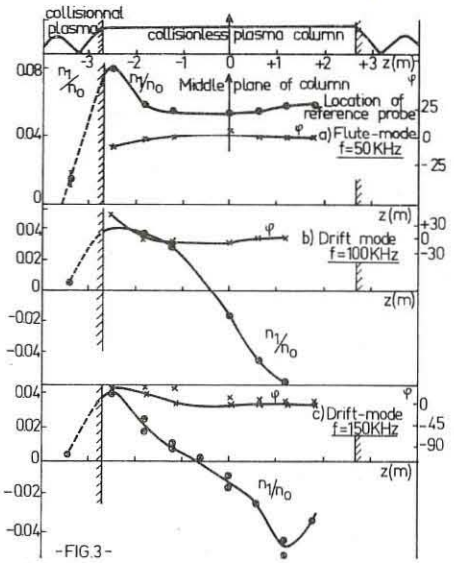

-FIG.3- PARALLEL WAVELENGTHS MEASUREMENT - PHASE AND AMPLITUDE VARIATIONS FOR EACH MODE - $B_z = 2000$Gs - $n_o = 2 \times 10^{10} cm^{-3}$

INFLUENCE OF TRAPPED PARTICLES ON THE DRIFT WAVES

by

A. Samain

ASSOCIATION EURATOM-CEA
Département de la Physique du Plasma et de la Fusion Contrôlée
Centre d'Etudes Nucléaires
Boite Postale n° 6 · **92 Fontenay-aux-Roses** (France)

Abstract : The stability of the drift modes of a collisionless magnetically confined plasma slab is considered when shear is present and the field intensity is modulated. In the absence of such a modulation the drift modes are generally convective and strongly localized in the direction of the plasma confinement. The field modulation introduces a coupling between these localized convective modes. Under proper conditions, unstable eigenmodes consisting of a sequence of convective localized modes may exist throughout the plasma.

I. Introduction : The modulation of the magnetic field intensity in toroïdal configurations produces unstable modes [1] associated with the curvature of the lines of force. Their phase velocity $\frac{\omega}{K_T}$ across the field is of the same order as the curvature drift velocities V_c. The field modulation has also an influence on the stability of the drift modes caused by the plasma confinement only, [2], [3], whose phase velocity $\frac{\omega}{K_T}$ is of the same order as the diamagnetic velocity $V_d \gg V_c$. We consider this question in the case of a collisionless plasma slab at a uniform temperature T, confined in the direction ox $\left(\left[\partial n/n\partial x\right]^{-1} = L\right)$ by a magnetic field $\vec{B}$ parallel to the plane y, z. The slab is uniform along oz and periodic along oy with the period $2\pi/H_y \gtrsim L$. The angle $\theta = (\vec{B}, oz)$ is small but finite. Magnetic shear $\left([d\theta/dx]^{-1} = L_s \gg L\right)$ is present. The magnetic field intensity depends on the abscissa ℓ along the magnetic lines passing through (y = o, z = o) as $B - \frac{\Delta B}{2}\cos(H_{\parallel}\ell)$ where $H_{\parallel} = H_y \sin\theta \sim L_s^{-1}$ and $\left(\frac{m_e}{m_i}\right)^{1/2}\frac{1}{H_y L} \ll \left(\frac{\Delta B}{B}\right)^{1/2} \ll 1$.

II. Specification of the mode : An electrostatic mode perturbing this equilibrium corresponds to a potential of the form :

$$\psi(x,y,z,t) = \exp\left[i(\omega t + K_y y + K_z z)\right] \sum_n \varphi_n(x)\exp(i n H_y y) + \text{c.c.} \quad (1)$$

The component $K_{\parallel}$ of the vector (K_y, K_z) along the magnetic lines depends on x as: $K_{\parallel}(x) = K_T\frac{x}{L_s} + \text{cste}$, where $K_T \simeq K_y \gg K_z$ is the transverse component of this vector. We assume that $K_T \sim \frac{1}{\rho_{thi}} \gg L^{-1} \gtrsim H_y$. $\left(\rho_{th}^2 = \frac{v_{th}^2}{\omega_c^2} = \frac{2T}{m\omega_c^2}\right.$; $\left.\omega_c = \frac{qB}{mc}\right.$; q is the charge and m is the mass of the particles). Also : $\omega_{ci} \gg \omega \sim K_T V_{di} \sim \frac{v_{thi}}{L}$. $\left(V_d = \frac{cT}{qBL}\right)$. Then the bounce frequencies $\omega_T \sim \left(\frac{\Delta B}{B}\right)^{1/2} H_{\parallel} v_{th}$ of the trapped particles satisfy : $\omega_{Ti} \ll \omega \ll \omega_{Te}$. Using the variational method reported in [4] we obtain :

$$\left(2 - \alpha_{ni} - \alpha_{ne}\right)\varphi_n(x) - \sum_{n'\neq n}\mathcal{L}_{n',n}\,\varphi_{n'}(x) = 0 \quad (2)$$

In this equation α_{ni} is the usual operator $\frac{\omega + K_T V_{de}}{\omega}\mathcal{F}\left[\frac{\omega}{(K_{\parallel}(x) + nH_{\parallel})v_{thi}}\right]Z\left(\frac{K_{\perp}^2\rho_{thi}^2}{2}\right)$, where $\mathcal{F}(u) = \frac{u}{\pi^{1/2}}\int_{-\infty}^{+\infty}\frac{e^{-s}(-\omega^2)\,d\omega}{u-\omega}$, $Z(u) = e^{-u}I_0(u)$ and $K_{\perp}^2 = K_T^2 - \frac{d^2}{dx^2}$. The quantity α_{ne} is given by :

$$\alpha_{ne}(x) = (\omega + K_T V_{de})\sum_p\left[(1-\nu_T)\left\langle\frac{\left|\overline{\exp\left[iK_{\parallel}(x)\left(\ell - v_{\parallel}t\right) + iH_{\parallel}\left(n\ell - p\omega_T t\right)\right]}\right|^2}{\omega + (K_{\parallel}(x) + pH_{\parallel})v_{\parallel}}\right\rangle_t + \nu_T\left\langle\frac{\left|\overline{\exp\left[i\left(K_{\parallel}(x)+nH_{\parallel}\right)\ell - ip\omega_T t\right]}\right|^2}{\omega + p\omega_T}\right\rangle_T\right]$$

where $\nu_T \sim \left(\frac{\Delta B}{B}\right)^{1/2}$ is the fraction of trapped electrons ; —— means time averaging over the trajectory of an electron along the line of force passing through (y = o, z = o) ; $v_{\parallel}$ is the time average velocity of this electron if it is circulating and ω_T is its bounce frequency if it is trapped ; $\langle\ \rangle_t$ and $\langle\ \rangle_T$ means averaging over circulating and trapped electrons, respectively. Finally :

$$\mathcal{L}_{n,n'}(x) = \frac{\omega + K_T V_{de}}{\omega}\nu_T\left\langle\overline{\exp\left[i\left(K_{\parallel}(x) + n'H_{\parallel}\right)\ell\right]}\ \overline{\exp\left[-i\left(K_{\parallel}(x) + nH_{\parallel}\right)\ell\right]}\right\rangle_T$$

III. Discussion : If $\frac{\Delta B}{B} = 0$, $\mathcal{L}_{n,n'} = 0$ and (2) determines the potential of a drift mode localized near the plane $x = x_n$ where $K_{\parallel}(x_n) + nH_{\parallel} = 0$ [5]. Close to this plane it receives a power $\sim \alpha_{ne}$ from electrons. However generally this power is convected along ox without reflexion towards the region $|x - x_n| \gtrsim \delta = \frac{L_s}{K_T}\frac{\omega}{v_{the}} \sim \frac{L_s}{L}\rho_{thi}$ where it is strongly absorbed by ion Landau damping. This circumstance generally prevents the mode from existing as an unstable eigenmode. If $\frac{\Delta B}{B} \neq 0$, the function $\alpha_{ne}(x) = \alpha_e(x - x_n)$ is found to be more localized along ox, in intervals $\delta' \sim \frac{L_s}{K_T}\frac{\omega}{v_{the}}\left(\frac{B}{\Delta B}\right)^{1/2} \ll \rho_{thi}$ close to the abscissae $x = x_n$, $x = x_{n\pm1}$, $x = x_{n\pm2}$, ... Also, the coupling coefficients $\mathcal{L}_{n,n'}(x) = \Lambda(x - x_n, x - x_{n'})$ are not zero. They have their maximum $\left(\sim\left(\frac{\Delta B}{B}\right)^{1/2}\frac{1}{|n-n'|}\right)$ for $x = \frac{x_n + x_{n'}}{2}$, and retain this value in an interval $\sim \delta'' = x_{n+1} - x_n = \frac{H_n L_s}{K_T} \sim \rho_{thi}$. Eventually, they allow the power driven from electrons near the plane $x = x_n$ by the component $\varphi_n(x)$, to be partly transferred to the components $\varphi_{n'}(x)$ before being damped in the regions $|x - x_n| \gtrsim \delta$. Therefore they allow the existence of unstable eigenmodes of the form (1), consisting of a sequence of coupled components $\varphi_n(x)$. Then

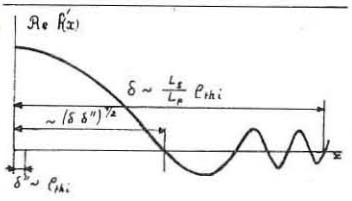

The structure of the function f'(x)

$\varphi_n(x) = \exp(in\theta)\,f(x - x_n)$, where θ is a constant, and f(x) satisfies :

$$\left[2 - \alpha_i - \alpha_e(x)\right]f(x) - \sum_{n\neq 0}\Lambda\left(x, x - n\delta''\right)f(x - n\delta')\exp(in\theta) = 0 \quad (3)$$

where α_i is the operator $\frac{\omega + K_T V_{di}}{\omega}\mathcal{F}\left(\frac{\omega L_s}{K_T x\, v_{thi}}\right)Z\left(\frac{K_{\perp}^2\rho_{thi}^2}{2}\right)$. The function $\alpha_i f(x)$ has a characteristic scale $\gtrsim \rho_{thi}$ for any function f(x). Writing f = f' + f", where f' and f" have a characteristic scale $\gtrsim \rho_{thi}$ and $\sim \delta'$, respectively, we have : $f''(x) = 2\left(\frac{1}{2 - \alpha_e(x)} - \frac{1}{2}\right)f'(x)$ and the function f'(x) is determined by :

$$\left(2 - \alpha_i\right)f'(x) = \alpha_i f''(x) + \sum_{n\neq 0}\Lambda\left(x, x - n\delta''\right)f'(x - n\delta'')\exp(in\theta) \quad (4)$$

Assuming that $2 - \frac{\omega + K_T V_{di}}{\omega}Z'\left(\frac{K_T^2\rho_{thi}^2}{2}\right) = 0$, the operator $2 - \alpha_i$ may be replaced in the L.H.S. of (4) by $-Z'\left(\frac{K_T^2\rho_{thi}^2}{2}\right)\rho_{thi}^2\frac{d^2}{dx^2} - \frac{x^2}{\delta^2}$, $\left(Z'(u) \simeq -\frac{dZ}{2\,du}\right)$, under the condition that f(x) be a divergent wave for $x = \pm\infty$. Then the equation (4) may be solved using a Green's function when its R.H.S. is known. Using an iterative method, we find that the considered unstable eigenmodes actually exist, (with $\theta = \pi$), if :

$$\frac{L_s}{L} > \frac{2.5}{\left[\text{Log}\left(\frac{L_s}{L}\frac{B}{\Delta B}\right)\right]^{2/3}}\left(\frac{m_i}{m_e}\right)^{1/3} \quad \text{and} \quad \frac{L_s}{L} > \frac{3}{(H_{\parallel}L_s)^2}\frac{B}{\Delta B}$$

References :

/1/ B.B. Kadomtsev - O.P. Pogutze
Sov. Phys. JETP 24 1172 (1967)

/2/ O.P. Pogutze
Nuclear Fusion 9 157 (1969)

/3/ K. Rohlena
Plasma Phys. 11 751 (1969)

/4/ P.H. Rebut - A. Samain
Compt. Rend. 268B 607 (1969)
and 268B 783 (1969)

/5/ B. Coppi - G. Laval - R. Pellat - MN. Rosenbluth
Plasma Phys. 10 1 (1968)

ELECTRON TEMPERATURE OSCILLATIONS IN DRIFT WAVES AND THEIR EFFECT ON POTENTIAL MEASUREMENTS

by

R. W. Motley, R. F. Ellis, and D. L. Jassby

Plasma Physics Laboratory, Princeton University
Princeton, New Jersey 08540 U.S.A.

Abstract: Electron temperature oscillations in drift waves can greatly modify the relation between density and probe floating potential. Evidence for such effects in Q machine plasmas is presented.

The relationship between the fluctuating density, $\tilde{n}$, and potential, $\tilde{V}$, of drift waves is of importance, since there is a net radial transport of plasma if $\tilde{n}$ and $\tilde{V}$ are not exactly in phase. Phase relations of drift wave quantities in Q machine alkali plasmas have been reported by Chu, Hendel, and Politzer [1], Chen [2], and Rowberg and Wong [3]. The experimental results are confusing, with various values of δ (phase angle by which density leads potential), such as 40°, $\sim 0^{\circ}$, and 5 to 20° being reported by different groups.

Such measurements of phase and magnitude of fluctuating quantities have traditionally been done with Langmuir probes. We believe that errors can arise from the identification of the floating potential $\tilde{V}_f$ (which is actually measured with a probe) with the space potential $\tilde{V}_s$ (given by theory). The space and floating potential fluctuations are not identical if the electron gas is not isothermal, but are related by the equation

$$\tilde{V}_s = \tilde{V}_f + \frac{k\tilde{T}_e}{e} \ln (v_e/\alpha v_i) \simeq \tilde{V}_f + 5\frac{k\tilde{T}_e}{e} . \qquad (1)$$

From this relation it is clear that a significant phase angle may exist between floating and space potential unless the electron temperature fluctuations are much less than $1/5\ e\tilde{V}_f/k$. Recent theoretical work by Tsai, Perkins, and Stix [4] and Gravier, Laval, Pellat, and Renaud [5] have shown that temperature fluctuations are important in determining the properties of collisional drift waves in Q machines. A typical amplitude of the temperature oscillation, $\tilde{T}/T$, is $\sim$ 10 - 20% of the potential, $e\tilde{V}/kT_e$, with a phase shift between temperature and density greater than 90°.

In the absence of definitive experimental information on temperature fluctuations we have calculated the phase angles between density, space potential, and temperature from the linear slab model theory. The theory, similar to that of Tsai et al., [4] drops the isothermal approximation for the electron fluid. The relationship between electron temperature and the other variables is calculated from the electron heat flow equation given by Braginskii [6]. The amplitude and phase of the floating potential are then calculated from Eq. (1). Typical results in the form of vector diagrams of the density, potential and temperature oscillations are shown in Fig. 1, for conditions of maximum wave growth ($n = 10^{11}$ cm^{-3}, $\lambda_{\parallel} = 250$ cm, $\nabla n/n = -1\ cm^{-1}$). The density fluctuation leads the space potential by 21° in approximate agreement with the previous results of the isothermal theory. The temperature, however, lags the space potential by a large angle and the vector sum of Eq. (1) then implies that the density lags the floating potential, which is the quantity actually measured, by about 10°.

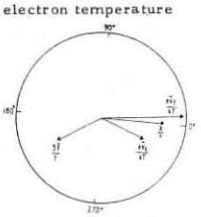

We have measured the relationship between density and floating potential for the collisional drift mode over a wide range of conditions in a Q machine plasma of length 110 cm and diameter 4 cm. The measurements are in approximate agreement with the nonisothermal theory on the following points:

(1) The amplitude of the fluctuating potential $e\tilde{V}_f/kT \approx 1.4\ (\tilde{n}/n)$.

(2) In the rest frame of the rotating plasma ($E_r = 0$) the density lags the floating potential by an angle between 0 and 8°. If the isothermal theory were employed this would imply a net radial influx of plasma, contrary to experiment, which shows an increase in the radial loss rate if drift waves are present.

(3) The phase angle between density and space potential, inferred from the theory, is sufficient to predict the magnitude of the radial loss measured experimentally. If electron temperature fluctuations are omitted (ignoring the difference in sign), the predicted flux is about 3 - 4 times too small.

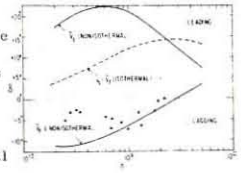

Figure 2 shows detailed results of experimental and theoretical phase angles as a function of plasma density and illustrates points (2) and (3), yielding agreement on both direction and magnitude of the phase angle. The results of the isothermal theory are also displayed, and are not compatible with experiment.

These data provide indirect experimental support for the occurence of temperature oscillations in drift waves and show that it is not possible, in general, to identify floating and space potential oscillations in long parallel wavelength instabilities.

References

[1] T. K. Chu, H. W. Hendel, and P. A. Politzer, Phys. Rev. Letters 19, 1110 (1967).

[2] F. F. Chen, Princeton Plasma Physics Laboratory MATT-717 (1969).

[3] R. E. Rowberg and A. Y. Wong, Phys. Fluids 13, 661 (1970).

[4] S. Tsai, F. W. Perkins, and T. H. Stix, Princeton Plasma Physics Laboratory MATT-700 (1969).

[5] R. Gravier, G. Laval, R. Pellat, and Renaud, International Conference on Physics of Quiescent Plasmas (Ecole Polytechnique, Paris, 1969).

[6] S. I. Braginskii, Reviews of Plasma Physics, Vol. 1 (Consultants Bureau Enterprises, Inc., New York, 1965), p. 205.

COLLISIONAL DRIFT INSTABILITY IN A BOUNDED PLASMA

by

Aldo Nocentini

Istituto di Meccanica dell'Università di Trieste, 34127 Trieste, ITALY, and Laboratori Gas Ionizzati del CNEN, 00044 Frascati, Rome, ITALY.

Abstract: We consider the influence of the cathodes on the drift instability of a Q-machine plasma, in which ions are collisionless, while electrons are collision dominated. We prove that only ion rich plasmas can support drift waves with parallel wavelength of the order of the length of the machine.

The influence of the cathodes of a Q-machine on the drift instability has been studied both in the collisional regime, using fluid equations[1], and in the collisionless regime, using Vlasov equation[2]. The influence of the plates in the two cases is different: in the intermediate frequency region, for a collisionless plasma no difference is found between ion and electron rich sheaths, while in the collisional regime it is found that only ion rich plasmas can support drift instabilities with wavelength of the order of the length of the machine. In this note we extend the treatement of ref.2 to the collisional regime, introducing the effect of electron collisions by a Krook term which conserves the number of particles.

The equilibrium distribution functions for ions and electrons are locally maxwellian, with slight density and temperature gradients in the x direction. Charge neutrality holds at the equilibrium. The low β, constant and uniform, external magnetic field points in the z direction; z=0 and z=L are the plasma boundaries. The equation for the perturbed electron distribution function f reads:

$$\frac{df}{dt} = \frac{e}{m}\nabla\phi\frac{\partial F}{\partial v} - \nu f - \nu\frac{F}{N_0}\int f\,d\underline{v} \qquad (1)$$

where F is the equilibrium distribution function, N the equilibrium number density, ν the electron-ion collision frequency. The perturbation is electrostatic. All perturbed quantities are Fourier analized in space and time. The equation (1) can then be solved by integration along the unperturbed orbits. In the limit $\omega,\nu \ll \Omega$ we obtain the following expression:

$$\sum_{k_z} f(\underline{k},v,\omega)\exp(ik_z z) = \sum_{k_z}\left\{a_1\phi(\underline{k},\omega) + a_2 n(\underline{k},\omega) + c(z)\left[b_1\phi(\underline{k},\omega) + b_2 n(\underline{k},\omega)\right]\exp(ik_z z)\right\} , \qquad (2)$$

where a_1, a_2, b_1 and b_2 are coefficients independent of z, and $n(\underline{k},z)$ is the Fourier coefficient of the perturbed electron density. The expression of c can be noticeably simplified choosing along z a Fourier series of cosines on the length 2L, so that: $k_z = n/L$, $\phi_n = +\phi_{-n}$. With this choice we get:

$$f_n = a_n\phi_n + b_n n_n + \sum_{-\infty}^{+\infty}{}_m\,(a_{nm}\phi_m + b_{nm} n_m) , \qquad (3)$$

and integrating over velocities leads to:

$$n^e_n = M^e_n\phi_n + N^e_n n^e_n + \sum_m (M^e_{nm}\phi_m + N^e_{nm} n^e_m) , \qquad (4)$$

where we introduced the superscript e to mark quantities referring to electrons. For the ions, which are assumed collisionless, we get:

$$0 = n^i_m - M^i_m\phi_m - \sum_l M^i_{ml}\phi_l . \qquad (5)$$

Poisson's equation reads:

$$\left\{\left(\frac{\pi n}{L}\right)^2 - k_\perp^2\right\}\phi_n = 4\pi(e^e n^e_n + e^i n^i_n) . \qquad (6)$$

We insert now the expressions (4) and (5) for n^e and n^i on the r.h.s. of (6) and add eq.(5) multiplied by $e^i(N^e_{mnm} + N^e_{nm})$ and summed up over m. Using again eq.(6) we get the following equation for ϕ:

$$\tilde{D}(n,\omega)\phi_n + \sum_0^\infty{}_m\,\tilde{\alpha}_{nm}\phi_m = 0 . \qquad (7)$$

The dispersion relation reads then:

$$\det\left|\tilde{D}(n,\omega)\delta_{nm} - \tilde{\alpha}_{nm}\right| = 0 , \qquad (8)$$

Where δ_{nm} is the Kroneker symbol. We do not give here the general expression for $\tilde{D}$ and $\tilde{\alpha}$, which are extremely massive. We simply notice that for $\nu\to 0$ the dispersion relation (8) reduces to that of ref.2. The effect of the cathodes is contained in the $\tilde{\alpha}$'s, while $\tilde{D}=0$ is the dispersion relation of the unbounded problem.

For simplicity we consider here only the case of no temperature gradient. At intermediate frequencies, in the usual limit $\nu \gg nu_e/L$, $\omega\nu \ll (nu_e/L)^2$, the expression of $\tilde{D}(n,\omega)$ is, for n≠0, the following one:

$$\tilde{D}(n,\omega) = \frac{1}{2\nu^2}\left\{\left[\left(\frac{\pi n u_e}{L}\right)^2 - 2i\omega\nu\right]\left[\lambda_D^2 k_\perp^2 + 1 - b\left(1+\frac{\omega_d}{\omega}\right)\right] + \left[\left(\frac{\pi n u_e}{L}\right)^2 - 2i\omega_d\nu\right]\right\} , \qquad (9)$$

Where: $k_\perp^2 = k_x^2 + k_y^2$; $b = I_o(Z)\exp(-Z)$; $Z = k_\perp^2 R_i^2/2$; J_o is the Bessel function of order zero, u_e the electron thermal speed, R_i the ion Larmor radius, λ_D the Debye length, ω_d the usual drift frequency. Let us notice that the terms of order $(\pi n u_e/L\nu)^2$ give the real part of the frequency, while the much smaller terms of order ω/ν give the growth rate. The solution ω_n of $\tilde{D}=0$ is:

$$\omega_n = b\omega_d/(\lambda_D^2 k_\perp^2 + 2 - b) + 2i\nu\omega_d^2 L^2 b(\lambda_D^2 k^2 + 2 - 2b)/(\pi n u_e)^2(\lambda_D^2 k^2 + 2 - b)^3 . \qquad (10)$$

For n=0 we get:

$$\tilde{D}(0,\omega) = \left\{\lambda_D^2 k^2 + (1-b)\left(1+\frac{\omega_d}{\omega}\right)\right\}\omega/(\omega+i\nu) . \qquad (11)$$

The solution ω_o of $\tilde{D}(0,\omega)=0$ is the following one:

$$\omega_o = -\omega_d(1-b)/(\lambda_D^2 k^2 + 1 - b) . \qquad (12)$$

Let us see now how far these modes are affected by the cathodes. We consider here only the two extreme cases of completely trapped electrons (ion rich plasma) and completely trapped ions (electron rich plasma). By "completely trapped" we mean that the trapping speed is much larger than the thermal speed of the trapped species. In these two cases the $\tilde{\alpha}$'s can be evaluated explicitely.

In the first case only the ions contribute to the $\tilde{\alpha}$'s, and we get:

$$\tilde{\alpha}_{nm} = \frac{iu_i}{\pi\omega L}\left[1+(-)^{n+m}\right]\delta_n\delta_m b\left(1+\frac{\omega_d}{\omega}\right) \qquad , \qquad (\delta_0 = 1/\sqrt{2},\ \delta_{n\neq 0} = 1) .$$

These terms do not influence the drift modes (neither frequency nor growth rate) if: $u_i/\omega L \ll \omega/\nu$. This condition is compatible with the preceding ones, so that a regime exists in which the Fourier terms with low n are modes of the bounded plasma, with the same characteristic features of the analogous modes of the unbounded problem. It is also easy to show that the n=0 mode is not destabilized by the sheaths.

Let us consider now an electron rich plasma. In this case the order of magnitude of the $\tilde{\alpha}$'s turns out to be $u_e/\nu L$. The condition that these terms be unimportant reads: $u_e/\nu L \ll \omega/\nu$, which is clearly incompatible with our previous assumptions unless n is large. Then the usual drift instability of an electron rich plasma is not modified by the cathodes (neither in frequency, nor in growth rate) only in the trivial case of a parallel wavelength much smaller than the length of the machine.

References:

1 F.F.Chen, Plasma Phys. 7, 399 (1965).

2 B.Bertotti & A.Nocentini, Plasma Phys. 12, 39 (1970).

COLLISIONAL DRIFT WAVES IN THE PRESENCE OF NON UNIFORM RADIAL ELECTRIC FIELDS

G. Bardotti and M. Dobrowolny

Laboratori Gas Ionizzati (Associazione EURATOM-CNEN), C.P. 65 - 00044 Frascati, Rome, Italy

Abstract: Numerical results are presented on the stability of a low-β magnetized plasma column, in collision-dominated regime, in the presence of radial non-uniform electric fields.

There has been recently much work on the influence of radial non uniform electric fields on the stability of a low-β plasma column in a uniform magnetic field. Q-machine experiments have pointed out the existence of oscillations located in regions of large electric field gradients and not identifiable with drift type instabilities driven by gradients in density or temperature / 1 ÷ 5 /. Theoretical work on the influence of such non uniform fields on stability, based on WKB approximation, /6,7/ has not given significant changes in the properties of the wave with respect to the field-free case. Local solutions cease however to be valid / 7 / for electric fields and electric field gradients such as those present in the experiments. Very recently results of exact solutions of the eigenvalue problem of stability have been reported / 4, 5 /, aiming at explanation of experimental observations of flute type oscillations at the edge of the plasma. We have undertaken the numerical solution of the eigenvalue problem of stability of collisional drift waves in the presence of radial non uniform electric fields. In the usual cylindrical coordinates r, Θ, z with magnetic field B along z, and for electrostatic perturbations of the form $\tilde{A}(r,\vartheta,z,t) = A(r)e^{i\ell\vartheta + ik_z z + i\omega t}$, the r dependent part of the electrostatic potential φ is governed by the following equation / 7, 8 /:

$$\frac{1}{2}\frac{a_i^2}{L_H^2}\frac{d^2\tilde{\varphi}}{d\xi^2} + \frac{1}{2}\frac{a_i^4}{L_H^4}p(\xi)\frac{d\tilde{\varphi}}{d\xi} + q(\xi)\tilde{\varphi} = 0 \qquad (1)$$

where $\tilde{\varphi} = \frac{e\varphi}{kT}$, $a_i = \sqrt{\frac{2m_i kT}{e^2B^2}}$, $\xi = \frac{r}{L_H}$, L_N is the scale of variation of density profile and the coefficients $p(\xi), q(\xi)$ are given by the following expressions

$$p(\xi) = \frac{1}{\xi} + \frac{n'}{n} + \frac{\omega_D}{\dot{\omega}(\dot{\omega}+\omega_D)}\omega_E' - 2\frac{\omega_E'}{\dot{\omega}} + \frac{2\omega_E' + \omega_D'}{\dot{\omega}+\omega_D} \qquad (2)$$

$$q(\xi) = \frac{\omega_D - \dot{\omega}}{(\dot{\omega}+\omega_D)(\ell+2i\epsilon^*\frac{\dot{\omega}}{\omega_D})}\frac{i}{k}\frac{a_i^4}{L_H^4}\left\{-\frac{\ell^2}{\xi^2}\frac{i}{\xi}\frac{n'}{n} + \frac{i}{\dot{\omega}(\dot{\omega}+\omega_D)}\left[\omega^2\frac{i}{\xi}\frac{n'}{n} - \omega_E'(2\omega_E' + \omega_D') - \frac{i}{\xi}\omega_D\omega_E'\right] - \right.$$
$$\left. - \frac{i}{\dot{\omega}}\left[\omega_E'\left(\frac{i}{\xi}+\frac{n'}{n}\right) + \omega_E''\right] - \frac{i}{\xi}\frac{i}{\dot{\omega}+\omega_D}\left[2\omega_E' + \omega_D'\right] + \frac{2}{\dot{\omega}^2}(\omega_E')^2 - \frac{\omega_D}{\dot{\omega}+\omega_D}\frac{\omega_E'^2}{\dot{\omega}^2}\right\} \qquad (3)$$

where primes denote ξ derivatives, $\omega_D = \frac{kT}{eB}\frac{\ell}{r}\frac{i}{n}\frac{dn}{dr}$ is the ion drift frequency, $\omega_E = -\frac{\ell}{r}\frac{E_0(r)}{B}$ is the frequency of rotation due to the radial electric field E_0, $\dot{\omega} = \omega + \omega_E$ and $\epsilon^* = \frac{\omega_D}{k_z^2}\frac{\nu_{ei}}{v_{the}^2}$ with ν_{ei} the electron-ion collision frequency. Solutions of (1) are to be subject to the boundary conditions $|\tilde{\varphi}| \longrightarrow 0$ at $\xi \longrightarrow +\infty$, $|\tilde{\varphi}| \longrightarrow \xi^\ell$ as $\xi \longrightarrow 0$.

We report here some preliminary results on the solution of this problem.

Both density and electric field were taken in Gaussian form (distance between respective maxima being taken $= \frac{1}{2}L_H$ and $\frac{L_H}{L_E} = 3$ with L_E typical electric field scale length). Unstable eigenvalues of (1) are examined in terms of the two parameters $W_E \sim \frac{(\omega_E)_{max}}{(\omega_D)_{max}}$ and ϵ^*.

In the case without electric field results seems to be in rather good agreement with what can be calculated from local theory (one has two branches, one of which is stable, the other unstable). We have followed the stable branch after introduction of a Gaussian shaped electric field, upon increasing its maximum amplitude.

In cases $W_E > 0$, corresponding to an electric field drift in the same direction as the ion diamagnetic drift, the unstable collisional drift wave (present at $W_E = 0$, if $\epsilon^* \neq 0$) appears to be modified upon increasing the electric field: both the frequency β and the growth rate γ are decreased with respect to the field-free case. One example of this is shown in Fig. 1 where β and γ (normalized to maximum drift frequency) are plotted as functions of ϵ^* for $W_E = 0$ and $W_E = +3$ (these curves refer to $\ell = 2$, $\frac{a_i}{L_H} = \frac{1}{6}$ and n = number of radial nodes of the eigensolutions = 0) There is thus a tendency to stabilization by the radial electric fields (at least up to values of W_E where electric drifts are still comprable with diamagnetic drifts).

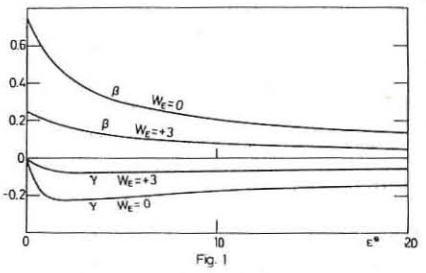

Fig. 1

Further work, both extending the range of electric field amplitudes considered and isolating the electric field effect from the effect of density inhomogeneity, is in progress.

REFERENCES

/ 1 / C.W. Hartmann and R.H. Munger, Proceedings of Conference on Physics of Quiescent Plasmas, Part I, Frascati 1967.

/ 2 / L. Enriques, A.M. Levine and G.B. Righetti, Proceedings of the Novosibirsk Conference on Plasma Physics, Vol. I Novosibirsk 1968.

/ 3 / F.F. Chen, Proceedings of the Novosibirsk Conference on Plasma Physics, Vol. I, Novosibirsk 1968.

/ 4 / G.I. Kent, N.C. Jen and F.F. Chen, Phys. Fluids 10, 2140 (1969).

/ 5 / D.L. Jassby and F.W. Perkins, Phys. Rev. Letts 6, 256 (1970).

/ 6 / A. Nocentini, Laboratori Gas Ionizzati, Frascati, Internal Report, LGI No. 68/30 (1968).

/ 7 / M. Dobrowolny, Proceedings of Conference on Physics of Quiescent Plasmas, Paris 1969.

/ 8 / M.N. Rosenbluth and A. Simon, Phys. Fluids 8, 1300 (1965).

CHARACTERISTICS AND CONTROL OF A DRIFT-TYPE INSTABILITY IN AN INHOMOGENEOUS LOW-β PLASMA

by

W. Friz, G. Müller*, J. C. Corbin, and R. S. Palmer,

Aerospace Research Laboratories, WPAFB, Dayton, Ohio, USA

Abstract: This paper is concerned with the stabilization of a drift-type instability at the edge of a Q-machine plasma column due to radial electric fields. Experimental results are compared with recent theories and the excitation and stabilization mechanism is discussed.

In a previous experimental work[1] it was shown that a drift-type instability can be stabilized due to non-uniform electric fields $\perp$ B. This paper presents recent investigations on the characteristics of this instability and the stabilization mechanism, performed in the Cs plasma column of a 2.5m long, single ended Q-machine. At plasma densities $n \gtrsim 1 \times 10^{10}$ cm^{-3} and at axial B-fields up to 3,500 Gauss, we observed density and potential low-frequency oscillations ($\omega < \omega_{ci}$) propagating with a dominating $m = 1$ mode and with a $k_\perp >> k_\parallel$ in the direction of the diamagnetic electron drift. The oscillation amplitudes $\tilde{n}$ peak at largest density gradient ∇n and largest non-uniformity of the radial electric field E_r, directed towards the plasma axis. Fig. 1 shows typical and directly recorded radial profiles measured with a radially driven probe near the center of the machine.

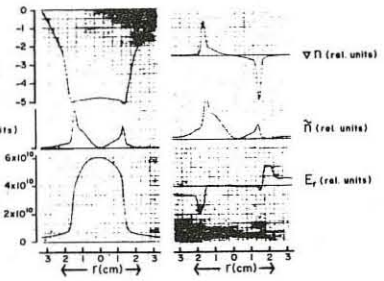

Fig. 1

By applying a d.c. voltage V_r between aperture ring and ionizer plate, the periphery potential and the radial electric field E_r in the edge region could be varied without any observable influence to the density gradient. As seen from Fig. 2, at small electric fields which correspond to negative V_r, the oscillations have smallest frequencies and largest amplitudes limited by the onset of a turbulence in the whole plasma column (noisy oscillations). The negative E_r grows with V_r, and the oscillations increase in frequency with simultaneously decreasing amplitude and disappear finally. Instability growth rates α/ω_o measured from the oscillation growing in time, when V_r is switched from the quiescent plasma state to more negative values, are shown in Fig. 2, bottom. The plasma is stable under collisionless conditions. In the collisional region the growth rates increase with the density and decrease with increasing V_r. Damping rates are shown in the lower portion of Fig. 3. They were derived from the oscillation decay, if V_r is switched from a fixed value to various more positive values, at which the plasma is quiescent under stationary conditions.

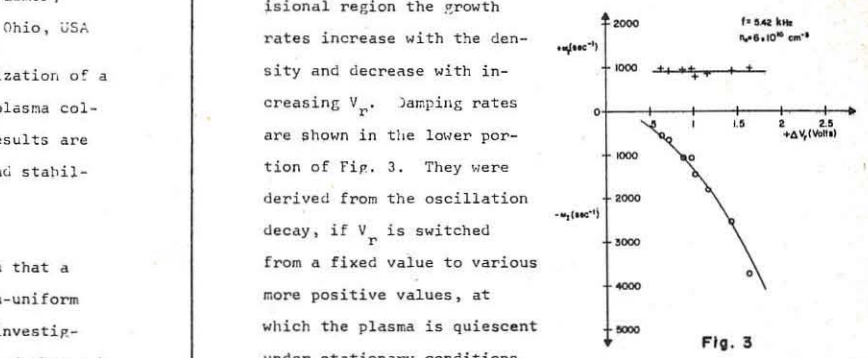

Fig. 2

Fig. 3

The increase in ΔV_r corresponds to an increase in the negative E_r. The upper curve of Fig. 3 shows growth rates of the same fixed instability states, which do not vary if they are switched on from different V_r in the quiescent state.

The instability causes enhanced radial ion fluxes which grow with $\tilde{n}^2$. Fig. 4 shows the radial plasma density variations Δn when the small amplitude instability is suppressed and amplified by a feedback method[4]. Much bigger plasma losses were observed in another machine in connection with azimuthal mode jumps m:2 → 1, constrained by either B-field or E_r variations[1].

From the experimental results of this investigation, we conclude that we observe a weak collisional drift-wave mode with a $\lambda \parallel$ B much larger than the machine length. In agreement with the theoretical work of Dobrowolny[2], we found increasing destabilization with growing plasma density and decreasing B-field. The drift-wave frequencies are Doppler shifted by an $E_r \times B$ drift due to the averaged negative E_r at the position of highest excitation. According to Nocentini[3], both ∇E_r (for $1/k_\perp >> r_L$) and $\nabla^2 E_r$, with the same sign as ∇n, should act as stabilizing terms. These stabilization conditions are fulfilled in our experiment. ∇n, ∇E_r, and $\nabla^2 E_r$ were found to be always negative and largest around the peak oscillations and the $\lambda_\perp$ is about 1 order larger than the Larmor radius r_L.

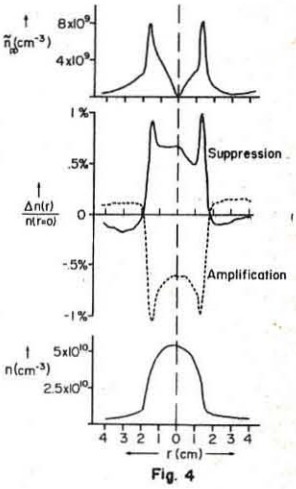

Fig. 4

*On leave from the Institut für Plasmaphysik, Garching, Germany

References:

1) G. Müller, Bull. Am. Phys. Soc. 14, 1055 (1969)

2) M. Dobrowolny, Proc. of the Int. Conf. on Phys. of Quiescent Plasmas, Paris, 1969, Pt. II, p. 11

3) A. Nocentini, J. Plasma Physics 3, 543 and 558 (1969)

4) G. Müller, J. C. Corbin, and R. S. Palmer, Symposium on Feedback & Dynamic Control of Plasmas, Princeton, N.J. (1970)

Invited Lecture

DYNAMIC STABILIZATION OF PERFECTLY DIAMAGNETIC PLASMAS

by

E.S. WEIBEL

Centre de Recherches en Physique des Plasmas
Lausanne . Switzerland

Abstract: As the word "perfectly" in the title implies this paper is primarily concerned with theoretical models. However experimental aspects of the problem are discussed briefly at the end.

There are many equilibrium configurations which describe the confinement of perfectly diamagnetic plasmas ($\beta = \infty$) by a magnetic field. However the configurations without cusps and of finite volume, that is all those of practical interest, are unstable. By varying periodically in time certain parameters of the confinement some or all of the surface deformation modes become stable. This is what we mean by Dynamic Stabilization. In practice the one parameter that can be oscillated is the magnetic Field. Three basically different types of dynamic stabilization of plasmas have been proposed. In the first type the confining field possesses no static component, its direction rotates in the plane tangential to the plasma surface. In the second type the field consists of a static and an oscillating component perpendicular to each other, so that the net field also changes its direction periodically. In the third type the magnetic field does not change direction but its intensity is varying periodically. Although it is probably not necessary we assume that the variations are sinusoidal. In all three cases the equation of motion for a given deformation mode has the form

$$(1) \qquad \int_0^t R(t-t')\,\dot{y}(t')\,dt' + (X + A\cos\omega t)\,y(t) = 0 \quad , \quad A > 0$$

(The labels on R, X, A and y, identifying the mode, have been suppressed). In this equation R(t) represents the pressure response of the plasma due to a deformation y(t) which has the form of a unit step in time. The Laplace transform $\hat{R}(s)$ of R(t) is the mechanical surface impedance of the plasma. The constants X and A depend only on the field configuration.
R(t) depends on the model of the plasma which one wishes to consider. If the model is incompressible and inviscid then $R(t) = M\dot{\delta}(t)$ so that (1) reduces to a Mathieu equation.

$$(2) \qquad M\ddot{y} + (X + A\cos\omega t)\,y = 0 \quad , \quad M > 0 \quad , \quad A > 0$$

In this case there will always be unstable modes.
If one assumes that the plasma consists of non interacting particles which are reflected from the plasma surface, but taking into account a single bounce, then $R = L\dot{\delta}(t)$ and the equation reduces to

$$L\dot{y} + (X + A\cos\omega t)\,y = 0 \quad , \quad L > 0 \quad , \quad A > 0$$

In this case the solution is obvious and the stability condition becomes simply $X > 0$ independent of A and of ω.
As one can see from these two examples the behaviour of the system is exceedingly sensitive to the type of response function R which is being used. To obtain realistic results it is necessary to calculate R from realistic plasma models. A better version of the free particle model is obtained if all successive bounces of the particles are taken into account. Then the pressure response becomes much more complicated but it still is highly dissipative. This is to be expected since the viscosity of a gas is proportional to the meanfree path. It is this dissipation which allows the dynamic stabilization of all modes.
We now turn our attention to the constants X and A which are determined by the geometry. In the first two types of confinement X can always be made positive for all modes by proper choice of the compression ratio. In this case dynamic stabilization of all modes is always possible. In the third type of confinement X is negative for an infinite number of modes. In this case, as Troyon* has shown, the stabilization of all modes is not always possible and in general difficult. This is intuitively understandable since $X > 0$ assures "average stability", that is stability for $\omega \to \infty$, while $X > 0$ leads to "average instability". Troyon's recent, yet unpublished work, which provides a general understanding of all previous work as well as numerical results for special cases will be summarized.
Experimental efforts to dynamically stabilize plasmas encounter two main difficulties: the need of large amounts of rf power and the screening of the oscillating field by low density residual plasmas outside the main body of the plasma. Recent progress on both fronts will be discussed.

References

E.S. Weibel, Phys. Fluids 3, 946 (1960). Earlier references on the subject can be found in this paper.

D.V. Orlinski, S.M. Osovets, V.I. Sinitsin, Plasma Physics and Controlled Fusion Research, Vol. II, 313. Proceedings of the Culham Conference (1964).

F.A. Haas and J.A. Wesson, Phys. Rev. Letters 19, 833 (1967).

F. Troyon, Phys. Fluids 10, 2660 (1967).

F.L. Ribe and W.B. Priesenfeld, Phys. Fluids 11, 2035 (1968).

J.A. Wesson and F.A. Haas, Phys. Fluids 12, 1271 (1969).

H.A.B. Bodin, E.P. Butt, J. Mc Cartan and G.H. Wolf, Third European Conference on Controlled Fusion and Plasma Physics, Utrecht, The Netherlands, 1969 (Wolters - Noordhoff Publishing - Groningen) p. 76.

R.F. Gribble, E.M. Little, W.E. Quinn, F.L. Ribe, G.A. Sawyer, K.S. Thomas D.M. Weldon, Utrecht, p. 79.

G. Berge, Phys. Fluids 13, 1031 (1970).

G.H. Wolf, Phys. Rev. Letters 24, 444 (1970)

STABILITY OF A ROTATING MAGNETIC FIELD PINCH

by

F. TROYON

Centre de Recherches en Physique des Plasmas

Lausanne - Switzerland

Abstract: The stability of a column of plasma, surrounded by a concentric conducting cylinder and confined by a rotating magnetic field is discussed in the collisionless and collision dominated limits. The assumption of a thin skinned plasma is discussed.

1. Introduction: An isothermal plasma column of radius a is confined by a rotating magnetic field obtained by superposing two oscillating magnetic fields

$$B_z = B\cos\omega t, \quad B_\theta = B\frac{a}{r}\sin\omega t$$

A conducting cylinder of radius b limits the magnetic field. The penetration of the field into the plasma is neglected (skin-effect).

A given mode of deformation of the plasma surface $\varepsilon_m(k,t)$ satisfies the equation [1,2].

$$(1) \qquad \{X_m(k) + A_m(k)\cos 2\omega t\}\,\varepsilon_m(k,t) + \int_o^t dt' R_m(k,t-t')\,\dot{\varepsilon}_m(k,t') = o$$

where m and k are the usual mode indexes. $R_m(k,t)$ is the plasma response function and $X_m(k)$ and $A_m(k)$ depend only on a, b, m and k. In a plane geometry $A_m(k) = X_m(k)$. In the cylindrical case we define $\Delta = (A_m(k)-X_m(k))/2$. It can be shown that $o \leq \Delta \leq 2p_o/a$, where p_o is the plasma pressure. The stability of Eq. (1) has been studied numerically, using the method of the determinant [2], for various models of the plasma. The following section summarizes the results.

2. Stability of the configuration

2.a. One fluid model: Neglecting viscosity and thermal conductivity, the equilibrium is always unstable. For any frequency there are modes which are "pumped" by the oscillating term of Eq. 1. The higher the frequency ω, the shorter the wavelengths which are unstable. The inclusion of a viscosity μ suffices to suppress these short wavelength instabilities, provided $\omega \gtrsim \cdot 07\ u^2/\mu$, where u is the sound velocity. Replacing μ by its expression in terms of the ion-ion collision frequency ν_i, this condition becomes $f = \frac{\omega}{2\pi} \gtrsim \cdot 01\ \nu_i$. The inclusion of thermal conductivity would lower the required frequency. These results apply only if $\nu_i \gg \frac{u}{a}$.

2.b. Collisionless models: When the mean free path becomes longer than the plasma radius a, the plasma is better described by the collisionless Vlasov equation. Even with the simplifying assumption of specular reflection at the plasma boundary the calculation of the response function in the long wavelength, low frequency range (ion waves domain) is still beyond our computational facilities. But it is possible to compute this function for a slab geometry, with the same assumptions. It has already been observed [2] that the response functions for symmetric and antisymmetric deformations of a slab of thickness 2a are very similar (qualitatively and quantitatively) to the response functions of the modes m = o and m = 1 respectively, if one neglects the electric field due to charge separation (bounce model). It is therefore reasonable to build a model for these two modes m = o and m = 1, using the correct expressions for $X_m(k)$ and $A_m(k)$ and the corresponding symmetric and antisymmetric response functions for a slab of thickness 2a, with the same value of k. Graphs showing the numerical results for a hydrogen plasma will be shown at the oral presentation. The most striking results are:

> The wall stabilizing effect: for $a/b \lesssim \cdot 9$ there is stability of all modes at a frequency $f \gtrsim \cdot 025\ u_i/a$ ($u_i = (2kT/m_i)^{\frac{1}{2}}$) and maybe at any frequency ω; for $a/b \lesssim 1/\sqrt{3}$ there is stability for $f \gtrsim u_i/a$.
>
> Only very long wavelengths ($\lambda \gtrsim 3.5\ a$) can become unstable for some values of ω and a/b.

This last result makes it very plausible that all the modes $m \geq 2$ are stable for all a/b and $f \geq \cdot 025\ u_i/a$ (smallest frequency considered). This conjecture is supported, on one hand by an examination of the bounce model response functions for these modes [2], which shows that they are very damped, and on the other hand by the fact that $X_m(k)$ is always positive for $m \geq 2$ and increases with m, for a fixed a/b.

3. Discussion: The results presented above are indeed very favourable. It is therefore crucial to look at the basic assumptions made which could invalidate the conclusions.

The main assumption is the possibility of obtaining such a configuration. It is not possible to prove that this configuration can be realized experimentally.

The creation of a vacuum field configuration around the plasma column may be impossible, because of the unavoidable residual plasma created by ionization of the neutral gas coming out of the walls or left behind during the formation of the column. Because the magnetic field components are alternating there is a continuous sweeping of this residual plasma. The speed of collection depends sensitively not only on the electrical properties of the residual plasma but also on the electrical properties of the plasma column itself. In some cases the residual plasma becomes hot before reaching the central column and holds the applied magnetic pressure alone, thus screening the field from the plasma column. This happens for example if the residual plasma has a higher resistivity than the plasma column. But there are also cases where the plasma is swept without appreciable heating and the magnetic pressure is indeed applied on the plasma column. Which one of these possibilities is realized experimentally will certainly depends on the history of the plasma and on the amount of residual plasma to be swept.

The neglecting of the penetration of the field into the plasma column is always justified, for any reasonable value of the plasma resistivity. In the collisionless regime the assumption of a specular reflection of particles at the plasma boundary is not essential. Turbulence or quasi-trapping of particles in the boundary will not affect the results since it leads to additional "mixing" of particles and thus to an increase in stability.

In conclusion it can be said that the stability of this configuration is established for a wide range of frequency ω and a/b.

4. References

1. E.S. WEIBEL Phys. Fluids 3, 946 (1960)

2. F. TROYON Phys. Fluids 10, 2660 (1967)

EXPERIMENTS ON THE ROTATING MAGNETIC FIELD PINCH

by

A. BERNEY, A. HEYM, F. HOFMANN, I.R. JONES and A. LIETTI

(Centre de Recherches en Physique des Plasmas,

Lausanne - Switzerland)

ABSTRACT: This paper presents the results and interpretation of measurements made on the 90 MW rotating magnetic field pinch and describes the progress made on a 720 MW experiment of the same type.

1. THE 90 MW EXPERIMENT

1.1 APPARATUS

The rotating magnetic field pinch is produced by the superposition of an alternating θ-pinch and an alternating Z-pinch. A detailed description of an apparatus constructed to generate such a pinch and some preliminary experimental results have previously been published[1]. The basic parameters are as follows:

Internal diameter of discharge tube	= 49 mm
Distance between Z-electrodes	= 488 mm
Length of θ-coil	= 430 mm
Maximum amplitude of $B_z(B_\theta)$ field at inner wall of discharge tube	= 2·1 (2·3) Kgauss
Frequency of rotation	= 3·1 MHz
Duration of rotating field	= 2·3 μsec

The experimental results which follow were obtained using helium as filling gas at initial pressures of 20, 60 and 180 mTorr.

1.2 MEASUREMENTS

The main conclusions of this experiment are based, primarily, on the following two measurements:

1.2.1 Electron line density profiles

The axial electron line density was measured by means of a Mach-Zehnder interferometer[2] which utilizes a He-Ne laser beam of 1 mm effective diameter. The time variation of the electron line density was measured with the laser beam located at a fixed radial position. Density profiles were obtained by repeating the measurement at a number of radial positions. Integration of these profiles over radius and length gave the total number of electrons, $N_e(t)$, present in the discharge tube at each instant.

1.2.2 Magnetic probe measurements

By making measurements with a double magnetic probe located at various radial positions, values of $B_\theta(r,t)$ and $B_z(r,t)$ were obtained with good space and time resolution. From a knowledge of the instantaneous magnetic field profiles, it was possible to calculate the rate of energy flow from the θ- and Z-circuits through the surface defined by the inner wall of the discharge tube as a function of time. Integration of these power curves gave the time variation of the energy, W(t), deposited in the discharge tube. The time dependence of the plasma surface resistivity, R_s, was also extracted from the magnetic probe data.

In addition to the above, streak and framing photographs of the pinch were made and electron and ion temperatures were measured (but with poor spatial resolution).

1.3 INTERPRETATION OF THE MEASUREMENTS

1.3.1 Plasma confinement

If the values of $N_e(t)$ and W(t) are known and if a reasonable hypothesis is made regarding the energy balance in the experiment, then it is possible to calculate the thermal energy of the plasma and hence the average plasma pressure, p(t). This quantity can be compared with the average magnetic pressure, $p_m(t)$, at the inner wall of the discharge tube.

If the ratio $p(t)/p_m(t) \leqslant 1{\cdot}0$, the plasma is magnetically confined. If, on the other hand, this ratio is greater than unity, then one can only have, at best, an inertial confinement of the plasma during the initial dynamic phase of the pinch. Once this phase has been passed, the plasma will only be partially confined by the magnetic field and thermal contact will be established between the plasma and the wall.

The results indicate that for the 20 and 60 mTorr He cases, the rate of plasma heating is such that before the end of the experiment, the plasma is no longer confined magnetically. For the 180 mTorr He case, however, the plasma remains magnetically confined throughout the duration of the rotating field pulse. The thermal energy of the plasma decreases with increasing filling pressure and is an immediate consequence of the fact that, whereas the input energy remains approximately constant for all the experimental conditions studied, ionization represents an energy sink which increases with filling pressure.

1.3.2 Electrical resistivity

During the first 1·5 μsec of the rotating field pinch, the plasma-field boundary is well characterized by a skin depth, δ, with which is associated an isotropic plasma resistivity, $\rho = R_s\delta$. Arguments based on energy considerations can be made to show that this isotropic resistivity has an anomalously high value. Furthermore, the existence of conditions favourable to the growth of micro-instabilities in the current-carrying skin layer can be inferred from the experimental data.

During the latter stage of the pinch ($t \geqslant 1{\cdot}5$ μsec), there is a momentary, enhanced penetration of the magnetic field which could be due to plasma motion and/or anisotropy of the plasma resistivity. It is plausible to assume that it is a velocity effect since it seems improbable that the plasma resistivity would suddenly become anisotropic.

2. THE 720 MW EXPERIMENT

Due to the high value of surface resistivity measured in the 90 MW experiment described above, the time interval during which magnetic overpressure exists is too short for the establishment of the desired magnetic field distribution. The required profile is one which approaches a vacuum field distribution near the tube wall and then falls to a negligible value within a thin plasma-field boundary. An experiment has been designed to investigate if such field profiles can be established in practice. Considerations of energy balance show that the duration of magnetic overpressure is proportional to the diameter of the discharge tube for a given magnetic field amplitude. The new experiment employs a discharge tube of 15 cm diameter and 80 cm length. Calculations show that with this tube diameter, magnetic overpressure should exist for the duration of the experiment, namely, 4 μsec.

2.1 APPARATUS

2.1.1 Preionization of the filling gas

A preionization system has been designed with the aim of obtaining the highest possible degree of ionization coupled with a minimum of impurity contamination. The scheme involves the successive discharging of two 180 KV Marx generators. The first of these produces a breakdown pulse (7·5 KA for 0·7 μsec) while the second generates the preionization pulse(15 KA for 1·5μsec).

2.1.2 Production of the rotating magnetic field

The large power which is required for this experiment is obtained from 24 line generators, each of which is capable of producing 30 MW[3]. The total power of 720 MW generates a 2·5 Kgauss, 3 MHz rotating field for a time duration of 4 μsec. A number of delicate technical problems have been overcome such as, for example, the synchronization of the generators (more than 300 spark-gaps are used) and rf isolation.

2.2 MEASUREMENTS

Measurements of the rf energy transfer and of the plasma resistivity are already underway. A preliminary study of the plasma dynamics is being made by means of streak photography.

ACKNOWLEDGEMENTS

The authors gratefully acknowledge the assistance of J.-M. Aeschlimann, P. Hafner, J.-P. Perotti, H. Ripper and M. Roux in the construction, maintenance and use of the experimental apparatus. They thank Prof. R.Keller, Prof. E.S. Weibel and Dr. F.S. Troyon for many fruitful discussions. This work was supported by the "Fonds National Suisse de la Recherche Scientifique".

REFERENCES

1. JONES I.R., LIETTI A. and PEIRY J.-M. (1968) Plasma Phys. 10, 213
2. HEYM A. (1968) Plasma Phys. 10, 1069
3. LIETTI A. (1969) Rev. Scient. Instrum. 40, 473

FOUR FLUID GENERALIZED M.H.D. COMPUTER CODE FOR A PARTIALLY IONIZED PLASMA

by F. Hofmann

Centre de Recherches en Physique des Plasmas, Lausanne

Avenue des Bains 21, 1007 Lausanne, Switzerland

Abstract: A computer program has been developed which solves the generalized M.H.D. equations (including electron inertia and drift velocity effects) for four fluids in one dimension. Results are presented and compared with measurements in the 90 MW rotating magnetic field pinch.

1. The Physical Model

The standard M.H.D. equations[1,2] implicitly contain the assumptions that electron drift velocities are small compared to thermal velocities, and that electron inertia is negligible. However, there are experimental situations where both of these conditions are violated. This is the case,for example, in a rotating magnetic field pinch experiment[3], where a high β plasma is confined by rapidly oscillating magnetic fields (~ 3MHz), and, hence, current densities are extremely high.

Such situations may be described by a generalized set of M.H.D. equations[4]. The generalization produces additional terms in the momentum equation for the charged particles, in the electron energy equation and in Ohm's law. The remaining equations are left unchanged.

In order to describe plasmas with two different kinds of ions (e.g. He),we introduce an additional continuity equation. The temperatures, however, as well as the fluid velocities, of the two ion species are assumed to be equal.

Consequently, in one dimension and cylindrical symmetry, we obtain a system of ten simultaneous equations, i.e., three continuity equations (one less than the number of fluids, due to charge neutrality), two momentum equations (charged particles and neutrals), three temperature equations (electrons, ions, and neutrals), and two equations for the magnetic field (B_θ, B_z).

Momentum and energy transfer between electrons, ions and neutrals due to ionization, recombination, charge exchange, and elastic scattering is taken into account. The transport and rate coefficients are assumed to be functions[2] of the local plasma parameters.

2. Numerical Methods

A one-dimensional computer code which solves the generalized M.H.D. equations described above, has been written. The program uses an implicit scheme in Lagrangian coordinates. The machine time requirement is approximately 0.5 sec per mesh point per time step on an I.B.M. 7040 computer.

3. Results

Fig. 1. shows the computed electron density as a function of radius, at various times. In this particular case, the following initial conditions were assumed: filling pressure = 60 mTorr He, 30% singly ionized, $T_e=T_i=T_o$ = 1 ev. Measured values were used as boundary conditions for the magnetic field components at the wall. Fig. 2. compares calculated and measured magnetic field profiles at various times (same conditions as in Fig. 1.). Similar comparisons were made for the electron density distributions, the degree of ionization, and the total energy contained in the plasma; these will be included in the oral presentation.

Acknowledgements

The author wishes to thank Dr. K.V. Roberts of Culham Laboratory and Dr. F. S. Troyon of Lausanne, for a number of discussions on the subject of this paper. This work was supported by the "Fonds National Suisse de la Recherche Scientifique".

References

1. K. Hain, G. Hain, K.V. Roberts, S.J. Roberts, Z. Naturforschung 15a,1039 (1960)
2. D. Düchs and H.R. Griem, Phys. Fluids 9, 1099 (1966)
3. A. Berney, et al., companion paper at this Conference
4. Shih-I Pai, "Magnetogasdynamics and Plasma Dynamics", Springer Verlag, Wien (1962).

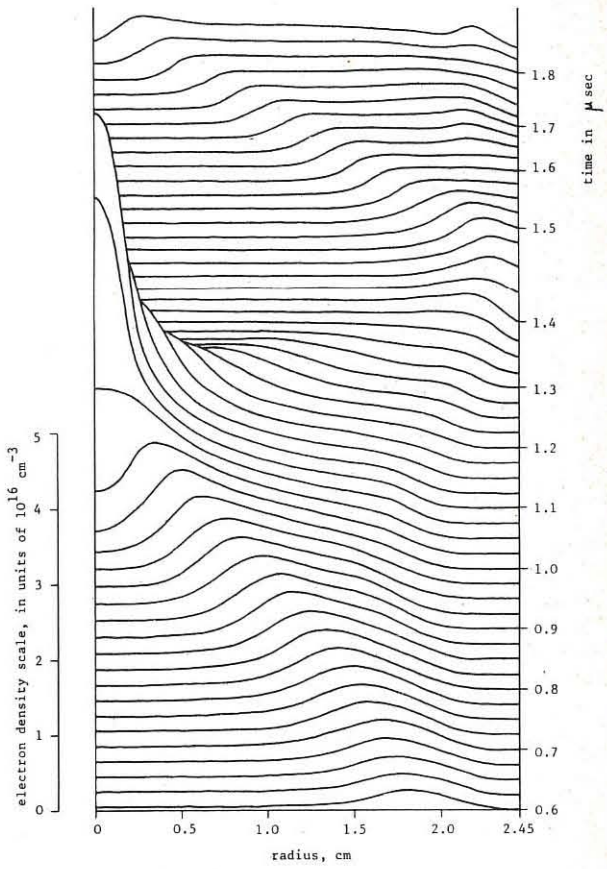

Fig. 1. Electron number density as a function of position and time

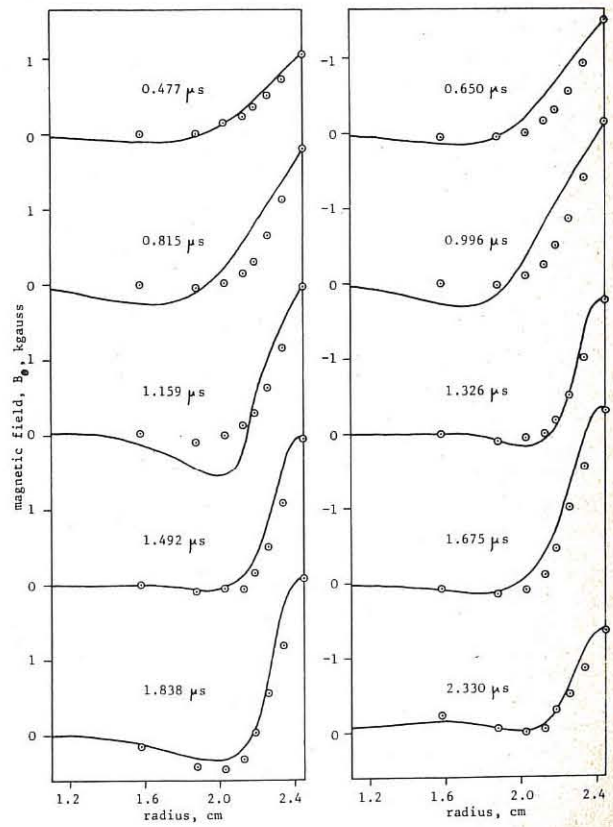

Fig. 2. Comparison between calculated (——) and measured (o) azimuthal magnetic fields (B_θ)

A linear screw pinch experiment with dynamic stabilization +)

by

G. Becker, O. Gruber, H. Herold

Institut für Plasmaphysik, Garching, Germany

Abstract: The growth of the helical m = 1 instabilities observed in a linear high β screw pinch can be reduced by means of a superposed oscillating B_z field if its amplitude and its frequency are chosen appropriately.

1) The object of the experiments to be described in this paper is to gain some insight into the experimental and technological possibilities for the stabilization of the most dangerous m = 1 (helical) instabilities of a linear high β screw pinch. In a first approach an oscillating superimposed B_z-field was applied for dynamic stabilization. Beforehand also the general stability behaviour of the linear screw pinch had to be studied in comparison with the results of theory /1,2/ and of a toroidal experiment /3/.

2) The screw pinch experiment with the basic circuits to produce B_z (up to 30 kG) and I_z (10 to 90 kA) is sketched in fig. 1. The ciruits for preionization and bias fields are omitted. The risetime ($T/4 \lesssim 4$ μsec) of the I_z and B_z are matched by variable inductances. The coil length and the electrode distance L are 1 m (i.d. 12 cm) resp. 1.2 m. The $\tilde{B}_z$ produced by a bank of high Q capacitors (Q = 90 at f = 2 Mc) is fed to the B_z coil via a foil switch with low inductance (2 nHy) and low resistance (< 1 mΩ at $\tilde{I}_\theta \gtrsim 200$ kA). A homogenous $\tilde{B}_z$ with an amplitude up to 3 kG, $\omega_s/2\pi = 1.1$ Mc and $\tau_{1/e} = 8$ μsec is achieved.

3) The plasma parameters in the screw pinch ($\tilde{B}_z = 0$) were: $T_e+T_i = 100$ to 500 eV; $n = 2$ to 10×10^{16} cm^{-3}. Helical m = 1 instabilities were observed in the pure screw pinch if $(I_z)_{max}$ was higher than a certain limit of about 15 kA. The growth rates ω_i determined by evaluating the exponential growth on steroscopic streak pictures agreed very well with those from constant pitch theory /2/ as well as with those derived from sharp boundary theory /1/ provided that values of μ measured at the boundary of the dense plasma column are inserted in:

$$\omega_i^2 = \left[-(2-\beta)\,k^2 + 2k\mu\right] \frac{(B_{z,ext}\cdot r_p)^2}{4\cdot \varrho_\ell} \;\Rightarrow\; \omega_{i\,max} = \frac{\mu \cdot v_A}{\sqrt{2-\beta}} \quad \text{at } k = \frac{\mu}{2-\beta}\,; \tag{1}$$

where ϱ_ℓ is the line mass and $\mu(r) = \frac{B_\theta(r)}{r\cdot B_z(r)}$; $\left(v_A = \frac{B\cdot r_p}{4\varrho_\ell}\right)$.

In all experiments, only one k mode was obersved for which just one wavelength fitted L. This is also supported by the "better agreement" using (1) and $k = \frac{2\pi}{L}$ as indicated in fig.2. So in the linear screw pinch a quasi periodicity condition holds, comparable to the Kruskal limit in a torus. A considerable fraction of I_z flows outside the dense plasma column. Constant pitch is only observed in the early stage of the discharge. It is lost in a characteristic way starting from the coil ends.

4) First the oscillating B_z was applied to a θ-pinch ($I_z = 0$) with ratio $\frac{(\tilde{B}_z)_{max}}{B_z}$ up to .2 and at times Δt_{HF} (see fig.4) up to 7 μsec. There was no deterioration of the θ-pinch stability i.e. no new modes were excited by parametric resonances (fig.3). Density measurements with a laser interferometer, with holographic interferometry and magnetic field measurements with probes indicated a radial surface motion which corresponds to $\frac{(\Delta r_p)_{max}}{r_p} \simeq \frac{(\tilde{B}_z)_{max}}{B_z}$ rather than $\frac{|\Delta r_p|}{r_p} \approx \frac{1}{2}\frac{|\tilde{B}_z|}{B_z}$ as expected for a relatively slow adiabatic motion with $\omega_s < \frac{v_A}{r_p}$. Moreover there was a shift of 120° to 150° between the forced oscillation of the plasma radius and the driving field.

5) If $\tilde{B}_z$ is applied to the screw pinch an appreciable decrease of m = 1 instability growth can be achieved, leading to a delay $\Delta t_c = t_c - \tilde{t}_c$ of wall contact. t_c and $\tilde{t}_c$ are the times between the start of the main discharge and wall contact without resp. with dynamic stabilization. This is shown in steroscopic streak pictures taken with 40 and 80 mtorr Deuterium in fig.5. Fig.4 gives a typical example for the currents and fields. In order to get an observable stabilizing effect, $(\tilde{B}_z)_{max}/B_z$ has to be greater than a critical value which depends on ω_i, provided that $\omega_s > \omega_i$; Table 1 gives examples.

ω_i [sec^{-1}]	$(\tilde{B}_z/B_z)_{crit}$	t_c [μsec]	$\tilde{t}_c$ [μsec]
$0.5 \cdot 10^6$	0.1 ÷ 0.12	10	15
$0.75 \cdot 10^6$	0.18 ÷ 0.2	7	12

There is not enough experimental material to confirm the expectation from theory that $(\tilde{B}_z/B_z)_{crit} \propto \frac{\omega_i}{\omega_s}$. The growth of the instability can still be reduced when the stabilizing field is switched on after an observable unstable displacement ξ ($\xi \lesssim r_p$) has taken place. This gives some hope for a potential application of feedback schemes.

6) Besides the stabilizing mechanism given by theory /4/ (the forced m = 0 motion of the plasma couples with the unstable m = 1 motion) there may be an additional stabilizing effect in our case. Probe measurements show that $B_\theta(r_p) \propto r_p$ and so $\mu(r_p) = \left(\frac{B_\theta}{r\cdot B_z}\right)_{r_p} \propto \frac{1}{B_z(r_p)}$.
Together with $\Delta r_p/r_p = \tilde{B}_z/B_z$ an inertially caused time dependence of μ/2-β at the plasma surface occurs, which should reduce the destabilizing time averaged potential of the unstable motion.

7) The efficiency of the stabilization is found to be dependent on the switch-on time of $\tilde{B}_z$ relative to the phase of the natural m = 0 plasma oscillation. Effective stabilization occurs, when the first maximum of $B_z+\tilde{B}_z$ coincides with a minimum of r_p. This can also be explained by the mechanism given in section 6.

/1/ M.D.Kruskal, and J.L.Tuck, Proc.Roy.Soc.Lond. A245, 222 (1958)
/2/ W.Schuurman, et al., Plasma Phys. 11, 495 (1969)
/3/ H.Zwicker, et al., presented at this conference
/4/ H.Wobig, and H.Tasso, to be published.

+) This work was performed as part of the joint research program between the Institut für Plasmaphysik, Garching and Euratom.

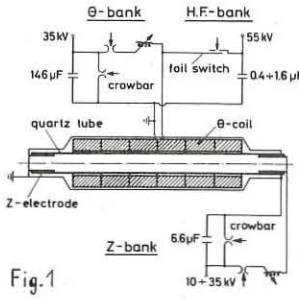

Fig.1

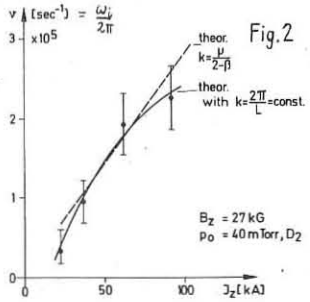

Fig.2

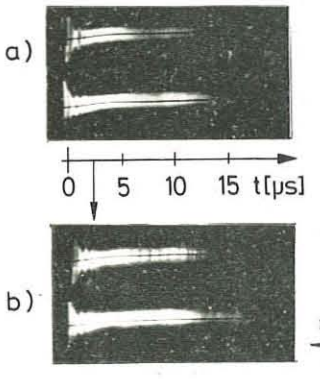

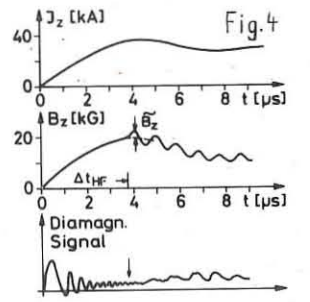

Fig.4

Fig.3: Linear θ-pinch (80 μD$_2$) without (a) and with (b) $\tilde{B}_z$.

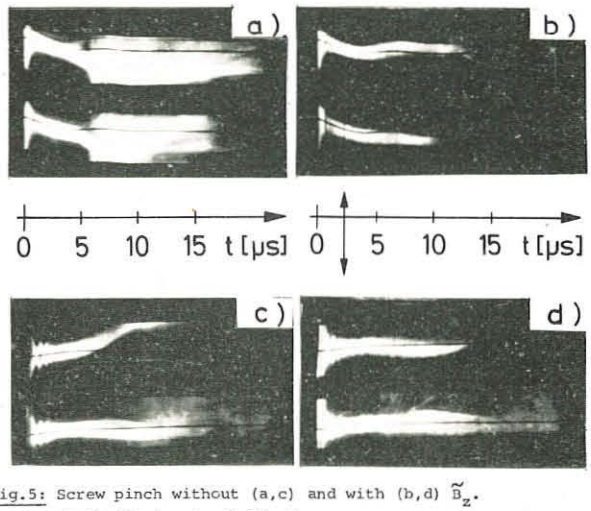

Fig.5: Screw pinch without (a,c) and with (b,d) $\tilde{B}_z$. (a,b) 40 μD$_2$; (c,d) 80 μD$_2$.

STUDY OF MAGNETIC FORCES FOR FEEDBACK STABILISATION OF HIGH BETA PLASMA

by

J. Junker[*], A.A. Newton[/] and H.A.B. Bodin[/]

/ U.K.A.E.A., Culham Laboratory, Abingdon, Berks., England.

* On attachment from Institut für Plasmaphysik, Garching, Germany.

Abstract: This paper reports an experimental study of the effects of magnetic forces due to a current dipole on a straight theta pinch plasma. The column remains cylindrical and its motion agrees with simple theory. The application of these results to the feedback control of the m = 1 instability of a bulged theta pinch[1,2] is discussed.

Introduction: Feedback control of M.H.D. instabilities in high β plasmas using magnetic forces is being studied[3,4]. In order to test the principles in a well-defined situation an experiment is being set up to study the suppression of the m = 1 mode of a bulged linear theta pinch[4]. It is necessary to know the nature and magnitude of these forces, and their influence on the plasma, and this paper describes a study of the effect of the forces from a single current dipole on a theta pinch plasma.

Nature of the Force: The method of producing the force by a current I_1 in a sector coil lying in a plane perpendicular to the coil axis is shown

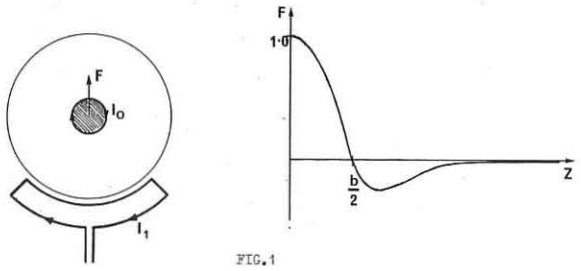

FIG.1

schematically in Fig.1. In addition to the diamagnetic current per unit length, I_o, a current, I', induced by I_1 flows in the plasma and gives a force per unit length of the form

$$F = F_1(I_o I_1) + F_2(I_o I') + F_3(I_1 I') \qquad \ldots (1)$$

F_1 and F_2 are linear in I_1 because $I' \propto I_1$ and F_3 is quadratic. It can be shown that $F_1 \gg F_2$ and for this experiment F_3 is negligible (except for $z \sim \frac{b}{2}$). For a straight plasma column

$$F(z) \cong F_1(z) = A_p A_d I_o I_1 (3b/r^5)(1 - 5 z^2/r^2) \qquad \ldots (2)$$

where A_p and A_d are the plasma and coil cross sectional areas, b is the perpendicular distance between the dipole and the plasma axis and $r^2 = b^2 + z^2$ where z is the distance along the axis measured from the coil plane. In the calculation we have assumed a sharp plasma boundary, a small circular current loop and neglected screening effects by conducting walls. The axial variation of F_1 is shown in Fig.1, where it can be seen that F_1 changes sign when $z = b/2$. The integrated linear force is zero, i.e. $\int_{-\infty}^{+\infty} F_1 \, dz = 0$. This result is expected since the mutual inductance between the dipole and an infinitely long plasma is zero. (The same holds for F_2 but not for F_3 which always has an integrated contribution.)

When the forces are time-varying propagation effects must be considered and a local plasma motion is possible. The equation for the plasma displacement, y(z,t),

$$\frac{\partial^2 y}{\partial t^2} = V^2 \frac{\partial^2 y}{\partial z^2} + F_1/M \qquad \ldots (3)$$

(M is the line mass and V the propagation speed) has been solved numerically for $F_1 \propto \sin \Omega t$ and the spatial variation of eq.(2). Fig.2 shows the displacement of the plasma with propagation superimposed. The displacement depends on the transit time of a wave compared to the period of the applied force. These results are for $V = 0.77\, b\Omega$.

Experiments have been carried out on a 2 M long theta-pinch using deuterium at 20 mtorr. Fig.3 shows that the driving field rises to 16 kG in 9 μsec and an alternating current in a three turn sector coil (geometry of Fig.1) of 10 kA peak and $\Omega = 2{\cdot}1 \times 10^6$ rad sec^{-1}. A streak photograph taken in a plane close to the coil shows an oscillatory motion of the plasma column (see Fig.3). Included for comparison is a picture taken with no current in the sector coil. The plasma motion is confined to a plane through the centre of the sector coil and the plasma axis. Its direction reverses, as expected with linear forces and quadratic effects are not observed. The plasma column retains its cylindrical symmetry.

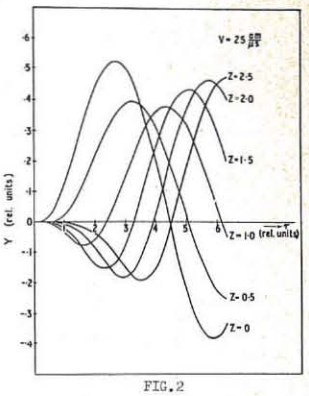

FIG.2

The observed displacement is consistent with the value calculated using eqs.(2) and (3) with corrections for the non-ideal geometry of the apparatus.

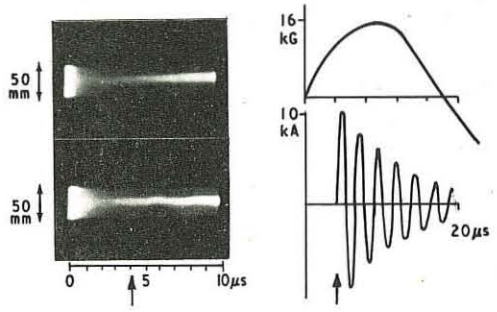

FIG.3

Conclusion and Application: The measured value of the linear force from a current dipole, deduced from the plasma motion it produces, agrees with theory for a uniform column. The calculation of the force has been extended to include a bulged plasma, and it is found that the bulge gives a large favourable local contribution to the force which therefore does not integrate to zero for a column of infinite length. For a bulge of length 2b with a maximum radius three times that of the remainder of the column and average beta 0.6 the linear force is a factor five greater than the unidirectional force (shaded curves, Fig.1) in the straight plasma.

We gratefully acknowledge J.B. Taylor and J.A. Wesson for discussions and C.A. Bunting, I.K. Pasco and A. Wootton for experimental assistance.

References

(1) H.A.B. Bodin, A.A. Newton, G.H. Wolf, J.A. Wesson. Culham Laboratory Preprint CLM-P 184, Phys. Fluids to be published.

(2) J. Junker, E. Fünfer, M. Kaufmann, J. Neuhauser, Bull. Am. Phys. Soc. Ser II 14 1049 (1969).

(3) A.I. Morozov, L.S. Solov'ev, Sov. Phys. Tech. Phys. 9 1214 (1965).

(4) A.A. Newton, J. Junker, H.A.B. Bodin. Symposium on the Dynamic and Feedback Control of Plasmas, Princeton, U.S.A., June 1970.

ON STABILITY OF A PLASMA IN THE HIGH-FREQUENCY AND CONSTANT MAGNETIC FIELDS

R.A.Demirkhanov, V.P.Sidorov, T.R.Soldatenkov, T.I.Gutkin, G.I.Boleslavskaya, S.N.Lozovsky, L.A.Utkina

Physico-Technical Institute of the State Committee on Utilization of Atomic Energy, Sukhumi, USSR

Abstract

In present paper the questions of the stability and confinement of the plasma in h.f. and constant magnetic fields are considered in two principal cases of the mutual orientation of the constant magnetic field and plasma surface-parallel and perpendicular (which correspond to some extent to the closed and open systems respectively).

I. We investigate in MHD approach the dynamic stabilization (DS) of the current-induced instabilities /I-3/ by means of helical multipole (HM) h.f. field which is created by the h.f. currents in the helical circuit. The circuit consists of helical windings placed on a cylindrical surface with radius b, the h.f. currents being $\vec{j} \sim exp\, i\{\Omega t + \ell_0 \varphi + k_0 z\}$. Such field configuration is realized in the RT-0 installation /4/. In particular we were interested in the question to which extent the h.f. circuit can be regarded as a stabilizing conducting wall. Due to HM currents in the plasma the h.f. magnetic field has a magnetic well form. Consequently we can expect an enhanced stability of the system. We have chosen the surface current distribution as the simplest one /5/. The skin-layer depth is assumed to be zero (this is valid if $\Omega > k_0 c_A$ /6/). For the sake of simplicity the helical circuit is replaced by the continuous current sheet with anisotropic conductivity.

Using the well-known technique /5/ we obtain after time-averaging the sufficient condition for DS of the helical perturbation modes:

$$\frac{(\ell+k_\parallel h_\ell)^2}{\varphi_1(\ell,k_\parallel)} + \frac{k_\parallel^2 h_r^2}{\varphi_2(\ell,k_\parallel)} - \frac{1}{2}\sum_{j=\pm 1}\left\{\beta_j^2 \frac{K_\ell'(\beta_j)}{K_\ell(\beta_j)} + \left(\sigma_j - \frac{\lambda_j M_j \tau_j}{b}\right)^2 \frac{1}{P_j}\frac{K_\ell'(\beta_j)}{K_\ell(\beta_j)} - \frac{\sigma_j^2 \tau_j^2 \beta_j}{P_j}\frac{K_\ell'(\beta_j)}{K_\ell(\beta_j)}\right\} + \tilde{E}_r^2 \gtrless 1 + \tilde{h}_\varphi^2 \qquad (I)$$

Here $\varphi_1 = k_\parallel \frac{K_{\ell-1}(k_\parallel)}{K_\ell(k_\parallel)} + \ell$; $\varphi_2 = k_\parallel \frac{I_{\ell-1}(k_\parallel)}{I_\ell(k_\parallel)} - \ell$; $\sigma_j = \frac{\ell_j}{\beta_j^2}\left(k_\parallel \tilde{h}_\varphi + \ell_j \tilde{E}_r\right) + \tilde{h}_z$; $\tau_j = \tilde{h}_\varphi + \frac{k_\parallel \tilde{E}_r}{\ell_j}$

$P_j = Q_j + \frac{\beta_j^2 M_j^2}{\ell^2 \rho^2} \lambda_j R_j$; $M_j = \frac{k_\parallel \ell_j}{\beta_j^2} - \frac{\ell_0}{k_0}$; $\beta_j^2 = k_j^2 - \rho_j^{-2}$; $\ell_j = \ell \pm \ell_0$; $k_j = k_\parallel \pm k_0$; $\ell_j = \pm\frac{\Omega}{c}$

Q_j, R_j, λ_j – are combinations of the modified Bessel functions, $\ell, k_\parallel$ – are the components of the perturbation wave vector.

The analysis of the DS criterion /I/ leads to the following conclusions:

a) The convective with respect to the h.f. magnetic field perturbations are absent in the quasi-stationary limit if $\ell_0 \neq 0$, $k_0 \neq 0$.

On increasing ℓ_0 the stabilizing effect increases.

b) There exist the resonant perturbations $M_j = 0$ $(\ell / k_\parallel = \ell / k_0)$ for which the helical h.f. circuit may be regarded as a perfectly conducting wall.

c) The most dangerous $(q = \frac{k_z H_{0z}}{\ell H_\varphi} = 1)$ perturbations can experience a stabilizing effect from the circuit its parameters being chosen such as to make the perturbations resonant.

d) $\tilde{H}_\varphi$ component of the h.f. field is responsible for the stabilization of long wave modes, $\tilde{H}_z$ component being responsible for the stabilization of the short wave ones.

e) If the zero helical mode ($\ell_0 = 0$, $k_0 = 0$) is used the convective perturbations are allowed. In this case the destabilization is possible.

We conclude that:

I. Multipole currents in a plasma are more stable than zero mode currents (d.c. in particular).

2. Using the multipole currents allows for lower values of q.

3. If these currents penetrate into a plasma they can simultaneously heat it /7/.

II. The effect of the h.f. field with components $\tilde{E}_z = E_{0z}(z)\sin\Omega t$ and $\tilde{H}_y = -\frac{c}{\Omega}\frac{\partial E_{0z}}{\partial x}\cos\Omega t$ on the drift instabilities of the slightly inhomogeneous plasma in the constant magnetic field H_{0z} is investigated, taking into account the h.f. field pressure, the oscillations of the resulting magnetic line of force and the electric h.f. component effect. The perturbed electric field is considered to be potential. If plasma is nonisothermic ($\tau = \frac{T_i}{T_e} < 1$) and the ion temperature gradients are not large, two eigenmodes of waves exist in a plasma; namely fast and slow ion-sound waves with frequencies $\omega_1 = \frac{\omega_{ce}^2}{\Omega}\omega^* - \omega_{ce}$ and $\omega_2 = -\frac{\beta^2}{\tau}\omega^* - \omega_{ce}$ and growth rates $\gamma_1 = -\frac{\sqrt{\pi}\,\omega^{*2}}{|k_z|v_{Te}}\left[\frac{\omega_{ce}^2}{\ell_e^2} + \frac{\ell}{\ell} + 1 - \frac{1}{2}\eta_e\right]\frac{\beta^4 \ell_e^4}{\tau^2 \omega_{ce}^4}$ and $\gamma_2 = -\frac{\sqrt{\pi}\,\omega^{*2}}{|k_z|v_{Te}}\left[\frac{\beta^2}{\tau} - \frac{\ell}{\ell} + 1 - \frac{1}{2}\eta_e\right]$.

Here $\omega_{ce} = k_y v_{de}^{eff}/\omega_{He}$, $\vec{g}_e^{eff} = -\nabla(\Phi_e + \Psi_e)$ is the effective "gravity acceleration", $\Phi_e = \frac{e^2 E_{0e}^2}{4 m_e^2 \Omega^2}$ is the h.f. potential /8/, Ψ is the electrostatic potential, $\frac{\ell}{\ell} = \frac{\omega_{ce}}{\omega^*} \approx \frac{\tilde{H}^2}{16\pi N T}$, $\eta_e = \frac{d(\ell n T_e)}{d(\ell n N)}$, $\omega^* = \frac{k_y T_e}{m_e \omega_{He} N'}$, $\omega_{He} = \frac{e H_{0z}}{m_e c}$, $\beta^2 = \frac{k_z^2 T_e}{m_i \omega^{*2}}$; $a_e = \frac{e \tilde{E}_{0e} k_z}{m_e \Omega^2}$, $\ell_e = \frac{k_y H_{0y} v_{Te}}{\Omega H_{0z}}$ are parameters which are determined by electric and magnetic h.f. components, respectively. For the drift waves we have $a_e, \ell_e \gg 1$. Plasma is stable against the excitation of the ion-sound mode if $\left(\frac{a_e^2}{\ell_e^2} + \frac{\ell}{\ell} + 1 - \frac{1}{2}\eta_e\right) > 0$. The stability region of the ion-sound wave is essentially enlarged. It is connected with the increase of the frequency of oscillations due to h.f. field effect on the plasma which results in increasing the electron Landau damping. The growth rate of the slow ion-sound wave does not change its sign, however its magnitude which is proportional to $\frac{\beta^2}{a_e^2}$ is considerably reduced. Although the terms due to the magnetic component of the h.f. field are small compared with those corresponding to the electric one still they essentially contribute to the oscillations growth rates if the frequencies of the h.f. field are not very far from the parametric resonance.

III. Let us consider a plasma occupying the half-space $z<0$ in a slightly inhomogeneous constant magnetic field $\vec{H}_0$ with $H_{0z} \gg H_{0x}, H_{0y}$. The h.f. field has the components: $\tilde{H}_x = \tilde{H}_0(z)\cos\Omega t$, $\tilde{H}_y = \tilde{H}_0(z)\sin\Omega t$. Due to effects connected with the inhomogeneity of the constant magnetic field it is possible to achieve some self-consistent equilibrium configurations for which $\tilde{\beta} = \frac{16\pi N T}{H_{0z}^2}$ can reach the values up to several units (in contrast with the statement made in /9/ that $\tilde{\beta} \approx 50$ in thermonuclear conditions). Supposing that plasma with $\beta = \frac{8\pi N T}{H_{0z}^2} \ll 1$ has the sharp boundary and the zero skin-layer, and that the inhomogeneity of the d.c. magnetic field can be neglected, we conclude that the plasma boundary is stable against the low-frequency ($\omega \ll \Omega$) MHD perturbations if the frequency of the h.f. field satisfies the condition $\Omega < \frac{k_\perp c}{\sqrt{2}} \equiv \Omega_{cr}$, where $k_\perp = \sqrt{k_x^2 + k_y^2}$ is the component of the perturbation wave vector on the xy-plane. When Ω exceeds Ω_{cr}, an alternation of stable and unstable regimes takes place. Note that the problem of the plasma boundary stability for the case considered has been previously investigated in /10/ but the consideration in this work is incorrect.

The authors are thankful to A.G.Kirov and L.I.Rudakov for useful discussions.

References

/1/. T.F.Volkov. Zh.T.F., 30, 497 (1960).
/2/. E.Weibel. Phys. of Fluids, 3, 946 (1960).
/3/. N.A.Bobyrev, O.I.Fedyanin. Zh.T.F., 33, 1187 (1963).
/4/. R.A.Demirkhanov et al. Plasma Physics and Controlled Nuclear Fusion Research, v.II, Vienna (1966).
/5/. V.D.Shafranov. Atomnaya Energiya, 5, 38 (1956); R.J.Taylor. Proc.Phys.Soc., 70B, 31 (1957).
/6/. T.I.Gutkin, S.N.Lozovsky, G.I.Boleslavskaya. Nuclear Fusion, 8, 109 (1968).
/7/. L.V.Dubovoi, V.I.Pistunovich, K.V.Khodatayev. The International Symposium on Closed Confinement Systems. Dubna, USSR (1969).
/8/. R.A.Demirkhanov, T.I.Gutkin, S.N.Lozovsky. Zh.E.T.F., 55, 2195 (1968).
/9/. C.J.H.Watson. In Culham Report CIM-R94 (1969).
/10/. V.A.Petržilka, J.Teichmann. Czech.J. of Phys. 14B, 485 (1964).

Invited Lecture

SUPRA-THERMAL ELECTRIC FIELD FLUCTUATIONS FROM SPECTRAL LINE PROFILE MEASUREMENTS

by

Hans R. Griem

UNIVERSITY OF MARYLAND

College Park, Maryland, U.S.A.

Most experimental and theoretical work on the broadening of spectral lines by interactions between charged particles in a plasma and radiating atomic systems has been concerned with Stark effects from particle-produced microfields. Compared to the latter, wave-produced fields are indeed small for equilibrium plasmas having a large number of electrons in the Debye sphere. However, for wave excitation much beyond equipartition at the particle temperatures, collective fields can influence spectral line profiles very strongly, so that in conjunction with line broadening theory supra-thermal field fluctuations and their frequency spectra may be obtained from observed line profiles. (Wave number spectra cannot be determined, the size of the probing atomic systems being negligible compared with plasma wave lengths.) Two distinct methods have evolved, one utilizing one-electron systems (linear Stark effect) and based on theoretical work by Blochinzew [1], the other utilizing two-or more-electron systems (quadratic Stark effect) and based on theoretical work by Autler and Townes [2] and, more specificly, Baranger and Mozer [3]. In the first case, all plasma frequencies are often small compared with Stark shifts so that the line shape reflects the distribution of wave-field amplitudes (regardless of frequency). This gives then near Gaussian line shapes, rather than suitably modified [4] Holtsmark profiles, and has been demonstrated experimentally [5]. More information on plasma waves or turbulence can be obtained by the second method which, to lowest order, gives the power spectrum of the electric field if measured frequencies are referred to those of forbidden ($\Delta\ell = 0, \pm 2$) lines and if the so-called plasma satellites are measured relative to the corresponding allowed ($\Delta\ell = \pm 1$) lines. Such satellites displaced from the forbidden lines by + or - the plasma frequency were predicted by Baranger and Mozer [3] and first found experimentally [6] in a helium-filled theta pinch. Since then much more experimental work has been done on plasma satellites of neutral helium lines in several laboratories and also some theoretical work, both on higher order effects and on the prediction of satellite shapes for certain idealized non-equilibrium plasmas. This work will be reviewed and the complementarity of the new method to that of cooperative light scattering emphasized.

[1]. D. I. Blochinzew, Physik. Z. Sowjetunion 4, 501 (1933).

[2]. S. H. Autler and C. H. Townes, Phys. Rev. 100, 703 (1955).

[3]. M. Baranger and B. Mozer, Phys. Rev. 123, 25 (1961).

[4]. P. Kepple and H. R. Griem, Phys. Rev. 173, 317 (1968).

[5]. H. R. Griem and H.-J. Kunze, Phys. Rev. Letters 23, 1279 (1969).

[6]. H.-J. Kunze and H. R. Griem, Phys. Rev. Letters 21, 1048 (1968).

Non-Linear Effects Involving Electron Plasma Waves

by

R.N. Franklin and G.J. Smith
Engineering Laboratory, Oxford University

and

S.M. Hamberger, G. Lampis
U.K.A.E.A., Culham Laboratory, England.

Abstract: Observations are presented of the frequency spectrum in a plasma when large amplitude electron plasma waves are excited. The spreading to side band frequencies is shown and the development of structure in the lower sideband detected. Parametric processes are also discussed.

It is now well established experimentally that electron plasma waves are damped by the collisionless phase-mixing process normally described as Landau damping. An early interpretation of the physical process underlying the wave-particle distribution-function interaction was that of electrons being trapped in the potential well of the wave[1]. This, while not appropriate to the linear regime of Landau damping, has been shown by Wharton, Malmberg and O'Neil[2] to describe effects observed when large amplitude waves propagate in a plasma.

Their interpretation was in terms of 'sidebands' being produced at frequencies $\omega \pm \Omega$ where $\Omega = (eEk/m)^{\frac{1}{2}}$ is the frequency of oscillation of an electron in the potential well of the wave. ω, ω is the frequency of the imposed signal with wave number k and associated field strength E. Recently Eldridge[3] has calculated the spectrum of frequencies in the range $\omega - \Omega$ to $\omega + \Omega$ for a potential V propagating through a plasma. For eV/k_BT_e finite, there is a spread of frequencies with local maxima at $\omega \pm 0.8\,\Omega$.

We have measured the frequency spectrum for the parameter eV/k_BT_e between zero and unity. Fig.1 shows the output of an X-Y recorder driven by a spectrum analyser for frequencies near the wave frequency, 30 MHz, when a wave was excited in the plasma column of a single ended Q-machine. The plasma frequency determined from the propagation of small amplitude waves[4] was 45 MHz. Results are given for different values of r.f. voltage applied to the exciting probe. The frequency spreading is clearly non linear and the primary wave energy is converted predominantly to lower frequencies in agreement with theory[3]. The linear damping was negligible over the length of the plasma column (65 cm). Fig.2 shows the variation of signal at the centre of the lower sideband with distance from the exciter when the excitation voltage was 9.0 volts corresponding to V ≈ 0.15 Volts. The signal rises to a maximum in a distance smaller than the linear damping length. Fig.2 shows that the sideband signal does not rise monotonically but depends on the local level of the large amplitude signal as found previously[3].

The new results, shown clearly in Fig.1, are (i) the observation of the upper sideband, with smaller magnitude, and (ii) the development of structure within the lower sideband with distance both as predicted by Eldridge.

Spectra were studied in the range 0-100 MHz. There is no detectable signal at the frequency of oscillation of the electrons in the potential well. Parametric decay into other electron waves is not observed for wave powers transmitted $\lesssim$ 10 mW. The conditions of Laval, Pellat, and Perulli[5] who observed such parametric decay differed from ours in that they had several wave modes available within the frequency band ω to $\omega - \Omega$ at the power levels used.

We have, however, observed at much smaller amplitudes, an apparent parametric decay involving the generation of a heavily damped ($\gamma/\omega \simeq 0.4$) ion acoustic wave. There was a threshold at a probe voltage ~ 1 mV and saturation occurred for a probe voltage ~ 200 mV. We have shown that ion waves have a dominant wavelength one half that of the pumping wave for a range of electron wave frequencies. This is to be expected since the pump and idler wave numbers are almost equal in magnitude so that $k = k_p - k_i \sim 2\,kp$. We have not as yet obtained quantitative results to compare with the calculations of Dysthe and Franklin[6]. Oscillations were also excited at the ion cyclotron frequency (133 kHz for a sodium plasma at 2.0 kG).

The effects observed are of significance in assessing the importance of different processes in the development of a spectrum of frequencies from a single coherent electron plasma wave.

References

1. Bohm, D., and Gross, E.P., Phys.Rev. (1949) 75, 1864.
2. Wharton, C.B., Malmberg, J.H., and O'Neil, T.M., Physics of Fluids (1968) 11, 1761.
3. Eldridge, O., Physics of Fluids (1970) 13, 738.
4. Barrett, P.J., Jones, H.G., and Frankoin, R.N., Plasma Physics (1968), 10, 911.
5. Laval, G., Pellat, R., and Perulli, M., Plasma Physics (1969) 11, 579.
6. Dysthe, K.B., and Franklin, R.N., Plasma Physics (1970) (in the press).

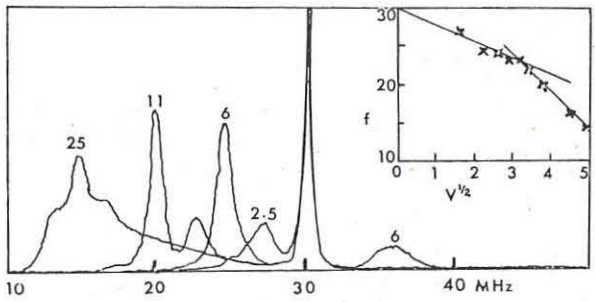

Figure 1 Frequency spectrum observed 30 cm from the exciter when rf voltages of the values indicated at 30 MHz are applied to the exciter. The inset shows that the dominant lower sideband frequency tends to a linear variation with probe voltage at large applied voltages.

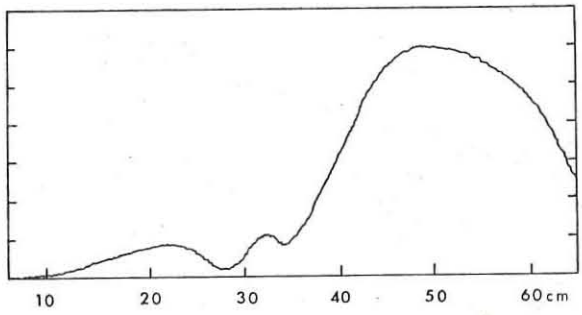

Figure 2 The power at the central lower sideband frequency, 36.25 MHz, in arbitrary units as a function of distance from the exciter when an rf voltage of 9.0 V at 40 MHz was applied. Similar shaped curves were obtained for other applied frequencies at this level of voltage.

INTERACTION OF LOW FREQUENCY WAVES WITH MICROTURBULENCE

André Rogister
European Space Research Institute
Frascati (Italy)

We have investigated in the framework of kinetic theory, the interaction of low frequency, large scale (compared to the ion Larmor radius R_i and frequency Ω_i) oscillations with high frequency, short wavelength ($\lambda \ll R_i$, $\omega \gg \Omega_i$) electrostatic microturbulence. In the general case, the relaxation of a weakly turbulent homogeneous plasma proceeds according to different time scales corresponding to different processes: quasi-linear relaxation of high-frequency oscillations build-up, non-linear spectral energy transfer and absorption of turbulent pulsations in plasmon-particle interactions. Two other time scales appear in the present problem: $\tau_{\ell.f.}$ corresponding to the low frequency wave and τ_i corresponding to its interaction with the turbulence (plasmon-wave-plasmon interaction).

The fundamental hypothesis to be made is that the energy spectrum of the turbulence, $\mathcal{E}_q$, and the one-particle distribution functions, F_r, relax to a non trivial ($\mathcal{E}_q \neq 0$) quasi-linear "equilibrium" on a time-scale τ_s *which is much shorter than the time-scales of interest*, $\tau_{\ell.f.}$ and τ_i which in turn, are very short compared to the time-scale for absorption of turbulent pulsations.

It was shown in a recent paper[1] that in the drift approximation, even relatively weak electrostatic (Langmuir) turbulence may lead, for example, to stabilization of drift waves. This effect is associated with the presence of particles which resonate with the low frequency wave. Although related processes could be understood in the context of the following theory, we are concerned here with another type of stabilization, or excitation, mechanism which results from the combined effects of turbulence and finite ion Larmor radius (f.l.r) and frequency (f.l.f.). We have shown that the turbulence leads to spatial diffusion (or antidiffusion) of the low frequency wave. In high and low β plasma alike the diffusion coefficient is found to scale like Bohm's:

$$D \sim \lambda \frac{c\Theta}{qB} \quad , \tag{1}$$

where Θ is the temperature in energy units, B the magnetic field, q the charge and c the velocity of light. In the example considered here of the interaction of an Alfvén wave with ion-sound turbulence, λ is the ratio to thermal energy of the *total* energy of the turbulence.

Since only non resonant particles play a role in the process just described, the theory of the interaction is akin to a macroscopic formulation; this remark helps clarifying the following point. In general the distribution functions will be functional of the energy spectrum of the turbulence. We have neglected that functional dependance and indeed assumed that scattering by plasmons is a rather inefficient process to randomize most of the particles. That assumption, which at the very least is justified for not too strong turbulence, plays here a role equivalent to Boltzman H-theorem for binary collisions.

Following the discussion given above, we have kept in the collision integral only those terms which describe the coupling with the turbulence of the electromagnetic field and the spatio-temporal gradients of the organized wave. The exact structure of the terms describing the interaction of course depends on the properties of the quasi-linear "equilibrium" spectrum of the turbulence after the initial relaxation is over. We have postulated, merely for the purpose of convenience, that the turbulence,

i) is one-dimensional, with its wave vectors orthogonal to a plane ($\hat{i}_z - \hat{i}_x$) spanned by the background gradients,

ii) can be approximated by a wave packet of central wave number q_c, frequency $\omega_c \gg \Omega_c$ (the electron gyrofrequency) and phase velocity $V_c = \omega_c/q_c$.

Under those conditions, the collision term takes the form

$$\frac{q_r}{m_r}\frac{\partial}{\partial \underline{v}} \cdot \underset{\sim}{\mathcal{C}}_r \equiv \frac{q_r^2}{m_r^2}\frac{\partial}{\partial v_y}\frac{1}{v_c - v_y}\left[\frac{q_r}{m_r}(\underline{E} + \frac{\underline{v}}{c} \times \underline{B}) \cdot \frac{\partial}{\partial \underline{v}} + \frac{1}{2}\underline{V} \cdot \frac{\partial}{\partial \underline{x}}\Big|_{F,v_c} + \right.$$

$$\left. + \frac{\partial}{\partial t}\Big|_{I_c} + \Gamma_c + \Delta_c\right]$$

$$\frac{1}{v_c - v_y}\frac{\partial}{\partial v_y} F_r I_c \tag{2}$$

$$+ \frac{1}{2}\frac{q_r^2}{m_r^2}\left[\frac{\partial}{\partial v_y}\frac{1}{v_c - v_y}\frac{\partial}{\partial \underline{v}} \cdot \frac{\partial}{\partial \underline{x}}\Big|_{F,v_c} - \frac{\partial}{\partial \underline{v}} \cdot \frac{\partial}{\partial \underline{x}}\Big|_{F,v_c}\frac{1}{v_c - v_y}\frac{\partial}{\partial v_y}\right] F_r I_c$$

where $\hat{i}_y \equiv \underline{q}_c/q_c$; $V_y \equiv \hat{i}_y \cdot \underline{v}$; $\partial/\partial \underline{x}|_{F,v_c}$ operates only on I_c and $\partial/\partial t|_{I_c}$ on F_r and V_c. The other notations but Γ_c and Δ_c are standard; in particular I_c is related to the total energy of the microturbulence by the relation $\mathcal{E}_c = \frac{1}{8\pi}\omega_c\left(\frac{\partial \varepsilon'(\omega,q_c)}{\partial \omega}\right)_{\omega_c} q_c^2 I_c$ where $\varepsilon'(\omega,q_c)$ is the (real part) of the dielectric function of the turbulence.

It is of course understood that the denominators in these expressions must be considered as Cauchy principal values. Lastly,

$$\Gamma_c \equiv -\left(\frac{\partial \varepsilon'(\omega,q_c)}{\partial \omega}\right)^{-1}_{\omega_c}\left(\frac{\partial}{\partial t}\Big|_{v_c} + \frac{1}{2}\frac{\partial}{\partial t}\Big|_{F_r}\right)\left(\frac{\partial \varepsilon'(\omega,q_c)}{\partial \omega}\right)_{\omega_c} \tag{3a}$$

and

$$\Delta_c \equiv q_c^{-1}\left(\frac{\partial \varepsilon'(\omega,q_c)}{\partial \omega}\right)^{-1}_{\omega_c} 4\pi \sum \frac{q_r^2 n_r}{m_r q_c^2}\int dv \frac{1}{v_c - v_y}\frac{q_r}{m_r}(\underline{E} + \frac{\underline{v}}{c} \times \underline{B}) \cdot \frac{\partial}{\partial \underline{v}}\frac{1}{v_c - v_y}\frac{\partial}{\partial v_y} F_r \tag{3b}$$

In order to complete the definition of the collision term, we note that

$$\frac{1}{2}\frac{\partial^{(i)}}{\partial t} I_c = (\Gamma_c + \Delta_c) I_c \quad ; \tag{4}$$

the use of the superscript (i), for interaction, is necessary for, during the early process of quasi-linear relaxation, the turbulent spectrum becomes a functional of the background distribution function, and thus also varies in space and time accordingly. In these equations, the terms associated with the presence of large scale spatial inhomogeneities, and with the time variation of the background can be seen to agree with the results of references (2) and (3,4) respectively if one notes that the last term of equation (2) disappears in one-dimension ($\underline{q}_c // \partial/\partial \underline{x}$). The other terms of equations (2) and (4) describe the interaction of the "weak" ($\Omega_i \ll \omega_c$) background electromagnetic field with the microturbulence. The spatio temporal evolution of the background distribution function is of course connected to the evolution of the electromagnetic field through Maxwell's equations.

The above problem is intended to serve as a guide for more general types of interaction of microturbulence with low frequency waves, or eventually with a spatially inhomogeneous stationary background plasma. Particular fields of application include "collisionless" shock waves (in high β plasma) and anomalous diffusion, due to microturbulence, of otherwise stationary non-uniform plasma in fusion devices.

REFERENCES

1) Krivoroutsky, E.N., V.G. Makhankov and V.N. Tsytovich, Nucl. Fus. 9, 97, 1969.

2) Drummond, W.E., Phys. Fluids 7, 816, 1964.

3) Rogister, A. and C. Oberman, J. Plasma Phys. 3, 119, 1969.

4) Frieman, E. and P. Rutherford, Ann. Phys. 28, 134, 1964.

TEST WAVES IN A TURBULENT PLASMA

by

Christian Thomas Dum

Cornell University, Ithaca, New York, U. S. A.

Abstract: The conductivity tensor of a turbulent plasma is computed from the coherent response of the plasma to an external test wave. We include nonexpandable effects due to scattering of particles and modification of dielectric properties by the turbulent spectrum, which may become important, even at low levels of turbulence.

A test wave propagating through a turbulent plasma may experience an enhanced damping which is similar to collisional damping. The effective collision frequency, however, may be enhanced by several orders of magnitude, even at low levels of turbulence. It, thus, appears that scattering of particles and the modification of dielectric properties by "turbulent collisions" should be included in a perturbation theory as nonexpendable effects. Scattering of particles may be included by perturbing the equation for the average distribution function, retaining terms to first order in the external electric field $\langle E_q \rangle$ of the testwave

$$\left[\frac{\partial}{\partial t} + \underline{v}\cdot\frac{\partial}{\partial \underline{x}} + \frac{e_j}{m_j}(\underline{v}/c \times \underline{B}_o)\cdot\frac{\partial}{\partial \underline{v}} - D\right]\langle f_q\rangle =$$

$$-\frac{e_j}{m_j}\langle E_q\rangle\cdot\frac{\partial}{\partial \underline{v}}\langle f\rangle + D^{(1)}\langle f\rangle \qquad (1)$$

where $\langle f_q \rangle$ is the coherent response of the plasma to $\langle E_q \rangle$, D is the diffusion operator and $D^{(1)}$ is the perturbation of this operator induced by the test wave. The solution of (1) with the right hand side set equal to zero determines the average propagator $\langle U(t,t')\rangle$ of a test particle distribution in the turbulent plasma. Eq. (1) may be solved in terms of $\langle U \rangle$. This procedure is frequently used to find ordinary collisional conductivity. In applying it to a turbulent plasma, it must be noted that turbulent diffusion depends on the electric field as seen by a test particle moving along its perturbed orbit. Thus we take D to be given by [1]

$$D\langle f(t)\rangle = \frac{\partial}{\partial \underline{v}}\cdot\left(\frac{e_j}{m_j}\right)^2 \sum_{\underline{k}} \underline{E}_{-\underline{k}}(t)\int_{-\infty}^{t} dt' \langle U(t,t')\rangle \underline{E}_{\underline{k}}(t')\cdot\frac{\partial}{\partial \underline{v}}\langle f(t')\rangle \qquad (2)$$

D allows a particle to pull itself into resonance with waves if the turbulent field exceeds a certain threshold.[2,3] Conventional perturbation theory, based upon unperturbed orbits cannot predict such a behavior. The modification of the linear wave-particle resonance by orbit perturbation leads to a rapid stabilization of a number of instabilities [2,3]. For the purpose of estimating the saturation level of these instabilities, it is then probably not too important to include mode coupling effects.

Coupling between the test wave and the background waves is, however, responsible for a coherent response of the plasma which is described by the term $D^{(1)}$. The coupling between waves is also modified by the presence of other waves. Using (2) in (1) we can obtain an equation for the coherent current in terms of $\langle E_q \rangle$ the spectrum $\underline{E}_{\underline{k}}$ and the induced spectrum $\underline{E}^{(1)}_{\underline{k}+\underline{q}}$.

$$\langle J\rangle = \underline{\underline{\kappa}}^{(1)}(\underline{q},\omega)\cdot\langle E_q\rangle + \sum_{\underline{k}} \underline{\underline{\kappa}}^{(2)}(\underline{q}+\underline{k},-\underline{k}) : \langle \underline{E}^{(1)}_{\underline{q}+\underline{k}}\, \underline{E}_{-\underline{k}}\rangle + \underline{\underline{\kappa}}^{(3)}(-\underline{k},\underline{q},\underline{k}) :$$

$$\langle \underline{E}_{-\underline{k}}\underline{E}_{\underline{k}}\rangle\langle \underline{E}_{\underline{q}}\rangle \equiv \underline{\underline{\kappa}}(\underline{q}\omega)\cdot\langle E_q\rangle \qquad (3)$$

where the conductivity tensors are obtained from the usual expressions after replacing the unperturbed propagators by $\langle U \rangle$. $\underline{\underline{\kappa}}^{(1)}$ is due to the linear wave particle interaction and $\underline{\underline{\kappa}}^{(2)}$, $\underline{\underline{\kappa}}^{(3)}$ lead to coupling between waves. The beat wave $\underline{E}^{(1)}_{\underline{q}+\underline{k}}$ is the coherent response of the turbulent plasma to the source current $\underline{J}^{(2)}_{\underline{q}+\underline{k}} = \underline{\underline{\kappa}}^{(2)}(\underline{q},\underline{k}) : \langle E_q \rangle \underline{E}_{\underline{k}}$ and, thus, should be computed using that turbulent condutivity $\underline{\underline{\kappa}}$ obtained from (3) and Maxwell's equations. Choosing the electrostatic case $\underline{E}_{\underline{k}} = -i\underline{k}\phi_{\underline{k}}$ for simplicity, we obtain explicitly

$$\varepsilon(\underline{q},\omega) = \varepsilon^{(1)}(\underline{q},\omega) + \sum_{\underline{k}} |\phi_{\underline{k}}|^2 \left\{\varepsilon^{(3)}(-\underline{k},\underline{q},\underline{k}) - \varepsilon^{(2)}(\underline{q}+\underline{k},-\underline{k})\cdot\right.$$

$$\left.\varepsilon^{(2)}(\underline{q},\underline{k})/\varepsilon(\underline{q}+\underline{k})\right\} \qquad (4)$$

for the dielectric constant of a turbulent plasma. Eq. (4) is equivalent to selective summing of an infinite number of terms in the usual perturbation series which is generated by a simple iteration from the unperturbed state. The first term in (4) is obtained from the solution of (1), neglecting the nonlinear coupling terms and can frequently be approximated by an expression of the form ($B_o = 0$) [2,3]

$$\langle f_q\rangle = -\frac{e_j}{m_j}\langle E_q\rangle\frac{\partial\langle f\rangle}{\partial v}\frac{i}{\omega - \underline{q}\cdot\underline{v} + i\nu} \qquad (5)$$

where ν is an effective collision frequency which depends on velocity, the turbulent spectrum and on frequency and wavenumber of the test wave. The reactive approximation which is commonly used in calculations of high frequency conductivity requires $\nu \ll \omega$. Anamolous resistivity, in this case, arises solely from the coupling between the test wave and the background spectrum. It is described by the remaining terms in (4). The resonant contribution from these terms yields the damping of the test wave due to scattering into wave modes $\underline{k}' = \underline{k}+\underline{q}$, $\omega_{\underline{k}'} = \omega_{\underline{k}}+\omega$ and the nonresonant contribution describes nonlinear Landau damping. For resonance, $1/\varepsilon$ may be still be replaced by a delta function. No significant changes from the usual resonant mode coupling result are to be expected. Even small changes in $\varepsilon(\underline{q}+\underline{k})$, however, may be important in the nonresonant case if $\varepsilon(\underline{q}+\underline{k}) \neq 0$ but small. If e.g. a driftwave interacts with high frequency turbulence, we have $\varepsilon(\underline{q}+\underline{k}) = \varepsilon(\underline{k},\omega_{\underline{k}}) + \partial\varepsilon/\partial\omega_{\underline{k}}(\omega - \underline{q}\cdot\partial\omega_{\underline{k}}/\omega\underline{k}$ but $\varepsilon(k,\omega_{\underline{k}}) = 0$ is the high frequency dispersion relation. Small changes in the imaginary parts of $\varepsilon^{(2)}$, $\varepsilon^{(3)}$ which enter nonlinear Landau damping could also be significant.

None of the above modifications of the usual perturbation theory are important for the high frequency ($\omega \gg \nu$) conductivity of a stable plasma. It may be shown that our result contains this case if the turbulent spectrum is replaced by the thermal spectrum $|\phi_{\underline{k}}|^2 \to |\phi_{\underline{k}\omega}|^2 \to 0$. The approach in this paper allows the discussion of high frequency resistivity in terms of mode-coupling theory. Calculation of the anamolous damping of specific transverse test waves in a turbulent plasma are under way.

This work has been supported by the U.S. Atomic Energy Commission under Contract AT-(30-1)-3782.

1. T. H. Dupree, Phys. Fluids, 9, 1733, (1966).

2. T. H. Dupree, Phys. Fluids, 11, 2684, (1968).

3. C. T. Dum and T. H. Dupree, Phys. Fluids, 13, August 1970.

LAGRANGIAN DERIVATION OF WAVE-WAVE COUPLING COEFFICIENTS

by

J. J. Galloway and F. W. Crawford

INSTITUTE FOR PLASMA RESEARCH

Stanford University, California, U.S.A.

Abstract: A Lagrangian technique is applied to the determination of plasma wave-wave coupling coefficients. It depends on space-time averaging of an expanded Lagrangian density, rather than the conventional iteration of the corresponding Euler equations, and is considerably more economical in effort. As an example, explicit results are given for three-wave coupling at arbitrary propagation angles in a cold infinite magnetoplasma.

Introduction: An impediment in the derivation of wave-wave coupling coefficients is the algebraic complexity of the iterative process leading from Maxwell's equations and an equation of motion to the canonical coupled mode equations. For three-wave interaction satisfying the synchronism conditions $\omega_1 + \omega_2 = \omega_3$, $\underset{\sim}{k}_1 + \underset{\sim}{k}_2 = \underset{\sim}{k}_3$, the latter may be written as[1]

$$\frac{i}{\omega_{1,2}}\left(\frac{\partial}{\partial t} + \underset{\sim}{v}_{g1,2}\cdot\nabla\right)\hat{A}_{1,2} = \chi^{*}\hat{A}^{*}_{2,1}\hat{A}_3 \ , \quad \frac{i}{\omega_3}\left(\frac{\partial}{\partial t} + \underset{\sim}{v}_{g3}\cdot\nabla\right)\hat{A}_3 = \chi\hat{A}_1\hat{A}_2 \ , \qquad (1)$$

where the normalized complex amplitudes, $\hat{A}_n$, are defined so that $\hat{A}_n\hat{A}^{*}_n$ is a generalized energy density; $\underset{\sim}{v}_{gn}$ is the group velocity, and χ is the wave coupling coefficient.

Since (1) can be derived from the Lagrangian density, $\mathcal{L}$, of the system,[1] the possibility arises that χ might be obtainable more directly by manipulation of $\mathcal{L}$. We shall show that this is so, and apply the method to a specific example.

Method: We assume a homogeneous plasma with $\mathcal{L}(q^i_t, \underset{\sim}{x})$ a function of the scalar variables $q^i_t (i=1,\ldots m)$: their first spatial and temporal derivatives $\partial q^i_t/\partial x_j$, $\dot{q}^i_t$, and position, $\underset{\sim}{x}$. For weak coupling, the small-signal solutions are perturbed slowly in time and space, so that for some wave parameter $a_n = \mathrm{Re}(\hat{a}_n) = \mathrm{Re}(\hat{a}_n \exp i(\omega_n t - \underset{\sim}{k}_n\cdot\underset{\sim}{x}))$ the amplitude $\hat{a}_n$ may only vary by $\delta\hat{a}_n/|\hat{a}_n\hat{a}_n| \ll 1$ over intervals of order $1/\omega_n$ and $1/k_n$.

We now replace q^i_t by $q^i_e(\underset{\sim}{x}) + q^i$ in $\mathcal{L}$, and the corresponding Hamiltonian density, $\mathcal{E}(q^i_t, \underset{\sim}{x}, t)\left[\equiv \sum_i \dot{q}^i_t\,\partial\mathcal{L}/\partial\dot{q}^i_t - \mathcal{L}\right]$, where the $q^i_e(\underset{\sim}{x})$ represent an equilibrium solution to the equations, and the q^i are small perturbations. Expansion to third order is sufficient for three-wave interactions and yields

$$\mathcal{L}(q^i, \underset{\sim}{x}) \approx \mathcal{L}_0 + \mathcal{L}_1 + \mathcal{L}_2 + \mathcal{L}_3 \ , \quad \mathcal{E}(q^i, \underset{\sim}{x}) \approx \mathcal{E}_0 + \mathcal{E}_1 + \mathcal{E}_2 + \mathcal{E}_3 \ . \qquad (2)$$

The q^i may be split into their wave components $q^i_1 + q^i_2 + q^i_3\left[\equiv \mathrm{Re}(q^i_1 + q^i_2 + q^i_3)\right]$, and a generalized energy density may be defined for the nth wave as $\epsilon_n = \mathcal{E}_2(q^i_n, \underset{\sim}{x})$, where the bar denotes space-time averaging over intervals long compared to $1/\omega_n$ and $1/k_n$, but short compared to the variations of the wave amplitudes. The kth spatial component of the corresponding generalized energy flux vector is

$$\phi_{nk} \equiv \overline{\sum_i \dot{q}^i_n\,\partial\mathcal{L}_2(q^i_n, \underset{\sim}{x})/\partial[\partial q^i_n/\partial x_k]} = v_{gnk}\epsilon_n \ . \qquad (3)$$

Finally, the three-wave coupling energy is defined by

$$\epsilon_0 \equiv (1/3)\,\overline{\mathcal{L}_3(q^i_1 + q^i_2 + q^{i*}_3, \underset{\sim}{x})} + (\text{complex conjugate, c.c.}) \ . \qquad (4)$$

The next step is to express ϵ_0 , ϵ_n and ϕ_n in terms of $\hat{a}_n$ for each wave, using only the small-signal relations derivable from $\mathcal{L}_2$. This procedure gives[2]

$$\epsilon_0 = \Gamma_0\,\hat{a}_1\hat{a}_2\hat{a}^{*}_3 + (\text{c.c.}) \ , \quad \epsilon_n = \Gamma_n\hat{a}_n\hat{a}^{*}_n \ , \quad \phi_n = v_{gn}\epsilon_n \ , \qquad (5)$$

where the Γ's are functions of the ω_n and k_n , and are related to the quantities of (1) by

$$\hat{A}_n = \hat{a}_n\,\Gamma_n^{1/2} \ , \quad \chi = \Gamma_0/|\Gamma_1\Gamma_2\Gamma_3|^{1/2} \ . \qquad (6)$$

Thus, to obtain the coupling coefficient χ , we first evaluate the generalized energy densities and fluxes, ϵ_0 , ϵ_n , ϕ_n . We then obtain Γ_0 , Γ_n from (5) and substitute them in the expressions for χ , and the $\hat{A}_n$.

Example: We now consider a cold homogeneous magnetoplasma, for which

$$\mathcal{L} = \dot{A}^2 - [V_t - \underset{\sim}{\dot{A}}\cdot\underset{\sim}{A}_t]^2 + (\nabla V_t + \underset{\sim}{\dot{A}}_t)^2/2 - (\nabla\times\underset{\sim}{A}_t)/2 \ , \qquad (7)$$

and dimensionless variables have been used for the scalar and vector potentials $V_t (\equiv eV_t/mc^2)$, $\underset{\sim}{A}_t (\equiv e\underset{\sim}{A}_t/mc)$: the particle displacement $\Lambda (\equiv \delta\underset{\sim}{x}\,\omega_0/c)$ from the equilibrium position $\underset{\sim}{X} (\equiv \underset{\sim}{x}\omega_0/c)$, and for the time $T (\equiv \omega_0 t)$. Here, ω_0 is the plasma frequency. Both V_t and $\underset{\sim}{A}_t$ in the square brackets are functions of $\underset{\sim}{X} + \underset{\sim}{\Lambda}$. All other terms are functions of $\underset{\sim}{X}$ only. Expansion of (7) yields

$$\mathcal{L}_2 = \dot{\Lambda}^2 + \underset{\sim}{\dot{\Lambda}}\cdot\left(\underset{\sim}{A} + \sum_k \Lambda_k\frac{\partial\underset{\sim}{A}_0}{\partial X_k}\right) + \frac{[\dot{A}^2 - (\nabla\times\underset{\sim}{A})^2]}{2} \ , \quad \mathcal{L}_3 = \underset{\sim}{\dot{\Lambda}}\cdot\Sigma_k\Lambda_k\frac{\partial\underset{\sim}{A}}{\partial X_k} \ , \qquad (8)$$

where we have chosen a gauge such that V_t is constant $(\nabla\cdot\underset{\sim}{A} = -\int^t \dot{N}dt')$.

For small-signal propagation as $\exp i(\Omega T - \underset{\sim}{K}\cdot\underset{\sim}{X})$ we have

$$\begin{bmatrix} S-\Pi^2\cos^2\theta, & iD & \Pi^2\cos\theta\,\sin\theta \\ -iD, & S-\Pi^2, & 0 \\ \Pi^2\cos\theta\,\sin\theta, & 0 & P-\Pi^2\sin^2\theta \end{bmatrix}\cdot\underset{\sim}{E} = 0 \qquad \begin{array}{l} \Pi^2 \equiv K^2/\Omega^2, \ P \equiv 1-1/\Omega^2 , \\ S \equiv 1-1/(\Omega^2-\Omega_c^2) , \\ D \equiv \Omega_c/\Omega(\Omega^2-\Omega_c^2) , \end{array} \qquad (9)$$

where $\underset{\sim}{K}$ lies in the x-z plane at θ to the z-axis. A rotation operator, R , will be used to generalize the propagation to the spherical angles θ,ϕ . For $0 < \theta < \pi/2$, all $\underset{\sim}{E}$ components are nonzero. We will choose to express $\underset{\sim}{\Lambda}$ and $\underset{\sim}{A}$ in terms of the component E_p perpendicular to $\underset{\sim}{K}$ and the z-axis. We then have $\Lambda_n = \Sigma_n E_{pn}$, $A_n = T_n E_{pn}$, $\underset{\sim}{\Sigma} = R\,\underset{\sim}{\Sigma}'$, $\underset{\sim}{T} = R\,\underset{\sim}{T}'$,

$$R \equiv \begin{bmatrix} \cos\phi, & -\sin\phi, & 0 \\ \sin\phi, & \cos\phi, & 0 \\ 0, & 0, & 1 \end{bmatrix}, \quad \underset{\sim}{\Sigma}' \equiv \begin{bmatrix} i[(\Omega/\Omega_c)(S-\Pi^2)+D] \\ \Pi^2 - S - (\Omega/\Omega_c)D \\ -i\,\dfrac{\Pi^2(S-\Pi^2)\cos\theta\sin\theta}{\Omega^2 D(P-\Pi^2\sin^2\theta)} \end{bmatrix}, \quad \underset{\sim}{T}' \equiv \begin{bmatrix} S-\Pi^2/\Omega D \\ i/\Omega \\ -\dfrac{\Pi^2(S-\Pi^2)\cos\theta\sin\theta}{\Omega D(P-\Pi^2\sin^2\theta)} \end{bmatrix}, \qquad (10)$$

Use of these in (3) and (4) yields

$$\epsilon_0 = (1/8)\overline{\mathcal{L}_3(\Lambda_1 + \Lambda_2 + \Lambda^{*}_3, A_1 + A_2 + A^{*}_3, \underset{\sim}{x})} + (\text{c.c.}) = i\Gamma_0\hat{E}_{p1}\hat{E}_{p2}\hat{E}^{*}_{p3} + (\text{c.c.})$$

$$\phi_n = -\,\dot{\underset{\sim}{A}}_n\times(\nabla\times\underset{\sim}{A}_n) = v_{gn}\Gamma_n\hat{E}_{pn}\hat{E}^{*}_{pn} \ ,$$

$$\Gamma_0 = \frac{1}{8}\begin{Bmatrix} \Omega_1\Sigma_1\cdot[(\underset{\sim}{\Sigma}_2\cdot\underset{\sim}{K}_2)\underset{\sim}{T}^{*}_3 - (\underset{\sim}{\Sigma}^{*}_3\cdot\underset{\sim}{K}_2)\underset{\sim}{T}_2] \\ + \Omega_2\underset{\sim}{\Sigma}_2\cdot[(\underset{\sim}{\Sigma}_1\cdot\underset{\sim}{K}_1)\underset{\sim}{T}^{*}_3 - (\underset{\sim}{\Sigma}^{*}_3\cdot\underset{\sim}{K}_1)\underset{\sim}{T}_1] \\ + \Omega_3\underset{\sim}{\Sigma}^{*}_3\cdot[(\underset{\sim}{\Sigma}_1\cdot\underset{\sim}{K}_2)\underset{\sim}{T}_2 + (\underset{\sim}{\Sigma}_2\cdot\underset{\sim}{K}_1)\underset{\sim}{T}_1] \end{Bmatrix}, \quad v_{gn}\Gamma_n = \Omega_n^2\begin{Bmatrix} T^2_{n-n}/2 \\ -(\underset{\sim}{\Pi}_n\cdot\underset{\sim}{T}_n)\underset{\sim}{T}^{*}_n/4 \\ -(\underset{\sim}{\Pi}_n\cdot\underset{\sim}{T}^{*}_n)\underset{\sim}{T}_n/4 \end{Bmatrix} \qquad (11)$$

The small-signal dispersion relation gives v_{gn} , so Γ_0, Γ_n are known and hence χ . The coupled mode equations for spatial wave growth are

$$(i\Gamma_{1,2}v_{g1,2}/\Omega_{1,2})\cdot\nabla\hat{E}_{p1,2} = \Gamma_0\hat{E}^{*}_{p2}\hat{E}^{*}_{p3} \ , \quad (i\Gamma_3 v_{g3}/\Omega_3)\cdot\nabla\hat{E}_{p3} = \Gamma_0\hat{E}_{p1}\hat{E}_{p2} \ . \qquad (12)$$

There is a well known elliptic integral solution of (12) for collinear propagation.[3] If one (pump) wave is much stronger than the other two, simpler solutions result for parametric amplification and frequency conversion. For all $\theta_n \approx 0$, results for coupling of three RH-polarized waves are obtained. For all $\theta_n = \pi/2$, and all ϕ_n equal, extraordinary mode coupling results are obtained. Comparison of previous analyses of these cases[4] demonstrates the efficacy of the Lagrangian method.

Discussion: Here, a cold magnetoplasma example has been treated. Our unpublished results extend the work to warm plasma wave coupling, using a Lagrangian based on macroscopic plasma theory. The most desirable future development is the inclusion of hot plasma effects, perhaps using Low's Lagrangian[5] as a starting point. This forms the subject of our current studies, and would allow inclusion of collisionless damping, and explosive instability.[6]

(1) A. E. Siegman, Proc. IEEE, 54, 756 (1966).

(2) J. J. Galloway, Stanford University IPR Report No. 362 (1970)[unpubl.].

(3) R. Z. Sagdeev and A. A. Galeev, Nonlinear Plasma Theory (Benjamin, N. Y., 1969).

(4) K. J. Harker and F. W. Crawford, J. Geophys. Res. 74, 5029 (1969); J. Appl. Phys. 40, 3247 (1969).

(5) F. E. Low, Proc. Roy. Soc. A248, 282 (1954).

(6) M. N. Rosenbluth, B. Coppi, and R. N. Sudan, Proc. Third International Fusion Conf., Novosibirsk (IAEA, Vienna, 1969) 1, 771.

THE STOCHASTIC MODEL OF MODE-COUPLING-THEORIES

by

K. Elsässer and P. Gräff*

Max-Planck-Institut für Physik und Astrophysik, München

Institut für Plasmaphysik, Garching b. München, Germany

Abstract: The hierarchy equations describing weakly interacting waves in a fluid are solved by the method of characteristic functionals, combined with the time asymptotic method of Krylov-Bogoljubov-Mitropolski. All fluid quantities look - in the stochastic sense - like solutions of a Langevin equation; they consist of a "friction" term into which the initial values (at t=0) enter and a stochastically independent Gaussian noise (turned on at t=0).

The hierarchy problem of homogeneous weak turbulence can be solved within the framework of a time asymptotic perturbation theory [1)2)]. To represent the hierarchy we introduce the generating functional Z of the wave correlations, given by [2)]

$$Z(t,a) = \log \left\langle \exp\left[\sum_\alpha \int d^3k \; a_\alpha(k)\, c_\alpha(k,t)\right]\right\rangle$$

Here α labels the different frequencies $\omega_\alpha(k)$ corresponding to a wave vector k, $c_\alpha(k,t)$ is a (stochastic) wave amplitude, and $a_\alpha(k)$ is an (arbitrary) test function. The brackets $\langle\ \rangle$ denote "taking the expectation value", which can be done, for instance by averaging over the phases of the waves at time t=0. The simplest examples of nonlinear wave interaction lead to the following type of equation for the wave amplitudes:

$$\frac{\partial}{\partial t} c_\alpha(k,t) = \varepsilon \sum_{\alpha'\alpha''} \int d^3k' \int d^3k'' \, \overset{\circ}{v}_{\alpha\alpha'\alpha''}(k k' k'')\, \delta^3(k-k'-k'')\, e^{i(\omega_\alpha(k)-\omega_{\alpha'}(k')-\omega_{\alpha''}(k''))t} \cdot \left(c_{\alpha'}(k',t)\, c_{\alpha''}(k'',t) - \langle c_{\alpha'}(k',t)\, c_{\alpha''}(k'',t)\rangle\right)$$

where the smallness parameter ε is a measure of the largest wave amplitudes, and $\overset{\circ}{v}_{\alpha\alpha'\alpha''}(kk'k'')$ is the interaction matrix. From this we obtain an equation for the time variation of $Z(t,a)$ which can be solved by the following ansatz:

$$Z = \bar{Z} + \sum_{\nu>0} \varepsilon^\nu \tilde{Z}^\nu(t,\bar{Z})$$

$$\frac{\partial}{\partial t}\bar{Z} = \sum_{\nu>0} \varepsilon^\nu P^\nu(\bar{Z})$$

The "main part" $\bar{Z}$ of Z is uniquely defined by the following two requirements: 1) $\bar{Z}$ generates correlations which are "smooth functions" in k-space, and 2) $Z-\bar{Z}$ is not secular with respect to the explicit time dependence. In the limit $\varepsilon\to 0$, $t\to\infty$, $\varepsilon^2 t$ = finite we obtain the following solution for $\bar{Z}$:

$$\bar{Z}(t,a) = Z_G(t,a) + Z_0\left(a\cdot \exp\{H(t)\}\right)$$

where $Z_G(t,a)$ is the functional of a Gaussian process and $Z_0(a)$ is the functional which generates the initial correlations (at t=0). The function $H_\alpha(k,t)$ depends on the spectrum $J_\alpha(k,t)$ in the following way:

$$H_\alpha(k,t) = \sum_{\alpha'\alpha''} \int d^3k' \int d^3k'' \, \frac{4i\,\delta^3(k-k'-k'')}{(\omega_\alpha(k)-\omega_{\alpha'}(k')-\omega_{\alpha''}(k''))^+} \, \overset{\circ}{v}_{\alpha\alpha'\alpha''}(k k' k'') \cdot \overset{\circ}{v}_{\alpha''\alpha\alpha'}(k'',k,-k') \cdot \varepsilon^2 \int_0^t dt' \, J_{\alpha'}(k',t')$$

The correlation $J_\alpha(k,t)$ of the Gaussian functional Z_G is given by

$$G_\alpha(k,t) = J_\alpha(k,t) - \exp\left\{2\,\mathrm{Re}\, H_\alpha(k,t)\right\} J_\alpha(k,t=0)$$

where $J_\alpha(k,t)$ obeys the usual kinetic wave equation. To interpret these results we consider a vector $\psi(x,t) = (\psi^j(x,t))$ whose elements are identical with the perturbations of the fluid quantities (density, velocity, electric field, ...). The x-space representation of our functional $\bar{Z}$ is equivalent to the following stochastic equation for $\psi(x,t)$:

$$\psi(x,t) = \int d^3x' \, K(x-x',t)\cdot \psi_0(x') + \gamma(x,t) \qquad (1)$$

The kernel $K(\xi,t)$ is given by its Fourier transform:

$$\sum_\alpha (2\pi)^{-1} \chi_\alpha(k)\, \tilde{\chi}_\alpha(k)\, \exp\left\{H_\alpha(k,t)\right\}$$

where $\chi_\alpha(k)\,\tilde{\chi}_\alpha(k)$ is the dyadic product of the orthogonal normalized eigenvectors of the linearized problem. $\psi_0(x)$ is the initial value of $\psi(x,t)$, and $\gamma(x,t)$ is a Gaussian variable whose variance is essentially determined by $G_\alpha(k,t)$. Equation (1) can be interpreted as a Langevin equation of Brownian motion, suitably generalized to describe the stochastic state of a fluid. The first term on the r.h.s. of (1) is analogous to the "friction" term, whereas $\gamma(x,t)$ is due to a stochastic force with Gaussian statistics. The latter is due to the resonant three wave processes. If the resonance condition cannot be fulfilled we have

$$\frac{1}{2}\frac{\partial}{\partial \varepsilon^2 t} G_\alpha(k,t) = \mathrm{Re}\left(\frac{\partial}{\partial \varepsilon^2 t} H_\alpha(k,t)\right) G_\alpha(k,t)$$

and therefore $G_\alpha(k,t)\equiv 0$, i.e. no Gaussian noise. In this case no information is lost.

* This work has been undertaken as part of the joint research programme of the Institute of Plasmaphysik and Euratom.

1) K. Elsässer, MPI-PAE/Astro 24 (1969) submitted to J. Plasma Phys.

2) K. Elsässer and P. Gräff, MPI-PAE/Astro 32 (1970) submitted to Ann. Phys.

AN APPROACH TO A THEORY OF STRONG TURBULENCE

by

Daniel R. Wells

Department of Physics, University of Miami, Coral Gables, Florida, U.S.A.

Abstract: A new approach to magnetohydrodynamic flow stability is outlined. The concept of space-time and gauge symmetries of the flow fields are utilized in developing a nonlinear global theory of stability.

A new theory of nonlinear global magnetohydrodynamic stability is described. The formalism is not an extension of quasi linear or normal mode cascade theory, but an entirely new approach to the problem which leads to a theory of strong turbulence. One invokes the concept of space-time and various gauge symmetries of the flow fields in order to find constants of the motion. These constants of the motion are used in conjunction with the principle of least constraint to find the Euler-LaGrange equations corresponding to stable plasma motion. For every symmetry there is a corresponding conserved integral (Noether's theorem). If that symmetry is broken, then that integral constraint must not be applied to the problem. Once all the symmetries and constraint integrals have been found, one applies the principle of least constraint. This principle states that if the total energy of the flow field is varied, subject to a set of constraint integrals, then the fewer the number of constraint integrals applied, the more stable the resulting flow. The minimum number of constraint integrals which apply to a linear (superposable) field results in a set of equations which describe a collinear flow. If linearity is sacrificed, then fewer constraints can be used and the resulting structure is a rigid rotator or rigid drift equilibrium centered on the magnetic guide field lines. Many types of plasma flow structure are possible depending on what symmetries are broken and thus on what constraint integrals must be applied. It is possible to have different types of stable structure existing and interacting in a given region of the flow field at the same time.

The symmetries and corresponding structures are easily classified because the space-time symmetries generate a finite parameter Lie group. The gauge symmetries generate a continuous parameter Lie group. The group formalism then leads to uniqueness theorems which are necessary in order to calculate the types of eddy present for a given set of boundary conditions.

A procedure is outlined for calculating the growth of strong turbulence by combining the symmetry approach with the theory of "compensating fields". The time rate of growth of the spectrum of eddys represented by the interacting stable flow structures are studied.

ON A POSSIBILITY OF PARAMETRIC RESONANCE IN ELECTRON PLASMA

N.L.Tsintsadze

Institute of Physics, Academy of Sciences of the Georgian SSR, Tbilisi, USSR

Abstract: Electron plasma placed into a strong high frequency electric field is studied. It has been shown that the electron mass oscillations in the external high frequency field lead to parametric excitation of both potential and nonpotential high frequency oscillations.

This paper considers the stability of electron plasma relative to its proper oscillations in a strong high frequency field. It is assumed that ions do not participate in oscillations but only compensate the equilibrium volume charge of electrons. Taking account of relativistic effect of electron motion in an external field leads to the fact that the parameter of the medium, which oscillates in the external field, is the electron mass. Oscillations of electron masses lead to parametric excitation of both potential and nonpotential high frequency oscillations. It is shown that at certain plasma parameters the increment of potential oscillations may exceed the maximum increment obtained in ref.2.

Let us represent the field applied to plasma in the form $\vec{E}(t)=\vec{E}_0\sin\omega_0 t$ assuming that the wave length of the proper oscillations is much less than the characteristic length of plasma inhomogeneity and less than the length of the external high frequency wave. Since we are interested in the parametric excitation of proper high frequency oscillations in a purely electron plasma, we use relativistic equations of one liquid electron hydrodynamics of cold plasma and Maxwell equations:

$$\begin{aligned}
&\operatorname{rot}\vec{H}=\frac{1}{c}\frac{\partial\vec{E}}{\partial t}-\frac{4\pi}{c}en\vec{V},\\
&\operatorname{rot}\vec{E}=-\frac{1}{c}\frac{\partial\vec{H}}{\partial t},\qquad \frac{\partial n}{\partial t}+\operatorname{div}n\vec{V}=0\\
&\operatorname{div}\vec{E}=4\pi e(n_{oi}-n),\\
&\left[\frac{\partial}{\partial t}+(\vec{V}\nabla)\right]\frac{\vec{V}}{\sqrt{1-V^2/c^2}}=-\frac{e}{m_0}\left(\vec{E}+\frac{1}{c}[\vec{V}\vec{H}]\right)
\end{aligned}\qquad (1)$$

The velocity of plasma electrons in the equilibrium state is determined by the expression

$$\vec{V}_0(t)=\frac{\vec{V}_E\cos\omega_0 t}{\sqrt{1+\frac{V_E^2}{c^2}\cos^2\omega_0 t}}$$

where

$$\vec{V}_E=\frac{e\vec{E}_0(0)}{m_0\omega_0}$$

Linearizing the set of equations (1) over small deviations from the equlibrium state ($n_0\gg n_1$, $V_0\gg V_1$, etc) and assuming for non equilibrium magnitudes the dependence on coordinates in the form $e^{i\vec{k}\vec{r}}$, we obtain a set of equations describing the parametric excitation of plasma proper oscillations.

Later we confine ourselves to the analysis of the mentioned equations in the two limiting cases: when the wave vector $\vec{k}$ is parallel to the external field $\vec{E}_0$ and when it is perpendicular to the field $\vec{E}_0$.

2. Let us consider the case of the parallel $\vec{k}_0$ and $\vec{E}_0$. Then we get two equations, the first of which describes the longitudinal oscillations and has the form

$$\frac{\partial^2 y}{\partial t^2}+\omega_{Le}^2\left(1-\frac{V_0^2}{c^2}\right)^{3/2}y=0, \qquad (2)$$

where $\omega_{Le}=\sqrt{\frac{4\pi e^2 n_{oe}}{m_e}}$ is the Langmuir frequency of electrons in the laboratory system of coordinates and

$$y=\left(1-\frac{V_e^2}{c^2}\right)^{-1/2}\frac{\partial}{\partial t}\left(n_1 e\varphi_1(\vec{k}\vec{V}_0+\omega)^{-1}\right) \qquad (3)$$

The second equation is the equation of magnetic field oscillations (a purely transverse wave) and is written in the form

$$\frac{\partial^2\vec{H}_1}{\partial t^2}+\left(k^2c^2+\omega_{Le}^2\left(1-V_0^2/c^2\right)^{1/2}\right)\vec{H}_1=0 \qquad (4)$$

Due to difficulties of the analytical study of equations (2) and (4) let us consider the case $\frac{V_E}{c}<1$, leading to Mathieu equations [4]. Then equation (2) takes the form

$$\frac{\partial^2 y}{\partial t^2}+\omega_{Le}^2\left(1-\frac{3}{4}\frac{V_E^2}{c^2}\cos 2\omega_0 t\right)y=0 \qquad (5)$$

The parametric excitation of electron Langmuir oscillations follows from eq. (5) and the main resonance is on the frequency ω_0 of the external field of the order of electron Langmuir frequency ω_{Le}, and the oscillation excitation increment has the following form

$$\gamma=\frac{3}{16}\omega_{Le}\frac{V_E^2}{c^2} \qquad (6)$$

At the comparison of increment (6) with the maximum increment, obtained in ref.2

$$\gamma_{max}\approx\omega_{Le}\left(\frac{m_e}{M}\right)^{1/3} \qquad (7)$$

one finds that increment (6) may become larger than expression (7) if the equilibrium electron density is of the order 10^8–10^9 l/cm^3, the amplitude of the external field of the order of some $\frac{kV}{cm}$ and the ion mass of the order of some tens of hydrogen masses.

From equation (4) at $\frac{V_E}{c}<1$ it follows that the maximum increment of transverse waves is

$$\gamma=\frac{1}{16}\omega_{Le}\frac{V_E^2}{c^2}$$

3. Consider now the case $\vec{k}\perp\vec{E}_0$. Then we obtain the following equations: for purely transverse wave

$$\frac{\partial^2 U}{\partial t^2}+k^2c^2U+\omega_{Le}^2\left(1-V_E^2/c^2\right)^{1/2}U=0 \qquad (9)$$

where

$$U=\frac{V_\perp}{\sqrt{1-V_E^2/c^2}},\qquad V_\perp=V\frac{[\vec{E}_0\times\vec{k}]}{E_0k}$$

and for longitudinal transverse wave of the 4th order

$$k^2c^2\frac{c}{V_0}\left[\frac{\partial}{\partial t}\frac{\frac{\partial E_x}{\partial t}}{\sqrt{1-V_0^2/c^2}}+\omega_{Le}^2\left(1-V_0^2/c^2\right)E_x\right]+\left[\frac{\partial^2}{\partial t^2}+\omega_{Le}^2\left(1-\frac{V_0^2}{c^2}\right)^{3/2}\right]\frac{c}{V_0}\left[\frac{\partial}{\partial t}\frac{\frac{\partial E_x}{\partial t}}{\sqrt{1-V_0^2/c^2}}+\omega_{Le}^2E_x\right]=0 \qquad (10)$$

At $kc\ll\omega_0,\omega_{Le}$ equation (10) is simplified and gives the equation of longitudinal oscillations $E_x\parallel k_0$ and has the same form as equation (2).

References

1. Yu.N.Aliev, V.P.Silin, JETP (USSR) 48, 901 (1965).
2. V.P.Silin, JETP (USSR) 48, 1679 (1965).
3. L.M.Gorbunov, V.P.Silin, JETP (USSR) 49, 1972 (1965)
4. N.N.Bogoliubov, Yu.A.Mitropolski. Asymptotic Methods in the Theory of Nonlinear Oscillations. Gostekhizdat, Moscow, 1963.

PARAMETRIC EXCITATION OF AN IONIC INSTABILITY BY A STRONG H.F. FIELD.

by

P. Leprince and M. Moisan,

LABORATOIRE DE PHYSIQUE DES PLASMAS,

91 - Orsay, France.

Abstract : Experimental results are presented which show a theoretically predicted ionic instability parametrically excited by an electric field with frequency $f_o = f_{pe}/\sqrt{2}$, where f_{pe} is the electron plasma frequency.

1 - Introduction

Aliev and Silin [1] have studied theoretically the effect of a strong high-frequency field on a plasma. They have determined the existence conditions for stable and unstable oscillations, given the relation between the frequency of the H.F. field, f_o, and the electron plasma frequency, f_{pe}. For what they call parametric excitation, i.e.

$$n f_o = f_{pe}$$

(where n is an integer), such an infinite-medium theory predicts the appearance of a new ionic branch, whose frequency is in general close to the ionic plasma frequency, f_{pi}, especially when the excursion length of the electrons in the H.F. field is of the order of the electron Debye length.

More recently, Aliev and Ferlenghi [2] have done a similar calculation for a bounded plasma (plasma slab). Assuming an electric field E_x parallel to the plasma boundary, they predicted an instability to occur when

$$n f_o = f_{pe}/\sqrt{2} \qquad (1)$$

This instability can be either periodic or aperiodic depending on whether f_{pe} is slightly below or above the critical frequency $f_o\sqrt{2}$. Let us consider the periodic case, where the frequency of the instability is of order f_{pi}. The threshold of this instability is given by

$$n f_o = \frac{f_{pe}}{\sqrt{2}} \left(1 + \left[4 J_n^2(a) \frac{f_{pi}^2}{f_{pe}^2} \right]^{1/3} \right) \qquad (2)$$

where

$$a = \frac{c\, k_x\, E_x}{m\, (2\pi)^2\, f_o^2} \qquad (3)$$

(J_n is the Bessel function of order n and k_x is the wave-number in the direction of E_x). If we further increase the plasma frequency f_{pe}, the growth increases and we reach a maximum for

$$n f_o = \frac{f_{pe}}{\sqrt{2}} \left(1 + \left[\tfrac{1}{4} J_n^2(a) \frac{f_{pi}^2}{f_{pe}^2} \right]^{1/3} \right) \qquad (4)$$

after which the periodic instability decreases and disappears at the critical point(1). We thus define an instability domain Δf_{pe} as the interval of f_{pe} lying between the threshold value(2) and the critical point(1).

$$\frac{\Delta f_{pe}}{f_o\sqrt{2}} = \left[4 J_1^2(a) \frac{f_{pi}^2}{f_{pe}^2} \right]^{1/3} \qquad (n = 1) \qquad (5)$$

II - Experimental results

In our experiments, we have detected an ionic oscillation, f_{m1}, close to f_{pi}, in the neighborhood of the critical point. However, in addition to the frequency f_{m1}, we have detected a second frequency f_{m2}(II band) which always appears for a smaller value of f_{pe} than f_{m1}(I band), and which is not explained by [2].

The experimental arrangement is that of [3], where the plasma is created directly by the H.F. field. The TM_{010} mode of the cavity provides us with an average electron plasma frequency, $f_{\overline{pe}}$, over the volume of the cavity.

i) $f_o = C f_{\overline{pe}}/\sqrt{2}$ ($C \leq 1$ is a constant for a given pressure)

In figure 1, where we have plotted the $f_{\overline{pe}}$ intervals over which the ionic frequencies (fig. 2) are observed, the relation between f_o and $f_{\overline{pe}}$ is absolutely linear. The value of C depends on the electronic profile, which depends in turn upon the pressure.

ii) Position of the instability over the Tonks-Dattner resonance.

Figure 3 gives the overall width of $f_{\overline{pe}}$ over which the plasma is self-sustaining. We know that such a plasma is sustained on the "stable" portion of the plasma resonance curve [4] i.e. it goes essentially from the top of that curve and down the higher density side. This means that the lower part of our diagram corresponds to the top of the resonance curve. Figure 3 shows that the instability regions do not occur at a particular point of the resonance curve at which the plasma is self-sustaining, but rather depend entirely on the linear relationship between f_o and $f_{\overline{pe}}$. In this particular case, the plasma resonance is the first Tonks-Dattner resonance.

iii) Variation of C as a function of pressure.

Figure 4 presents a typical plot of the frequency $f_{\overline{pe}}$ as a function of pressure. We note that a maximum of density is attained as the ambipolar regime is approached ; however, there exists a pressure limit above which the instability will disappear. In all the gases studied(Xe, Kr, A, Ne, He and H_2), the maximum of $f_{\overline{pe}}$ was located within ± 5 % of $f_o\sqrt{2}$.

iv) Instability domain Δf_{pe}.

We have been able to qualitatively verify the variation of the instability domain Δf_{pe} in three gases as a function of the ionic mass. The values obtained were

Gas	$\frac{\Delta f_{pe}}{f_o\sqrt{2}}$ (theoretical)	$\frac{\Delta f_{pe}}{f_o\sqrt{2}}$ (experiment)
Xenon	2.6 %	1.5 %
Krypton	3 %	1.9 %
Argon	3.8 %	2.8 %

The model does not take into account electron-neutral collisions which certainly require a growth rate larger than the threshold one, thus reducing Δf_{pe}.

We wish to thank Dr. E. Ferlenghi for many fruitful discussions.

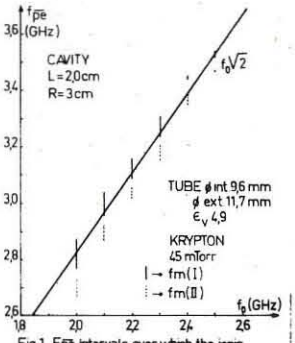

Fig.1 $F_{\overline{pe}}$ intervals over which the ionic instabilities are observed.

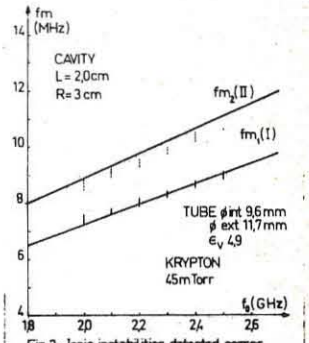

Fig.2 : Ionic instabilities detected corresponding to the $f_{\overline{pe}}$ intervals of Fig.1

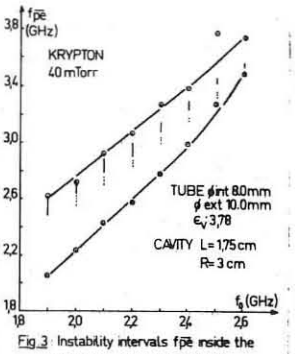

Fig.3 : Instability intervals $f_{\overline{pe}}$ inside the HF plasma operating width.

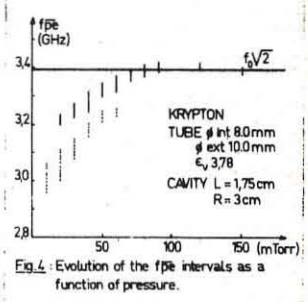

Fig.4 : Evolution of the $f_{\overline{pe}}$ intervals as a function of pressure.

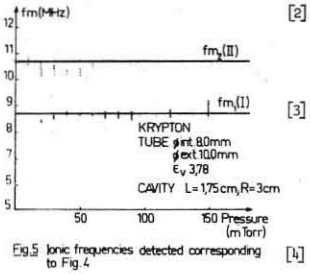

Fig.5 Ionic frequencies detected corresponding to Fig.4

References.

[1] V.P.Silin,"A survey of Phenomena in Ionized Gases.(Invited papers). IAEA, Vienna, p.205-237(1968). Gives a resumé of Silin and Aliev works.

[2] Yu.M.Aliev and E.Ferlenghi, Report LGI 69/4(April 69), Ionized gas laboratory,CNEN,Frascati(Rome). To appear in J.E.T.P.

[3] a) M.Moisan and P.Leprince, Phys. Letters 27A, 545(1968).
b) P.Leprince and M.Moisan, Proceedings of the IXth International Conference on Phenomena in Ionized Gases, Bucarest, paper 4.3.7.9(69)

[4] P.Leprince, Phys. Letters 26A, 431 (1968).

OBSERVATION OF NON-LINEAR LANDAU DAMPING OF ELECTRON PLASMA WAVES

Kenneth W. Gentle and Anthony Malein*

Center for Plasma Physics and Thermonuclear Research, University of Texas, Austin, Texas, U. S. A.

Abstract A non-linear interaction between two electron plasma waves in a collisionless plasma has been observed. A test wave at ω_1, k_1, is propagated in a plasma column, and damping or growth of this wave is measured in the presence of a second wave at ω_2, k_2 under conditions where the beat wave $\Delta\omega$, Δk does not satisfy the dispersion relation for any wave mode. The results agree with the predictions of Aamodt and Drummond (1).

Theory These predictions are based on a perturbation theory, where the wave energy must be much less than the particle energy, and spread over many modes. In particular no strong non-linear effects may occur for any one mode and each wave is nearly described by linear theory with only weak additional interactions. The theory predicts two important types of interaction; the resonant wave-wave type, (where the beat wave lies on the dispersion curve) and non-linear Landau damping where the phase velocity of the beat wave is near the thermal velocity. The prediction is that the higher frequency wave decays while the lower frequency grows and is represented by the following expression, the magnitude of the reciprocal damping length (α) of the wave at ω_1 being given by:

$$\alpha = \frac{v_1}{v_{g_1}} \frac{4.4 \times 10^{41} P_2}{(V_1 - V_g)^4 V_{g_2}} \cdot \frac{\lambda_1^2}{\lambda_2^2} \cdot \frac{W_1}{W_2} \frac{T}{N.A} I_{ooo} R_e\left(\frac{i}{W_g}\right) \left\{ 2 \frac{W_{1-2}}{W_1} \left[\frac{\lambda_2 - \lambda_1 W_2/W_1}{\lambda_2 - \lambda_1} - \frac{W_{1-2}}{2W_1} \right] - \left[\frac{\lambda_2 - \lambda_1 W_2/W_1}{\lambda_2 - \lambda_1} \right]^2 \right\}$$

Subscripts 1 indicate the wave observed to damp or grow non-linearly and subscripts 2 indicate the second large amplitude wave causing the interaction. Most other symbols can be inferred, but W_1, W_2 and W_g are the "W" functions evaluated at V_1, V_2 and V_g, the phase velocities and difference group velocity. W_{1-2} is the function evaluated at the phase velocity of a wave on the dispersion curve at $k=k_1-k_2$. I_{ooo} is the correction for finite geometry and is approximately unity. The expression for α is evaluated for each experimental point at which non-linear Landau damping is observed.

*Now at U.K.A.E.A. Culham, Abingdon, Berkshire, U.K.

Experiment The apparatus, shown diagrammatically in Fig. 1, below, comprises a 2 metre long cylinder, 10 cm in diameter, forming a waveguide beyond cut off for electromagnetic propagation at wave frequencies. Four longitudinal slots, equi-spaced round the circumference, allow antennae to be moved

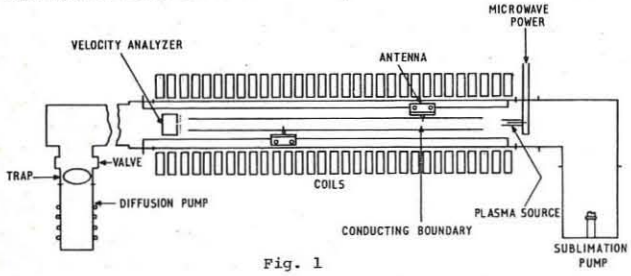

Fig. 1

radially and longitudinally through the plasma volume, coaxial with the cylinder, which is supported in the centre of a 40cm diameter vacuum vessel 3 metres long. Closely fitting the external surface are the axial magnetic field coils which provide a uniform field of up to 1 Kgauss. This, theoretically 'infinite', field assists in production of the plasma and confines the beam. The plasma is generated by ionization of hydrogen gas in a coaxial stub arrangement, coupled to a c.w. magnetron. Biassing of the source potential and a cusp magnetic field at the plasma orifice allow electron density and density gradient to be manipulated as required. Typical plasma conditions are $n_e = 4 \times 10^2$ cm^{-3}, $T_e = 15$ eV for a 4 cm diameter column (at half density points). The plasma beam is terminated at the far end of the apparatus on a plate behind which an energy analyser samples electrons through a small hole. A grid prevents the emergence of secondary electrons. The high vacuum is normally maintained by a diffusion pump but during operation of the source, a Ti getter pump provides a neutral background pressure of less than 2×10^{-5} torr.

Operation Normally, plasma conditions are first stabilized and the density and radial profile are checked. A velocity analyzer measurement fixes the value for T_e and a dispersion curve is plotted. For non-linear experiments, wave frequencies are selected which do not show damping but are far enough over the knee of the dispersion curve to have low phase velocities. The V^{-4} dependence of α indicates that high velocities do not exhibit significant effects but unfortunately as damping is approached, at very low phase velocities, the efficiency of coupling is drastically reduced and the power (P_2) in the second wave is severely limited. The transmitted frequency for wave 1 is selected and the output of the tuned receiver is taken via the synchronous detector to an x,y recorder. Fig. 2

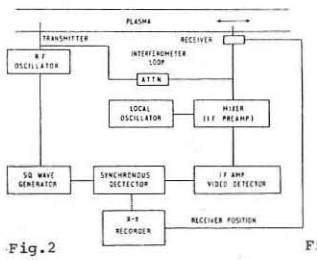

Fig.2

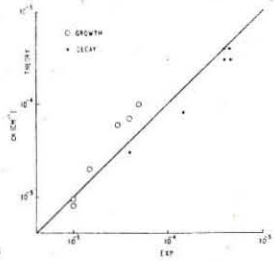

Fig.3

shows the layout of the transmitter and receiver circuits. The interferometer loop is needed for plotting the dispersion curve. The second high power wave, modulated by a square wave locked to the synchronous detector is then turned on and the receiving antenna traversed along the plasma column. The two wave frequencies are separated by at least 20 MHz so that with r.f. filtering and narrow i.f. bandwidth only one wave is received. Typically, the magnitude of the non-linear interaction changes by a few millivolts per metre, for a received signal of 500 millivolts. Since the experimental value of α is so small, $e^{-\alpha z} = 1 - \alpha z$ proves sufficient in the expansion and is thus linear with z. Most of the rest of the terms in the theoretical expression can be obtained from the dispersion curve, leaving only P_2 to be determined. Separate experiments are carried out to determine the coupling.

Results The experimentally observed damping or growth is plotted against the theoretical result expected from the measured plasma parameters. The range of values includes results for the same wave frequency at different power levels P_2 and also the effect of waves at different frequencies, for which all the arguments in the expression for α change. Because α does not depend on a simple way with anything that can be controlled directly, except P_2, the data are represented in this rather simple way. The open circles indicate the growth in the low frequency wave, and the dots the damped high frequency wave. The errors of about $\pm$ 3dB, not indicated in Fig. 3 are primarily caused by the difficulty in measuring the actual power P_2.

This research was funded by the National Science Foundation.

References

Aamodt, R.E. and Drummond, W.E., Paper CN 21/83 I.A.E.A. Conference on Plasma Physics & Controlled Nuclear Fusion Research, Culham, 1965.

INFLUENCE OF WAVE AMPLITUDE ON THE COLLISIONLESS DAMPING AT DIFFERENT PHASE VELOCITIES.

T. Matitti, E.P. Barbian and B. Jurgens

Euratom-FOM Association Contract.
FOM-Instituut voor Atoom- en Molecuulfysica, Kruislaan 407 Amsterdam/Ngm.

ABSTRACT: We studied the collisionless damping of electrostatic Langmuir waves as a function of the wave amplitude. We can distinguish two cases: a) waves with such a phase velocity that the linear Landau damping is moderate; b) waves for which the linear Landau damping is strong. In the first case we observe a recovering of the wave at a certain distance from the exciting probe. In the second case the wave is definitely damped.

The purpose of this paper is to study experimentally the damping of large amplitude Langmuir waves at various phase velocities. It may be considered as an extension of the work done in [1] and [2] where the behaviour of large amplitude waves with phase velocity corresponding to a moderate linear Landau damping was investigated. Differently from the work in [1] and [2] we look also at waves with such phase velocities that the linear Landau damping is rather strong.

Our plasma column (~ 2 cm in diameter and ~100 cm long) is created in a single ended Q-machine (see ref. [3]) with a 1500 G axial magnetic field and a background pressure better than 1×10^{-7} Torr. The plasma density used is typically of the order of $1 \times 10^{7}/cm^{3}$. Fig. 1 shows the circuit used for measuring the wavelengths and wave amplitudes. The h.f.-signal is applied to probe 1 and it is picked up by probe 2 which is movable along the plasma column. By providing a reference signal we get an interferometer of which the output is connected with an x-y-recorder. In this way we get a plot of the phase and amplitude dependence of the wave propagating in the plasma. We use a Phase Sensitive Detector in order to measure also very small amplitude waves. Attenuators A1 and A2 are introduced to keep constant the sensitivity of the detecting system when we change the wave amplitude. To know the plasma parameters like T_e, n_e and radius r_p, we measure the plasma dispersion characteristic and we interpret it as shown in ref. [3].

Due to the not completely quiescent state of the plasma the wavelength of the propagating wave changes with time. This fact introduces an apparent damping because the measurement of the wave amplitude is time integrated. The value of this apparent damping can be measured in the case in which Landau damping can be neglected (i.e. for $\omega \ll \omega_p$). Then, knowing the dispersion diagram, it is possible to calculate the value of the apparent damping also in the case in which Landau damping is not negligible, so that the measured values can be corrected. Time-resolved measurements confirm the validity of this correction. However these measurements can be done only if the wave amplitude is not too small. The wave E-field is calculated by equalizing the effectively injected energy per unit volume to the wave energy. Of course we take into account the coupling factor between probe and plasma (which is known by measuring the attenuation between probe 1 and probe 2 when apparent damping and Landau damping are negligible) and the wave E-field form (which is known from the dispersion diagram).

Fig. 2 shows a typical example of the results obtained. Recorder charts of two cases are shown. Case a: The ratio v_p/v_t (i.e. between phase velocity and thermal velocity) is large ($v_p/v_t = 5.3$). Case b: The ratio v_p/v_t is small (= 2.8). In the first case, by increasing the wave E-field, we observe at the beginning a slightly but monotonously damped wave. However, when the E-field is large enough (in the example given E= 0.4 V/cm) we observe a recovering of the wave at a certain distance from the exciting probe. This distance becomes shorter as the E-field increases. In the example given the recovering distance is ~ 25 cm, if the apparent damping is taken into account. In the second case for any value of the wave E-field we observe only a monotonously damped wave.

To discuss the results we may recall that the damping of the wave is caused by the so called trapped electrons, which absorb energy from the wave. We indicate by R the ratio between the energy that the electrons can absorb and the wave energy. If R > 1 the wave will be completely damped. As it is shown in ref. [4] R depends on the value of the wave E-field. However, for waves with $v_p/v_t < 4$, R remains always larger than 1. Therefore these waves will be completely damped independently of their amplitude. The example given in fig. 2b falls within this category. On the contrary, for waves with $v_p/v_t > 4$, R becomes smaller than 1 if the wave E-field is larger than a certain value. The wave is no longer completely damped but shows periodical amplitude oscillations in space. This is the case of the example given in fig. 2a. For the same example we can calculate the period of these oscillations by using the formula (given in ref. [1]):

$$k_{osc.} = \frac{2\pi}{\lambda_{osc.}} = \frac{1}{v_p}\left(\frac{e\,2\pi E}{m_e \lambda}\right)^{\frac{1}{2}}$$

We find a value of 19 cm which is in reasonable agreement with the measured value of 25 cm.

Fig. 3 shows the initial damping as a function of the wave E-field for three different values of v_p/v_t (2.8, 3.8, 5.3). We see that the damping increases with the E-field and that the rate of increase is larger for smaller values of v_p/v_t. This is in qualitative agreement with the calculations in [4]. Indeed we are in a range where R increases with the E-field and it is larger for smaller values of v_p/v_t. Finally we observe that for $v_p/v_t = 2.8$ the damping measured at very low E-field is in agreement with the calculated linear Landau damping ($k_i = 0.2\ cm^{-1}$).

References

1 Malmberg, J.H. and Wharton, C.B., Phys. Rev. Lett. 19, 775 (1967).
2 Wharton, C.B., Malmberg, J.H. and O'Neill, T.M., Phys.Fluids 11, 1761, (1968).
3 Matitti, T., Barbian, E., Goede, A. and Hopman, H.J., IX Int.Conf. on Phenomena in Ionized Gases. Contributed papers, p. 471, Bucharest, (1969).
4 Dawson, J.M. and Shanny, R., Phys.Fluids 11, 1506 (1968).

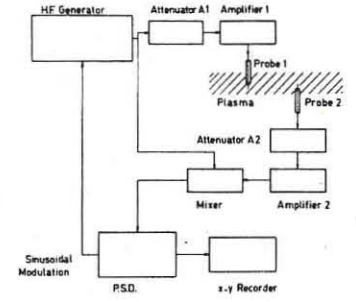

Fig.1

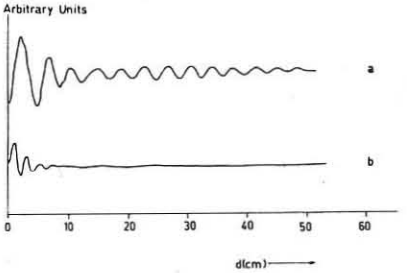

Fig.2
a) $v_p/v_t = 5.3$
b) $v_p/v_t = 2.8$
$E_{wave} = 0.4$ V/cm.

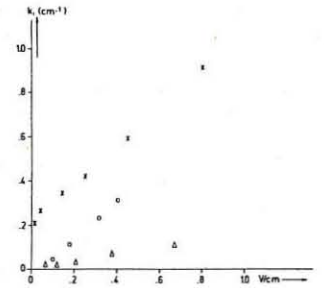

Fig.3
× $v_p/v_t = 2.8$
o $v_p/v_t = 3.8$
Δ $v_p/v_t = 5.3$.

ELECTRON HEATING BY LARGE-AMPLITUDE PLASMA WAVES IN A QUIESCENT PLASMA

by

E. Barbian, T. Matitti and B. Jurgens

Association EURATOM-F.O.M.

FOM-Instituut voor Atoom- en Molecuulfysica, Kruislaan 407, Amsterdam/Wgm.

The Netherlands

ABSTRACT:

Longitudinal Langmuir waves are used to heat the electrons in a Cs-plasma. We compare a narrow band excitation where the axial temperature dependence shows a modulation correlated with a standing wave pattern, and a broad band excitation that gives a smooth temperature curve together with a moderate noise level.

THE EXPERIMENT:

The Cs-plasma is produced in a single-ended Q-machine with the hot plate at about 2000°C and in which the collector is kept floating. The plasma column is confined in a magnetic field of 1500 Gauss and has a length of 100 cm and a diameter of 2 cm. The used density values are below 1×10^{8} cm^{-3} and the density decreases slightly in axial direction with an e-folding length of 75 cm. The neutral gas pressure is below 1×10^{-7} Torr.

The high frequency voltage signal which is used for excitation in the range between several MHz and 80 MHz is produced by an oscillator and symmetrically mixed with a small band (0.02 MHz) or a broad band (5 MHz) noise spectrum (see fig. 1). A broad band amplifier provides a continuous high amplitude signal up to a peak to peak value of 15 V across 50 Ω at the collector. Then at frequencies below the plasma frequency longitudinal waves are excited in the plasma column. With movable probes the wavenumber k and the values of T_e (r,z) and n(r,z) can be measured. From the dispersion diagram the plasma frequency $\omega_p/2\pi$ is derived in the way described in [1].

RESULTS:

A nearly linear increase of the temperature value from the 0.2 eV level of the non-excited plasma up to several eV can be observed when the applied voltage signal is varied from the noise level up to 15 Volt (fig. 2). This dependence is found with a fixed probe outside the direct coupling region near to the

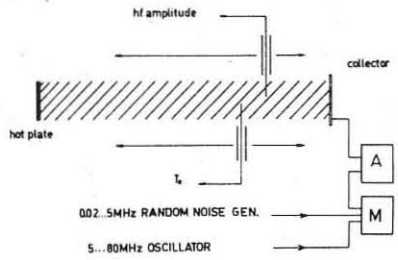

Fig. 1.

collector and with an excitation frequency of 10 MHz. The radial variation is weak, probes moved along z, however, reveal a significant z-dependence of the T_e-value which is correlated with the variation of the amplitude of the excited wave.

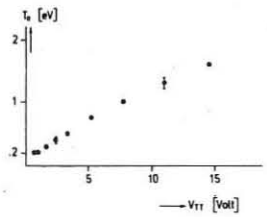

Fig. 2.

If the longitudinal wave is only slightly damped a standing wave can be formed by reflection of the wave at the hot plate. In fig. 3a an example is shown of the time averaged T_e-values (these values are determined from probe characteristics with sweep times of about 1 ms), which are measured along the z-axis, together with 20 MHz standing wave amplitudes. The narrow band (20 ± 0.02 MHz) excitation is equivalent to a practically monochromatic wave. As is seen from fig. 3a the maxima of T_e are correlated with the maxima of the wave amplitude with higher values nearer to the collector.

From the simplified dispersion relation: $\omega^2 = k^2 p^{-2} (\omega_p^2 - \omega^2)$ [2] we see that for $\omega^2 \ll \omega_p^2$ we get $k \sim \omega$. If plasma waves are excited within this linear region of the dispersion curve, the general picture remains the same.

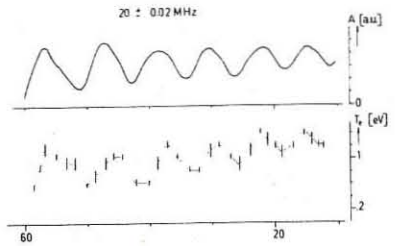

Fig. 3a.

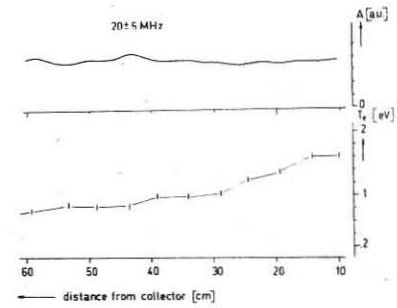

Fig. 3b.

Only for high ω-values near to the plasma frequency the situation changes. Then the plasma waves become strongly damped already near to the collector and no standing wave exists.

We should attend to previous experimental work [3] which was done with a sinus wave excitation. But it has to be considered that because of the higher densities reported there, the wave length of the excited plasma wave may have been much longer than the length of the plasma column.

When the broad band excitation (20 ± 5 MHz) is used as an alternative to case a), the wave amplitude along z becomes smooth (see fig. 3b) and the T_e-value decreases monotonously and slightly from the collector towards the hot plate side. In addition the noise level remains considerable below that in case a) though it is higher than when no excitation is applied.

DISCUSSION:

The increase in energy of the electrons can be understood in the way that the electrons are accelerated by the electric field of the longitudinal wave from velocities less than the phase velocity to velocities greater than that. As is shown in numerical experiments about Landau damping [4] the energy transfer from the wave to the electrons becomes efficient only for large amplitude waves (i.e. when the electric field energy is not much less than the thermal energy) if the phase velocity is several times the thermal velocity of the electrons. These conditions are fulfilled in our case. Then also, as [4] shows, the energy transferred from the wave to the electrons can become larger with increasing wave amplitude and this may cause the growth of the T_e-value as demonstrated in fig. 1.

In comparing the sinus wave excitation with the broad band excitation we have to concede that in the first case the electrons undergo coherent motion in the standing wave field which may cause the induction of additional electric fields of a two-stream instability. The chance, however, that electrons become trapped is small as the potential periodically passes zero and further there is the possibility as was shown in [5] that the energy of large-amplitude plasma oscillations may become randomized even in a collisionless plasma by non-linear effects. In the second case the amplified noise spectrum provides a direct randomization of the phases which contributes to a thermalization of the particles. We assume that in this many waves case particles which may have been trapped in one of the waves, soon will be transferred to another wave with a slightly different phase velocity and in this way go from one part of the velocity space to another. This is why for the purpose of electron heating the broad band excitation is to be preferred.

REFERENCES

[1] T. Matitti, E. Barbian, A. Goede and H.J. Hopman,
Proc. 9th Int. Conf. on Phen. in Ion. Gases, Bucharest, 471 (1969).

[2] A.W. Trivelpiece,
Slow-Wave Propagation in Plasma Waveguides, Ch.II - San Francisco Press, Inc. (1967).

[3] R.A. Demirkhanov, G.L. Khorasanov, J.K. Sidorova,
Proc. 9th Int. Conf. on Phen. in Ion. Gases, Bucharest 225 (1969).

[4] I.M. Dawson and R. Shanny,
Phys. Fluids 11, 1506 (1968).

[5] O. Buneman,
Phys. Rev. 115, 503 (1959).

ELECTRON CURRENT AND DISTRIBUTION FUNCTION ASSOCIATED WITH AN ELECTRON PLASMA WAVE

by

M. Guillemot, J. Olivain, F. Perceval, A. Quémeneur and J. Scharer*

ASSOCIATION EURATOM-CEA
Departement de la Physique du Plasma et de la Fusion Contrôlée
Centre d'Etudes Nucleaires
Boite Postale n° 6 - **92 Fontenay-aux-Roses** (France)

* On research leave from and supported in part by the University of Wisconsin, Madison.

Abstract : The second order time-independant electron current and distribution function have been derived theoretically and measured experimentally. The results show that there is a deformation in the vicinity of the phase velocity of the wave. This deformation is related to the wave amplitude, wave spectrum, and distance from the source.

We have calculated the difference between the time-independent current when a spatially damped wave is on and when it is off by a method similar to that of Malmberg et al [1]. The coherent current was calculated assuming a wave source located at $z = 0$, a plasma source at $z = -\infty$, and the analyzer at $z_o > 0$. We take into account waves propagating to the right and left and the interaction length. Under these conditions the coherent current density as a function of the cut off velocity of an electron energy analyzer was found to be : $J_o^{(2)}(z_o, t, v_c) = J_o$(with wave) $- J_o$ (without wave)

$$= -\frac{e^3}{m^2}\left(k_r^2 + k_i^2\right)\phi_w^2\, v_c \left(\frac{\partial f_o}{\partial v}\right)_{v=v_c}\left[\frac{1-e^{-2k_i z_o}}{(\omega - k_r v_c)^2 + (k_i v_c)^2} - \frac{1}{(\omega + k_r v_c)^2 + (k_i v_c)^2}\right]$$

where ϕ_w is the wave potential at $z = 0$.

The deformation of the time independant distribution function is :

$$f_o^{(2)}(z_o, t, v_c) = -\frac{1}{e v}\,\frac{\partial J_o^{(2)}(z_o, t, v)}{\partial v}\bigg|_{v=v_c} \qquad (2)$$

We have measured the coherent current on the EOS facility[2] with an electrostatic energy analyzer and using synchronous detection. Fig.1 illustrates a resonance structure shown by the solid curve in the neighborhood of the energy - eV associated with the wave phase velocity ($- eV = \frac{1}{2} m \left(\frac{\omega}{k}\right)^2$). The dashed curve in Fig.1 corresponds to the solution of Eq (1). The measured half-width of the current $J_o^{(2)}$ is too large to be explained by that monochromatic wave theory and was found to increase with increasing wave power. This increased width can be attributed to the existence of a spectrum of wave phase velocities in the experiment. To see the influence of this spectrum we have assumed a Gaussian form with $\frac{\Delta k}{k} = 9\%$ and this results in a theoretical width shown by the alternate dashed solid line. This results in the same half-width as that measured experimentally. We have also measured the deformed distribution function ($f_o = f_o^{(o)} + f_o^{(2)}$). Fig.2 presents the effect of a 120 MHz wave on the distribution function for different wave power levels (10^{-4} W corresponds to $\phi_w = 1$V). For a given separation between the probe and analyzer a plateau is created in the neighborhood of -eV. This width is also too large to be explained by a monochromatic wave theory and one must consider the effect of a wave spectrum as mentioned previously. Fig.3 shows that as the antenna is moved farther away from the analyzer the change in the velocity distribution is stronger indicating a wave-particle interaction through space. In conclusion we have shown that the effect of a damped plasma wave on the velocity distribution leads to the formation of a plateau with a width larger than that predicted by monochromatic wave theory. The increase of the deformation with distance has shown the wave-particle nature of the interaction.

Acknowledgement : The authors wish to thank Dr. C. Etiévant who has encouraged this work.

References :

1. J.H. Malmberg, T.H. Jensen and T.M. O'Neil, CN-24/E-8, Novosibirsk - URSS (1968)
2. R. Cano et al, CN-24/E-9, Novosibirsk - URSS (1968)

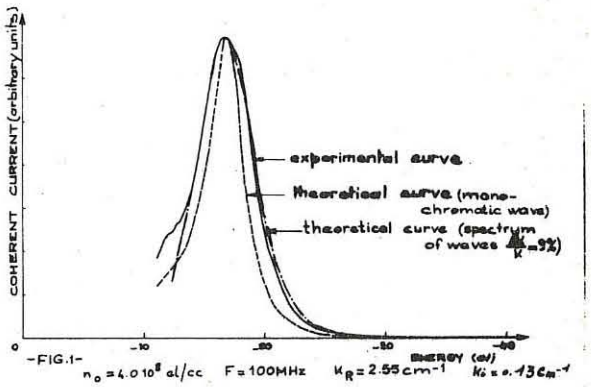

-FIG.1- $n_o = 4.0\,10^8$ el/cc F = 100MHz $k_R = 2.55\,cm^{-1}$ $k_i = 0.13\,cm^{-1}$

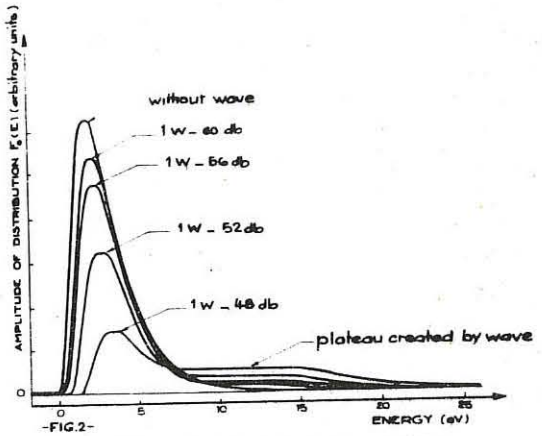

-FIG.2- $n_o = 4.0\,10^8$ el/cc $T_e \simeq 2$eV $B_o = 1.5$KG L = 50 cm

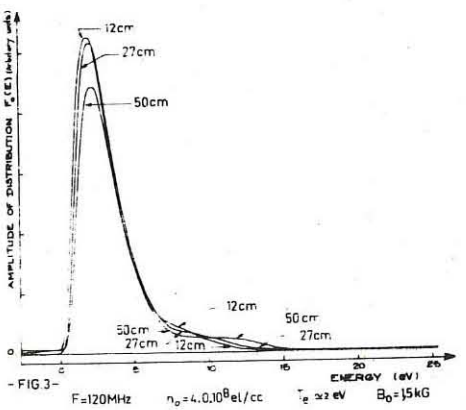

-FIG.3- F=120MHz $n_o = 4.0.10^8$ el/cc $T_e \simeq 2$ eV $B_o = 1.5$kG

RESONANT WAVE PARTICLE INTERACTIONS IN AN ELECTROSTATIC PULSE IN AN INHOMOGENEOUS MEDIUM

BY
D. Nunn
Dept. Physics, Imperial College, London.

Abstract: We consider the resonant beam excitation of a wave pulse whose wave number is spatially varying. After one trapping period, stably trapped second order resonant particles are dominant, and give rise to very large growth rates, and a steady change in the frequency and wave number of the pulse.

The system under study is a narrow band electrostatic wave pulse with a spatially varying wave number. The field is of the form:

$$E_0 = E(x)\cos\left(\Pi t + k_0 x - \tfrac{1}{2}k' x^2\right)$$

where E(x) is the envelope of the pulse, and is taken to be square with Gaussian ends. The system is excited by a weak resonant beam whose distribution function is a linear function of velocity. Assuming the plasma to be essentially collision free, for a weak beam Fres is given by

$$\left(\frac{\partial}{\partial t} + v\frac{\partial}{\partial x} - \frac{e}{m}E_0\,\partial/\partial v\right) F_{res} = 0$$

and may be thus obtained by numerically integrating particle trajectories in the field Eo. The equation of motion in dimensionless units is

$$\frac{dv}{dt} = -R\cos\left(x' + t' - \tfrac{1}{2}k^* x'^2\right) = -R\cos\phi$$

where: $R = +eEk/m\Pi^2$, $x' = k_0 x$, $t' = \Pi t$, $k^* = k'/k_0^2$

Now it can be shown that the condition for exact second order resonance $V_z = V_{res}$; $\dot{V}_z = \dot{V}_{res}$ is satisfied if

$$\phi = \phi_0 = \cos^{-1}\left(k^*/R\bar{k}^3\right);\ \bar{k} = 1 - k^*\bar{x};\ V_z = -1/\bar{k}$$

Defining $V' = V - V_{res}$, $\phi' = \phi - \phi_0$, we procure for small V',

$$\ddot{V}' - R\bar{k}\sin\phi_0 V' = 0$$

of for $0 < \phi_0 < -\pi$, second order resonant particles are stably trapped and oscillate around the point $V_z = V_{res}$, $\phi = \phi_0$ at the trapping frequency $(R\bar{k}\sin\phi_0)^{1/2}$. The region in ϕ, V space occupied by trapped particles is delineated by the limiting "ellipse" centred on ϕ_0, Vres that just reaches $\phi = -\phi_0$. Thus for $k^* > R\bar{k}^3$ the trap vanishes, but second order resonant effects will manifest themselves for higher K*. Since these trapped particles undergo very large changes in energy, after one or two trapping periods they will dominate the resonant particle distribution function. An example of Fres at phase ϕ_0 is shown here:-

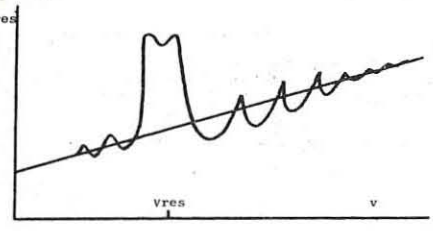

We are particularly interested in the component of resonant particle charge density that varies as $e^{i\Pi t}$ ($\tilde{\rho_1}$). This acquires a roughly constant phase at ϕ_0, and increases linearly with trapping time. The in phase component (ρ_R) gives the power input into the field, and is shown below as a function of position for various K*. Note the contrast to the homogeneous problem where the growth rate dies away in an oscillatory fashion(1). The greatest growth rates occur for $k^*/R \sim 7$. and for $k^*/R > 1$ it levels off at about the linear value. Note that for a pulse n trapping lengths long the growth rate will reach a value about n times the Landau growth rate. This points to the existence of explosive resonant particle instabilities in inhomogeneous media.

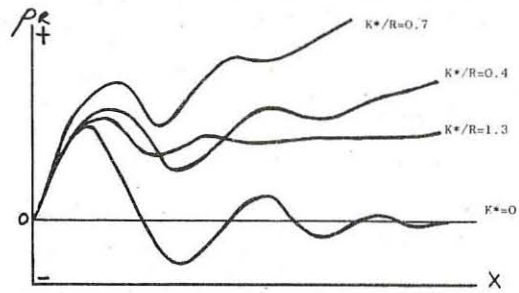

Of considerable interest is the reactive component of $\tilde{\rho_1}$ (ρ_I). It is possible to show that this can cause a steady change in the wave frequency and wave number. Assuming a warm ambient plasma the equation governing the time development of E can be shown to be of the form(2)

$$\frac{\partial}{\partial x}\left(\frac{\partial^2}{\partial t^2} + \Pi^2 - A\,\partial^2/\partial x^2\right)E = 4\pi\,\partial^2\rho/\partial t^2$$

To first order in the weakness of the beam it is possible to obtain an exact solution to this equation if we assume the following. (1) L and K are at all times independent of x, as is ρ_R. (2) The reactive component ρ_I is linearly dependent upon x. Such a solution predicts a growth of amplitude given by the expression

$$\frac{\partial E}{\partial t} = 2\pi\rho_R\Pi/k$$

and a rate of change of wave number going as

$$\frac{\partial k}{\partial t} = \frac{-2\pi\Pi}{Ek}\frac{\partial}{\partial x}\rho_I\ ;\quad \frac{\partial\omega}{\partial t} \approx \frac{-2\pi A}{E}\frac{\partial\rho_I}{\partial x}$$

A physical argument based on the way in which the density continuously generates fields which are added on to the existing ones, suggests that this frequency shift occurs more generally, and that the expression should really be modified to

$$\frac{\partial k}{\partial t} = \frac{-2\pi\Pi}{k}\frac{\partial}{\partial x}\left(\rho_I/E\right)$$

The theory here developed is a fairly general one and should be extendible to the case where any type of narrow band wave propagates in an inhomogeneous medium, and is excited by a resonant beam under collision free conditions. Note that the concept of inhomogeneity is here being introduced in a very general sense (3). It is taken to mean any situation where any of the quantities determining Vres has a space or time dependence.

REFERENCES

(1) Nunn D. Non linear wave particle processes in an electrostatic wave packet. Imperial College report. (1970)

(2) Houghton M.J. The linear theory of wave packets propagating in the whistler mode. J. Plasma Phys. ,3,611 (1969)

(3) Schram, D.C., Strijland, W., and Ornstein, L.Th.M.. The energy gain of particles pulled through cycloiron resonance. Proceedings of the third European conference on Controlled Fusion and Plasma Physics (Utrecht 1969)

QUASILINEAR APPROXIMATION TO THE TWO-STREAM INSTABILITY

R. H. HIRSCH, Institut für Plasmaphysik der Kernforschungsanlage Jülich, Jülich, Germany and J. DENAVIT, Naval Research Laboratory, Washington, D.C., U.S.A.

Abstract. The quasilinear approximation to the two-stream instability is investigated using a numerical solution of the Vlasov equation neglecting mode coupling. A case for which the trapping time is much longer than the correlation time is considered and the results are compared with quasilinear theory.

The one-dimensional Vlasov equation yields, after Fourier transformation in space

$$\frac{\partial f_k}{\partial t} + ikv f_k - E_k \frac{\partial f_o}{\partial v} = \sum_q E_{k-q} \frac{\partial f_q}{\partial v} \quad , \quad k = 0, k_o, 2k_o, \ldots$$

In these equations, time is measured in units of ω_p^{-1}, length in units of $\sqrt{2}\lambda_D$ and velocity in units of $\sqrt{2}v_{th}$, where ω_p is the plasma frequency, λ_D is the Debye length and v_{th} is the thermal velocity. The terms in the right members of the equations for $k \neq 0$ are the mode coupling terms.

The quasilinear theory of weak turbulence[1] proceeds on the basis of the following assumptions, (1) mode coupling is neglected, (2) the distribution function is expanded in powers of the electric field, and (3) the electrostatic energy spectrum is continuous in k space. This theory cannot account for electron trapping because of the expansion of the distribution function in powers of the electric field. It is expected, however, to be valid if $\tau_{tr} \gg \tau_c$, where $\tau_{tr} \cong 2\pi/k_c^{1/2} U^{1/4}$ is the electron trapping period and $\tau_c \cong 2\pi/k_c(v_2 - v_1)$ is the correlation time. U is the electrostatic energy, k_c is the central wave number, and v_1 and v_2 are the phase velocities of the slowest and fastest waves[2].

This work seeks to clarify the meaning of these assumptions by presenting a numerical solution of the Vlasov equation, with mode coupling neglected, for a case of two-stream instability for which $\tau_{tr} \gg \tau_c$. It should be noted that neglecting mode coupling does not result in the loss of trapped electron effects, as was demonstrated by Al'tshul and Karpman[3].

The numerical solution used is the Fourier-Fourier transform method originated by Knorr[4]. The above equations, with mode coupling terms set to zero, are Fourier transformed with respect to velocity. The resulting equations, coupled with Poisson's equation, are then integrated in time along their characteristics.

An initial distribution function of the form

$$f_o(v) = \frac{e^{-v^2} + e^{-A(v-v_b)^2} + e^{-A(v+v_b)^2}}{\sqrt{\pi}(1 + 2D/\sqrt{A})} D$$

is used, with A = 4.0, D = 0.01, v_b = 3.0. Eleven modes corresponding to $k = 0.3 + jk_o$, with k_o = 0.03 and j = 0, 1, ... , 10 were considered. These modes were excited with equal initial electrostatic energies.

The numerical solution was carried out to t = 180, during which the fractional energy error remained less than $8\ 10^{-7}$. The approach to equilibrium of the distribution function is illustrated in Fig. 1. At t = 180 the distribution function in the region of the small beam forms the plateau predicted by the quasilinear theory. The distribution function, however, approaches the initial distribution function gradually near the ends of the plateau instead of having sharp corners at v_1 and v_2. The resulting

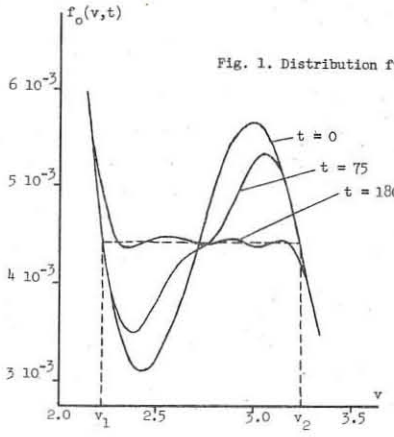

Fig. 1. Distribution function

kinetic energy is therefore smaller than predicted by the quasilinear theory. The distribution function at t = 180 also shows small ripples, which are still fluctuating in time. This effect is attributed to electron trapping which still exists with the moderate value of τ_{tr}/τ_c used in the present case ($\tau_{tr}/\tau_c \cong 4$).

The envelopes of the density fluctuations $n_k(t)$ for each mode are shown in Fig. 2. After an initial damping period the central modes grow in time and seem to approach steady state amplitudes as predicted by the theory. We observe that the modes seem to have been chosen sufficiently dense in the present computation. No single mode became overwhelming as in the case studied by Armstrong and Montgomery[5].

Fig. 3 shows a plot of the electrostatic energy spectrum against phase velocity at t = 180. This plot is compared with the result of the quasilinear theory which is shown as a continuous curve. We observe a shift of the spectrum (particularly due to the strength of mode k = 0.36) and a larger electrostatic energy than predicted.

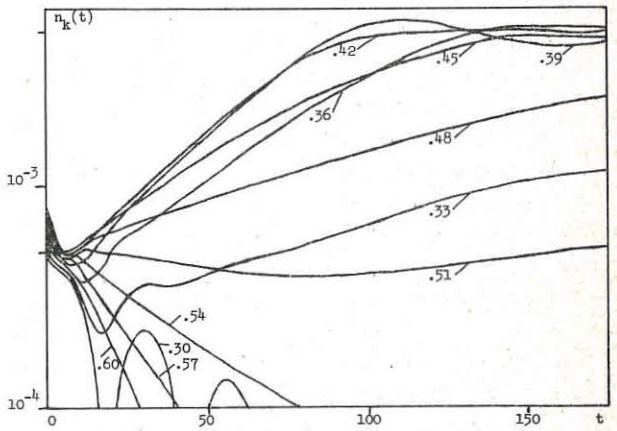

Fig. 2. Envelopes of the density fluctuations

In summary, trapped electron effects are considerably reduced in the present case, due to the decorrelation of the several waves of the spectrum. The distribution function approaches the prescribed plateau, but the energy spectrum deviates from the result of the quasilinear theory.

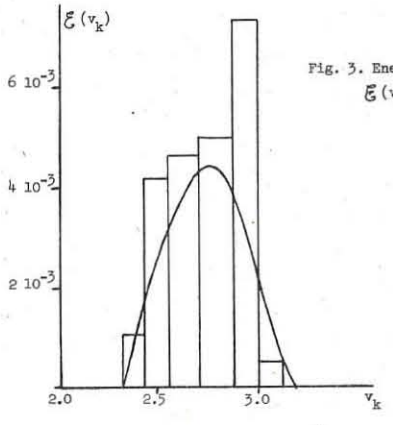

Fig. 3. Energy spectrum $\mathcal{E}(v_k) = n_k^2/k_o k^2$

Acknowledgement. This work was supported in part by the National Science Foundation under Grant GK-1857 to Northwestern University.

References.

1. W. E. Drummond and D. Pines, Nuclear Fusion, 1962 Supplement, Part 3, page 1049
2. T. Dupree, Phys. Fluids 9, 1773 (1966)
3. L. M. Al'tshul and V. I. Karpman, JETP 2, 361 (1966)
4. G. Knorr, Z. Naturforsch. 18a, 1304 (1963)
5. T. P. Armstrong and D. Montgomery, Phys. Fluids 12, 2094 (1969). Note that these authors included mode coupling in their computations.

NUMERICAL EXPERIMENTS ON THE CONTRA-STREAMING INSTABILITY IN A FINITE-LENGTH SYSTEM

by

A. T. Lin and J. E. Rowe

Electron Physics Laboratory
Department of Electrical Engineering
The University of Michigan
Ann Arbor, Michigan U.S.A.

Abstract: The effects of a finite-length system and particle thermal spread on the contra-streaming instability are investigated by computer simulation using a sheet model. It is found that the rate of formation of vortices is reduced by the thermal spread, the vortex is eventually destroyed in a finite-length system and a hysteresis loop in velocity space develops just before the destruction of the vortex.

The nonlinear development of the contra-streaming instability in a periodic system has been reported in many previous papers [1,2]. In the present paper, the effects of finite-length system and particle thermal spread on the instability are investigated by numerical simulation using a sheet model [3] for the electrons and assuming the ions to constitute an immobile neutralizing background. Electron sheets are injected at a fixed rate into the interaction region from opposing emitter planes and are collected whenever they reach boundary planes. The system is approximately ten wavelengths long. A wavelength is defined as $2\pi V_o/\omega_p$ where ω_p is the total plasma frequency and V_o is the stream mean velocity which is equal to 40 in all experiments reported here. The model consists on the average of 2600 sheets divided into two streams with equal densities but oppositely directed mean velocities. The results are given as computer generated plots. Distance is normalized to the average plasma intersheet spacing and time is normalized to $1/\omega_p$. Four cases with different particle thermal velocities are reported. The linear growth rates are plotted as a function of wavenumber for several cases in Fig. 1; these were calculated from the plasma dispersion equation [4].

The first experiment is for electron beams with zero thermal spread. In order to excite the fastest growing mode in the system, the stream traveling to the right is velocity modulated before it enters the interaction region with a 1 percent modulation depth at plasma frequency. The velocity modulation is converted into charge bunching in a short distance and thereupon induces bunching in the other stream. The two streams slow down and tend to bring one another to rest. In the process, they give a portion of their streaming energies to the instability. According to the linear analysis, the fastest growing mode should occur at a wavenumber $k = 0.62\ \omega_p/V_o$ and have a growth rate $\gamma = 0.353\ \omega_p$. The results from our computer simulation give $k = 0.6\ \omega_p/V_o$ and $\gamma = 0.33$ at $t = 20/\omega_p$; thus there is good agreement with the predictions of linear theory. At a later time ($t = 25/\omega_p$) a vortex in the velocity space is formed as can be seen from Fig. 2a and the growth rate drops to $0.29\ \omega_p$ but the wavenumber still remains at $0.6\ \omega_p/V_o$. At this instant the stream acceleration, which is equivalent to the electric field, is rich in harmonics of even order due to nonlinear effects as indicated in the wavenumber spectra analysis shown in Fig. 2b. The fundamental mode occurs at $k = 0.6\ \omega_p/V_o$ as predicted by the linear theory and the harmonics as far as the sixteenth still has significant amplitude. The vortex is unstable in a finite-length system and is eventually destroyed. At the same time, a great number of collective modes other than harmonics of the fastest growing mode are excited and the system turns into a turbulent state. A hysteresis loop in velocity space develops just before the destruction of the vortex.

Several other cases have been calculated for the purpose of investigating the effects of beam thermal spread on the instability. In these cases, the coherent phases needed for oscillation are partly destroyed by thermal spread and the growth rate is reduced. Maxwellian velocity distributions about mean streaming velocities are generated using random number generators so that all components of collective modes are initially excited in the system. Thermal spreads of $V_{th}/V_o = 0.1$, 0.2 and 0.5 have been investigated. The system length is approximately six wavelengths of the maximum growing mode which is defined as $\lambda_{max} = \lambda_{nom}/0.6$ from the linear theory. The number of vortices developed in the system starts with approximately six and reduces to four at $t = 25/\omega_p$ in all cases as shown in Figs. 3. The thermal spread naturally decreases the instability growth rate and consequently reduces the rate of formation of vortices. Figure 3c indicates that the vortex is hardly developed at $t = 25/\omega_p$ due to the small growth rate of the fastest growing mode. In all runs, the electric field energy is saturated at about 16 percent of the total system energy and the double bump velocity distribution diffuses to a flat shape in the central region when saturation occurs.

References

[1] Roberts, K. V. and Berk, H. L., "Nonlinear Evolution of a Two-Stream Instability," Phys. Rev. Letters, vol. 19, No. 6, pp. 297-300; August 1967.

[2] Morse, R. L. and Nielson, C. W., "One-, Two-, and Three-Dimensional Numerical Simulation of Two-Beam Plasmas," Phys. Rev. Letters, vol. 23, No. 19, pp. 1087-1090, November 1969.

[3] Dawson, J., "One-Dimensional Plasma Model," Phys. Fluids, vol. 5, No. 4, pp. 445-459, April 1962.

[4] Fried, B. D. and Conte, S., The Plasma Dispersion Function, Academic Press, Inc., New York: 1961.

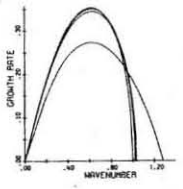

FIG. 1 LINEAR GROWTH RATE AS A FUNCTION OF WAVE-NUMBER. ($V_{th} = 0$, $V_{th} = 0.1\ V_o$, $V_{th} = 0.2\ V_o$, $V_{th} = 0.5\ V_o$)

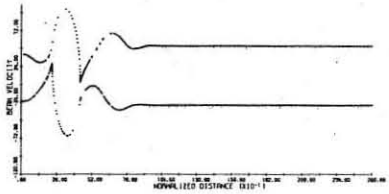

FIG. 2a VELOCITY SPACE FOR RUN NO. 1, $V_{th} = 0$, T = 25.

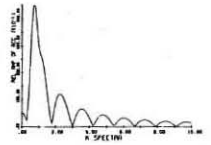

FIG. 2b WAVENUMBER SPECTRUM ANALYSIS OF RUN NO. 1 AT T = 25.

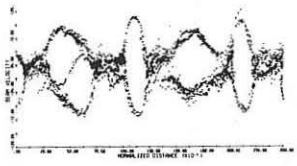

FIG. 3a VELOCITY SPACE FOR WARM STREAM CASES AT T = 25. $V_{th} = 0.1\ V_o$.

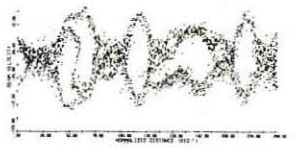

FIG. 3b VELOCITY SPACE FOR WARM STREAM CASES AT T = 25. $V_{th} = 0.2\ V_o$.

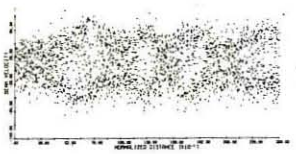

FIG. 3c VELOCITY SPACE FOR WARM STREAM CASES AT T = 25. $V_{th} = 0.5\ V_o$.

NUMERICAL EXPERIMENTS ON PLASMA HEATING VIA A CONVECTIVE BEAM-PLASMA INSTABILITY IN A FINITE-LENGTH ONE-DIMENSIONAL SYSTEM

by

A. T. Lin and J. E. Rowe

Electron Physics Laboratory
Department of Electrical Engineering
The University of Michigan
Ann Arbor, Michigan U.S.A.

Abstract: A sheet model is used to investigate the effects of plasma thermal spread and inhomogeneity in the plasma density distribution on plasma heating due to a beam-plasma interaction. The electric field is found to be amplitude modulated and the inhomogeneity reduces the interaction but increases the average electron thermal velocity.

The use of a convective beam-plasma instability to heat a plasma has been investigated by numerous authors [1,2]. In this investigation a sheet model for electrons and ions is used to follow the time-dependent, nonlinear, and inhomogeneous evolution of the beam-plasma instability in a finite-length system. The effects of plasma thermal spread and inhomogeneity in the plasma density distribution on plasma heating are also investigated. Electron beam sheets are injected continuously at the left of the system, pass through the plasma region, and are collected at the right. The system is situated in an idealized "square well" mirror magnetic field. The mirror ratio is assumed to have such a value that all beam sheets are lost at the ends whereas plasma sheets are reflected back into the system. This is equivalent to the assumption that all beam-sheet velocities lie in the loss-cone region and all plasma sheet velocities lie outside of it. A number of experiments for different plasma parameters have been completed. The model consists of 2000 plasma sheets and on the average approximately 100 beam sheets. The interaction length is approximately three nominal wavelengths ($2\pi V_o/\omega_p$). In the calculations distance is normalized to the average plasma intersheet spacing and time to $1/\omega_p$.

The first case is for the velocity-modulated electron beam (3 percent modulation) interacting with an initially uniform warm plasma (V_{th} = 0.075 V_o). The beam density is 1/79 that of plasma density. Some of the results are shown in Figs. 1. The electric field is observed to be highly inhomogeneous in the interaction region. The amplitude of the high electric field increases and travels upstream with a decreasing velocity. The spatial growth is caused by the ordinary convective instability in a two-stream system. The temporal growth arises from the fact that energy is fed into the plasma by the electron beam at a rate larger than that for which thermal conduction or other dissipative processes carry energy away. There is no dissipative mechanism in the model considered. The electric field will cease growth and stop traveling only if the energy carried into the high field region by the electron beam is balanced by the energy diffused away by plasma oscillations. This high field region is essentially the meniscus observed by many experimentalists in discharge experiments. The plasma sheet velocity distribution stays Maxwellian for all time although the width of the distribution function increases with time. The frequency spectrum analysis shows that only the first and second harmonics have been excited and only these two harmonics have amplitudes significantly above the noise level in the nonlinear region. The electric field evolution in time as shown in Fig. 1b indicates an amplitude modulation. The mechanism of this phenomenon is unfortunately not completely understood. We may apply O'Neil's [3] mechanism to explain the amplitude modulation by considering the electron beam as trapped particles which cause amplitude modulation and the plasma as untrapped particles which produce the oscillatory motion. The results also show that the electron beam has given up 8 percent of its energy to the plasma at the end of the run. Figure 1d shows that the plasma electron thermal velocity has achieved one fifth of the beam dc velocity and eventually oscillates at twice the plasma frequency.

Case No. 2 is for an initially uniform cold plasma. In this instance there is a rapidly increasing region, from t = 20 to t = 40, in the plasma electron thermal velocity plot. The interaction is more intense than the warm plasma case which is in agreement with the prediction of linear theory. The electron beam has given up 10 percent of its energy at the end of the run and the plasma thermal velocity has reached 10 percent of the beam dc velocity. The rest of the cases have been calculated in order to study the effects of inhomogeneities on the plasma heating process. In these cases the ions are simulated by mobile charge sheets with a charge/mass ratio of 1/100 that of electron sheets. A parabolic density distribution is generated for both plasma electrons and ions by initially assigning appropriate intersheet spacings. The ratios of maximum density to minimum density are 0.9 and 0.5 for Cases No. 3 and No. 4 respectively. The interaction in Case No. 4 is less intense than in Case No. 3 as can be seen from the comparison of electron beam velocity distributions although the plasma electron thermal velocity reaches a higher level in Case No. 3 due to large Landau damping [4] in this case. There is still an anomalous heating region from t = 20 to t = 40. The plasma ion thermal velocity oscillates at one half the frequency of the electron thermal velocity oscillations as shown in Figs. 2.

References

[1] Smith, C. and Dawson, J., "Some Computer Experiments with a One-Dimensional Plasma Model," MATT-151, Plasma Physics Laboratory, Princeton University, Princeton, New Jersey; 1963.

[2] Lin, A. T. and Rowe, J. E., "Numerical Experiments on a One-Dimensional Finite-Length Beam-Plasma System," Bull. Am. Phys. Soc., p. 1070; November 1969.

[3] O'Neil, T., "Collisionless Damping of Nonlinear Plasma Oscillations," Phys. Fluids, vol. 8, No. 12, pp. 2255-2262; December 1965.

[4] Jackson, E. A. and Raether, M., "Landau Damping in Inhomogeneous Plasmas," Phys. Fluids, vol. 9, No. 7, pp. 1257-1259; 1966.

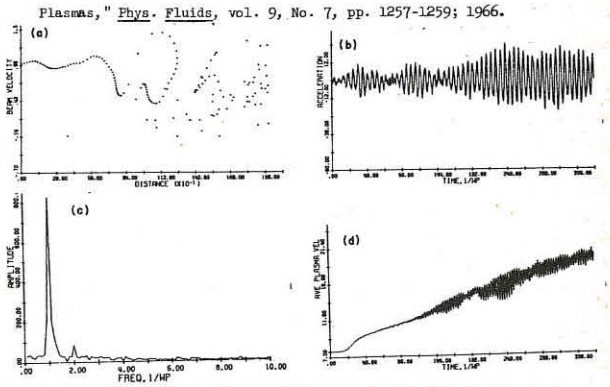

FIG. 1 MODULATED BEAM (3 PERCENT MODULATION) INTERACTING WITH WARM ONE-COMPONENT PLASMA (V_{th} = 0.075 V_o). (a) BEAM VELOCITY-SPACE AT t = 320. (b) BEAM ACCELERATION AS A FUNCTION OF TIME AT Z = 1500. (c) FREQUENCY SPECTRUM ANALYSIS AT Z = 1500, t = 320. (d) ELECTRON THERMAL VELOCITY AS A FUNCTION OF TIME.

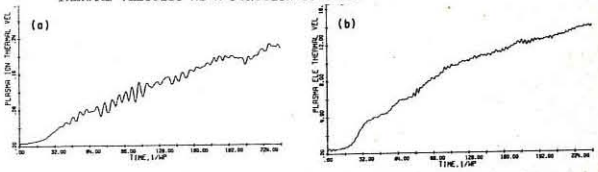

FIG. 2 MODULATED BEAM (3 PERCENT MODULATION) INTERACTING WITH COLD TWO-COMPONENT NONUNIFORM PLASMA (n_{min}/n_{max} = 0.5). (a) PLASMA ELECTRON THERMAL VELOCITY AS A FUNCTION OF TIME. (b) PLASMA ION THERMAL VELOCITY AS A FUNCTION OF TIME.

MODULATED SOLITARY WAVES PROPAGATING IN A THREE COMPONENT PLASMA IN A MAGNETIC FIELD

D.G.Lominadze, A.D.Pataraya

Institute of Physics, Academy of Sciences of the Georgian SSR, Tbilissi, USSR

Abstract: Modulated solitary waves of compression are considered in a three component plasma containing negatively charged ions when the electron inertia may be neglected. Numerical calculations to determine characteristic magnitudes of plasma have been carried out on a computer.

As is known [1] the stable solitary waves of compression in a cold collisionless plasma arise due to the existence of two effects: dispersion of linear waves and nonlinearity.

Waves formed from the well known in linear theory fast magnetosound waves [2-4] belong to nonmodulated compression solitary waves. These waves are characterized only by one frequency.

The modulated solitary waves of compression [5-7] are elliptically polarized in the general case and variations of plasma magnitudes are characterized then by two frequencies. The larger of them ω_ϑ characterizes the frequency of a modulated solitary wave, while the smaller one represents the modulation frequency of a solitary wave. For weak waves the modulation frequency is proportional to $\omega_\vartheta(M-M_\vartheta)$ where $M=V/V_A$, $M_\vartheta=V_\vartheta/V_A$; V and V_A are the solitary wave and Alfven velocity respectively, V_ϑ and ω_ϑ are characteristic velocity and the frequency of the solitary wave.

In a two component cold plasma [5] modulated solitary waves of compression arise from helical waves well known in linear theory .

In a three component cold plasma containing negatively charged ions, two types of modulated compression solitary waves may propagate. In the waves of the first type the characteristic frequency and wave velocity coincide by the order of magnitude with the corresponding magnitudes for the two component plasma. In the waves of the second type the electron inertia may be neglected.

The purpose of this work is the study of the second type modulated waves in the three component plasma containing negatively charged ions.

Let us consider the behaviour of the characteristic magnitudes in plasma in the coordinate system of the wave $(\zeta=x+Vt)$ on the infinity $(\zeta=-\infty)$. In the region $\zeta=-\infty$ the excited magnitudes are considered to be proportional to $\exp(p\zeta/\ell_1 M)$ where $\ell_i=V_A/\omega_i$, $\omega_i=\frac{Z_i e H_0}{m_i c}$ is the cyclotron frequency of the i-th kind particles m_i and $Z_i e$ are the mass and the value of the charge respectively, H_0 is the unperturbed magnetic field forming the angle ϑ with the x axis.

Using the equation of motion and Maxwell equation, we obtain the following equation for P

$$P=0.5q_2^{-\frac{1}{2}}\sec^{\frac{1}{2}}\vartheta\left\{\left[-q_2 d_1^{-2}\sec\vartheta(M^2-M_+^2)(M^2-M_-^2)+2(M^2-1)^{\frac{1}{2}}(M^2-\cos^2\vartheta)^{\frac{1}{2}}\right]^{\frac{1}{2}}\pm\right.$$
$$\left.\pm\left[-q_2 d_1^{-2}\sec\vartheta(M^2-M_+^2)(M^2-M_-^2)-2(M^2-1)^{\frac{1}{2}}(M^2-\cos^2\vartheta)^{\frac{1}{2}}\right]^{\frac{1}{2}}\right\} \quad (1)$$

Here

$$M_\pm^2=0.5d_1d_{-1}\left\{1+\cos^2\vartheta\pm\left[(1+\cos^2\vartheta-2d_1^{-1}d_{-1}^{-1})^2+\right.\right.$$
$$\left.\left.+4q_2^{-2}d_3d_1^{-1}d_{-1}^{-1}(\cos^2\vartheta\mp\cos^2\vartheta)\right]^{\frac{1}{2}}\right\}, \quad (2)$$

where $\cos^2\vartheta^*=\alpha_1\alpha_2q_2(1+q_2)^2d_1^{-1}d_3^{-1}$, $d_K=\alpha_1+\alpha_2q_2^K$, $q_2=\omega_1/\omega_2$, $\alpha_1=Z_1n_{10}/n_{e0}$, $\alpha_2=Z_2n_{20}/n_{e0}$, $\alpha_1-\alpha_2=1$, n_{i0} is the number of particles per volume unit in the unperturbed state.

In the case of weak solitary waves we obtain from eq.(1)

$$P=\pm i\omega_\vartheta/\omega_1+P_1(M^2-M_\vartheta^2)^{\frac{1}{2}} \quad (3)$$
$$\omega_\vartheta/\omega_1=q_{12}^{-\frac{1}{2}}\sec^{\frac{1}{2}}\vartheta\left[(M_\vartheta^2-1)(M_\vartheta^2-\cos^2\vartheta)\right]^{\frac{1}{4}}, \quad (4)$$

where

$$P_1=0.5q_{12}^{\frac{1}{2}}\sec^{\frac{1}{2}}\vartheta\left\{-d_1^{-2}q_2\sec\vartheta\left[2M_\vartheta^4-d_1d_{-1}(1+\cos^2\vartheta)\right]+\frac{2M_\vartheta^6-(1+\cos^2\vartheta)}{(M_\vartheta^2-1)^{\frac{1}{2}}(M_\vartheta^2-\cos^2\vartheta)^{\frac{1}{2}}}\right\}^{\frac{1}{2}}>0 \quad (5)$$

and M_ϑ is determined by means of the following eq. [7]

$$2(M_\vartheta^2-1)^{\frac{1}{2}}(M_\vartheta^2-\cos^2\vartheta)^{\frac{1}{2}}=q_2d_1^{-2}\sec\vartheta(M_\vartheta^2-M_-^2)(M_\vartheta^2-M_+^2). \quad (6)$$

Let us consider now the structure of large amplitude modulated solitary waves propagating along a magnetic field.

In this case the maximum value of the magnetic field $h=(H_y^2+H_z^2)^{\frac{1}{2}}/H_0$ is connected with the Mach's number M by the following relationship [7]

$$(d_1h_m^2)^3+8d_1\left[(\alpha_1+\alpha_2)(\alpha_1^{\frac{1}{2}}+\alpha_2^{\frac{1}{2}})^{-2}-M^2\right](d_1h_m^2)^2+16\left\{d_1^2(\alpha_1^{\frac{1}{2}}+\alpha_2^{\frac{1}{2}})^{-4}-2d_1^2(\alpha_1^{\frac{1}{2}}+\alpha_2^{\frac{1}{2}})^{-2}M^2+\right.$$
$$\left.+(d_1^2+\alpha_1\alpha_2q_{12})M^4\right\}(d_1h_m^2)+64\alpha_1\alpha_2d_1M^4\left[d_1(1+q_2)(\alpha_1^{\frac{1}{2}}+\alpha_2^{\frac{1}{2}})^{-2}-q_2M^2\right]=0 \quad (7)$$
$$(h_m\neq h_{max})$$

The magnitude M is limited below by M_0 [6,7]

$$M_0^2=1+q_{12}(\omega_*/\omega_1)^2, \text{ where } \omega_*/\omega_1=(\alpha_1^{\frac{1}{2}}-\alpha_2^{\frac{1}{2}}q_2)(\alpha_1^{\frac{1}{2}}+\alpha_2^{\frac{1}{2}})^{-1}q_{12}^{-1}. \quad (8)$$

When $\omega_*>0$, M is limited above by M_{max} then electrons are ejected from the central region of the wave. And in the case $\omega_*<0$, when $M=M_{max}$, negatively charged ions are.

Using the computer HESM-4 numerical calculations have been carried out to find the dependence $h_m=f(M)$ and $M_\vartheta=\varphi(\vartheta)$ The results are given in Figs. 1-2 for different values of mixtures.

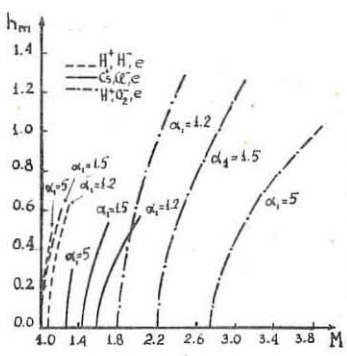

Fig.1

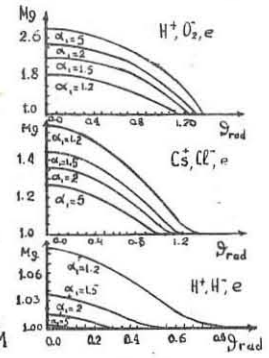

Fig.2

References.

[1] A.A.Vedenov, E.P.Velikhov, R.Z.Sagdeev, Nuclear Fusion 1, 82 (1961).

[2] J.H.Adlam, J.E.Allen, Phil.Mag. 3, 448 (1958).

[3] R.Z.Sagdeev. Plasma Physics and Problems of Controlled Thermonuclear Reactions. v.IV. Moscow. Izd.AN SSSR, 1958.

[4] Yu.A.Beresin, R.Z.Sagdeev PMTF (USSR) 2, 8 (1966); A.D.Pataraya, Nuclear Fusion 9, 121 (1969).

[5] P.G.Saffman, J.Fl.Mech. 11,16 (1961); B.A.Tverskoi, JETP (USSR) 42,833 (1962); A.D.Pataraya, JTF (USSR) 32,139 (1962); A.P.Kazantsev, JETP (USSR) 34, 1283 (1963); A.Mizutani, T.Taniuti, Ph.Fl. 12, 1167 (1969).

[6] A.D.Pataraya, JTF (USSR) 39, 1714 (1969).

[7] A.D.Pataraya, JTF (USSR) 40, N8 (1970).

PROPAGATION OF SOLITARY DRIFT WAVES OF SMALL AMPLITUDE IN A COLLISIONLESS PLASMA

A. Orefice and R. Pozzoli
Laboratorio di Fisica del Plasma e di Elettronica Quantistica del CNR. Istituto di Fisica, via Celoria 16, Milano (Italia)

Abstract A generalized Kortweg - de Vries equation is derived for nonlinear drift waves propagating with a nonzero angle with respect to the external uniform magnetic field. A relation is presented between amplitude and propagation velocity of solitary drift waves.

The K.d.V. equation has been obtained from a wide group of nonlinear systems, in the approximation of weak nonlinearity. A numerical analysis of the K.d.V. equation, supplemented by a certain class of boundary and initial conditions was given in Refs.[1],[2]. K.d.V. equations have been derived, in the case of a collisionless cold plasma, for hydromagnetic waves [3],[4] and for ion acoustic waves [5]. It is to be observed that the problem was always reduced to an essentially unidimensional one. We consider in this work the nonlinear evolution of drift waves sustained by temperature and density gradients. A study of the stationary regime for nonlinear drift waves was performed, with an approach similar to the present one, in Ref. [6]. Our aim is to derive a generalized K.d.V. equation, including propagation along the external magnetic field, and to find a relation between the amplitude and the propagation velocity of solitary drift waves.

We consider here low-frequency waves, sustained by equilibrium gradients, along x, in density and temperature, in a collisionless magnetoplasma. The external, strong and uniform, magnetic field is directed along z. The electron and ion temperatures are taken to be the same, T(x). The electrons move freely along z, fast enough to get their equilibrium distribution. We normalize all quantities in terms of the following ones : a characteristic density n_0 ; a length L , typical of the x-gradients; the characteristic electric potential kT_0/e , being T_0 a typical temperature; and the diamagnetic velocity $V = (ckT_0)/(eLB)$.

In our scheme, the electrostatic potential ϕ adjusts itself, at each time, so that, in adimensional notations

$$n_i = n_e = n(x,y,z,t) = n_e(x) \exp\left\{ T^{-1}(x)\ \phi(x,y,z,t) \right\} \qquad (1)$$

In order to fix ideas, we take the gradient $n_0'/n_0 < 0$.

The ion continuity equation is

$$n_t + \nabla\cdot(n\underline{v}) = 0 \qquad (2)$$

Keeping into account the low-frequency nature of our problem, the ion velocity $\underline{v}$ is assumed to be given approximately by the following equations

$$\underline{v}_\perp = \underline{b}\times\nabla\phi + n^{-1}\,\underline{b}\times\nabla(nT) - \omega/\Omega\ \nabla_\perp\phi_t \qquad (3)$$

$$v_{/\!/} = -(V_T/V)^2 \int_{t_0}^{t} \phi_z\ dt' \qquad (4)$$

where Ω is the ion gyrofrequency, $\underline{b} = \underline{B}/B$, V_T is the thermal ion velocity, and $\omega = V/L$. Eq. (3) contains a sum of electric, pressure gradient, and polarization drifts.

From Eqs. (1) to (4) an evolution equation is obtained for $\phi(x,y,z,t)$.

We analyze a situation characterized by the following scaling :

$$\omega/\Omega \sim (V/V_T)^2 \sim \epsilon \qquad (5)$$

being ϵ a smallness parameter.

We perform the following transformation to a frame moving with the diamagnetic velocity :

$$\eta = y - t \qquad (6)$$

We make moreover a stretching in x,z,t assuming the n-th order derivatives in such variables to be of order ϵ^n .

Expanding ϕ around the equilibrium value $\phi^{(0)} = 0$:

$$\phi = \phi^{(1)} + \phi^{(2)} + \ldots \qquad (7)$$

with $\phi^{(n)} \sim \epsilon^n$, and retaining in the equation for ϕ the nonzero terms of the lowest order, we obtain :

$$\phi^{(1)}_t + T'/T\ \phi^{(1)}\phi^{(1)}_\eta + T\,\omega/\Omega\ \phi^{(1)}_{\eta\eta\eta} + - (V_T/V)^2\, T \int_{t_0}^{t} \phi^{(1)}_{zz}\ dt' = 0 \qquad (8)$$

In this equation the variable x is contained only as a parameter.

Eq. (8) is a generalized form of the K.d.V. equation, including a term due to ion motion along z . It may be observed that linearizing Eq. (8) one obtains the dispersion relation given e.g. in Ref. [7].

We search now for a solution of the form $\phi(\eta + \alpha z - \beta t)$, that is for a disturbance propagating in the moving frame with a phase velocity $W = \beta(1+\alpha^2)^{-\frac{1}{2}}$, at an angle $\vartheta = \arctg\alpha$ with respect to the η-axis. If $T'/T > 0$ we obtain, imposing the standard conditions for solitary waves of Ref.[2], a soliton of the usual sech^2 form, for which the relation between the amplitude A and the velocity W is now :

$$A = 3\,W\,(1+\alpha^2)^{\frac{1}{2}}\,T/T'\left\{1 - (V_T/V)^2 T\,(\alpha/W)^2\,(1+\alpha^2)^{-1}\right\} \qquad (9)$$

We observe that, in the next order of approximation of the complete evolution equation for ϕ, an equation for $\phi^{(2)}$ can easily be obtained where the x-derivatives play an essential role.

References

(1) Y.A.Beresin, V.I.Karpman: JETP 46, 1880(1964)
(2) N.J.Zabusky, M.D.Kruskal: Phys.Rev.Lett. 15, 240(1965)
(3) C.S.Gardner, G.K.Morikawa: TID 10-6184, NYU(1960)
(4) K.W.Morton: Phys.Fluid. 7, 1800(1964)
(5) H.Washimi, T.Taniuti: Phys.Rev.Lett. 17, 996(1966)
(6) V.N.Oraevsky, H.Tasso, H.Wobig: IAEA Proc. CN 24/E-6, Novosibirsk 1968
(7) B.B.Kadomtsev: Plasma Turbolence, Academic Press 1965

PHASE-LOCKING OF COUPLED MODES

IN NONLINEARLY UNSTABLE PLASMAS

by

H. Wilhelmsson and K. Östberg

INSTITUTE OF PHYSICS

UPPSALA, Sweden

Abstract: The purpose of the paper is to discuss phase-locking of three coupled modes for plasma systems which are explosively unstable. The study is carried out within the frame-work of the well-defined phase description. It turns out that appreciable phase-locking occurs in a period of time shorter than the time the explosive instability needs to develop.

It has been noticed [1] that phase effects may have considerable importance for the dynamics of nonlinearly unstable plasma systems. The so - called explosive instabilities in such systems have been studied theoretically by several authors, utilizing either the random-phase approach [2-4] or the well-defined phase description [5] . The random-phase method [6,7] amounts to repeated phase-randomization at every instant of time during the development of the instability, whereas the well-defined phase description preserves the details of the internal dynamic phase-changes in the process. The results of the two methods differ [1,5] with regard to the characteristic time developments of the unstable systems. The purpose of the present paper is to describe the phase-locking of coupled modes for an explosively unstable plasma system. Dissipative effects are neglected.

Let us consider the coupling of three modes and assume that their interaction is resonant, i.e. that the conditions $\omega_0 = \omega_1 + \omega_2$ and $k_0 = k_1 + k_2$ for the frequencies and wave-numbers, respectively, are fulfilled.

In the well-defined phase description the basic equations for the explosively unstable case [1,5] are

$$\frac{du_0}{dt} = u_1 u_2 \cos\Phi \quad ,$$

$$\frac{du_1}{dt} = u_0 u_2 \cos\Phi \quad , \qquad (1)$$

$$\frac{du_2}{dt} = u_0 u_1 \cos\Phi \quad ,$$

$$\frac{d\Phi}{dt} = -\left[\frac{u_1 u_2}{u_0} + \frac{u_0 u_2}{u_1} + \frac{u_0 u_1}{u_2}\right] \sin\Phi \quad ,$$

where the u_j are the moduli of the wave amplitudes and

$$\Phi = \phi_0 - \phi_1 - \phi_2 \quad , \qquad (1a)$$

with ϕ_j the phase of the j-th amplitude.

In the following we regard the quantity x, defined by

$$x = u_j^2(t) - u_j^2(0) \quad , \quad (j = 0, 1, 2) \qquad (2)$$

as a primary variable, independent of the index j, due to the conservation laws [1] of Eqs.(1). From x the time t and the phase $\Phi(t)$ can be obtained by means of the following relations:

$$t = \begin{cases} I(x) - I(0) & (0 \le \Phi(0) \le \pi/2) \\ I(0) - I(x) & (\pi/2 \le \Phi(0) < \pi \text{ and } \Phi(t) \ge \pi/2) \\ I(0) + I(x) & (\text{ - " - and } \Phi(t) \le \pi/2) \end{cases} \qquad (3)$$

and

$$\sin\Phi(t) = u_0(0)u_1(0)u_2(0)\sin\Phi(0) \left\{ \prod_{j=0}^{2} [x + u_j^2(0)] \right\}^{-1/2} \qquad (4)$$

In (3) the function I(x) is

$$I(x) = \frac{1}{2} \int_{x_0}^{x} \frac{d\xi}{\sqrt{R(\xi)}} \qquad (3a)$$

where x_0 is the largest real root of the equation $R(\xi) = 0$, and

$$R(\xi) = \prod_{j=0}^{2} [\xi - u_j^2(0)] - u_0^2(0)\, u_1^2(0)\, u_2^2(0) \sin^2\Phi(0) \qquad (3b)$$

Furthermore, in (3) the time t is always less than the explosion time t_∞, defined by $t_\infty = \lim_{x \to \infty} t$.

In Fig. 1 is plotted the results of computer calculations from (2-4).

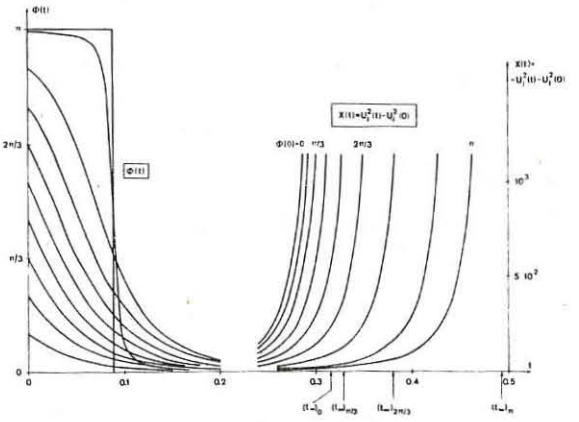

Fig. 1. Demonstrating the variation of $\Phi(t)$ and $x = u^2(t) - u^2(0)$ with time for different initial values of Φ , (1a). The explosion times $(t_\infty)_{\Phi(0)}$ are indicated in the figure for different initial phase values.

We have also plotted, as shown in Fig. 2, the development in time of the probability distribution $P_t(\Phi)$ assuming at t=0 that all phases are equally probable.

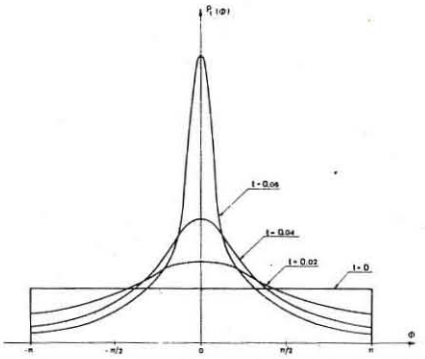

Fig. 2. Probability distribution $P_t(\Phi)$ for different time values. (The correspondong explosion times range between $(t_\infty)_0 = 0.3$ to $(t_\infty)_\pi = 0.5$ for the normalization used in Eq. (1)).

The effect of phase-locking is clearly seen from the above figures. We want to emphasize that the approach used to determine the curves in Fig. 2 assumes a random distribution of phases only initially, whereas in the random-phase method the phases are randomized at every moment of time.

References:

1. ENGELMANN, F. & WILHELMSSON, H 1969 Z. Naturforsch 24a, 206
2. KADOMTSEV, B.B., MIKHAILOVSKII, A.B. TIMOFEEV, A.V. 1965 Soviet Phys. JETP 20, 1517
3. DIKASOV, V.M., RUDAKOV, L.I. & RYUTOV, D.D. 1965 Soviet Phys. JETP 21, 608
4. ROSENBLUTH, M.N., COPPI, B. & SUDAN, R.N. 1968 3rd Conf. on Plasma Phys. and Contr. Fusion Research, Novosibirsk paper CN-24/E-13
5. WILHELMSSON, H., STENFLO, L & ENGELMANN 1970 J. Math. Phys. (in press)
6. TSYTOVICH, V.V., 1967 Soviet Phys. Uspekhi 9, 805
7. SAGDEEV, R.Z. & GALEEV, A.A. 1969 Nonlinear Plasma Theory, Benjamin Publ, p. 20-24

NONLINEAR ELECTROSTATIC INSTABILITIES IN A MAGNETOPLASMA

J.A. Tataronis - J. Teichmann

ASSOCIATION EURATOM-CEA
Département de la Physique du Plasma et de la Fusion Contrôlée
Service I.6n. Centre d'Etudes Nucléaire
Cedex 85. 38 Grenoble Gare (France)

The existence of nonlinear instabilities in plasmas and the characteristics of parametric amplification of waves is discussed for the case of asymmetric coupling coefficients.

Recently, attention has been given to the problem of the generation of explosive instabilities [1,2] and parametric amplification [3,4] resulting from nonlinear interaction of positive and negative energy waves in plasmas. As far as we can determine, previous treatments have delt with systems in which the coupling coefficients exhibit some form of symmetry. Here we shall show that symmetry does not always exist and that this fact could have a strong influence on the excitation of nonlinear instabilities and parametric amplification. The analysis will be restricted to the case of electrostatic modes in a magnetoplasma. Assuming we have $\omega'' = \omega - \omega'$, $\vec{k}'' = \vec{k} - \vec{k}'$, the interacting waves are described by

$$\frac{d}{dt}\phi_k = -i\sigma_k \left|\frac{\partial \varepsilon_0}{\partial \omega}\right|^{-1}_{\omega_k} S(k,k',k'')\,\phi_{k'}\phi_{k''}\,e^{i\Delta\omega t}$$

$$\frac{d}{dt}\phi_{k'} = -i\sigma_{k'} \left|\frac{\partial \varepsilon_0}{\partial \omega}\right|^{-1}_{\omega_{k'}} S(k',-k'',k)\,\phi_k\,\phi^*_{k''}\,e^{-i\Delta\omega t}$$

$$\frac{d}{dt}\phi_{k''} = -i\sigma_{k''} \left|\frac{\partial \varepsilon_0}{\partial \omega}\right|^{-1}_{\omega_{k''}} S(k'',k,-k')\,\phi_k\,\phi^*_{k'}\,e^{-i\Delta\omega t} \qquad /1/$$

where ε_0 is the dielectric constant, ϕ_k the potential, $\Delta\omega = \omega - \omega' - \omega''$ and $\sigma_k = \mathrm{sgn}\left.\partial\varepsilon_0/\partial\omega\right|_{\omega_k}$. The energy for an electrostatic monochromatic mode is defined as $W_k = \frac{1}{16\pi}\sigma_k \left|\partial\varepsilon_0/\partial\omega\right|_{\omega_k} \omega_k \phi_k \phi_k^*$.
The coupling coefficients are [5] : $S(k,k',k'') = R(k,k',k'') + R(k,k'',k')$,

$$R(k,k',k'') = \sum_{e,i} 2\pi \frac{e\omega_p^2}{m n_0} k^{-2} \int dv_\parallel dv_\perp v_\perp \sum_{s,s'} e^{-i(s+s')\psi_k + is'\psi_{k'} + is\psi_{k''}} J_{s+s'}(\mu_k) \cdot$$

$$\cdot \left[\omega - k_\parallel v_\parallel - (s+s')\omega_c\right]^{-1} \left[-s\frac{k'_\perp}{v_\perp} J_{s'}(\mu_{k'}) + \frac{i}{\omega_c}\left(\vec{k}\times\vec{k}'\right)_\parallel J_{s'}(\mu_{k'}) + J_{s'}(\mu_{k'})\left(\frac{s'\omega_c}{v_\perp}\frac{\partial}{\partial v_\perp} + k'_\parallel \frac{\partial}{\partial v_\parallel}\right)\right] \cdot$$

$$\cdot \left[\omega'' - k''_\parallel v_\parallel - s\omega_c\right]^{-1} \left[J_s(\mu_{k''})\left(\frac{s\omega_c}{v_\perp}\frac{\partial}{\partial v_\perp} + k''_\parallel \frac{\partial}{\partial v_\parallel}\right)\right] f_0 \qquad /2/$$

where $f_0 = f_0(v_\perp, v_\parallel)$, $\mu_k = \frac{k_\perp v_\perp}{\omega_c}$ and $\psi_k = \mathrm{arctg}\, k_y/k_x$. The solution of /1/ is well known [1,2,6] when the signs of the coupling coefficients are equal. It can be shown that when $S(k,k',k'')$, $S(k',-k'',k)$, $S(k'',k,-k')$ are complex and unequal, as is the case for /2/, eq. /1/ has the following invariant:

$$(\sigma_k\varepsilon_{k'}A_k^2 - \sigma_{k''}\varepsilon_{k''}A_{k''}^2)\,tg\beta_k - (\sigma_k\varepsilon_{k'}A_k^2 + \sigma_{k''}\varepsilon_{k''}A_{k''}^2)\,tg\beta_{k'} + (\sigma_k\varepsilon_k A_k^2 + \sigma_{k'}\varepsilon_{k'}A_{k'}^2)\,tg\beta_{k''} = C \qquad /3/$$

where $\phi_k = A_k e^{i\Psi_k}\left(M_k, M_{k'}\cos\beta_{k'}, \cos\beta_{k''}\right)^{-1/2}$, $\left|\frac{\partial\varepsilon_0}{\partial\omega}\right|_{\omega_k} S(k,k',k'') = \epsilon_k M_k e^{i\beta_k}$,

$\epsilon_k = \mathrm{sign\ Re}\, S(k,k',k'')$, $M_k > 0$, $-\pi/2 \le \beta \le \pi/2$, $\theta = \Delta\omega t + \varphi_{k'} + \varphi_{k''} - \varphi_k$ / similarly for $\phi_{k'}$ and $\phi_{k''}$ /. The three expressions in parenthesis in eq. /3/ are in fact the Manley-Rowe invariants of a system with real $S(k,k',k'')$, $S(k',-k'',k)$ and $S(k'',k,-k')$. For the system /1/ the total wave energy is not an invariant since

$$\frac{d}{dt}\left(\sigma_k\epsilon_k\omega_k A_k^2 + \sigma_{k'}\epsilon_{k'}\omega_{k'}A_{k'}^2 + \sigma_{k''}\epsilon_{k''}\omega_{k''}A_{k''}^2\right) = -2A_kA_{k'}A_{k''}\left(\omega_k tg\beta_k + \omega_{k'}tg\beta_{k'} + \omega_{k''}tg\beta_{k''}\right)\cos\theta \qquad /4/$$

Clearly, the solution of /1/ depends strongly on the signs $\sigma\epsilon$. For eq. /2/ the following cases can be distinguished:

1. $\epsilon_k = \epsilon_{k'} = \epsilon_{k''}$, $\mathrm{Im}\, S = 0$ which leads to

$$k^2\, S(k,k',k'') = k'^2\, S(k',-k'',k) = k''^2\, S(k'',k,-k')$$

This case occurs for parallel propagation and for perpendicular propagation when the three wave vectors are in the same direction, $\Psi_k = \Psi_{k'} = \Psi_{k''}$.

2. $\epsilon_k = \epsilon_{k'} = \epsilon_{k''}$, $\mathrm{Im}\, S \neq 0$ giving us

$$k^2\, S^*(k,k',k'') = k'^2\, S(k',-k'',k) = k''^2\, S(k'',k,-k')$$

This case occurs for perpendicular propagation when the wave vectors are not parallel, $\Psi_k \neq \Psi_{k'} \neq \Psi_{k''}$.

3. $\epsilon_k \neq \epsilon_{k'} \neq \epsilon_{k''}$, $\mathrm{Im}\, S \neq 0$. This is the general case of oblique propagation. It can be established from eq. /2/ that no symmetry exists in the coupling coefficients, i.e. with $\Psi_k \neq \Psi_{k'} \neq \Psi_{k''}$ and $k_x \neq k'_x \neq k''_x$ we have the following:

$$k^2\,\mathrm{Re}\, S(k,k',k'') + k'^2\,\mathrm{Re}\, S(k',-k'',k) + k''^2\,\mathrm{Re}\, S(k'',k,-k')$$
$$k^2\,\mathrm{Im}\, S(k,k',k'') + k'^2\,\mathrm{Im}\, S(k',-k'',k) + k''^2\,\mathrm{Im}\, S(k'',k,-k')$$

These three cases show that the nonlinear interaction between electrostatic modes in a magnetoplasma is highly asymmetric. Consequently in order to predict the existence of instability, it is necessary to modify the rules which have been used in the past to study symmetric interactions. Considering first cases 1. and 2., we see that since S are symmetric, the nature of the interaction can be predicted solely by the sign of the wave energy. Thus in those cases, explosive instability can exist only if one wave has negative energy while the remaining two have positive energy [1] . This interaction exists for perpendicular propagation when the electron velocity distribution is a δ function [2] . Three positive energy waves cannot have simultaneously growing amplitudes.

For oblique propagation , case 3, the asymmetric form of the coefficient implies that the sign of the energy cannot be used alone to determine the nature of the interaction. It is necessary to take into consideration the exact form of $S(k,k',k'')$, $S(k',-k'',k)$, $S(k'',k,-k')$. Hence, a general instability criterion cannot be established analytically for this case. We can see, however, new possibilities of instability and parametric excitation of obliquely propagating waves. For example, we can envisage explosive instabilities resulting from the nonlinear interaction of three positive energy waves.or three negative energy waves. Another example is parametric wave excitation resulting from the interaction between a positive and negative energy wave. If the wave ϕ_k is the pump mode, $\phi_{k'}$ the idler mode, $\phi_{k''}$ the Stokes' mode, the growth rate γ is given by

$$\gamma^2 = \sigma_{k'}\sigma_{k''}\left|\frac{\partial\varepsilon_0}{\partial\omega}\right|^{-1}_{\omega_{k'}} \left|\frac{\partial\varepsilon_0}{\partial\omega}\right|^{-1}_{\omega_{k''}} S^*(k',-k'',k)\, S(k'',k,-k')$$

From this expression it follows that parametric excitation may be possible if $\epsilon_{k'} \neq \epsilon_{k''}$ and $\sigma_{k'} = \sigma_{k''}$.

It should be noted that in the new interactions mentioned above, the sum of the wave energies is no longer a constant . Conservation of energy would give us

$$\omega_k\sigma_k A_k^2 + \omega_{k'}\sigma_{k'}A_{k'}^2 + \omega_{k''}\sigma_{k''}A_{k''}^2 = C_5$$

which is in contradiction with eq. /4/. This implies that another energy source, which is not included in the equations describing the wave interaction, must exist in the plasma.

References:

1. Rosenbluth N.N., Coppi B., Sudan R.N., Annals of Physics /USA/ 55 /1969/, 207.
2. Fukai J., Krishan S., Harris E.G., Phys. Rev. Letters 23 /1969/, 910.
3. Goldman R., Davidson R., Hasegawa A., Physics of Fluids 12 /1969/, 1247.
4. Harker K.J., Crawford F.W., Journ. of Appl. Physics 39 /1968/, 5959.
5. Teichmann J., Journ. Plasma Physics 2 /1968/, 353.
6. Armstrong J.A., Bloembergen N., Ducuing J., Pershan P.S., Phys. Rev. 127 /1962/, 1918.

KINETIC THEORY OF ANOMALOUS DIFFUSION DUE TO A DRIFT DISSIPATIVE INSTABILITY

by

P.ROLLAND

ASSOCIATION EURATOM - CEA
Département de la Physique du Plasma et de la Fusion Contrôlée
Service S.G.N. Centre d'Etudes Nucléaire
Cedex 05. 38 Grenoble Gare (France)

Abstract : A kinetic theory of classical and anomalous diffusion is presented, taking into account the average of the quadratic effects associated with the presence of a drift dissipative instability. The obtained results enable us to study some of the saturation mechanisms of the instability.

1. Introduction : One knows already several semi-empirical formulae giving an order of magnitude of the flux of anomalous diffusion arising from the drift dissipative instability (1) but no exact quantitative expressions have yet been given. We want to calculate the diffusion fluxes as functions of the wave amplitude, by taking into account the exact features of the instability. First, we integrate the zero order kinetic equation for the electrons, to obtain an equilibrium state in which we see the plasma motion at the drift velocity, and also the classical diffusion. The integration of the first order perturbed equation enables us incidently to confirm the validity of the fluid equations. Then we integrate the second order perturbed equation, in which appears the average quadratic term $\langle \frac{e}{m} E_1 . \nabla_v f_1 \rangle$, in order to obtain the new equilibrium state, in the presence of the wave. This state is caracterized by an enhanced diffusion, already obtained in some limit using a fluid theory. The mechanism of this diffusion appears clearly, an we can see why its upper limit is given by Bohm's formula. This result enables us to study quantitatively certain saturation processes, of important practical interest.

2. Equilibrium state : We assume that electron-neutral collisions are dominant, and that the relaxation can be described by Krook's model (2). The kinetic equation can be written, for the electrons :

$$(1)\qquad \partial_t f + v.\nabla_r f + \frac{e}{m}\left[E + v \wedge B\right].\nabla_v f = -\nu\left[f - \frac{N}{N_0} F_0\right] \qquad \text{where}$$

$$(2)\qquad F_0 = A \exp -b\left(v_x^2 + v_y^2 + v_z^2\right) \;,\; N_0 = A\pi^{\frac{3}{2}} b^{-\frac{3}{2}},\; N = \int f \, dv \;,\; 2b = \frac{m}{T}$$

In the absence of the wave, E = 0, B = B_0. The characteristic system is :

$$(3)\qquad \frac{dt}{1} = \frac{dx}{v_x} = \frac{dy}{v_y} = \frac{dz}{v_z} = \frac{dv_x}{\Omega v_y} = \frac{dv_y}{-\Omega v_x} = \frac{dv_z}{0} = \frac{df}{-\nu\left[f - \frac{N}{N_0} F_0\right]} \qquad (\Omega = \frac{eB_0}{m})$$

The "Trajectories" are defined by the 6 invariants :

$$(4)\qquad C_1 = v_x \cos \Omega t - v_y \sin \Omega t \qquad C_2 = v_x \sin \Omega t + v_y \cos \Omega t \qquad C_3 = v_z$$

$$C_4 = x + \frac{v_y}{\Omega} \qquad C_5 = y - \frac{v_x}{\Omega} \qquad C_6 = z - v_z t$$

We integrate df/dt on these trajectories and we get, for $t - t_0 \gg \nu^{-1}$:

$$(5)\qquad f_{eq} = \left[1 + \varepsilon\left(\gamma - \frac{v_x}{\Omega}\right)\right] F_0 - \frac{\nu\varepsilon}{\Omega^2 + \nu^2}\left[v_y - \frac{\nu}{\Omega} v_x\right] F_0 \qquad \text{where : } \varepsilon = \frac{1}{N}\frac{dN}{dy}$$

The first term in eq. (5) gives the drift motion of the electrons with the velocity $V_0^x = -\frac{T\varepsilon}{m\Omega}$. The second term coming from the combined effects of collisions and the variation of N along the Larmor circle, gives the classical diffusion :

$$V_0^y = -\frac{T}{m}\frac{\nu\varepsilon}{\Omega^2} \;.$$

3. Perturbed state of first order. We put $f = f_{eq} + f_1$ and we linearize the equation (1). The characteristic system is still given by eq. (3) except for the last term. The trajectories are still given by eq. (4). On these trajectories we have :

$$(6)\qquad \frac{df_1}{dt} = -\nu f_1 + \nu \frac{n_1}{N_0} F_0 - \frac{e}{m} E_1 . \nabla_v f_{eq}$$

In the quasi-electrostatic approximation, $E_1 = -\nabla \phi_1$. We suppose that all the per-turbed quantities vary like exp$i$ $(\omega t + k.r)$ and we integrate eq. (6) along the trajectories. We obtain :

$$(7)\qquad \begin{aligned} f_1(\omega,k) = {} & \frac{1}{(\nu + i\omega + ik_z v_z)}\left\{\frac{\nu n_1}{N_0} F_0 - i\frac{e\phi}{T} F_0\left[k_x v_z\left(1 + \varepsilon\left(\gamma - \frac{v_x}{\Omega}\right)\right) + \frac{Tk_x\varepsilon}{m\Omega}\right]\right\}\left(1 - \frac{i}{\Omega}\left(k_y v_x - k_x v_y\right)\right) \\ & - \frac{i\Omega}{\Omega^2 + (\nu + i\omega + ik_z v_z)^2}\left\{\frac{\nu n_1}{N_0}\frac{F_0}{\Omega}\left(k_x v_x + k_y v_y\right) - \frac{e\phi}{T} F_0\left[\left(1 + \varepsilon\left(\gamma - \frac{v_x}{\Omega}\right)\right)\left[\frac{ik_z v_z}{\Omega}\left(k_x v_x + k_y v_y\right)\right.\right.\right. \\ & \left.\left.\left. - \left(1 - \frac{i}{\Omega}\left(k_y v_x - k_x v_y\right)\right)\left(k_y v_x - k_x v_y\right)\right] + i\frac{T\varepsilon k_x}{m\Omega^2}\left(k_x v_x + k_y v_y\right)\right]\right\} \\ & + \frac{i\nu}{\Omega^2 + (\nu + i\omega + ik_z v_z)^2}\left\{\frac{\nu n_1}{N_0}\frac{F_0}{\Omega}\left(k_y v_x - k_x v_y\right) - \frac{e\phi}{T} F_0\left[\left(1 + \varepsilon\left(\gamma - \frac{v_x}{\Omega}\right)\right)\left(1 - \frac{i}{\Omega}\left(k_y v_x\right.\right.\right.\right. \\ & \left.\left.\left.\left. - k_x v_y\right)\right) + \frac{iT\varepsilon k_x}{m\Omega^2}\left(k_y v_x - k_x v_y\right)\right]\right\} \end{aligned}$$

By the way, on can verify that eq. (7) gives the expressions for v and n already obtained by using the fluid theory based on the equation of motion (8) in which T = cte :

$$(8)\qquad N\left\{-\frac{e}{m} E - v \wedge \Omega + \nu v + \partial_t v + (v.\nabla) v\right\} + \frac{T}{m}\nabla N = 0$$

This proves that the pressure term in eq. (8) is correct up to the first order, [illegible] trivial.

4. Perturbed state of second order. In the presence of the wave, supposed to be single, the equilibrium state is modified. As long as the wave amplitude is small enough, we can still express f_1 by neglecting the non linear effect and calculate the modification g of the equilibrium distribution f_{eq} , retaining in the second order perturbed equation only the time average of the non-linear term $E_1 . \nabla_v f_1$. We write $f = f_{eq} + f_1 + g$ where g is given by the equation :

$$(9)\qquad \partial_t g + v.\nabla_r g + \frac{e}{m} v \wedge B . \nabla_v g + \langle \frac{e}{m} E_1 . \nabla_v f_1 \rangle = -\nu\left[g - \frac{\delta N}{N_0} F_0\right] \qquad (\delta N = \int g \, dv)$$

The trajectories are still given by eq. (4). On these trajectories we have :

$$(10)\qquad \frac{dg}{dt} = -\nu\left[g - \frac{\delta N}{N_0} F_0\right] - \langle \frac{e}{m} E_1 . \nabla_v f_1 \rangle \qquad \text{so that :}$$

$$(11)\qquad g = \int_0^\infty ds \, e^{-\nu s}\left\{\nu \frac{\delta N}{N_0} F_0 - \langle \frac{e}{m} E_1 . \nabla_v f_1 \rangle\right\}'$$

Using eq. (7) we calculate the product $\frac{e}{m} E_1 . \nabla_v f_1$ and its time average. Let us put :

$$(12)\qquad \frac{n_i}{N_0} = -\frac{e\phi}{T}\mu \qquad \text{and} \qquad D = \frac{T}{m\nu} \;. \qquad \text{We obtain, when } \omega \ll k_z v_z \ll \nu \ll \Omega :$$

$$(13)\qquad \begin{aligned} g = {} & \frac{\delta N}{N_0} F_0 + \frac{F_0}{\nu}\langle\left(\frac{e\phi}{T}\right)^2\rangle\left\{k_x v_z\left(\mu_i + 2\frac{\omega_*}{\nu}\right) + \frac{k_x^2 v_z^2}{\nu}\left(1 - \mu_r\right) - Dk_z^2\left(1 - \mu_r\right)\right\} + \\ & \frac{F_0}{\Omega}\langle\left(\frac{e\phi}{T}\right)^2\rangle\left\{\left(k_y v_x - k_x v_y\right) + \frac{\nu}{\Omega}\left(k_x v_x + k_y v_y\right)\right\}\left\{\mu_i + \frac{\omega_*}{\nu} + \frac{k_z v_z}{\nu}\left(1 - \mu_r\right) + \ldots\right\} \end{aligned}$$

Integrating eq. (13) we obtain the fluxes of anomalous diffusion :

$$(14)\qquad \begin{aligned} \Psi_x &= \int v_x g \, dv = \frac{N_0 T}{m\Omega}\left(\mu_i + \frac{\omega_*}{\nu}\right)\left(k_y + \frac{\nu}{\Omega} k_x\right)\langle\left(\frac{e\phi}{T}\right)^2\rangle \\ \Psi_y &= \int v_y g \, dv = -\frac{N_0 T}{m\Omega}\left(\mu_i + \frac{\omega_*}{\nu}\right)\left(k_x - \frac{\nu}{\Omega} k_y\right)\langle\left(\frac{e\phi}{T}\right)^2\rangle \qquad \left(\omega_* = \frac{k_x T\varepsilon}{m\Omega}\right) \\ \Psi_z &= \int v_z g \, dv = \frac{N_0 T}{m\nu} k_z\left(\mu_i + 2\frac{\omega_*}{\nu}\right)\langle\left(\frac{e\phi}{T}\right)^2\rangle \qquad \left(\omega_s = \frac{\Omega_e \Omega_i k_z^2}{\nu k_\perp^2}\right) \end{aligned}$$

In the limit $\omega_s \ll \nu$, $\mu_i \gg \omega_* \nu^{-1}$ we have $\mu_r \approx 1$ and $\mu_i \approx \frac{\omega_*}{\omega_s}$; then eq. (14) agrees with the result of fluid theory.

5. A saturation mechanism. This enhanced diffusion must be limited because the variation g itself modifies f_1 , and especially modifies the phase μ_i between the fluctuations of density and potential, and this phase plays an essential role in the diffusion given by eq. (14). The modification of f_1 is :

$$(15)\qquad \delta f_1 = \int_0^\infty ds\, e^{-\nu s}\left\{\frac{\nu F_0}{N_0}\delta n_1 + i\frac{e\phi}{m} k . \nabla_v g\right\}'\left(1 - \frac{i}{\Omega}\left(k_y v_x' - k_x v_y'\right)\right) e^{-ik_z v_z s - i\omega s}$$

In the limit of small Larmor radius, we obtain :

$$(16)\qquad \frac{\delta n_1}{N_0}\left(i\omega + Dk_z^2\right) = \frac{e\phi}{m} k_z^2\left\{-\frac{\delta N}{N_0} + 2i\frac{Dk_z^2}{\nu}\left(\mu_i + 2\frac{\omega_*}{\nu}\right)\langle\left(\frac{e\phi}{T}\right)^2\rangle\right\}$$

We combine eq. (16) with the well known expression (17) :

$$(17)\qquad \frac{n_i}{N_0}\left(i\omega + Dk_z^2\right) = -\frac{e\phi}{T}\left(i\omega_* + Dk_z^2\right)$$

This leads to a new dispersion equation, differing from that of Kadomtsev ((3) eq. IV. 90) only by a term in $\langle\phi^2\rangle$:

$$(18)\qquad \omega^2 - i\omega\left[Dk_z^2 + \omega_s - 2i\omega_s\frac{Dk_z^2}{\nu}\left(\mu_i + 2\frac{\omega_*}{\nu}\right)\langle\left(\frac{e\phi}{T}\right)^2\rangle\right] + i\omega_s\omega_* = 0$$

The instability is satured when $\mathrm{Im}(\omega) = 0$. Then eq. (16) (17) (18) show that $\mu_i = 0$, that is to say that the density and potential have the same phase. Using eq. (18) we find that the amplitude of the perturbation reaches the value :

$$(19)\qquad \langle\left(\frac{e\phi}{T}\right)^2\rangle = \frac{\nu^2}{4Dk_z^2\left(\omega_s + Dk_z^2\right)} \qquad \text{(assumed to be } \ll 1\text{).}$$

The diffusion fluxes reach the values :

$$(20)\qquad \Psi_y = -\frac{N_0\omega_* \nu^2 k_x}{4\Omega k_z^2\left(\omega_s + Dk_z^2\right)} \qquad \Psi_z = \frac{N_0\omega_* \nu}{4k_z\left(\omega_s + Dk_z^2\right)}$$

This saturation process leads to a diffusion smaller than Bohm's value. It appears only if the non-linear effects remain small enough so that eq. (9) can be used. Other effects do exist : in particular, if $\nu^2 \geq \left(\omega_s + Dk_z^2\right)Dk_z^2$ the lack of electrons ($\frac{e\phi}{T} \approx 1$) limits the wave amplitudes, and the Bohm diffusion can be reached when $\omega_* \approx \omega_s$ and $k_x \approx \varepsilon$.

References : (1) M.Bernard - G.Briffod - R.Frank - M.Grégoire - J.Weisse. Conference Novosibirsk (1968).
(2) P.L.Bhatnagar, E.P.Gross - M.Krook - Phys. Rev. 94, 3 may 1954.
(3) B.B.Kadomtsev - Plasma Turbulence (Acad. Press London).

THE TEMPERATURE PROFILE IN A STEADY-STATE THERMONUCLEAR REACTOR

by

J. Rem and G.K. Verboom

Association Euratom-FOM/FOM-Instituut voor Plasma-Fysica
Rijnhuizen, Jutphaas, the Netherlands

Abstract

A steady-state, thermonuclear D-T plasma column, surrounded by a cold plasma has been investigated by solving the MHD equations numerically. A solution in which the temperature falls to a low value at the boundary is found to exist only in a limited range of values for the characteristic parameters. Fuel is supplied and ash removed at the boundary.

In reactor studies carried out these last years the thermonuclear plasma is usually assumed to be a steady-state plasma cylinder in a strong longitudinal magnetic field surrounded by a vacuum (for an extensive list of references see Ref. 1). The temperature of this column is then taken constant while the associated refueling problem is hardly considered. In this paper we treat a thermonuclear plasma surrounded by a high-density relatively cold, plasma. In such a plasma the heat conduction to the wall is one of the mechanisms that determine a radial temperature profile. It has the advantage that if the temperature at the wall is sufficiently low the fuel can be supplied at the boundary. Since the transport processes are similar to those in an arc in a magnetic field, the electron-ion collisions must be expected to have a large influence on the temperature profile[2,3].

To investigate whether the appropriate MHD equations permit such a thermonuclear plasma to exist we consider an infinitely long, fully ionized, plasma cylinder in a strong magnetic field in which the energy is supplied by thermonuclear reactions and is lost through Bremstrahlung and heat conduction. An equal mixture of deuterium and tritium burns into helium (^{4}He) and is the only energy source. The neutrons created in the reaction are assumed to be absorbed somewhere outside the plasma. The plasma being fully ionized we have to restrict the analysis to the region where the temperature is higher than a certain minimum, for which we have taken 1×10^5 K.

The plasma is described by the continuity equations and the equations of motion for the species, one energy equation[4], the equations of state for the species, and Maxwell's equations. In these equations we make the following assumptions: quasi-neutrality, one temperature for all species, no reabsorption of Bremstrahlung, no viscosity, no inertia effects, no momentum transfer by inelastic collisions, all velocities are small compared to the thermal speeds, the product of the cyclotron frequency and the collision time for all species is much larger than unity, the magnetic field B has an axial component only. The magnetic field strength must be sufficiently large to insure that the larmor radius of the helium is small compared to the half width of the temperature profile, defined as the distance from the axis of the plasma column ($r = 0$) to the place where the temperature has fallen to half its value on the axis. Only then it is permitted to assume that the helium ions obtain their energy at the same place as where they give it off to the plasma.

The temperature profile found upon solving the equations must satisfy the following conditions to be acceptable: 1) the temperature of 1×10^5 K must be reached and 2) the assumptions made above must hold of which the one concerning the velocities of the species turns out to be the most critical. Both these conditions are found to limit the range of solutions. Figure 1 shows for which axis values (indicated by the subscript o) of n_4/n_d and T at $p_o = 50$ atm and $B_o = 1$ tesla a solution exists. The line $Q_P = Q_R$ forms a lower limit on T_o, on the left of which condition 1) is not satisfied, while condition 2) forms a lower limit on the admissible value of n_{4o}/n_{do} (line $V_{4r} = \sqrt{\frac{kT}{m_4}}$). Below this line the radial velocity of helium goes to infinity before the required temperature of 1×10^5 K is reached. For high values of n_{4o}/n_{do} the solution is restricted by the condition $q_{P_o} > q_{R_o}$, i.e. the nuclear energy given to the plasma must be larger than the radiated energy per unit volume. In this way we have limited the possible solutions to those in which on the axis $d^2T/dr^2 > 0$. The lines $q_P = q_R$ and $V_{4r} = \sqrt{\frac{kT}{m_4}}$ are not influenced by a change in B_o; the line $Q_P = Q_R$ moves to higher temperatures if B_o is increased, i.e. the range of possible axis temperatures becomes smaller. Since the neutrons carry 4 times as much energy as the helium ions (Q_P) the total energy production is easily read out of this figure, i.e. it is 5 Q_P. In fig. 2, Q_P and Q_R are given as function of T_o for different values of n_{4o}/n_{do} at $B_o = 1$ tesla and $p_o = 50$ atm. The enveloping curves, -.- for Q_P and -..- for Q_R, indicate the region in which a solution exists. The energy carried to the wall can also be read from this figure as it is equal to the difference between Q_P and Q_R. An example of the radial dependence of various quantities is presented in fig. 3. It shows how the temperature profile changes if B_o is changed. Increasing the parameter n_{4o}/n_{do}, while keeping the other parameters constant generally has the effect of broadening the profile. Since a lowering of B_o has a similar effect as increasing n_{4o}/n_{do}, the power production at a fixed T_o and p_o is maximal at low B_o and high n_{4o}/n_{do}. Increasing the pressure p_o with a factor of two broadens the temperature profile approximately 10 percent. Hence, the total nuclear power becomes ~ 5 times larger, making a production of 10^8 W/m easy to obtain. Since the radial velocity of the fuel is low, ~ 10^{-3} m/s, the fuel can easily be supplied at the boundary of our model.

The authors wish to express their gratitude to Dr. J.C. Terlouw and Dr. M.P.H. Weenink for valuable discussions.

This work was performed under the Euratom-FOM association agreement with financial support from ZWO and Euratom.

References

1. Rose, D.J., Nucl. Fusion 9 (1969) 183.
2. Verboom, G.K., Plasma Phys. 11 (1969) 903.
3. Klüber, O., Z. Naturforsch. 18a (1963) 1151.
4. Braginskii, S.I., Reviews of Plasma Physics 1 (Consultants Bureau Enterprises, New York, 1965).

n_4 = helium density
n_d = deuterium density
m_4 = helium mass
Q_P = total nuclear energy given to the plasma
Q_R = total energy radiated away by Bremstrahlung
q_P = nuclear energy per unit volume given to the plasma
q_R = energy per unit volume radiated away by Bremstrahlung

subscript o refers at $r = 0$.

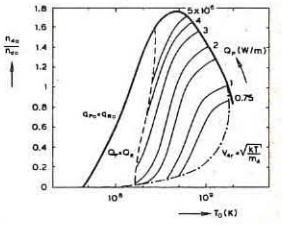

Fig.1. Permissible values of T_o and n_{4o}/n_{do} at $p_o = 50$ atm, $B_o = 1$ tesla

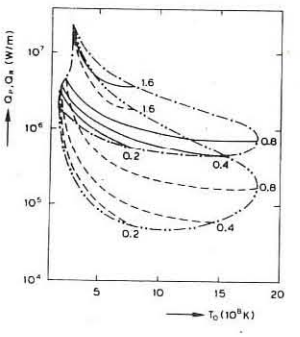

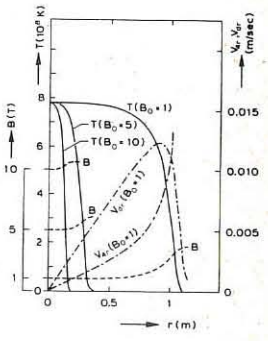

Fig.2. Q_P(-) and Q_R(--) as function of T_o for several values of n_{4o}/n_{do} at $p_o = 50$ atm and $B_o = 1$ tesla (left fig.)

Fig.3. Temperature and magnetic field profiles for different B_o; the radial velocity profile of helium and deuterium for $B_o = 1$ T, $p_o = 50$ atm, $T_o = 7.8 \times 10^6$ K, and $n_{4o}/n_{do} = 1.6$

PLASMA INSTABILITIES CONNECTED WITH THERMONUCLEAR REACTIONS

Ya.I.Kolesnichenko, V.N.Oraevsky

Institute of Physics of the Ukrainian SSR Academy of Sciences, Kiev, Union of Soviet Socialist Republics

Abstract. The paper presents a consistent analysis of the main types of instabilities in high temperature plasma, which stem from the accumulation of thermonuclear reaction (TNR) products in thermonuclear devices.

In the course of operation of TNR devices high energy charged particles may be accumulated in the plasma due to TNR. These particles "introduce" an additional thermodynamic nonequilibrium into the plasma systems (an explicit form for the TNR products distribution function was calculated in /1/). Then, the following problem arises, whether this nonequilibrium is sufficient for the emergence of new instabilities. Paper /1/ gives an answer to the question: the plasma becomes, in fact, unstable when the TNR products density exceeds a certain critical value. Furthermore, some new instabilities due to the TNR products accumulation were recognized in /2/-/6/.

Naturally, the case of small TNR products density is of the primary concern. Therefore, one may apply perturbation theory to the stability problem the TNR product density used as a small parameter.

It is well known, that equation describing the plasma oscillations can be presented as /7/:

$$\Lambda_{ik} E_k = 0; \quad \Lambda_{ij} \equiv N^2\left(\frac{k_i k_j}{k^2} - \delta_{ij}\right) + \varepsilon_{ij}. \qquad (1)$$

With tensor ε_{ij} put down as a sum of two terms $\varepsilon_{ij} = \varepsilon_{ij}^{(0)} + \varepsilon'_{ij}$ where ε'_{ij} is a term due to the TNR products, one can rewrite expressions (1) as follows:

$$\Lambda_{ik}^{(0)} E_k = -\varepsilon'_{ik} E_k; \qquad (2)$$

Hence assuming ε'_{ik} to be small, we obtain an expression for the corrections to the magneto-active plasma eigenfrequencies, associated with TNR products (roof-crossing is neglected for simplicity):

$$\Delta\omega = -\frac{\langle e_i^* | \varepsilon'_{ik} | e_k \rangle}{\langle e_i^* \left| \frac{\partial \Lambda_{ik}}{\partial \omega} \right| e_k \rangle}; \qquad (3)$$

where $\vec{e}$ is a polarization vector of the respective wave.

For toroidal systems (which seems most advantageous at present) where plasma pressure is supposed to be small in comparison with the magnetic one, we assume in following that $8\pi P/H^2 \equiv \beta << 1$.

Starting from (3) and explicit form for calculated in /6/, /5/ we get the following results, which are arranged in the Table*):

Oscillation mode	Instability "threshold"	Maximum value of instability growth rate
$\omega = k_z V_s$	$\frac{n'}{n} > \sqrt{\frac{m_e}{m_i}} \cdot \frac{\omega_i^2}{k_\perp^2 V_s^2}$, $k_\perp \gtrsim \frac{\omega_i}{U}$	$\gamma \sim \frac{n'}{n} \cdot \frac{k_\perp^2 V_s^2}{\omega_i}$
$\omega = k_z V_A$	$\frac{n'}{n} > \frac{m_e}{m_i}\left(\frac{V_A}{U}\right)^2 \frac{V_e}{U}$	$\gamma \sim \frac{n'}{n}\omega_i$
$\omega = k V_A$	$\frac{n'}{n} > \frac{m_e}{m_i} \cdot \frac{V_e}{U}$	$\gamma \sim \frac{n'}{n} \cdot \frac{U}{V_A} \cdot \omega_i$
$\omega \approx l\omega_i$	$\frac{n'}{n} > \frac{\omega_i^2 U}{k_\perp^2 V_i^3} I_l(z) \cdot$ $\cdot \exp\{-x_l^2 - z\}$, $x_l > 1$	$\gamma \sim \left(\frac{m_e}{m_i}\right)^2 \cdot \frac{n'}{n} \cdot$ $\cdot \frac{l^6 \omega_i^4 I_l e^{-z} k_\perp^2}{V_i^2 U \lvert k_z \rvert^5}$
$\omega \sim \Omega_i$	$\frac{n'}{n} > 10^{-3}$	$\gamma \sim \frac{n'}{n}\omega_* \gtrsim \omega_i$

*) Part of results in the Table are obtain in /1/, /3/ - /5/.

Here, n and n' stand for plasma and TNR products densities; U is an rms velocity of TNR products:

$$V_s = \sqrt{\frac{T_e}{m_i}}; \quad V_A = \sqrt{\frac{H^2}{4\pi n m_i}}; \quad \omega_i = \frac{e_i H}{m_i c}; \quad \Omega_i = \sqrt{\frac{4\pi n e_i^2}{m_i}};$$

$$\omega_* = -\frac{k_y U^2}{\omega_i} \cdot \frac{d \ln n}{dx}; \quad z = \frac{k_\perp^2 V_i^2}{\omega_i^2}; \quad x_l = \frac{m_e}{m_i}\left(\frac{l\omega_i}{k_z V_i}\right)^3 I_l(z) e^{-z};$$

$I_l(z)$ are modified Bessel functions of the l -order. Inequality $T_e \gtrsim T_i$ is used for evaluation of the thresholds.

References

1. Kolesnichenko Ya.I., Oraevsky V.N., Atomnaja energija, 23, 289 (1967)
2. Korablev L.V., Zh. eksp. teor. Fiz., 53, 1600 (1967)
3. Korablev L.V., Rudakov L.I., Zh. eksp. teor. Fiz., 54, 818 (1968)
4. Belikov V.S., Kolesnichenko Ya.I., Oraevsky V.N., Zh.eksp. teor. Fiz., 55, 2210 (1968)
5. Kolesnichenko Ya.I., Ukr. Fiz. Zh., 14, 1070 (1969)
6. Belikov V.S.,Kolesnichenko Ya.I., Oraevsky V.N., Ukr. Fiz. Zh., 14, 1242 (1969)
7. Sitenko A.G., Stepanov K.N., Zh. eksp. teor. Fiz., 31, 642 (1956)

VARIATIONAL ANALYSIS OF LINEARIZED VLASOV PLASMAS*

by

H. Ralph Lewis

University of California, Los Alamos Scientific Laboratory
P. O. Box 1663, Los Alamos, New Mexico 87544
USA

Abstract: Analysis of linearized Vlasov plasmas by means of Hamilton's principle is illustrated by application to the initial-value problem for a neutralized, single-species plasma in one spatial dimension with periodic boundary conditions. For any degree of approximation and for arbitrary equilibrium velocity distributions, the problem is reduced to the solution of a system of ordinary differential equations in time with constant coefficients and time-dependent driving terms, and an exact particular solution has been found. Numerical results will be presented both for Maxwellian and nonMaxwellian equilibrium velocity distributions.

Application of Hamilton's variational principle to Vlasov plasmas was originally formulated for use in investigating nonlinear behavior [1], and this continues to be an area of active research. The variational principle has also been used to approximate the linearized description of Vlasov plasmas, including electromagnetic effects, in terms of a system of linear ordinary second-order differential equations in time with constant coefficients and time-dependent driving terms. The size of the system of equations is determined by the degree of approximation that is desired. These equations are suitable for numerical computation of the linearized behavior of even complicated physical situations. The constant coefficients of the homogeneous part of the equations depend on the equilibrium distribution functions, but they do not depend on knowledge of the equilibrium particle orbits. The time-dependent driving terms depend on the perturbations of the equilibrium distribution functions and on some knowledge of the unperturbed orbits. Therefore, to compute the linear eigenfrequencies, no integration along unperturbed orbits is required. To do the complete initial value problem, some knowledge of the unperturbed trajectories is required, as would be expected.

This method has been successfully applied to the problem of electrostatic oscillations of a neutralized, single-species plasma in one spatial dimension with periodic boundary conditions. The equilibrium velocity distribution functions can be arbitrary, and the ones used have included a single Maxwellian distribution, sums of two Maxwellian distributions, and nonanalytic distributions that are bounded in velocity and represented by cubic spline functions. A particular solution of the basic equations has been found for an arbitrary equilibrium velocity distribution. The Landau damping rates and growth rates observed for some of the cases in which the equilibrium velocity distribution was a Maxwellian or a sum of two Maxwellians were compared with precise numerical solutions of the usual dispersion relation [2]. The rates observed with the variational method reported here agree well with those computed from the dispersion relation. Specific results of numerical computation with the variational method will be given in the oral presentation.

In the variational method, the basic functions that enter are the particle positions as functions of initial conditions and time and the electromagnetic potentials as functions of space and time. The initial distribution functions are specified as initial data, but the distribution functions at later times do not enter into the equations.

For the case of a neutralized, single-species plasma in one spatial dimension with periodic boundary conditions, we take the normalized equilibrium velocity distribution function to be $F(v)$, and we write the initial distribution function of position x and velocity v as

$$f(x, v, 0) = F(v) + \left[G(v)e^{iKx} + G^*(v)e^{-iKx} \right] . \tag{1}$$

The scalar potential is represented as

$$\phi(x, t) = 2\mathrm{Re}\left[\alpha(t)e^{iKx} \right] , \tag{2}$$

and the x-coordinate of a particle whose initial position and velocity are x' and v', respectively, is represented as

$$X(x', v', t) = x' + v't + 2\mathrm{Re}\left[\sum_j \gamma_j(t)e^{iK(x'+v't)} \chi_j(v') \right] . \tag{3}$$

The initial conditions on $\gamma_j(t)$ are $\gamma_j(0) = \dot{\gamma}_j(0) = 0$. For convenience in the formulation, we normalize the equilibrium particle density, n_o, to unity ($n_o = 1$), and we take the functions $\chi_j(v')$ to be orthonormal to one another with respect to $F(v')$ as a weight function. If the $\chi_j(v')$ form a complete set, then the representation of $\phi(x,t)$ and $X(x',v',t)$ are exact. The quantities to be determined are $\gamma_j(t)$ and $\alpha(t)$; these quantities, along with $G(v)$, are considered small for the purposes of linearization.

The Euler-Lagrange equations, written in terms of a column matrix γ whose j^{th} element is γ_j, are

$$\ddot{\gamma} + i2KV\dot{\gamma} - K^2V^2\gamma + \omega_o^2 P\gamma = \omega_o^2 g(t)\sigma \tag{4}$$

and

$$\alpha(t) = (4\pi Q/iK)\left[\sum_j \sigma_j\gamma_j(t) - g(t)\right] , \tag{5}$$

where σ is a column matrix, V and P are square matrices, Q and M are the charge and mass per particle, and $\omega_o^2 = (4\pi n_o Q^2/M)$. The quantities σ, V, P, and $g(t)$ are defined as

$$\begin{aligned} &\sigma_j = \int dv F(v)\chi_j(v), \quad V_{j\ell} = \int dv F(v)\chi_j(v)v\chi_\ell(v) , \\ &P_{j\ell} = \sigma_j\sigma_\ell, \quad \text{and } g(t) = \frac{1}{iK}\int dv G(v)e^{-iKvt} . \end{aligned} \tag{6}$$

If the $\chi_j(v)$ form a complete set, then the solution of Eq. (4) can be written as

$$\gamma_j(t) = \eta_j(t) + \frac{1}{iK}\int dv\, G(v)e^{-iKvt}\chi_j(v) , \tag{7}$$

where the quantities $\eta_j(t)$ satisfy the homogeneous form of Eq. (4). It has been demonstrated that this formulation is completely equivalent to the usual linearized theory in terms of a time-dependent distribution function when the $\chi_j(v)$ form a complete set.

For the numerical computations, the $\chi_j(v)$ have been chosen as the orthonormal polynomials with weight function $F(v)$. Then the matrix V is tridiagonal and it can be written in terms of the coefficients of the three-term recursion formula for the orthonormal polynomials; these coefficients are easily found numerically for arbitrary $F(v)$.

---

* Work performed under the auspices of the United States Atomic Energy Commission.

[1] H. Ralph Lewis, chapter in Methods in Computational Physics (Academic Press, Inc., New York, 1970), Vol. 9.

[2] D. W. Forslund, private communication.

PLASMA MOTION AND EQUILIBRIUM IN UNSYMMETRIC MAGNETIC FIELDS

by

Bo Lehnert

ROYAL INSTITUTE OF TECHNOLOGY
S-10044 Stockholm 70, Sweden

Abstract: Stationary plasmas confined by a magnetic field of short connection length and arbitrary shape are treated in terms of average motions in $\alpha\beta$ space defined by the field lines. Local fluid motions are allowed to take place. An average macroscopic fluid velocity is deduced in terms of which plasma equilibria can be investigated.

1. The Local Plasma Balance. The present treatment is restricted to a plasma having a small energy density compared to a strong confining magnetic field $\underline{B}$ in which both the equivalent magnetic moment M and the longitudinal invariant J can be treated as constants of the motion. In a hot confined plasma dissipation will cause the local fluid velocity of the centre of mass $\underline{v}=(m_i\underline{v}_i+m_e\underline{v}_e)/(m_i+m_e)$ to decay at essentially the same rate as the pressure gradients and the electric current density $\underline{j}$. We shall neglect dissipation here and remove the unnecessary restriction of "local static equilibria" where $\underline{v}=0$ all over the plasma. We assume $\underline{v}$ to be small and treat the electric field $\underline{E}=-\nabla\phi$ as a quantity of the same order as the terms arising from the pressure gradients in the momentum balance of the plasma. The transverse part $u_\perp$ of the guiding centre velocity should also be small compared to its component $u_\parallel$ along the magnetic field and to the velocity W of the gyro motion.

In a stationary state div $(n\underline{v})=0$, div $\underline{j}=0$ and curl $\underline{E}=0$ can be considered as subsidiary conditions for a plasma of density n which has to satisfy the equation of motion, Ohm's law, and the corresponding heat balance equations. There is a larger class of equilibria which satisfy these conditions when $\underline{v}\neq 0$ and fluid motions are allowed to exist, than that corresponding to local static equilibria with $\underline{v}=0$.

2. Average Drifts and Fluid Motions. With the present approximations the energy $H_\parallel=q\phi+MF$ of a particle of mass m, charge q, and with $F=B(1+u_\parallel^2/W^2)$ will become a constant of the motion (1,2). For a monoenergetic plasma with ions and electrons having the same velocity vectors at all points in space, both ϕ and F then become constant along a field line (3,4), as well as the longitudinal particle flux functions $G_\nu=u_{\parallel\nu}n/B$ where $\nu=i,e$ stands for ions and electrons.

We introduce a system α,β,s of curvilinear coordinates where s is in the direction of magnetic field $\underline{B}=\nabla\alpha\times\nabla\beta$. Then $H_\parallel$, F, G and J become functions of α and β only. Further, mean values are taken of the guiding centre motions along a field line, using the expressions for the corresponding contravariant components. We introduce the metric tensor g_{ij} and its determinant $g=|g_{ij}|$, as well as the longitudinal period $t_s=\oint dl_s/u_\parallel$ of the particle motion along a field line, where $dl_s=\sqrt{g_{ss}}ds$. Taking into account that $H_\parallel$ is a constant of the motion, we obtain the average guiding centre drift $\underline{U}=\underline{U}_E+\underline{U}_B$ where

$$\underline{U}_E=-\frac{\partial\phi}{\partial\beta}\underline{a}_\alpha+\frac{\partial\phi}{\partial\alpha}\underline{a}_\beta\ ;\quad \underline{U}_B=\frac{M}{q}\left(-\frac{\partial F_J}{\partial\beta}\underline{a}_\alpha+\frac{\partial F_J}{\partial\alpha}\underline{a}_\beta\right) \tag{1}$$

are the contributions from the gradients of the electric potential and the magnetic field, subscript J refers to the explicit dependence of J, and $\underline{a}_\alpha$ and $\underline{a}_\beta$ are unitary vectors in $\alpha\beta$ space.

To determine the analogous contribution to the total macroscopic particle flux from the gyro motion we introduce $Q=n/B$, the particle density $N=\oint Q dl_s$ in $\alpha\beta$ space, $G=u_\parallel Q$, and use the relations $t_s=N/G$, $\oint dl_s/Q=J/mG$, and $B=F-(m/2M)(G/Q)^2$. The corresponding average contribution to the particle flux then becomes

$$N\underline{U}_W=\left(-\underline{a}_\alpha\frac{\partial}{\partial\beta}+\underline{a}_\beta\frac{\partial}{\partial\alpha}\right)\left(\frac{M}{q}FN-\frac{1}{2q}JG\right). \tag{2}$$

Consequently, div $N\underline{U}_W=0$ in $\alpha\beta$ space, as expected since the gyro motion should not produce any changes in particle density in this approximation.

Finally, the average macroscopic fluid velocity $\underline{V}_\nu$ of one species and the corresponding centre of mass velocity $\underline{V}$ are

$$\underline{V}_\nu=\underline{U}_E+\underline{U}_{B\nu}+\underline{U}_{W\nu}\ ;\quad \underline{V}=(m_i\underline{V}_i+m_e\underline{V}_e)/(m_i+m_e)\ . \tag{3}$$

From eqs. (1)-(3) we obtain

$$\operatorname{div} N\underline{V}_\nu=\underline{U}_\nu\cdot\nabla N=U_\nu^\alpha\frac{\partial N}{\partial\alpha}+U_\nu^\beta\frac{\partial N}{\partial\beta} \tag{4}$$

which implies that density changes are only produced by the convective motion due to the average guiding centre drifts.

3. Plasma Equilibria. To establish a stationary equilibrium in the present approximation it is sufficient to realize a situation where charge separation is avoided by the average guiding centre drifts in $\alpha\beta$ space, without imposing any restriction on $\underline{v}$. This is the case when $\phi=\phi(N)$ and $F=F(N)$ and the ion and electron drifts are parallel or antiparallel (5) and directed along the surfaces N=const. In a closed magnetic bottle where F forms closed nested lines in $\alpha\beta$ space there will then be no particle leakage from the confinement region in a stable state.

If, in addition, we require $G_i=G_i(N)$ and $G_e=G_e(N)$ there should exist "average static equilibria" where the fluid velocity $\underline{V}$ can be made to vanish. An electric potential is then set up which compensates the average contributions from the magnetic gradient drift and the gyro motion and is determined by

$$\frac{d\phi}{dN}=-\frac{m_i-m_e}{m_i+m_e}\frac{M}{e}\left[\frac{dF_J}{dN}+\frac{1}{N}\frac{d}{dN}(FN)\right]+\frac{1}{2eN(m_i+m_e)}\frac{d}{dN}(m_iJ_iG_i-m_eJ_eG_e). \tag{5}$$

Local fluid motions $\underline{v}$ are allowed to exist in this case.

The present results indicate that plasma equilibrium should become possible in internal ring (or ring-current) configurations with magnetically screened supports, provided that there are no excessive losses in the small weak field regions close to the supports where this analysis is inapplicable.

References

1. B.B. Kadomtsev, Plasma Physics and the Problem of Controlled Thermonuclear Fusion, Akad. Nauk USSR, Vol. III, p. 285 (1958).

2. T.G. Northrop and E. Teller, Phys. Rev. 117 (1960) 215.

3. H. Alfvén and C.G. Fälthammar, Cosmical Electrodynamics, Second Edition, Oxford Univ. Press (1963).

4. H. Persson, Phys. Fluids 6 (1963) 1756 and 9 (1966) 1090.

5. B. Lehnert, Plasma Physics 10 (1968) 263.

ASYMPTOTIC MAGNETIC SURFACES *)

by

G.O. Spies and D. Lortz

INSTITUT FÜR PLASMAPHYSIK

D-8046 Garching bei München, Germany

Toroidal magnetic fields $B = \sum_{\nu \geq 0} \varepsilon^\nu \vec{B}_\nu$ where the unperturbed field $\vec{B}_0$ has zero rotational transform are considered. On rather weak assumptions it is shown that single-valued formal solutions $F = \sum_{\nu \geq 0} \varepsilon^\nu F_\nu$ of the equation $\vec{B} \cdot \nabla F = 0$ exist, and that the asymptotic magnetic surfaces F= const are unique to all orders. Recursion formulae are derived which allow any order of F to be calculated from its lower orders, and explicit expressions are given for F_0. These depend on the order of the rotational transform ι, which can either be the same as, or higher than, the order of the perturbing field. In the former case, i.e. if $\vec{B} - \vec{B}_0 \sim \iota$, $F_0(X)$ is simply the flux of the lowest order perturbing field through the closed line of force of the unperturbed field passing through the point X. The latter case occurs if, and only if, this flux is a constant.

For the special cases of stellarator-like vacuum fields, i.e. for vacuum fields having circular lines of force in the limit $\varepsilon \to 0$, it is shown that the asymptotic magnetic surfaces can be toroidally closed without encircling any current carrying wires only if ι is of higher order than the perturbing field. This necessary condition is fulfilled by classical stellarators with alternating helical windings, but it is violated by any torsatron configurations.

As another application the lowest order of an adiabatic invariant is constructed for the longitudinal guiding centre motion. This invariant applies if ι is comparable with the usual expansion parameter of the adiabatic orbit theory. It reduces to the usual longitudinal invariant if ι is much smaller. If $\iota \sim \vec{B} - \vec{B}_0$, then it agrees with an adiabatic invariant previously constructed by Hastie et al. on the assumption that exact magnetic surfaces exist, taking an entirely different form in general.

---

*Submitted to "Plasma Physics".

FLUCTUATION LEVELS CONNECTED WITH REACTIVE MARGINAL INSTABILITIES OF A MAGNETIZED PLASMA

by

E. Minardi

Association Euratom-FOM/FOM-Instituut voor Plasma-Fysica
Rijnhuizen, Jutphaas, the Netherlands

Abstract

Some physical aspects and applications are discussed of an expression giving the probability distribution for special collective resonant electrostatic fluctuations. The latter should include the marginal reactive instabilities associated with bodily energy transportation from the polarized plasma into the collective field.

Let $\varepsilon(\omega,\vec{k})$ be the effective dielectric coefficient fixing the plasma electrostatic oscillations and ω_m, $k_m^2=-\lambda^{-2}>0$ a real solution of the equation $\varepsilon(\omega,\vec{k})=0$ (where $\mathrm{Re}\,\varepsilon(\omega_m,k)\equiv\varepsilon_r(\omega_m,k)=1+(k\lambda)^{-2}$) representing a marginal point of the dispersion relation. Consider, in a reference system moving with the velocity ω_m/k_m, a collective charge density fluctuation $\delta\sigma=V_1^{-\frac{1}{2}}\sum_{\vec{k}}\delta\sigma_{\vec{k}}\exp i\vec{k}\vec{x}$ occurring inside the volume V_1. As shown elsewhere[1] the probability density for $\delta\sigma_k$ is then given by

$$p=p_e\exp-\frac{\lambda^2}{4\pi\tau}\left(\sum_{\vec{k}>0}|\delta\sigma_k|^2+\sum_{\vec{k}>0}\frac{|\delta\sigma_k|^2}{k^2\lambda^2}-\frac{1}{2\pi N\tau}\sum_{\vec{k}>0}\frac{|\delta\sigma_k|^2}{k^2}\sum_{\vec{k}>0}|\delta\sigma_{\vec{k}}|^2\right). \tag{1}$$

In the cases described by the Harris dispersion relation one has (for $k_\parallel\neq0$)

$$\tau=4\pi^2\left(\frac{\sum_{\text{species}}q^2n\sum_n C_n^j F_\parallel\left(\frac{\omega-n\Omega}{k_\parallel}\right)}{kk_\parallel|d\ \mathrm{Im}\,\varepsilon/dy|}\right)_{\omega_m,\vec{k}_m}, \tag{2}$$

where $y=(\omega-\omega_m)/k$ and a distribution function of the form $f(\vec{v})=ng_o^j(v_\perp)F_\parallel(v_\parallel)$ is assumed, the quantities g_o^j and C_n^j being defined as in Ref. 2.

It can be shown that the probability density (1) has an absolute maximum corresponding to all $|\delta\sigma_k|=0$ with the exception of the $|\delta\sigma_k|$ associated with the minimum unstable k. For simplicity, we shall consider only this case, where Eq. (1) takes the form

$$p=p_e\exp-\frac{\lambda^2|\delta\sigma_k|^2}{4\pi\tau}\left[1+(k\lambda)^{-2}-\frac{|\delta\sigma_k|^2}{2\pi\tau Nk^2}\right]. \tag{3}$$

To obtain Eq. (1) the state of the plasma is supposed to be specified by the coarse-grained values of the charge density (related both to the collective and the individual-particle fluctuations) in each volume ΔV in which the plasma volume V is subdivided by a coarse graining inherent to the measuring process. In Eq. (1) $N=V/\Delta V$, while the fourth-order term in $\delta\sigma_k$, proportional to N^{-1}, represents an interaction between the collective and the individual fluctuations; it is important for $k^2<-\lambda^{-2}$, which defines the unstable region. As shown in Ref. 1 the mean square deviations $\overline{\Delta\sigma^2}$ ($\overline{\Delta E^2}$) of the random fluctuations of $\sigma(E)$ as measured in each ΔV are connected with τ according to $\tau/2=V\lambda^2\overline{\Delta\sigma^2}/8\pi N<0$ ($|\tau/2|=\overline{\Delta E^2}\Delta V/8\pi$). The "fluctuation temperature"[3] τ must be independent of the collective fluctuations ("isothermic" system). This involves $\lambda|\partial\lambda^{-2}/\partial k_i|_m\ll1$ (condition (a)), since then λ^{-2} is independent, at first order, of variations of the considered component k_i away from the equilibrium point (which is the marginal point in the considered reference frame). Moreover, while one can take $V=V_1$ at equilibrium, in the stable region ($k^2>-\lambda^{-2}$) the condition $V\gg V_1$ must hold, outside equilibrium, for the volume V_1 of the subsystem where "isothermic" fluctuations are considered (thermodynamic limit).

Equation (3) involves stringent bounds for $\overline{\delta\sigma^2}$ in view of the restrictions $N\ll nV$ and $k\simeq k_m$ in the unstable region, as shown in Ref. 1. We next discuss some physical aspects and possible applications of Eq. (3).

The quantity $1+(k\lambda)^{-2}-|\delta\sigma_k^2|/2\pi\tau Nk^2$ constitutes an effective non-linear dielectric constant $\varepsilon_{n\ell}$, taking into account, in the last term, the reaction of the polarized plasma to the collective instability. Indeed, the part of the polarization energy due to the individual fluctuations equals $\Phi=\tau N(\varepsilon_r-1)/2$. When the instability develops in V, the energy of the collective field δE associated with the mode introduced above becomes $W=\delta E^2V/8\pi=|\delta\sigma_k^2|/4\pi k^2$. Assuming that this energy is absorbed from Φ, the polarization energy reduces to $\Phi_{n\ell}=\Phi-W$, while $\varepsilon_{n\ell}$ follows from the relation $\Phi_{n\ell}\equiv\tau N(\varepsilon_{n\ell}-1)/2=\tau N(\varepsilon_r-1-\delta\sigma_k^2/2\pi\tau k^2N)/2$.

If the system is neither dispersive at the considered marginal point, where (condition (b)) $(d\varepsilon_r/d\omega)_m=0$, nor in the adjacent unstable region, the relation $U=\varepsilon_{n\ell}\delta E^2V/8\pi\simeq-\varepsilon_{n\ell}|\delta\sigma_k^2|\lambda^2/4\pi$ can be used for calculating the time-averaged total collective energy of the plasma. Moreover, it is assumed that $\varepsilon_r(\omega)$, and therefore U, increases (condition (c)) for those $\delta\omega=i\gamma$ ($\gamma>0$) which are associated with perturbations from the marginal point to the unstable region ($k^2<-\lambda^{-2}$). These are just the physically relevant perturbations which are more probable than those moving the system towards the stable region described by Eq. (3). Since U is to be minimized with respect to the relevant variations, it constitutes a "good" thermodynamical potential under the conditions (b) and (c). In fact, the discussion of the dispersion relation assuming (b) and (c) shows that instability occurs when $k^2<-\lambda^{-2}$ which is just the unstable region predicted by Eq. (3), which can be written $p=p_e\exp-U/|\tau|$. It is also verified that the most probable $\delta\sigma_k$ minimizes $U(\delta\sigma_k)$.

The above considerations can be applied e.g. to the loss-cone instability of Guest and Dory[2] which admits a branch point (related to a marginal value of ω_{pe}), where $(\partial\lambda^{-2}/\partial k_\parallel)_m=0$ (condition (a)), while (b) and (c) are satisfied when $\tilde{\varepsilon}_r(\omega,\omega_{pe})\equiv\varepsilon_r(\omega,\omega_{pe},k_\parallel(\omega,\omega_{pe}))$ ($k_\parallel=k_\parallel(\omega,\omega_{pe})$ is the marginal relation for fixed $k_\perp$; see Figs. 2 and 3 of Ref. 2).

A further example concerns the flute instability ($k_\parallel=0$, see Ref. 4 for the notations) in a Maxwellian plasma (so that $|\tau|=k(T_i+T_e)/2$). The condition (a) here implies $|dn/ndx|\ll2\alpha_i|g_i-g_em/M|$ (equilibrium near the marginal point $dn/dx=0$) and, moreover, $4\pi nMc^2/B^2\ll1$.

The author is indebted to Professor H. Bremmer for his comments.

This work was performed under the EURATOM-FOM association agreement with financial support from ZWO and Euratom.

References

1. E. Minardi, Internal Report 69/033, Jutphaas, August 1969 (to be published).
2. G.E. Guest and R.A. Dory, Phys. Fluids 8 (1965) 1853.
3. G. Bekefi in Radiation Processes in Plasmas (J. Wiley & Sons Inc., New York, 1966) 129.
4. N.A. Krall in Advances in Plasma Physics, Vol. I (Interscience Publ., New York, 1968) 168.

LOCAL POTENTIAL AND NONLINEAR STABILITY IN HYDROMAGNETICS

by
F. Herrnegger
INSTITUTE FOR THEORETICAL PHYSICS
Innsbruck University, A-6020 Innsbruck, Austria

Abstract: The concept of a thermodynamic local potential is applied to the Bénard problem of hydromagnetics. In this way a new functional is derived which may be viewed as a generalized entropy production due to various dissipative and convective processes. Based on this result a stability analysis including arbitrary nonlinearities is given.

1. Introduction. The stability of a hydromagnetic system in a stationary equilibrium depends essentially on nonlinear effects due to the interaction between the dynamic variables which determine the evolution of the system, or due to the dependence of the phenomenological transport coefficients at the instantaneous state of the system. In this paper a general evolution criterion and a thermodynamic local potential is given. Based on that a thermodynamic stability theory is derived valid for a magnetofluid of infinite electrical conductivity where the viscosity and the thermal conductivity vary with temperature T. The electrical conductivity is assumed to be infinite. Prigogine[1,2] introduced the concept of local potential into the phenomenological equations of an electrically nonconducting continuum without electromagnetic field being in nonequilibrium.

2. Local potential. The flow configuration of the Bénard problem corresponds to a horizontal layer of plasma with volume V, in which a temperature gradient is maintained by heating it from below in a constant gravitational field $\vec{g}$ and in a variable magnetic field $\vec{B} = (B_1, B_2, B_3)$. It is assumed that the Boussinesq approximation is valid. We start from the ideal MHD basic equations including effects due to the viscosity $\bar{\nu}$ and the heat conductivity λ, and construct a negative semidefinite function Φ

$$\Phi = -\left[\frac{\rho_o c_v}{T_o^2}\left(\frac{\partial T}{\partial t}\right)^2 + \frac{\rho_o}{T_o}\left(\frac{\partial \vec{v}}{\partial t}\right)^2 + \left(\frac{\partial \vec{B}}{\partial t}\right)^2\right] \tag{1}$$

(where $\vec{v}$, ρ and c_v are flow velocity, density and specific heat; the index o corresponds to the plane $x_3 = 0$). Let us denote the physical quantities of the equilibrium state of the plasma configuration whose stability will be investigated by barred quantities $\bar{q}$ and let us write the nonlinear disturbances without bar: $q(\vec{x},t) \to \bar{q}(\vec{x},t) + q(\vec{x},t)$. If one integrates (1) over the whole volume V bounded by the surface Σ, then, using the MHD basic equations, one obtains the following relation[3]

$$\int_V \Phi dV = \frac{\partial}{\partial t}\left[\int_V \mathcal{L}_V dV + \int_\Sigma \mathcal{L}_\Sigma d\Sigma\right] \equiv \frac{\partial}{\partial t}\,\Psi(t) \tag{2}$$

where the Lagrangians $\mathcal{L}_V$ and $\mathcal{L}_\Sigma$ are given by ($\vec{n}$ normal to the surface):

$$\begin{aligned}\mathcal{L}_V = {} & \frac{\rho_o c_v}{T_o^2}(\bar{\vec{v}}.\nabla\bar{T})T + \frac{\rho_o c_v \lambda}{2T_o^2}(\nabla T.\nabla T) - \frac{\bar{\rho}}{T_o}(\vec{g}.\vec{v}) + \frac{\bar{\nu}}{2T_o}\sum_{i=1}^{3}(\nabla v_i.\nabla v_i) + \\ & + \frac{1}{T_o}(\nabla.\bar{\vec{v}})p + \frac{\rho_o}{2T_o}(\bar{\vec{v}}.\nabla\vec{v}^2) - \frac{\rho_o}{T_o}\sum_{i=1}^{3}\bar{v}_i(\bar{\vec{v}}.\nabla v_i) + \frac{1}{T_o}(\nabla\bar{p}.\vec{v}) + \\ & - \frac{1}{T_o\mu_e}\left\{\sum_{i=1}^{3} v_i[\nabla.(\bar{\vec{B}}\,\bar{B}_i)] - \frac{1}{2}(\vec{v}.\nabla\bar{\vec{B}}^2)\right\} - \sum_{i=1}^{3} B_i[\nabla.(\bar{\vec{B}}\,\bar{v}_i)] + \\ & + \frac{1}{2}(\bar{\vec{v}}.\nabla\bar{B}^2) + \sum_{i=1}^{3}\bar{B}_i(\bar{\vec{v}}.\nabla B_i) + \frac{\rho_o}{T_o}(\vec{v}.\frac{\partial\bar{\vec{v}}}{\partial t}) + \frac{\rho_o c_v}{T_o^2}T\frac{\partial\bar{T}}{\partial t} + (\vec{B}.\frac{\partial}{\partial t}\bar{\vec{B}})\end{aligned} \tag{3}$$

$$\mathcal{L}_\Sigma = -\frac{\rho_o c_v \lambda}{T_o}T(\nabla\bar{T}.\vec{n}) - \frac{\bar{\nu}}{T_o}\sum_{i=1}^{3} v_i(\vec{n}.\nabla\bar{v}_i). \tag{4}$$

After carrying out the integration over the space coordinates in (2), the resulting quantity $\Psi(t)$ is a function of t only. The form Φ given by (1) contains derivatives with respect to time t and is smaller than zero or vanishes for the stationary state. Consequently there follows for the time-derivatives of Ψ:

$\frac{\partial\Psi(t)}{\partial t} \leq 0$; the equality sign holds for the steady equilibrium state. Therefore Ψ can only decrease with time and takes its minimum value at the steady state. This quantity Ψ is called the local potential[1,3]. It is important to note that the integrand of Ψ depends on the equilibrium quantities $\bar{q}$ and on the nonlinear perturbations q, the former being supposed to be known. Taking now $\Psi(\bar{q},q)$ as a functional of the unknown functions q, one obtains the extremal principle

$$\Psi(\bar{q},q) = \text{extremum}, \tag{5}$$

the variational derivatives of which produce the unsteady MHD basic equations in the form of the Euler-Lagrange differential equations with the subsidiary conditions $\bar{q} = q$. In this way we have derived a new general variational principle applicable to time-dependent processes, the solution of which may be considered as a consistent scheme of successive approximations and is useful for stability investigations.

3. Stability analysis. The integrals in (2), representing a volumetric contribution and a surface contribution, may be viewed as a generalized entropy production in the volume V per unit time. They contain an expression of entropy production due to dissipative processes and an expression due to convective processes. This fact is the reason for the fact that a thermodynamic theory of magnetohydrodynamic stability is feasible. This concept is much more important for the case that the dissipation mechanisms are arbitrary functions of temperature. Analogies and relations between the free energy and the local potential for dissipative effects of thermal and mechanical origin without magnetic field and without ohmic dissipation are given by Glansdorff[3].

We now assume that the plasma configuration whose stability we are investigating has been perturbed according to $q = q^o + f(x)\Omega(\omega t)$ (analogously for the $\bar{q}$), where q^o is the value of q in the stationary state, the f(x) is the spatial perturbation of this state, and the parameter ω occurring in the function Ω is a measure of the stability of the system. If we specify $\Omega(\omega t) = \exp(-\omega t)$, then a positive ω would indicate a stable system. If the perturbed system is in nonequilibrium, then the function is not identically zero. Therefore the functional of the total energy dissipated during the time interval τ is obtained by integration $\Psi(t)$ with respect to t. For small time intervals we may expand the resulting functional in a Taylor series, and after introducing the assumption made above we get a condition for the parameter ω where only known functions enter. In order to obtain information about stability, it is sufficient to determine the sign of ω.

The author thanks Professor F. Cap for many discussions. This work has been sponsored in part by the United States Government under Contract No. F61052-67-C-0014.

1 Glansdorff P., Prigogine I., Physica 30 (1964) 351

2 Donnelly R.J., Herman R., Prigogine I., Nonequilibrium Thermodynamics, Variational Techniques and Stability, University of Chicago Press 1966

3 Herrnegger F., Innsbruck University UNICP-SR64 (1970)

LINEAR WAVES IN INCOMPRESSIBLE BEAM-PLASMA SYSTEMS

by

Frank Verheest

SEMINARIE VOOR ANALYTISCHE MECHANICA, RIJKSUNIVERSITEIT GENT

Jozef Plateaustraat 22, B-9000 Gent, Belgium

Abstract: *The dispersion law for linear waves in incompressible beam-plasma systems is derived. Several special cases are discussed.*

If a magnetofluiddynamical treatment is given of waves in a plasma (in the broadest sense), an additional assumption is required about the pressure tensor in order to close the set of magnetofluiddynamical equations[1]. Very often the pressure is assumed isotropic and hence the pressure tensor becomes a multiple of the unit tensor. This almost invariably goes together with the supplementary assumption that the plasma pressure varies barotropically, which includes both isothermal and adiabatic behavior[2]. There is, however, no valid physical reason why the hypotheses of a scalar pressure and a barotropic behavior of the fluid should be coupled. We therefore propose to investigate here how the dispersion law for linear waves is changed for non-barotropic plasmas. We will do this for simplicity for a specific class, namely the *incompressible plasmas*. We start from the set of magnetofluiddynamical equations for incompressible plasmas and have per kind of particles[3]:

$$\vec{\nabla}\cdot\vec{v} = 0, \qquad \frac{\partial\vec{v}}{\partial t} + \vec{v}\cdot\vec{\nabla}\vec{v} + \frac{1}{\rho}\vec{\nabla}p - \frac{q}{m}(\vec{E} + \vec{v}\times\vec{B}) = 0,$$

$$\vec{\nabla}\times\vec{E} = -\frac{\partial\vec{B}}{\partial t}, \qquad \vec{\nabla}\times\vec{H} = \frac{\partial\vec{D}}{\partial t} + \vec{J}, \qquad \vec{\nabla}\cdot\vec{D} = \sigma. \tag{1}$$

The subscript s indicating the species componing the plasma will be omitted whenever possible. Before linearizing these equations about a ***uniform equilibrium***, we remark that such an equilibrium must satisfy the conditions

$$\vec{E}_0 + \vec{v}_0\times\vec{B}_0 = 0, \qquad \vec{J}_0 \equiv \sum_s N_0^s q^s \vec{v}_0^s = 0,$$

$$\sigma_0 \equiv \sum_s N_0^s q^s = 0. \tag{2}$$

This indicates that, even if the plasma is composed of more than one kind of particles, all steady-state velocities have the same component $\vec{E}_0\times\vec{B}_0/B_0^2$ perpendicular to the static magnetic field. By a suitable choice of the reference frame (already taken with the z-axis along $\vec{B}_0$) we can transform away all $V_{0x,y}^s$ as well as $\vec{E}_0$. We now apply the linearization procedure with a Fourier transform of all first-order perturbed quantities and get:

$$\vec{k}\cdot\vec{v} = 0, \qquad \phi\vec{v} = \frac{1}{\rho_0}\vec{k}p + i\frac{q}{m}(\vec{e} + \vec{v}_0\times\vec{b} + \vec{v}\times\vec{B}_0),$$

$$\vec{k}\times\vec{e} = \omega\vec{b}, \qquad c^2\vec{k}\times\vec{b} = -\omega\vec{e} - \frac{i}{\epsilon_0}\vec{j}. \tag{3}$$

Here $\phi = \omega - k_z V_0$ is the Doppler-shifted frequency (per species). It is worth mentioning that since $\vec{k}\cdot\vec{e} = 0$, we always have that $\vec{k}$, $\vec{e}$, $\vec{b}$ form a positive orthogonal triad. We now solve the set (3) for $\vec{v}$ and p and find:

$$v_x = i\frac{q\phi}{m\omega}\frac{k^2\phi e_x + i\Omega k_z^2 e_y}{k^2\phi^2 - k_z^2\Omega^2},$$

$$v_y = i\frac{q\phi}{m\omega}\frac{-i\Omega k^2 e_x + k^2\phi e_y}{k^2\phi^2 - k_z^2\Omega^2},$$

$$v_z = i\frac{q\phi}{m\omega}\frac{-i\Omega k_x k_z e_y + k^2\phi e_z}{k^2\phi^2 - k_z^2\Omega^2},$$

$$p = i\frac{q\rho}{m\omega}\frac{-i\Omega\phi^2 k_x e_y + (\omega k_z\Omega^2 - \phi^2 k^2 V)e_z}{k^2\phi^2 - k_z^2\Omega^2}. \tag{4}$$

From the substitution of the values for $\vec{v}$ into the wave equation,

$$(\omega^2 - c^2k^2)\vec{e} + i\frac{\omega}{\epsilon_0}\sum_s N_0^s q^s \vec{v}^s = 0, \tag{5}$$

the dispersion law follows as

$$\left(\omega^2 - c^2k^2 - \sum_s \frac{\Pi_s^2\phi_s^2 k^2}{k^2\phi_s^2 - k_z^2\Omega_s^2}\right)\left(\omega^2 - c^2k^2 - \sum_s \frac{\Pi_s^2 k\phi_s}{k\phi_s \pm k_z\Omega_s}\right) = 0. \tag{6}$$

While discussing this dispersion law, we have to keep in mind that $\vec{k}\cdot\vec{e} = 0$, which means that we are dealing with transverse electromagnetic waves, modified by the presence of the incompressible beam-plasma system immersed in a static magnetic field. We have to distinguish the following different cases:

-i- *Propagation along the external magnetic field*: From (4) and (6) it is clear that the dispersion law evolves into

$$\omega^2 = c^2k^2 + \sum_s \Pi_s^2(\omega - k_z V_0^s)/(\omega - k_z V_0^s \pm \Omega_s). \tag{7}$$

This result is essentially the same as obtained from a cold plasma treatment[4], especially since here $p = 0$, indicating that these parallel electromagnetic waves do not affect the static pressure.

-ii- *Propagation across the external magnetic field*: (6) becomes

$$\omega^2 = c^2k^2 + \sum_s \Pi_s^2 . \tag{8}$$

Here even the effect of the static magnetic field and of the possible beam velocities is no longer felt.

-iii- *Arbitrary propagation*: The general dispersion law is now

$$\omega^2 = c^2k^2 + \sum_s \Pi_s^2 k(\omega - k_z V_0^s)/(k\omega - k_z k V_0^s \pm k_z\Omega_s). \tag{9}$$

This varies appreciably from analyses given for a plasma with a scalar barotropic or even anisotropic pressure variation[5]. Because of the incompressibility the longitudinal plasma waves (essentially of compressional nature) are absent, and hence no coupling phenomena can occur between the transverse electromagnetic and the longitudinal plasma waves.

[1] *T.J.M. Boyd & J.J. Sanderson,* Plasma dynamics *(London 1969: Nelson), p. 45.*

[2] *P.C. Clemmow & J.P. Dougherty,* Electrodynamics of particles and plasmas *(Reading Mass. 1969: Addison-Wesley), p. 175.*

[3] *I.P. Shkarofsky, T.W. Johnston & M.P. Bachynski,* The particle kinetics of plasmas *(Reading 1966: Addison-Wesley), p. 426.*

[4] *K.N. Stepanov & A.B. Kitsenko, Zh. tekh. Fiz.* 31, *167 (1961).*

[5] *F. Verheest (to be published).*

INDEX OF AUTHORS